

Green Energy and Technology



Jan Kośny

David W. Yarbrough *Editors*

# Thermal Insulation and Radiation Control Technologies for Buildings

 Springer

# **Green Energy and Technology**

Climate change, environmental impact and the limited natural resources urge scientific research and novel technical solutions. The monograph series Green Energy and Technology serves as a publishing platform for scientific and technological approaches to “green”—i.e. environmentally friendly and sustainable—technologies. While a focus lies on energy and power supply, it also covers “green” solutions in industrial engineering and engineering design. Green Energy and Technology addresses researchers, advanced students, technical consultants as well as decision makers in industries and politics. Hence, the level of presentation spans from instructional to highly technical.

**\*\*Indexed in Scopus\*\*.**

**\*\*Indexed in Ei Compendex\*\*.**

More information about this series at <https://link.springer.com/bookseries/8059>

Jan Kośny · David W. Yarbrough  
Editors

# Thermal Insulation and Radiation Control Technologies for Buildings

 Springer

*Editors*

Jan Košny  
Mechanical Engineering  
University of Massachusetts  
Lowell, MA, USA

David W. Yarbrough  
R&D Services, Inc.  
Watertown, TN, USA

ISSN 1865-3529

ISSN 1865-3537 (electronic)

Green Energy and Technology

ISBN 978-3-030-98692-6

ISBN 978-3-030-98693-3 (eBook)

<https://doi.org/10.1007/978-3-030-98693-3>

© The Editor(s) (if applicable) and The Author(s), under exclusive license to Springer Nature Switzerland AG 2022

This work is subject to copyright. All rights are solely and exclusively licensed by the Publisher, whether the whole or part of the material is concerned, specifically the rights of translation, reprinting, reuse of illustrations, recitation, broadcasting, reproduction on microfilms or in any other physical way, and transmission or information storage and retrieval, electronic adaptation, computer software, or by similar or dissimilar methodology now known or hereafter developed.

The use of general descriptive names, registered names, trademarks, service marks, etc. in this publication does not imply, even in the absence of a specific statement, that such names are exempt from the relevant protective laws and regulations and therefore free for general use.

The publisher, the authors, and the editors are safe to assume that the advice and information in this book are believed to be true and accurate at the date of publication. Neither the publisher nor the authors or the editors give a warranty, expressed or implied, with respect to the material contained herein or for any errors or omissions that may have been made. The publisher remains neutral with regard to jurisdictional claims in published maps and institutional affiliations.

This Springer imprint is published by the registered company Springer Nature Switzerland AG  
The registered company address is: Gewerbestrasse 11, 6330 Cham, Switzerland

# Preface

Thermal insulation technologies play an important role in today's buildings. They equally affect the general architectural design, building envelope configurations, as well as, building energy conservation, and internal thermal comfort. The editors with decades of research and application experience in the field of thermal insulations and building envelopes undertook the organization of this book on thermal insulations to provide a milestone for the status of the field and to provide useful discussions about research areas that are active at this time. The twenty contributors to this volume on thermal insulation representing three continents are due our praise and appreciation for their time and effort to prepare chapters based on their experience and expertise. The intent of this work is to provide industrial and academic researchers a resource for entry to a diverse collection of thermal insulation types and related subjects. The chapters contain discussion that has value for a wide variety of professions in the area of insulation technologies, building envelopes, material engineering, building science, as well as those who would simply like to know the status of the science at this point in history.

In the opening section, this book offers a short history of thermal insulation and later, it contains discussions about conventional materials such as mineral wool, reflective insulations, and cellular plastics used to insulate buildings. An effort has been made to include chapters on insulation products, for example, reflective insulations and bio-based materials, that are not commonly allocated much space in publications on thermal insulation materials. Areas that support the effective use of thermal insulations in buildings such as resistance to fire, biological considerations, and assembly evaluation are included in this book to further document the current status of thermal insulations used in buildings.

Major advances in the field of thermal insulation have appeared in recent years. Evacuated panels and aerogels have come into use with thermal resistivities (R-value per unit thickness) that are far greater than conventional air-based insulations. The term "super-insulation" is sometimes applied to these materials especially in the case of nano-based and vacuum insulations. A chapter on low-density concretes that have significant thermal resistance is included as well. Areas important to the performance of thermal insulations have not been neglected. This category includes topics such

as dynamic performance and the concept of thermal mass, the impact of thermal bridging, and material designs to reduce flammability. The impact of moisture on thermal performance is an important area that will expand user understanding. In every case, the chapter authors have included key references that provide additional coverage and insight for the subjects being discussed. The chapters as a result offer multiple avenues for evaluating and characterizing thermal insulations in the present decade.

The category “conventional insulating materials” is ably represented by chapters on mineral fiber insulations (glass, rock, and ceramic wools), reflective insulations, cellular plastic insulations, and cellular concrete by Z. Chen, T. Lui; H. Saber, C. Lim and M. Ashhar, A. Stepien, R. Dachowski, and J. Piotrowski. Advanced insulations that make use of reduced dimensions or vacuums (super insulations) are described and discussed in chapters by P. Mukhopadhyaya, Z. Chen, B. Jelle, and E. Kossecka. Environmental factors and assembly details that affect insulation performance are the subject of contributions from H. Kunzel, as well as E. Kossecka, D. Yarbrough, and J. Kośny. Unique subjects for those deep in this area of building science are represented by chapters on bio-based insulation by H. Kunzel and S. Czlonka, bio-resistance by N. Sienkiewicz, and reduced flammability by J. Lubczak and R. Lubczak.

The editors of this book and publisher are indebted to experts, who contributed to this book, for sharing their knowledge and insights.

Please bear in mind that publications of this type inevitably reflect the opinions and prejudices of their authors. That is why some readers may inevitably disagree with our opinions, book structure, and of course the choice of subject matter presented. Past experience indicates that such disagreements usually represent healthy reflections coming from the diversity of the technology under discussion and are essential for its evolution. Nevertheless, we hope that all future readers will find something of interest.

Happy Reading!

Lowell, USA  
Watertown, USA

Jan Kośny  
David W. Yarbrough

# Contents

<b>1</b>	<b>Short History of Thermal Insulation and Radiation Control Technologies Used in Architecture</b> .....	<b>1</b>
	Jan Kośny and David W. Yarbrough	
<b>2</b>	<b>Long-Term Thermal Performance of Insulations Under Moisture Loads</b> .....	<b>37</b>
	Hartwig M. Künzel	
<b>3</b>	<b>Overview of Thermal Performance of Air Cavities and Reflective Insulations</b> .....	<b>55</b>
	Hamed H. Saber	
<b>4</b>	<b>Reflective Insulation in South-East Asia Region</b> .....	<b>83</b>
	Lim Chin Haw and Muhamad Zahin Bin Mohd Ashhar	
<b>5</b>	<b>Development and Application Status of Glass Wool, Rock Wool, and Ceramic Wool</b> .....	<b>129</b>
	Zhaofeng Chen and Tianlong Liu	
<b>6</b>	<b>Characteristics of Bio-based Insulation Materials</b> .....	<b>163</b>
	Hartwig M. Künzel	
<b>7</b>	<b>Bio-based Foam Insulation</b> .....	<b>177</b>
	Sylwia Członka, Agnė Kairytė, and Anna Strąkowska	
<b>8</b>	<b>Improvements of Polyurethane (PU) Foam’s Antibacterial Properties and Bio-resistance</b> .....	<b>217</b>
	Natalia Sienkiewicz	
<b>9</b>	<b>Increased Thermal Stability and Reduced Flammability of Polyurethane Foams with an Application of Polyetherols</b> .....	<b>241</b>
	Jacek Lubczak and Renata Lubczak	



**10 High Performance Thermal Insulations—Vacuum Insulation Panels (VIPs) . . . . . 275**  
Phalguni Mukhopadhyaya

**11 Application of Vacuum Insulation Panels (VIPs) in Buildings . . . . . 289**  
Zhaofeng Chen and Qiong Wu

**12 The Concept of Nano Insulation Materials—Challenges, Opportunities, and Experimental Investigations . . . . . 347**  
Bjørn Petter Jelle

**13 Insulated Autoclaved Cellular Concretes and Improvement of Their Mechanical and Hydrothermal Properties . . . . . 393**  
Anna Stepień, Ryszard Dachowski, and Jerzy Z. Piotrowski

**14 Dynamic Thermal Performance of Insulation Combined in Different Formations with Thermally Massive Components . . . . . 421**  
Jan Kośny, Elisabeth Kossecka, and David W. Yarbrough

**15 Thermal Efficiency of Insulation in Building Structures—The Impact of Thermal Bridging . . . . . 443**  
Jan Kośny and David W. Yarbrough

# Chapter 1

## Short History of Thermal Insulation and Radiation Control Technologies Used in Architecture



Jan Kośny and David W. Yarbrough

**Abstract** This chapter discusses the history of major and most common types of building thermal insulation, which is probably as long as human civilization. Different types of thermal insulation materials have been used in buildings to reduce heat transfer between different building components or structures of varying temperatures, with best known applications in building envelopes. In practice, the exterior building skin should perform a variety of different roles that include keeping the exterior climate outside by limiting the transfer of heat, water, and air, in order to maintain comfortable interior conditions. A particular role, however, is reserved for thermal insulation, which is responsible for minimizing the heat exchange between the exterior environment and the interior space of a building. The mitigation of heat transport is the primary reason for thermal insulation materials being so widely used in buildings. The use of thermal insulation materials greatly impacts the following:

- Energy consumed for heating and cooling of buildings' internal spaces.
- The thermal and hygrothermal performance of specific envelope and construction materials or structures that require thermal insulation such as opaque walls and roofs, damp-proof courses, waterproof membranes, related joints or sealants, and others.

In these applications, thermal insulation is a key component of the building interior fabric or exterior envelope. Additional functions often provided by thermal insulation include: a visual and daylight connection to the outdoors (windows and skylights), reduction of noise transmission, support of structural loads, and aesthetically pleasing appearance on both sides of the building envelope. Furthermore, a number of configurations of thermal insulation and heat conducting components, generate thermal bridging effects in various parts of the building skin and architectural interfaces. They can significantly impact thermal performance of building envelopes and also

---

J. Kośny (✉)  
University of Massachusetts Lowell, Lowell, MA, USA  
e-mail: [Kosny\\_Jan@uml.edu](mailto:Kosny_Jan@uml.edu)

D. W. Yarbrough  
R&D Services, Watertown, TN, USA

their long-term durability. During the last two centuries thermal insulation technologies have changed significantly, and the chapter below discusses these changes for the most popular categories of insulation.

## 1.1 Introduction

Since the beginning of civilization, people have understood the need for both warm cloths as well as insulated, comfortable dwellings. In prehistoric ages, members of hunting tribes covered themselves with a variety of natural materials including wool and skins from animals. At the same time, humans built shelters using readily available ordinary materials such as stone, mud, wood, grass, leaves, and other accessible materials for protection from cold winters and hot summers. These materials not only protected people from the elements: sun, wind, and rain, but also from animals, insects, and sometimes intruders. That is why the history of thermal insulations is so strongly coupled with the history of our civilization and parallels, for example, the history of tools. As soon as prehistoric people learned how to make tools, they used them to hunt, prepare food, build shelters, and fashion clothes.

The history of thermal insulation is easily as long as that for other common man-made items. It is fair to say, however, that the development of building insulation is no doubt as old as human construction activity. Prehistoric people used natural caves or built shelters to protect themselves from the elements, originally using a variety of inorganic and organic materials, including those naturally available in regions from the tropics to the arctic. Types of natural thermal insulations used in primitive construction were region-specific, ranging from leaves, reeds, and grass in the tropics, and porous stones, adobe structures, clay straw/grass mixtures, to snow and ice blocks in the far north areas of North America and Europe.

Later, during the subsequent thousands of years, building insulation technologies have been closely following changes in construction techniques and occupant preferences in different parts of the world. Builders have not been limited to materials found in nature since the continuously growing demand for comfortable structures coincided with discoveries yielding a variety of new processes and materials suitable for use as thermal insulation. The great variety of modern building insulations such as mineral wool, fiberglass, and cellular plastic foams have their roots either during the second great industrial revolutions of the nineteenth century or during the years between WWI and WWII. The high-performance insulations based on vacuums or nanomaterials are relatively recent innovations.

## 1.2 Thermal Insulation Used in Early Age Constructions

Undoubtedly, the earliest forms of human shelters were just trees, which were expected to provide some protection from rain, snow and the searing heat of the sun. Similarly, trees protected primeval people from large animals that could not climb the trees. The first man-made shelter was most likely made from stones and tree branches, where leaves served as a rain and sun shield. The stones were placed at the base of the structure to hold the branches in place. No doubt, animal skins, fur, or wool were also used. But, due to limited durability, the most common applications were temporary tent-like structures. The first native Americans encountered by Europeans, for example, lived in structures roofed with bark or animal skins.

### 1.2.1 *Natural Materials Used in Primitive Shelters*

When the early nomadic lifestyle advanced into the more settled existence and after the introduction of agriculture, people realized that they needed sturdy permanent shelters. The common choices for construction were stones, wood and a variety of earth-based materials. Both earth-sheltered houses and cave-based living accommodations were popular because of their inherent thermal comfort and excellent protection against wild animals and fire. Due to the suitable thermal resistance and significant heat-storage capacity of thick stone or earth-based structures, people could stay in warm interiors during the winter and enjoy relatively cool conditions in summer. The oldest example of such shelters are the earth-covered stone-age Neolithic structures located on the Bay of Skail on the west coast of the Mainland Island that is part of the Orkney Archipelago of Northern Scotland.<sup>1</sup> The Skara Brae settlement, for example, consists of a cluster of eight houses that were occupied from roughly 3180 to 2500 BC. Similarly constructed buildings can be found in other Nordic locations spreading from Greenland, Iceland, Scandinavia, and Russia, to Alaska. Many indigenous people around the world, such as the Maya, the Inca, and the Aztec, lived in buildings made with grass or straw. During the late Paleolithic period, wild vegetation was probably used to cover shelters and primitive dwellings in Europe, but so far, no direct archaeological evidence for this has been recovered. Similarly, people probably began to use straw in the Neolithic period when they first grew cereals.

Walls made from tied bundles of long lengths of straw, stacked in mud mortar, or compacted loose straw coated with a clay-based slurry, have been constructed for centuries throughout Asia and Europe. Straw might seem like a very fragile material, but it is important to note that straw was one of the key construction/insulation materials used during the Middle Ages. Building enclosures made of straw provided an excellent insulation that was available at the end of summer making an excellent choice for rural construction. Sadly, they were also quite flammable, which seriously affected their lifespan.

---

<sup>1</sup> <http://www.orkneyjar.com/history/skarabrae/>.

A few of these ancient construction methods and materials are still used in many developing countries. These old construction methods found their rebirth in some cases following developments in other technological areas. For example, in the United States, a new era of building with straw and grasses began in the late 1800s with the development of the mechanically powered balers, which made it possible to compress hay and straw into so-called bales. It didn't take too long for early homesteaders in the timber-poor region of the North American Great Plains to realize that they can utilize straw bales as oversized construction blocks and blocks of sod for earth houses.

It was not until the advent of the industrial revolution of the late nineteenth century that deliberate commercial application of thermal insulations become mainstream. For example, blanket-type insulations were being developed throughout the 1890s. One such product, known as "Cabot's Quilt", was introduced by Samuel Cabot in 1891. The material consisted of a matting of *Zostera Marina*, a marine plant also known as Eel Grass, sandwiched, or stitched between two layers of Kraft paper.

Thatching is a very old method of building sloped roofs (and sometimes walls) using dry straw, grass, or swamp reed. Thatching has been successfully practiced in many climates worldwide for thousands of years. It is based on layering the straw or grass so as to shed water down from the roof without wetting internal surfaces. Remarkably, thatched roofs can be still found both in many developing countries exemplifying a low-cost construction and at the same time, in some developed countries, an attractive architectural style for affluent homeowners desiring a rustic look for their homes.

While discussing roofing structures utilizing natural bio-based materials, it is important to include palm leaves, which are commonly used as a roofing material in the tropics. Palm leaves have been widely used for centuries in many equatorial countries, and they are still considered a viable construction material. For example, in Fiji, builders combine palm-leave roofs with layered-reed walls. Palm-leaf roofs are also found in Hawaii and Bali. Sugar-cane leaf roofs are common in Kenya.

### ***1.2.2 Adobe and Dry Clay Structures***

Sun-dried clay/mud bricks or clay-straw mixture are well-known natural insulating and structural materials with the oldest evidence of such constructions dating back to 8000 B.C.—Houben and Guillard (1994). According to the Oxford English Dictionary (2009), the word adobe—"mud brick" has been used for around 4000 years with relatively little change in either pronunciation or meaning. It can be traced from the Middle Egyptian (c. 2000 BC) word *j bt* "mud brick." The word adobe was introduced in the Americas by Spaniards from Africa via Mozarabic—American Heritage Dictionaries (2007). Homes built of sun-dried clay and mud can be found around the world in West Asia, North Africa, West Africa, South America, Southwestern North America, Spain, England, and Eastern Europe. A diversity of adobe construction methods has been used for thousands of years by indigenous peoples of the Southwestern United States, Mesoamerica, and the Andes. In precolonial times,

Native Americans initially built their adobe structures manually using baskets to carry ingredients. Later, they adopted skills from the Spanish for making and assembling adobe bricks—Beck et al. (1999). In Europe, adobe bricks were used in Spain as early as the Late Bronze and Iron Ages—Chazelles-Gazzal (1997). Wide use of this technology can be attributed to its simplicity of design, ease of manufacture, and affordability.

Today, adobe construction technologies are very common in Latin America, Africa, the Indian subcontinent and other parts of Asia, the Middle East, and southern Europe. It is estimated that around 30% of the world's population live in earth-made construction—Blondet et al. (2003). Interestingly enough, approximately 50% of the population in developing countries, including the majority of rural population and at least 20% of the urban and suburban population, live in earthen dwellings—Houben and Guillard (1994). In various publications, thermal conductivity, a key physical property of thermal insulations, of adobe is reported to be between 0.3 and 0.6 W/(m K), depending on the density:—Chávez-Galán et al. (2007), Hagan and Trujillo (2011).

### ***1.2.3 Wood for Structure and Thermal Insulation***

Wood has a relatively low thermal conductivity between 0.1 W/m-K for cedar and cottonwood and 0.19 W/m-K for oak and hickory wood (at 12 wt% water content—TenWolde et al. 1988). In addition, wood has significant heat storage capacity. For thousands year, wood has been regarded around the world as a primarily structural material for residential construction that has insulating value primarily because of its mass. Construction of solid log structures has its roots in Central and Eastern Europe and Scandinavia. Log cabins were widely used in the forested regions of North America. Through centuries, log construction had undergone an evolutionary process from the crude gabled-roof cabins, made of round logs with an opening in the roof to vent smoke to more sophisticated squared logs with interlocking double-notch joints with timber extending beyond the corners. Log-home construction, however, has been always based on stacking tree trunks one on top of another with overlapping of the logs at the corners with cracks and irregularities filled with locally available substances. In different regions, increasingly complex joints have been developed to ensure weather-tight joints between the logs. Wall profiles have been largely based on the round log. In addition, log builders developed a variety of interlocking corners by notching the logs at the ends to create strong structures. All these developments made it easy to achieve a relatively weather-tight structure. Most often the connections between logs were chinked (sealed) by inserting horsehair, moss, mud, or other soft materials into the joints.

An active discussion still exists about the exact origin and the period when log homes appeared, the first log structures were probably being built somewhere in Northern Europe by the Bronze Age (about 3500 BC)—Weslager (1969). The origin of these types of structures is often associated with the Pomeranian culture of the Late

Bronze Age and the Early Iron Age, which developed from Lusatian culture—Coles and Harding (1979), Dabrowski (1989). One of the best examples of the Pomeranian wooden architecture from the Iron Age is the fortified settlement of Biskupin in North-Central Poland—Archeological Records of Europe.<sup>2</sup> In Danish-controlled areas, the earliest constructions of laying and crossing logs were found in the fortifications of Danevirke in southern Jutland, built in the eighth and ninth centuries. A similar construction technique has been found in a few houses in Haithabu (Hedeby) near Danevirke and in a well in Kaupang in Norway. These examples were built in the beginning of the ninth century—Syrett (2004). Construction with solid wood logs was first recorded by the Roman architect Marcus Vitruvius Pollio (80–15 BC) in his architectural essay *De Architectura*. He noted that in Pontus (today North-Eastern Turkey), dwellings were constructed by laying logs horizontally on top of each other and filling the gaps with “wood chips and mud”—Pollio (1914). Log homes have been built in North America for over 500 years. It was the log house that sheltered the Pilgrims from the weather when they first came to America. Early loggers and trappers-built log homes for basic shelter. In the early days of log-home buildings were limited to local materials such as oak, maple, ash, cedar, and pine. The log cabin actually marked the beginning of American architecture.

#### ***1.2.4 Cork, a Natural Porous Material***

The origins of the use of cork are lost in time though used by prehistoric peoples who for thousands of years before Christ discovered the potential material from the cork oak (*Quercus Suber* L.) and used it in endless everyday objects. The proof lies in the countless remnants found in some Mediterranean countries. Cork is a historically used thermal insulation, which is impermeable to water and buoyant. It is harvested for commercial use from cork oak trees, which are endemic to southwest Europe and northwest Africa. Ancient Egyptians used cork to insulate the soles of their sandals. In Roman times cork was also used as a closure for vessels (amphorae) used to transport liquids and as a construction material to cover roofs and ceilings. Cork’s usefulness as thermal insulation was recognized at the time. Cork became widely used in medieval times as an interior wall insulation in monasteries for year-round protection against the elements.

Cork is composed of dead cells that accumulate on the outer surface of the cork oak tree. Because of its porous honeycomb-like structure, cork consists largely of empty space; its density (weight per unit volume) is one-fourth that of water. Unlike a honeycomb, however, cork consists of irregularly shaped and spaced cells having an average of 14 sides. With 625 million of these empty cells per cubic inch (40 million per cubic centimeter), cork is like many layers of microscopic bubble wrap, making it an effective cushioning material. Its low density makes cork useful in life preservers and buoys. The large amount of air space makes cork an effective

---

<sup>2</sup> [http://www.muzarp.poznan.pl/zewnetrzne/arena/Biskupin/dok\\_eng.html](http://www.muzarp.poznan.pl/zewnetrzne/arena/Biskupin/dok_eng.html).

insulation material for both temperature and noise. Furthermore, it is fire resistant; flames only char the surface, and no toxic fumes are generated. Cutting the surface of cork turns many of the microscopic cells into tiny suction cups, creating an effective non-slip surface. In addition to being flexible, cork is highly resilient. After being crushed under a pressure of 96,000 kPa, cork will regain 90% of its original size in 24 h. Cork absorbs neither dust nor moisture, and it resists both rot and insects. Highly resistant to wear, it is used for polishing diamonds. Cork bottle stoppers have been found in Egyptian tombs that date back thousands of years. Ancient Greeks used cork to make fishing net floats, sandals, and bottle stoppers. Two thousand years ago, Romans used cork in a variety of ways, including life jackets for fishermen but also in their houses to cover roofs and ceilings. For hundreds of years, Mediterranean cottages have been built with cork roofs and floors to keep out summer heat and winter cold and to provide a comfortable walking surface. Finally, cork stoppers are treasured for successfully closing wine bottles for decades.

## 1.3 Technological Discoveries Leading to Mineral Wool, Glass Fiber and Foam-Glass Insulation

### 1.3.1 *Mineral Wool*

Mineral wool is the general name for a family of fibrous materials that are manufactured by spinning or drawing molten minerals at high temperature. A product of this process, mineral wool or stone wool, is a non-metallic, inorganic thermal insulation produced from volcanic rock (typically basalt or dolomite). This type of insulation has a thermal conductivity of  $\sim 0.0345$  W/m-K at 24 °C. It has been widely used for decades as a building and industrial insulation—ASHRAE Handbook of Fundamentals (2017).

Slag wool, another material in this family, was first made in 1840 in Wales by Edward Parry, “but no effort appears to have been made to confine the wool after production; consequently, it floated around the works with the slightest breeze, and became so injurious to the crew that the process had to be abandoned”—Spon et al. (1883). A method of making mineral wool was patented in the United States in 1870 by John Player (Appleton’s Annual Cyclopedic 1981) and first produced commercially in 1871 at Georgsmarienhütte in Osnabrück Germany. The process involved blowing a strong stream of air across a falling flow of liquid iron slag which was similar to the natural occurrence of fine strands of volcanic slag from Kilauea called Pele’s hair created by strong winds blowing apart the slag during an eruption. Mineral wool was produced for the first time in the United States in 1875. In 1897, C. C. Hall, a chemical engineer, produced rock wool. By 1901, he was producing the insulation commercially at a plant in Alexandria, Indiana—Kärner (2012). Hall formed a partnership to make the new product and later founded Banner Rock Products Co. (which was purchased by Johns Manville Co. in 1929). By 1928, there were eight



plants manufacturing either rock wool or slag wool insulation in the United States. By the 1950s, this number had increased to approximately 90.

The process of production and handling of mineral wool, however, has been viewed as a health hazard, as the fine threads can easily penetrate the skin, causing inflammation, and the dust when inhaled irritates the respiratory organs. Due to numerous health problems reported by their employees some manufactures had to abandon this production during the second and third decades of the twentieth century.

Today, during the manufacturing of mineral wool insulation, rock and two slag materials (blast-furnace slag and steel slag) are melted together in cupola furnaces operating at approximately 1500 °C. The two types of slag act as a flux to help the molten rock flow and lower the melting temperature. ‘Formstones’ are also added; these are manufactured “briquettes” composed of mineral wool process and product waste that are processed by rod-milling the waste into dust and binding it together with starch or lime. The molten mixture is spun to give the mineral wool a fiber-like structure.

### ***1.3.2 Glass Fiber***

Production of glass fiber had its beginnings in ancient times when glass makers discovered that they could draw hot glass into threads. The ancient Phoenicians and Egyptians were two civilizations that made glass and pulled glass into fibers. Glass shops were in most cases able to make only small amounts of relatively coarse glass thread at a time. Ancient craftsmen used glass fibers almost exclusively for decoration being unaware of other potential applications for this material.

The real history of fiberglass manufacturing started in 1836 when a Parisian craftsman Ignace Dubus-Bonnel was issued a patent for using a loom to weave molten glass. John Player refined the process in 1870 by using a steam jet to mass produce glass fibers—Appleton’s Annual Cyclopedia (1981). Herman Hammesfahr was awarded a patent for a type of fiberglass cloth—US 232,122 A (1880). This fiberglass cloth was interwoven with silk. The resulting composite was durable and flame retardant. Libbey Glass purchased the fiberglass patent among others from Hammesfahr with the intention of displaying the fabric in a spectacular manner at the 1892 Chicago World’s Fair. In 1893, the Libbey Glass Company exhibited lampshades at the World’s Columbian Exposition in Chicago that were made of coarse glass thread woven together with silk—Close (1947).

The method currently used for producing fiberglass, like most technological advances, was discovered coincidentally. In 1932, Dale Kleist a graduate student at Ohio State University, who worked as a researcher for Corning Glass produced fine glass fibers for the first time. This happened while he was trying to create a vacuum-tight seal between two glass blocks when he used a jet of high-pressure air. Surprisingly, the high-pressure air turned a stream of molten glass into fine fibers. As a result, Kleist had accidentally discovered an effective method to produce

large amounts of fiberglass fibers, a method that he would refine in later years—Jester (1995). Fiberglass was trademarked in 1938 as Fiberglas® and was subsequently used in clothing, boat hulls, fishing rods, and eventually automobile bodies, when in 1953 Fiberglas® partnered with Chevrolet. Between 1931 and 1939, the Owens Illinois Glass Company and the Corning Glass Works developed practical methods of making fiberglass commercially and the North American industry began to produce glass fiber for thermal insulation and air filters. In 1935, Corning Glass joined with Owens-Illinois, another company that had been experimenting with fiberglass, to continue develop the product. In 1936, they patented the product “Fiberglas”, with only 1 “s.”, and then in 1938 the two companies merged to become Owens-Corning, which is still in existence today—Owens Corning Records, The University of Toledo—MSS-222.<sup>3</sup>

### 1.3.3 *Foam Glass*

There were three similar patents to produce foam glass in the 1930s: The American Albert L. Kern patented a method in 1931 based on silica with a 20 wt% combustible mixture of lignite, coal, wood and foaming agents hydrochloric acid and sodium hydroxide. He heated this mixture to 1500 °C resulting in a porous product—Dämmstoffarten (2007). A Russian engineer I. I. Kitaigorodsky of the Mendeleev Institute developed another method to create foamed glass in 1932. He took a mixture of finely powdered glass and calcium carbonate as a foaming agent and heated it to 850 °C then cooled it in steel molds—Oakseson et al. (1977).

Another process for making foam glass using a mixture of finely powdered silica, borax, and zinc oxide was developed in 1934. Heating used trapped gases to be given off leaving a cluster of bubbles with a cellular structure. This technology was further developed by William O. Lytle, a laboratory technician at Pittsburgh Plate Glass and Corning Glass Works (Pennsylvania, USA). In 1940, Lytle was granted a patent for a process using air and water vapor as additional foaming agents to create an increased number of pores. Foam glass products produced at this time were lightweight, rigid, fire, water, rodent and insect resistant. At this time, Foam glass was introduced as a thermal insulation. The mass production of foam glass started in 1943 in Port Allegany (Pennsylvania, USA)—Scheffler and Colombo (2003).

## 1.4 Past Developments of Cellulosic Fiber Insulation

Cellulose is among the oldest types of insulation used in buildings. Many forms of cellulosic materials have been used for insulating purposes. This includes newsprint, cardboard, cotton, straw, sawdust, hemp and corncobs. The third U.S. President,

---

<sup>3</sup> <https://www.utoledo.edu/library/canaday/findingaids1/MSS-222.pdf>.

Thomas Jefferson, used a form of cellulose to insulate his Monticello residence (from Italian—“Little Mountain”). In 1768, Jefferson began constructing his primary residence on a hilltop overlooking his 5,000-acre plantation. He moved into the Monticello’s South Pavilion in 1770. It should be recognized that what is frequently cellulose insulation on modern construction sites has been in use in North America and Europe since the 1920’s—see Plundstein (2007).

In Canada, the first commercial cellulose insulation was made from macerated paper in 1919—Bomberg and Solvason (1980). Wall cavities in Canadian wood-framed buildings at this time were filled with wood chips stabilized with limewater, later with shredded newspapers, and ultimately with mineral fiber batts. In 1922, the University of Saskatchewan performed a pioneering field test using test huts. The research focused on the thermal performance of different types of fibrous insulation installed in wall cavities—Greig (1922). Candidate insulations including sawdust, wood shavings, straw, seaweed, and mineral fibers (rock wool) were evaluated. In 1926, the first-ever pneumatic equipment for installation of cellulose insulation was used to install “loose-fill” cellulose in wall cavities. The cellulose used at that time was not chemically treated, except for small quantities of lime and boron salts that were added as a protection against mold growth and rot, no significant moisture damage was found after 50 years. These wall cavities were opened and examined in 1975—Bomberg and Solvason (1980).

Simultaneously, Scandinavia cellulose insulation products were introduced in the 1920s. These products were fabricated from both newsprint and forestry by-products. Cellulose was initially used as a cavity insulation in traditional timber-framed walls and sometimes as an attic-floor insulation. In Germany, the first factory producing cellulose insulation was opened in 1928. This kind of thermal insulation became quite popular in residential housing sector during the period 1920–1930. The first mobile equipment for cellulose installations was developed at that time.<sup>4</sup>

As the U.S. paper industry grew significantly in the 1940s, it was a natural consequence that wastepaper was utilized for production of thermal insulation. Cellulose was originally manufactured as a sound insulation. It was not long, however, until wastepaper started to be used as a dense thermal insulation material. At that time, cellulose shared only a small portion of the building material market, as fiberglass insulation had become increasingly popular after World War Two. The reason for all of this was relatively simple—since 1958, when the modern glass fiber production process was developed, glass fiber insulation batts and blankets became more cost effective than cellulose in building envelope applications.

As a result of the 1970s energy crisis, heavy demand for insulation induced many to enter the cellulose industry, causing a resurgence of cellulose insulation popularity. Once the crisis passed, however, only a few companies remained in the U.S. committed to refining the product and production technology.

During the 1980s, several interesting technological developments took place in North America, such as an addition of supplementary polymer fibers (e.g. polypropylene)—US Patent US4468336 A (1984), Bataille et al. (1989), a use of the mixing

---

<sup>4</sup> <http://ekoiso.com/en/history/>.

cyclones with steam treatment during application—Bomberg and Solvason (1980), a use of latex based or starch-based adhesives during manufacturing process—US Patents WO2005007984 A1 (2005), and US6262164 B1 (2001). The major development in the mid-1980s was an introduction of fiberization technology a replacement for the earlier hammer-mill process which dramatically changed the cellulose production process—US Patent US5011091 A (1991). An introduction of rotational fiber mills, similar to those used in the wet wood-fiber board production, but operating in a dry environment, replaced hammer mills in either the second or both stages of cellulose fiber production—Bomberg and Solvason (1980). This upgrade of manufacturing lines improved the production process and enhanced the performance of cellulose insulation by reducing the product settled density by about 50%.

Modern cellulose insulation is made from either ground up newsprint or cardboard (usually recycled), or denim (also usually recycled). It is heavily treated (up to 15 wt%) with combinations of boric acid, borax, and ammonium sulfate. These chemicals are used for improvement of the fire resistance and reduce potential issues with pests.

## 1.5 Development of Cellular Plastic Foam Insulation

The term “cellular plastics” encompasses a wide range of polymeric materials with varying thermal and mechanical properties and different fields of application. Virtually any polymer, thermoplastic or thermoset, can be made into a cellular or foamed form with the resulting products having densities ranging from 3.2 kg/m<sup>3</sup> up to 640 kg/m<sup>3</sup>. Ultimately, cellular plastics can have either of two cellular configurations: (a) the closed-cell type, in which each individual cell, more or less spherical in shape, is completely enclosed by a wall of plastic, or (b) the open-cell type, in which the individual cells are interconnected. To achieve internal cellular structure the following two foaming methods are widely used: (a) in physical foaming, where a gas is the cell-forming agent and (b) in chemical foaming, where the expanding agent is produced by the reaction of two or more chemicals. Depends on the internal structure and on density, the foams can be ridged, semirigid, or flexible. Cellular plastics can be produced in the form of slabs, blocks, boards, sheets molded shapes, and sprayed layers. The introduction of cellular polystyrene and polyurethane in the 1940s and 1950s created a real revolution in the areas of building and industrial thermal insulation. Two of three currently used methods for producing plastic foams originated in the nineteenth century.

Polymerization as a natural process was first utilized in 1838 by a French chemist and physicist, Henri Victor Regnault (1810–1878), a Lecturer of Chemistry at the University of Lyon and the École Polytechnique, and a Professor of Physics in the Collège de France. Although he first reported the formation of polyvinyl chloride (PVC), the historical credit for the discovery of the polymer has been awarded to the German chemist Eugen Baumann (1846–1896). Furthermore, it is widely assumed that the first human-made polymer was made by the American self-taught chemist

and engineer, Charles Nelson Goodyear (1800–1860). In 1839, Goodyear tried to vulcanize rubber gum on a hot stove and discovered that it changed into a durable and flexible material. In reality, the Mesoamericans used stabilized rubber for balls and other objects as early as 1600 BC—Hosler et al. (1999). Finally, a British chemist Thomas Hancock received a patent eight weeks before Goodyear for a vulcanization process using sulfur.

Polycondensation is another important technology for producing plastic foams. It was invented by Johann Friedrich Wilhelm Adolf von Baeyer (1835–1917), the 1905 recipient of the Nobel Prize in Chemistry. In 1871, Bayer prepared phenolphthalein, with the condensation of phthalic anhydride and phenol under acidic conditions. In 1872, he also experimented with phenol and formaldehyde; the resinous product, which later led to the development of Bakelite and phenolic foam—Reboul (1994).

### 1.5.1 *Polystyrene Foams*

Styrene is a liquid hydrocarbon that is important primarily for its tendency to undergo spontaneous polymerization (a process in which individual molecules are linked to produce large, multiple-unit molecules). Styrene is widely employed today in the manufacture of polystyrene products, as well as a number of specialty plastics and synthetic rubbers. Pure styrene is a clear, colorless, flammable liquid that boils at 145 °C and freezes at –30.6 °C. Polystyrene had been known as a natural bio-based compound well before the twentieth century (Denis and Castor 2007). Its original monomer, a natural oil, can be attained from the resin (called “styrax balsam”) of the American sweetgum tree (*Liquidambar styraciflua*—the *Altingiaceae* plant family)—Berthelot (1866).

In 1839, a German pharmacist, Eduard Simon (1789—1856) working in Berlin distilled an oily, colorless, fragrant and refractive substance from styrax and named it styrene. After a couple of days, Simon observed that this material had changed into a thick, jelly-like substance. He presumed that it happened as a result of oxidation, so he called this compound styrene-oxide—Semmler (1907). In 1922, the German organic chemist Hermann Staudinger (1881–1965), a 1953 Nobel Prize recipient in the area of chemistry and Chemistry Professor at the University of Freiburg, realized that heating styrene to a high temperature starts a chain reaction that produces macromolecules.

Today, the monomer of polystyrene is manufactured in commercial scale from petroleum, which is a blend of around 500 compounds. Styrene obtained from crude oil, for example, began in the 1850s. Bakelite, the first plastic made from petroleum was economically produced by the Belgium chemist Leo Hendrik Baekeland (1863–1944) in 1907—Bowden (1997). Therefore, it is no wonder that consumers had to wait until the third decade of the twentieth century for the development of synthetic polystyrene. The modern method for commercial production of styrene by dehydrogenation of ethylbenzene was first introduced in the 1930s. In 1929 in Ludwigshafen, Germany, a chemist from the IG Farbenindustrie AG (today Badische Anilin und Sodafabrik—BASF) Hermann Franz Mark (1895–1992) produced synthetic styrene

with the catalytic dehydrogenation of ethyl-benzene at a temperature of 500–600 °C. In 1930, two researchers from the Karl Wulff and Eugen Dörrer, performed a successful polymerization of polystyrene from styrene. Thereafter, the industrial production of polystyrene began and the utilization of it as plastic foam followed shortly after—James and Castor (2007). Polystyrene is a vinyl polymer. Structurally, it is a long hydrocarbon chain, with a phenyl group attached to every other carbon atom. Today, polystyrene is produced by free radical vinyl polymerization from the monomer styrene.

Polystyrene foam was first made in 1931 in the USA. The Swedish inventor Carl Georg Munters (1897–1989) cooperating with John Tandberg (1896–1968) patented the method for foaming polystyrene. Applying their technology, the first polystyrene foam was produced in 1941 by Otis Ray McIntire (1918–1996), an engineer with the Dow Chemical Company. It was an accidental invention, which came as he was trying to find a flexible electrical insulator. Polystyrene, a known material, was a good insulator but it was too brittle for electrical applications. McIntire tried to make a new rubber-like polymer by combining, under pressure, styrene with isobutylene, a volatile liquid. He heated the milk white polystyrene granulate up to 200 °C in an extruder using a chlorinated hydrocarbon (chloromethane) as a foaming agent. The result was a foam polystyrene was 30 times lighter than regular polystyrene. Following this development, the first polystyrene insulating product was put on the market by the Dow Chemical Company in 1943—James and Castor (2007). Another thermal insulation product—the expanded polystyrene foam (EPS)—was invented in Germany by the engineers of IG Farbenindustrie AG in 1950.

In late 1940s, Fritz Stastny (1908–1985), a Czech chemical engineer working for BASF AG, developed pre-expanded polystyrene beads by incorporating aliphatic hydrocarbons, such as pentane. These beads are used today as the raw material for molding or extruding the foam. The foam molding process was demonstrated during the Plastics Fair in Dusseldorf (Art Museum—Kunststoff Messe). A molded ship model made of expanded foam was displayed. The Styropor brand was introduced in 1951, by BASF AG. Following this fair, BASF began with manufacture of expanded polystyrene (popularly known as Styrofoam).

### ***1.5.2 Polyurethane, Polyisocyanurate, and Bio-Based Foams***

A surge of activity in polyurethane foam technology took place during World War II. Polyurethane foams were introduced as a replacement for rubber which at that time was expensive and hard to get. The versatility of this new organic polymer and its ability to substitute for scarce materials spurred development of numerous applications. Early work focused on the production of polyurethane fibers and flexible foams. In addition, during World War II, polyurethane coatings were used for the impregnation of paper and the manufacture of mustard gas resistant military uniforms, high-gloss airplane finishes and corrosion-resistant coatings to protect metal, wood, and masonry.

The real origin of polyurethanes, however, dates earlier being associated with the discovery of the polyaddition reaction, which is a key step in the polymerization process. Polyaddition takes place as a step-growth reaction involving molecules with low degrees of polymerization. In 1933, it was discovered accidentally by Reginald Gibson and Eric Fawcett, scientists at the Imperial Chemical Industries (ICI) in Northwich, England—Bozsaky (2010). This development also led to the development of polyethylene.

Applying the earlier research findings of Gibson and Fawcett, Otto Bayer (1902–1982) was the first to prepare polyurethane samples in the research laboratory of IG Farbenindustrie AG in Leverkusen, Germany (today Bayer AG). Polyurethane was achieved as a result of a reaction of glycol and polyisocyanate—Bayer (1947). The new polymers had some advantages over existing plastics that were made by polymerizing olefins or by polycondensation. During World War II polyurethane foam was applied as an aircraft coating but the final breakthrough came in the 1950s, when the production of polyisocyanates became possible. Commercial scale production of polyisocyanates was achieved in 1952, followed with production of flexible polyurethane foam. This began in 1954 using toluene diisocyanate (TDI) and polyester polyols. The above precursors were also used to produce rigid foams, gum rubber, and elastomers. In addition, by the late 1950s, polyurethanes began to be used in the production of adhesives and elastomers.

The first commercial insulating foam boards made of polyurethane appeared in 1954. In those days, polyurethane foam panels lacked dimensional stability and tended to distort. The development of rigid board polyurethane panels has made it possible to use them as a building insulation. The commercial production of polymer fibers from hexamethylene diisocyanate (HDI) and 1,4-butanediol (BDO) began during the 1950s.

In North America, in 1956, DuPont introduced polyether polyols, specifically poly(tetramethylene ether) glycol. Following this development, BASF and Dow Chemical started selling polyalkylene glycols in 1957. Polyether polyols were cheaper, easier to handle and more water-resistant than polyester polyols, and that is why they became more popular than the DuPont product. Union Carbide and Mobay (U.S. Monsanto/Bayer joint venture) also began making polyurethane chemicals—see Seymour and Kauffman (1992). More than 45,000 metric tons of flexible polyurethane foams were produced in 1960. The availability of chlorofluoroalkane blowing agents, inexpensive polyether polyols, and methylene diphenyl diisocyanate (MDI) allowed polyurethane rigid foams to be used as high-performance insulation materials. During the 1960s, automotive interior safety components, such as instrument and door panels, were produced by back-filling thermoplastic skins with semi-rigid foam.

Polyisocyanates became commercially available in 1952, soon after the commercial scale production of PU occurred (after World War II) from toluene diisocyanate (TDI) and polyester polyols. In the years that followed (1952–1954), different polyester-polyisocyanate systems were developed by Bayer.

In 1967, urethane-modified polyisocyanurate rigid foams were introduced, offering even better thermal stability and flammability resistance. Polyisocyanurate

foams are one of the most popular insulating board products in construction. Polyisocyanurate foam is a thermoset plastic typically produced as a foam and used as rigid thermal insulation. Its chemistry is similar to polyurethane foams, except that the proportion of methylene diphenyl diisocyanate (MDI) is higher and a polyester-derived polyol is used in the reaction instead of a polyether polyol. This reaction takes place at higher temperatures than polyurethane foam. Catalysts and additives used in polyisocyanurate formulations also differ from those used in polyurethane foams.

Polyester polyols were gradually replaced by polyether polyols owing to their several advantages such as low cost, ease of handling, and improved hydrolytic stability over the former. Poly(tetramethylene ether) glycol (PTMG), was introduced by DuPont in 1956 by polymerizing tetrahydrofuran, as the first commercially available polyether polyol. Later, in 1957, BASF and Dow Chemical produced polyalkylene glycols—Rudnick (2013). Based on PTMG and 4,4'-diphenylmethane diisocyanate (MDI), and ethylene diamine, a Spandex fiber called Lycra was developed in 1962 by chemist Joseph Shivers at DuPont's Benger Laboratory in Waynesboro, Virginia, U.S. Spandex is stronger and more durable than natural rubber—see U.S. Patent 3,023,192 (1962). With the decades, PU graduated from flexible PU foams (1960) to rigid PU foams (polyisocyanurate foams-1967) as several blowing agents, polyether polyols, and polymeric isocyanate such as poly methylene diphenyl diisocyanate (PMDI) became available. These PMDI based PU foams showed relatively good thermal performance and flame resistance.

In 1969, Polyurethane Reaction Injection Moulding [PU RIM] technology was introduced. This allowed production of high-performance polyurethane products, including a fabrication of the first plastic-body automobile in the United States, in 1983—see Bryce (1996). In 1990s, due to the rising awareness towards the hazards of using chloroalkanes as blowing agents and as a result of the Montreal Protocol agreement in 1987, several other blowing agents flowed into the market (e.g., carbon dioxide, pentane, 1,1,1,2-tetrafluoroethane, 1,1,1,3,3-pentafluoropropane)—Grundmann (2007).

The next interesting development was the utilization of vegetable oil-based polyols for production of polyurethane foam. Natural oils have great potential to compete with petroleum in producing polyols used to make polyurethanes. However, except for a few oils like castor oil and lesquerella oil, most natural oils do not have hydroxyl groups which are needed to form urethane links with isocyanate—Carlson et al. (1990). The unsaturated sites in natural oils can be used to introduce hydroxyl groups, and a number of methods have been developed to synthesize natural oil-based polyols. As early as in 1974, Lyon prepared polyurethane rigid foams from hydroxymethylated castor oil, safflower oil, and polyol esters of castor acids—Lyon et al. (1974).



### 1.5.3 *Development of Phenolic Foams*

Phenolic foam exhibits unique characteristics and can't be compared with other cellular plastics. Phenolic foam combines good ignition and fire resistance with low smoke production, relatively good mechanical strength with one of the lowest thermal conductivities of all close cell plastic foam insulations reaching (after aging) between  $\lambda = 0.017$  W/m-K and  $\lambda 0.021$  W/m-K.

Phenolic resins are the key components in the production of phenolic foams. Phenolic resin was first investigated in the 1870s by Adolf von Bayer during his work on phenolic dyes. In 1872, A. Von Bayer found that phenol reacting with formaldehyde was converted to a colorless resin. He discovered the first thermoset polymer when heating phenol with formaldehyde. Still, the first patent dealing with phenolic resins (as substitute for hard rubber) belongs to A. Smith in 1899 (British Patent 16,275). During the following decade, the phenol-formaldehyde reaction was investigated mainly in academic labs. However, the processing technique was further advanced and patented by Leo H. Baekeland in 1907—see Knop and Pilato (1985). This technique made possible the worldwide application of the first wholly synthetic polymer material (only cellulose derivatives were known before). Since then, thermoset phenolics have been used in variety of industrial and commercial applications—see Whitehouse et al. (1968). Today, phenolic foam is produced by catalytic curing of a phenol-formaldehyde resin incorporating blowing agent. It is available in two distinct forms: open cell and close cell. Open cell phenolic foams were first produced in the U.S. in 1937—Lasman (1965). However, closed-cell phenolic foams were not introduced until 1982—Dvorchak (1985). Due to excellent thermal and fire performance combined with good structural integrity, phenolic products have been used as high-performance thermal protection applications, such as for example nose caps and exit cones for rocket nozzles—Knop and Pilato (1985), Segal (1967), Schmidt and Graig (1982).

Traditionally, in the production of phenolic foam, highly acidic aromatic sulfonic acids has been used as the catalyst. This yields a low pH level of the resulting foam product. The low pH foam is not an issue by itself, rather the low pH leachate that is created as moisture comes in contact with the foam. Unfortunately, this acidic leachate has a strong potential to corrode any metal in close proximity. The corrosion issue is compounded by poor mechanical properties that cause formation of crevices and gaps in the cellular structure, thereby increasing exposure of foam surface to moisture. Phenolic foams produced in the U.S. during 1980s used a relatively high level of sulphonic acid resulting in high acidity foam with corrosive leachates in the presence of water. The acidity level of early phenolic foams produced in the US was very low i.e. in the range of 1.5–2.8—Smith et al. (1993).

During 1992–94, after a series of commercial roof catastrophes caused by the corrosion of metal decks, which were directly associated with phenolic foam applications, building applications of phenolic foam in North America were completely discontinued. Corrosion was the result of a combination of the foam's high acidity and poor cellular structure that caused creation of cracks and gaps in the foam board,

allowing ingress of water. During the last two decades, however, phenolic foam insulation has been successively manufactured in Europe and Asia and widely used in construction for roofing and wall applications and as industrial insulation.

## **1.6 Development of Thermally Insulating Wood Composites and Wood Concretes**

### ***1.6.1 Insulating Fiber Boards and Early Wood Composites***

The origin of wood-based composite products reaches back to ancient times. Archeologists have found traces of laminated wood in the tombs of the Egyptian pharaohs. About 5500 years ago, Egyptians used animal glue to bond hardwood veneer—Altenmüller (2001). They also discovered that the orientation of wood grains plays an important role in the improvement of the mechanical strength of wood composites. They oriented adjacent layers so that the grains were perpendicular. At least a thousand years ago, the Chinese and Japanese also knew this principle. They shaved wood and glued it together for use in furniture. The best-known laminated wood product, however, was the Roman scutum—a lightweight laminated wood shield used by Roman Legions—Sabin et al. (2007). Also, the English and French are reported to fabricate a product similar to plywood during the seventeenth and eighteenth centuries. The production of wood-based composites increased significantly during the eighteenth and nineteenth centuries. This followed the development of wood chip and wood veneer processing equipment. In 1797, Samuel Bentham applied for patents covering several machines to produce veneers. In his patent applications, he described the concept of laminating several layers of veneer with glue to form a thick piece—the first example of what is now called plywood. About fifty years later, Immanuel Nobel, the father of Alfred Nobel who recognized the industrial potential for wood-based composites, invented the rotary lathe machine, which later became a basic equipment for production of plywood—Dickson and Parker (2014).

The production of wood fiber boards dates back to Japan in the sixth century B.C. In the nineteenth century, so called heavy-paper boards were used in Japan as wall sheathing in residential construction. In Europe and North America, the first insulation boards were developed as a byproduct of paper production. Efforts to utilize the large quantities of oversize fiber bundles (called screenings) removed from ground-wood pulp led to the establishment of the first European company producing insulating wood-based boards. Sutherland's plant was built in 1898 in Sunbury-on-Thames, England—Asplund (1956). Similar plants were built a few years later in Trenton, New York, U.S.A and in Thorold, ONT, Canada. In 1914, approximately 10 years after Sutherland's developments, a pilot plant was built at International Falls, MN in the USA, by the Ontario Paper Company for production of insulation boards. This small plant produced a rigid insulation board from ground-wood and sulfite screenings. A second larger and more advanced plant (with a separate

ground-wood line) was built there in 1916 to produce an insulating board. This board product was sold under the name Insulite. It was used for wall sheathing, interior finish, and roof insulation—Muench (1947). The next insulation board plant using ground-wood as a raw material was built in Greenville, MS, in 1931. At this time, in order to further reduce the production and material costs, pioneers of the insulation board industry, including Muench, explored different sources of bio-fiber originating from a variety of agricultural byproducts such as corn, wheat straw, and bagasse, the waste after extraction of the sugar from cane— Dickson and Parker (2014). In the 1920s, the Celotex Corporation of America and its subsidiary, the Celotex Company of Great Britain, established themselves as a supplier of bagasse fiberboard products. Bagasse, also called cane waste, is the fibrous pulpy residue that remains after sugarcane or sorghum stalks are crushed to extract their juice. The first Celotex plant producing fiber boards was built at Marrero, LA, USA. In the 1920s bagasse fibers became the core material for Celotex insulating boards. As one of the first companies in this industry, Celotex utilized natural gas for heat production and in the evaporating process. During the 1970s and 80s, the Celotex Company was one of the largest producers of insulation and acoustic fiber boards in the U.S.—Suchsland and Woodson (1986), Kollmann et al. (2012).

### ***1.6.2 Wood Concrete Products***

Wood and cement are combined in a variety of composite products that are used extensively in many countries. Wood and concrete mixtures of wood shavings, lime, and cement has been used in Central, Eastern, and North European building construction since 1940s with first production taking place in Switzerland—Mielczarek and Lange (1989). In the former Soviet Union, wooden concrete production exceeds 150 million m<sup>3</sup> of wooden concrete products in 1980—Filimonow and Nanazasvili (1981). Also, in other Central European countries like Austria, Germany, Slovakia, and Poland, wood-based concrete is a popular bio-based structural and insulation material used in small residential buildings. It has been used to produce lightweight concrete blocks and wall-forms or as lost-in-place forms for bond-beams and headers. In spite of many advantages, this material is almost unknown in North America. Mid- density wood-cement boards are used in Europe and in Japan wood-concrete form work—Shigekura (1989). In Latin America wood-cement boards are used for general-purpose wall sheathing—Ramirez-Coretti et al. (1998).

The basic wood concrete components are wood shavings, mineralizers, cement, and lime. Only coniferous tree shavings can be used without limit in wood-concrete production. Deciduous tree wood contains too many sugars, which inhibit the concrete setting process. Sometimes, these wood components are called “cement poisons.” The content of deciduous tree wood was eventually limited to be less than 10 wt% of the wood shavings input. The wood shaving moisture was limited to 20 wt%. Portland cement is used as a binder In the production of wood concrete. A mineralization process helps protect the wood from decay and also provides better

mixing of the wood with the cement. The most commonly used mineralizers are a 3–5% water solution of calcium chloride or a 3–6% water solution of aluminum sulfate  $Al_2(SO_3)$ —Dabrowski (1961). In the U.S., a modern mineralization process was developed using kaolin to hold “cement poisons” in the wood pores—US Patent US 5019170 A—(1991). Thanks to this technology, it was possible to increase the deciduous wood content of wood-concrete mixtures. Another advantage of this process is that decayed wood can be used. Slaked lime is used for a calcium chloride treatment, and burnt lime is used for aluminum sulfate treatments—Kosny (1994).

## 1.7 Sad History of Asbestos Fiber Insulation

Asbestos has been known since ancient times in both the western world and Asia as a natural wonder and a source of fiber for very expensive, and therefore rare, textile objects such as shrouds, napkins, tablecloths, and special purpose clothing. Most likely, it was first used by humans in the Neolithic age as a temper for ceramics. Prehistoric shards and ware containing asbestos have been found in Finland, central Russia, Norway, and Sweden. Asbestos was first mentioned in Greek written documents about 300 B.C., calling asbestos “inextinguishable”. Interestingly enough, the Greeks and Romans not only noted that asbestos had low thermal conductivity as well as it was resistant to fire and acids, but they also knew that asbestos had harmful health impacts. In addition to western sources, Chinese, Sinhalese and Indian sources attest to the use of asbestos in antiquity. The first definite identification of asbestos fabric in Asian sources occurs in a writing dated towards the end of the fifth century B.C. about a fireproof cloth that was cleaned by exposure to fire—Rackham (1961), Rose and Nolan (2003), Alleman and Mossman (1997).

For hundreds of years, asbestos was woven into cloth linings, for suits of armor, asbestos paper and very expensive textiles. In Europe, the use of asbestos waned during the Middle Ages. It reappeared in England in the 1700s but did not become popular until the Industrial Revolution of the late 1800s. The Industrial Revolution represented a huge boom for the asbestos industry. At this time, asbestos started to be used as thermal insulation. For example, asbestos was found to be especially useful as thermal insulation for pipes, boilers, and fireboxes in that era’s steam locomotives. Similarly, shipbuilders made extensive use of asbestos for insulating steam pipes, boilers, hot water pipes, and incinerators. In fact, asbestos was so widely used aboard ships that those who worked in the industry are among the most affected by asbestos-related diseases such as mesothelioma and asbestosis—Gee and Greenberg (2002).

The greatest demand for asbestos worldwide, however, was created by construction. Since, all homeowners or office users, expected their homes and offices to be fire resistant and warm, so fire-resistant asbestos seemed like the perfect product both for residential homes and commercial buildings. Asbestos fiber was used in various forms as wall insulation, for floor and ceiling tiles, in exterior siding, and in roofing tar and shingles. Asbestos could also be found in stucco, drywall tape, gaskets, cement pipes, rain gutters, plaster, putty, caulk, and a host of other building

products. Schools and theatres even boasted that curtains containing asbestos were safer than other standard fabrics because of its strength and heat resistance—Don (2011). When the use of asbestos was at its peak—probably in the 1940s to 1970s—an estimated 3,000 products made use of its unique properties.

At the turn of the twentieth century, researchers began to notice a large number of deaths and lung problems in asbestos mining towns. In the period 1917–1918, it was observed that asbestos workers were dying at an unnaturally young age. The first diagnosis of asbestosis was made in 1924. A woman had been working with asbestos since she was thirteen. She died when she was thirty-three years old, and an English doctor determined that the cause of death was what he called “asbestosis”—Selikoff and Lee (1978), Stanton and Layard (1978), Voytek et al. (1990), Toyokuni (2009). The health problems’ warnings and code regulations of the 1970s and later put an end to much of the worldwide asbestos industry. A few countries continued mining asbestos with chrysotile content with subsequent export of asbestos containing products.

## 1.8 Development of Aerogel Insulations

Aerogel is a nanopore thermal insulation with thermal resistance superior to what is achievable by plastic foams or fiber insulations. Aerogels are derived from a gel by replacing the liquid regions with a gas. The result is a solid material with extremely low density and low thermal conductivity. Aerogels can be made from a variety of chemical compounds. The apparent thermal conductivity of silica aerogel has been reported in the range 0.012 to 0.036-W/m K at atmospheric pressure and 25 °C—Wei et al. (2007), Beatens et al. (2011), Bheekhun et al. (2013).

The general idea, the name aerogel, and the first production method, all were developed by Samuel S. Kistler-Kistler (1931), Aegerter et al. (2011). Though, the history of development of aerogel insulation is somewhat enigmatic with its origin in the late 1920s at the College of the Pacific in Stockton and Stanford University in California where Kistler started his doctoral program in 1927. The myth is that Kistler made a bet with his colleague, Charles Learned, over what mainly contributes to the defining characteristics of a gel: its liquid properties or its structure.<sup>5</sup> Kistler believed that a gel substance was confined by a continuous solid structure of the same size and shape as the container in which the wet gel was contained. The obvious way to prove this hypothesis was to remove the liquid from the wet gel and demonstrate the remaining solid structure. So, the object of the game between Kistler and Learned was to replace the liquid in the gel substance with air without causing damage to the solid structure. In first Kistler’s first experiments, however where a wet gel was allowed to dry on its own, it shrank to a fraction of its original size. This shrinkage was often accompanied by severe cracking of the gel. It is important to mention

---

<sup>5</sup> [https://www.elsevier.com/\\_\\_data/assets/pdf\\_file/0006/166785/R\\_D\\_Solutions\\_Chemicals\\_use\\_case\\_AlphaMoment\\_Aerogel\\_DIGITAL.pdf](https://www.elsevier.com/__data/assets/pdf_file/0006/166785/R_D_Solutions_Chemicals_use_case_AlphaMoment_Aerogel_DIGITAL.pdf).

here, that Kistler properly deduced at that time that the solid component of the gel was microporous, and that the liquid-vapor interface of the evaporating liquid exerted strong surface tension forces that collapsed the pore structure. Kistler also understood that in order to produce aerogel, a liquid needs to be replaced with air by some means in which the surface of the liquid is never permitted to recede within the gel. Then, he found that when a liquid component of a gel was held under the pressure greater than the vapor pressure of the liquid phase and with the temperature was raised, it transformed at the critical temperature into a gas without two phases present at any time—Kistler (1932). This outcome was the discovery of the first aerogel production method.

The first gels investigated by Kistler were silica gels, prepared by the acidic condensation of aqueous sodium silicate. Kistler, after a series of unsuccessful attempts with water exchange, was able to wash the silica gels with water (to remove salts from the gel), and then he exchanged the water with alcohol. After converting the alcohol to a supercritical fluid and allowing it to escape, he produced his first aerogel. Over the next several years, Kistler investigated a variety of precursors and prepared aerogels from alumina, tungsten oxide, ferric oxide, tin oxide, nickel tartrate, cellulose, cellulose nitrate, gelatin, agar, egg albumen, and rubber—US Patent US2093454 (1937), Aegerter et al. (2011).

The first commercial aerogel was produced in 1942 by the Monsanto Corporation (at the Everett plant in Massachusetts, USA), after Kistler took a research and development position with them. Monsanto's aerogel was a friable granular silica material, containing about 95% of air by volume. It was sold under the trade name Santocel—Carragher (2005). The process involved contacting a sodium silicate solution with sulfuric acid, then repeatedly washing it in alcohol before drying it at high pressure—US Patents US 2,660,564 A (1953). Monsanto claimed to have produced aerogels with densities of  $29 \text{ kg/m}^3$ , but their regular output was between 48 and  $80 \text{ kg/m}^3$  Torgal et al. (2016). Monsanto marketed Santocel mainly as a flattening agent for paints and varnishes. In addition, Santocel was used as a thixotropic (thinning) additive in cosmetics and toothpastes. At this time, aerogel's thermal insulation application was in household freezers. The U.S. military used Monsanto's aerogel as an ingredient in Napalm. Nevertheless, from the business perspective, production of aerogel by Monsanto was not a success. Because of its high manufacturing cost, Monsanto discontinued aerogel production in 1970—Aegerter et al. (2011), Bheekhun et al. (2013), Kretzer (2016).

In the late 1960-ies/early 1970s, the fast-growing aerospace industry was seeking a highly porous medium, capable of storing oxygen and liquid rocket fuel. In the late 1970s, the French government funded a research program focused on porous materials and one of the grant recipients was Professor Stanislaus Teichner from Universite Claud Bernard, Lyon. There is a tale circulating within the aerogel community, that Teichner assigned one of his students the task of preparing the aerogel specimens for the project. The original plan was to use the existing Kistler's method which involved two time-consuming solvent exchange steps. That is why the Teichner's team was

highly motivated to improve the aerogel synthetic process and cut the required time—Vicarini et al. (1970), Pajonk and Teichner (1985). This led directly to the development of the single-solvent-exchange sol-gel chemistry. This process replaced the sodium silicate used by Kistler with an Tetramethoxysilane (TMOS) and eliminated two key disadvantages of the Kistler's method: (i) the water-to-alcohol exchange step and (ii) the presence of inorganic salts in the gel. In addition, drying aerogel under supercritical alcohol conditions produced high-quality silica aerogels. In following years, the Teichner's approach was utilized for preparation of a wide variety of metal oxide aerogels—see: Nicolaon and Teichner (1968), Pajonk and Teichner (1985), Aegerter et al. (2011). A number of new developments in aerogel technology followed quickly this ground-breaking innovation, because the aerogel production process became faster, simpler, and less expensive. Also, because of its unique optical characteristics, aerogel almost immediately became employed in several nuclear research applications. For example, in the 1980s and 1990s, as a part of the European particle physics research programs, two large detectors (containing large transparent tiles made of silica aerogel) were fabricated—see Nappi (1998). One was built at the Deutsches Elektronen Synchrotron (DESY) in Hamburg, Germany. It was using about 1700 L of silica aerogel. The other one located at the CERN research facility near Geneva, Switzerland (Organisation Européenne pour la Recherche Nucléaire—European Organization for Nuclear Research). It used 1000 L of silica aerogel, which was prepared at the University of Lund in Sweden—Aegerter et al. (2011). Later, the Lund group built aerogel pilot plant in Sjobo, Sweden. This facility produced silica aerogel monoliths using the TMOS as a precursor. The plant included a 3000 L autoclave, designed to handle the high temperatures and pressures encountered for supercritical methanol (240 °C and 80 atmospheres). However, in 1984 the facility was damaged, because the autoclave explosion caused by the methanol vapor leak. The plant was later rebuilt and is currently operated by the Airglass Corp.<sup>6</sup>

In the 1980-ties, Arlon Hunt and the research team at the Microstructured Materials Group at the Lawrence Berkeley National Laboratory found that the high toxic Tetramethoxysilane (TMOS) can be substituted with Tetraethylorthosilicate (TEOS), a much safer reagent, without compromising aerogels physical properties—Zhan and Zhao (2016). In addition, the supercritical drying technique was made safer by replacing supercritical alcohol with supercritical carbon dioxide. Consider that alcohol poses a significant explosion hazard, while carbon dioxide does not. Furthermore, the critical point of carbon dioxide (31 °C and 724 kPa) occurs at much less severe conditions than the critical point of methanol (240 °C and 1103 kPa). This groundbreaking modification of process chemistry yielded a major safety improvement in aerogel production—Aegerter et al. (2011). In parallel, BASF in Germany developed their original CO<sub>2</sub> substitution method for the preparation of silica aerogel beads from sodium silicate. This material was in production until 1996 and was marketed as “BASOGEL”—Stark et al. (1998). Finally, in the late 1980s, researchers at Lawrence Livermore National Laboratory (USA) lead by Larry Hrubesh prepared the world's lowest density silica aerogel—Tillotson and Hrubesh (1992). This aerogel

---

<sup>6</sup> [https://p25ext.lanl.gov/~hubert/aerogel/agel\\_suppliers.html](https://p25ext.lanl.gov/~hubert/aerogel/agel_suppliers.html).

had a density of only  $0.003 \text{ g/cm}^3$ , which is only three times greater from air density. Shortly thereafter, a team led by Rick Pekala, developed a unique preparation method of organic aerogels made with use of resorcinol-formaldehyde and melamine-formaldehyde. This method, in conjunction of pyrolysis, yielded pure carbon aerogels—Pekala et al. (1992). With all above developments, the interest in aerogel products reemerged, followed with a significant volume of new international research in this area.

Between in 1989 and 1992, Thermalux, L.P. produced in Richmond California silica aerogel monoliths from TEOS, using the carbon dioxide-based process. Thermalux operated the 300 L autoclave in their production. A few years later, the same autoclave and a carbon dioxide substitution process were used by the Aerojet Corp. in Sacramento, California.

In 1992, in Frankfurt, Germany, the Hoechst Corp. (aerogel division of Aventis Research and Technologies) began a research focused on low-cost granular aerogels. In 1998, Cabot Corporation's acquired the Hoechst Corp. The U.S.-based global company secured the rights to a patented method for the manufacture of aerogels on an industrial scale. Cabot also used the Hoechst's pilot plant, where first aerogel specimens were produced. In late 1980s and early 1990s, BASF in Germany simultaneously developed  $\text{CO}_2$  substitution methods for the preparation of silica aerogel beads from sodium silicate. This material was in production until 1996 and was marketed as "BASOGEL"—Marko and Braun (2013).

In the 1990s, aerogel also started its aero-space "carrier". Silica aerogel, prepared by the Jet Propulsion Laboratory (Pasadena, California, USA) has flown on several NASA space missions. In 1997, aerogel was used as thermal insulation on the Sojourner Mars Rover.<sup>7</sup> During the period 1999—2006, a very low- density aerogel was used to collect and return specimens of high-velocity cosmic dust, during the Star Dust Mission.<sup>8</sup>

In the 1990s, a research team led by C. Jeff Brinker and Doug Smith from the University of New Mexico, Albuquerque, NM, USA, initiated work focused on elimination of the supercritical drying step used in aerogel production. In 1992, Brinker and Smith developed a unique aerogel production process, based on chemical modification of the gel surface prior to its drying—Aegerter et al. (2011). This work led to the founding of Nanopore, a spin-off company, in 1994. The result was commercializing of lower-cost aerogels than previously available. The Cabot Company purchased rights to the NanoPore aerogel production process in 1998.

In 1993, Aspen Systems Inc. of Marlborough, Massachusetts, USA started development of a flexible aerogel under a contract with NASA (The National Aeronautics and Space Administration—U.S.A.). The original concept of a flexible nano-pore insulation was introduced by James Fesmire, of the Cryogenics Test Laboratory at NASA's Kennedy Space Center—Fesmire et al. (1998), Fesmire and Augustynowicz (2003). At that time, he was responsible for cryogenic fueling systems design. Fesmire envisioned an elastic aerogel-based material that would be practical, but

---

<sup>7</sup> [https://science.nasa.gov/science-news/science-at-nasa/1997/msad08jul97\\_2](https://science.nasa.gov/science-news/science-at-nasa/1997/msad08jul97_2).

<sup>8</sup> [http://stardust.jpl.nasa.gov/aerogel\\_factsheet.pdf](http://stardust.jpl.nasa.gov/aerogel_factsheet.pdf).



would still demonstrate high thermal resistance, coming from the nano-pore internal structure.<sup>9</sup> The world's first aerogel composite blanket-like material was produced in 1993 with centimeters-wide laboratory specimens. In 1999, Aspen Systems developed with NASA support, a manufacturing process for flexible aerogel blanket insulation. It was used later in NASA Space Suits. In order to commercialize flexible aerogel insulation and to scale up the aerogel production, Aspen Aerogels was founded in Northborough, Massachusetts, USA in 2001.

During the second decade of the 20-th century BASF, worked on commercialization of its new high-performance insulation product using aerogel—see International Patent WO 2013182506 (2013). This insulating material was based on a polyurethane (PU) aerogel that had open pores with sizes between 50 and 100 nm. At about the same time, PU aerogel was investigated by the other research centers as well—U.S. Patents US 2,014,147,607 (A1) (2014) and US 2,015,266,983 A (2015), International Patent WO 2,015,109,488 (2015), Diascornia (2015). The first insulation specimens were produced in mid-2014 at the BASF's pilot plant in Lemförde, Germany. In 2015, BASF commissioned the manufacturing facility for production of PU aerogel insulation board products, which were introduced to the market under the name of SLENTITE®. With apparent thermal conductivity value of less than 17 mW/(m·K), it is one of the best performing insulation board products available in 2016 on the building materials market. The compressive strength of more than 300 kPa is twice that of standard PU-foam insulation panels.<sup>10</sup>

## 1.9 Enclosed Reflective Air Spaces (Reflective Insulation)

Thermal insulation materials termed “reflective insulations” derive their thermal resistance primarily by significantly reducing the radiative heat transport across an enclosed air space. Fibrous and particulate thermal insulations eliminate convection and reduce radiation. For all three insulation types, the objective is to reduce or eliminate convection and radiation without undue increase in conductive transport. The limiting thermal resistance, as a result, is provided by the relatively low thermal conductivity of air (0.026 W/m·K at 23.9 °C). The common definition of a reflective insulation assembly is a material with surface(s) having a low thermal emittance,  $\epsilon$ , with an adjacent enclosed air space. The low emittance is often taken to be  $\epsilon < 0.1$ —Dwight (1963). For opaque materials, the emittance plus the reflectance,  $r$ , equals one. The  $r$  for a reflective insulation, therefore, is greater than 0.9. “Reflective insulation” is the popular term for thermal insulations with low thermal emittance and high reflectance surfaces facing an air space.

<sup>9</sup> [https://spinoff.nasa.gov/Spinoff2010/cg\\_2.html](https://spinoff.nasa.gov/Spinoff2010/cg_2.html).

<sup>10</sup> [http://www.polyurethanes.basf.com/pu/solutions/en\\_GB/content/group/innovation/products/slentite/intro](http://www.polyurethanes.basf.com/pu/solutions/en_GB/content/group/innovation/products/slentite/intro).

The term thermal emittance refers to the ratio of emitted radiant energy to that emitted by a black body at the same temperature. Radiation in the “thermal” category is generally taken to include radiation given off at all wavelengths less than 100  $\mu\text{m}$ —Seigel and Howell (1972). The radiation of interest is generally taken to be in all directions from the surface and as a result is called a “total hemispherical property”. A number of metals have thermal emittances that are less than 0.1 at room temperature—Gray (1963). Aluminum foil or metallized film have been used almost exclusively for manufacturing reflective insulation materials. The emittance of aluminum is highly dependent on the surface conditions—Touloukian (1970).

The use of air spaces has no doubt been used for centuries without formal recognition in the literature. One of the earliest written recognitions of reflective air spaces was published in 1878 by J.E.C. Pecllet—Goss and Miller (1989). John Dewar’s invention (Dewar Flask) that used an enclosure with a low emittance surface appeared a few years later—Soulet (1996). The early research and developments was followed by dozens of technical papers in the early twentieth century that dealt with heat transfer and thermal resistance for air spaces bounded by low-emittance surfaces—Goss and Miller (1989). A paper on the “Thermal Resistance of Air spaces” in 1929 is an excellent example of early analysis of the thermal resistance of enclosed air spaces—Rowley and Agen (1929).

Reflective insulation is represented in the literature of the 50s by a publication from the UK entitled “The Thermal Insulation of Buildings”—Nash et al. (1955) that contained installation diagrams and thermal performance numbers. The text “Heat Insulation”—Wilkes (1950) included reflective insulation as a topic. The publications of the 50 s contained detailed information about performance of single and multiple airspace application and recognition of the fact that thermal performance was a function of heat-flow direction in most cases. The use of reflective insulation in North America became established in 1955 as the result of a major effort by the U.S. National Bureau of Standards to provide a significant data base of measured thermal resistance values obtained from a hot-box facility—Robinson and Powell (1956). Data from the NBS project were published in the 1st revision of the ASHRAE Handbook -Fundamentals, a reference widely used by mechanical engineers and air-conditioning specialists—ASHRAE (1972).

Reflective insulation products appeared in the 40s and 50s in North America, especially in the western Regions and in Europe as evidenced by the publication from the UK (referenced above). Multilayer reflective insulation was in use during this period. Use of reflective insulation in commercial buildings were more common than use in residential applications because spacing of structural elements in commercial buildings was more regular than that found in residential structures.

The major contribution to the field of reflective air spaces that occurred with the publication of work by Robinson and Powell at the U.S. National Bureau of Standards that included the results from 96 hot-box tests and analyses that identified the convective component of heat transfer across enclosed reflective and non-reflective air spaces boosted confidence in the thermal performance of reflective insulations. The data base for enclosed reflective air spaces was significantly extended by a U.S.DOE project reported in a National Laboratory Report—Desjarlais and Tye

(1991) and later published in the open literature—Desjarlais and Yarbrough (1991). The acceptance of reflective insulation for use in buildings was supported by the publication of a “Standard Specification” by the American Society for Testing and Materials in 1993—ASTM (2017). The product is now used around the world most notable in Europe, Southeast Asia, Australia/New Zealand and S. Africa.

Thermal insulation materials and assemblies are evaluated using steady-state, one-dimensional standard tests carried out at specified temperatures. Standardization at the international level (an ISO product Specification, for example) has not yet been achieved after many years of effort. In recent years, the evaluation of reflective insulation assemblies has moved to multidimensional evaluations involving computer simulations (CFD) that characterize the convective component of heat flow are represented by—Han et al. (1988), and numerous papers of which the following are examples—Saber (2013), Saber (2014), and Saber (2020).

The reflective insulation manufacturers in some parts of the world have shifted from exclusive use of aluminum foil to metallized aluminum films for low emittance. The use of metallized films was motivated by improved fire test results in the U.S. Metallized films must be protected by a coating that blocks reaction of the metallized film with oxygen without significant increase in the thermal emittance. This design challenge has been largely met.

Radiant barriers applications are ventilated and consequently, differ from reflective insulations which are enclosed (not ventilated). Radiant barriers are included here since they have become a popular technique that uses low-emittance materials to reduce the heat gain by structures in cooling dominated regions. Attic or roof-deck radiant barrier applications reduce the day-time temperature in occupied areas that are not conditioned or reduce the energy used for air-conditioning. Significant effort has been made to evaluate the geographically dependent performance of attic radiant barriers.

### ***1.9.1 Vacuum Insulation Panels***

Vacuum insulation is a “region” containing a rigid porous material enclosed by a gas impermeable skin, from which air has been evacuated. It has been used for decades in a variety of applications to provide better thermal performance than conventional fiber or plastic foam insulations. After decades of development, vacuum Insulation Panels (VIPs) today deliver improved energy efficiency and space benefits for home appliances, temperature-controlled packaging, refrigerated transportation systems and any other applications that require limited heat loss or gain.

VIPs are based on the same principle as the famous Vacuum Flask, invented in 1892 by Sir James Dewar, Professor at Cambridge University in England. By maintaining a vacuum between concentric walls of glass Sir James Dewar demonstrated that a very effective thermal insulation can be achieved. Dewar’s vacuum flasks were fabricated using glass and metal, which could support the compression force generated from the pressure difference between the vacuum layer between the walls of

the flask and the external atmospheric pressure. It was also found that an application of a reflective coating on the impermeable enclosure surfaces reduced infrared heat transmission—Fricke et al. (2008). It is a basic process that has been used in VIPs today, where the glass is replaced with a metallized plastic or thin metal film and a low conductivity material is used to make a core that holds the exterior skins apart—Reichenauer et al. (2007). Interestingly enough, Dewar's Vacuum Flask was not produced until 1904, when two German glass blowers, Reinhold Burger and Albert Aschenbrenner founded Thermos GmbH.

The first VIP prototype originated around 1930 when a German patent on a rubber enclosed porous body was granted to O. Hemman of Sterchamolwerke, Dortmund—German Patent Nr. 516,377 (1930). Around 20 years later, the first metal enclosed VIP was invented. A patent application describing a glass fiber core enclosed into the welded steel foil satchel, was filed in the U.S. by H. P. Bovenkerk of General Electric Company, New York—U.S. Patent US 2,700,633 (1955). It was a continuation of an earlier work performed in the GE Schenectady Laboratories by H.M. Strong and F.P. Bundy—Fricke et al. (2007). In 1963, the first patent of an evacuated panel with a core of a nanostructured material was filed by Alfred G. Emslie, Peter E. Glaser, and Warren A. Salmon of the Arthur D. Little company of Cambridge, Massachusetts—US Patent US 3,151,365 A (1964). The development of VIPs intensified, and the first VIPs made of precipitated silica began to appear in the 1990s, thanks to the development of more durable plastic composites that provided an efficient impermeable barrier that minimized diffusion of atmospheric gases ( $O_2$ ,  $N_2$  and  $H_2O$ ). It was a significant technological advance that allowed further developments of the VIP industry. The availability of new plastic packaging methods eliminated the need for more conductive metal foils. Elimination of metal materials reduced the thermal bridge effects around the edges of a VIP—Schwab et al. (2005), Thorsell (2006). Further development in this area came from the rapid advance of new packaging methods in the food and pharmaceutical industries as well as more restrictive energy code regulations, in the building sector. The VIP skin material is often called a barrier, because it protects the VIP from air and water transmission. Still, it also provides mechanical strength to withstand atmospheric pressure and handling stresses during transportation and installation. The overall performance of the VIP skin depends mainly upon its barrier properties. Low-thermal conductivity of the skin material is also welcomed since it effects to level of the VIP's edge thermal bridging. A significant volume of research on barrier materials took place during last three decades—Kunzel (1998), Schonhardt et al. (2003), Wang et al. (2007), Fricke et al. (2007), Grynning et al. (2009). The main goal was to reduce the water vapor transmission rate (WVTR) to approximately  $0.0001 \text{ g/m}^2 \text{ d}$  and oxygen transmission rate (OTR) of  $0.001 \text{ cm}^3/\text{m}^2 \text{ d}$  to yield a useful lifetime of 30–50 years for building applications. However, the range of useful lifetime of 30 to 50 years is wide and lifetime needs to be specified more precisely to build confidence with manufacturers and users—Simmler et al. (2005). A variety of polymer membranes and thin metalized plastic films or metal foils are currently employed to package VIPs for various applications. In addition, the growing aero-space sector has created a demand for high

performance insulations, and this has yielded a variety of new vacuum insulation applications—U.S. Patent US 3,094,071 A (1963), Kogan et al. (2010).

VIPs that can be currently found in buildings were produced in the early 1990s—Binz et al. (2005), Grynning et al. (2009). These products contained fumed or pyrogenic silica, silica aerogels and expanded perlite individually or as a blend as core material. Fumed silica panels were frequently tested due to the low thermal conductivity of 0.003–0.006 W/m K. These VIPs required an internal pressure of about 20–100 mbar. The above physical characteristics are a result of a fumed silica pore size of 300 nm and relatively specific surface area in the range of 50–600 m<sup>2</sup>/g—Fricke et al. (2007), Wang et al. (2007).

A substantial amount of research focused on VIP core materials took place during the 30-year period between 1960 and 1990—Fricke et al. (2007). During this period, the greatest motivation for the development of advanced insulations was the need to replace closed-cell foam insulations containing chlorofluorocarbons (CFCs), which were restricted or banned in many countries following the acceptance of the 1989 Montreal Protocol on substances that deplete the ozone layer.

In the 1960s, for example, Whirlpool Company investigated VIPs enclosed with metal sheets and a core of milled perlite powder—U.S. Patent US 2989156A (1961). Perlite powder was also investigated as a VIP core by LaHousse of Massachusetts Institute of Technology, Cambridge, Massachusetts—LaHousse (1993). The mentioned earlier work performed by the Arthur D. Little company of Cambridge, Massachusetts, was focused on VIPs using a mixture of silica powder and carbon black—U.S. Patent US 3,151,365 A (1964). Carbon black was used in this case in order to reduce radiation heat transfer across the VIP core. In addition, the internal reflective foil shields and an emissivity-reducing silver coating were utilized for the same purpose. In a similar effort, undertaken by the General Electric research team, the use of a very fine fiberglass mat having oriented glass fibers was investigated. Fiberglass mats were sealed inside the welded metal enclosure, which was evacuated. U.S. Patent US 3,179,549 A (1964). In the follow-on work by the same company, fiberglass was still used as a VIP core. However, more interest was paid to sealing the panel on the edges to reduce the gas intrusion (plastic edge sill strips were used)—U.S. Patent US 4,444,821 A (1984). Fiberglass mats placed inside the welded stainless-steel VIPs were also used in the research and development work performed by Hitachi Ltd. from Tochigi, Japan. These glass mats were stitched with glass fibers that ran perpendicularly to the plane of the mat. The goal was to support the external atmospheric pressure load on the panel walls to keep them from collapsing—U.S. Patent US 4,486,482 (1983). In addition, glass fiber cores were also considered for high temperature applications due to the glass high thermal stability.

VIP designers found that open-cell foams such as polyurethane and polystyrene with pore sizes in the range 30–250 μm can be also used as a core in VIPs—U.S. Patent US 6,106,449 A (2000). These foams have low thermal conductivity in evacuated conditions due to their low density (60–100 kg/m<sup>3</sup>) and small pore sizes. Unfortunately, a quite high vacuum level, well below 0.1 mbar (Kwan et al. 2009), which is required to achieve a reasonable thermal resistance in the case of foams used as VIP core material. The lifetime of a VIP is negatively impacted by the need

to maintain low absolute pressures. Another approach, in protecting VIP skins from collapsing inwards, is a usage of low conductive space separators. German engineer, Friedrich Hensberg in his VIP design is using plastic spacers and low-conductive edge profiles—German Patent DE 3,707,768 A1 (1988).

## References

- Aegerter, M. A., Leventis, N., & Koebel, M. M. (2011). *Aerogels handbook*. Springer Publishing. ISBN 978-1-4419-7477-8.
- Alleman, J. E., & Mossman, B. T. (1997). Asbestos revisited. *Scientific American*, 277, 54–57.
- Altenmüller, H. (2001). Studien zur altägyptischen Kultur. Band 29. Gebunden: Buske Verlag. ISBN: 978-3-87548-267-6.
- Appleton's Annual Cyclopaedia. (1981). Mineral wool or mineral cotton. In *Appleton's annual cyclopaedia and register of important events of the year 1891*, vol. 16 (p. 528). New York: Publ. D. Appleton and Company (1892).
- ASHRAE Handbook of Fundamentals. (1972). *Thermal conductances and resistances of a plane air space* (pp. 358–359). New York: American Society of Heating, Refrigerating and Air-Conditioning Engineers, Inc.
- Asplund, A. J. A. (1956). The beginning and development of the fiberboard industry. *Svensk Papperstidning*, 59(12), 441–448.
- ASTM C1224 (2017) Standard specification for reflective insulation for building applications. In *Annual Book of ASTM Standards*, vol. 04.06 (pp. 695–699).
- Bataille, P., Ricard, L., & Sapiaha, S. (1989). Effects of cellulose fibers in polypropylene composites. *Polymer Composites*, 10(2), 103–108.
- Bayer, O. (1947). Das Di-Isocyanat-Polyadditionsverfahren (Polyurethane). *Angewandte Chemie*, 59, 257–272.
- Baetens, R., Jelle, B. P., & Gustavsen, A. (2011). Aerogel insulation for building applications: A state-of-the-art review. *Energy Building*, 43(4), 761–769.
- Beck, R. B., Black, L., Krieger, L. S., Naylor, P. C., & Shabaka, D. I. (1999). World history: Patterns of interaction. Evanston, IL: McDougal Littell. ISBN 978-0-395-87274-1.
- Berthelot, M. (1866). Sur les caractères de la benzine et du styrolène, comparés avec ceux des autres carbures d'hydrogène. *Bulletin de la Société Chimique de Paris, 2nd series*, 6, 289–298.
- Bheekhun, N., Abu Talib, A. R., & Roshdi Hassan, M. (2013). Aerogels in aerospace: an overview. In *Advances in materials science and engineering*, vol. 2013, Article ID 406065, 18 p. Hindawi Publishing Corporation.
- Binz, A., Moosmann, A., Steinke, G., Schonhardt, U., Fregnan, F., Simmler, H., Brunner, S., Ghazi, K., Bundi, R., Heinemann, U., Schwab, H., Cauberg, J. J. M., Tenpierik, M. J., Jóhannesson, G. A., Thorsell, T. I., Erb, M., & Nussbaumer, B. (2005). Vacuum insulation in the building sector. Systems and Applications (Subtask B): IEA/ECBCS Annex 39 High Performance Thermal Insulation (HiPTI).
- Blondet, M., Villa Garcia, G. M., Brzev, S. (2003). Earthquake-resistant construction of adobe buildings: A tutorial. Published as a contribution to the EERI/IAEE World Housing Encyclopedia, <http://www.world-housing.net>, March 2003. Earthquake Engineering Research Institute, Oakland, California, USA (pp. 94612–1934).
- Bomborg, M., & Solvason, K. R. (1980). How to ensure good thermal performance of cellulose fiber insulation. I. Horizontal Applications, II. Exterior Walls. *Journal of Building Physics*, 4, 93 and 119AN.
- Bowden, M. E. (1997). Leo Baekeland. Chemical achievers: The human face of the chemical sciences. Philadelphia, PA: Chemical Heritage Foundation. ISBN 9780941901123.

- Bozsaky, D. (2010). The historical development of thermal insulation materials. *Periodica Polytechnica Architecture*, 41(2), 49–56.
- Bryce, D. M. (1996). Plastic injection molding: Manufacturing process fundamentals. Society of Manufacturing; First edition. ISBN-10: 0872634728.
- Carlson, K. D., Chaudhry, A., Bagby, M. O. (1990). Analysis of oil and meal from Lesquerella Fendleri seed. *Journal of the American Oil Chemists' Society*, 67(7), 438–442.
- Carmer, K. (2012). Father of rock wool from Alexandria. TheHeraldBulletin.com, Community Newspaper Holdings, Publisher beverly.joyce@heraldbulletin.com, Inc. Feb 11, 2012.
- Carraher, C. E., Jr. (2005). General topics. *Polymer News*, 30(2), 62–64.
- Chávez-Galán, J., Almanza, R., & Rodríguez, N. (2007). Experimental measurements of thermal properties for Mexican building materials to simulate thermal behavior to save energy. In *Proceedings of ISES World Congress 2007* (Vol. I – Vol. V, pp. 496–501). Springer.
- de Chazelles-Gazzal, C.-A. (1997). The earth houses of Southern Gaul. In *French: Les maisons en terre de la Gaule méridionale. Montagnac* (pp. 49–57). France: Éditions Monique Mergoïl.
- Close, P. D. (1947). *Thermal insulation of buildings* (p. 7). New York: Reinhold.
- Coles, J. M. & Harding, A. F. (1979). *The bronze age in Europe: An introduction to the prehistory of Europe c.2000–700 BC*. London: Methuen.
- Dabrowski, J. (1961). Beton Struzkowy - Produkcja, Wyroby i Zastosowanie ich w Budownictwie—(Wooden concrete—Production and application in building). Biuletyn Informacyjny Budownictwa 4/1961, Warsaw - Poland (in Polish).
- Dabrowski, J. (1989). Nordische Kreis und Kulturen Polnischer Gebiete. Die Bronzezeit im Ostseegebiet." Ein Rapport der Kgl. Schwedischen Akademie der Literatur-Geschichte und Altertumsforschung über das Julita-Symposium 1986.
- Dämmstoffarten, P. M. (2007). *Detail Praxis—Dämmstoffe (Grundlagen, Materialien, Anwendungen)*. Institut für internationale Architektur- Dokumentation GmbH & Co. KG.
- Denis, H. J., & Castor, W. M. (2007). Styrene. In *Ullmann's encyclopedia of industrial chemistry* (7th ed., p. 1). Wiley. [https://doi.org/10.1002/14356007.a25\\_329.pub2](https://doi.org/10.1002/14356007.a25_329.pub2).
- Desjarlais, A. O., & Tye, R. P. (1991). Research and development data to define the thermal performance of reflective materials used to conserve energy in building applications. Oak Ridge National Laboratory Report ORNL/Sun/88-SA 835-1 (1990) Available from the National Technical Information Services, U.S. Department of Commerce.
- Desjarlais, A. O., & Yarbrough, D. W. (1991). Prediction of the thermal performance of single and multi-air-space reflective materials. *American Society for Testing and Materials, STP, 1116*(1991), 24–49.
- Dickson, M., & Parker, D. (2014). *Sustainable timber design* (p. 248). Routledge—Architecture. ASIN: B00R623GMY.
- Diascorina, N., Calasb, S., Salléec, H., Acharda, P., & Rigacci, A. (2015). Polyurethane aerogels synthesis for thermal insulation—Textural, thermal and mechanical properties. *The Journal of Supercritical Fluids*, 106, 76–84. Aerogels: Synthesis and applications. Elsevier.
- Don, A. (2011). Asbestos: The hidden health hazard in millions of homes. *The Guardian*.
- Dvorchak, M. J. (1985). Use of phenolic foam in low-slope roofing. In *Proceedings of the Second International Symposium on Roofing Technology* (p. 360). Gaithersburg, MD, USA.
- Dwight, G. E. (Coordinating Editor) (1963). *Total emissivity of metals, surface unoxidized*. American Institute of Physics Handbook, 2nd edn (pp. 6–164).
- Editors of the American Heritage Dictionaries. (2007). *Spanish word histories and mysteries: English words that come from Spanish* (p. 5). Houghton Mifflin Co.
- Fesmire, J. E., Rouanet, S., & Ryu, J. (1998). Aerogel-based cryogenic superinsulation. In *Advances in cryogenic engineering*. Springer.
- Fesmire, J. E., & Augustynowicz, S. D. (2003). Improved thermal-insulation for low temperatures (pp. 54–55). NASA Tech Briefs, September 2003.
- Filimonow, P. J., & Nanazasvili, I. C. (1981). Problemy Rassirenija Proizvodstva i Primenenija Arbolita v Stroitelstvie. (Problems of production development and application of wooden concrete in building). Stroitelnyje Materialy 11/1981. Moscow - Russia (in Russian).

- Fricke, J., Heinemann, U., & Ebert, H. P. (2007). Vacuum insulation panels—From research to market. *Vacuum*, 82(2008), 680–690.
- Gee, D., & Greenberg, M. (2002). Asbestos: From 'Magic' to Malevolent Mineral. Late lessons from early warnings: the precautionary principle 1896–2000. Copenhagen: EEA Report, European Energy Agency (22) (pp. 52–63). ISBN 92-9167-323-4.
- Goss, W. P., & Miller, R. G. (1989). Literature review of measurement and predictions of reflective building insulation system performance; 1900–1989. *ASHRAE Transactions*, 95(2), 651–664.
- Gray, D. E. (Ed.). (1963). *American Institute of Physics Handbook*, Table 6k-7 (2nd ed., pp. 6–164). McGraw-Hill Book Company, Inc.
- Grynning, S., Baetens, R., Jelle, B., Gustavsen, A., Uvsløkk, S., & Meløysund, V. (2009). Vakuumsolasjonspaneler for bruk i bygninger – Egenskaper, krav og muligheter” [Vacuum insulation panels for building applications: Properties, requirements and possibilities]; (Project number: B22479.18 Report ISSN 1504-6958 ISBN 9788253610504). Oslo: SINTEF Byggforsk.
- Greig, A. R. (1922). Wall insulation. U. of Saskatchewan, College of Engineering, Bul. No. 1.
- Grundmann, R. (2007). Climate change and knowledge politics. *Environmental Politics*, 16(3), 414–432.
- Hagan, D., & Trujillo, H. (2011). 2009 New Mexico energy conservation code: Residential applications manual. State of New Mexico Energy, Minerals and Natural Resources Department Energy Conservation and Management Division (ECMD), Santa Fe, New Mexico, USA.
- Han, B. J., Yarbrough, D. W., & Han, S. M. (1988). Thermal resistance of wall cavities containing reflective insulation. *Journal of Solar Energy Engineering*, 108(1988), 338–341.
- Hosler, D., Burkett, S. L., & Tarkanian, M. J. (1999). Prehistoric polymers: Rubber processing in ancient Mesoamerica. *Science*, 284(5422), 1988–1991.
- Houben, H., & Guillaud, H. (1994). *Earth construction—A comprehensive guide*. ITDG Publishing.
- James, D. H., & Castor, W. M. (2007). *Styrene. Ullmann's encyclopedia of industrial chemistry*, 7th edn (p. 1). Wiley. [https://doi.org/10.1002/14356007.a25\\_329.pub2](https://doi.org/10.1002/14356007.a25_329.pub2).
- Jester, T. C. (1995). *Twentieth century building materials* (p. 122). New York: McGraw-Hill.
- Kistler, S. S. (1931). Coherent expanded aerogels and jellies. *Nature*, 127(3211), 741. Bibcode: 1931Natur.127.741K. <https://doi.org/10.1038/127741a0>.
- Kistler, S. S. (1932). Coherent expanded-aerogels. *Journal of Physical Chemistry*, 36(1), 52–64. <https://doi.org/10.1021/j150331a003>
- Knop, A., & Pilato, L. A. (1985). *Phenolic resins* (p. 313). Springer Verlag, Technology and Engineering.
- Kogan, A., Fesmire, J., Johnson, W., & Minnick, J. (2010). Cryogenic vacuum insulation for vessels and piping. In *Proceedings of International Cryogenic Engineering Conference 23 - International Cryogenic Materials Conference 2010 (ICEC 23 - ICMC 2010)*, 19–23 July 2010; Wroclaw, Poland.
- Kollmann, F. P., Kuenzi, E. W., & Stamm, A. J. (2012). *Principles of wood science and technology: II wood based materials*. Springer Science & Business Media, 703 p.
- Kosny, J. (1994). Wooden concrete—High thermal efficiency using waste wood. In *Proceedings of 1994 ACEEE Summer Study on Energy Efficiency in Buildings, Pacific Grove, CA, USA*.
- Kretzer, M. (2016). *Information materials: Smart materials for adaptive architecture*. Springer, p. 86. ISBN 3319351508.
- Künzel, H. (1998). Effect of interior and exterior insulation on the hygrothermal behaviour of exposed walls. *Materials and Structures*, 31(2), 99–103.
- Kwon, J. S., Jang, C. H., Jung, H., & Song, T. H. (2009). Effective thermal conductivity of various filling materials for vacuum insulation panels. *International Journal of Heat Mass Transfer*, 52, 5525–5532.
- LaHousse, S. W. (1993). Vacuum insulation using perlite powder sealed in plastic and glass. Thesis, Massachusetts Institute of Technology, Department of Mechanical Engineering, Cambridge, Massachusetts, February 1993.
- Lasman, H. R. (1965). . 2, 532–556. New York: Interscience.



- Lyon, C. K., Garrett, V. H., & Franker, E. N. (1974). Rigid urethane foams from hydroxymethylated castor oil, safflower oil, oleic safflower oil, and polyol esters of castor acids. *Journal of the American Oil Chemists Society*, 51(8), 331–334.
- Marko, A., Braun, P. (2013). *Thermische Solarenergienutzung an Gebäuden*. Springer-Verlag, Business & Economics, 440 p. ISBN 3642591205.
- Mielczarek, Z., & Lange, M. (1989). *Wlasciwosci i Zastosowanie Wiorobetonow w Budownictwie*. (Properties of wood concrete and its application in building). Centralny Osrodek Informacji Budownictwa, Warsaw, Poland 1989 (in Polish).
- Muench, C. G. (1947). An outline of the insulation board industry. *Paper Trade Journal*, 125(5), 48–50.
- Nappi, E. (1998). Aerogel and its applications to RICH detectors. *Nuclear Physics B—Proceedings Supplements, Proceedings of the Fifth International Conference on Advanced Technology and Particle Physics*, 61(3), 270–276.
- Nash, G. D., Comrie, J., & Broughton, H. F. (1955). *The thermal insulation of buildings—design data and how to use*. Her Majesty's Stationery Office (London).
- Nicolaon, G. A., & Teichner, S. J. (1968). Preparation of silica aerogels from methyl orthosilicate in alcoholic medium, and their properties. *Bulletin of Societe Chimique de France*, 1906–1911
- Oakseson, W., Lee, J., Goyal, S., Robson, T., & Cutler, I. (1977). *Foam glass insulation from waste glass*. Environmental Protection Agency, Washington, D.C., EPA/600/3-77/030.
- Oxford English Dictionary Second Edition on CD-ROM (v. 4.0) © Oxford University Press 2009.
- Pajongk, G., & Teichner, S. J. (1985). On some recent applications of aerogels. In *Aerogels: Proceedings of the First International Symposium, Würzburg, Fed. Rep. of Germany, September 23–25, 1985*, Springer Science & Business Media, Dec 6, 2012—Science, 208 p. ISBN 3642933130.
- Pekala, R. W., Alviso, C. T., Kong, F. M., & Hulsey, S. S. (1992). Aerogels derived from multifunctional organic monomers. *Journal of Non-Crystalline Solids*. Elsevier.
- Plundstein, M. (2007). *Dämmstoffarten. Detail Praxis—Dämmstoffe (Grundlagen, Materialien, Anwendungen)*”, Institut für Internationale Architektur-Dokumentation GmbH & Co. KG, München, Deutschland.
- Vitruvius, P. M. (1914). *Ten books on architecture*. Harvard University Press, p. 39.
- Rackham, H. (1961). *Pliny natural history*, English translation in ten volumes, v. 5, (Books 17–19). Cambridge, MA: Harvard University Press, 544 pp.
- Ramirez-Coretti, A., Eckelman, C. A., & Wolfe, R. W. (1998). 'Inorganic-bonded composite wood panel systems for low-cost housing: A central American perspective. *Forest Products Journal*, 48(4), 62–68.
- Reboul, P. (1994). Britain and the Bakelite revolution. In S. T. I. Mossman & P. J. T. Morris (Eds.), *The development of plastics* (pp. 26–37.5.1). Cambridge: Royal Society of Chemistry.
- Reichenauer, G., Heinemann, U., & Ebert, H.-P. (2007). Relationship between pore size and the gas pressure dependence of the gaseous thermal conductivity. *Colloids and Surfaces A Physicochemical and Engineering Aspects*, 300(1–2), 204–210.
- Robinson, H. E., & Powell, F. J. (1956). The thermal insulating value of airspaces. Housing Research Paper 32, U.S. National Bureau of Standards Project ME-12.
- Ross, M., & Nolan, R. P. (2003). History of asbestos discovery and use and asbestos-related disease in context with the occurrence of asbestos within the ophiolite complexes. In Dilek Y. & Newcomb S. (Eds.), *Ophiolite concept and the evolution of geological thought*. Special Paper 373. Boulder, Colorado: Geological Society of America. ISBN 0-8137-2373-6.
- Rowley, F. B., & Algren, A. B. (1929). Thermal resistance of air spaces. *Transactions of the American Society of Heating and Ventilating Engineers*, 35(1929), 165–181.
- Rudnick, L. R. (2013). *Synthetics, mineral oils, and bio-based lubricants: Chemistry and technology*, 2nd edn (p. 147). CRC Press. ISBN 978-1-4398-5537-9.
- Saber, H. H. (2013). Practical correlations for thermal resistance of vertical enclosed airspaces for building applications. *Journal of Building and Environment*, 59(2013), 379–396.
- Saber, H. H. (2014). Practical correlations for thermal resistance of horizontal enclosed airspaces with downward hot flow for building applications. *Journal of Building Physics*, 37(4), 403–435.

- Saber, H. H., Maref, W., & Hajiah, A. E. (2020). Effective R-value of enclosed reflective space for different building applications. *Journal of Building Physics*, 43(5), 398–427.
- Sabin, P., van Wees, H., & Whitby, M. (2007). *The Cambridge history of Greek and Roman warfare*. 1 (p. 196). Cambridge University Press.
- Scheffler, M., & Colombo, P. (2003). Cellular ceramics: Structure, manufacturing, properties and applications. Weinheim, (Germany): Wiley-WCH Verlag GmbH & Co.KGaA.
- Schmidt, D. L., & Graig, R. D. (1982). Advanced carbon fabric-phenolic for thermal protection application. Air Force Wright Aeronautical Laboratories, US AFWAL-TR-81-4136, USA.
- Schonhardt, U., Binz, A., Wohler, M., & Dott R. (2003). Ökobilanz eines Vakuum-Isolations-Paneels (VIP). Muttenz, Switzerland: Institut für Energie, Fachhochschule beider Basel.
- Schwab, H., Stark, C., Wachtel, J., Ebert, H.-P., & Fricke, J. (2005). Thermal bridges in vacuum-insulated building façades. *Journal of Thermal Envelope & Building Science*, 28(4), 345–355.
- Segal, C. L. (1967). *High temperature polymers*. Marcel Dekker.
- Selikoff, I. J., & Lee, D. H. K. (1978). *Asbestos and disease, environmental sciences: An interdisciplinary monograph series*. Academic Press, Inc.
- Semmler, F. W. (1907). Die ätherischen Öle nach ihren chemischen Bestandteilen unter Berücksichtigung der geschichtlichen Entwicklung, vol. 4 (Leipzig, Germany, Veit & Co., 1907), § 327. Styrol (pp. 24–28).
- Seymour, R. B., & Kauffman, G. B. (1992). Polyurethanes: A class of modern versatile materials. *Journal of Chemical Education*, 69, 909.
- Shigekura, Y. (1989). Wood fiberboards bonded with inorganic binders in Japan. In *Proceedings of Fiber and Particle Boards Bonded With Inorganic Binders*, Forest Products Research Society, Madison, Wis (pp. 141–150).
- Seigel, F., & Howell, J. R. (1972). *Thermal radiation heat transfer*. New York: McGraw Hill Book Company.
- Simmler, H., Brunner, S., Heinemann, U., Schwab, H., Kumaran, K., Mukhopadhyaya, P., Quénard, D., Sallée, H., Noller, K., Kücükpinar-Niarchos, E., Stramm, C., Tenpierik, M. J., Cauberg, J. J. M., Erb, M. (2005). Vacuum insulation panels. Study on VIP-components and panels for service life prediction of VIP in building applications (Subtask A): IEA/ECBCS Annex 39 High Performance Thermal Insulation (HIPTI).
- Smith, T., Carlson, J., & Walzak, T. (1993). Steel deck corrosion associated with phenolic roof insulation: Problem causes, prevention, damage assessment & corrective action. In *10th Conference on Roofing Technology*, NRCA, National Roofing Contractors Association (pp. 108–122).
- Soulet, R. (1996). James Dewar, His flask and other achievements. *Physics Today*, 49(3), 32–37.
- Spon, E., Haldane, R., Lock, C. G. W. (1883). *Workshop receipts* (p. 439). London: E. & F. N. Spon.
- Stanton, M. F., & Layard, M. (1978). The carcinogenicity of fibrous minerals. National Bureau of Standards, Special Publication 506—From Gaithersburg Conference of July 1977.
- Stark, R. W., Drobek, T., Weth, M., Fricke, J., & Heckl, W. M. (1998). Determination of elastic properties of single aerogel powder particles with the AFM. *Ultramicroscopy*, 75(1998), 161–169.
- Suchsland, O., & Woodson, G. E. (1986). *Fiberboard manufacturing practices in the United States*. United States Department of Agriculture, Forest Service Agriculture, Handbook No. 640
- Syrett, M. (2004). Scandinavian History in the Viking Age—A select bibliography. Department of Anglo-Saxon, Norse, and Celtic, University of Cambridge. ISSN 1475-8520.
- TenWolde, A., McNatt, I., & Krahn, L. (1988). *Thermal properties of wood and wood panel products for use in buildings*. USDA Forest Products Laboratory Report for Oak Ridge National Laboratory, Oak Ridge, TN. U.S. Department of Energy, Report ORNLSub/87- 21697/1, September 1988
- Thorsell, T. I. (2006). Edge loss minimization in vacuum insulation panels. *Research in Building Physics and Building Engineering*, 251–256.
- Tillotson, T. M., & Hrubesh, L. W. (1992). Transparent ultralow-density silica aerogels prepared by a two-step sol-gel process. *Journal of Non-Crystalline Solids*. Elsevier.
- Torgal, F. P., Buratti, C., Kalaiselvam, S., Granqvist, S. G., & Ivanov, V. (2016). Nano and biotech based materials for energy building efficiency. Springer, February 4, 2016—Technology & Engineering, 484 p.

- Touloukian, Y. S., & Dewitt, D. P. (1970). *Thermal radiation properties—Metal elements and alloys, Thermophysical properties of matter* (Vol. 7). IFI/Plenum Press.
- Toyokuni, S. (2009). Mechanisms of asbestos-induced carcinogenesis. *Nagoya Journal of Medical Sciences*, 71(1–2), 1–10. PMID 19358470.
- U.S Department of Energy. Attic radiant barrier fact sheet. DOE/CE-0335P, Washington, D.C.
- Vicarini, M. A., Nicolaon, G. A., & Teichner, S. J. (1970). Propriété's texturales d'aérogels mine'raux mixte pré'paré's par hydrolyse simultané'e de deux alcoolates mé'talliques en solution dans un milieu organique. *Bulletin de la Socié'té Chimique de France*, 10, 3384–3387.
- Voytek, P., Anver, M., Thorslund, T., Conley, J., & Anderson, E. (1990). Mechanisms of asbestos carcinogenicity. *International Journal of Toxicology*, 9(5), 541–550. <https://doi.org/10.3109/10915819009078762>
- Wang, X., Walliman, N., Ogden, R., & Kendrick, C. (2007). VIP and their applications in buildings: A review. *Construction Materials*, 160, 145–153.
- Wei, T. Y., Chang, T. F., Lu, S. Y., & Chang, Y. C. (2007). Preparation of monolithic silica aerogel of low thermal conductivity by ambient pressure drying. *Journal of the American Ceramic Society*, 90(7), 2003–2007.
- Weslager, C. A. (1969). *The log cabin in America*. New Jersey, Rutgers University Press.
- Whitehouse, A. A. K., Pritchett, E. G. K., & Barnett, G. (1968). Phenolic resins. Iliffe Books Ltd., London; American Elsevier, New York, 1968. 143 pp. *Journal of Polymer Science, A-2 Polymer Physics*, 7, 2139–2140.
- Wilkes, G. B. (1950). *Heat insulation-chapter 6: Reflective insulation*. John Wylie and Sons.
- Zhang, S., & Zhao, D. (2016). Aerospace materials handbook. In *Advances in materials science and engineering*. CRC Press—Technology & Engineering, 781 p. ISBN 1439873305.

## Patents

- U.S. Patent US 232122 A. (1880). Glass Cloth or Fabric," Patented Sept, 14th 1880. Herman Hammesfahr.
- German Patent Nr. 516377. (1930). Patentschrift Nr. 516377, Klasse 80b, Gruppe 9 des Reichspatentamt, Deutsches Reich, Sterchamolwerke Dortmund and Hemman O, Bad Durenberg.
- U.S. Patent US 2093454. (1937). Method of Producing Aerogels." Samuel S. Kistler.
- U.S. Patent US 2700633. (1955). Insulating Structure and Method of Forming Same." New York, 1955. - Bovenkerk H. J. General Electric.
- U.S. Patent US 2989156A. (1961). Heat Insulating Panels, Pastuhov Alexis, Brooks Frank P, Glaser Peter E.
- U.S. Patent US 3094071 A. (1963). Vacuum insulated storage tanks for missile use. Beckman John Heller.
- US Patent US 3151365 A. (1964). Insulation material and structures containing same. In Emslie A. G., Glaser P. E., Salmon W. A., & Little A. D. (Eds.). Cambridge, MA.
- U.S. Patent US 3179549 A. (1964). Thermal insulating panel and method of making the same. In Strong Herbert M., & Bundy Francis P (Eds.), *General electric*.
- U.S. Patent US 4486482. (1983). Vacuum Heat Insulator. Kobayashi Nobuyuki, Abe Yoritsune, Shibata Katuo, Watanabe Yukio; Hitachi Ltd. (Tochigi, JP).
- U.S. Patent US 4468336 A. (1984). Low density loose fill insulation. Ivan T. Smith.
- German Patent DE 3707768 A1. (1988). Vakuum Waermeisolation, Friedrich Hensberg.
- U.S. Patent US 5011091 A. (1991). Cellulose fiberization apparatus. Ivyl D. Kopecky.
- U.S. Patent US 5019170 A—Coated Tree Aggregate Usable in Wood Concrete Technology and Method of Making the Same, Walter H.
- U.S. Patent US 6106449 A. (2000). Vacuum insulated panel and container and method of production. Nicholas Wynne, Vacupanel, Inc.

- WO2005007984 A1. (2005). Cellulose fibre insulation and method of application. In Schmidt A.O., Krendl D.J., & Molcar, K (Eds.).
- U.S. Patent U S6262164 B1. (2001). Method of installing insulation with dry adhesive and/or color dye, and reduced amount of anti-static material. In Church J.T., Chenoweth C., Romes G.E., & Vegedes M.H. (Eds.).
- WO 2013182506. (2013). Aerogel containing polyurethane composite material. In Eling, B., & Auffarth S. (Eds.).
- US 2014147607 (A1). (2014). Porous polyurethane networks and methods of preparation. In Leventis N., Sotiriou-Leventis C., & Chidambareswarapattar C. (Eds.).
- US 2015266983 A. (2015). Flexible to Rigid Nanoporous Polyurethane-Acrylate (PUAC) Type Materials for Structural and Thermal Insulation Applications. In Leventis N., Sotiriou-Leventis C., & Band A. (Eds.).
- WO 2015109488. (2015). Rigid polyurethane foam having a small cell size. In Bertucelli L., Parenti V., Li D., Liu W., Chai N., Wang B., Chen C., Guo H.F., Chen J., Yin Y., Costeux S., & Smith B.G. (Eds.).

# Chapter 2

## Long-Term Thermal Performance of Insulations Under Moisture Loads



Hartwig M. Künzel

**Abstract** The performance of thermal building envelope insulation systems may be severely impaired by moisture. The best solution would be to keep insulation materials dry at all times. Alas, building practice has proven time and again that this is wishful thinking. Even if the insulation materials are enclosed by vapor barriers on both sides, there is a fair chance that moisture will get inside eventually through imperfections and small leaks emerging during normal use. Once inside, moisture will be trapped there for a long time. Thus, understanding the long-term performance of insulation materials is vital for sustainable and energy efficient building design. This chapter analyzes and quantifies the impact of moisture on the thermal resistance of insulation systems and explains the interdependence of heat and moisture transfer. This helps to develop durable envelope solutions and appropriate test methods for insulation materials.

### 2.1 Theoretical Background

Under dry conditions, heat transfer in insulation materials is mainly governed by conduction in the solid and gas phase as well as by thermal radiation within the pore space. Convection by external pressure or buoyancy effects should be minimized by air and wind barriers and the pore structure of the insulation material. If the gas phase is partly replaced by water with its rather high thermal conductivity ( $0.6 \text{ W}/(\text{m}\cdot\text{K})$ ), the thermal transmittance of the whole system will increase accordingly. This is called the sensible heat effect of moisture. However, there is a second moisture impact on thermal transmittance, the so-called latent heat effect. It is caused by water evaporation and condensation at different location of the assembly. In vapor permeable materials, this effect may transfer more energy than the sensible heat flux by conduction, at least for short periods of time.

---

H. M. Künzel (✉)

Department of Hygrothermics, Fraunhofer Institute for Building Physics IBP, Holzkirchen, Germany

e-mail: [hartwig.kuenzel@ibp.fraunhofer.de](mailto:hartwig.kuenzel@ibp.fraunhofer.de)

Both effects are relevant to quantify the impact of moisture on the thermal performance of insulation systems. There may be other effects such as heat transfer by liquid flow or thermal storage by ice formation. However, they are usually of minor importance in insulation materials and therefore not considered here. This does not mean that liquid flow has no impact at all, but it is mostly more indirect, e.g. in mineral, capillary active insulation materials whose particular properties enhance vapor diffusion, which will be addressed later.

While sensible heat flux is a linear phenomenon and proportional to temperature gradient and thermal conductivity of the material, the latent heat flux is non-linear and depends only indirectly on the temperature gradient, because it is proportional to the vapor pressure gradient and the vapor diffusion coefficient of the material. Since variations in vapor pressure depend strongly on the moisture stored in the insulation layer but also in the adjacent layers, the latent heat flux may become very dynamic, and a precise analysis requires hygrothermal (heat and moisture transfer) considerations. To quantify its impact in relation to thermal conductance under realistic practice conditions, means to carry out a more long-term investigation to evaluate its dynamic behavior. Short snapshots as in Hedlin (1988) may demonstrate peak values but not necessarily the mean impact over the whole heating or cooling period. In contrast to thermal conduction which also depends on stationary moisture in the insulation layer, the dynamic latent heat effect is only significant in very vapor permeable insulation materials. In vapor retarding materials, such as closed cell foam insulation, there is only very little vapor transport and thus hardly any latent heat contribution to the total heat flux. However, over several years vapor diffusion and interstitial condensation may lead to moisture accumulation in the insulation layer and therefore also to a considerable increase in its thermal conductivity—Zirkelbach (2011).

Independent of the kind of insulation material, it is important to assess the long-term thermal performance of the whole system in response to environmental moisture loads. Short-term investigations and those that consider only parts of the entire building system may be misleading because of the complex nature of the interaction between energy and moisture. Therefore, it is not enough to consider the relevant heat transfer phenomena in insulation materials individually, as in most guarded hot plate tests. To grasp the whole picture, it is crucial to do a long-term hygrothermal analysis of the entire building envelope system subject to real climatic boundary conditions. This may be achieved by an elaborate field test or more cost-effectively by validated hygrothermal simulation models.

The following section summarizes the background of the coupled heat and moisture transfer mechanisms that determine moisture dependent heat transmission through insulated envelope systems. It identifies the relevant material properties and explains how they should be measured. Finally, the importance of moisture related effects is demonstrated by two practice cases with vapor retarding and vapor permeable insulation materials.

## 2.2 Analysis of Moisture Effects on Heat Transfer in Thermal Insulation Materials

Heat transfer in dry insulation materials is a mixture of thermal conduction in the solid and the gas phase as well as radiation exchange and some convection effects within the gas phase. The latter is usually very small and may only become relevant if there are external air pressure differences or large temperature gradients. Thus, under normal conditions the term thermal conduction in insulation materials includes only physical conduction and internal thermal radiation exchange in the solid matrix and the gas-filled voids. The type of gas and the size of the voids has also an influence on the thermal resistance of the material. Small pores and heavy gases decrease the thermal conductivity because the momentum propagation between gas molecules and the solid matrix, respectively between the individual gas molecules is reduced. Evacuating the voids inhibits thermal conduction in the pore space altogether, leaving only the conduction in the solid matrix and thermal radiation as heat transfer mechanisms. Adding compounds that absorb radiation and/or reduce the emissivity of the solid matrix increases the thermal resistance by reducing the radiative heat transfer.

The presence of moisture will always lower the thermal resistance of porous materials by adding another phase to the material with a considerable thermal conductivity (liquid water  $\approx 0.6 \text{ W}/(\text{m}\cdot\text{K})$ , ice  $\approx 2.1 \text{ W}/(\text{m}\cdot\text{K})$ ), water molecules adsorbed by the solid matrix). The thermal conductivity of water in the adsorbed phase is not really known, however, this doesn't really matter because the thermal conductivity of insulation materials is measured as a lumped quantity of different heat transfer phenomena anyway. The impact of moisture on the internal radiation exchange is largely unknown. As long as the moisture in the material is stationary, i.e. not moving about by vapor diffusion or liquid flow (capillary flow and surface diffusion—see Künzel, 1995), the impact of moisture on the heat flux by effective thermal conduction can be described by:

$$q = -k(w) \cdot \Delta\theta / \Delta x \quad (2.1)$$

where,

$q \text{ [W/m}^2\text{]}$	heat flux
$k(w) \text{ [W}/(\text{m}\cdot\text{K})\text{]}$	moisture dependent effective thermal conductivity
$\theta \text{ [K]}$	temperature

Equation (2.1) describes the steady state heat flux through a homogenous insulation material subjected to a constant temperature difference, a common situation under winter conditions. As long as the exterior and interior surface temperatures do not change, this heat flux doesn't change either, provided that the moisture distribution within the insulation layer remains the same. If the boundary conditions change over time, the heat flux becomes dynamic and its size changes not only with time but also with the position within the insulation layer due to thermal inertia. This transient process may be described by the following partial differential equation:

$$\frac{\partial H}{\partial t} = -\nabla \cdot q + S_h \tag{2.2}$$

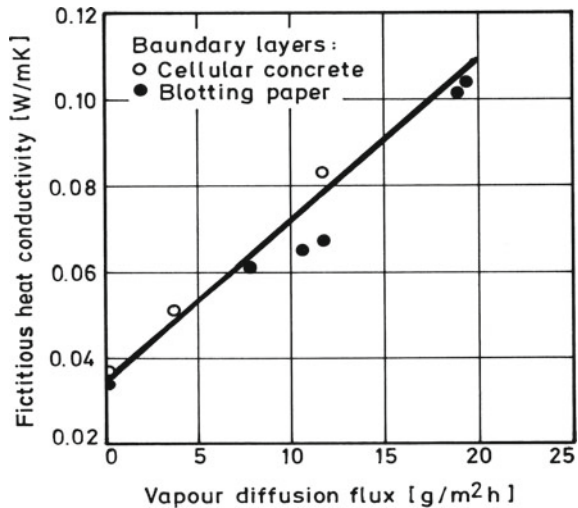
where,

$H$  [J/m<sup>3</sup>]      enthalpy of the material and the moisture inside  
 $S_h$  [J/(m<sup>3</sup>·s)]    heat source/sink related to moisture movement

For insulation materials with very low vapor permeability such as closed cell organic foams, the term  $S_h$  on the right-hand side is negligible, i.e. close to zero. In this case we get Fourier’s heat transfer equation. In materials with high vapor permeability, however, another heat transfer effect, the so-called enthalpy flux or latent heat flux may become dominant. This phenomenon is caused by water evaporating at the warm side and moving by vapor diffusion through in the gas phase to the cold side where it condenses again. It has nothing to do with thermal conduction and the driving force is only indirectly the temperature gradient. In reality it is a diffusion flux driven by vapor pressure differentials and fed by evaporating water and condensing vapor within the insulation material or in resp. on the material layers adjacent to the insulation layer.

An experiment using a modified guarded hot plate apparatus measuring the heat transfer through a mineral wool insulation slab between two wet layers of either blotting paper or cellular concrete (AAC) in Achtziger (1984), demonstrated the mechanism of latent heat transfer and its importance for the overall thermal performance of insulation systems. Figure 2.1 shows the “fictitious” thermal conductivity of the insulation layer (determined from measuring the total heat flux and the surface temperature difference over the mineral fiber insulation slab) as a function of the vapor flux calculated from the weight changes of the respective boundary layer

**Fig. 2.1** Apparent thermal conductivity of mineral fiber insulation slabs between wet layers of porous materials, determined from heat flux and surface temperature measurements, as function of vapor diffusion flux through the insulation—Achtziger (1985)





materials. The thermal conductivity increases almost linearly with the vapor diffusion flux, reaching values that are three times as high as the thermal conductivity of the dry material.

These results of Achziger (1985) are in line with the findings in Hedlin (1988). However, in this case the moisture was initially not in the insulation material itself but in the adjacent boundary layer materials. This demonstrates that the latent heat transfer is neither part of thermal conduction, nor is it a specific material property but rather the response of a whole system to certain boundary conditions. In contrast to thermal conduction, it is also highly dynamic. While the conduction heat flux remains almost constant for a long period of time—as long as the boundary conditions are left unchanged—the latent heat flux decreases to zero as soon as the wet layer at the warm side has dried out.

Since vapor diffusion in building envelope systems can have such an important influence on heat transfer, it must be accounted for, to understand and quantify the relevant thermal phenomena in insulated building assemblies—see: EN 15026 (2007), ANSI/ASHRAE Standard 160 (2016), and ASHRAE Handbook of Fundamentals (2017). The enthalpy flows through vapor movement and phase transition can be described by specifying the source term in the heat balance equation:

$$S_h = -h_v \nabla \cdot g_v \quad (2.3)$$

where,

$S_h$ [J/m <sup>3</sup> ·s]	heat source/heat sink caused by condensation/evaporation
$h_v$ [J/kg]	latent heat of phase change
$g_v$ [kg/m <sup>2</sup> ·s]	vapor diffusion flux density

The latent heat of phase transition consists of the evaporation enthalpy of pure water ( $h_v \approx 2500$  kJ/kg) and the material specific sorption enthalpy which is negligible for most building materials compared to the evaporation enthalpy of water if  $RH \geq 50\%$ . To determine  $S_h$ , the remaining unknown is the vapor diffusion flux density  $g_v$  which can only be calculated by solving the transient moisture transfer equation.

### 2.3 Interaction Between Heat and Moisture Transfer—Hygrothermal Phenomena

As soon as moisture is present in porous materials, its migration in building envelope systems has an influence on heat transfer that must be accounted for. Analogous to heat transfer, transient moisture transfer can be described by the following partial differential equation—Künzel (1995):

$$\frac{\partial w}{\partial t} = -\nabla(g_w + g_v) \quad (2.4)$$

where;

- $W$  [kg/m<sup>3</sup>] water content of the building material layer
- $g_w$  [kg/(m<sup>2</sup>·s)] liquid transport flux density
- $g_v$  [kg/(m<sup>2</sup>·s)] vapor diffusion flux density

Liquid transport flux has generally only a minor effect on heat transfer—see: Künzle (1995), Gawin et al. (2004). Most conventional insulation materials such as organic foams or mineral fibers do not support liquid flow. However, there are also exceptions, e.g. capillary active insulation materials. They have been developed for interior wall insulation applications that work without a vapor retarder. Their capacity to support liquid flow helps to wick any water back from the condensation plane, because vapor and liquid flow are driven by different potentials (vapor pressure vs. capillary pressure respectively RH). These driving forces are generally opposed to each other in the insulation layer when condensation occurs (Binder et al., 2010) as shown in Fig. 2.2. In this case, the liquid flux may be relevant because it enhances the vapor diffusion flux. This happens by wicking back condensation water from the cold to the warm side, a bit like a low performing heat pipe—Gawin et al. (2004). However, this effect should not be overestimated because it is only relevant in materials whose structure is dense enough to support liquid flow, which means the thermal resistance is usually not that large anyway. Since liquid flow is absent or insignificant in most conventional insulation materials, only vapor diffusion is considered here by the

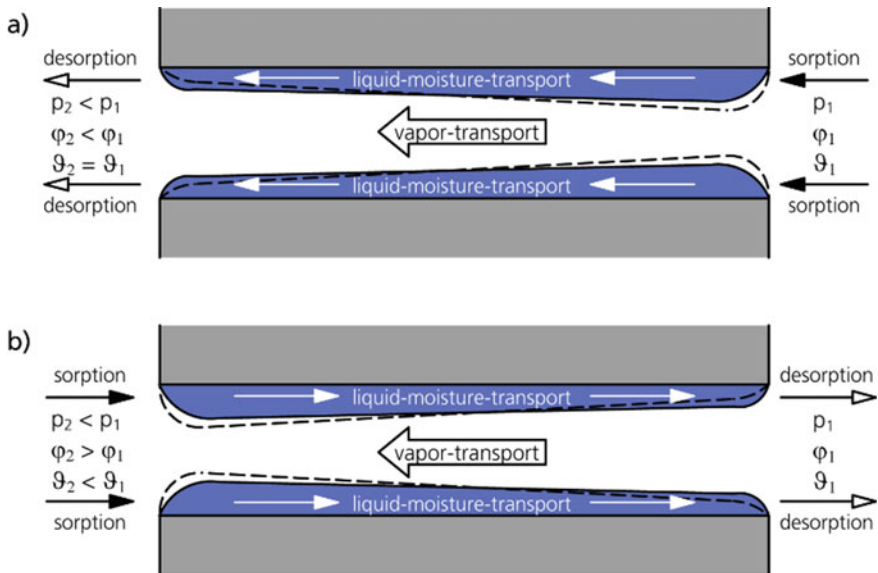


**Fig. 2.2** Moisture transport phenomena in pores of hydrophilic media under **a** isothermal and **b** non-isothermal boundary conditions. In case (**b**) the driving potentials and thus the related moisture fluxes of vapor diffusion and liquid transport in the surface water layer (aka surface diffusion) are often opposing each other—Binder et al. (2010)

following gas diffusion equation:

$$q_v = -\delta \cdot \nabla p_v = -\delta \cdot \nabla \varphi p_{sat} \quad (2.5)$$

where:

$\delta$  [kg/(m·s·Pa)] water vapor permeability of building material  
 $p_v/p_{sat}$  [Pa] water vapor partial/saturation Pressure.  $\varphi$  [–] relative humidity (RH)

According to Eq. (2.5), the vapor diffusion flux through porous materials depends on the RH in the pores and the saturation pressure which is an exponential function of the local temperature. This means, heat transfer is also affecting moisture transfer and vice versa and it also demonstrates that both transfer mechanisms are strongly coupled. Therefore, we talk about hygrothermal transfer, because one doesn't exist without the other, as long as moisture is present, and in real buildings, moisture is always present.

The fundamentals and working principles of these hygrothermal transfer models have been standardized in EN 15026 (2007), as well as in ANSI/ASHRAE Standard 160 (2016), and ASTM E3054/E3054M (2016) for wider application, i.e. many national moisture control standards refer to them. Neglecting transfer by air convection in porous insulation materials—if convection effects occur, more sophisticated approaches would be necessary that take account of joints and imperfections—the one-dimensional heat and moisture transport through the building envelope components may be represented by the following partial differential equations:

$$(\rho_s c_s + \rho_w c_w) \cdot \partial \theta / \partial t = \nabla \cdot [k(w) \nabla \theta] + h_v \nabla \cdot [\delta \nabla (\varphi \cdot p_{sat})] \quad (2.6)$$

$$dw/d\varphi \cdot \partial \varphi / \partial t = \nabla \cdot [D_w dw/d\varphi + \delta \nabla (\varphi \cdot p_{sat})] \quad (2.7)$$

where

$\rho_s, \rho_w$  density of solid matrix, water [kg/m<sup>3</sup>]  
 $c_s, c_w$  specific heat of solid matrix, water [J/kg K].  
 $w$  moisture content, [kg/m<sup>3</sup>]  
 $k(w)$  moisture dependent thermal conductivity, [W/(m·K)].  
 $D_w$  liquid diffusivity, [m<sup>2</sup>/s]

Equations (2.6) and (2.7) are strongly coupled. The stationary water in the material pores increases the thermal storage  $\rho_w c_w$  and the thermal conductivity  $k(w)$  in Eq. (2.6). The divergence of the vapor transport from in Eq. (2.7) multiplied by the heat of evaporation, represents the latent heat transfer in Eq. (2.6). The temperature distribution calculated by Eq. (2.6) has a small effect on the liquid flux in Eq. (2.7) due to changes in water viscosity (part of  $D_w$ ) but a significant impact on the vapor transport term because the saturation pressure increases exponentially with temperature, while the relative humidity in the pore air changes only slightly as long as

enough sorption moisture is present on the pore surfaces to compensate the effect of temperature fluctuations.

An important aspect of the exponential increase of saturation pressure with temperature concerns the magnitude of the latent heat effect. Under winter conditions with 20 °C indoors and 0 °C outdoors it can be of the same size as the heat flux due to thermal conduction in a fibrous insulation layer of 10 cm as long as there is enough moisture on the warm side. In the temperature range between 20 °C and 40 °C there is only a slight increase in the conduction heat flux, however, the latent heat flux can be almost three times as high. However, the moisture in the assembly will also dry out much faster, unless it is trapped between two vapor tight layers, e.g. vapor barrier and roofing membrane.

This may challenge our common sense, but the good news is, we possess the tools that show us what is really going on, when heat and moisture intertwine. Until now, hygrothermal simulation tools were mainly employed to predict the moisture conditions in building assemblies, e.g. to avoid moisture related damage like mold growth, rot, corrosion, etc. There are only very few studies that employed these tools for heat transfer investigations such as interpreting guarded hot plate measurements, e.g. Gawin et al. (2004), Kehrer et al. (2003). In those tests only the total heat flux density can be measured. To separate the latent heat flux from the sensible heat flux resulting only from thermal conduction in the solid, liquid, and gaseous phase is very difficult. Comparing the measured heat flux to hygrothermal simulation results that mimic the course of the guarded hot plate test is a possible way out, because hygrothermal models calculate both heat fluxes independently. Therefore, their sum must coincide with the measured heat flux as long as material parameters, boundary and initial conditions are the same for measurement and simulation. Since the latent heat flux is not part of thermal conduction, the only remaining unknown—the moisture dependent thermal conductivity—can be determined that way.

## 2.4 Measuring Thermal Conductivity of Moist Materials

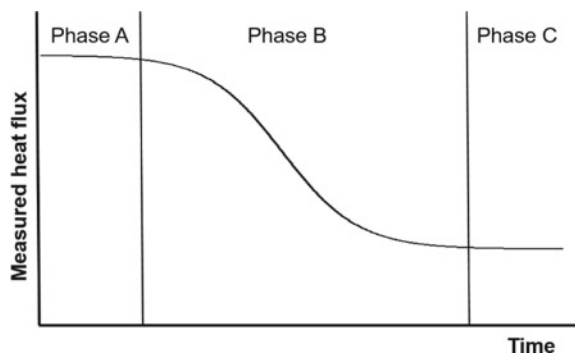
As already mentioned above, there must be a clear separation between thermal conduction in wet materials and heat transfer by vapor diffusion and evaporation/condensation. This has already been recognized several decades ago, e.g., by Sandberg (1986). While the true thermal conductivity of a moist material can be seen as a material property, the latent heat flux is neither part of it, nor is it a thermal property at all. It is true that the latent flux is usually a function of another material property, the vapor permeability, however, since the driving force for vapor diffusion is partial vapor pressure which is not directly related to temperature, there is no way of combining sensible and latent heat transfer in one single transfer equation. For this reason, it is impossible to measure the true moisture dependent thermal conductivity in highly vapor permeable materials independent of moisture transfer. In materials with low vapor permeability the latent heat transfer becomes so small that its impact

falls within the measuring accuracy. Therefore, a standard guarded hot plate test will provide reliable results for most closed cell insulation materials (Fig. 2.3).

Many solutions have been proposed to get around the latent heat dilemma with thermal conductivity measurements of vapor permeable insulations materials. In the ISO Standard 10051 (1996) the moisture effects on heat transfer during guarded hot plate measurements have been analyzed and the test period has been divided into 3 phases. The initial Phase A is characterized by a rather uniform moisture distribution in the carefully sealed test sample (moisture is not allowed to dry-out during the test—moisture loss should be below  $0.01 \text{ kg}/(\text{m}^3 \cdot \text{h})$ ), when there is still an over hygroscopic water content at the warm side of the sample. Phase A is followed by the transition Phase B when the heat flux decreases because the warm side is slowly drying out until a dynamic moisture equilibrium is reached in Phase C. This moisture equilibrium results from opposing vapor and liquid flow processes in hygroscopic and capillary active insulation materials as explained in Fig. 2.2. These fluxes are in balance with each other when a constant moisture profile is achieved which is characterized by zero net moisture movement under the prevailing boundary conditions. It should be noted that care must be taken to avoid liquid flow due to gravity. Therefore, the standard states that downward heat flow is preferred. However, before doing the thermal transmissivity test on a moist material in the downward direction, we propose to first make sure that there is no difference in results between upward and downward direction when testing the same material in dry state, unless buoyancy and edge effects can be totally excluded.

To evaluate Phase A, the standard recommends A for materials with low vapor permeability because the effects of moisture movement are small. For all other materials Phase C is the preferred evaluation range and the moisture distribution at the beginning and at the end of the test should be measured and if possible, the rate of moisture redistribution should be determined by calculation. Alas, the standard does not present a comprehensible explanation on how to calculate  $k(w)$  for highly vapor permeable materials exactly. Therefore, we propose to accompany the heat transmission tests of materials with high vapor permeability by hygrothermal simulations and determine the true  $k(w)$  by comparing the measured and the calculated dynamic heat flux results, e.g. as demonstrated in Gawin et al. (2004) and Kehrer et al. (2003).

**Fig. 2.3** Evolution of the measured heat flux during thermal transmissivity tests of moist materials according to ISO 10051 (1996)



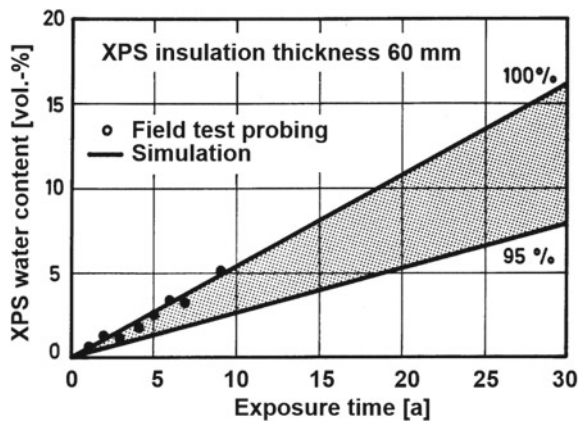
## 2.5 Practice Case: Water Accumulation in Closed-Cell Foam Insulation of an Inverted Roof

Garden roofs are on the rise because they provide some natural space in an urban environment and may help to alleviate the urban heat island effect. Since gardening activities may damage the waterproofing membrane so-called inverted or protected membrane roofs appear to be a good solution. This type of flat roof where the waterproofing membrane is directly attached to the concrete deck, covered by extruded polystyrene insulation (XPS) and ballasted by gravel has been applied in Europe for decades. Because precipitation water penetrates the insulation layer before it is drained off on the roofing membrane there is a risk of interstitial condensation in the insulation slabs.

While numerous investigations have shown that there is no moisture accumulation when extruded polystyrene is used as insulation material, there has been some doubt whether replacing the gravel ballast by plant substrates will not lead to critical conditions. From practical experience it is known that the bottom surface of the insulation is permanently in contact with water. While the extrusion skin of the insulation slabs is impermeable to liquid water, its vapor permeability is not zero. This means some vapor will enter the insulation layer and if it cannot leave through the upper surface, long-term moisture accumulation may occur which results in a reduction of the roof's thermal resistance.

Based on field tests and hygrothermal simulations on inverted flat roofs with plant cover, the long-term moisture uptake of XPS insulation slabs of 60 mm thickness has been determined for Central European climate conditions. Figure 2.4 shows the measured water content in the XPS insulation as dots compared to the simulated water accumulation (solid lines) over a period of 30 years. The simulations were performed, because the measured results were questioned, and it was hoped that the moisture accumulation would level off after some years.

**Fig. 2.4** Water content due to vapor condensation in the insulation layer of an inverted roof over time as a function of the relative humidity in the substrate above the insulation—Künzel and Kießl (1998). The dots show the measured values and the solid lines the simulated annual increase, assuming average substrate moisture of 95% and 100% RH



As boundary conditions for the simulations the controlled indoor conditions during the field test and the outdoor temperature variations of an average year at the test location were employed. The moisture conditions beneath and above the insulation layer have not been monitored during the field test. Therefore, they had to be estimated from observations during probing. There had been ample of proof that the lower surface of the insulation was always in contact with residual precipitation water, therefore RH was set to constant 100% at this position. The upper surface covered by the plant substrate also appeared to be wet most of the time according to observations during probing. Therefore, an average RH of 95% respectively 100% was selected for the simulation. The comparison between measurement and simulations demonstrated that the relative humidity in the substrate layer above the insulation remained around 100% all year round at that location. Since most plants need liquid water to survive, the relative humidity in the soil must be on average at least 99%. In later field tests this result has been confirmed by monitoring the dewpoint and the surface temperature at the top of the insulation layer—Künzel and Kiebl (1998).

The consequences for the thermal performance of the observed long-term moisture accumulation are significant. According to Achtziger and Cammerer (1984), the thermal conductivity of the XPS insulation rises from 0.03 W/(m·K) in dry state to about 0.045 W/(m·K) at 16 vol.-% water content after 30 years. This increases the heat transfer through the insulation layer by about 50%. Over the estimated 30-year service life of the roof, the additional conduction heat transfer due to moisture in the XPS amounts to 25%. This could be easily compensated by installing insulation slabs that are 20 mm thicker. The moisture uptake is a function of the vapor pressure gradient (which is proportional to the temperature gradient in this case). Thus, inverted roofs designed to have a higher R-value (insulation thickness) will pick-up moisture more slowly and hence increase their thermal conductivity less quickly.

## **2.6 Practice Case: Latent Heat Effect Caused by Water Trapped in the Mineral Fiber Insulation Layer of a Light-Weight Flat Roof**

In order to study the hygrothermal behavior of envelope assemblies with mineral fiber insulation, a light-weight flat roof has been installed at the Fraunhofer IBP open-air test site in Holzkirchen—see: Bludau et al. (2010). The 90 mm thick insulation layer, installed between an aluminum vapor barrier and a vapor-tight roofing membrane was equipped with temperature and humidity sensors at the bottom (on the vapor barrier) at the top (underneath the roofing membrane) and half-way between top and bottom within the mineral fiber insulation slabs. To simulate the effect of moisture trapped during the installation process, about 2 kg/m<sup>2</sup> of water was added on top of the insulation before enclosure. With the temperature variations during changing seasons or during a night and day cycle, the moisture was expected to migrate between

bottom and top of the insulation slabs which could be monitored by the humidity sensors.

During the test period from August until January, the indoor temperature was kept at 20 °C, while the recorded roof surface temperature cycled between minimum and maximum values of -20 °C and 20 °C in winter, respectively, between 0 °C and more than 60 °C in summer. The resulting RH recordings within the roof are shown in Fig. 2.5. The overall agreement between measured and calculated curves is rather good and justifies further evaluations based solely on simulation results. In summer the RH at the top position varies between 20% at noon (when the sun shines and heats up the exterior surface) and 100% at night. With lower temperatures and shorter days in autumn and winter the RH at noon stays higher and remains from midmonth of November permanently at 100%. At the bottom of the insulation layer, the relative humidity stays at 100% during the whole summer until the middle of November. Afterward, it cycles between maximal 10% at night and 100% on sunny days.

The position in the middle of the insulation layer shows cycles with smaller amplitudes compared to the other two positions, but most importantly, there is almost no time period with constantly 100% RH all day round. This means the bulk of the water in the flat roof is either stored at the top of the insulation layer (winter situation) or at the bottom (summer situation), but not somewhere in between. It also shows that there are two separate cycles overlapping each other, a daily and a seasonal cycle.

The thermal consequences may only be evaluated by hygrothermal simulation since no heat flux transducers had been installed for this test. However, there had been another roof set-up with moisture introduced in the insulation layer before, that did not show the expected increase in heat transfer measured at the bottom of the concrete roof deck. For that reason, the thermal consequences of the roof described above was analyzed in more detail. Figure 2.6 shows the simulated heat flux densities including and excluding the latent heat effect determined for the bottom of the insulation layer, plotted as daily and weekly mean values over one year. Excluding the latent heat effect means here, that the heat of evaporation is set to zero in the simulations, i.e., the resulting heat flux is only due to thermal conduction. From the difference, it

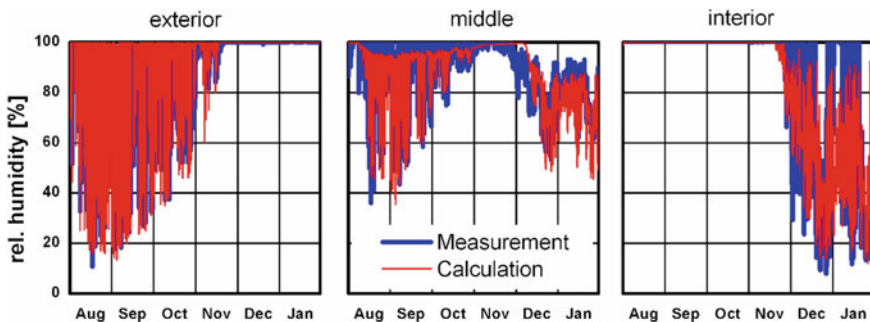
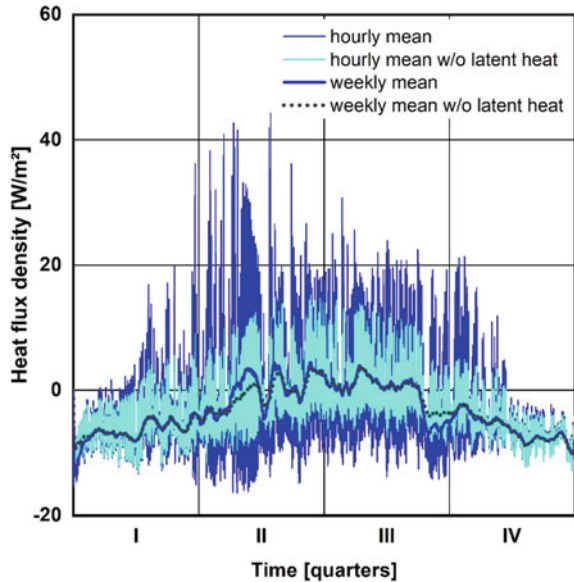


**Fig. 2.5** Comparison of measured and calculated relative humidity variations at the three sensors' position in the mineral fiber insulation layer of the investigated flat roof



**Fig. 2.6** Hourly and weekly means of the heat flux density calculated for the indoor surface of the flat roof with latent heat effect and without (heat of evaporation set to zero)



becomes obvious that the latent heat effect plays an important part leading to heat flux peaks in summer that are three times as high as the conduction heat flux. However, in the winter month the latent heat effect may still be significant, but it is not dominating the total heat flow anymore.

The most important energetic consequences for the building can be derived from the net heat losses and gains. Since most buildings have a rather high thermal inertia, the daily heat flux fluctuations through the building envelope are reaching the indoor spaces with a phase shift compared to the solar radiation input through the windows. The thermal storage also helps to dampen indoor temperature swings. Therefore, the energy balance of the building depends more on daily or even longer averages of the envelope heat fluxes. In order to clearly see the net effects of sensible and latent heat transfer through the roof, weekly averages of the heat flux with and without latent effects have also been plotted in Fig. 2.6.

During the cold winter month with a rather high negative heat flux density (heat loss through the building envelope), there is no difference between the mean heat flux densities with and without latent heat effect. Thanks to the reversible nature of the latent effect (night-time losses are compensated by daytime gains), moisture in the insulation layer does not have any significant impact on the energy consumption. During the hot summer month with net heat gains through the roof, the same results can be observed.

Only during the swing seasons, when the heat flux density is close to zero, both curves diverge slightly. In spring, the latent heat effect seems to increase the heat gains, and in fall it increases the heat losses. However, the net influence of the latent heat effects last only about a month and appears to be rather small. An explanation for

the impact of the latent heat effect in spring and fall could be the bulk of condensate migrating from top to bottom respectively from bottom to top of the insulation layer. While the water during the heating and cooling season remains either at the top or the bottom with only little moisture moving back and forth during daily cycles, there seem to be two periods per year when the whole water in the roof moves mainly in one direction—up or down—which has a net effect on the average heat flux. Luckily, in the investigated case, this happens during the seasons when the thermal performance of the building envelope is of minor importance, because the indoor and outdoor temperatures are not far apart from each other.

It should be noted, however, that this positive view of the latent heat effects in vapor permeable insulation materials is only valid for insulated building assemblies without liquid counterflow in any form, e.g., due surface diffusion, capillary action or gravity. Also, the consideration of the net fluxes integrated over several days is only appropriate for buildings with high thermal storage capacity. Buildings with light-weight structure and well insulated envelope may not benefit from the reversing latent heat fluxes and suffer net heat losses, because intermediate heat gains are only partly or not at all usable without overheating the building.

## 2.7 Conclusions

Excessive moisture in building assemblies is always a matter of concern, because it may not only degrade the thermal performance but more importantly it represents a hazard for the hygienic conditions in the building and the durability of its structure. From a purely energetic point of view, temporary or localized moisture peaks are generally not a big issue. Construction moisture may affect the initial thermal performance of building assemblies but only the long-term moisture conditions have a lasting impact and should be considered in more detail. Laboratory and field tests may help to assess the long-term hygrothermal performance to some extent, however, they are expensive and not generally applicable—insulation manufacturers are hardly inclined to sponsor tests that may demonstrate thermal degradation of their products over time. Therefore, hygrothermal simulations are usually the simplest and most efficient way of predicting the long-term thermal performance of building envelope insulation systems for the climatic design loads.

Hygrothermal models that comply with the existing standards treat heat transfer by thermal conduction and latent heat flow separately and comprehensively, which means they also take the moisture in neighboring materials and the dynamic changes in boundary conditions into account. As an input, they require thermal storage capacity as well as thermal conductivity including its dependence on stationary moisture  $k(w)$  without any latent heat contribution. Further necessary input are the moisture transfer characteristics of all the materials involved, the so-called hygrothermal properties. Since most of the hygrothermal simulation tools on the market have been broadly experimentally validated, their application can be regarded as state-of-the-art for moisture control design purposes. However, there are only limited applications

where the main focus has been on thermal performance rather than moisture safety issues. Therefore, the focus on the thermal properties in the hygrothermal databases has been less pronounced, which means, the actual data may contain all sorts of safety margins. The tabled thermal conductivity may also contain some contributions of latent heat effects resulting from standard thermal conductivity tests performed on moist materials.

Despite these shortcomings, rather accurate thermal performance predictions seem feasible at least in relative terms, i.e., the impact of moisture in building envelope assemblies on latent heat transfer may be quantified. To assess the overall effect of latent heat transfer in building assemblies on the energy performance of buildings, hygrothermal whole building simulation analysis is recommended. In cases of stationary moisture effects in materials with low or moderate vapor permeability, hygrothermal component simulation seems sufficient. For these materials which are present in many building components, it would be helpful to define limits for the allowable water content based on acceptable thermal performance degradation margins. Similar limits already exist for timber and timber-based products to prevent rot or other forms of material degradation. However, exceeding moisture limits to safeguard design thermal resistance should not necessarily signal failure but could be remedied during the design process by adding more insulation to compensate for performance degradation during the expected service life of the building assembly.

In practice, moisture in foam insulation has become a controversial issue. Most concerned are flat roofs—inverted and conventional—where moisture has accumulated either naturally or due to unintended leaks. But similar problems have also been reported from externally insulated walls, where rainwater leakage occurred. Obviously, this impairs the thermal performance of the assembly concerned. However, in most cases the remaining thermal resistance is still significant and costly removal of the wet insulation may be unnecessary. Some experts even recommend leaving the old insulation material in place and top it up by a new insulation layer. Long-term monitoring of roofs retrofitted this way has demonstrated that this works very well regarding thermal performance and sustainability aspects—see: Spilker and Oswald (2003), Zöllner and Sprengard (2018).

In summary, it may be concluded that moisture in insulation materials has an impact on thermal performance, but it is predictable and mostly less dramatic than often assumed. The presence of moisture in building assemblies is mostly unavoidable but it can be controlled by good design that focusses on minimizing the loads and maximizing the drying potential. Because heat and moisture transfer are always coupled, it makes little sense to analyze heat transfer individually. This holds for measuring the thermal conductivity of moist materials, but it is equally true for evaluating the consequences for the thermal transmissivity under practice conditions.

Since moisture may have more severe implications than just increasing heat transfer, hygrothermal simulations are often performed anyway. Including an energy performance evaluation would, therefore, not require much additional effort. One important prerequisite is the availability of thermal conductivity data of insulation materials being determined excluding latent heat effects. Otherwise, the impact of

moisture may be counted twice which would penalize vapor permeable insulation materials.

## References

- Achtziger, J., & Cammerer, J. (1984). Einfluss des Feuchtegehalts auf die Wärmeleitfähigkeit von Bau- und Dämmstoffen. FIW-report B15-800183-4.
- Achtziger, J. (1985). Kerndämmung von zweischaligem Mauerwerk; Einfluß des Wassergehalts und der Feuchtigkeitsverteilung auf die Wärmeleitfähigkeit der Dämmschicht. (*Core insulation of a two-layered masonry wall; Effect of the water content and moisture distribution on the thermal conductivity of the insulation layer.*) Bauphysik 7, 4, 121–124.
- ANSI/ASHRAE Standard 160. (2016). *Criteria for moisture control design analysis in buildings*.
- ASHRAE. (2017). *ASHRAE handbook of fundamentals*. Chapter 25 Heat, air and moisture control in building assemblies.
- ASTM. (2016). ASTM E3054/E3054M-16, Standard guide for characterization and use of hygrothermal models for moisture control design in building envelopes, ASTM International, West Conshohocken, PA, 2016
- Binder, A., Zirkelbach, D., & Künzle, H. M. (2010). Test method to quantify the wicking properties of insulation materials designed to prevent interstitial condensation. In *Proceedings of Building XI Conference on Clearwater Beach December 5–9, 2010*. ASHRAE publication Atlanta, 12 pp.
- Bludau, Ch., Künzle, H. M., & Zirkelbach, D. (2010). Hygrothermal performance of flat roofs with construction moisture. In *Proceedings of Building XI Conference on Clearwater Beach December 5–9, 2010*. ASHRAE publication Atlanta, 7 pp.
- EN 15026. (2007). Hygrothermal performance of building components and building elements—Assessment of moisture transfer by numerical simulation.
- Gawin, D., Kosny, J., & Wilkes, K. (2004). Thermal conductivity of moist cellular concrete—Experimental and numerical study. In *Proceedings of Building IX Conference on Clearwater Beach December 5–10, 2004*. ASHRAE publication Atlanta, 10 pp.
- Hedlin, C. P. (1988). Heat transfer in a wet porous thermal insulation in a flat roof. *Journal of Thermal Insulation*, 11, 165–188. <https://doi.org/10.1177/2F109719638801100305>.
- ISO (1996)-ISO 10051. (1996 E). Thermal insulation—Moisture effects on heat transfer.
- Kehrer, M., Künzle, H. M., & Sedlbauer, K. (2003). Ecological insulation materials—does sorption moisture affect their insulation performance? *Journal of Thermal Envelope Building Science*, 26(3), 207–212. <https://doi.org/10.1177/2F109719603027869>.
- Künzle, H. M., & Kießl, K. (1998). Moisture behavior of protected membrane roofs with greenery. In *Proceedings CIB W40 Symposium Publication 213, University Kyoto, October 7–10, 1997, edited April 1998* (pp. 329–338).
- Künzle, H. M. (1995). Simultaneous heat and moisture transport in building components. One- and two-dimensional calculation using simple parameters. Dissertation University of Stuttgart 1994, English publication IRB-Verlag Stuttgart. [http://www publica.fraunhofer.de/eprints/urn\\_nbn\\_de\\_0011-px-566563.pdf](http://www publica.fraunhofer.de/eprints/urn_nbn_de_0011-px-566563.pdf).
- Sandberg, P. (1986). Thermal resistance of wet insulation materials. Nordtest Technical Report 063, Swedish National Testing Institute, 1986, 52 pp.
- Spilker, R., & Oswald, R. (2003). Flachdachsanieerung über durchfeuchteter Dämmschicht. Bauforschung für die Praxis, Band 61, Fraunhofer IRB Verlag, Stuttgart.
- Zirkelbach, D., Schafaczek, B., & Künzle, H. M. (2011). Thermal performance degradation of foam insulation in inverted roofs due to moisture accumulation. In *Proceedings of 12th International Conference on the Durability of Building Materials and Components 12dbmc, Porto, April 12–15, 2011* (pp. 529–536).

Zöller, M., & Sprengard, C. (2018). Langzeitverhalten feuchter Dämmstoffe auf Flachdächern - Praxiserfahrungen und Wärmestrommessungen. Aachener Institut für Bauschadensforschung und angewandte Bauphysik, Aktenzeichen: SWD – 10.08.18.7-15.27 Fraunhofer IRB Verlag, Stuttgart, Report F 3075. [http://www.wp13698212.server-he.de/wp-content/uploads/2019/06/2018-05-17\\_AIBau\\_Langzeitverhalten\\_feuchter\\_Daemmstoffe.pdf](http://www.wp13698212.server-he.de/wp-content/uploads/2019/06/2018-05-17_AIBau_Langzeitverhalten_feuchter_Daemmstoffe.pdf).

# Chapter 3

## Overview of Thermal Performance of Air Cavities and Reflective Insulations



Hamed H. Saber

**Abstract** Many parts of the building components such as walls, and flat and sloped roofs contain enclosed airspaces. In addition, the Insulating Glass Units (IGUs) in fenestration systems such as curtain walls, windows and skylight devices contain enclosed spaces that are normally filled with air or heavy gas such as Argon, Xenon or Krypton. The thermal resistance (R-value) of an enclosed space depends mainly on the type of the filling gas, emissivity of all surfaces that bound the space, the size and orientation of the space, the direction of heat flow through the space, and the respective temperatures of all surfaces that define the space. Assessing the energy performance of building envelopes with reflective insulations and fenestration systems, subjected to different climatic conditions, require accurate determination of the R-values of the enclosed spaces. In this chapter, a review was conducted on the thermal performance of enclosed airspaces for different building applications. As well, the different parameters that affect the thermal performance of enclosed airspaces were discussed. These parameters include: (a) dimensions, (b) inclination angles, (c) directions of heat flow, (d) emissivity of all surfaces that bound the space, and (e) operating conditions.

**Keyword** Reflective insulations · Effective emittance · Airspace aspect ratio · R-value correlation · Low emissivity materials · Insulating glass units

### 3.1 Background

Reflective insulation has been discussed in the literature for over 100 years and is presently manufactured in countries around the world. Reflective insulation material consists of low-emittance material usually aluminum foil or metallized film bonded to a substrate such as paper or plastic sheet for support. The following three figures

---

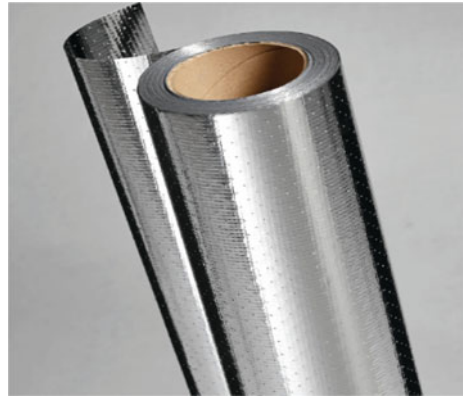
H. H. Saber (✉)

Mechanical Engineering Department, Prince Saud Bin Thuniyan Research Center, Jubail University College, Royal Commission for Jubail and Yanbu, P.O. Box: 10074, Jubail Industrial City 31961, Saudi Arabia  
e-mail: [saberh@ucj.edu.sa](mailto:saberh@ucj.edu.sa)

**Fig. 3.1** Foil or film faced polyethylene bubble pack



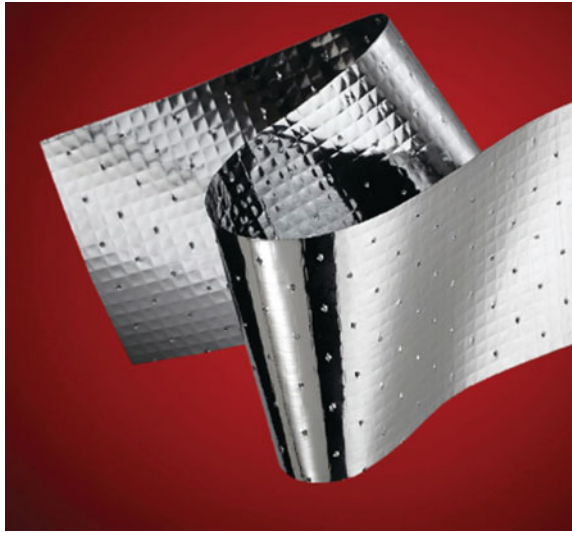
**Fig. 3.2** Single sheet with paper or plastic support material



(Figs. 3.1, 3.2 and 3.3) show three common reflective insulation products. Figure 3.1 is a polymer substrate (bubble pack) usually 4–8 mm in thickness with aluminum foil facing. This product type has a small material RSI-value that is in the range 0.1–0.2  $\text{m}^2\cdot\text{K}/\text{W}$  depending on the thickness. The single-sheet products in Figs. 3.2 and 3.3 are generally less than 1.0 mm in thickness with negligible thermal resistance. The perforated version in Fig. 3.3 is water vapor transmitting. This product type is intended for locations that must allow water vapor to pass through and not accumulate. Single-sheet material can be combined with spacers to produce multilayer reflective insulation products, enclosed reflective airspaces in series.

Reflective insulation materials used in buildings are installed in enclosed airspaces on one or both sides to produce a reflective insulation system or assembly. A low-emittance surface facing an enclosed airspace significantly reduces radiation across the airspace thus establishing thermal resistance. The phrase “enclosed reflective airspace” is commonly used to describe a reflective insulation system.

**Fig. 3.3** Single sheet-perforated reflective insulation material



Reflective insulation material is installed in a region to be perpendicular to the direction of heat flow. The material can be attached to one side of a region to form a single enclosed reflective airspace or in the interior of the region to form two enclosed reflective airspaces provided that both sides of the reflective insulation material are faced with material having a total hemispherical emittance typically no more than 0.05. The lower the emittance results in greater thermal resistance (RSI) that can be provided by the reflective insulation system. Reflective insulation systems with two or three enclosed airspaces are common. There are reflective insulation systems with more than three enclosed airspaces.

The thermal resistance of a reflective insulation system can be measured using a hot-box apparatus or evaluated using advanced computational techniques, which is the subject of this chapter.

### 3.2 Reflective Insulation Overview

Reflective Insulation (RI) products are typically being used in conjunction with mass insulation products, such as glass fiber, expanded polystyrene foam (EPS), and other similar insulation products. The RI products can be installed in wall cavities, between ceiling and floor joists, and in metallic buildings that cannot readily accommodate loose-fill or batt-type insulations. Also, RI products can be used as part of a roofing system either below the decking between rafters, within small air gaps between decking and roofing, and in air gaps created, for example, by paneling interior masonry walls (Yarbrough, 1983). As well, RI can be used in fenestration



systems such as windows, curtain walls and skylight devices (Saber & Laouadi, 2011; Saber et al., 2013, 2020).

A review about the use of reflective materials to reduce heat transfer by radiation across enclosed airspaces was conducted by Gross and Miller (1989). Fricker and Yarbrough (2011) conducted literature review on four computational methods for evaluating the R-values of enclosed reflective airspaces that involved an assumption of one-dimensional heat transfer between large parallel surfaces (infinite parallel planes). In an actual building enclosure, however, there are surfaces connecting the parallel planes (e.g., framing). These surfaces absorb, emit and reflect thermal radiation. Glicksman (1991) has shown that the heat transfer process that included radiation interaction between the parallel surfaces and the framing resulted in a decrease in the overall thermal performance (i.e., lower R-values).

It is important to accurately determine the effective R-values of the airspaces of different dimensions, effective emittances, inclination angles, directions of heat flow, mean temperature of the airspace, and temperature differences across the airspaces. Many studies were conducted to determine the R-values of RI products, and debate is still ongoing whether the claims about high thermal resistance of RI products are correct because hot plate measurements performed in laboratories often resulted in lower R-values. Tenpierik and Hasselaar (2013) conducted an extensive literature review to identify the causes for the different results among different research organizations. D’Orazio et al. (2012) conducted field study under hot climatic conditions to investigate the thermal performance of an insulated roof with RI product. The results of that study showed that the benefits of RI product are quite limited when using the insulation level imposed by actual laws, which consider insulation as the main strategy for energy saving in temperate and hot climates.

This chapter focuses on the thermal performance of enclosed airspaces under different operating conditions (see Fig. 3.4). Note that the term “enclosed” is critical since the major distinction between RIs and Radiant Barriers (RBs) is the airspace condition, where the RB system is defined as a building construction that consists of a low emittance surface bounded by an “open” airspace. The key parameters that affect the R-value of an enclosed airspace are: (a) the physical properties of the air filling the space, (b) temperature of all surfaces of the airspace, (c) emissivity of all surfaces of the airspace, (d) temperature differences across the airspace, (e) dimensions of the airspace, (f) direction of heat flow through the airspace, and (g) orientation of the airspace. The R-values of enclosed airspaces were calculated by many investigators (e.g., see Robinson et al. (1954, 1956) for various orientations of airspaces and reflective boundaries by using heat transfer coefficient data obtained from measurements of panels of different thicknesses using the test method described in the ASTM C236-53. In those studies, the steady-state heat transmission data were corrected for heat transfer occurring along parallel paths between hot and cold boundaries. Thereafter, the convective heat transfer coefficients were obtained from the data by subtracting a calculated radiative heat transfer rate from the total corrected heat transfer rate; and the radiative heat transfer was calculated using an emissivity of 0.028 for the aluminum surfaces.

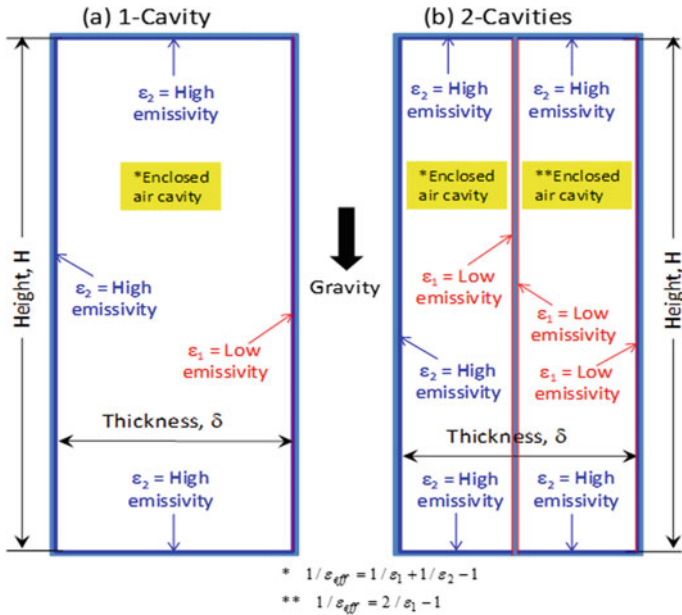


**Fig. 3.4** Schematics of enclosed airspace with and without thin sheet of low emissivity on both sides, placed in the middle of the airspace

The 2009 ASHRAE Handbook of Fundamentals (Chapter 26) provides a table that contains the R-values for enclosed airspaces of three inclination angles ( $\theta$ ) of  $0^\circ$ ,  $45^\circ$  and  $90^\circ$ , which were determined on the basis of the heat transfer data reported by Robinson et al. (1954) and (1956). These R-values are being extensively used by modelers, architects and building designers to determine the R-values of building enclosures. The ASHRAE R-values (ASHRAE, 2009) were obtained by combining the convective and radiative components of heat transfer from which the effective R-value for an enclosed airspace was provided for airspaces of different: (a) thickness ( $\delta$ ) of 13, 20, 40 and 90 mm, (b) mean temperature ( $T_{avg}$ ) of  $-45.6$ ,  $-17.8$ ,  $10.0$ ,  $32.2$   $^\circ\text{C}$ , (c) temperature difference across the airspace ( $\Delta T$ ) of 5.6, 11.1 and 16.7  $^\circ\text{C}$  (d) effective emittance ( $\epsilon_{eff}$ ) of 0.03, 0.05, 0.2, 0.5 and 0.82, and (e) direction of heat flow through the airspace (heat flow up and heat flow down).

Note that the effective emittance ( $\epsilon_{eff}$ ) of an enclosed airspace is given as:

$$1/\epsilon_{eff} = 1/\epsilon_1 + 1/\epsilon_2 - 1 \tag{3.1}$$

where,  $\epsilon_1$  and  $\epsilon_2$  are the emissivity of the hot and cold surfaces (see Fig. 3.4a). It is worth mentioning that the R-values of low-sloped enclosed airspaces are not available in the ASHRAE table. As well, the effect of the aspect ratio (height (H)/thickness ( $\delta$ )) of the enclosed airspace on the R-value is not accounted for in the ASHRAE table. Saber’s model was extensively used in many studies to assess the thermal

performance and moisture performance of different building components (walls, roofs and fenestration systems) with and without RI products. A brief discription of this model is provided next.

### 3.3 Model Discription and Validations

The previously developed and extensively validated model was used to predict the R-values of vertical (Saber, 2013a), horizontal with heat flow up (Saber, 2013b), horizontal with heat flow down (Saber, 2014a) high-sloped (45°) with heat flow up (Saber, 2021), high-sloped (45°) with heat flow down (Saber, 2013c), and low-sloped (30°) with heat flow down (Saber, 2014b) enclosed airspaces for a wide range of airspace thickness, aspect ratio, mean temperature, temperature differential across the airspace, and effective emittance. Most recently, the model was extensively used to develop a user-friendly evaluation and design tool of enclosed airspaces called “Reflective Airspace Tool” that can be used by modelers, architects and building engineers to determine the R-values of enclosed airspaces of various design parameters and subjected to different operating conditions. The full capabilities and features of this tool that was recently presented to the Reflective Insulation Manufacturers Association International (RIMA-I, 2020). The details of this tool related to using it as “Evaluation Tool” and as “Design Tool” will be published at later date.

Briefly, the model solves simultaneously the 2D and 3D moisture transport equation, energy equation, surface-to-surface radiation equation (e.g., surface-to-surface radiation in enclosed airspace such as shown in Fig. 3.4, and as well surface-to-surface and surface-to-ambient radiation for the case of open airspace such as that in radiant barriers) and air transport equation in the various material layers of building components (walls, roofs, windows, curtain walls and skylight devices). The air transport equation is the Navier-Stokes equation for the airspace (e.g., air cavity), and Darcy equation (for Darcy Number,  $DN < 10^{-6}$ ) and Brinkman equation (for  $DN > 10^{-6}$ ) for the porous material layers. This numerical model had been benchmarked in a number of building applications for full-scale and small-scale building components with and without a reflective insulation products (e.g., see, Saber, 2012, 2013d; Saber et al., 2010a, 2011a, b, 2012a, b, c).

For building applications that are similar to this study, the model was benchmarked against thermal performance data for a wall assembly featuring a reflective insulation product (Saber et al., 2011b). The data were obtained using a guarded hot box (in accordance with the test method of ASTM C-1363, 2006) for a full-scale wall system. The results showed that the R-value predicted by the model was in good agreement with the measured R-value (within 1.2%). The model also was benchmarked against test data of test specimens with reflective insulation products that were obtained using heat flow meter (in accordance with the test method of ASTM C-518, 2003). As shown in Saber (2012) and Saber et al. (2012b), the heat fluxes predicted by the model were in good agreement with all measured heat fluxes from these tests (within

$\pm 1.0\%$ ). The next sections discuss the effect of different parameters on the R-values of enclosed airspaces.

### 3.4 Effect of Airspace Aspect Ratio on the R-Value

The studies by Saber (2013a, 2013b, 2013c, 2014a, 2014b, 2021) for enclosed airspaces of different operating conditions, dimensions, orientations and directions of heat of flow have included the dependence of the R-value on the aspect ratio,  $A_R$  ( $A_R = \text{height } (H)/\text{thickness } (\delta)$ ). These studies showed that the aspect ratio could have a significant effect on the R-value. Figure 3.5 shows an example for the R-values of vertical enclosed airspace of different aspect ratios. In this example, for a wide range of effective emittance ( $\epsilon_{\text{eff}}$ ) of 0–0.82, numerical simulations were conducted for vertical enclosed airspace having a thickness of 40 mm with a height range of 102–2438 mm. This represents an aspect ratio range of 2.54–60.96. The results shown in Fig. 3.5 are for the case of airspace average temperature ( $T_{\text{avg}}$ ) of

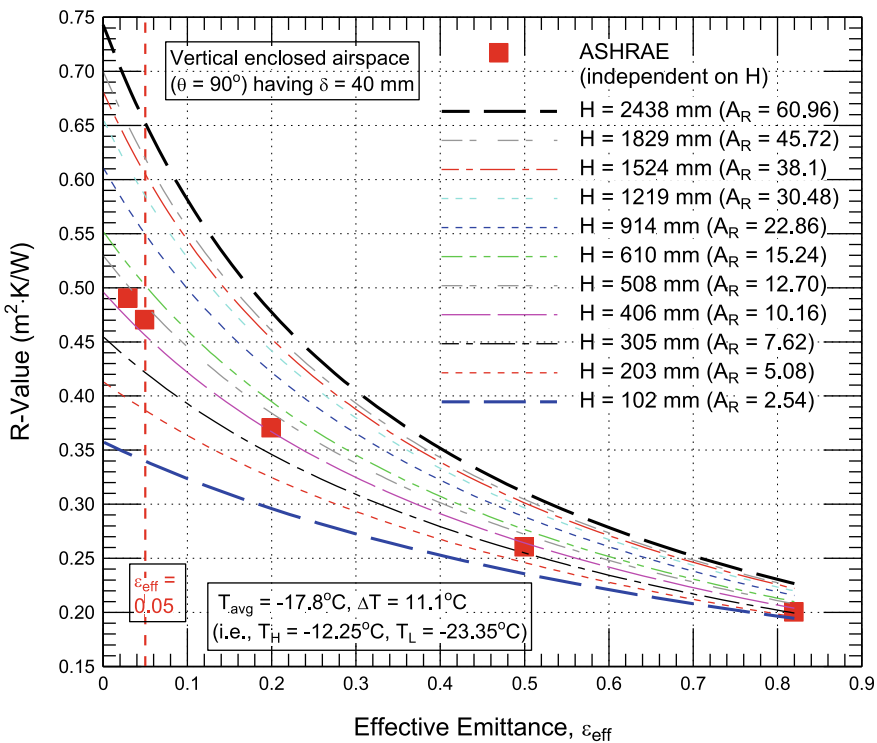


**Fig. 3.5** Effect of aspect ratio on the R-value for the case of vertical enclosed airspace ( $\delta = 40$  mm,  $H = 305$  mm,  $T_{\text{avg}} = -17.8$  °C,  $\Delta T = 11.1$  °C)

−17.8 °C and a temperature different ( $\Delta T$ ) of 11.1 °C in which the hot-side temperature ( $T_H$ ) is −12.25 °C and the cold-side temperature ( $T_L$ ) is −23.35 °C. For the purpose of comparison, the ASHRAE R-values (independent on the aspect ratio) are also shown in Fig. 3.5.

Figure 3.5 shows that the ASHRAE R-values of different effective emittances are in closest agreements with the predicted R-value for airspace height of 406 mm (i.e.,  $A_R = 10.16$ ). Also, this figure shows that the R-value increases significantly with increasing the aspect ratio for the range of low effective emittance. For the range of high effective emittance, however, the R-value increases insignificantly with increasing the aspect ratio. For example, at low effective emittance of 0.05, the R-value increases by 92% with increasing the aspect ratio from 2.54 ( $H = 102$  mm and  $R = 0.341$  m<sup>2</sup>·K/W) to 60.96 ( $H = 2438$  mm and  $R = 0.655$  m<sup>2</sup>·K/W). At this low effective emittance (0.05), ASHRAE R-value (2.669 m<sup>2</sup>·K/W) overestimated the R-value by 28% at aspect ratio of 2.54 (compared to 3% for effective emittance of 0.82). Furthermore, at this low emittance (0.05), ASHRAE R-value understated the R-value by 39% at aspect ratio of 60.96 (compared to 13% for effective emittance of 0.82).

### 3.5 Effect of Inclination Angle and Direction of Heat Flow

The model was used in a previous study to quantify the contribution of reflective insulation to the R-value of specimen with different orientations (Saber, 2012). In that study, after validating the model against the test results, it was used to conduct a parametric study in order to investigate the effect of inclination angle ( $\theta$ ) and direction of heat flow on the effective R-value of EPS sample stack shown in Fig. 3.6. Note that the rate of heat transfer by both convection and radiation in the air cavity depends on its size and the temperature difference across the sample stack ( $\Delta T$ ). As such, the effective R-value depends on both  $\Delta T$  and the size of the air cavity. The results

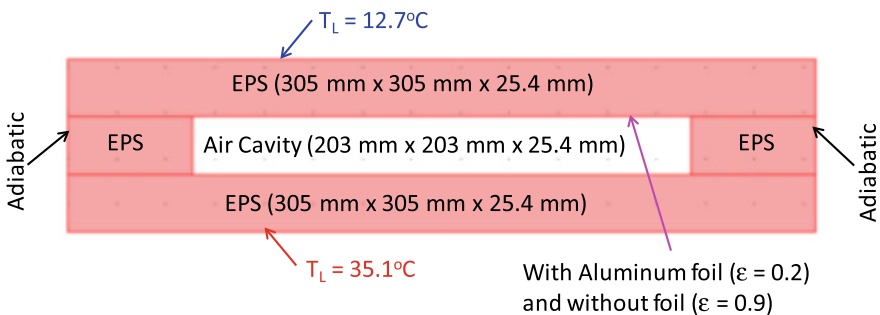


**Fig. 3.6** Sample stacks with enclosed air cavity

presented in Saber (2012) were obtained for *only* one  $\Delta T$  of 22.4 °C ( $T_c = 12.7$  °C, and  $T_h = 35.1$  °C) and one size of the air cavity as shown in Fig. 3.6.

The results showed that for all values of foil emissivity, the horizontal sample stack heated from the top (i.e., heat flow down) resulted in the highest R-values while the horizontal sample stack heated from the bottom (i.e., heat flow up) resulted in the lowest R-values. These two cases represent the application of reflective insulations in flat roof in the summer season and winter season. During the service life, the foil emissivity may increase because of the oxidation, accumulation of dust and/or water vapor condensation on the surface of the foil. Increasing the foil emissivity from 0.05 to 0.9 (maximum) resulted in a decrease in the R-value by 20.7% and 8.2% for horizontal sample stack heated from the top and bottom, respectively. Observe that the emissivity of 0.9 represents the case of no foil in the system. As the foil emissivity increases from 0.05 to 0.9, the contribution of the air cavity to the R-value decreases by 118% and 49% for horizontal sample stack heated from the top and bottom, respectively. In the case of foil surface fully covered by dust or water vapor condensate (i.e.,  $\epsilon = 0.9$ ), both inclination angle and direction of heat flow through the specimen have insignificant effect on the effective R-value. In this case, the maximum change in the contribution of air cavity to the R-value is only 6%.

For a wide range of inclination angle ( $\theta$ ) of 0° (horizontal)–90° (vertical), numerical simulations were conducted recently for enclosed airspace having  $\delta$  of 40 mm, H of 305 mm at operating condition with  $T_{avg}$  of  $-17.8$  °C and  $\Delta T$  of 11.1 °C (i.e.,  $T_H = -12.25$  °C and  $T_L = -23.35$  °C). These simulations were conducted for the full range of effective emittance (0–0.82) for both heat flow up and heat flow down. For clarity, it is important to point out that for vertical enclosed airspace presented in this chapter ( $\theta = 90^\circ$ ), heat flow up or heat flow down means that the enclosed airspace is heated from the left side (i.e., heat flow horizontally to the right direction “ $\rightarrow$ ”) or heated from the right side (i.e., heat flow horizontally to the left direction “ $\leftarrow$ ”). In the absence of heat transfer by convection inside the enclosed airspaces, Figs. 3.7a and 3.8a show the R-value for a wide range of effective emittance. By accounting for all modes of heat transfer inside the enclosed airspaces (conduction, radiation and convection), the obtained R-values are provided in Fig. 3.7b for heat flow up and Fig. 3.8b heat flow down.

At an effective emittance of 0.05, the distributions of the temperature (T), vertical velocity ( $V_y$ ), horizontal velocity ( $V_x$ ), resultant velocity ( $V_{res}$ ) and velocity field streamlines are shown in Figs. 3.9, 3.10, 3.11, 3.12 and 3.13 for the case of heat flow down. The corresponding results for the case of heat flow up are shown in Figs. 3.14, 3.15, 3.16, 3.17 and 3.18. Because of the large differences in the air velocities ( $V_x$ ,  $V_y$  and  $V_{res}$ ) inside the enclosed airspaces at different inclination angles, auto-scale contour level was used for each enclosed airspace in Figs. 3.10, 3.11, 3.12, 3.15, 3.16 and 3.17. As shown in these figures, only one contour legend was used for all enclosed airspaces of different inclination angles in which the “Max” value in red color and the “Min” value in blue color are listed alongside each enclosed airspace for  $V_x$ ,  $V_y$  and  $V_{res}$ .

In absence of heat transfer by convection in all enclosed airspaces of the same effective emittance, thickness and height with heat flow up and heat flow down when

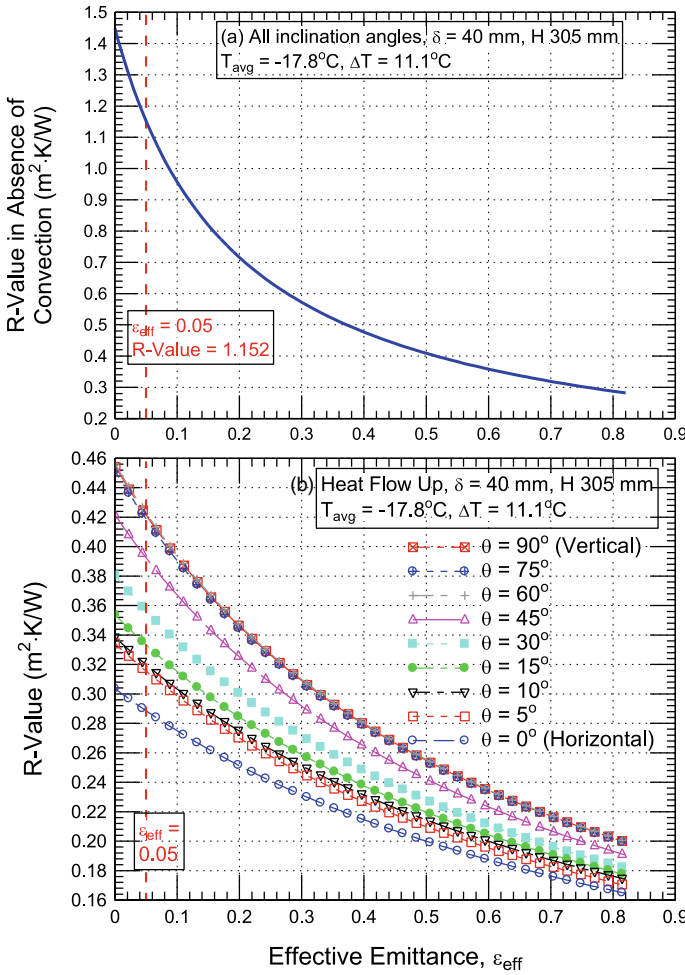


**Fig. 3.7** Effect of inclination angle on the R-value for the case of heat flow down ( $\delta = 40$  mm, H = 305 mm,  $T_{avg} = -17.8^\circ C$ ,  $\Delta T = 11.1^\circ C$ ): **a** with heat transfer by conduction and radiation only, and **b** with all modes of heat transfer

they are subjected to the same operating conditions (e.g.,  $T_H = -12.25^\circ C$  and  $T_L = -23.35^\circ C$ ), the rates of heat transfer by conduction and radiation through the enclosed airspaces must be the same for different inclination angles. In this case, the R-values for a given effective emittance of the enclosed airspaces of different inclination angles must also be the same for all inclination angles as shown in Fig. 3.7a and Fig. 3.8a.

For horizontal enclosed airspace ( $\theta = 0^\circ$ ) with heat flow down, two vortex cells airflow are developed in the air cavity with quite small air velocity in relation with other enclosed airspaces of different inclination angles. As such, the rate of heat

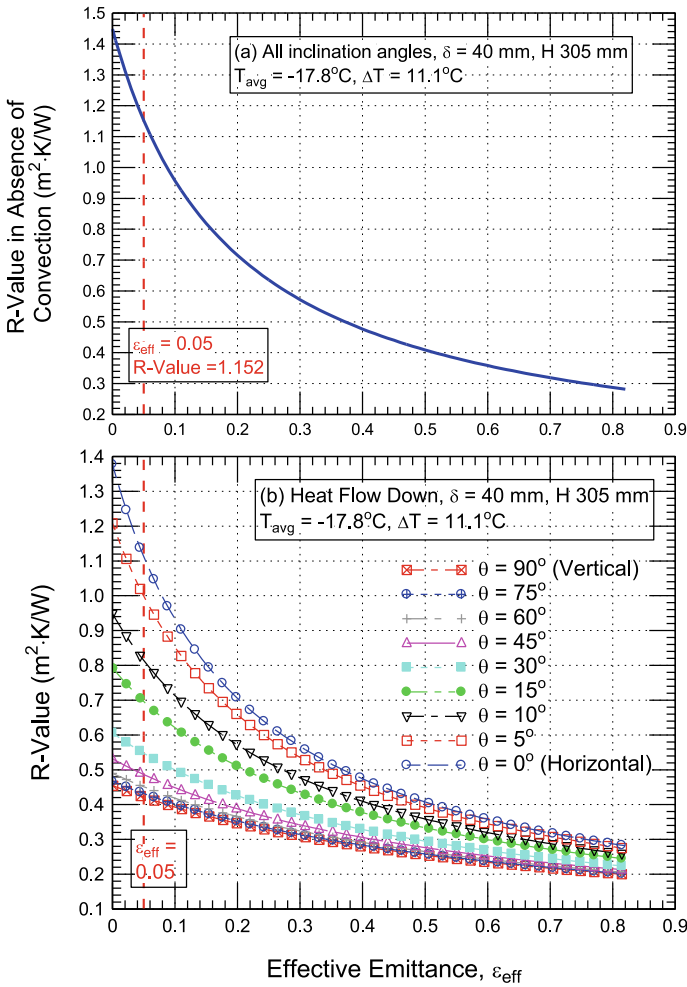


**Fig. 3.8** Effect of inclination angle on the R-value for the case of heat flow up ( $\delta = 40$  mm,  $H = 305$  mm,  $T_{avg} = -17.8^\circ\text{C}$ ,  $\Delta T = 11.1^\circ\text{C}$ ): **a** with heat transfer by conduction and radiation only, and **b** with all modes of heat transfer

transfer by convection would be insignificant in relation with the other rates of heat transfer by conduction and radiation. Consequently, the R-value of the enclosed airspace would be slightly lower than that in the absence of heat transfer by convection. For example, at an effective emittance of 0.05, the R-value ( $1.112 \text{ m}^2\cdot\text{K}/\text{W}$ , Fig. 3.7b) is only 3.5% lower than that in the absence of heat transfer by convection ( $1.152 \text{ m}^2\cdot\text{K}/\text{W}$ , Fig. 3.7a).

As shown in Fig. 3.9, 3.10, 3.11, 3.12 and 3.13, in the case of enclosed airspaces heated from the top (i.e., heat flow down) with  $\theta = 15^\circ, 30^\circ, 45^\circ, 60^\circ, 75^\circ$  and vertical enclosed airspace heated from the left ( $\theta = 90^\circ$ ), a mono-cellular with one vortex



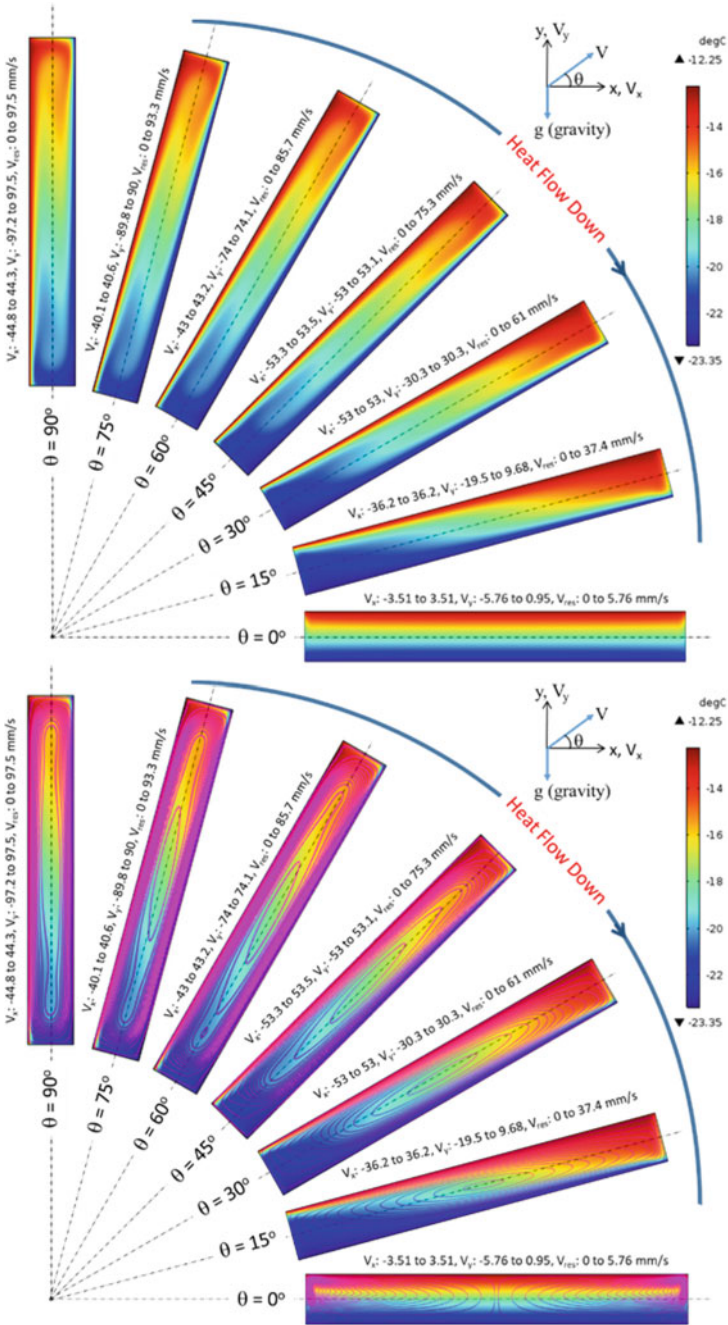


**Fig. 3.9** Temperature distribution and velocity field streamlines in enclosed airspace of different orientations for the case of heat flow down ( $\delta = 40$  mm,  $H = 305$  mm,  $\epsilon_{eff} = 0.05$ ,  $T_{avg} = -17.8$  °C,  $\Delta T = 11.1$  °C)

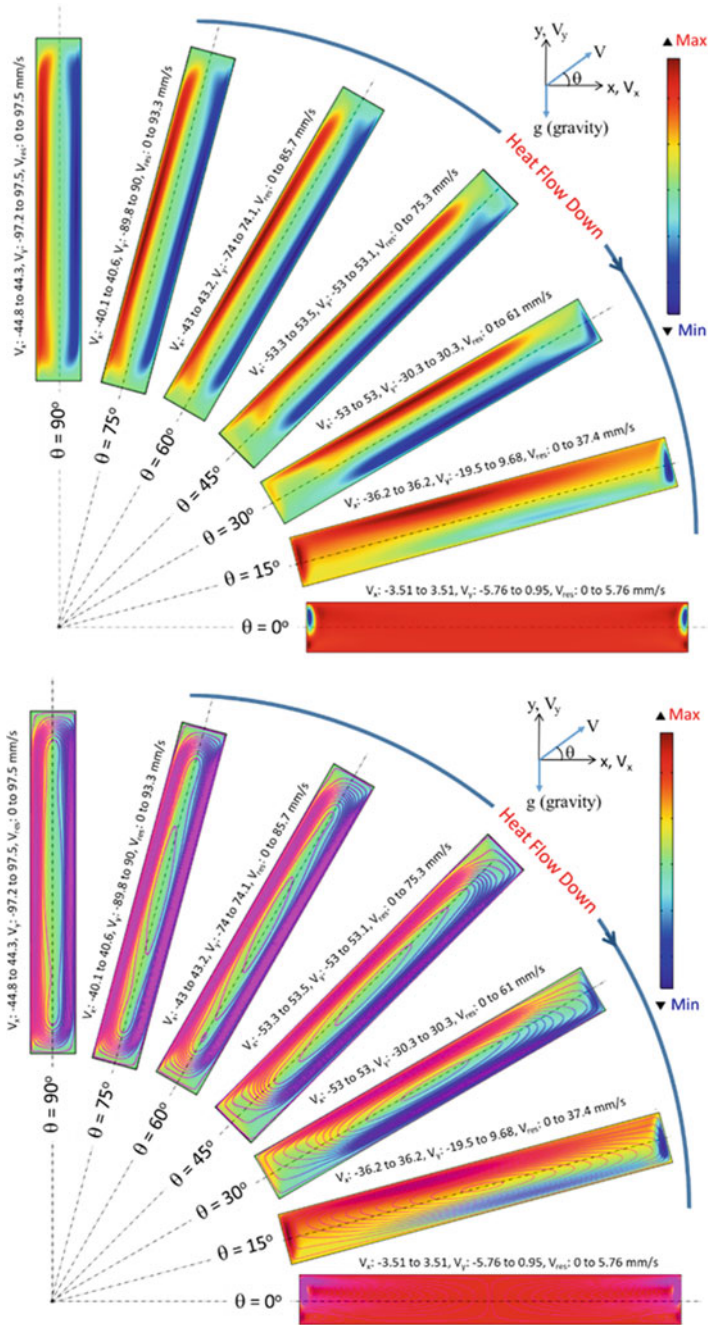


**Fig. 3.10** Vertical velocity distribution and velocity field streamlines in enclosed airspace of different orientations for the case of heat flow down ( $\delta = 40$  mm,  $H = 305$  mm,  $\epsilon_{eff} = 0.05$ ,  $T_{avg} = -17.8$  °C,  $\Delta T = 11.1$  °C)

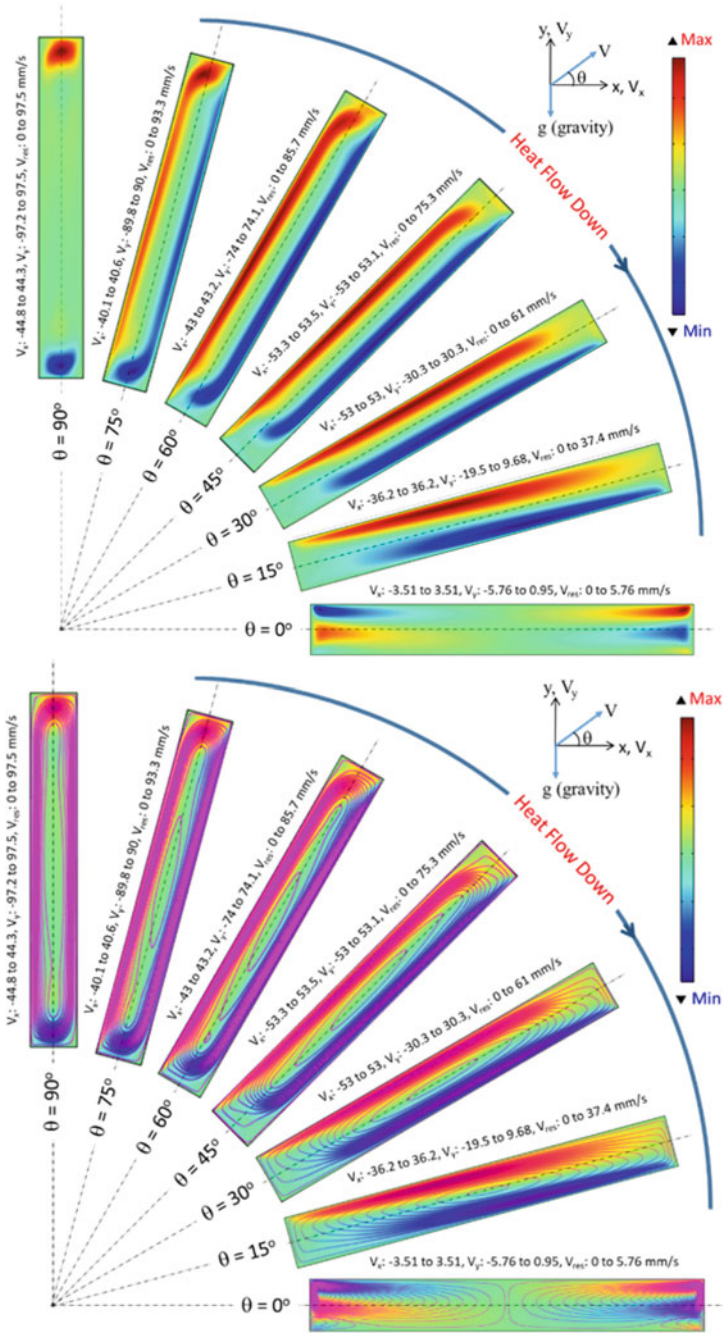


**Fig. 3.11** Horizontal velocity distribution and velocity field streamlines in enclosed airspace of different orientations for the case of heat flow down ( $\delta = 40$  mm,  $H = 305$  mm,  $\epsilon_{eff} = 0.05$ ,  $T_{avg} = -17.8$  °C,  $\Delta T = 11.1$  °C)

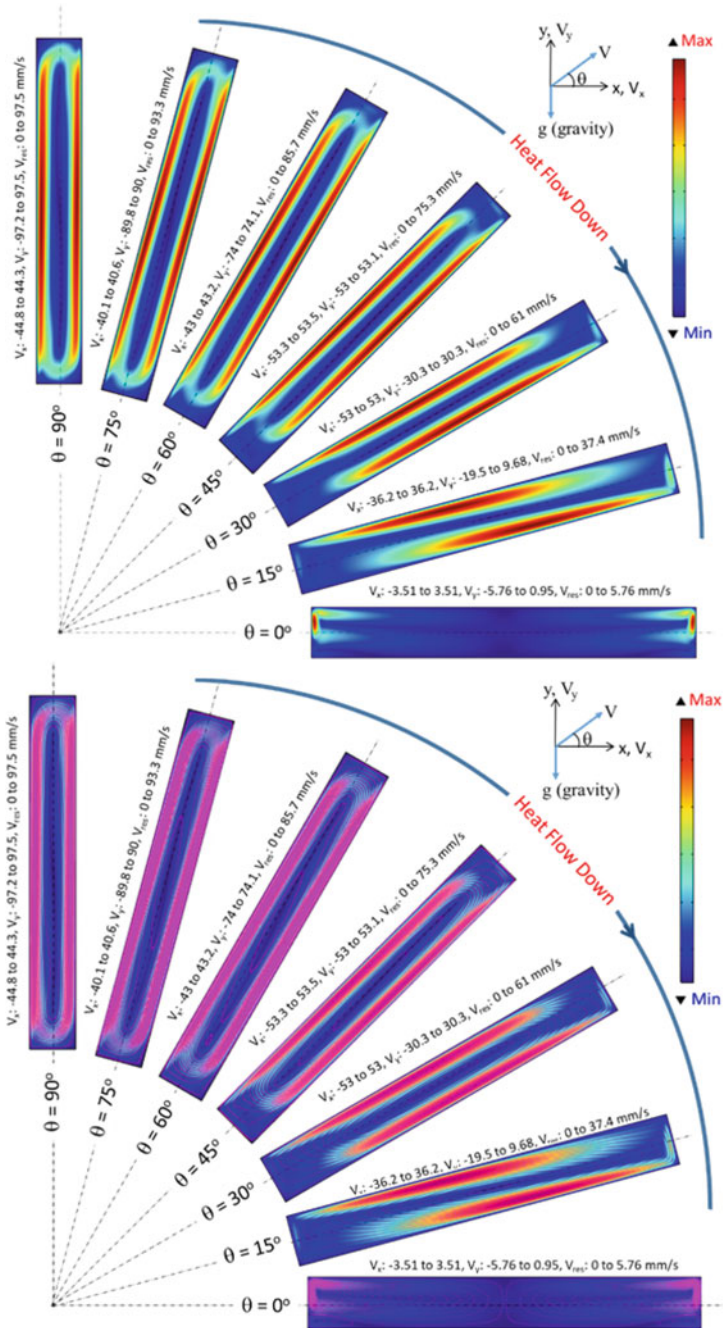


**Fig. 3.12** Resultant velocity distribution and velocity field streamlines in enclosed airspace of different orientations for the case of heat flow down ( $\delta = 40$  mm,  $H = 305$  mm,  $\epsilon_{eff} = 0.05$ ,  $T_{avg} = -17.8$  °C,  $\Delta T = 11.1$  °C)

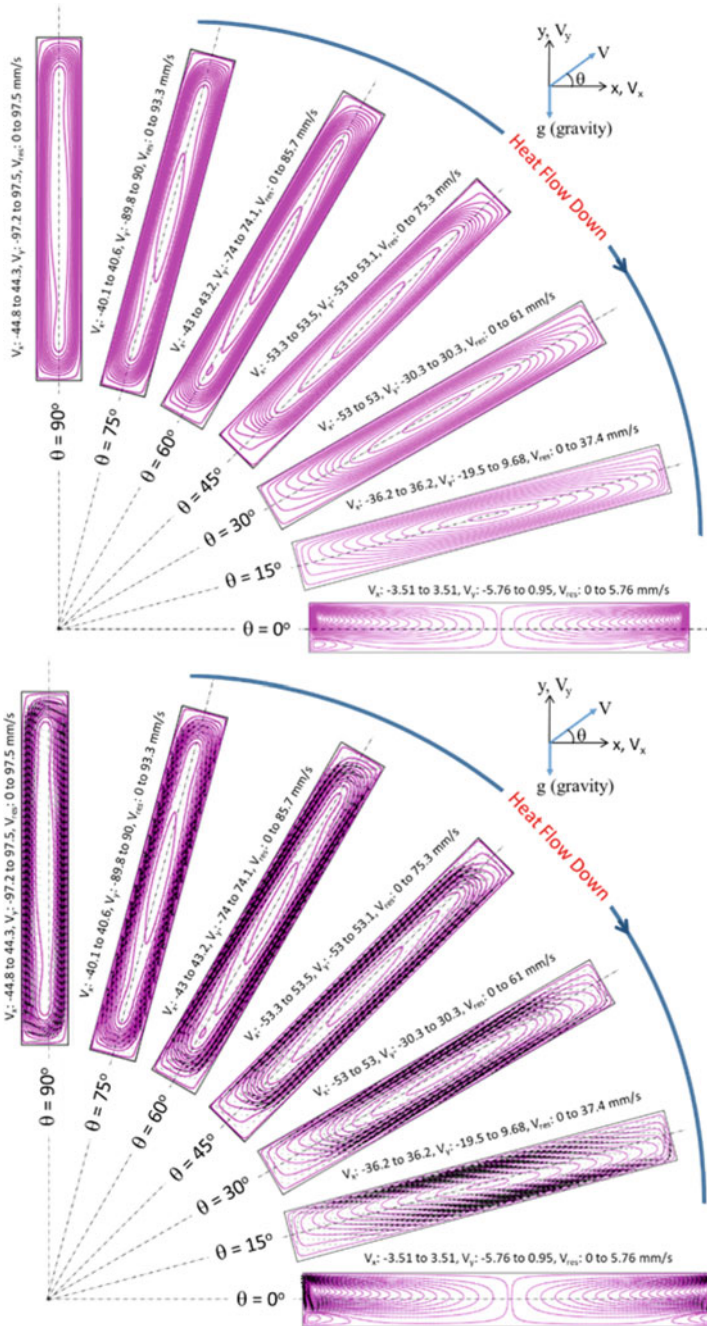


**Fig. 3.13** Velocity field streamlines and arrows in enclosed airspace of different orientations for the case of heat flow down ( $\delta = 40$  mm,  $H = 305$  mm,  $\epsilon_{\text{eff}} = 0.05$ ,  $T_{\text{avg}} = -17.8$  °C,  $\Delta T = 11.1$  °C)

cell airflow is developed in the air cavity. Increasing the inclination angle, however, results in increasing the air velocity, and thus increasing the rate of heat transfer by convection. Hence, the R-value decreases with increasing the inclination angle as shown in Fig. 3.7b. For example, at an effective emittance of 0.05, the heat transfer by convection has resulted in a reduction in the R-value by:

- 3.5% for  $\theta = 0^\circ$  ( $R = 1.112 \text{ m}^2 \cdot \text{K/W}$ ),
- 13.3% for  $\theta = 5^\circ$  ( $R = 1.000 \text{ m}^2 \cdot \text{K/W}$ ),
- 29.3% for  $\theta = 10^\circ$  ( $R = 0.814 \text{ m}^2 \cdot \text{K/W}$ ),
- 39.5% for  $\theta = 15^\circ$  ( $R = 0.697 \text{ m}^2 \cdot \text{K/W}$ ),
- 52.4% for  $\theta = 30^\circ$  ( $R = 0.548 \text{ m}^2 \cdot \text{K/W}$ ),
- 57.7% for  $\theta = 45^\circ$  ( $R = 0.487 \text{ m}^2 \cdot \text{K/W}$ ),
- 60.8% for  $\theta = 60^\circ$  ( $R = 0.452 \text{ m}^2 \cdot \text{K/W}$ ),
- 62.5% for  $\theta = 75^\circ$  ( $R = 0.432 \text{ m}^2 \cdot \text{K/W}$ ), and
- 63.3% for  $\theta = 90^\circ$  ( $R = 0.423 \text{ m}^2 \cdot \text{K/W}$ ).

As such, the full range of the reduction in the R-value due to heat transfer by convection inside the enclosed airspace of different inclination angles with heat flow down is 3.5% ( $\theta = 0^\circ$ )–63.3% ( $\theta = 90^\circ$ ).

At an effective emittance of 0.05 for the case of enclosed airspace heated from the bottom (i.e., heat flow up) with  $\theta = 0^\circ, 15^\circ, 30^\circ$  and  $45^\circ$ , Fig. 3.14, 3.15, 3.16, 3.17 and 3.18 show that a multi-cellular airflow is developed in the cavity with 10 vortex cells of approximately same size for  $\theta = 0^\circ$ , 5 vortex cells of different sizes for  $\theta = 15^\circ$  and  $30^\circ$ , and 3 vortex cells of different sizes for  $\theta = 45^\circ$ . For enclosed airspace with  $\theta = 60^\circ, 75^\circ$  and  $90^\circ$ , a mono-cellular with one large vortex cell airflow is developed in the air cavity. Unlike the case of heat flow down, the R-value for the case of heat flow up increases with increasing the inclination angle as shown in Fig. 3.8b. For example, at an effective emittance of 0.05, the heat transfer by convection has resulted in a reduction in the R-value by:

- 75.0% for  $\theta = 0^\circ$  ( $R = 0.288 \text{ m}^2 \cdot \text{K/W}$ ),
- 72.6% for  $\theta = 5^\circ$  ( $R = 0.316 \text{ m}^2 \cdot \text{K/W}$ ),
- 72.2% for  $\theta = 10^\circ$  ( $R = 0.320 \text{ m}^2 \cdot \text{K/W}$ ),
- 71.1% for  $\theta = 15^\circ$  ( $R = 0.333 \text{ m}^2 \cdot \text{K/W}$ ),
- 69.0% for  $\theta = 30^\circ$  ( $R = 0.357 \text{ m}^2 \cdot \text{K/W}$ ),
- 65.9% for  $\theta = 45^\circ$  ( $R = 0.393 \text{ m}^2 \cdot \text{K/W}$ ),
- 63.7% for  $\theta = 60^\circ$  ( $R = 0.419 \text{ m}^2 \cdot \text{K/W}$ ),
- 63.4% for  $\theta = 75^\circ$  ( $R = 0.422 \text{ m}^2 \cdot \text{K/W}$ ), and
- 63.3% for  $\theta = 90^\circ$  ( $R = 0.423 \text{ m}^2 \cdot \text{K/W}$ ).

At this condition, the full range of the reduction in the R-value due to heat transfer by convection inside the enclosed airspace of different inclination angles with heat flow down is 63.3% ( $\theta = 90^\circ$ )–75.0% ( $\theta = 0^\circ$ ).

Figures 3.10, 3.11 and 3.12, 3.15, 3.16 and 3.17 show that the values of the air velocities ( $V_x$ ,  $V_y$  and  $V_{res}$ ) in the cavity is greatly affected by both the inclination angle and the direction of heat flow through enclosed airspace. For small inclination

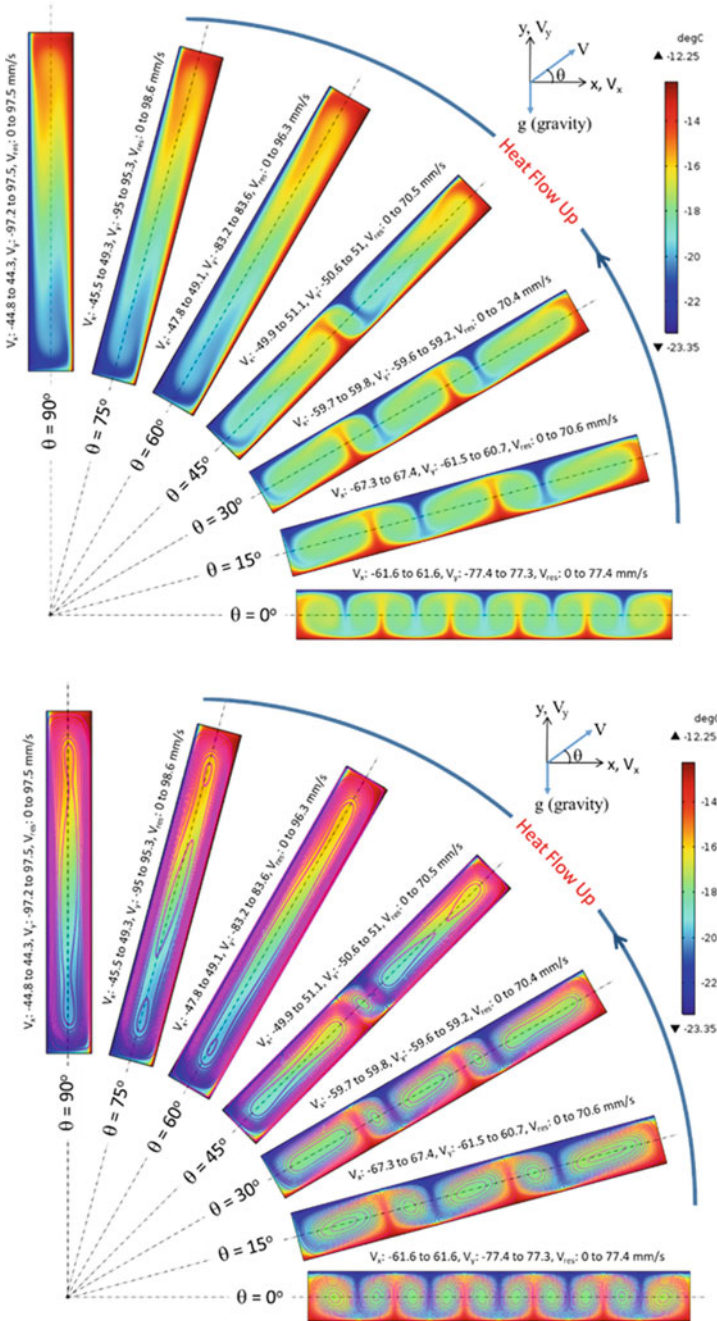


**Fig. 3.14** Temperature distribution and velocity field streamlines in enclosed airspace of different orientations for the case of heat flow up ( $\delta = 40$  mm,  $H = 305$  mm,  $\epsilon_{eff} = 0.05$ ,  $T_{avg} = -17.8$  °C,  $\Delta T = 11.1$  °C)

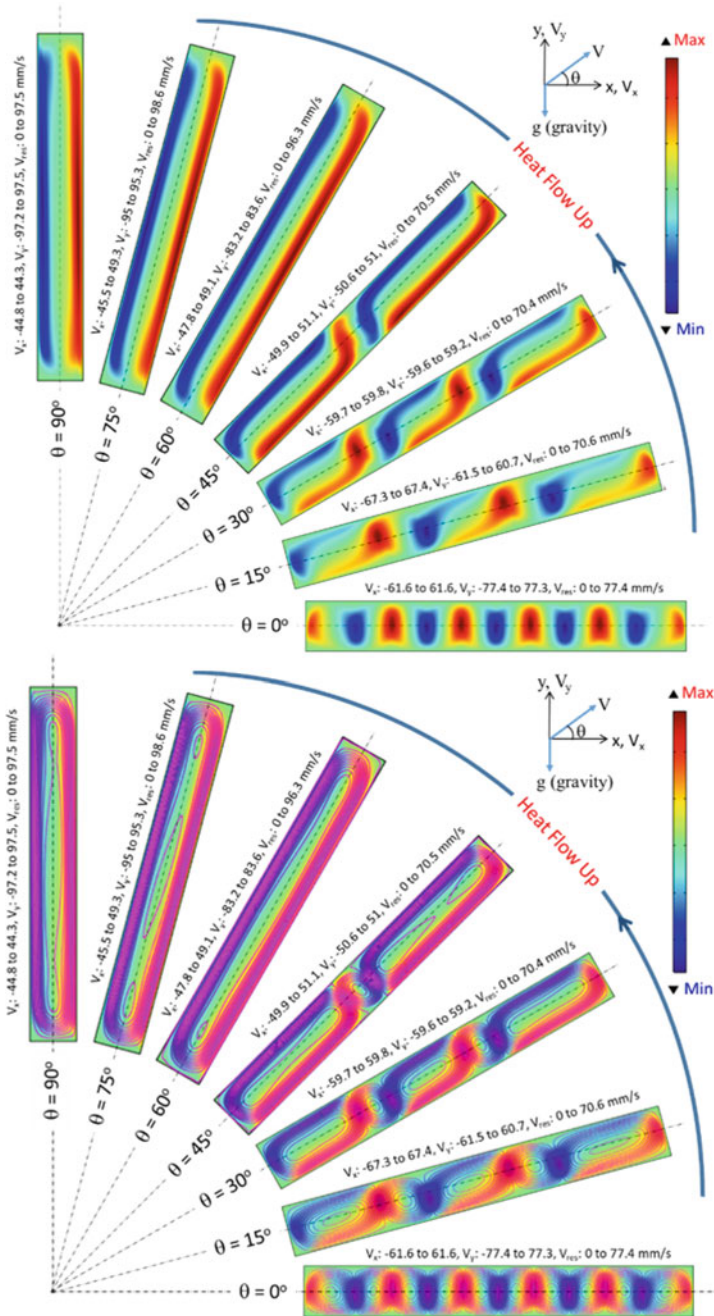


**Fig. 3.15** Vertical velocity distribution and velocity field streamlines in enclosed airspace of different orientations for the case of heat flow up ( $\delta = 40$  mm,  $H = 305$  mm,  $\epsilon_{eff} = 0.05$ ,  $T_{avg} = -17.8$  °C,  $\Delta T = 11.1$  °C)



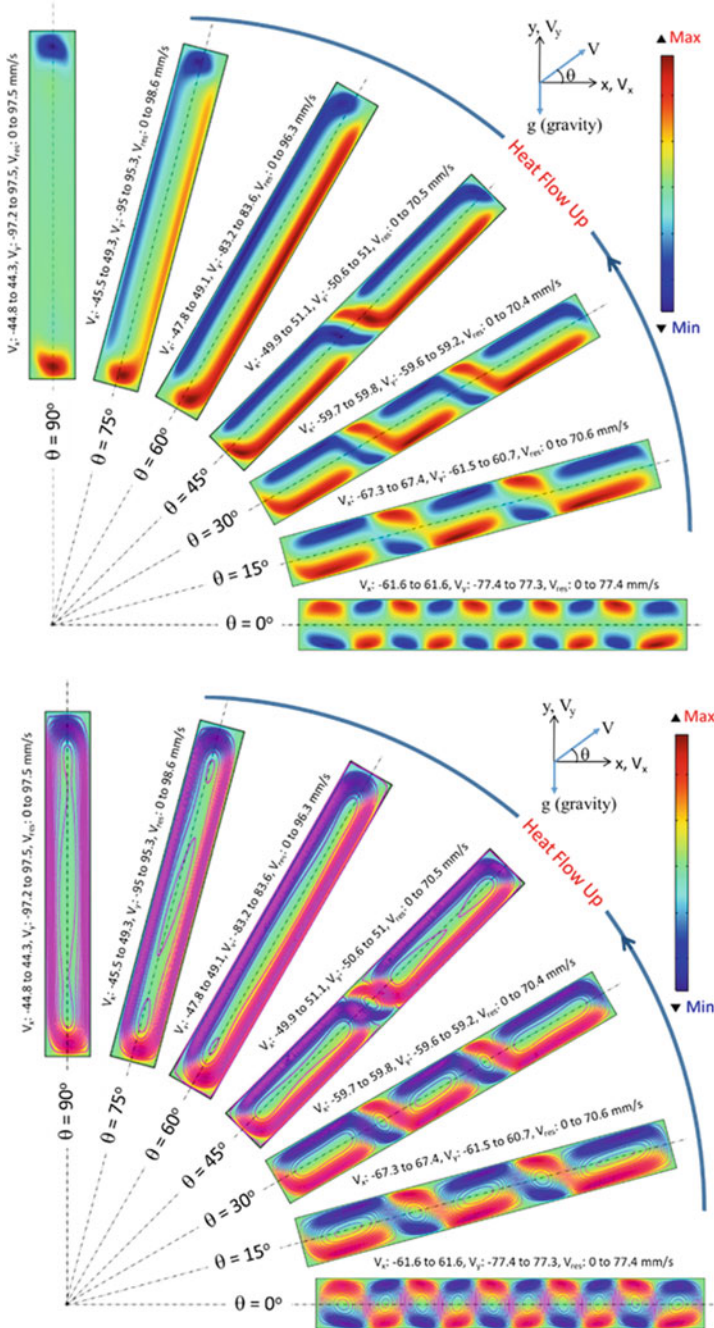


**Fig. 3.16** Horizontal velocity distribution and velocity field streamlines in enclosed airspace of different orientations for the case of heat flow up ( $\delta = 40$  mm,  $H = 305$  mm,  $\epsilon_{eff} = 0.05$ ,  $T_{avg} = -17.8$  °C,  $\Delta T = 11.1$  °C)

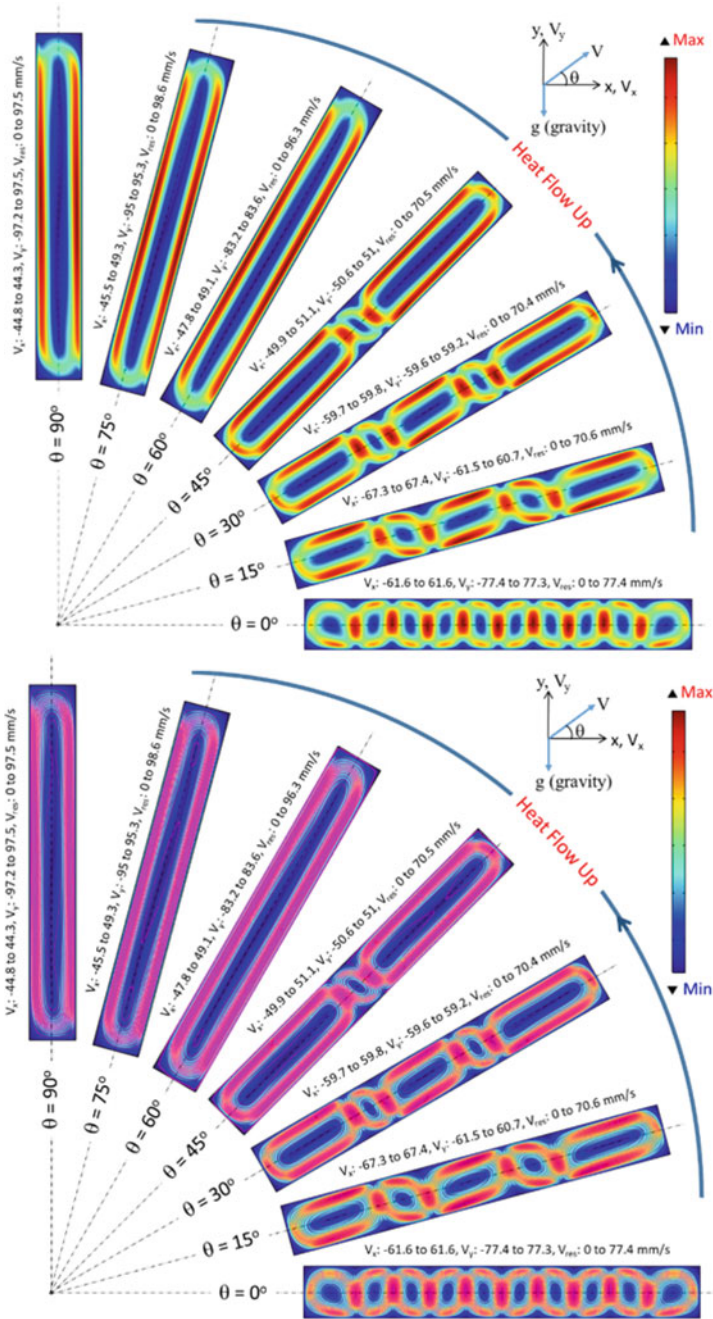


**Fig. 3.17** Resultant velocity distribution and velocity field streamlines in enclosed airspace of different orientations for the case of heat flow up ( $\delta = 40$  mm,  $H = 305$  mm,  $\epsilon_{eff} = 0.05$ ,  $T_{avg} = -17.8$  °C,  $\Delta T = 11.1$  °C)

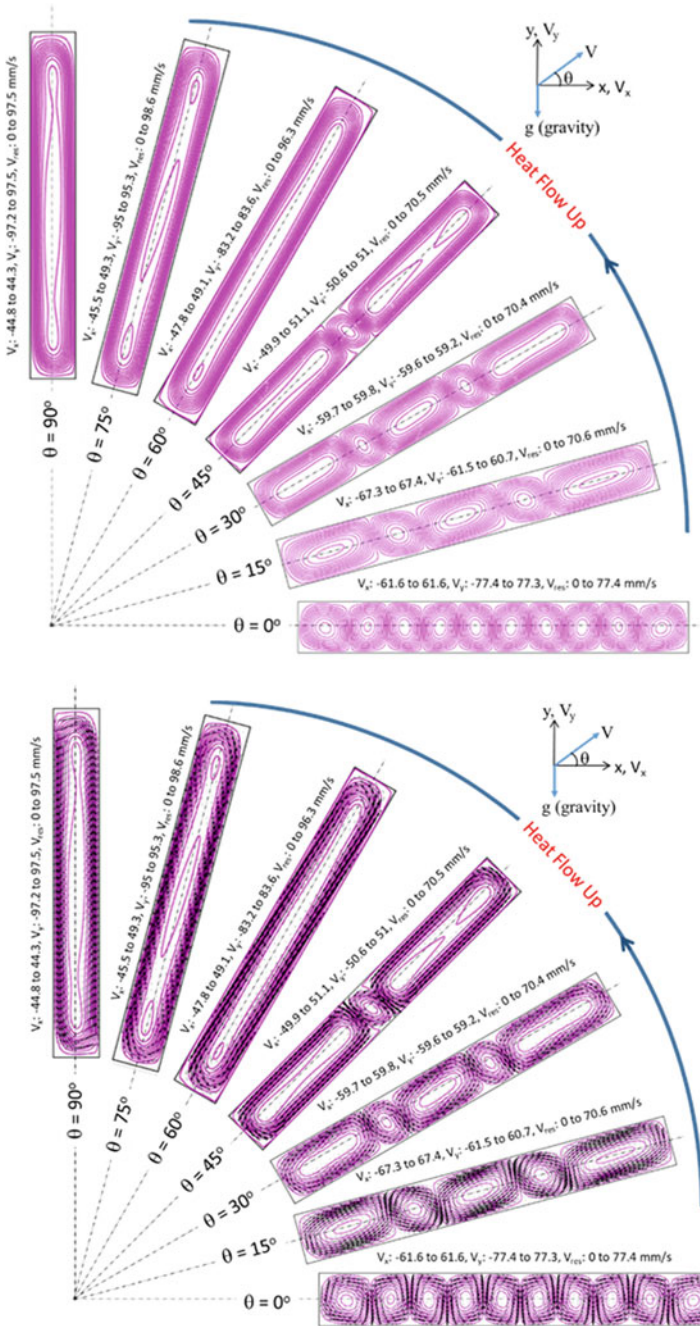


**Fig. 3.18** Velocity field streamlines and arrows in enclosed airspace of different orientations for the case of heat flow up ( $\delta = 40$  mm,  $H = 305$  mm,  $\epsilon_{eff} = 0.05$ ,  $T_{avg} = -17.8$  °C,  $\Delta T = 11.1$  °C)

angle (e.g.,  $0^{\circ}$ – $30^{\circ}$ ), the air velocity in the case of heat flow down is much smaller than that in the case of heat flow up. This is due to the case of heat flow down encourages a relatively stable stratification of air due to differences in buoyancy compared to the case of heat flow up. Effectively, for same effective emittance, dimensions and operating conditions, an enclosed airspace with heat flow down results in a greater R-value (Fig. 3.7b) than that with heat flow up (Fig. 3.8b). The cases of heat flow down and heat flow up represent the application of reflective insulations in building components (walls, roofs and fenestrations) during the summer season and winter season, respectively.

As indicated earlier, the emissivity of low-e surface (e.g., foil) may increase because of the oxidation, accumulation of dust and/or water vapor condensation on the surface. Increasing the emissivity of the low-e surface has resulted in a significant decrease in the R-value of enclosed airspace with both heat flow up and down. In the case of low-e surface fully covered by dust or water vapor condensate (i.e.,  $\varepsilon = 0.9$  at which  $\varepsilon_{\text{eff}} = 0.82$ ), both inclination angle and direction of heat flow through the enclosed airspace have insignificant effect on the effective R-value (i.e. resultant lines in Figs. 3.7b and 3.8b tend to converge as  $\varepsilon_{\text{eff}}$  tends to reach 0.82). Therefore, in order to maximize the benefits of reflective insulations, it is important to investigate whether or not water vapor condensation occurs on the low-e surface of building components with reflective insulations. This can be done by conducting hygrothermal modeling (instead of thermal modeling) for such building component when it is subjected to the weather conditions of different climatic zones.

In closing, the rate of heat transfer by convection due to airflow inside the enclosed airspace could result in a significant reduction in its R-value. For example, reduction ranges in R-value by 3.5–63.3% for heat flow down and by 63.3–75.0% for heat flow up occurred for the enclosed airspace shown in Figs. 3.9, 3.10, 3.11, 3.12, 3.13, 3.14, 3.15, 3.16, 3.17 and 3.18). So, it is important to precisely characterize the airflow inside the airspace so as to accurately determine its R-value. In turn, this will lead to accurately assessing the energy performance of building components with reflective insulations (walls, roofs and fenestrations), and consequently predicting accurately the overall energy performance of whole buildings.

On a side note, all results presented in this chapter for the R-values (see Figs. 3.5, 3.7b and 3.8b) can be easily obtained (within  $\pm 1.5\%$ ) using the “Reflective Airspace Tool” that was recently developed. This tool, to be published later, covers different types of enclosed airspaces that can exist in building components (walls, roofs, windows, curtain walls and skylight devices) with reflective insulations and subjected to a wide range of climatic conditions across the globe. In addition, it can be used as “Evaluation Tool” and as “Design Tool” for different building applications with enclosed airspaces.

### 3.6 Effect of Installing Thin Sheet in the Middle of Enclosed Airspace

Dividing an enclosed airspace into 2 or more cavities by thin sheet(s) would increase the R-value of the enclosed airspace. Figure 3.4a shows a case of 1-Cavity (i.e., without thin sheet) and Fig. 3.4b shows a case of 2-Cavities (i.e., with one thin sheet). A practical example for the case “2-Cavities” is to install a thin sheet with low emissivity at the middle of the enclosed airspace. For the applications of planar skylights, windows and curtain wall systems, the thin sheet should be transparent that can be coated with a transparent material of low emissivity. However, for the applications of wall and roofing systems with enclosed airspaces, the thin sheet could be opaque (e.g., aluminum foil). The benefits of installing thin sheet(s) with low-e inside the enclosed airspaces can lead to: (a) reducing heat transfer by convection, and (b) reducing heat transfer by radiation due to low effective emittance. Many previous studies have shown that these benefits have resulted in obtaining higher R-value for the “2-Cavities” case compared to the “1-Cavity” case.

As provided in Saber (2013a, 2013b, 2013c, 2014a, 2014b, 2021), the R-value could be doubled due to installing a thin sheet in the middle of all horizontal or sloped enclosed airspaces with heat flow down and vertical enclosed airspace. The R-value could be even tripled in case of horizontal airspace with heat flow up. Effectively, thin reflecting sheet(s) of low-e could be installed in the enclosed airspace of planar skylights, windows, curtain walls, and walls and roofs with Furred-Airspace Assemblies (FAAs).

### 3.7 Practical Correlation for the R-Values of Enclosed Airspaces

For enclosed airspaces of different orientations with heat flow up and heat flow down, the correlation of all parameters that affect the thermal performance of the enclosed airspaces, namely: average temperature ( $T_{avg}$ ), temperature difference across the airspace ( $\Delta T$ ), aspect ratio ( $A_R = H/\delta$ ) and effective emittance ( $\varepsilon_{eff}$ ) is given in Eq. (3.2) as (Saber, 2013a, 2013b, 2013c, 2014a, 2014b, 2021):

$$R - value = R_c(T_{avg}) + a_0 A_R^{\alpha_1} T_{avg}^{a_1} (\Delta T)^{c_1} + a \varepsilon_{eff}^{\beta} T_{avg}^{a_2} (\Delta T)^{c_2} \sum_{i=1}^4 g_i A_R^i + A_R^{\alpha_2} T_{avg}^{a_3} (\Delta T)^{c_3} \sum_{i=1}^4 b_i \varepsilon_{eff}^i \quad (3.2)$$

where,  $R_c(T_{avg})$  is the conductive R-value in ( $\text{ft}^2\text{hr}^{\circ}\text{F}/\text{BTU}$ ) of the enclosed airspace, which is given as:

$$R_c(T_{avg}) = \delta/\lambda(T_{avg}), \quad (3.3)$$

$$\lambda(T_{avg}) = \sum_{i=0}^4 f_i T_{avg}^i, \quad f_0 = -2.276 \times 10^{-4}, \quad (3.4)$$

$$f_1 = 1.155 \times 10^{-4}, \quad f_2 = -7.903 \times 10^{-8},$$

$$f_3 = 4.117 \times 10^{-11}, \quad f_4 = -7.439 \times 10^{-15}$$

Note that  $\lambda(T_{avg})$  in Eq. (3.4) is the average thermal conductivity of still air in (W/m.K), which is evaluated at the average temperature of the airspace,  $T_{avg}$  in (K). It is important to point out that the calculated value of  $R_c(T_{avg})$  from Eqs. (3.3) and (3.4) must be converted to (ft<sup>2</sup>hr°F/BTU) in order to be used in Eq. (3.2).

In Eq. (3.2), the units of  $T_{avg}$  and  $\Delta T$  must be in (K). The other coefficients in this equation ( $a_0, a, b_1, b_2, b_3, b_4, \alpha_1, \alpha_2, \beta, a_1, a_2, a_3, c_1, c_2, c_3, g_1, g_2, g_3,$  and  $g_4$ ) are provided by Saber (2013a, 2013b, 2013c, 2014a, 2014b, 2021) for enclosed airspace of different inclination angles and directions of heat flow. The R-values calculated from Eq. (3.2) for different inclination angles and directions of heat flow agreed with model in the range of  $\pm 3\%$  to  $\pm 5\%$ .

### 3.8 Concluding Remarks

The outcome of this chapter showed that the aspect ratio of the enclosed airspace can have a significant effect on its R-value. Also, this chapter showed that depending on the value of the effective emittance and the thickness of the airspace, the R-value could be doubled or tripled by incorporating thin sheet in the middle of the enclosed airspace. Accurate practical correlation for determining the R-value of enclosed airspaces for different building applications was provided. For different inclination angles and directions of heat flow through enclosed airspaces, this correlation covered wide ranges of values for various parameters, including: (a) aspect ratio, (b) temperature difference across the airspace, (c) mean temperature, and (d) effective emittance. Also, this correlation can be used by architects and building designers to determine the R-values of enclosed airspaces at different operating conditions. Finally, the correlation can be easily implemented in the currently available energy simulation models such as ESP-r, Design Builder and EnergyPlus. The simplicity of the recommended correlation suggests that it could be included in a future edition of ASHRAE Handbook of Fundamentals.

## References

- ASHRAE. (2009). *ASHRAE handbook—Fundamentals. Chapter 26: Heat, air, and moisture control in building assemblies—Material properties* (SI). ASHRAE Inc.
- ASTM C1363. (2006). Standard test method for the thermal performance of building assemblies by means of a hot box apparatus. In *2006 Annual book of ASTM standards*, 04.06 (pp. 717–759).
- ASTM C518. (2003). Standard test method for steady-state heat flux measurements and thermal transmission properties by means of the heat flow meter apparatus. In *Annual Book of Standards*, 04.06 (pp. 153–164). Philadelphia, PA: ASTM.
- D’Orazio, M., Di Perna, C., Di Giuseppe, E., & Morodo, M. (2012). Thermal performance of an insulated roof with reflective insulation: Field tests under hot climatic conditions. *Journal of Building Physics*, 36(3), 229–246.
- Fricker, J. M., & Yarbrough, D. W. (2011). Review of reflective insulation estimation methods. In *Proceedings of Building Simulation, 12th Conference of International Building Performance Simulation Association*, Sydney, November 14–16 (pp. 1989–1996).
- Glicksman, L. R. (1991). Two-dimensional heat transfer effects on vacuum and reflective insulations. *Journal of Thermal Insulation*, 14, 281–294.
- Gross, W. P., & Miller, R. G. (1989). Literature review of measurement and predictions of reflective building insulation system performance. *ASHRAE Transactions*, 95(2), 651–664.
- RIMA International. (2020). Be Our Zoom Guest for Dr. Hamed Saber November 5<sup>th</sup>. <https://www.rimainternational.org/news/press-room/09-20-be-our-zoom-guest-for-dr-hamed-saber-november-5th/>. Accessed Feb 2021.
- Robinson, H. E., & Powlitch, F. J. (1954). The thermal insulating value of airspaces. Housing Research Paper No. 32, National Bureau of Standards Project ME-12, U.S. Gov Printing Office, Washington, D.C.
- Robinson, H. E., Cosgrove, L. A., & Powell, F. J. (1956). Thermal resistance of airspaces and fibrous insulations bounded by reflective airspace. Building Material and Structures Report 151, United States National Bureau of Standards, 1956.
- Saber, H. H. (2012). Investigation of thermal performance of reflective insulations for different applications. *Journal of Building and Environment*, 55, 32–44.
- Saber, H. H. (2013a). Practical correlation for the thermal resistance of vertical enclosed airspaces for building applications. *Journal of Building and Environment*, 59, 379–396.
- Saber, H. H. (2013b). Practical correlation for thermal resistance of horizontal enclosed airspaces with upward heat flow for building applications. *Journal of Building and Environment*, 61, 169–187.
- Saber, H. H. (2013c). Practical correlation for thermal resistance of 45° sloped enclosed airspaces with downward heat flow for building applications. *Journal of Building and Environment*, 65, 154–169.
- Saber, H. H. (2013d). Thermal performance of wall assemblies with low emissivity. *Journal of Building Physics*, 36(3), 308–329.
- Saber, H. H. (2014a). Practical correlation for thermal resistance of horizontal enclosed airspaces with downward heat flow for building applications. *Journal of Building Physics*, 37(4), 403–435.
- Saber, H. H. (2014b). Practical correlation for thermal resistance of low-sloped enclosed airspaces with downward heat flow for building applications. *HVAC&R Research Journal*, 20(1), 92–112.
- Saber, H. H., & Laouadi, A. (2011). Convective heat transfer in hemispherical cavities with planar inner surfaces (1415-RP). *Journal of ASHRAE Transactions*, 117(2), 713–724.
- Saber, H. H., Maref, W., & Swinton, M. C. (2012a). Thermal response of basement wall systems with low-emissivity material and furred airspace. *Journal of Building Physics*, 35(4), 353–371.
- Saber, H. H., Maref, W., Sherrer, G., & Swinton, M. C. (2012b). Numerical modeling and experimental investigations of thermal performance of reflective insulations. *Journal of Building Physics*, 36(2), 163–177.

- Saber, H. H., Maref, W., Elmahdy, A. H., Swinton, M. C., & Glazer, R. (2012c). 3D heat and air transport model for predicting the thermal resistances of insulated wall assemblies. *International Journal of Building Performance Simulation*, 5(2), 75–91.
- Saber, H. H., Laouadi, A., Galasiu, A. D., & Arsenault, C. D. (2013). Convective heat transfer correlations for low-profile spherical cavities with planar bottom surfaces (1415-RP). *HVAC&R Research Journal*, 19(1), 10–23.
- Saber, H. H., Maref, W., Elmahdy, A. H., Swinton, M. C., & nd Glazer, R. (2010a). 3D thermal model for predicting the thermal resistances of spray polyurethane foam wall assemblies. In *Building XI Conference*, December 5–9, Clearwater, Florida, USA.
- Saber, H. H., Maref, W., Lacasse, M. A., Swinton, M. C., & Kumaran, M. K. (2010b). Benchmarking of hygrothermal model against measurements of drying of full-scale wall assemblies. In *International Conference on Building Envelope Systems and Technologies, ICBEST 2010b*, Vancouver, British Columbia, Canada, June 27–30 (pp. 369–377).
- Saber, H. H., Maref, W., & Swinton, M. C. (2011a). Numerical investigation of thermal response of basement wall systems with low emissivity material and furred—Airspace. In *13th Canadian Conference on Building Science and Technology (13th CCBST) Conference*, May 10–13, Winnipeg, MB, Canada.
- Saber, H. H., Maref, W., Swinton, M. C., & St-Onge, C. (2011b). Thermal analysis of above-grade wall assembly with low emissivity materials and furred-airspace. *Building and Environment*, 46(7), 1403–1414.
- Saber, H. H., Maref, W., & Hajiah, A. E. (2020). Effective R-value of enclosed reflective space for different building applications. *Journal of Building Physics*, 43(5), 398–427.
- Saber, H. H. (2021). Practical correlation for thermal resistance of 45° sloped enclosed airspaces with upward heat flow for building applications. *Journal of Building Physics*, 1–26. <https://doi.org/10.1177/17442591211009922>.
- Tenpierik, M. J., & Hasselaar, E. (2013). Reflective multi-foil insulations for buildings: A review. *Journal of Energy and Buildings*, 56, 233–243.
- Yarbrough, D. (1983). Assessment of reflective insulations for residential and commercial applications. ORNL/TM-8891, Oak Ridge National Laboratory, Oak Ridge, TN (pp. 1–63).



# Chapter 4

## Reflective Insulation in South-East Asia Region



Lim Chin Haw and Muhamad Zahin Bin Mohd Ashhar

**Abstract** The use of reflective insulation as roof insulation has become increasingly popular in Southeast Asian countries. It is proven to be effective at reducing heat gain through the roof and building energy consumption, as well as improving indoor thermal comfort. The present work is divided into three sections: field measurements of the thermal performance of reflective insulation in Malaysia, Computational Fluid Dynamics (CFD) analysis of reflective insulation in a gable roof system, and techno-economic analysis of roof thermal insulations for a hypermarket under the equatorial climate of Malaysia. Reflective insulation has proven to be an effective type of roof insulation for buildings in Southeast Asia, where the predominant heat flow direction is downward. Measured thermal resistance (RSI values) of roof assemblies with reflective insulations showed results in the range from 2 to 3 m<sup>2</sup>·K/W. A ceiling heat flux reduction of 80% was obtained for roofs with reflective insulation as compared to uninsulated roof attic. A validated CFD model showed that increasing the reflective air gap from 25 to 100 mm increases the RSI value of the roof assembly by 26%. Besides that, increasing the roof pitch from 30° to 45° increases the RSI value of the roof assembly by 30%. The techno-economic analysis showed that small bubble aluminum foil has the highest life-cycle savings and internal rate of return, as well as the shortest payback period. Although it does not yield the lowest annual cooling energy consumption, it is the most cost-effective type of insulation to be used as roof insulation under the hot and humid climate of Malaysia.

### 4.1 Introduction

Implementing energy conservation in buildings is important because energy consumption in buildings account for about 40% of the total world energy use. Approximately 60% of the world's electricity is consumed by residential and commercial buildings—see: UN (2016). Consequently, buildings have become the

---

L. C. Haw (✉) · M. Z. Bin Mohd Ashhar  
Solar Energy Research Institute, Universiti Kebangsaan, Bangi, Malaysia  
e-mail: [chinhaw.lim@ukm.edu.my](mailto:chinhaw.lim@ukm.edu.my)

© The Author(s), under exclusive license to Springer Nature Switzerland AG 2022  
J. Košny and D. W. Yarbrough (eds.), *Thermal Insulation and Radiation Control Technologies for Buildings*, Green Energy and Technology,  
[https://doi.org/10.1007/978-3-030-98693-3\\_4](https://doi.org/10.1007/978-3-030-98693-3_4)

main source of global greenhouse gases emissions. Therefore, the benefits of implementing building energy use reductions are twofold. The first being a reduction in the use of fossil fuels to generate electricity and second, the protection of our environment by reducing greenhouse gas emissions. There has been a positive correlation between economic growth and energy usage. Emerging economies in developing nations in Southeast Asia, the Middle East, South America, and Africa show an average annual energy use growth rate of 3.2%. This growth rate is expected to exceed that for the developed countries in North America, Western Europe, Japan, Australia and New Zealand by the year 2020—Pérez-Lombard et al. (2007). Malaysia being one of the fastest growing countries in Southeast Asia has recorded a significant increase in energy consumption in recent years. The electricity consumption per capita in Malaysia has increased from 1,101 kWh in 1990 to 4,110 kWh in 2013—Suruhanjaya Tenaga Energy Commission (2015). The increase of almost fourfold in less than 25 years is very alarming. Based on the 2015 outlook report by the International Energy Agency (IEA), electricity demand in Malaysia's building sector is expected to grow at an average of 3.7% annually from 2013 to 2040. Cooling equipment and appliances account for about 50% of the electricity demand in buildings in 2013 and this is expected to increase to 57% by 2040—see: IEA (2015). This statistic agrees with those reported by Saidur (2009) and the project conducted by Centre for Environment, Technology & Development Malaysia (CETDEM) (“Creating Awareness on issues related to Climate Change, Energy Usage and Transport in Kajang and Petaling Jaya (CACCT)” 2007) which found that among the categories of electricity usage, air conditioners for cooling is the largest consumer of electricity in commercial and residential buildings in Malaysia.

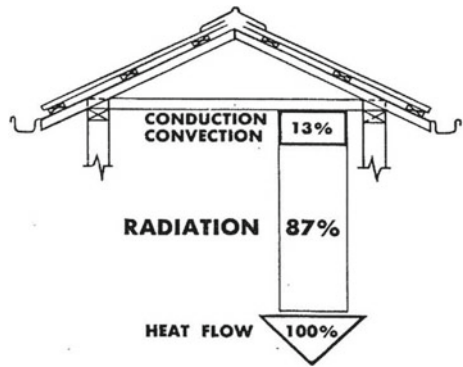
Weather conditions which include outdoor air temperature and solar radiation are the major factors that impact building energy consumption—see: Steemers and Young Yun (2009), Kavousian et al. (2013), Zhun et al. (2011). Malaysia is located in the Southeast Asia near the equator (Fig. 4.1), a region characterized as hot and humid all year round. According to the Malaysian Meteorological Department, “it is rare to have a stretch of a few days without sunshine except during the northeast monsoon seasons” (“General Climate of Malaysia” n.d.). This clearly reflects the abundance of sunshine and thus solar radiation Malaysia receives. Malaysia on average receives about 6 h of sunshine per day. As a result, most of the heat gain by buildings is in the form of radiation rather than conduction or convection. Vijaykumar et al. (2007) and Michels et al. (2007) agree that the greatest heat transfer into a building in tropical countries occurs through the roof. Suehrcke et al. (2008) further observes that heat gain through roof due to solar radiation can reach  $1 \text{ kW/m}^2$  during clear sky conditions, and 20–95% of this radiation is absorbed by roof surface. This downward heat transfer by radiation (refer to Fig. 4.2) from a roof surface is undesirable in a tropical country like Malaysia as it increases the load on air-conditioning equipment which will increase the electricity bill.

The roof is the most important structural element of a building for reducing energy consumption—see Jim (2014), Florides et al. (2002), Kumar et al. (1989). A major part of the building thermal load comes from the roof. As illustrated in Fig. 4.3, heat absorbed by the roof is transferred to the interior conditioned space impacting the

**Fig. 4.1** Map showing location of Malaysia near the equator. Source <http://www.worldatlas.com>



**Fig. 4.2** Illustration of heat flow into an indoor space from a domestic roof system in a hot and humid climate. Source Hassal (1977)



energy used for cooling. It is therefore obvious that the great potential for lowering energy consumption in buildings involves the roof.

For this reason, it is imperative to include a passive cooling strategy as part of the roof design. One of the passive strategies is thermal insulation. Dylewski and Adamczyk (2011) and Daouas (2011) both agreed that thermal insulation is one of the most effective way to conserve energy in building. Suehrcke et al. (2008) stated that one of the ways to reduce downward heat transmission from the roof is through the use of reflective foil. On average, radiant barriers which use reflective foil installed in the attic space can reduce heat flow to the conditioned space by 26–50% during summer season—see: Lee et al. (2016). This is because reflective technology that

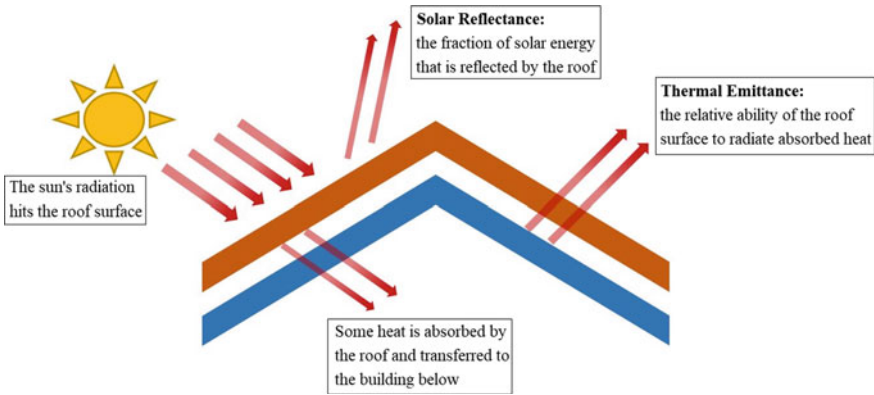


Fig. 4.3 Radiant heat transfer into building

uses very thin layer of low-emittance aluminum foil is very effective in blocking heat transfer by radiation across adjacent air spaces. This is illustrated in Fig. 4.4.

The use of thermal insulation in building roofs in an equatorial climate like Malaysia is a common practice. There are various types of thermal insulation materials available in the local market. However, supplier of each material claim that their product is superior to others in terms of thermal resistance. They often provide the thermal resistance value for the insulation material alone and not in the roof assembly. This is because more often than not the thermal resistance value will be different after installation due to the way it is being installed. In addition, the general public is unaware of how much savings they can derive from their investment in installing roof thermal insulation in the long run and often view this as an unnecessary expense. Therefore, there is a need to test and compare the thermal resistance of commonly used roof thermal insulation material in a roofing assembly to determine economic benefits of the available insulation materials and determine the cost-benefit of the investment. The building industry need to determine the most cost-effective roof thermal insulation material among the commonly used ones.

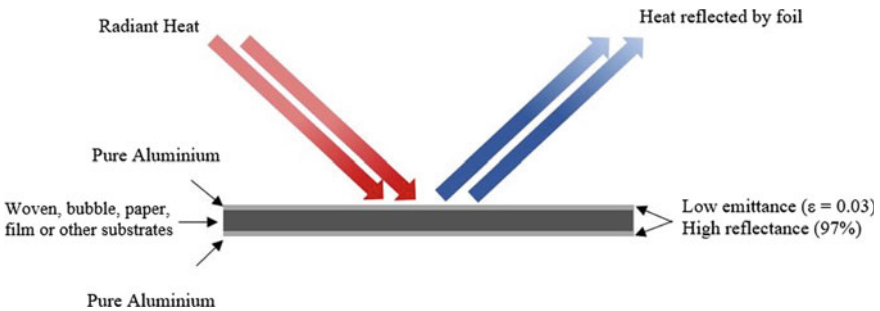


Fig. 4.4 Radiant heat reflected by low emittance aluminum foil

In Malaysia, two commonly used energy conserving systems based on reflective technology are identified as radiant barriers or reflective insulations.

## 4.2 Application of Reflective Insulation in Building

Radiant barrier systems are commonly installed in the roof system while reflective insulation systems are often found in walls. Radiant barriers are associated with large usually ventilated air spaces while reflective insulations are defined as enclosed air spaces with at least one low-emittance surface.

Vrachopoulos et al. (2012) conducted an evaluation of reflective insulations in wall using a small-scale test chamber exposed to outdoor conditions. Reflective insulation material was inserted to create a 10 mm air gap on each side of the reflective material. During a winter period, the reflective insulation system helped to retain heat in the test chamber by reflecting heat into the interior causing stabilization of the indoor temperature. The inner wall temperature remained quite constant from 10 to 12 °C while greater temperature fluctuations of 4–16 °C were seen on the outer wall temperatures. During the summertime, reflective insulation block the radiation heat from entering the interior hence helping to maintain temperatures on the surface of the internal wall to 23–27 °C throughout the whole day while temperatures on the external wall surface vary from 17 °C in the morning to about 32 °C in the afternoon. The control of temperatures during both seasons reduce the thermal load for the air-conditioning system and lead to cost savings.

Field measurements using test cells conducted by Baldinelli (2010) to evaluate the thermal performance of reflective insulations in walls showed a RSI value of 1.236 m<sup>2</sup>·K/W.

Fricker and Yarbrough (2011) did RSI calculations in accordance with data in the Australian Institute of Refrigeration, Air Conditioning and Heating (AIRAH) Handbook<sup>1</sup> for reflective insulation applied to roof and wall systems under both winter and summer conditions. Results clearly showed that with addition of a reflective airspace the overall thermal resistance of these two building sections increased the most for installations below the roof while calculated RSI values for walls were similar for both seasons.

However, based on the assemblies tested in Cold Climate Housing Research Center, Craven and Garber-Slaght (2011) concluded the contribution of RSI value created by reflective insulation system to overall RSI value of a wall assembly was very modest compared to the minimum prescriptive values by local law in cold climates like Alaska.

Figure 4.5 illustrates reflective insulation facing an enclosed air cavity in the roof batten while radiant barrier faces an open air space in actual roof assemblies.

---

<sup>1</sup> [https://www.airah.org.au/Technical\\_Handbook/Default.aspx](https://www.airah.org.au/Technical_Handbook/Default.aspx).

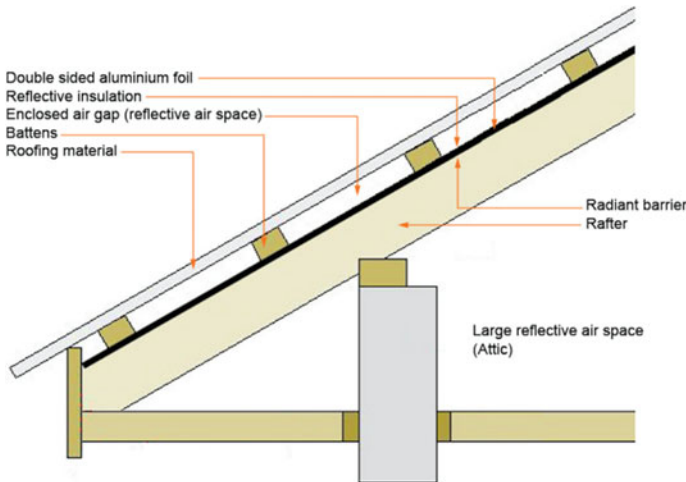


**Fig. 4.5** Radiant barrier and reflective insulation in a typical roof construction

The distinction between reflective insulation and radiant barrier can be explained in two ways. Firstly, in terms of the material itself, reflective insulation has a measurable material RSI value of the product due to additional bubble or foam that provides a thermal break between the two outer aluminum foil layers, while radiant barrier products themselves have insignificant material RSI value due to the very thin foil layer. Secondly, in terms of installation location in the roof assembly, reflective insulations face an enclosed air space while radiant barrier face an open attic air space as shown in Fig. 4.5. However, radiant barrier can become “reflective insulation” if it faces an enclosed air space since the system RSI value can be measured.

### 4.3 Standards, Guidelines and Building Rating Systems for Roof Thermal Insulation in Malaysia

In the last decade, there has been an increasing awareness and thus emphasis on the importance of thermal insulation for building roofs in Malaysia. Considerate effort has been made to reduce the thermal conductance of roof sections through the use of thermal insulation. In this section, recent development of green initiatives implemented in Malaysia that focus on roof thermal insulation is introduced.

**Table 4.1** Minimum RSI and maximum  $U$ -value for roofs

Roof weight group	Min RSI ( $m^2K/W$ )	Max $U$ -value ( $W/m^2K$ )
Light < 50 $kg/m^2$	2.5	0.4
Heavy > 50 $kg/m^2$	1.67	0.6

### 4.3.1 Malaysian Standard MS1525

The introduction of the Malaysian Standard (MS) 1525 Code of Practice on Energy Efficiency and Use of Renewable Energy for Non-residential Buildings in 2001 provides guidance on application of renewable energy and energy efficient designs in new and existing non-residential buildings—MS 1525 (2014). This standard was subsequently revised with the latest revision being, *MS1525:2014 Energy efficiency and use of renewable energy for non-residential buildings—Code of Practice (Second revision)* 2014. This standard clearly spells out the maximum thermal transmittance, also known as  $U$ -value of lightweight and heavyweight roofs shall be no greater than 0.4 and 0.6  $W/m^2\cdot K$ , respectively. In recent developments, the Malaysian Government on 10 July 2017 proposed making compliance with MS1525 mandatory for non-residential buildings—see: KPKT (2017).

### 4.3.2 Malaysian Standard MS2680

In the same year, another standard MS2680:2017 “Energy efficiency and use of renewable energy for residential buildings—Code of practice” was introduced. This standard provides guidance on the design, material selection, electrical appliances selection, and the efficient use of energy. This included the importance of using renewable energy in new and existing building. The roofing materials being recommended have low thermal conductivity, low solar absorptivity, low thermal emissivity, and high solar reflectance index. The entire roof construction must include appropriate and sufficient insulation materials in order to achieve low thermal transmittance ( $U$ -value) and high thermal resistance (RSI value). The recommended  $U$ -value and RSI value for roof construction is contained in Table 4.1.

### 4.3.3 Malaysian Standard MS 2095

MS, 2095 details the requirements for materials for use as radiant barriers and reflective insulations intended for use in buildings—see: MS 2095 (2014). This standard is intended for use by manufacturers that produce these products. Adequate radiant barriers. The standard is also users to aid identification of grade or quality of the radiant barrier and reflective insulation materials intended for specific purposes.

MS, 2095 defines reflective insulation as thermal insulation system consisting of one or more low emittance surfaces which is bounded to one or more enclosed air space with a measurable RSI value. As stated, reflective insulation and radiant barrier are effective in reducing radiant heat flow into the indoor space of a building.

The advantages of reflective insulation and radiant barrier are:

1. Both reflective insulation and radiant barrier are effective in reducing radiant heat transfer from the roof into the indoor space of a building.
2. Materials are lightweight and do not add weight to the roof system.

MS, 2095 also details the standard laboratory test methods for determining the thermal resistance for reflective insulation. The first apparatus used for evaluation is the Heat Flow Meter as given by the ISO 8301 standard, or a guarded hot plate apparatus as given in ISO 8302 with the heat flow from top to bottom. The second apparatus is two wooden frames with thickness of 25 mm. The frames are not more than 10 mm in width. The test method is summarized below.

1. Test method as detailed in MS, 2095:
2. Cut the specimen size of 500 mm × 500 mm.
3. Place the specimen on the first piece of wooden frame, and then place the second piece of wooden frame on top of the specimen, as the test specimen is sandwiched between the two wooden frames.
4. The specimen shall be installed in a heat-flow meter apparatus or hot plate apparatus with an air gap of 40 mm on the hot side and 60 mm on the cold side with the reflective side of the specimen facing the hot side. The temperature difference between the hot and cold side shall be 15 °C.
5. The calculated thermal resistance shall include the combination of test specimen and air gaps.
6. The reported values for thermal resistance shall be the equivalent thermal resistance ( $m^2 \cdot K/W$ )—see MS 2095 (2014).

Motivated by the requirement of local Malaysian standards and by-laws, many developers and architects in Malaysia started to include thermal insulation in the design of building roofs. However, having thermal insulation in the building roof is an investment from an economic point-of-view. This investment includes the cost of material, transport, and labor to install the insulation, whereas the economic benefits are linked to the monetary savings from decreases in utility use. The motivation for the economic evaluation of a roof thermal insulation is to find the most cost-effective option.

#### ***4.3.4 Green Building Index (GBI)***

Another important initiative called the Green Building Index (GBI) applied the same requirement for roof *U*-values as the mandatory compliance criterion. GBI is a green rating tool and certification system designed specifically for the tropical climate and



**Table 4.2** Classifications of GBI rating

Points	GBI rating
86–100 points	Platinum
76–85 points	Gold
66–75 points	Silver
50–65 points	Certified

Source Warta Kerajaan (2012)

Malaysia's current social, infrastructure and economic development. GBI is also to encourage sustainability in the constructed buildings and also to spread awareness amongst the developers, designers, engineers, architects, contractors, planners, and the public. Besides that, GBI offers an opportunity for the developers and contractors to plan, design, and build sustainable structures. It is similar to BREEAM in UK, LEED in USA, Green Star in Australia and Green Mark in Singapore—Chua and Oh (2011). In addition, the same maximum roof  $U$ -value for both residential and non-residential building is further enforced by Uniform Building (Amendment) (No. 2) By-Laws 2012 gazette by local government of Selangor State—see: Warta Kerajaan (2012). GBI has four classifications that represents the level of compliance with the requirements—Table 4.2.

## 4.4 Construction and Applications of Reflective Technology in Malaysia

South-East Asian countries like Malaysia have a hot and humid climate throughout the year, except those countries like Myanmar and northern Vietnam that are further north of the equator, experience cooler year-end period. Buildings are generally constructed to reduce the solar heat gain, especially through the roof. There are two types of roofs generally used in South-East Asia—Tile roof (concrete/clay) and Metal roof.

### 4.4.1 Tile Roof (Concrete and Clay)

The majority of the residential building roofs are constructed using concrete and clay tiles, due to its availability, aesthetic, and inherent soundproof properties. Roof pitch is typically greater than  $30^\circ$  to prevent water leakage during heavy rain with strong wind. Ceiling is constructed between the living space and the roof to create a non-ventilated attic space. Often, there is no insulation material underneath the tiles. However, new houses may have reflective insulation installed as illustrated in Fig. 4.6.

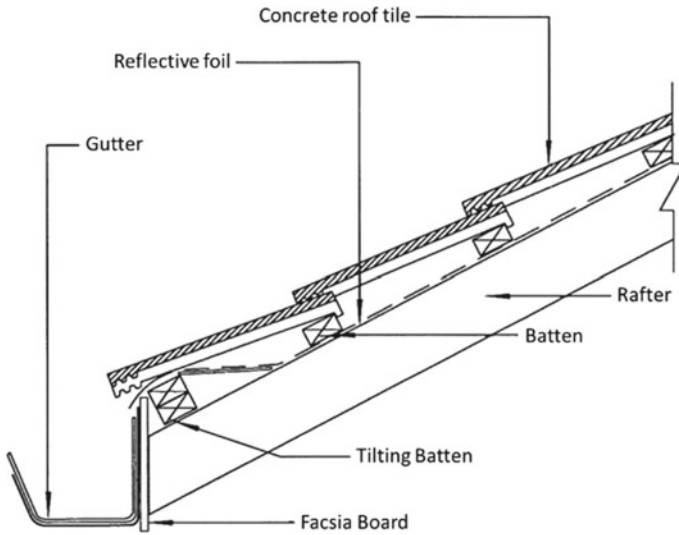


Fig. 4.6 Tiled roof with reflective insulation. Source Teh et al. (2017)

### 4.4.2 Metal Roof (Concrete and Clay)

Metal roofing is used in residential, industrial, and commercial buildings. For residential buildings, metal roofing is gaining in popularity due to its versatile design and is able to prevent water leakage even in heavy storms. Typical roof pitch is usually less than 10°. This results in smaller non-ventilated attic space in comparison with concrete and clay tile roofs. Metal roofs are commonly insulated against sound and heat using insulation materials such as mineral wool and fiberglass, supported by reflective insulation material as shown in Figs. 4.7 and 4.8.

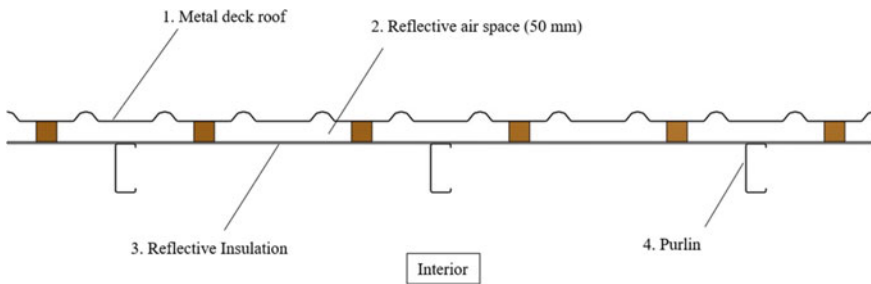
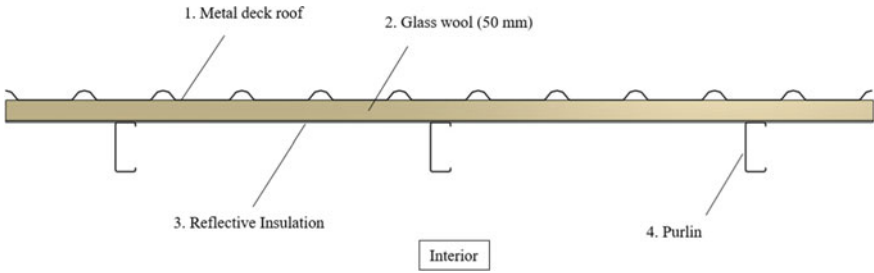


Fig. 4.7 Metal deck roof with reflective insulation



**Fig. 4.8** Metal deck roof with mass insulation and reflective insulation

### 4.5 Field Evaluation of Reflective Insulation and Radiant Barrier in Malaysia

Test huts were constructed to study the performance of radiant barriers and reflective insulations for actual environmental conditions. The test huts shown in Fig. 4.9 were built in an open area with natural weather in Melaka, Malaysia. The dimensions of each hut are 2.2 m × 2.5 m × 3.3 m (height). The distance between the test huts is 1.9 m. The test huts face the West to prevent self-shading. The walls, including the attic area, are constructed using hollow metal frames and covered on the outside with 6 mm of cement board with 12 mm of gypsum board as interior sheathing. The floor assembly is faced with 12-mm thick plywood on the top and bottom. The wall and floor cavities contain 100 mm thick mineral wool with density of 80 kg/m<sup>3</sup> to reduce heat gain or heat loss through the walls and floor. Hence, temperature changes in the attic and interior of the test huts are mainly affected by heat from the roof. The attic for the test huts uses a gable-roof design. Reflective insulation with low-emittance



**Fig. 4.9** Test huts in Melaka, Malaysia. *Source* San et al. (2017)



**Fig. 4.10** Wall insulation material. *Source* Yarbrough et al. (2016)

surfaces on both sides is laid on the rafters. Battens with specific dimensions are used to create an enclosed reflective air space between the reflective insulation and the roof tiles. The enclosure is completed by fascia boards installed around the eaves. Figure 4.10 shows the attic space from the inside with the ceiling removed. A shed-roof design is used for the metal-roof structures. Reflective insulation and/or rock wool insulation is placed or draped above the battens with roofing panels installed above the insulation. The bottom side of the reflective insulation material creates an enclosed reflective air space.

The project was carried out in seven phases over a period of 12 months (May 2015–April 2016). Each phase consisted of different insulation configurations in the three test huts. In this study, roof materials commonly found in Malaysia, i.e. concrete tile, clay tile and metal deck, were used. For insulation, woven foil (double sided Aluminum), bubble foil (8 mm thick with double sided Aluminum), foam-foil (8 mm thick with double sided Aluminum) and mineral wool (50 mm thick with density 40 kg/m<sup>3</sup>) were used.

### 4.5.1 Instrumentation

The test huts were instrumented with a pyranometer, thermocouples, heat flux transducers and portable data loggers. The pyranometer was placed in the exterior on top of the roof ridge of the test hut to record the irradiance throughout the day. Type-K thermocouples with precision  $\pm 1$  °C were installed and positioned as shown in Fig. 4.11 and were used to monitor the material surface temperatures. Each of the test huts contained 12 thermocouples—six underneath the roof tiles or metal deck, three underneath the insulation material, and three thermocouples on top of

**Fig. 4.11** Diagram of thermocouple location. Source Teh et al. (2017)

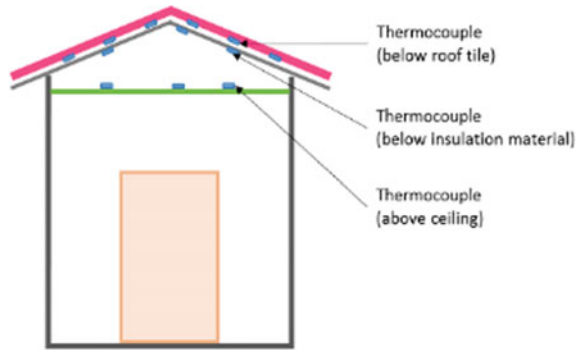
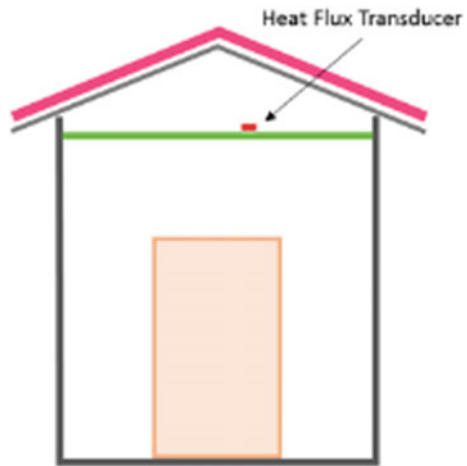


**Fig. 4.12** Heat flux transducer on ceiling. Source Teh et al. (2017)



the ceiling. Every test hut contained a transducer attached to the ceiling with silicon thermal adhesive (as shown in Fig. 4.12) to determine the heat flux across the ceiling. Portable data loggers recorded the attic air temperature.

### 4.5.2 Calculation of RSI from Transient Data

Temperatures, heat flux and irradiance were recorded at 2-min intervals for 10 days. Figure 4.13 shows the average temperature for roof tiles (red line), woven foil (blue line) and ceiling (grey line) in the same 10-day time frame (29 May–7 Jun 2015). The average outdoor temperature ranged from 25 to 38 °C. Figure 4.14 is the temperature comparison of three test huts in the same 1-day time frame, whereby Test Hut 2 was without any insulation material underneath the roof.

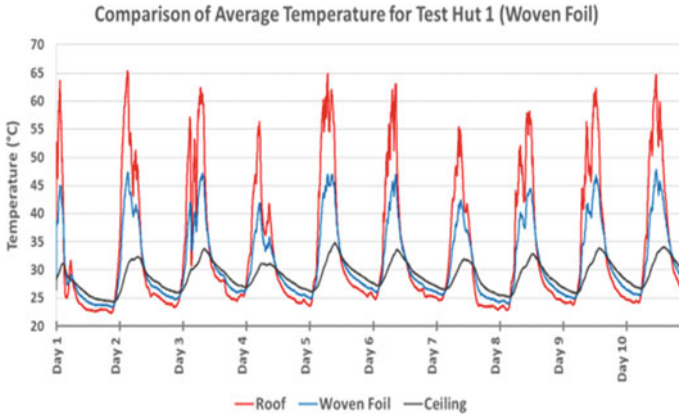


Fig. 4.13 Average temperatures for roof tiles, woven foil, and ceiling—see: Teh et al. (2017)

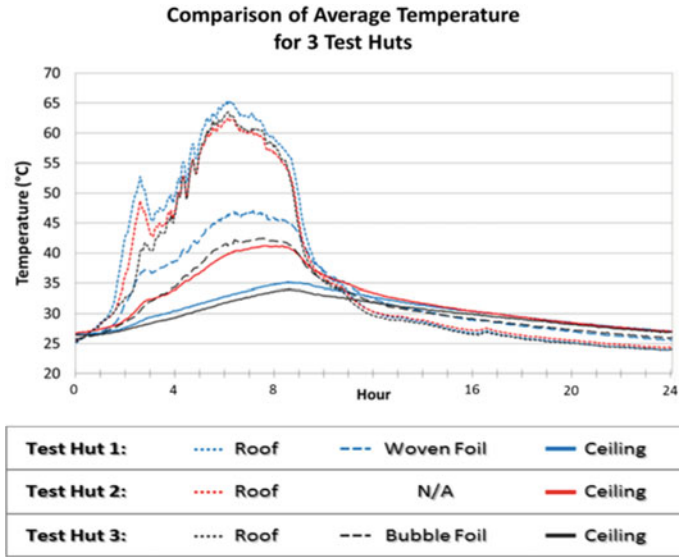


Fig. 4.14 Comparison of temperatures—see: Teh et al. (2017)

It is noted that the ceiling temperatures for Test Hut 1 and Test Hut 3 are significantly lower than Test Hut 2 during daytime.  $RSI_t$  is the total thermal resistance of two enclosed regions of the attic as indicated by Eq. (4.1). The heat fluxes for the upper attic region were obtained from the transducer mounted on the ceiling using Eq. (4.2).  $RSI_{block}$  is then calculated by averaging temperature and heat flux data for ten two-minute intervals, as expressed in Eq. (4.3). For instance, if there are 1,000 2-min intervals, then there will be 100  $RSI_{block}$  values.

$$RSI_t = RSI_A + RSI_B \quad (4.1)$$

$$Q_A = Q_B \cdot (\text{ceiling area}/\text{Roof area}) \quad (4.2)$$

$$RSI_{\text{block}} = \sum_i \left\{ \frac{T_1 - T_2}{Q_A} + \frac{T_2 - T_3}{Q_B} \right\}_i \cdot \Delta t_i / \sum_i \Delta t_i \quad (4.3)$$

where:

$RSI_A$  is for air space between roof and insulation material;  $RSI_B$  is for air space between insulation material and ceiling;  $T_1$  is the average temperature of the roof;  $T_2$  is the average temperature of the insulation material;  $T_3$  is the temperature of the top of the ceiling;  $Q_A$  is the heat flux across the roof;  $Q_B$  is the heat flux across the ceiling;  $\Delta t$  is a 2-min interval;  $RSI_{\text{block}}$  is the average of  $RSI_i$ -values.

An  $RSI_{\text{block}}$  value is retained if the following criteria are satisfied:

1. Data indicate heat flow down
2. Irradiance is at least 600 W/m<sup>2</sup>
3. Heat flux is at least 1.0 W/m<sup>2</sup>
4. Temperature difference across an air space is at least 0.1 °C
5.  $\{RSI_{\text{block}}\}_{(n+1)}$  is within 25% of the running average for RSI (Eq. 4.4).

$$RSI_{\text{running - average}} = \sum_n \{RSI_{\text{block}}\}_n / n \quad (4.4)$$

### 4.5.3 Results and Findings

The RSI (m<sup>2</sup>·K/W) for each roof configuration for each phase are detailed in Tables 4.3 and 4.4. The results for Test Hut 2 with no insulation show RSI value of 0.40 for the region between the roof and the ceiling. The agreement seems reasonable given the wide variety of attic designs. The time-averaged RSI values in Table 4.3 for insulated attic spaces are significantly greater than the uninsulated value. The reduction in heat flow across the ceiling results in lower maximum air temperatures in the region below the ceiling when the space is not conditioned, or in reduced utility used for air conditioning in the occupied space. The reduction in interior air-space temperatures due to attic-space insulation was discussed in Sect. 4.2.3. The percentage reduction in ceiling heat flux (HFR) is estimated using Eq. (4.5), where RSI is for the insulated attic.

$$\text{HFR} (\%) = (1 - 0.4/RSI) \cdot 100 \quad (4.5)$$

**Table 4.3** RSI for the huts

Phase	Type of roof	Configuration	Test Hut 1 (RSI)	Test Hut 2 (RSI)	Test Hut 3 (RSI)
1	Concrete tile	25 mm air space	Woven foil (2.37)	Without foil (0.37)	Bubble foil (2.93)
2	Concrete tile	50 mm air space	Woven foil (2.16)	Without foil (0.40)	Bubble foil (2.69)
3	Concrete tile	Woven foil	50 mm air space (2.31)	25 mm air space (2.15)	75 mm air space (3.08)
4	Concrete tile	Bubble foil	50 mm air space (2.41)	25 mm air space (2.41)	75 mm air space (3.09)
5	Clay/Concrete tile	25 mm air space (woven foil)	Concrete tile (2.26)	Clay tiles without foil (0.40)	Clay tiles (2.40)
6	Metal deck	No air space	Woven foil/Mineral wool (2.23)	Foam foil (2.37)	Bubble foil (1.77)
7	Metal deck	No air space	Woven foil/Mineral wool (2.77)	Mineral wool (1.61)	Bubble foil (2.02)

**Table 4.4** Maximum attic air temperatures

Phase	Type of roof	Configuration	Test Hut 1 (°C)	Test Hut 2 (°C)	Test Hut 3 (°C)
1	Concrete tile	25 mm air space	Woven foil (37.2)	Without foil (46.1)	Bubble foil (36.7)
2	Concrete tile	50 mm air space	Woven foil (38.3)	Without foil (45.7)	Bubble foil (36.6)
3	Concrete tile	Woven foil	50 mm air space (37.3)	25 mm air space (38.4)	75 mm air space (35.8)
4	Concrete tile	Bubble foil	50 mm air space (36.7)	25 mm air space (37.8)	75 mm air space (35.4)
5	Clay/Concrete tile	25 mm air space (woven foil)	Concrete tile (36.7)	Clay tiles without foil (43.8)	Clay tiles (36.0)
6	Metal deck	No air space	Woven foil/Mineral wool (39.2)	Foam foil (38.7)	Bubble foil (39.5)
7	Metal deck	No air space	Woven foil/Mineral wool (37.6)	Mineral wool (39.1)	Bubble foil (38.1)

Teh et al. (2017)



Table 4.3 indicates a reduction in heat flows across the ceiling ranging from 80 to 90%, which translates to a reduction in electrical use when a conditioned space is maintained. The estimated annual savings for a change from 0.4 to 2.4 in attic RSI is 109 kW·h/(y·m<sup>2</sup>).

Table 4.4 lists the maximum attic air temperatures for all phases. It shows that there is about 9 °C difference for roof with and without insulation (Phases 1 and 2). There will be a reduction of attic air temperature of about 1–1.5 °C with every increment of 25 mm of enclosed reflective air space (refer to Phases 3 and 4). In general, attic air temperature for clay tiles (without insulation) is cooler than concrete tiles. However, there is no significant difference in terms of attic air temperature when clay tiles and concrete tiles are insulated (refer to Phase 5). For phase 6, Hut 3 insulated with Bubble Foil gave the highest attic air temperature. For phase 7, there is a 1.5 °C attic air temperature difference for mass insulation with and without reflective insulation.

Reflective technology is effective as attic insulation in South-East Asia buildings, especially in locations where the predominant heat flow direction is downward. Measured RSI for typical attic applications of reflective products showed results in the range of 2–3 m<sup>2</sup>·K/W. Measured thermal resistances for attics with reflective insulations are higher than for mass insulations in the same structure. Ceiling heat-flux reduction for attics with reflective insulation were determined to exceed 80% relative to an uninsulated attic. Small-scale field measurements using custom-built test huts can provide thermal resistance values from transient heat flux and temperature data.

#### 4.6 Thermal Performance of Roof Assembly with Reflective Technology Using Computational Fluid Dynamics (CFD) Analysis

Siemens FloEFD CFD software package tool<sup>2</sup> was used to solve the 3D steady-state model condition. All three modes of heat transfer (conduction, convection, and radiation) were considered in the simulation. Solar radiation was directed towards the roof tiles, to mimic the actual condition of a typical hot and humid Malaysian weather. FloEFD software can predict both laminar and turbulent flows. To predict the laminar-turbulent flows, the conservation of energy, mass, and momentum (Favre-averaged Navier–Stokes) equations were employed. To solve the system of equations, FloEFD uses *thek – emodel* to employ transport equations for the turbulent kinetic energy and its dissipation rate. Unlike other traditional CFD solver, FloEFD uses only one system of equations to solve both laminar and turbulent flows.

---

<sup>2</sup> <https://www.plm.automation.siemens.com/global/en/products/simcenter/floefd.html>.

### 4.6.1 CFD Model

In the CFD model, the heat transfer through the gable roof assembly was studied independently, as the influence of other building structures was not included. The modelled roof structures replicate the roof of the test huts as detailed in the experimental measurements. In addition, a roof pitch of  $45^\circ$  was also modelled to investigate the effect of varying the roof pitch on the thermal performance of the insulated roof assembly. The geometries of the analyzed gable roof assemblies are shown in Figs. 4.15 and 4.16.

Figure 4.16 above shows the main components of the investigated gable roof assembly incorporating reflective insulation and radiant barrier systems. The assembly configuration is the same for both  $30^\circ$  roof pitch and  $45^\circ$  roof pitch. The total length, width, and height of the roof assemblies are  $4.2\text{ m} \times 3.3\text{ m} \times 1.7\text{ m}$  and  $3.5\text{ m} \times 3.3\text{ m} \times 2.1\text{ m}$  for the roof pitch of  $30^\circ$  and  $45^\circ$  respectively which can be seen in Fig. 4.15. The roof pitch of  $45^\circ$  has taller height and shorter length as the pitch was increased while keeping the same total surface area of roof tiles.

Table 4.5 details the investigated roof configurations considered in this research where reflective air space thickness of 25, 50, 75, and 100 mm for roof pitches of  $30^\circ$  and  $45^\circ$  were studied. The materials used in the CFD simulation were:

- Air as the fluid domain
- Clay tiles or concrete tiles as roof tiles
- Aluminum foil as the reflective insulation material
- Wood as the rafters, battens, and ridge
- Gypsum board as the ceiling

The properties of the materials obtained from FloEFD database that were used in the simulation are listed below in Table 4.6.

As the CFD simulation aims to simulate the heat transfer through the gable roof assembly at an outdoor environment, external type analysis was used. The CFD computational conditions used to simulate Malaysia outdoor environment are summarized in Table 4.7:

The mesh quality affects the sensitivity and accuracy of the results when compared to measurements. Hence, to achieve the accurate analysis of the roof assemblies, a finer mesh was employed in regions with more geometry complexity such as the roof tiles. Finer mesh was also used on the materials that require higher sensitivity for accurate results such as the aluminum foil and the ceiling. Coarser mesh was used on the other roof structures such as the rafters, ridge, and in all other regions. Finer mesh was also used in corners and small edges of the roof structures as seen in Fig. 4.17. One of the features of FloEFD employs local mesh refinement on the intended components. This feature was used on the roof tiles, the aluminum foil, and the ceiling, with the highest level of refinement was employed on the roof tiles due to the geometric complexity. This results in tetrahedral mesh cells on the roof tiles which is a better mesh type in capturing results in complex geometry. The number

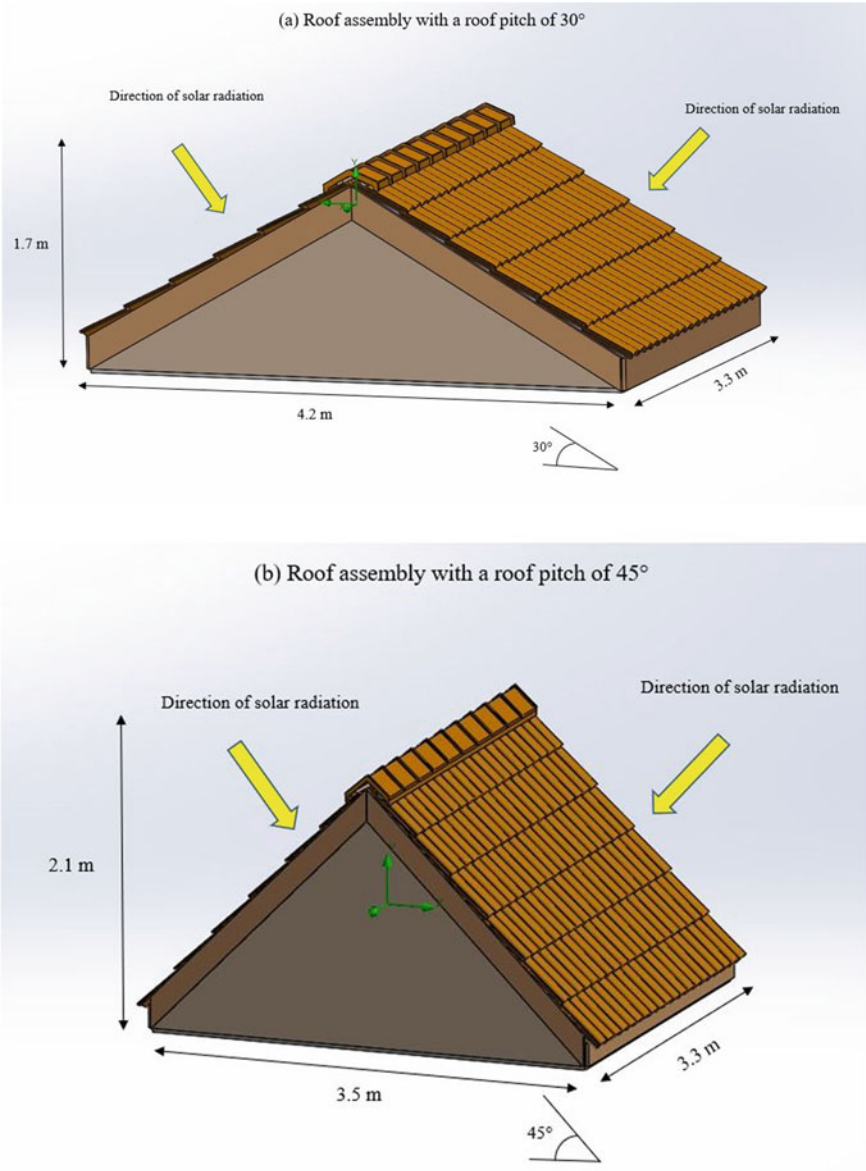


**Fig. 4.15** a Roof assembly with a roof pitch of 30°; b roof assembly with a roof pitch of 45°. Source Ashhar and Lim (2020)

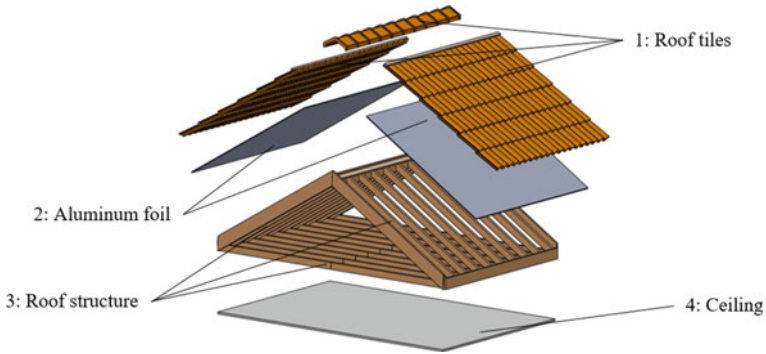


**Fig. 4.16** Exploded view of the typical gable roof assembly with radiant barrier system (1: Roof tiles; 2: Aluminum foil; 3: Roof structure; 4: Ceiling). *Source* Ashhar and Lim (2020)

**Table 4.5** The investigated configurations using CFD simulation

Roof type	Reflective air space thickness (mm)	Roof pitch (°)
Clay tile	25, 50, 75, and 100	30 and 45
Concrete tile	25, 50, 75, and 100	30 and 45

**Table 4.6** List of material properties used in the simulation

Material	Emissivity, $\epsilon$	Thermal cond. (W/m·K)	Specific heat (J/K·kg)	Density (kg/m <sup>3</sup> )
Clay tiles	0.9	0.83	800	1,900
Concrete tiles	0.9	1.10	837	2,100
Gypsum	0.85	0.16	840	950
Wood	0.9	0.14	1,200	650
Aluminum	0.03	0.896	167	2,689

Ashhar and Lim (2020)

**Table 4.7** The input used in the CFD simulations

CFD computational condition	Value
Ambient temperature	33 °C
Heat radiation directed towards the roof	600–1,000 W/m <sup>2</sup>
Atmospheric pressure	101.3 kPa
Wind velocity	0.5 m/s
Relative humidity	60%
Cloudiness index	0.3

Ashhar and Lim (2020)

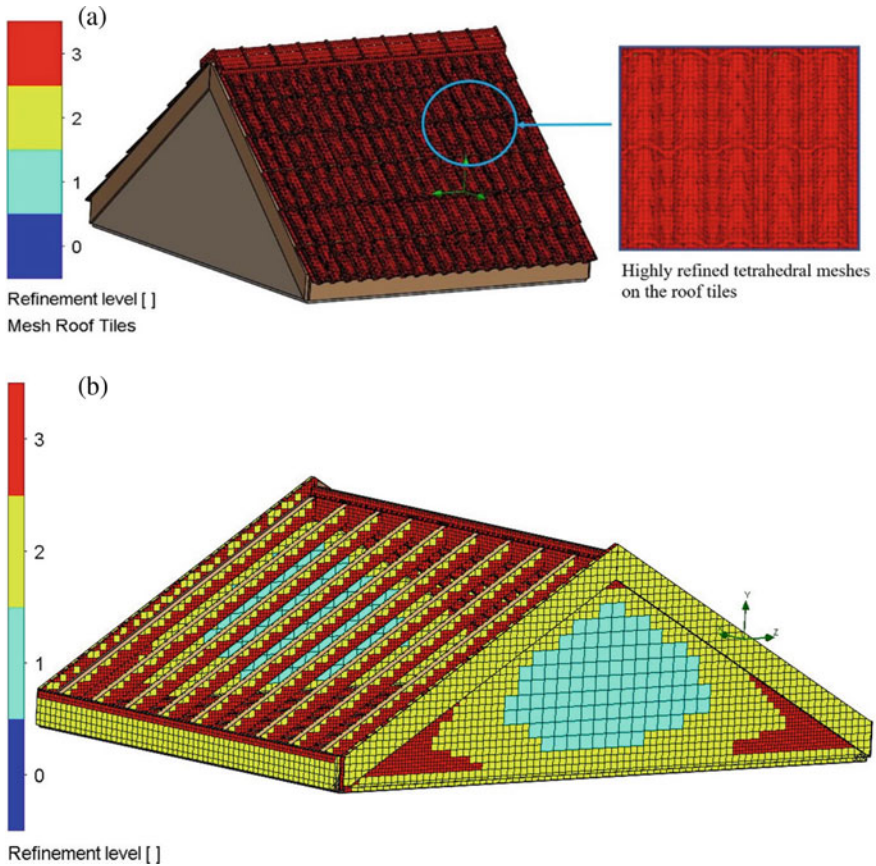


**Fig. 4.17** a Tetrahedral meshes type on the roof tiles; b hexahedral mesh type on the roof structure. Source Ashhar and Lim (2020)

of total cells used in the simulations was over 200,000 fluid cells and solid cells, and the results converge after 200 or more iterations.

### 4.6.2 CFD Results Validation Against Experimental Measurements

To ensure that the results obtained by CFD simulation are acceptable, the CFD results must first be validated against some of the test results obtained by the field test conducted by Teh et al. (2017). Due to limitations in conducting the field experiment, the RSI values obtained from CFD simulation and experimental measurements can only be compared against available data which are shown in Table 4.8.

**Table 4.8** Cases used for CFD results validation against test data

Case	Roof type	Air space thickness (mm)	Roof pitch (°)	RSI value (m <sup>2</sup> ·K/W) from experimental measurement [9]		Predicted RSI value (m <sup>2</sup> ·K/W) from CFD simulation	Percentage error (%)
1	Clay tiles	25	30	2.40	2.37		1.25
2	Concrete tiles	25	30	2.15		2.33	8.37
3	Concrete tiles	25	30	2.26		2.33	3.10
4	Concrete tiles	25	30	2.37		2.33	1.69
Mean absolute percentage error							3.6

Figure 4.18 shows a comparison between the predicted RSI values using FloEFD and the measured RSI values for various configuration in different phases. The predicted RSI values obtained from CFD simulation for all configurations are in good agreement with the measured RSI values as the predicted RSI values are within the ±95% confidence band. Furthermore, the mean absolute percentage error between the CFD simulation and experimental measurements is 3.60%, which is acceptable. Once the results are validated, then it can be said that the 3D model, assumptions, and boundary conditions are able to predict accurate values with high confidence. From here, the exact same 3D model, along with the assumptions and boundary conditions will be used to investigate the other roof configurations.

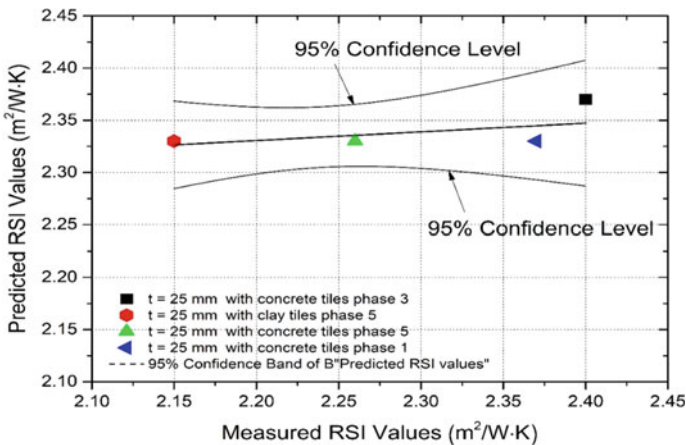
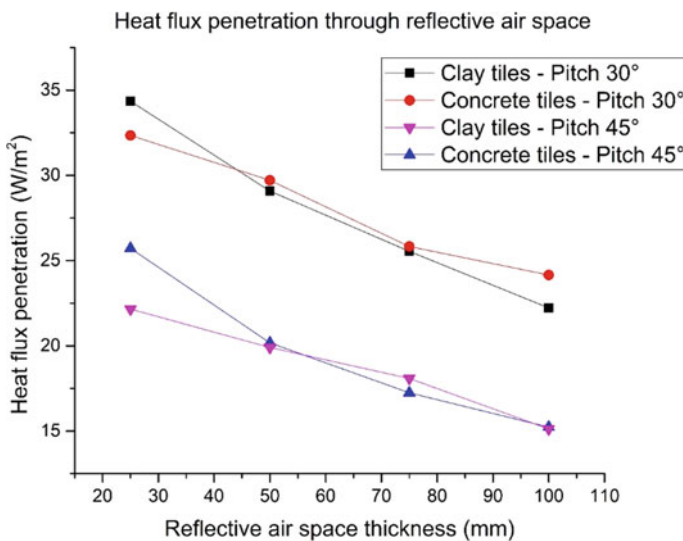


**Fig. 4.18** Comparison of the predicted RSI values with the measured RSI values. *Source* Ashhar and Lim (2020)

### 4.6.3 Heat Flux Penetration Through the Gable Roof Assemblies

In this section, the heat flux penetration will be analyzed in two parts: (a) heat flux penetration through the reflective air space and (b) heat flux penetration through the attic. The percentage of heat flux reduction will also be presented for all roof configurations.

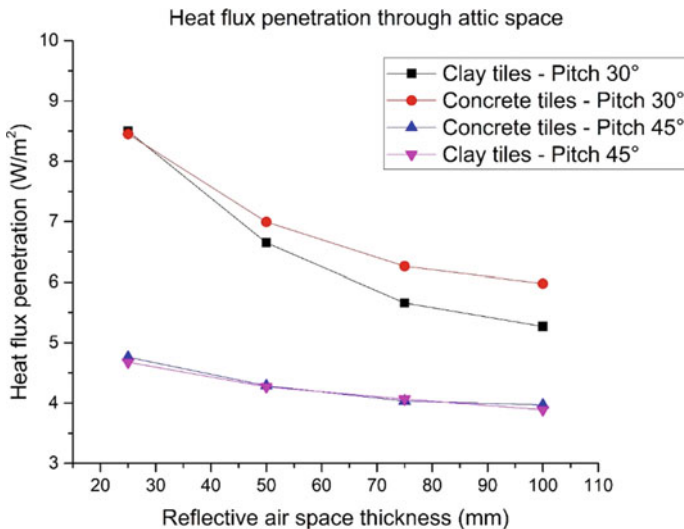
Figure 4.19 illustrates the heat flux penetration through the reflective air space area of the roof assemblies. It can be noted that the heat flux penetration through the reflective air space decreases exponentially as the air space thickness increases from 25 to 100 mm. This is because the air ventilation inside the reflective air space area increases as the thickness of reflective air space increase from 25 to 100 mm. This causes the rate of hot air flow from the eaves to ridge to increase—see: Roels and Deurinck (2011). Stronger air flow rate inside the reflective air space area increases the convective heat transfer. Therefore, heat loss through convective heat transfer increases and the heat flux penetration into the roof assembly due to solar radiation decreases. However, when a smaller thickness of reflective air space is used, the drag force that causes friction to become larger and contributes to restricting the air movement and hence reduces convective heat transfer—see: Alzwayi and Paul (2014). As a result, the heat radiation traps inside the reflective air space and transmits into attic. As the reflective air space is further inclined to 45° from 30°, the heat flux transmitted through the reflective air space area is much lesser and this phenomenon agrees with an empirical measurement done by Tong and Li (2014).



**Fig. 4.19** Heat flux penetration through the reflective air space of the roof assemblies. *Source* Ashhar and Lim (2020)

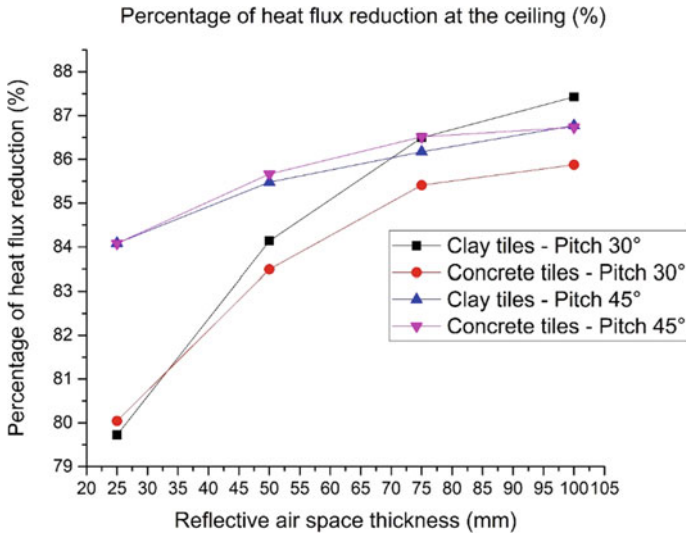
Figure 4.20 shows the heat flux penetration through the attic space of the roof assemblies for a gable roof pitch of 30° and 45°. The heat flux penetration through the attic space for a gable roof pitch of 45° was consistently lower than roof pitch of 30° for both types of roof tile materials. Hence, it can be argued that the pitch of the attic space contributes to a higher impact in the reduction of heat flux penetration through the gable roof assembly. While increasing the thickness reflective air space from 25 to 100 mm have a bigger effect on reducing the heat flux transmission through the attic air space for a gable roof pitch of 30°, a much lesser impact can be noted for a gable roof pitch of 45°. One possible reason is that the rate of convective heat transfer inside the attic space area overshadows the impact of convective heat transfer inside the reflective air space.

Figure 4.21 shows the percentage of heat flux reduction at the ceiling when an aluminum foil was installed in the roof assembly. The percentage of heat flux reduction varies between 84 and 87% for a gable roof pitch of 45° whereas the percentage of heat flux reduction was between 79 and 88% for a gable roof pitch of 30° for reflective air space between 25 and 100 mm. It can be noted that the roof assemblies show a logarithmic increment of heat flux reduction as the reflective air space was increased from 25 to 100 mm. At reflective air space thickness of 25 mm, gable roof pitch of 45° shows a higher percentage of heat flux reduction compared to a gable roof pitch of 30°. However, as the reflective air space was increased from 25 to 100 mm, the percentage of heat flux reduction converges to a value between 85 and 88%. This can be explained by the fact that as the reflective air space was increased from 25 to 100 mm, the temperature gradient between roof surfaces (i.e. Roof tiles and the ceiling) get smaller and hence buoyancy force increases at a lower rate. Thus, the



**Fig. 4.20** Heat flux penetration through the attic space of the roof assemblies. *Source* Ashhar and Lim (2020)





**Fig. 4.21** Percentage of heat flux reduction at the ceiling of the roof assemblies. *Source* Ashhar and Lim (2020)

rate of airflow and convective heat transfer increase at a slower rate despite having a thicker reflective air space [36].

#### 4.6.4 Thermal Resistance (RSI Values) of the Gable Roof Assemblies

Figure 4.22 shows the predicted total RSI values of the entire roof assembly for roof assemblies with reflective air space thickness from 25 to 100 mm for clay tiles and concrete tiles. The total predicted RSI values are significantly higher for roof assemblies with roof pitch of 45° than roof assemblies with roof pitch 30°. Besides that, the total predicted RSI values increased as the thickness of the reflective air spaces increased from 25 to 100 mm, and the total RSI value for concrete tiles are consistently slightly lower than clay tiles for both roof pitches assembly. This is because clay tiles have lower thermal conductivity than concrete tiles. Hence, concrete tiles are able to transfer heat by heat conduction better than clay tiles which causes the heat flux penetration is slightly higher for roof assembly with concrete tiles. The CFD simulation predicts that the total RSI value passes the minimum RSI value as regulated in UBBL Sect. 38A-(2) when the reflective air space thickness is 50 mm and 60 mm for clay tiles and concrete tiles respectively for roof pitch of 30°. As for roof pitch of 45°, the RSI value passes the minimum regulated RSI value for all roof configurations.

Table 4.9 summarizes the predicted RSI values for all configuration of roof assem-

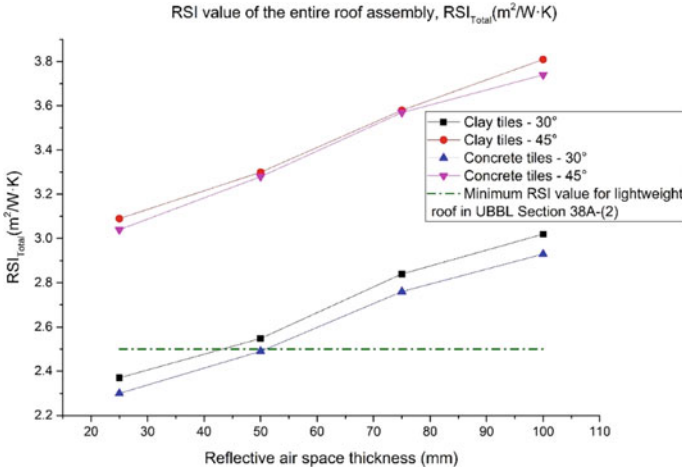


**Fig. 4.22** The predicted total RSI value of the entire roof assembly. *Source* Ashhar and Lim (2020)

blies with roof pitch 30° and roof pitch 45° using clay roof tiles and concrete roof tiles respectively.

From Table 4.9, it can be noted that:

1.  $RSI_A$  for roof pitch of 45° are consistently slightly lower than roof pitch 30° for all reflective air space thicknesses.
2.  $RSI_B$  for roof pitch of 45° are massively higher than roof pitch of 30° for all reflective air space thicknesses.

While  $RSI_A$  increases as the thickness of reflective air space increases, the  $RSI_B$  decreases as the thickness reflective air space increases.

### 4.6.5 CFD Graphical Results

This section shows the CFD images obtained from the simulation. Note that the two parallel plates above the roof are the heat source directed towards the roof. This is to simulate heat radiation between 600 and 1,000  $W/m^2$  to the roof.

Figures 4.23 and 4.24 show the plots of temperature in a 30° roof pitch assembly without and with aluminum foil. The figures shows that there is a massive temperature reduction when an aluminum foil is installed. A majority of the heat was trapped inside the reflective air space and reflected by the aluminum foil. Because of buoyancy force, the heat flows upwards and escapes through the ridge vent.

Comparing Figs. 4.24 and 4.25, reveals a larger amount of heat that moves upwards towards the ridge when the thickness of the reflective air space is increased from 25 to 100 mm. Hence, lower heat penetration through reflective air space and the ceiling

**Table 4.9** Summary of predicted RSI values

Roof type	Roof Pitch	Reflective air space thickness											
		25 mm			50 mm			75 mm			100 mm		
		RSI <sub>A</sub>	RSI <sub>B</sub>	RSI <sub>Total</sub>	RSI <sub>A</sub>	RSI <sub>B</sub>	RSI <sub>Total</sub>	RSI <sub>A</sub>	RSI <sub>B</sub>	RSI <sub>Total</sub>	RSI <sub>A</sub>	RSI <sub>B</sub>	RSI <sub>Total</sub>
Clay tiles	30°	0.9	1.47	2.37	1.24	1.31	2.55	1.55	1.29	2.84	1.76	1.26	3.02
	45°	0.78	2.31	3.09	1.19	2.12	3.30	1.46	2.12	3.58	1.65	2.16	3.81
Concrete tiles	30°	0.83	1.5	2.33	1.2	1.32	2.52	1.5	1.26	2.76	1.69	1.24	2.93
	45°	0.72	2.32	3.04	1.17	2.11	3.28	1.43	2.14	3.57	1.63	2.11	3.74

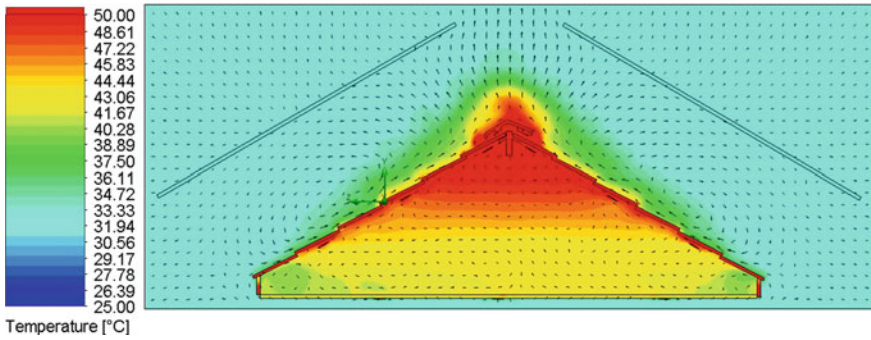


**Fig. 4.23** Temperature gradient cut plot of 30° roof assembly without aluminum foil. *Source* Ashhar and Lim (2020)

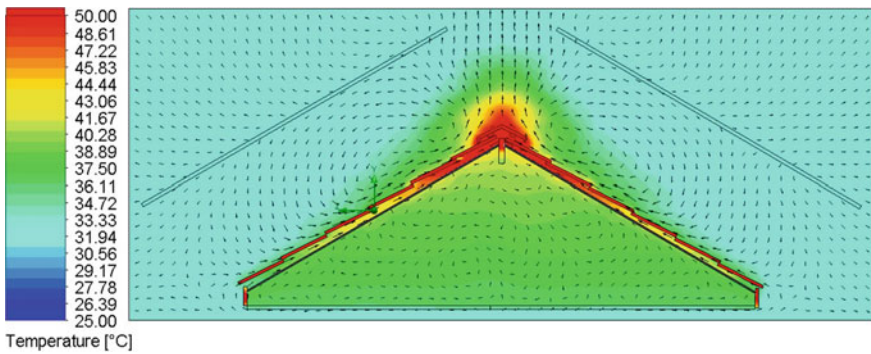


**Fig. 4.24** Temperature gradient cut plot of 30° roof assembly with aluminum foil and reflective air space of 25 mm. *Source* Ashhar and Lim (2020)

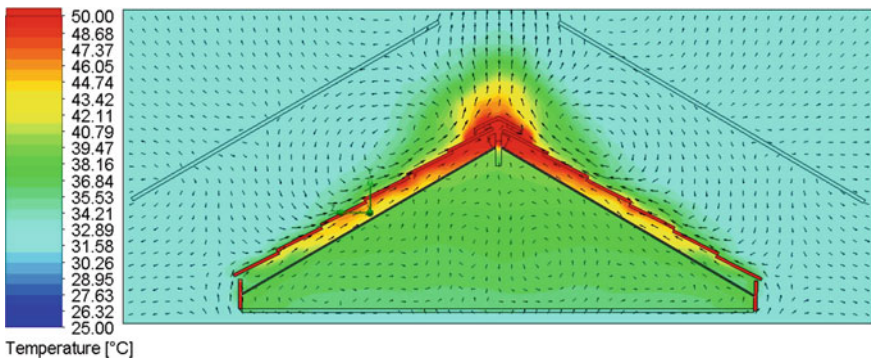


**Fig. 4.25** Temperature gradient cut plot of 30° roof assembly with aluminum foil and reflective air space of 100 mm. *Source* Ashhar and Lim (2020)

and this results in lower ceiling temperature when the thickness of reflective air space is increased from 25 to 100 mm.

Figures 4.26 and 4.27 show temperatures in a 45° roof pitch assembly without and with aluminum foil installed. In Fig. 4.26, the buoyancy effect has evidently taken place inside the attic space. Despite not having an aluminum foil installed, the hot air accumulates and escapes through the ridge due to buoyancy force. In Fig. 4.27,

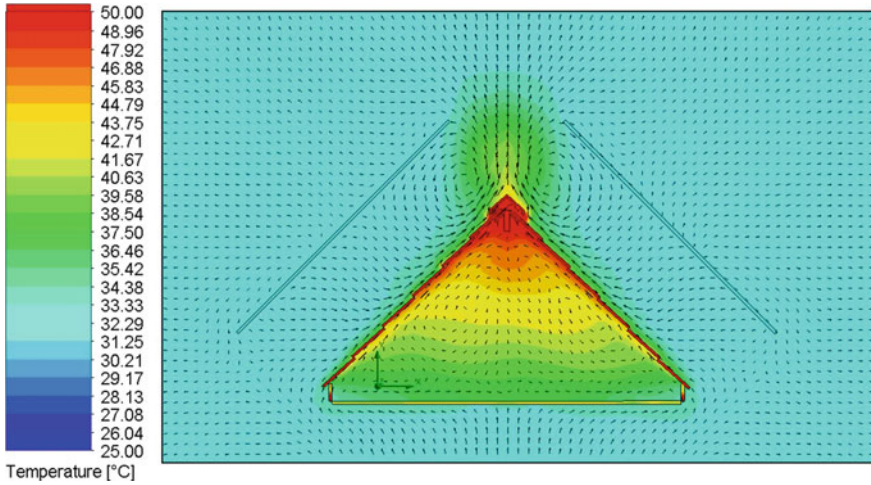


**Fig. 4.26** Temperature gradient cut plot of 45° roof assembly without aluminum foil. *Source* Ashhar and Lim (2020)

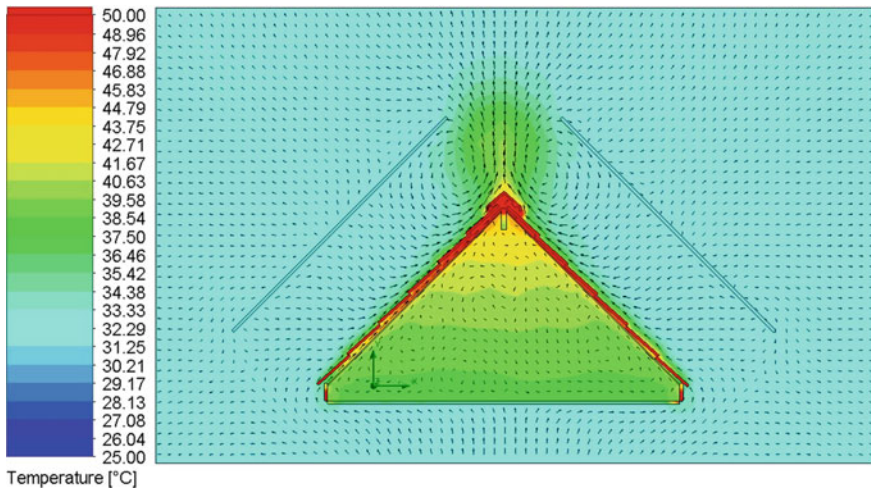


**Fig. 4.27** Temperature in a 45° roof assembly with an insulation layer and 25 mm of air space. *Source* Ashhar and Lim (2020)

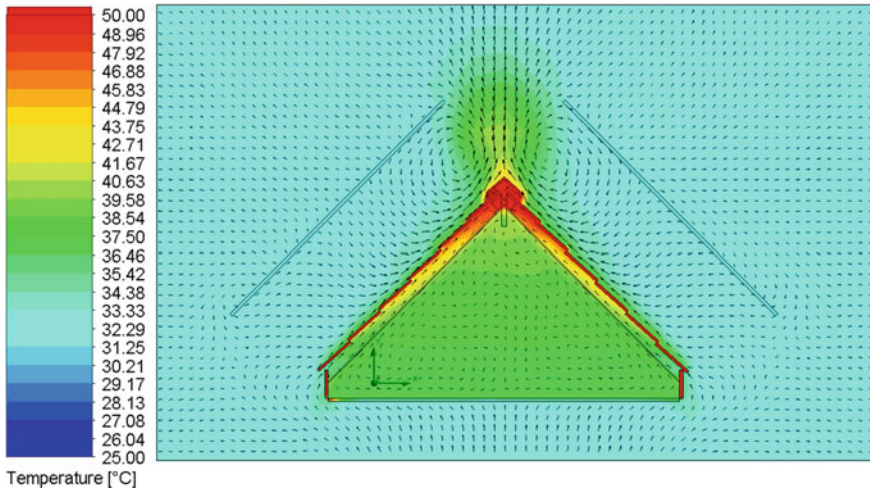


**Fig. 4.28** Temperature gradient cut plot of 45° roof assembly with aluminum foil and reflective air space of 100 mm. *Source* Ashhar and Lim (2020)

the results show that the hot air was trapped and reflected by the aluminum foil in the reflective air space area. In the reflective air space area, the heat flows upwards from the eaves and escapes through the ridge.

Comparing Figs. 4.27 and 4.28, it can be seen that there is a larger amount of heat that moves upwards towards the ridge when the thickness of the reflective air space is increased from 25 to 100 mm. In the attic space, it is obvious that the air temperature is much lower when the reflective air space increases from 25 to 100 mm. Hence, when the thickness of the reflective air space is increased from 25 to 100 mm, heat penetration through the reflective air space and the attic space decrease. Furthermore, due to the escalated buoyance force in gable roof pitch of 45°, the hot air inside the attic moves upwards and escapes through the ridge and hence massively reduces the ceiling temperature.

The thermal performance of thermal insulated pitched roof assembly incorporating reflective insulation and radiant barrier systems was investigated in this paper. The study was performed by means of 3D CFD simulation with the aid of FloEFD. The predicted CFD results were validated against experimental measurement that was conducted by Teh et al. (2017)—a researcher from SERI UKM. The predicted CFD results were in good agreement with the empirical measurement with a  $\pm 95\%$  confidence level, and a MAPE of 3.60%. The parameters investigated were the reflective air space thickness, roof pitch, and roof tile material. The thermal performance of the thermal insulated gable roof assembly was by evaluating the reduction of heat flux across the roof assembly, and by calculating the RSI value of the roof assembly. The experimental measurement and CFD simulation results have led to the following conclusions:

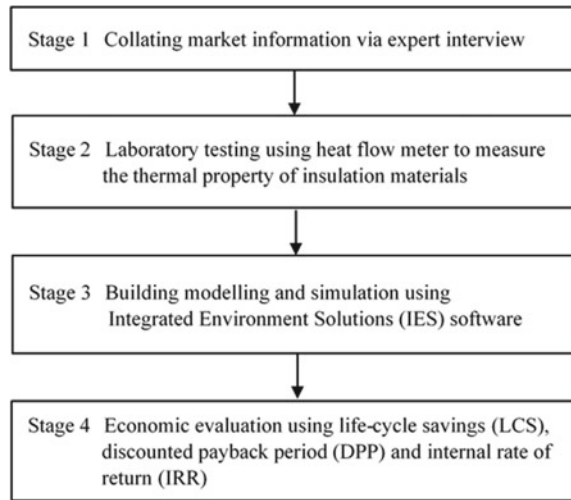
- For roof pitch of 30° the total predicted RSI value increases from 2.37 m<sup>2</sup>/W·K and 2.33 m<sup>2</sup>/W·K to 3.02 m<sup>2</sup>/W·K and 2.93 m<sup>2</sup>/W·K for clay tiles and concrete tiles respectively, with increasing the reflective air space thickness from 25 to 100 mm. For roof pitch of 45°, the total predicted RSI value increases from 3.09 m<sup>2</sup>/W·K and 3.04 m<sup>2</sup>/W·K to 3.81 m<sup>2</sup>/W·K and 3.74 m<sup>2</sup>/W·K for clay tiles and concrete tiles respectively, with increasing the reflective air space thickness from 25 to 100 mm. As the thickness of reflective air space increases from 25 to 100 mm, the decrease of heat gain increases from 79 to 88% and 84% to 87% for roof pitch of 30° and 45° respectively.
- Heat flux penetration through the reflective air space decreases as the thickness of reflective air space thickness increases from 25 to 100 mm as air flows from the eaves of the roof and escapes through the ridge.
- The RSI value of roof assembly with a roof pitch of 45° is significantly higher than roof assembly with a roof pitch of 30°. As the roof pitch is increased from 30° to 45°, the buoyancy effect increases in the attic space and reduces heat accumulation which results in lower heat flux penetration.
- The results also showed that there is only a slight difference in thermal resistivity of the roof assembly between clay tiles and concrete tiles. The overall behavior of heat transfer across the roof assembly was the same between the two materials of roof tiles.
- The CFD simulation predicts that roof pitch of 30°, the total RSI value passes the minimum RSI value of 2.5 m<sup>2</sup>/W·K when the reflective air space thickness is 50 mm and 60 mm for clay tiles and concrete tiles respectively for roof pitch of 30°. As for roof pitch of 45°, the RSI value passes the minimum regulated RSI value for all roof configurations.

#### 4.7 Techno-Economic Evaluation of Roof Thermal Insulation for a Typical Hypermarket in Malaysia

This subsection details the economic evaluation of various types of insulation implemented on a hypermarket. Briefly there are four methodological stages involved in order to achieve the objectives of this research. They are in chronological order, collating market information; laboratory measurement; building modelling and thermal simulation; and economic evaluation as shown in Fig. 4.29. Table 4.10 lists commonly used insulation materials, insulation systems, that are typically used for insulating sloped roofs in Klang Valley, Malaysia.

The cost of an insulation system includes the cost of material, labor charges and transportation fee for delivery within Klang Valley. This cost is used to calculate the investment cost of installing roof insulation for a hypermarket for our present study. The insulation system includes the insulation material and the air cavity for a typical hypermarket in Malaysia. For this study, eight common roof insulation systems (i.e. case 1–8 as shown in Table 4.11) were identified and investigated for a typical hypermarket roof in Malaysia. Each case of these 8 insulation systems is represented

**Fig. 4.29** Flow chart of the research activities



by the insulation materials used. Sample specimens of insulation materials for the eight examined cases were collected for laboratory testing to determine thermal resistance values.

#### **4.7.1 Thermal Resistance Evaluation of the Insulation Materials**

Table 4.11 below summarizes the results from heat flow meter measurements for the eight examined cases and the base case (case 0) in this study. Each case can be identified by the insulation material type which is commonly used for a typical hypermarket in Malaysia. Insulation system which includes low emissivity aluminum foil (typically  $\epsilon = 0.03$ ) insulation material and air cavity in the present study for each of the case 0–8. It can be seen that case 0 recorded the lowest RSI value and corresponding highest  $U$ -value when there is no insulation material to resist heat. On the contrary, case 8 using double big bubble foil achieved the highest RSI value and corresponding lowest  $U$ -value in comparison to the rest of the cases. However, this finding is only based on the technical aspect of the insulation system and may not be the best choice economically. Insulation system incorporating bubble foil insulation material as in the case 5–8 perform better in resisting heat as compared to case 1–4 which is using bulk materials.



**Table 4.10** Commonly used insulation materials, systems, and costing for a typical hypermarket roof in Klang Valley, Malaysia

Case	Insulation materials	Insulation system	Cost of insulation system (MYR/m <sup>2</sup> )
0	Base case (non-insulated roof)	Air gap of 80 mm	Nil
1	Rock wool + metallized foil	13.24 mm rock wool (after compressed) Foil 0.16 mm 50 mm lower air cavity	22.69
2	Rock wool + aluminium foil	12.46 mm rock wool (after compressed) Foil 0.16 mm 50 mm lower air cavity	28.44
3	Glass wool + metallized foil	4.46 mm glass wool (after compressed) Foil 0.16 mm 50 mm lower air cavity	17.01
4	Glass wool + aluminium foil	4.15 mm glass wool (after compressed) Foil 0.16 mm 50 mm lower air cavity	22.76
5	Small bubble aluminium foil	30 mm upper air cavity Foil 4 mm 50 mm lower air cavity	15.54
6	Big bubble aluminum foil	30 mm upper air cavity Foil 8 mm 50 mm lower air cavity	19.62
7	Bubble + foam foil	30 mm upper air cavity Foil 9 mm 50 mm lower air cavity	28.63
8	Double big bubble foil	30 mm upper air cavity Foil 16 mm 50 mm lower air cavity	29.59

**4.7.2 Building Modelling and Thermal Insulation Evaluation Using IESVE**

A 3D model hypermarket with area 15,607.46 m<sup>2</sup> (represents actual size of a hypermarket building found in Klang Valley) was designed and constructed in Integrated Environment Solutions—Virtual Environment (IES<VE> ) software. The model building of the hypermarket is shown in Figs. 4.30 and 4.31.

IES<VE> is a 3D building modelling and energy performance simulation software used to design energy efficient building. It is fully validated under a number of global standards including American Society of Heating, Refrigeration, and Air Conditioning Engineers (ASHRAE 140) and used by leading green rating systems

**Table 4.11** RSI value and corresponding *U*-value from heat flow meter measurement

Case	Insulation materials	RSI value m <sup>2</sup> ·K/W	<i>U</i> -value (1/R) W/m <sup>2</sup> ·K
0	Base case (non-insulated roof)	0.195	5.128
1	Rock wool + metallized foil	1.370	0.730
2	Rock wool + aluminium foil	1.841	0.543
3	Glass wool + metallized foil	0.946	1.057
4	Glass wool + aluminium foil	1.581	0.633
5	Small bubble aluminium foil	2.103	0.476
6	Big bubble aluminium foil	2.124	0.471
7	Bubble + foam foil	2.302	0.434
8	Double big bubble foil	2.529	0.395

**Fig. 4.30** Roof top view of an actual hypermarket (with GPS coordinates) (Source Google Map)



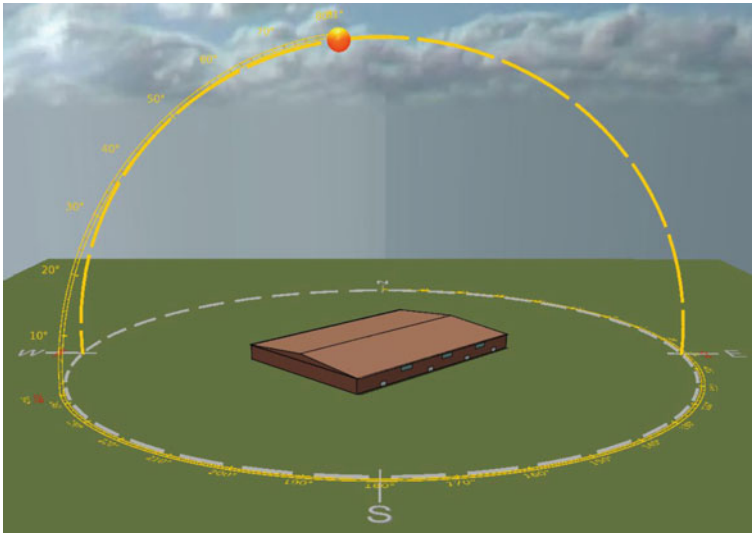


**Fig. 4.31** Model building of a hypermarket in this study (Source IES<VE> Integrated Software)

as well as national regulations for compliance purpose. Findings from Nikpour et al. (2013) revealed that the differences between experimental measurement and IES<VE> simulation results is not more than 10%, proving this software has enough validity to calculate the amount of heat gain in building. In addition, this software is one of the most up-to-date tools for dynamic simulation of energy consumption in building. In this study, our purpose of running the thermal simulation is to generate energy consumption when applying case 0–8 insulation system for the model hypermarket. To run the thermal simulation for this purpose, the main input data required by IES<VE> is  $U$ -value of insulation system obtained from Sect. 0. The weather file used in the simulation was based on the weather station nearest to the hypermarket (within 10 km radius) which is Subang Jaya weather station. In addition, daily profile for air-conditioning, lighting and equipment (i.e. freezer) operating hours and occupancy are set for the model hypermarket. Whole building simulations were performed for each case as shown in Table 4.12, where major building schedules are described.

Result from IES<VE> annual cooling energy consumption simulations performed for the hypermarket model are presented in Table 4.13. These simulations were performed for the base case scenario and under each examined building configuration cases.

It is apparent that with the use of thermal insulation system there are reductions in the cooling energy consumption. The reduction was computed by comparing the energy consumption for each case against the base case i.e. case 0. It is observed that more than 20% savings in cooling energy consumption can be achieved for all the examined cases. The highest percentage of savings i.e. 41% was attained when using double big bubble foil (i.e. case 8) as the insulation material. This corresponds to the highest RSI value achieved by the same material. The same correlation can be seen

**Table 4.12** Profiles set in IES<VE> for the model hypermarket

Type	Profile
Air-conditioning	00:00–10:00—only 30% of air-conditioning is switched on 10:00–22:00—100% of air-conditioning is switched on during the hypermarket operating hours 22:00–24:00—30% of air-conditioning is switched on
Freezer	00:00–24:00—all freezer is turned on 24 h to preserve the perishable foods
Lighting	00:00–09:00—no light is turned on as workers haven't arrive work 09:00–23:00—all lights are turned on 23:00–24:00—all lights are off after hypermarket closes and workers knock off work
Occupancy	<i>Weekend/public holidays</i> 00:00–08:00—hypermarket is empty 08:00–10:00—30% occupancy rate as workers start to report to work 10:00–22:00—occupancy rate gradually achieving 100% during the hypermarket operating hours 22:00–23:00—occupancy rate drops to 30% as shoppers leaving 23:00–24:00—hypermarket becomes unoccupied after workers knock off work  <i>Weekdays</i> 00:00–08:00—hypermarket is empty 08:00–10:00—30% occupancy rate as workers start to report to work 10:00–12:00—occupancy rate slowly achieving 100% as shoppers coming to shop for groceries 12:00–14:00—occupancy rate reaching 100% during lunch break 14:00–19:00—occupancy rate drops to 50% as consumers returning to work 19:00–21:00—shoppers start flocking into the hypermarket after office hours to have dinner or purchase groceries 21:00–23:00—occupancy rate drops to 30% as shoppers leaving 23:00–24:00—hypermarket becomes unoccupied after workers knock off work

with case 3 which uses glass wool together with metallized foil. This examined case achieved the lowest RSI value and correspondingly lowest percentage of reduction in energy consumption. If roof thermal insulation is installed energy consumption will be reduced. The higher the thermal resistance i.e. RSI value the lower the energy consumption. The aforesaid 2 hypothesis were supported by results shown in Table 4.13 and Fig. 4.32.

### 4.7.3 Economic Evaluation of the Thermal Insulations

The examined investments in this stage are for the case 1–8 of roof insulation system. As shown Fig. 4.33 each of the 8 cases of roof insulation system will be compared to the base case (case 0) scenario and only the investment cost i.e. money spent to add insulation system is considered in this economic evaluation. Annual savings is the

**Table 4.13** Annual cooling energy consumption and energy savings from simulation using IES

Case	Insulation materials	Annual cooling energy consumption (kWh)	Reduction of annual cooling energy consumption (kWh)	% Reduction of energy consumption
0	Base case (non-insulated roof)	256,805.70	–	–
1	Rock wool + metallized foil	183,074.30	73,731.40	29%
2	Rock wool + aluminum foil	163,891.80	92,913.90	36%
3	Glass wool + metallized foil	194,358.30	62,447.40	24%
4	Glass wool + aluminium foil	170,815.60	85,990.10	33%
5	Small bubble aluminium foil	158,270.60	98,535.10	38%
6	Big bubble aluminium foil	157,817.50	98,988.20	39%
7	Bubble + foam foil	154,378.00	102,427.70	40%
8	Double big bubble foil	150,520.80	106,284.90	41%

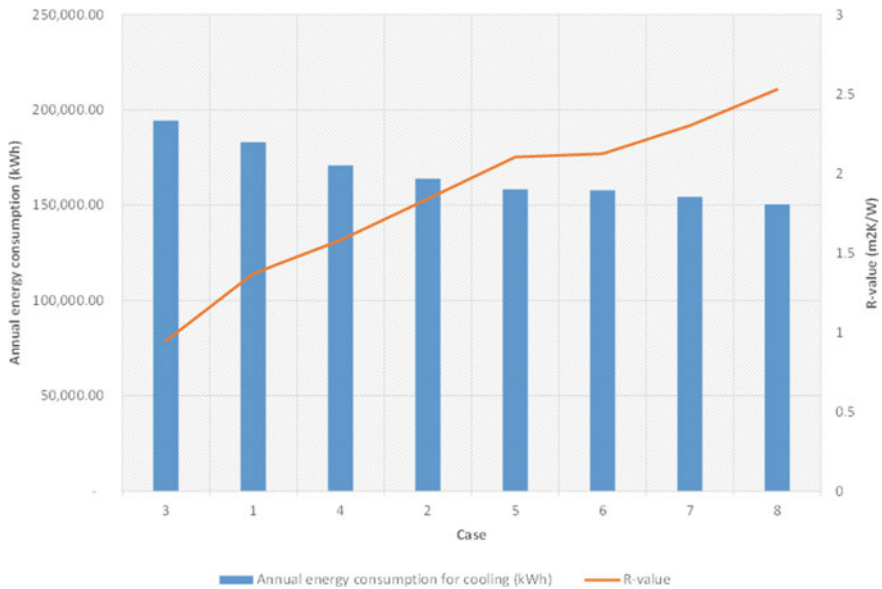
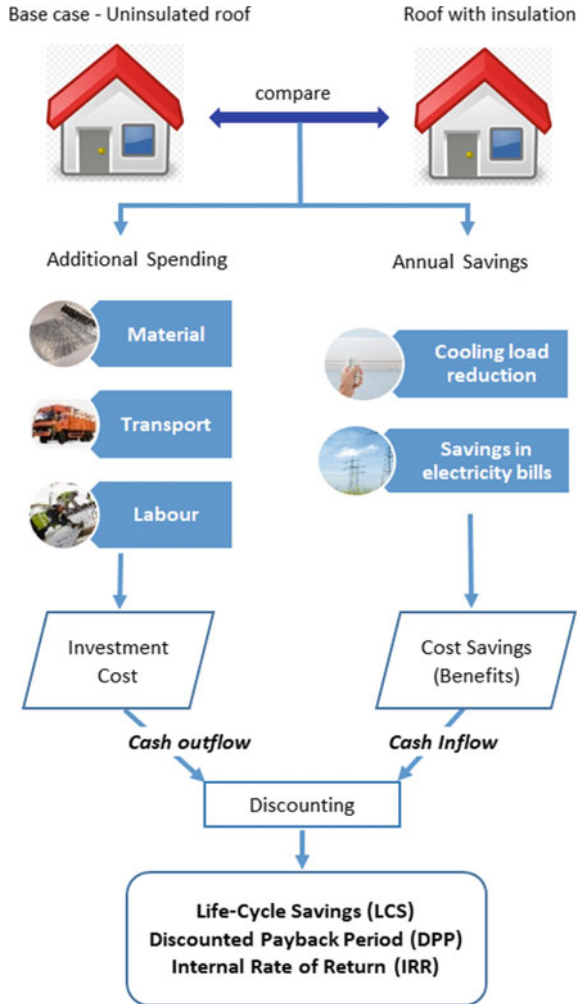


**Fig. 4.32** Annual energy consumption for cooling for the 8 examined cases against its RSI value

**Fig. 4.33** Economic evaluation methods



annual electricity savings resulted from cooling load reduction. This reduction is due to the improved thermal resistance after adding roof insulation system in relation to base case or non-insulated roof. The investment costs include the material, labour and transportation cost of installing roof insulation. The economic evaluation methods used to evaluate the 8 cases in this study are life-cycle savings (LCS), discounted payback period (DPP) and internal rate of return (IRR).

### 4.7.4 Life-Cycle Savings (LCS)

This method includes the sum of current investment costs and annual savings derived from installing roof insulation system over its lifetime in relation to the non-insulated roof. All the cost (cash outflow) and annual savings (cash inflow) over the insulation system lifetime will be discounted at a rate to convert the future cash flow of various time periods into money worth today or net present value. The formula for LCS calculation is:

$$LCS = \sum_{t=0}^n \frac{St - Ct}{(1 + d)^t} \tag{4.6}$$

where t is the time period in year; St and Ct is the annual savings (cash inflows) and investment cost (cash outflows) respectively for year t for the insulated roof compared with the base case; n is the roof insulation system lifetime usually in number of years; and d is the discount rate or cost of capital. LCS for each case studied in this paper is derived based on the assumptions that cash flows for the various time periods are spent or collected at the end of year t. It should be noted that although there is no actual money collected, the electricity bills saved resulted from installation of roof insulation system deemed to be cash inflow. The cost of capital, d is based on the average lending rate in Malaysia. As various roof insulation systems are compared in the present study, the best of them under this method of evaluation would be the one with the highest LCS value.

Table 4.14 presents the results of evaluation using LCS for all the 8 examined cases for a typical hypermarket in this study. Case 5 using small bubble aluminum foil recorded the highest LCS followed by case 6 which is using big bubble aluminum foil.

By ranking the 8 examined cases according to LCS as presented in Fig. 4.34, reveals that small bubble aluminum foil with the highest LCS is the most attractive insulation material economically. This means with every ringgit invested, using small bubble aluminum foil to insulate the roof of hypermarket will yield the highest

**Table 4.14** Results of economic evaluation using LCS

Case	Insulation materials	LCS (MYR)
1	Rock wool + metallized foil	51,368.85
2	Rock wool + aluminum foil	67,124.35
3	Glass wool + metallized foil	77,960.37
4	Glass wool + aluminum foil	117,695.76
5	Small bubble aluminum foil	299,375.60
6	Big bubble aluminum foil	238,189.09
7	Bubble + foam foil	116,482.18
8	Double big bubble foil	122,712.54

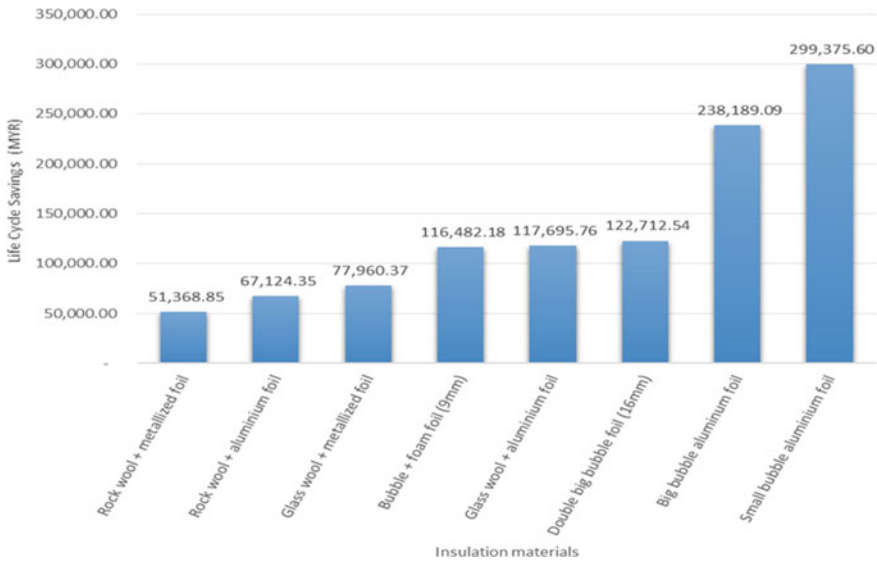


Fig. 4.34 Ranking of roof insulation systems according to LCS

savings. Big bubble aluminum foil becomes the second preferred option. On the contrary, insulating roof with rock wool + metallized foil is the least favored choice economically given the lowest LCS. This can be attributable to the higher initial cost of investment and the lower corresponding energy savings derived compared to other alternatives.

### 4.7.5 Discounted Payback Period (DPP)

This method determines the number of years that are required to recover the initial cash outflow of an investment. In this present study, the initial investment cost can be recouped through the electricity bills savings (cash inflow) that are expected after installing roof insulation system. The word ‘discounted’ simply means it takes into consideration time value of money like LCS where all cash flows are calculated to the present value. The formula for DPP calculation is:

$$DPP = (T - 1) + \frac{C0 - CumulativePVofcashflow(T-1)}{PVofcashflowT} \tag{4.7}$$

where  $T$  is the year in which the cumulative present value (PV) of cash flows from investment exceed the initial investment cost;  $(T - 1)$  is the year prior to  $T$ ; PV of cash flow  $T$  is the present value of net cash flow in year  $T$ ; Cumulative PV of cash



**Table 4.15** Results of economic evaluation using DPP

Case	Insulation materials	DPP (years)
1	Rock wool + metallized foil	16.75
2	Rock wool + aluminum foil	16.64
3	Glass wool + metallized foil	14.37
4	Glass wool + aluminum foil	13.87
5	Small bubble aluminum foil	7.60
6	Big bubble aluminum foil	9.85
7	Bubble + foam foil	14.84
8	Double big bubble foil	14.77

flow ( $T - 1$ ) is the cumulative present value of cash flow from investment at the end of year ( $T - 1$ ); and  $C_0$  represents the initial cost of investment.

Generally, if the DPP of an investment is less than the expected investment lifetime it is considered as cost effective. If alternative options are being compared, investment with the shortest payback period may be desired. However, this method of evaluation needs to be analyzed concurrently with LCS to give a more complete economic overview.

Examining the 8 insulation solutions using DPP again shows a similar finding. From Table 4.15 and Fig. 4.35 it is obvious that insulating hypermarket roof with small bubble aluminum foil enables the investment cost incurred to be recovered in

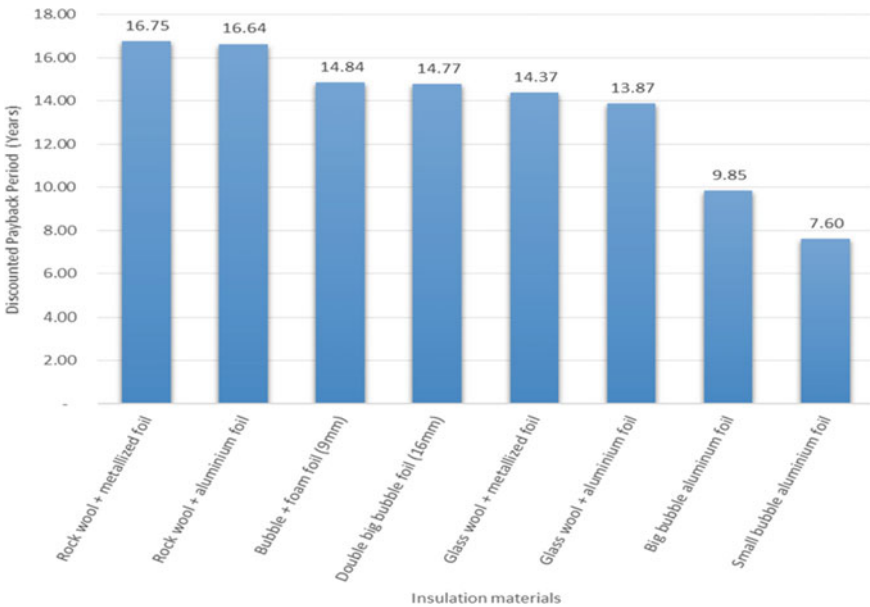


**Fig. 4.35** Ranking of roof insulation systems according to DPP

the shortest period i.e. 7.6 years. This indicates after 7.6 years of installation; this insulation system will generate profit in terms of energy savings in monetary form.

While big bubble aluminum foil takes approximately 10 years to breakeven, the remaining 6 insulation systems take more than 10 years with the longest about 17 years when using rock wool + metallized foil. Figure 7.12 also shows how fast an investment become profitable.

### 4.7.6 Internal Rate of Return (IRR)

IRR is an evaluation method to determine the rate of return earned on every money invested in each period of time in the entire evaluation time horizon. In other words, this method measures the yield or financial gains of an investment. IRR can be calculated by solving the discount rate,  $d$  when setting the PV of all cash flows of an investment equal to zero. Therefore, for our calculation in this present paper, simply set Eq. (4.6) to 0 as shown below:

$$\sum_{t=0}^n \frac{St - Ct}{(1 + d)^t} = 0 \tag{4.8}$$

The value  $d$  solved in Eq. (4.8) is the IRR. When evaluating each examined option using IRR, the general rule is to accept investments with IRR greater than the minimum required rate of return which in most cases is the cost of capital. In essence, investment that yield the highest IRR is the most attractive option.

By analyzing with the third evaluation method i.e. IRR, the results are presented in Table 4.16. All the 8 examined cases achieve IRR greater than the minimum required rate of return, 4.88% which is the cost of capital in this study. Hence, these investments can be pursued. However, if only one investment can be executed, the one that presents the highest IRR will be the best choice. Figure 4.36 shows ranking of the 8 examined insulation systems. It is apparent that small bubble aluminum foil produces the highest return i.e. 15.92%. It is about 2.5 times more profitable than

**Table 4.16** Results of Economic Evaluation using IRR

Case	Insulation materials	IRR (%)
1	Rock wool + metallized foil	6.41
2	Rock wool + aluminum foil	6.48
3	Glass wool + metallized foil	7.89
4	Glass wool + aluminum foil	8.25
5	Small bubble aluminum foil	15.92
6	Big bubble aluminum foil	12.22
7	Bubble + foam foil	7.57
8	Double big bubble foil	7.62

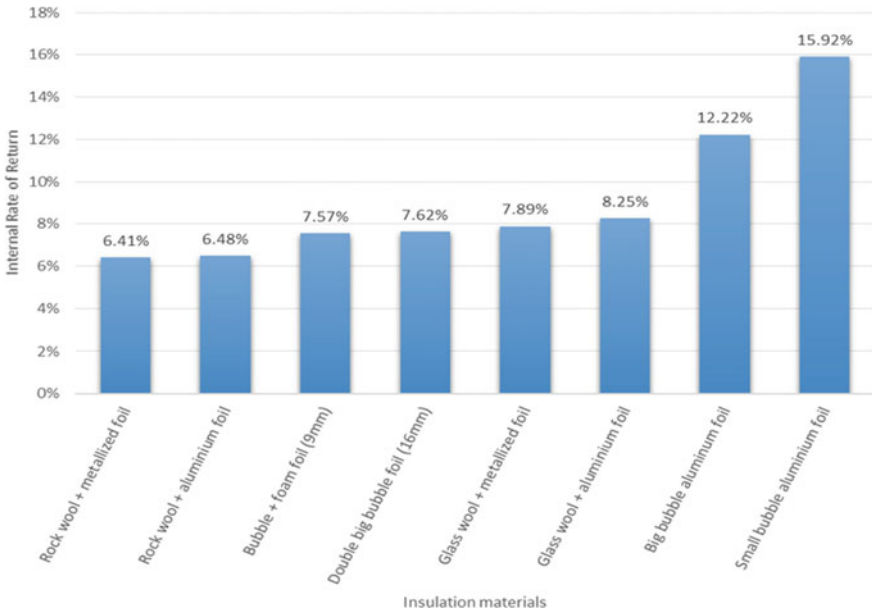


**Fig. 4.36** Ranking of roof insulation systems according to IRR

rock wool + aluminum foil. The second-best choice according to IRR is big bubble aluminum foil. IRR can also be used as a benchmark when sourcing capital for an investment. It represents the highest interest that the investor is willing to pay for financing the investment.

Three widely used economic evaluation methods which take into consideration the time value of money i.e. life-cycle savings, discounted payback period and internal rate of return have been used. Results from these three evaluations agreed quantitatively that choosing small bubble and big bubble aluminum foil as the thermal insulation solutions is the best and second best most cost-effective measures. Investing in these two solutions will each generate greater return while having shorter payback period relative to the other examined alternatives. However, there are bound to be uncertainty in the economic evaluation results by virtue of the variation in the parameters used in the calculation. In this regard, sensitivity analysis was conducted to ascertain the effect of changing key parameters i.e. cost of capital and lifetime period on the results of economic evaluations. Based on the analysis it becomes apparent that small bubble aluminum foil is the least affected by the changing cost of capital and lifetime period. This followed by big bubble aluminum foil as the next least sensitive option.

Although the commonly adopted thermal insulation materials in local market were studied in this paper, certain material may not comply with the local regulation requirements. For instance, Construction Industry Development Board (CIDB) of Malaysia requires the use and certification of insulation material that is fire resistant.

Hence, non-fire-retardant material will soon be phased out in the market. As stated in Sect. 1, the maximum thermal transmittance value ( $U$ -value) for a lightweight roof as in the case of hypermarket is  $0.4 \text{ W/m}^2\cdot\text{K}$ , small bubble and big bubble aluminum foils are slightly over this threshold. Insulating with double big bubble foil appeared to be the only option in this paper that achieved the  $U$ -value requirement in MS1525:2014.

## References

- Alzwayi, A. S., & Paul, M. C. (2014). Transition of free convection flow inside an inclined parallel walled channel: Effects of inclination angle and width of the channel. *International Journal of Heat and Mass Transfer*, *68*(2014), 194–202. <https://doi.org/10.1016/j.ijheatmasstransfer.2013.09.015>
- Ashhar, M. Z. M., & Lim, C. H. (2020). Numerical simulation of heat transfer in a roof assembly with reflective insulation and radiant barrier. *Building Simulation*, *13*(2020), 897–911. <https://doi.org/10.1007/s12273-020-0624-3>
- Baldinelli, G. (2010). A methodology for experimental evaluations of low-e barriers thermal properties: Field tests and comparison with theoretical models. *Building and Environment*, *45*(2010), 1016–1024. <https://doi.org/10.1016/j.buildenv.2009.10.009>
- Chua, S. C., & Oh, T. H. (2011). Green progress and prospect in Malaysia. *Renewable and Sustainable Energy Reviews*, *15*(2011), 2850–2861. <https://doi.org/10.1016/j.rser.2011.03.008>
- Craven, C., Garber-Slaght, R. (2011). *Reflective insulation in cold climates*. Technical Report TR 2011-01, (2011). Cold Climate Housing Research Center, p. 22. [https://www.insulationstop.com/resources/TR\\_2011-01\\_Reflective\\_Insulation\\_in\\_Cold\\_Climates.pdf](https://www.insulationstop.com/resources/TR_2011-01_Reflective_Insulation_in_Cold_Climates.pdf)
- Daouas, N. (2011). A study on optimum insulation thickness in walls and energy savings in Tunisian buildings based on analytical calculation of cooling and heating transmission loads. *Applied Energy*, *88*(2011), 156–164. <https://doi.org/10.1016/j.apenergy.2010.07.030>
- Dengan Kuasa, Government of Selangor Gazette, Malaysia, December 2012. <https://www.scribd.com/document/275093356/SELANGOR-UNIFORM-BUILDING-BY-LAWS-2012-SEL-P-U-142-2012-pdf>.
- Dylewski, R., & Adamczyk, J. (2011). Economic and environmental benefits of thermal insulation of building external walls. *Building and Environment*, *46*(2011), 2615–2623. <https://doi.org/10.1016/j.buildenv.2011.06.023>
- Florides, G. A., Tassou, S. A., Kalogirou, S. A., & Wrobel, L. C. (2002). Measures used to lower building energy consumption and their cost effectiveness. *Applied Energy*, *73*(2002), 299–328.
- Fricker, J. M., & Yarbrough, D. (2011). (2011) *Review of reflective insulation estimation methods* (pp. 14–16). 12th Conference of International Performance Simulation Association.
- Hassal, D. N. H. (1977). *Reflective insulation and the control of thermal environments*. St. Regis—ACI.
- IEA (2015). *Southeast Asia Energy Outlook 2015*. International Energy Agency, <https://www.iea.org/reports/southeast-asia-energy-outlook-2015>.
- Jim, C. Y. (2014). Air-conditioning energy consumption due to green roofs with different building thermal insulation. *Applied Energy*, *128*(2014), 49–59. <https://doi.org/10.1016/j.apenergy.2014.04.055>
- Kavousian, A., Rajagopal, R., & Fischer, M. (2013). Determinants of residential electricity consumption: Using smart meter data to examine the effect of climate, building characteristics, appliance stock, and occupants behavior. *Energy*, *55*(2013), 184–194. <https://doi.org/10.1016/j.energy.2013.03.086>

- Kumar, A., Ashutosh, S., & Sodha, M. S. (1989). Optimum distribution of insulation over various components of an air-conditioned building. *Building and Environment*, 24(1989), 169–178.
- KPKT (2017). *Kementerian Perumahan Dan Kerajaan Tempatan, Buletin Bandar* (pp. 1–10). Malaysian Government Bulletin publication. <https://www.kpkt.gov.my/index.php/pages/view/642>.
- Lee, S. W., Lim, C. H., & Salleh, E. (2016). Reflective thermal insulation systems in building: A review on radiant barrier and reflective insulation. *Renewable and Sustainable Energy Reviews*, 65(2016), 643–661.
- Michels, C., Lamberts, R., & Güths, S. (2007). Evaluation of heat flux reduction provided by the use of radiant barriers in clay tile roofs. *Energy and Buildings*, 40(2008), 445–451. <https://doi.org/10.1016/j.enbuild.2007.03.013>
- MS 2095 (2014). *Department of Standards Malaysia, MS2095 Radiant Barrier Building Materials, Department of Standards Malaysia*. <https://www.kisb.com.my/index.php?ws=ourproducts&cid=253422&cat=INSULATION-FOIL&subcat=Fire-Retardant-Radiant-Barrier-MS2095-2014>
- MS 1525 (2014). *Department of Standards Malaysia, MS1525:2014 Energy efficiency and use of renewable energy for non-residential buildings—Code of practice (Second revision)* (pp. 271–272). <https://doi.org/10.1002/9781118820186.ch15e>.
- Nikpour, M., Kandar, M. Z., & Mousavi, E. (2013). Empirical validation of simulation software with experimental measurement of self shading room in term of heat gain. *World Applied Sciences Journal*, 21(2013), 1200–1206. <https://doi.org/10.5829/idosi.wasj.2013.21.8.27>
- Pérez-Lombard, L., Ortiz, J., & Pout, C. (2007). A review on buildings energy consumption information. *Energy and Buildings*, 40(2008), 394–398. <https://doi.org/10.1016/j.enbuild.2007.03.007>
- Roels, S., & Deurinck, M. (2011). The effect of a reflective underlay on the global thermal behaviour of pitched roofs. *Building and Environment*, 46(2011), 134–143. <https://doi.org/10.1016/j.buildenv.2010.07.005>
- Saidur, R. (2009). Energy consumption, energy savings, and emission analysis in Malaysian office buildings. *Energy Policy*, 37(2009), 4104–4113. <https://doi.org/10.1016/j.enpol.2009.04.052>
- Stemmers, K., & Young Yun, G. (2009). Household energy consumption: A study of the role of occupants. *Building Research and Information*, 37(5–6), 625–637. <https://doi.org/10.1080/09613210903186661>
- Suehrcke, H., Peterson, E. L., & Selby, N. (2008). Effect of roof solar reflectance on the building heat gain in a hot climate. *Energy and Buildings*, 40(2008), 2224–2235. <https://doi.org/10.1016/j.enbuild.2008.06.015>
- Suruhanjaya Tenaga (2015). *Malaysia energy statistics handbook 2015*. Suruhanjaya Tenaga (Energy Commission). [https://www.st.gov.my/contents/publications/statistics\\_energy/MALAYSIA%20ENERGY%20STATISTICS%20HANDBOOK%202015.pdf](https://www.st.gov.my/contents/publications/statistics_energy/MALAYSIA%20ENERGY%20STATISTICS%20HANDBOOK%202015.pdf).
- Teh, K. S., Yarbrough, D. W., Lim, C. H., & Salleh, E. (2017). Field evaluation of reflective insulation in South East Asia. *Open Engineering*, 7(2017), 352–362. <https://doi.org/10.1515/eng-2017-0039>
- Teh Khar San, E., Yarbrough, D. W., Lim, C. H., Salleh, E. (2017). Reflective insulation for energy conservation in reflective insulation for energy conservation in South East. *International Conference on Energy Engineering*.
- Tong, S., & Li, H. (2014). An efficient model development and experimental study for the heat transfer in naturally ventilated inclined roofs. *Building and Environment*, 81(2014), 296–308. <https://doi.org/10.1016/j.buildenv.2014.07.009>
- UN (2016). United Nations Environmental Programme, *United Nations Environment Programme Environment for Development*, Annual Report, THE ENVIRONMENT IN NUMBERS, (2013). <https://wedocs.unep.org/bitstream/handle/20.500.11822/86071/-UNEP%202013%20Annual%20Report-2014UNEP%20AR%202013-LR.pdf?sequence=8&isAllowed=y>.
- Vijaykumar, K. C. K., Srinivasan, P. S. S., & Dhandapani, S. (2007). A performance of hollow clay tile (HCT) laid reinforced cement concrete (RCC) roof for tropical summer climates. *Energy and Buildings*, 39(2007), 886–892. <https://doi.org/10.1016/j.enbuild.2006.05.009>

- Vrachopoulos, M. G., Koukou, M. K., Stavlas, D. G., Stamatopoulos, V. N., Gonidis, A. F., & Kravvaritis, E. D. (2012). Testing Reflective insulation for improvement of buildings energy efficiency. *Central European Journal of Engineering*, 2(2012), 83–90. <https://doi.org/10.2478/s13531-011-0036-3>
- Warta Kerajaan (2012). Selangor Uniform Building (Amendment) (No.2) By-Laws 2012, NEGERI SELANGOR, Warta Kerajaan, DITERBITKAN.
- Yarbrough, D. W., Teh, K. S., Haw, L. C., Salleh, E., Mat, S., & Sulaiman, M. Y. (2016). Hybrid and reflective insulation assemblies for buildings. *Journal of Power and Energy Engineering*, 04(2016), 23–31. <https://doi.org/10.4236/jpee.2016.47004>
- Zhun, Y., Fung, B. C. M., Haghghat, F., Yoshino, H., & Morofsky, E. (2011). A systematic procedure to study the influence of occupant behavior on building energy consumption. *Energy and Buildings*, 43(2011), 1409–1417. <https://doi.org/10.1016/j.enbuild.2011.02.002>

# Chapter 5

## Development and Application Status of Glass Wool, Rock Wool, and Ceramic Wool



Zhaofeng Chen and Tianlong Liu

**Abstract** Inorganic insulations such as glass wool, rock wool, and ceramic wool have the characteristics of lightweight, low thermal conductivity, high sound-absorbing performance, chemical durability, and non-combustibility. Therefore, these inorganic insulation materials have been widely used as high-quality heat-insulating and sound-absorbing materials in transport systems, the nuclear power industry, and refrigeration as well as buildings. The centrifugal-blow process and flame-blow process are mainly used for the manufacturing of inorganic wools. The chemical composition, classification, fabrication technology, equipment, characteristics, and applications of glass wool, rock wool, and ceramic wool will be discussed in this chapter.

**Keywords** Glass wool · Rock wool · Ceramic wool · Fabrication technology · Fibrous insulation

### 5.1 Introduction

Glass wool, rock wool, and ceramic wool are all well-known insulation materials that exhibit remarkable material properties, including low bulk density, low thermal conductivity, corrosion resistance, and stable chemical properties—see: Marmoret (2016), Kudo et al. (2003), Zeng et al. (2002). These qualities have made glass wool, rock wool, and ceramic wool extremely desirable for pipe insulation, building insulation, industrial furnace insulation, and refrigerated transportation and medical hygiene applications. Inorganic insulation materials have unique advantages in fire-resistance, non-aging, low cost, and environmental benignity compared to organic insulation materials—as discussed in: Stazi et al. (2014), Chan-Ki et al. (2017).

---

Z. Chen (✉) · T. Liu  
College of Material Science and Technology, Nanjing University of Aeronautics and Astronautics,  
Nanjing 211106, P. R. China  
e-mail: [czf\\_msc@nuaa.edu.cn](mailto:czf_msc@nuaa.edu.cn)

T. Liu  
e-mail: [liu1061178707@nuaa.edu.cn](mailto:liu1061178707@nuaa.edu.cn)

The development of inorganic wool products has a history of more than 180 years. In 1840, the British discovered that melted slag could be sprayed to form fibers and thus began producing slag wool. In 1880, research on the properties and uses of slag wool led Germany and the United States to produce slag wool, which was then used and produced in other countries. From 1930 to 1950, large-scale production and application of inorganic wool insulation began.

Since the 1890s, the United States had used glass to make glass fibers, and in the 1930s, mechanical methods were used for its production. At that time, there were rod drawing and flat blowing methods. The fiber diameter was relatively thick, reaching more than 25  $\mu\text{m}$ . Due to the lack of imported asbestos during the First World War, Germany vigorously developed glass wool as a substitute. Because of glass wool's excellent heat and sound insulation properties, various countries rushed to develop similar products. In 1938, the first glass wool production line was constructed by Owens Corning Fiberglas Corporation. This marked the official beginning of the commercial development of glass wool. For over 80 years, glass wool has proven to be a safe and effective thermal insulation material for residential, commercial, and industrial applications. The low production volume of the rod drawing method was not enough to meet the high demand, so a new processing method was introduced. In 1956, Saint-Gobain in France successfully developed the centrifugal blow method (the TEL method) and sold licenses in more than a dozen countries.

At the present time, resource-saving development models are getting more attention due to the energy crisis. Building energy consumption accounts for more than one-third of the total world-wide energy consumption. Low-carbon buildings have gradually become a mainstream objective in the international construction industry to reduce building energy consumption. More importantly, the economic and social benefits are significant for the promotion of high-quality and highly efficient inorganic insulation materials. The prospects for the application of inorganic insulation materials are promising. Glass wool, rock wool and ceramic wool insulations will continue to play an important role in energy conservation and environmental protection.

## 5.2 Raw Materials and Chemical Composition

Glass wools, rock wool, and ceramic wool are man-made fibers, which are mainly composed of silicate, and small amounts of other elements. Glass wool is a cotton-like inorganic fiber material made by fiberizing molten glass. The raw materials for glass wool are mainly natural ores like quartz sand, dolomite, and pyrophyllite with small amounts of soda ash and borax. The chemical compounds in glass wool include  $\text{SiO}_2$ ,  $\text{Al}_2\text{O}_3$ ,  $\text{CaO}$ ,  $\text{MgO}$ , alkali metal oxides, and  $\text{B}_2\text{O}_3$ .

The impurities contained in glass wool are mainly slag balls, which greatly affect quality. Slag ball is a general term for non-fibrous glass in glass wool insulation. There are many reasons for their occurrence, such as insufficient combustion-chamber temperature, air injection speed, or improper gas to air ratio.



The  $\text{SiO}_2$  content in glass wool accounts for more than 60% of the total mass and constitutes the main body of the product.  $\text{SiO}_2$  reduces the thermal expansion coefficient of the glass and improves its thermal stability, chemical stability, heat resistance, hardness, mechanical strength, viscosity, and ultraviolet light transmission.  $\text{Al}_2\text{O}_3$  increases the viscosity of the glass reduces its crystallization tendency, improves the chemical and thermal stability, mechanical strength, hardness, refractive index of the glass, and reduces the corrosion of the glass to refractory materials. The main function of  $\text{CaO}$  in glass is as a stabilizer, which increases the chemical stability and mechanical strength of the glass. However, at high  $\text{CaO}$  concentration, the glass's crystallization tendency will increase, and products become brittle. Therefore, the content of  $\text{CaO}$  should not exceed 12.5%—see: Zhou (2012).

Viscosity is a characterization of the fluid's internal friction, which is determined by the nature of the fluid-structure, so it is the external manifestation of the internal structure of the fluid. At high temperatures,  $\text{CaO}$  reduces the viscosity of molten glass and promotes melting and clarification of the glass. The viscosity, however, increases rapidly when the temperature decreases, causing difficulty in molding.

$\text{MgO}$  partially replaces  $\text{CaO}$  in soda-lime silicate glass and slows down the hardening speed of the glass to improve the forming of glass fibers. In addition,  $\text{MgO}$  can reduce the tendency and speed of crystallization, increase the high-temperature viscosity of the glass, and improve the chemical stability and mechanical strength of the glass. Alkali metal oxides ( $\text{Na}_2\text{O}$ ,  $\text{K}_2\text{O}$ ) are good fluxing agents that reduce glass viscosity and help it melt easily. However, they will also increase the thermal expansion coefficient of the glass and reduce its thermal and chemical stability, along with the mechanical strength, so the amount generally should not exceed 18%—Zhou (2012).

$\text{B}_2\text{O}_3$  can reduce the thermal expansion of the glass, improve the thermal and chemical stability, refractive index, mechanical properties, and gloss of the glass—Jensen (2009). It can reduce the viscosity of the glass melt at high temperatures, accelerate the melting and clarification, and reduce the crystallization tendency of glass.

The raw materials for rock wool are mainly basalt and dolomite. The chemical composition of rock wool includes  $\text{SiO}_2$ ,  $\text{Al}_2\text{O}_3$ ,  $\text{CaO}$ ,  $\text{MgO}$ ,  $\text{Fe}_2\text{O}_3$ ,  $\text{Na}_2\text{O}$ , among which  $\text{SiO}_2$ ,  $\text{Al}_2\text{O}_3$ ,  $\text{CaO}$ ,  $\text{MgO}$  are the main components.  $\text{SiO}_2$  and  $\text{Al}_2\text{O}_3$  form the basic structure, while  $\text{CaO}$  and  $\text{MgO}$  can adjust and lower the melting point, but it is not conducive to fiber formation—Alves et al. (2015).

Ceramic wool generally refers to an aluminum silicate insulation consisting of high-purity clay clinker, alumina powder, silica powder, and chromite sand. The chemical compositions of ceramic wool are mainly  $\text{SiO}_2$  and  $\text{Al}_2\text{O}_3$ . The addition of  $\text{ZrO}_2$ ,  $\text{Cr}_2\text{O}_3$ , and  $\text{B}_2\text{O}_3$  can effectively suppress crystallization and grain growth of glassy aluminum silicate when added at high temperatures. The preceding compounds also reduce the linear shrinkage of ceramic wool at high temperatures and increase its application temperature. Ceramic wool has higher temperature resistance than glass wool or rock wool.

### 5.3 Classification

Depending on the classification basis (e.g., by origin, chemistry and structure, physical form and morphology, or application), glass wool, rock wool, and ceramic wool have multiple classifications. As shown in Table 5.1, glass wool can be categorized as alkali-free, medium-alkali, or high-alkali glass wool depending on the concentration of alkali metal oxides. The classification of ceramic wool according to chemical composition is shown in Table 5.2. Since the hazard classification of man-made vitreous fibers by IARC in 1988, glass wool and rock wool compositions with increased bio-solubility have been rapidly developed. It had been demonstrated in some vivo research that the fibers with low alumina content and high boron content have high bio-solubility. Most insulation wools currently being produced and marketed within the European Union and other European countries consist of fibers

**Table 5.1** Classification of glass fiber with different alkali metal oxide content

Classification	Basic situation	Characteristic	Application field
E-glass fiber	Alkali-free glass R <sub>2</sub> O content <0.5 wt.%	High temperature resistance, high strength, strong electrical insulation, poor resistance to inorganic acid corrosion	Glass fiber reinforced plastics materials, electrical insulation materials
C-glass fiber	Medium-alkali glass 11.5 wt.% < R <sub>2</sub> O content <12.5 wt.%	Low price, high temperature resistance, acid resistance, poor electrical insulation, low mechanical strength, poor water resistance	Acid filter cloth, Corrosion-resistant utensils
A-glass fiber	High-alkali glass R <sub>2</sub> O content >15 wt.%	Poor strength, poor water resistance, good acid resistance	Battery separator, Acid mist filtration, electroplating bath

Note R refers to K and Na

**Table 5.2** Classification of ceramic wool with different chemical composition

Ingredient type	Al <sub>2</sub> O <sub>3</sub>	Al <sub>2</sub> O <sub>3</sub> + SiO <sub>2</sub>
Normal (C)	≥40.0 wt.%	≥95.0 wt.%
Standard (S)	≥ 43.0 wt.%	≥97.0 wt.%
High-purity (P)	≥43.0 wt.%	≥98.5 wt.%
High-aluminum (A)	≥52.0 wt.%	≥98.5 wt.%
Zirconium-containing (Zr)	(Al <sub>2</sub> O <sub>3</sub> + SiO <sub>2</sub> + ZrO <sub>2</sub> ) ≥ 99.0 wt.%, (ZrO <sub>2</sub> ) ≥ 15.0 wt.%	
Chromium-containing (Cr)	(Al <sub>2</sub> O <sub>3</sub> + SiO <sub>2</sub> + TCr <sub>2</sub> O <sub>3</sub> ) ≥ 99.0 wt.%, (TCr <sub>2</sub> O <sub>3</sub> ) ≥ 1.2 wt.%, Cr(VI) ≤ 0.1 wt.%	

with high bio-solubility as required by regulations within the European Union. This development had been motivated by the knowledge that the potential hazard of a given fiber type was directly related to the long fibers ability to persist in lung tissue. The introduction of wools with high bio-solubility had increased the safety margins in manufacturing and use of these fibrous insulations—Alves et al. (2015). German regulatory bodies (TRGS 905) have developed a carcinogenicity index denoted  $K_i$  (also termed KI). The index is based purely on the chemical composition of fibers and is equal to the algebraic sum of the percentages by weight of oxides in fiber as follows—Moore et al. (2002):

$$K_i = \sum (\text{Na}_2\text{O} + \text{K}_2\text{O} + \text{CaO} + \text{MgO} + \text{B}_2\text{O}_3 + \text{BaO}) - 2(\text{Al}_2\text{O}_3). \quad (5.1)$$

In use, fibers with  $K_i \geq 40$  are considered to have low bio-persistence, while those with  $K_i < 40$  require further testing to assess bio-persistence or toxicity.

The huge number of fiber compositions reported in patents, scientific, and industrial literature can be categorized as vitreous silicates, as illustrated by the sample of fiber compositions provided in Table 5.3—see: Moore et al. (2002). In the table, the fiber compositions are arranged in descending order of the network forming component.

## 5.4 Fabrication Technology

Since the development of glass wool in the 1930s, manufacturing mainly relied on the rod drawing or flat blowing process, both with low-production capacity. In addition, the diameter of the fiber monofilament produced was tens or even hundreds of microns. In 1958, the development of the pool kiln wire drawing technology created conditions for large-scale glass wool production. The pool kiln is a kind of glass melting furnace in which raw materials are added from one end and after melting, clarification, and cooling, the molten glass flows out from the other end to form fibers. In the 1970s, the world energy crisis promoted the development of glass wool because of its light weight, high operating temperature, and excellent thermal insulation properties. It prompted fiber preparation methodologies, such as steam blow, flame blow, micro-cyclone, and centrifugal blow processes.

Nowadays, the fabrication technologies for glass wool, rock wool, and ceramic wool are mainly based on the centrifugal blow process and the flame blow process. The diameter of fibers is related to the composition and fiber-forming parameters, especially the temperature, cooling time, and atmospheric conditions during the fiber-forming process. The production technology for microfiber glass wool from Germany's Lauscha company and France's Saint Gobain company was internationally recognized as relatively advanced, leading the industry. Both used the centrifugal-blow process and flame-blow process.

Table 5.3 Selected inorganic wool compositions arranged by SiO<sub>2</sub> composition

	Generic other name	SiO <sub>2</sub>	Al <sub>2</sub> O <sub>3</sub>	CaO	MgO	Na <sub>2</sub> O + K <sub>2</sub> O	Fe <sub>2</sub> O <sub>3</sub> + Fe	B <sub>2</sub> O <sub>3</sub>	Other
IV	Glass	73	2	5.5	3.5	16	-	-	-
X7753	Glass	65.7	0.5	5.7	3.0	15.8	-	8.0	-
A	Glass	65.0	1.9	7.4	2.6	16.8	-	4.7	1.1 (P <sub>2</sub> O <sub>5</sub> )
II	Glass	65.0	4.0	14.0	3.0	8.5	-	5.5	-
M	Glass	65.4	4.5	6.0	3.5	10.0	-	5.0	-
753	Glass	63.5	4.0	5.5	2.5	15.0	-	5.5	-
MMVF 11	Glass	63.4	3.9	7.4	2.8	16.7	-	4.5	-
B	Glass	62.0	5.0	3.0	1.0	9.5	-	9.5	4 (Ba) 2.3 (Zn)
C	Glass	61.7	1.0	7.2	2.9	16.7	-	9.2	1.1 (P <sub>2</sub> O <sub>5</sub> )
B(B-01/09)	Glass	61.5	0.3	15.6	3.0	16.2	-	3.2	-
X7484	Glass	60.7	3.8	7.9	3.7	14.8	-	5.1	2 (Ba)
G	Rock	60.1	0.4	18.8	8.3	5.7	6.1	-	-
X7779	Glass	60.1	8.1	9.2	4.3	15.3	-	1.8	-
V	Glass	59.5	5.0	-	-	14.5	-	7.0	8(ZrO <sub>2</sub> )2(TiO <sub>2</sub> )
III	Glass	59.0	4.5	16.0	5.5	11.5	-	3.5	-
363	Glass	58.5	5.0	-	-	7.5	-	7.5	4 (Zr)
MMVF 33 (475 glass)	Glass	58.4	6.0	1.8	-	12.6	-	11.0	4.9 (Ba) 4.9 (Zn)
X-607	New	58.3	1.3	38.7	0.4	-	-	-	0.4 (P <sub>2</sub> O <sub>5</sub> )
MMVF 10	Glass	57.5	5.1	7.5	-	16.1	-	8.8	-
475	Glass	57.5	5.5	2.5	-	10.5	-	10.5	5 (Ba) 4 (Zn)
H	Rock	57.2	3.9	25.5	9.9	-	-	-	2.9 (P <sub>2</sub> O <sub>5</sub> )

(continued)

Table 5.3 (continued)

	Generic other name	SiO <sub>2</sub>	Al <sub>2</sub> O <sub>3</sub>	CaO	MgO	Na <sub>2</sub> O + K <sub>2</sub> O	Fe <sub>2</sub> O <sub>3</sub> + Fe	B <sub>2</sub> O <sub>3</sub>	Other
F	Rock	56.3	3.2	26.1	6.4	3.9	-	-	2.9 (P <sub>2</sub> O <sub>5</sub> )
MMVF 32 (E-glass)	Glass	55.2	14.8	18.7	3.3	-	-	7.3	-
I	Glass	54.5	14.5	22.0	-	-	0.5	8.5	-
Rockwool 1	Rock	52.9	6.5	30.3	-	3.9	2.5	-	0.5 (Ti)
RCF 2	Ceramic	50.0	35.0	-	-	-	-	-	15 (Zr)
RCF 1	Ceramic	47.7	47.0	-	-	0.7	1.0	-	2.1 (Ti)
Rockwool 2	Rock	47.5	13.0	16.0	-	3.6	7.5	-	1.5 (Ti) 0.5 (Mn)
Diabase 2	Rock	46.9	13.4	16.9	10.3	3.2	6.6	-	1.8 (Ti)
L	Rock	46.3	13.5	10.0	9.1	4.5	13.2	-	2.6(Ti)0.4(P <sub>2</sub> O <sub>5</sub> )
MMVF 21	Rock	46.2	13.8	17.0	9.5	3.8	6.2	-	3 (Ti) 0.4 (P <sub>2</sub> O <sub>5</sub> )
Rockwool 3	Rock	45.5	13.4	10.8	-	2.5	14.0	-	1.99 (Ti)
Diabase 3	Rock	44.3	12.5	11.5	10.5	5.4	11.1	-	2.4 (Ti)
Diabase 1	Rock	42.9	12.6	29.7	6.8	1.9	2.2	-	2.5 (Ti)0.7 (Mn)
Slagwool 1	Slag	41.0	11.8	40.0	-	0.6	0.9	-	0.4(Ti) 0.6 (Mn)
Darkwool 1	Slag	41.0	5.1	19.7	7.5	1.4	21.1	-	-
Slagwool 2	Slag	40.6	12.5	37.5	-	1.5	1.0	-	0.4 (Ti)
Darkwool 2	Rock	39.1	7.4	31.9	8.9	1.1	9.0	-	0.5 (Mn)
MMVF 34 (HT stone)	Rock	38.9	23.2	15.0	9.6	2.7	6.7	-	-
MMVF 22	Slag	38.4	10.6	38.0	9.9	0.9	-	-	(Mn)

### 5.4.1 Centrifugal-Blow Process

The current centrifugal blow process system was developed on the basis of the TEL centrifugal technology invented by Saint-Gobain in France in the 1950s. This process has low energy consumption, large capacity, and high quality—see: Mabru and Levecque (1964). Figure 5.1 contains a schematic diagram of the TEL process.

In 1964, Johns Manville Company, in the U.S., invented the annular combustion nozzle system, which transformed the centrifugal process into a centrifugal blow process—Stelmah (1968). After the glass liquid enters the centrifugal disk from the inlet, it is centrifuged out through the pores on the sidewall of the centrifugal disk. Meanwhile, a ring-shaped combustion nozzle is used instead of a high-frequency current. The gas and air are injected in the pipe, followed by mixing and burning at the open end of the ring nozzle that heats and stretches the fibers thrown out of the sidewall of the centrifugal disc. The drawing temperature is limited due to the gas mixing in the pipeline; thus, combustion flames cannot be arranged in an ideal annular shape, resulting in the larger fiber diameter distribution range of 8–20  $\mu\text{m}$ .

In 1981, the U.S. Owens Corning Company invented the centrifugal blow secondary drafting process to further refine the fiber diameter—see: Guffey and Schultz (1981). The molten glass enters the centrifugal disk and is spun out through the pores of the sidewall. The gas and air are premixed in the pipeline, then burned in the combustion chamber to form a high-temperature and low-speed airflow, heating the fibers thrown from the centrifugal disk. Finally, the fibers are stretched by the annular airflow, and glass wool with an average diameter of 7  $\mu\text{m}$  is obtained.

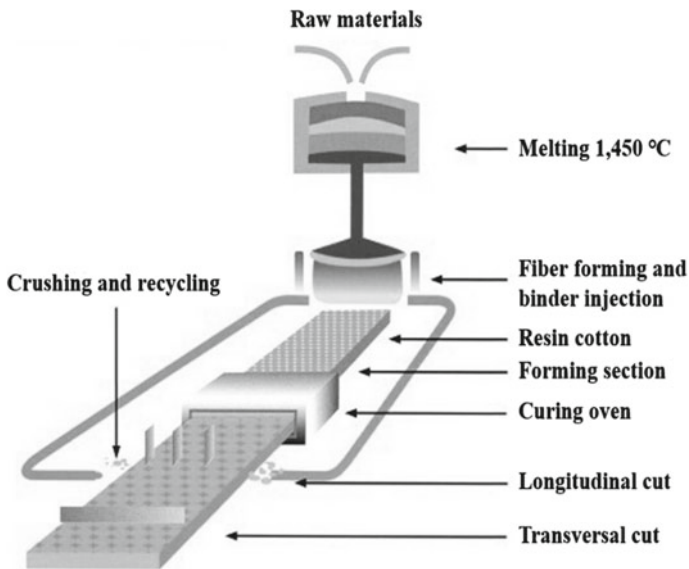


Fig. 5.1 Schematic diagram of the Saint-Gobain TEL

In 2001, Johns Manville Company adopted the internal heating centrifugal disc and high-temperature high-speed air flow in the combustion chamber to further optimize the centrifugal blow secondary drafting process—see: Baker and Smalley (2001). The upper part of the centrifugal disc is designed with an airflow channel that can be heated vertically and obliquely to ensure a relatively stable forming viscosity of the glass liquid in the centrifugal disc. The outlet of the combustion chamber outside the centrifugal disc is designed as a slit type. The primary fibers thrown out by the centrifugal disk are subjected to a secondary drawing process with high temperature and high-speed airflow, where the average fiber diameter could be around 5  $\mu\text{m}$ .

In 2011, Saint Gobain adopted a central feed distributor to further refine the fiber—Letourmy et al. (2016). The molten glass is introduced into the distributor with openings on the sidewall. The distributor rotates at high speed to distribute the molten glass to the centrifugal disk, and then spins it out through the pores on the side wall of the centrifugal disk to form fibers. The fiber diameter is reduced after stretching by the high annular temperature, high-speed airflow and the cooling airflow.

There are four main systems in the centrifugal production process: raw material system, melting system, fiber-forming system, and combustion system. First, the raw materials are mixed and moved to the furnace for high-temperature melting and homogenization. The molten material flows out through the platinum–rhodium alloy drain plate into the centrifuge. The molten material flows through small holes in the sidewall due to high centrifugal forces and forms a thin stream of fluid. It is then further stretched and cut under high-speed and high-temperature flame blow in the combustion chamber to form fibers of a certain length—as discussed by Li et al. (2012a). The glass wool produced through this technique is more uniform and finer than earlier products. There are no slag balls, and decomposed toxic gases, and mixing with the binder is improved. The diameter of the glass wool produced is generally about 2.5–8  $\mu\text{m}$ , which is made possible by controlling the rotation speed of the centrifuge and the diameter of the secondary drawing of the melt trickle. The centrifugal blow process has a promising edge because of its high output, low energy consumption, uniform fiber diameter, and continuous production. A diagram of the centrifugal injection process is shown in Fig. 5.2. A schematic diagram of glass wool centrifugal blow process is depicted in Fig. 5.3.

### 5.4.2 Centrifugal Rotation Process

A schematic diagram of the centrifugal rotation process for rock wool is shown in Fig. 5.4. The melt flowing out of the furnace flows to the 1# roll through the chute. The primary function of the 1# roll is to control the working state of the melt on the subsequent rollers and the dispersion of the melt, forming very little fiber. The high-speed rotation of the roller produced centrifugal force and the melt is partially dispersed. The melt is then moved to the second roller along the tangential direction.

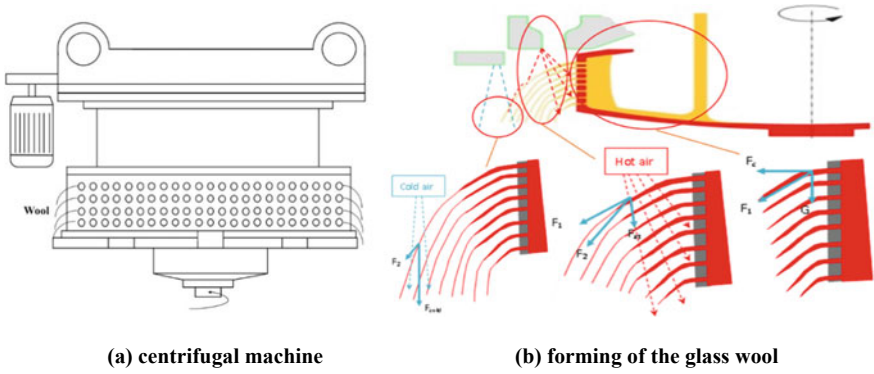
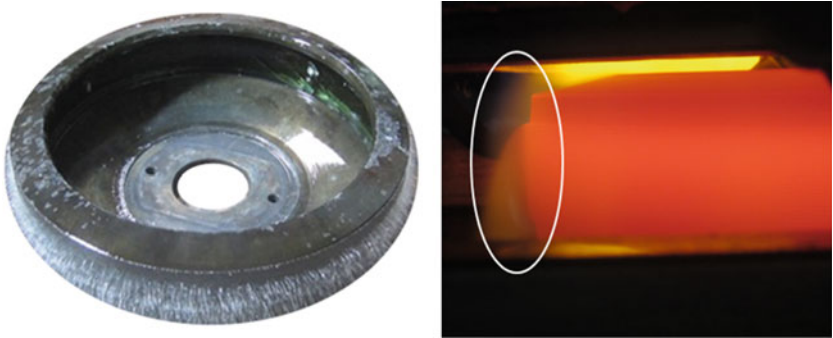


Fig. 5.2 Schematic diagram of centrifugal blow process



(a) Primary wool with the centrifugal disc (b) Secondary wool beside the centrifugal disc

Fig. 5.3 Schematic diagram of glass wool centrifugal blow process

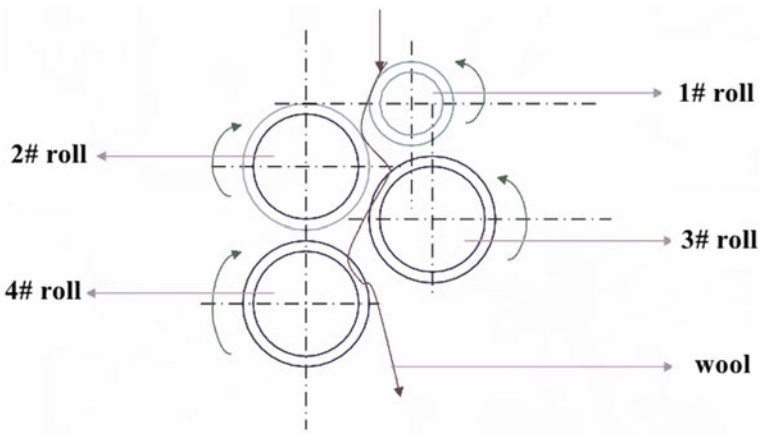


Fig. 5.4 Schematic diagram of rock wool centrifugal blow process



The temperature of the melt on the surface of 2# roll dropped due to the accelerated centrifugal effect of 1# roller. These factors produced greater adhesion and increased useful surface area by reducing its thickness, which is easily accomplished. As the surface area of the melt increases, the cooling speed and viscosity of the melt also increase, which results in unfavorable conditions for wool formation. Because of these reasons, the speed of the 2# roller needs to be increased. The melt without cotton formation on the 2# roller is dispersed and sent to 3# roller for further centrifugal dispersion. The melt enters the 3# roller, and the viscosity increases due to the further decrease in temperature, and the 3# roller has a higher speed than the 2# roller. Simultaneously, the 3# roller had a more suitable wool melt viscosity and the highest wool forming rate. The speed of the 4# roller is higher, and the 3# roller highly disperses the melt that is not spun into fibers on the 3# roller. The further decrease in temperature increased the viscosity increased with further reduction in temperature, but the speed of 4# roller is high, which further centrifuged the melt into wool. At the same time, the compressed air is blown horizontally from the centrifugal roll to let the rock wool out.

### 5.4.3 Flame Blow Process

During the Second World War, the United States began to develop ultra-fine flame glass wool to replace asbestos as a filter material. In the mid-1940s, Owens Corning invented the flame blow process to overcome the shortcomings of the steam blow process, such as thick diameter, short length, and high impurity content. As compared to the centrifugal blow process, the flame blow process consisted of simple equipment and was cost-efficient. The microfibers produced by the flame blow process had finer diameter than the steam blow product. However, it also has the disadvantages of high energy consumption, relatively poor operating environment, and large fiber diameter dispersion, which is a main challenge for their future development—see: Zou et al. (2020).

In the case of glass wool, the raw materials are first moved to the furnace and are melted into a molten state at 1400 °C. The molten glass then flows through an opening in the platinum–rhodium alloy drain plate or nickel–chromium alloy drain plate to form glass fiber. The glass microfibers are then formed under high temperature and high-speed flame blowing. Finally, it is collected on the mesh belt to form a cotton felt. Like the centrifugal blow process, the flame blow process also has a high-temperature and high-speed flame to stretch the primary glass fiber. This process can successfully refine the fiber diameter and reduce the impurity content up to 4%. The fiber length, however, is still relatively short. The diameter of prepared fibers varies in the range of 0.1–6 μm due to the frequent changes in parameters such as manual drawing, wire discharging, flame temperature, and air flow. At present, the average diameter of glass microfibers produced by flame blow process can be 0.5 μm or less.

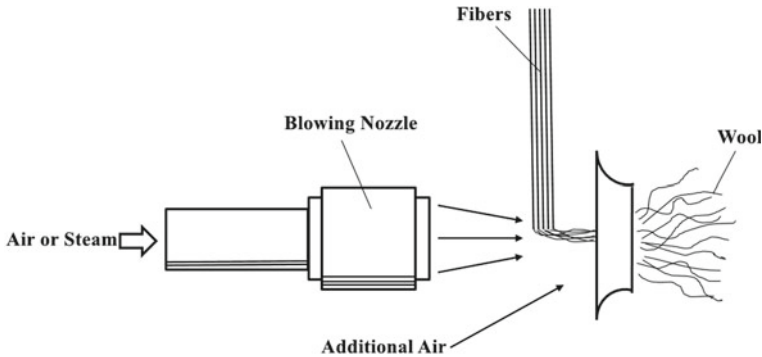


**Fig. 5.5** Schematic diagram of flame blow process

In the early 1950s, Johns Manville started to optimize the flame injection method to produce ultra-fine glass wool technology and successfully prepared 100% glass fiber paper for heat insulation, sound absorption, and filter materials. Germany also began to actively research glass wool preparation technology to replace asbestos after the Second World War. The Bayer company in Germany began to use a flame blow process to prepare glass wool in 1950. In the 1980s, the Johns Manville Company and the Evanite Company produced large quantities of ultra-fine glass wool products with diameters of 1.5–4.0  $\mu\text{m}$  using the flame blow process. The combined output accounted for more than 70% of the total output of the United States at that time, and the technology ranked the world leading position. But the energy consumption was still high and production capacity was low. Figure 5.5 shows the schematic diagram of flame blow process.

## 5.5 Centrifugal Equipment

The United States broke through the full-automatic control technology of centrifugal blow equipment first in 1967, resulting in the continuous large-scale production of centrifugal blow glass wool products. The energy consumption was much lower than the traditional steam and flame blow processes. The automatic feeding equipment included a mixing batching system and automatic feeding system, and it was an essential part of the production line. Automated feeding equipment improved the accuracy of batching and feeding speed, the safety and reliability of the raw material supply system, labor productivity and product quality. The feeding system was composed of a receiving hopper and conveying machinery. It could be used for receiving and transporting all kinds of raw material ores to expedite the classification and storage of raw materials. It also had the advantages of heavy load bearing, stable operation, and continuous conveying of materials.

In 2017, Saint-Gobain developed a new type of equipment for melting glass, that included a furnace equipped with electrodes in contact with the mass of vitrifiable materials. The furnace included a side opening connected to a feeder channel for the molten glass, a removable barrier dipping into the glass at or before the opening. A vertical plane passing through the upstream face of the barrier touches the biggest horizontal circle which could be inscribed downstream in the furnace, barrier excluded, the biggest circle being at the height of the highest side of the bottom of the channel. The device delivered a glass of good quality which could feed a fiberizing device—Clatot et al. (2017).

A centrifugal fiberizer is the main equipment of the centrifugal blow process, which determines the fiber quality, yield, and spray quality—Li et al. (2012b). The centrifuge consists of a refining furnace, discharging mechanism, fiber discharging mechanism, rotating drum, and rotating motor. It is also an important element of equipment to be maintained in the centrifugal blow process and an important area for improving the quality of product from the centrifugal blow process. The molten liquid flows out of the leakage plate at the end of the high temperature furnace and enters the centrifugal fiberizer. The melt ejected from the small holes by centrifugal force to form primary fibers when rotated at high speed and temperature. The primary fibers were stretched again through the gas of the annular combustion chamber to form the secondary wool. Figures 5.6 and 5.7 show the centrifuge fiberizer for glass wool and a four-roll high-speed centrifuge fiberizer for rock wool.

The working environment of the centrifugal fiberizer required strong resistance to high temperature creep and oxidation and corrosion resistance to molten glass in high temperature environments. The corrosion of molten glass to nickel–chromium alloy is a kind of high-temperature oxidation. The service life of the centrifuge can be increased by improving the alloy's oxidation resistance, reasonable control of the centrifuge's operating temperature, and optimization of the internal structure of the centrifuge. The performance of the centrifugal fiberizer is mainly improved from the following two aspects:

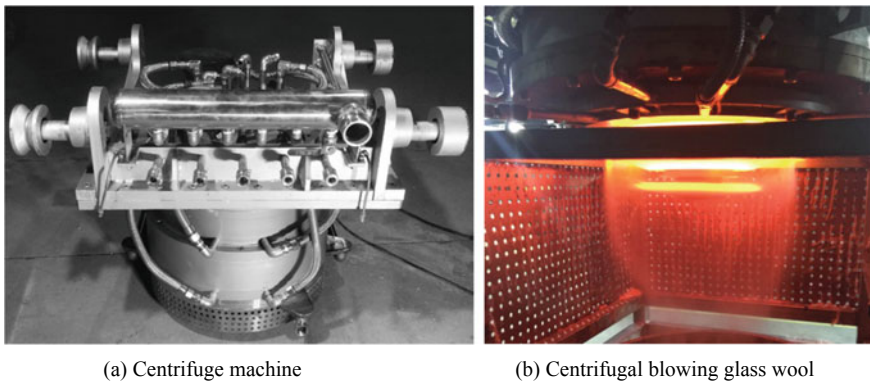


**Fig. 5.6** Centrifuge fiberizer for glass wool

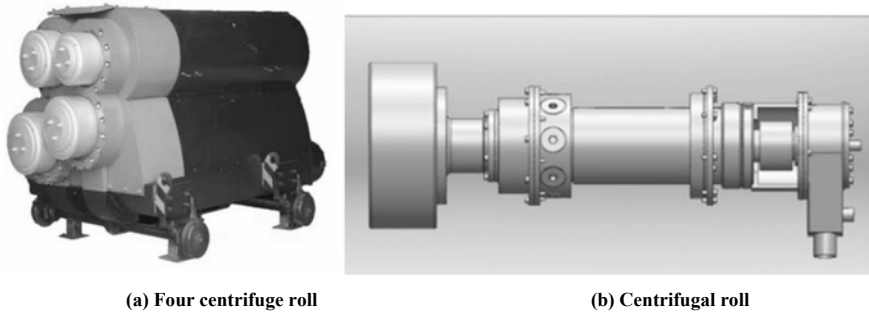


**Fig. 5.7** Centrifuge fiberizer for rock wool

- (1) The centrifugal fiberizer is mainly based on nickel–chromium alloy. Chromium has a solid solution strengthening effect, which stabilizes the surface state of the alloy by forming a  $\text{Cr}_2\text{O}_3$  rich protective layer on the nickel alloy matrix surface to resist high temperature oxidation. Adding solid solution strengthening elements such as tungsten and molybdenum slows down the diffusion rate of chromium at high temperatures and increases the diffusion activation energy and atomic bonding force in the solid solution. Moreover, molybdenum has the ability to resist glass corrosion at high temperatures, and the addition of an appropriate amount of molybdenum generally improves the durability of the alloy. The addition of niobium can increase the high temperature endurance strength of the centrifugal fiberizer and ensure the performance of the alloy for an extended period under high working temperatures.
- (2) The centrifugal fiberizer is made of high temperature alloy. The strength, oxidation resistance, and creep resistance of the nickel alloy at high temperature are limited. The endurance strength of the alloy at high temperature is based on the maximum axial section bending stress. The shoulder of the centrifugal fiberizer on a conical surface can reduce the bending stress in the edge area. The distribution hole diameter and position arrangement on the centrifugal fiberizer needs to be designed according to the stress distribution and to promote a uniform distribution of the glass melt on the peripheral wall of the centrifuge. The height of the centrifuge should be minimal to reduce internal stress. Therefore, the number of holes should not exceed 10–15 rows, improving the alloy's durability, oxidation corrosion resistance, and creep resistance performance indicators at high temperature.

The principle of the pendulum cloth cotton system is to re-stack and place the first cotton felt collected from the cotton collector to make the cotton structure clear and create favorable conditions for pleating the forming section. The forming conveyor consists of a transmission device, tension device, lifting device, sidewall device, and frame part. A trapezoidal temperature curing furnace is used for high-temperature pressurization of centrifugal glass fiber and adding various additives for curing and forming. The molten glass is processed into white cotton-like glass fiber by the

centrifugal blow process using a centrifugal fiberizer. This white cotton-like glass fiber falls on the cotton-collecting mesh belt and then passes through the trapezoidal temperature curing furnace for surface pretreatment and spraying adhesive in a continuous method. It is then compacted and cured at trapezoidal temperature (low, medium, and high temperature curing), baking processing and adding of various additives, and finally processed into centrifugal glass wool. The curing furnace is equipped with up and down rolling hollow chain plates and a hot air circulation system. The glass fiber enters the curing furnace and sprayed the binder. It is then pressurized by rolling hollow chain plates up and down and baked at high temperature to finally form centrifugal glass wool of certain thickness. The curing furnace transports and pressurizes the uncured wool felt through the upper and lower conveyor belts while the hot air is blown in for drying and curing a binder in the second felt. The roll felt machine is used to make felts of the insulation cotton such as rock wool and glass wool, which is convenient for cutting, packing, and transportation. The main function of the edge crusher is to cut the edges of the cotton felt precisely, and the cut waste edges are beaten into granules by a rotary cutter, which is moved to the cotton collector for reuse. The structure of different equipment is optimized, coordinated, and combined with advanced control methods to improve the accuracy, continuously improved technical indicators, and performance based on existing equipment according to actual production needs.

## 5.6 Characteristic and Application

Glass wool, rock wool, and ceramic wool showed different characteristics. It had been widely used in various fields based on different properties due to its different manufacturing materials, chemical components, and production processes. According to different product forms, it could be divided into cotton, board, belt, blanket, felt and tube shell.

Most insulation materials are porous, and the air stored in the holes has a low thermal conductivity, so they could play a role in heat insulation and heat preservation. Moreover, there are discontinuous bodies where the heat transfer including heat conduction between the solid framework and air, as well as air convection and thermal radiation is resisted. In engineering, the thermal conductivity created by this composite heat transfer is often called apparent thermal conductivity.

The apparent thermal conductivity was not only affected by material composition, pressure, and temperature, but also by material density and moisture content. As the density decreases, there are more small voids in the material, resulting in a decrease in apparent thermal conductivity. However, apparent thermal conductivity increases when the density is small to a certain extent, it indicated that the internal voids had increased or had been connected to each other, causing internal air convection and heat transfer enhancement. On the other hand, the pores in the insulation material easily absorb water, and the evaporation and migration of water under the action of a temperature gradient greatly increases the apparent thermal conductivity.

### 5.6.1 Glass Wool

Glass wool is made from glass fibers at temperatures in the range of 800–1450 °C and processed using a binder to form a texture-like wool. Fibers are spun from melted glass. This process uses high-speed spinning heads, somewhat like the process used to produce cotton candy. The process traps many small pockets of air between the glass, which results in high thermal resistance. During the spinning of the glass fibers, a binding agent is injected. Glass wool is then formed into rolls or slabs with different thermal and mechanical properties. It may also be produced as a material sprayed or applied directly on the surface to be insulated. A selection of national standards for glass wool for buildings is contained in Table 5.4.

The main characteristics of glass wool are as follows:

**Fire resistance:** The core material of glass wool panels is non-flammable and insulating. Thus, it prevents flames from spreading and is a viable choice for fire-resistant constructions.

**Thermal Insulation:** Glass wool is a material renowned for its thermal insulation properties.

**Table 5.4** Selected national standards of glass wool for building

Standard	Country	Standard Name
UNE-EN 14,303:2017	Spain	Thermal insulation products for building equipment and industrial installations—factory made mineral wool (MW) products—specification
DS EN 14,303:2015	Denmark	Thermal Insulation Products for Building Equipment and Industrial Installations—factory made mineral wool (MW) products—specification
BS EN ISO 23993:2010	UK	Thermal insulation products for building equipment and industrial installations—determination of design thermal conductivity
GB/T 13,350–2017	China	Glass wool and its products for thermal insulation
GB/T 17,795–2019	China	Glass wool thermal insulating products for building
ASTM C 726–2005	US	Standard specification for mineral fiber roof insulation board
ASTM C800	US	Standard specification for fibrous glass blanket insulation (Aircraft Type)
ASTM C1290	US	Standard specification for flexible fibrous glass blanket thermal insulation used to externally insulate HVAC ducts
ASTM C764	US	Standard specification for mineral fiber loose-fill insulation
ASTM C547	US	Standard specification for mineral fiber pipe insulation
EN 13,500–2003	EU	Thermal insulation products for buildings—external thermal insulation composite systems (ETICS) based on mineral wool—specification
ASINZS 4859.1	Australia	Materials for the thermal insulation of buildings—general criteria and technical provisions

Sound absorption: Glass wool panels absorb sound as the core structure consists of porous air pockets.

Anticorrosive properties: Glass wool is an inorganic thermal insulation material with stable physical and chemical properties and the ability to maintain its original form and shape.

### 5.6.1.1 Thermal Insulation for Pipes

Thermal insulation for pipes mainly refers to assemblies used to transport hot water, steam or other fluids. Thermal insulation layers are usually wrapped around a pipe to reduce heat loss or gain. Pipe insulation consists of three layers: an insulation layer, a protective layer, and a waterproof layer. A waterproof layer is often not required for indoor piping. The insulation layer must be composed of materials with low thermal conductivity to reduce heat loss or gain. Glass wool has the advantages of low thermal conductivity, high operating temperature, and minimal heat leakage from gaps. High-temperature glass wool had been successfully used as thermal pipeline insulation. For example, Owens Corning glass wool was used in the Fengxiang Thermal Power Project in Shaanxi, China. Effective insulation measures can reduce the heat loss of the heating system by more than 90%, and the key to insulation is to choose suitable insulation materials and an economical insulation thickness. A schematic diagram of a glass wool tube shell and thermal insulation schematic are shown in Fig. 5.8.

Studies have shown that convection outside the pipe is an important reason for the temperature differences on the surface of the insulation layer. The pipe surface temperature supports natural convection outside the insulation. Traditionally, the flow

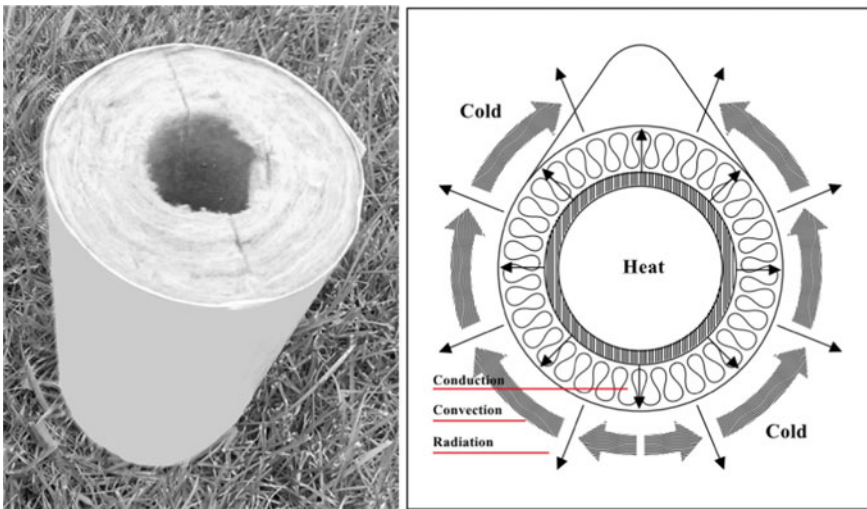


Fig. 5.8 Schematic diagram of glass wool tube shell and thermal insulation schematic

pattern of natural convection is judged by  $Ra$  (Rayleigh number) in large convection flow pattern. Now, engineers are more inclined to use  $Gr$  as a criterion for natural convection.

High-temperature glass wool insulations are mainly used for pipe insulation at or below 400 °C and have the following advantages:

- (1) High thermal insulation efficiency: The fibers are uniform, slender, and arranged perpendicular to the heat transfer direction, the existence of a large amount of air ensures the insulation effect of glass wool insulation that effectively prevents heat transfer and heat loss.
- (2) Lightweight, easy to construct, and could be cut into any size.
- (3) Strong shock resistance and high durability: The fibers are tightly interwoven with each other, avoiding the phenomenon where the fibers are stretched and voided due to the disjointed fibers, which causes heat loss to increase with age.
- (4) Low corrosiveness: The raw material of high temperature glass wool is glass, the pH value is between 7–8, and research by the Science Division National Aerospace Laboratories of India showed that the chlorine ion dissolved from glass wool would corrode stainless steel. So high-temperature glass wool is produced with very little chlorine content, which has no corrosive effect on equipment and pipelines—see: Kumar et al. (2008).
- (5) Strong Hydrophobicity: The hydrophobicity of the insulation material refers to the ability of insulation material to discharge absorbed water. The content of slag ball is extremely low, and the glass will not be broken due to soaking or raining, and the thermal insulation performance will not change after drying.
- (6) According to manufacturers, this insulation is environmentally friendly and healthy.

### 5.6.1.2 Building Insulation

Steel-structure buildings are an indispensable part of existing buildings. Due to the thermal bridging effect, the building envelope exchanges heat with the external environment. The heat transfer coefficient of some parts of the enclosed structure is significantly higher than other parts. Thus, heat is quickly transferred from high thermal concentration to the lower, increasing the building's air conditioning, heating load, and energy consumption. The energy efficiency of a building is improved by applying glass, or rock wool insulation layer to steel structure buildings. The heat flow in the building avoids condensation problems, provides a comfortable working environment, reduces the transmission of environmental noise, and meets the safety and fire protection requirements of steel structure buildings.

Japan vigorously promotes the concept of “zero-energy-consumption housing”. The “zero-energy-consumption house” does not mean that the house consumes no energy, but rather that the house could achieve an excellent thermal performance through its own external enclosure (for example, the use of new thermal insulation materials, increased the thickness of the insulation materials used, and using





**Fig. 5.9** Glass wool insulation installation

thermal breaks at key locations—see: Moore (2014). After 2030, all Japanese independent houses will be constructed in accordance with the “Zero Energy House ZEH” standard. Figure 5.9 shows an example of glass wool insulation construction.

The glass wool used in residential construction is made of slender and soft high-performance glass fibers evenly distributed and interwoven. The glass wool could effectively block the transmission of heat, absorbs sound wave energy, has excellent fire resistance, and provides efficient insulation and sound absorption, making it desirable is for use in residential buildings. Based on existing high-performance products, Saint-Gobain used 100% pure natural binders to produce formaldehyde-free high-quality glass wool, which could meet the ‘EU’s strictest requirements for formaldehyde content and volatile organic emissions in indoor air, greatly improving the quality of people’s living and working environments.

### 5.6.1.3 Sound Insulation

Ultra-fine glass wool is excellent thermal insulation and sound absorption, light weight, and chemically resistant Class A non-combustibility—see: Wang et al. (2019). Using this high-performance glass wool to insulate the fuselage reduces energy consumption and provides passengers with a comfortable temperature, quiet, and safe flight environment. At the same time, it could reduce the weight ratio, space ratio, and internal energy consumption of the aircraft.

The development of ultra-fine glass wool mat was a systematic and complex project—see: Nakayama et al. (2002). The sound and heat insulation performance of glass wool felt depends not only on the composition, diameter, and distribution of fibers but is also closely related to the bulk density, organizational form, and distribution structure of the glass wool felt. Hongda company successfully prepared ultra-fine glass wool in 2014 with fiber diameters in the range of 0.25–3  $\mu\text{m}$  using the centrifugal blow process. The thermal conductivity of glass wool felt with an average diameter of 1.1  $\mu\text{m}$  can be as low as 26  $\text{mW}/(\text{m}\cdot\text{K})$ . Figure 5.10 shows a SEM

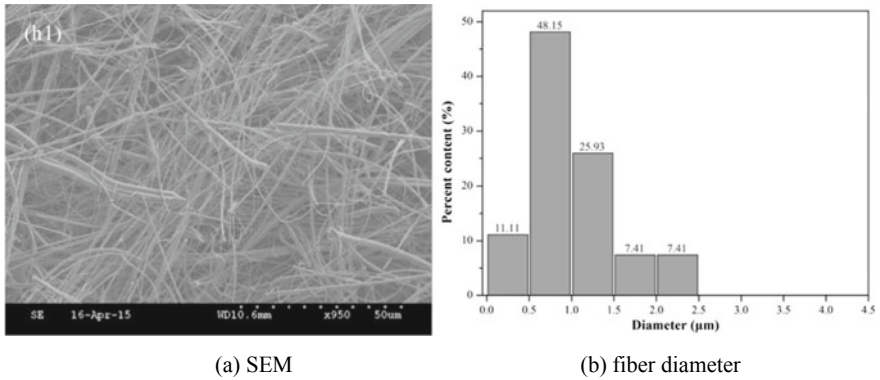


Fig. 5.10 SEM and fiber diameter of ultra-fine glass wool using centrifugal blow process

image and fiber diameter distribution of ultra-fine glass wool from the centrifugal blow process. XRD patterns of glass wool with different diameters are depicted in Fig. 5.11. The XRD patterns of glass wool with diameters of 1.1 and 6.5 μm were consistent in showing broadened amorphous peaks.

When a sound wave is incident on the surface of glass wool, a part of it is reflected away from the surface of the glass wool, and the remaining part of it propagates into the glass wool. The sound waves transmitted into the glass wool are only partly

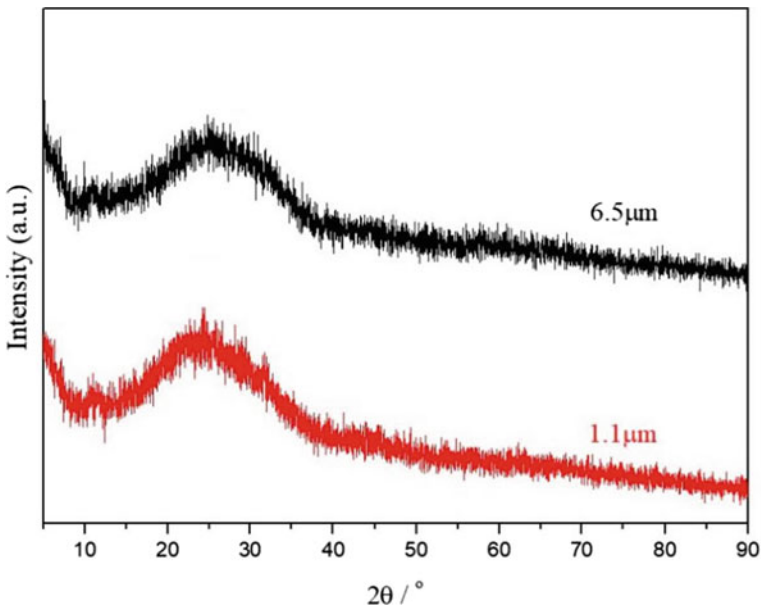


Fig. 5.11 XRD patterns of glass wool with diameters of 1.1 and 6.5 μm

absorbed inside the glass wool, while those not absorbed will pass through the glass wool and form noise. The friction between the sound wave entering the glass wool and the fiber and fiber vibration itself is also more intense as the density increases; the energy consumption is increased, and the intensity of the sound wave passing through the insulation is significantly reduced. The thinner the glass wool diameter, the denser will be the glass wool structure. The greater part of sound waves will be reflected at the glass wool surface layer resulting in improved sound insulation performance. Figure 5.12 shows the relationship between glass fiber diameter and sound insulation. The fiber diameters used for testing were  $3.4\ \mu\text{m}$ ,  $5.1\ \mu\text{m}$ , and  $7.0\ \mu\text{m}$ , respectively. As shown in the figure, the sound insulation was inversely proportional to the fiber diameter. As the fiber diameter decreases, the sound insulation of the glass fiber felt increases.

Furthermore, since, ultra-fine glass wool provides excellent thermal and acoustic properties, they are particularly well suited for thermal and sound insulation of commercial aircraft fuselage wall cavities. Figure 5.13 shows ultra-fine glass wool blankets from Johns Manville (JM).

At the same time, the compatibility of glass wool with the human body and potential health impact are also highly valued—see: Wilson et al. (1999). Nowadays, the bio-soluble ultra-fine glass wool with reduced acid resistance index and water resistance index was successfully prepared by Dr. Chen's team from Nanjing University of Aeronautics and Astronautics, which solved the health safety issues related to cancer in the lungs. The insulation passed the bio-soluble test from the Fraunhofer

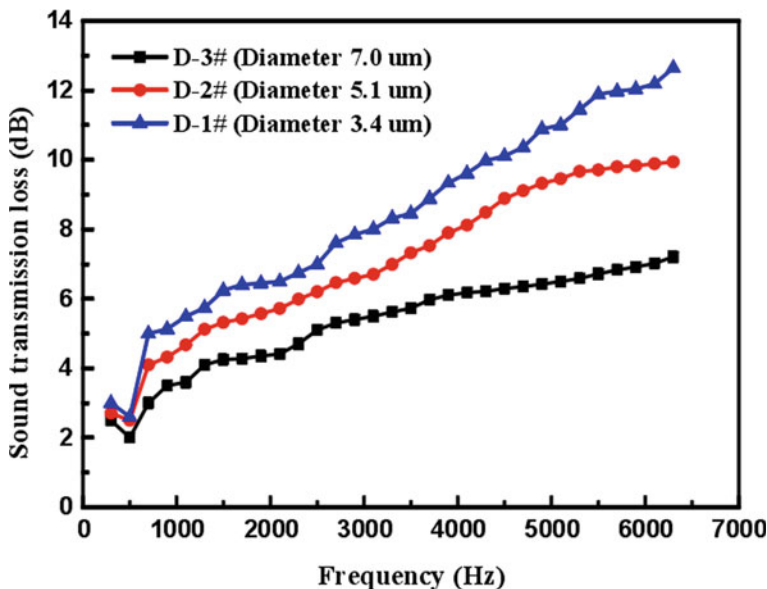
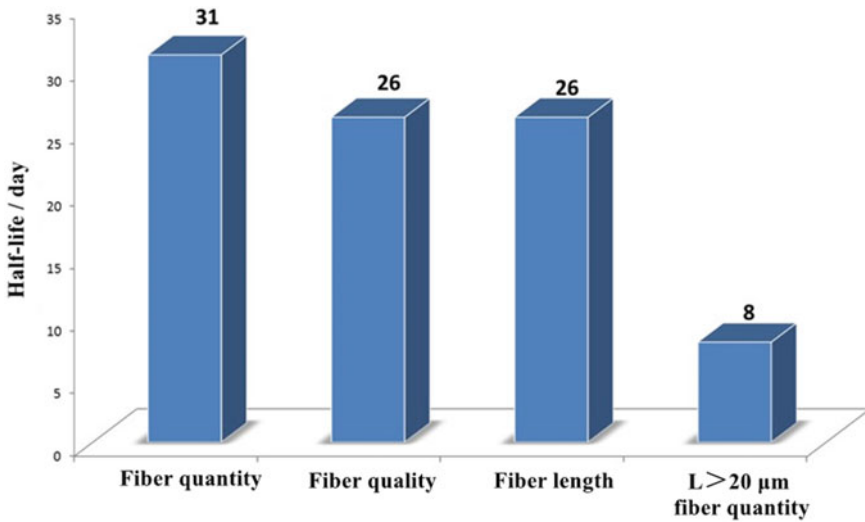


Fig. 5.12 The relationship between glass fiber diameter and sound insulation



**Fig. 5.13** Ultra-fine glass wool blankets from Johns Manville



**Fig. 5.14** Schematic diagram of glass wool half-life

Institute in Germany, showing the harmless of ultra-fine glass wool. The half-life of glass wool in rat lung fluid is 26 days, which is far less than the rat lung fluid half-life  $\leq 40$  days required by the EU bio-soluble fiber standard certification. The schematic diagram of glass wool half-life is shown in Fig. 5.14.<sup>1</sup>

<sup>1</sup> Chen Z. The research on the key fabrication process and properties of  $\text{Na}_2\text{O}-\text{CaO}-\text{B}_2\text{O}_3-\text{SiO}_2$  ultra-fine glass wool—Dissertation, Nanjing University of Aeronautics and Astronautics, 2016.

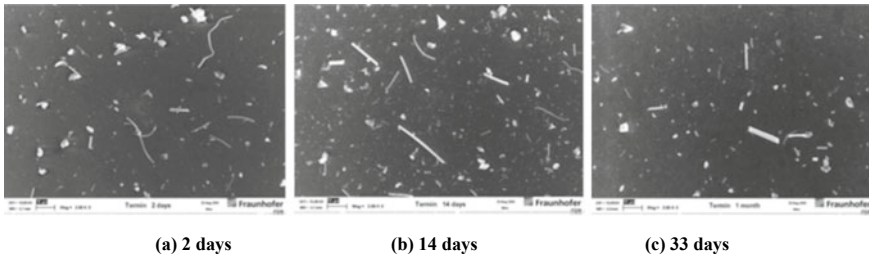


**Fig. 5.15** SEM micrographs of lungs of rats with tracheal instillation of glass wool at different stages

The bio-soluble ultra-fine glass wool is currently the only ultra-fine glass wool that has passed EU certification. Ultra-fine centrifugal glass wool can be used in many fields such as construction, refrigerator, and nuclear power insulation to solve the problem of bio-solubility. High bio-solubility could increase the safety margins in manufacturing and allow the use of glass wool. Figure 5.15 shows the SEM micrographs of the rat's lungs with tracheal instillation of glass wool at different stages.

### 5.6.2 Rock Wool

Rock wool is one of the inorganic thermal insulation materials that is highly favored by the construction industry due to its low price, fire insulation, and easy access to raw materials. Rock wool is usually manufactured from high-quality basalt that is melted at high temperatures. A four-roll centrifugal cotton-making process is used to spin the melt into 4–7  $\mu\text{m}$  diameter fibers. Binder, dustproof oil, and water repellent are added to the primary fibers. The fibers and the added components are processed to form batts or blankets.

Rock wool products can be prepared with different specifications for a variety of uses. The national standards of rock wool for buildings are shown in Table 5.5.

Rock wool board is a prefabricated product with a required minimum compressive strength—see: Li et al. (2020). Once the rock-wool fiber is layered and bonded with a resin binder, it is compacted with a pendulum hammer so that most of the internal fibers are arranged in the same direction. Rock-wool board has obvious stratification along the horizontal direction, resulting in low tensile strength perpendicular to the fiber arrangement direction. Rock-wool felt is packaged in rolls, which is easy to install in a large area. According to requirements, both products can be produced with different densities and thicknesses and can be laminated with different facing materials for construction applications. Rock-wool board and felt for construction are widely used in a variety of building applications. These products are used for fire protection, heat preservation, and energy saving, sound absorption and noise

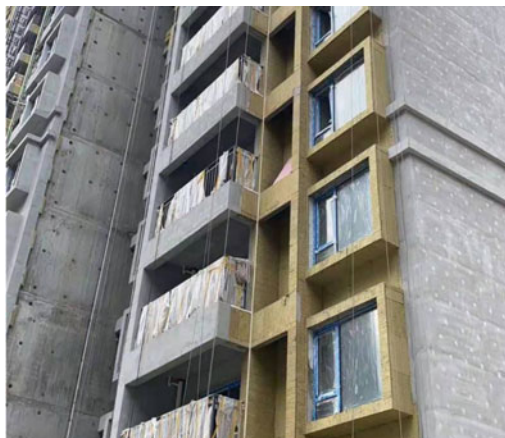
**Table 5.5** National standards of rock wool for building (partly)

Standard	Country	Standard name
GB/T 25,975–2018	China	Rock wool products for external thermal insulation composite systems
ASTM C726–17	US	Standard specification for inorganic wool roof insulation board
ASTM C1859-19	US	Standard practice for determination of thermal resistance of pneumatically installed loose-fill building insulation (behind netting) for enclosed applications of the building thermal envelope
ASTM C665	US	Standard specification for mineral fiber blanket thermal insulation for light frame construction and manufactured housing
ASTM C1014	US	Standard specification for spray-applied mineral fiber thermal and sound absorbing insulation
AUS/NZS 4859	US	Thermal insulation material for buildings
ASTM C892	US	Standard specification for high-temperature fiber blanket thermal insulation
ASTM C726	US	Standard specification for mineral wool roof insulation board
BS/EN 13,162	UK	Thermal insulation products for buildings-factory made mineral wool (MW) products—specification
MS 1020	Malaysia	Thermal insulation products for buildings-factory made mineral wool (MW) products—specification
EN 13,162–2008	EN	Thermal insulation products for buildings—Factory made mineral wool (MW) products—Specification

reduction, anti-condensation on steel structure roofs, external protective walls, indoor partition walls, sound-absorbing ceilings, and floating sandwich floors. Low-density (40–80 kg/m<sup>3</sup>) rock-wool board and felt are suitable for filling the gaps between steel structure frames for reducing heat transfer and absorbing sound. Elastic, medium-strength rock-wool board is suitable for building wall/roof insulation, fire protection, sound absorption, interior wall partitions, and elevator shafts. High-strength rock-wool board has good load-bearing and compressive properties in high and low-temperature environments and is suitable for heat preservation and insulation of large ships, storage rooms, ovens, pipes, and industrial equipment. Figure 5.16 shows the rock wool as an insulation layer on a building exterior wall.

Rock-wool board is often combined with metallic materials, inorganic mortar, and glass fiber mesh cloth to make sandwich panels and composite insulation systems. The rock-wool board is composed of a bonding layer, insulation layer, connector, enhanced protective layer, and finishing layer. The base wall is filled and flattened with 1:3 cement mortar. The base layer must be dry and have a specific mechanical strength. The sticking method for rock wool is used when the rock-wool structure is

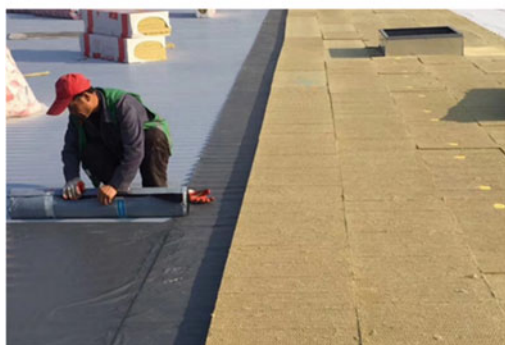
**Fig. 5.16** Rock wool as an insulation layer on building



**(a) Window insulation**



**(b) Wall insulation**



**(c) Roof insulation**

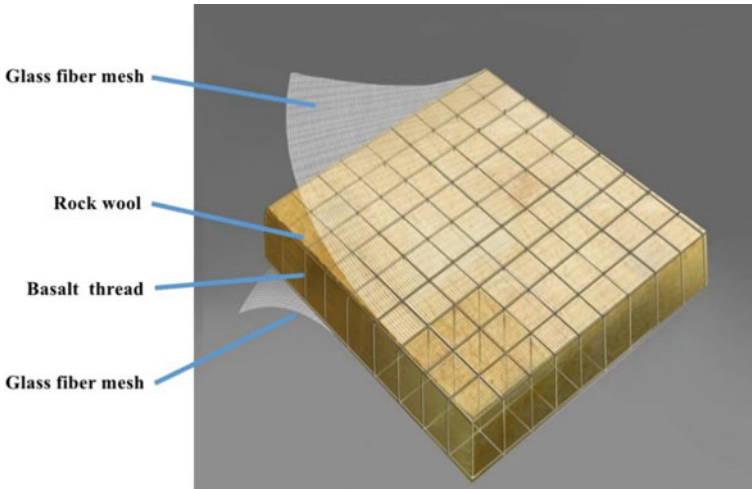


**Fig. 5.17** Schematic diagram of AW board structure

loose. Therefore, for reliable bonding, the anchor setting is essential for the installation of rock-wool boards. The number, specification, distribution, and pulling force test of anchor bolts must meet the design requirements.

A new type of mesh reinforced rock wool insulation board was formed (AW board), through the structural optimization of the rock wool board. The AW board is based on the rock-wool board physical structure. Using industrial sewing technology, continuous basalt fiber thread is used to cross-stitch the glass fiber mesh placed on both sides of the insulation board to form a high-strength insulation board. A schematic diagram of AW board is shown in Fig. 5.17. AW board performance parameters are shown in Table 5.6.

Compared to rock-wool board, the advantages of AW board as an external wall insulation system include higher tensile strength, durable and reliable, cost-effective system, and reduces construction complications. Figure 5.18 contains a schematic diagram of an exterior wall insulation system using AW board.

Net-woven reinforced thermal insulation decorative integrated board is composed of soft rock-wool felt and rigid decorative tile. The tensile strength perpendicular to the board surface is 0.10 MPa, thermal conductivity  $\leq 0.040$  W/(m·K), thickness  $\leq 200$  mm, and the thickness of 60 mm plate does not exceed 20 kg/m<sup>2</sup>. The net-woven reinforced thermal insulation decorative integrated board is shown in Fig. 5.19.

The thermal insulation performance of rock wool is extensively utilized in construction, and the durability of the product has been steadily improved. When used as an insulation layer in the building envelope, however, the composite board has a problem when water vapor from the environment diffuses into it, liquid water accumulates and reduces the boards' thermal resistance.



**Table 5.6** AW board performance parameters

Performance (AW board)	Parameter
Size	1200 × 600 mm
Thickness	≤200 mm
The tensile strength perpendicular to the board surface	≥0.10 MPa
Moisture and heat tensile strength retention rate	60%
Thermal conductivity (average temperature 25 °C)	0.035 W/(m·K)
Unit combustion growth rate index	0 W/s
Total heat release in the first 600 s during combustion	4.7 MJ
Burning drips in the first 600 s during combustion	No
Total heating value of combustion	0.7 MJ/kg
Total smoke production in the first 600 s during combustion	5 m <sup>2</sup>

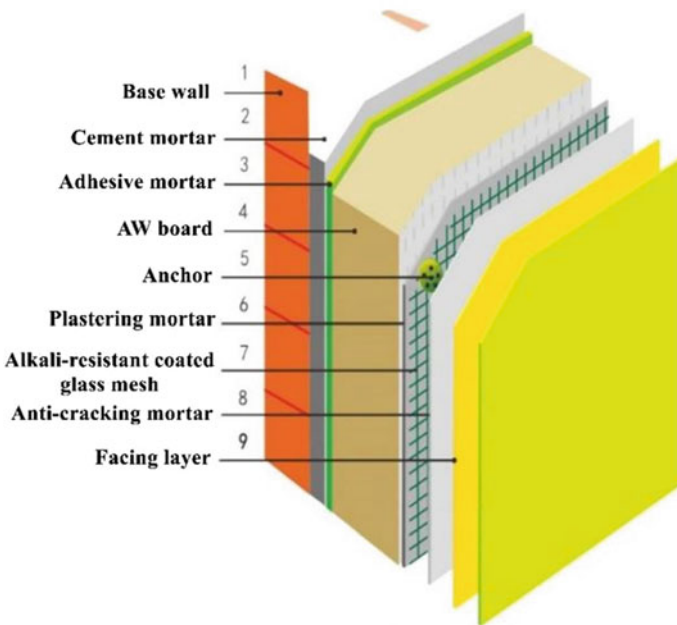


**Fig. 5.18** Schematic diagram of external wall insulation system

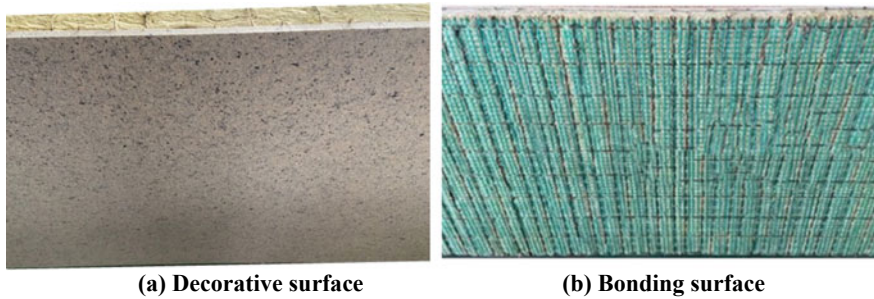


**Fig. 5.19** The net-woven reinforced thermal insulation decorative integrated board

### 5.6.3 Ceramic Wool

The selection of furnace lining material is one of the critical challenges for heating the furnace body. It was generally composed of refractory materials, thermal insulation materials, protective materials, and a steel structure. The main part of the furnace body bears the thermal load. When choosing furnace-lining material, it is not only sufficient strength and stability under high temperature and load conditions that must be maintained. Besides these, the insulation should resist furnace-gas flushing and slag erosion and provide thermal resistance and air tightness.

Ceramic wool is a fibrous thermal insulation material having light weight, low thermal conductivity, and good thermal stability compared to other fibrous light-weight insulation materials such as glass wool and rock wool. The major advantage of this material is its high temperature resistance—see: Chen et al. (2019). Based on its chemical composition and structure, it is safe to be used in the temperature range from 600 to 1300 °C. Ceramic wool, therefore, is widely used in high temperature kilns, heating devices, wall-lining gap fillers, and the filling of complex spaces in the electrical and automotive industries.

- (1) Ceramic wool has excellent wind-erosion resistance.
- (2) Ceramic wool is a stable thermochemical material: It is a porous product composed of interwoven fibers of 2–5  $\mu\text{m}$  diameter. Even if the temperature changes sharply, structural stress and peeling will not occur, and the material can effectively resist mechanical vibrations such as bending and twisting and other thermal vibrations.
- (3) Low heat loss: The thermal conductivity of the ceramic wool lining is about 0.17 W/m·K at 600 °C. The thermal conductivity of ceramic wool is 50% that of heavy refractory, enhancing the thermal insulation effect and reducing energy loss. The heat storage loss of a furnace lining is directly proportional to the bulk density of the lining material, and the bulk density of the aluminum silicate refractory fiber is 1/10th that of the heavy refractory. The use of ceramic wool as a furnace lining, therefore, reduces the heat loss of the furnace wall and reduces the weight of the stove and thickness of the furnace lining.

- (4) **Wide range of application temperature:** The working temperature range for ceramic wool is 600–1400 °C, which broadens the application of fiber linings. More significantly, the lining material can be composed of fiber products of different materials according to the temperature profile in the lining thickness direction. This reduces the cost of furnace construction, with improved furnace lining structure and insulation effect. The use of appropriate materials, safety, and economy can reduce energy consumption by 30%.

Ceramic wool is a crystalline phase binary compound composed of  $\text{Al}_2\text{O}_3$  and  $\text{SiO}_2$ . The thermal conductivity increases rapidly as the temperature increases. The required lining thickness could be calculated by Eq. (5.2).

$$\delta = \frac{1}{qB} (e^{A+Bt_1} - e^{A+Bt_0}) \quad (5.2)$$

Here,  $\delta$  is the thickness of the furnace wall,  $q$  is the heat transfer loss,  $t_1$  is the temperature of a certain point in the furnace wall,  $t_0$  is the temperature of the inner surface of the furnace wall,  $e$  is the base of the natural logarithm, and  $A$  and  $B$  are constants.

Under the same conditions, compared with the traditional furnace lining, ceramic-wool lining dramatically reduces heat loss, heat-storage loss, and reduced wall thickness. Due to the excellent insulation performance of the ceramic wool kiln lining, the heating speed is fast. These characteristics can reduce the heating time and improve production efficiency. Figure 5.20 shows ceramic wool used for furnace lining.



**Fig. 5.20** Ceramic wool used in furnace lining

Ceramic wool, however, has poor impact resistance, moisture absorption, serious fiber powdering and peeling, and is harmful to human skin and respiratory system. The material has been identified as a class 2B carcinogen. The mullite crystal precipitation occurs when the long-term working temperature of the ceramic wool exceeds 980 °C. When the mullite grains grow, they cause the fibers to shrink and break into the powder, which falls off. In recent years, a new three-layer anticorrosive fiber lining structure had been proposed. First, an anticorrosive sealing paint is applied to the hot surface of the furnace wall steel plate, the cold end of the anchor nail, and the welding point to form the first dense protective film on the hot steel plate surface and the surface of the anchor. In addition, a 50 mm thick layer of dense high-strength thermal insulation material is used on the backing of the fiber lining. A layer of gas barrier foil is laid on the hot surface of the dense thermal insulation material to prevent the gas from passing through the furnace lining effectively. The gas barrier foil also enhances the heat preservation effect. Finally, increasing the overall bulk density of the fiber lining to an appropriate value allows the fiber lining to prevent smoke penetration. At the same time, the ceramic fiber lining is sprayed with a surface-enhancing radiation coating on the fiber surface. After the coating is processed, a dense high-temperature resistant and erosion-resistant protective layer is formed on the surface of the fiber module. It prevents the penetration of flue gas and reduces the heat radiation from the furnace lining. A schematic diagram of three-layer anticorrosive fiber lining structure is shown in Fig. 5.21.

In addition to being used in the lining of furnace, ceramic wool is also used to insulate smoke exhaust and fire-proof ducts. The smoke exhaust duct is a pipe used in the mechanical smoke exhaust unit of the building ventilation systems to exhaust fire smoke from rooms, walkways, and other spaces to the outside of the building. It is also connected to the smoke exhaust fire damper. Smoke exhaust ducts usually require a temperature resistance above 600 °C and have good fire and thermal insulation performance. Temperature detection points are arranged at eight locations around the pipeline. When the average temperature rise exceeds 140 °C, or it exceeds 180 °C at any location, it is considered to have lost thermal insulation properties. Figure 5.22 shows a schematic diagram of the smoke exhaust duct section with ceramic wool as a thermal insulation layer.

## 5.7 Closing Statement

Glass wool, rock wool, and ceramic wool are all commonly used excellent thermal insulation materials, which can be processed into different products for various applications. As compared to rock wool, the glass wool has a low bulk density, low slag-ball content, low thermal conductivity, long service life, and high fiber toughness. Glass wool can be used in many fields, including thermal pipelines, residential insulation, VIP core materials, aviation sound insulation, and AGM partitions. Glass wool is generally used for heat preservation applications below 260 °C, however, the

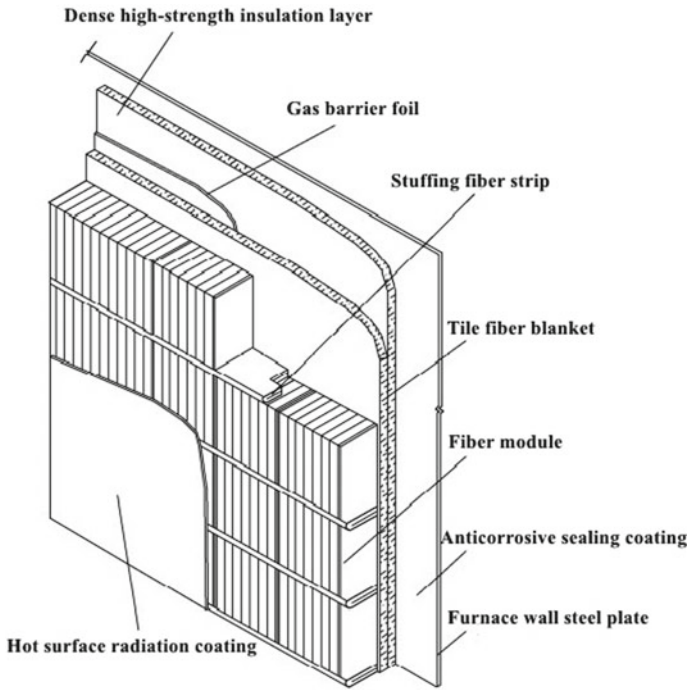


Fig. 5.21 Schematic diagram of three-layer anticorrosive fiber lining structure



(a) Smoke exhaust duct



(b) Schematic diagram of structural section

Fig. 5.22 Schematic diagram of smoke exhaust duct and insulation structure

maximum working temperature of rock wool and ceramic wool can reach 600 °C and 1600 °C, respectively.

**Acknowledgements** Thanks to all of those who supported the development of this chapter by writing and providing pictures, the specific picture providers or units were as follows:

- Fig. 5.2 Beijing Caifang Fuyuan Xinkemao Co., Ltd.;
- Fig. 5.6 Beijing Caifang Fuyuan Xinkemao Co., Ltd.;
- Fig. 5.7 Yinglai Machinery;

Fig. 5.16 (a) Wei Xiaoguang; (b) (c) Wang Liting;  
 Fig. 5.17 Shanghai Anwei Intelligent Technology Stake CO., LTD.;  
 Fig. 5.18 Shanghai Anwei Intelligent Technology Stake CO., LTD.;  
 Fig. 5.19 Shanghai Anwei Intelligent Technology Stake CO., LTD.

## References

- Alves, J. O., Espinosa, D. C. R., & Tenório, J. A. S. (2015). Recovery of steelmaking slag and granite waste in the production of rock wool. *Materials Research*, 18(1), 204–211. <https://doi.org/10.1590/1516-1439.324414>
- Baker, J.W., & Smalley, R.R. (2001). Apparatus and Method for Forming Fibers from Thermoplastic Fiberizable Materials. US, Patent US6245282B1, John's Manville, 2001. <https://patents.google.com/patent/US6245282B1/en>.
- Chan-Ki, J., Jae-Seong, L., Hoon, C., Ju-Ho, K., & Jong-Pil, P. (2017). A study on insulation characteristics of glass wool and inorganic wool coated with a polysiloxane agent. *Advances in Materials Science and Engineering*, 2017, 1–6. <https://doi.org/10.1155/2017/3938965>
- Chen, W., Ye, J., & Li, X. (2019). Fire experiments of cold-formed steel non-load-bearing composite assemblies lined with different boards. *Journal of Constructional Steel Research*, 2019, 158: pp. 290–305. <https://www.sciencedirect.com/science/article/abs/pii/S0143974X18308198>.
- Clatot, R., Maugendre, S., & Szalata, F. (2017). Device for melting glass comprising a furnace, a channel and a barrier. US, Patent 20170197859, Saint Gobain, 2017. <https://patents.justia.com/assignee/saint-gobain-isover?page=5>.
- Guffey, L. J., & Schultz W. W. (1981). Method and apparatus for forming mineral fibers [P]. US, Patent US4302234A, Owens Corning, 1981. <https://patents.google.com/patent/US4302234A/en>.
- Guldberg, M., de-Meringo, A., Kamstrup, O., Furtak, H., & Rossiter, C. (2000). The development of glass and stone wool compositions with increased biosolubility [J]. *Regulatory Toxicology and Pharmacology Rtp*, 32(2), 184–189. <https://doi.org/10.1006/rtph.2000.1418>.
- Jensen, A. A. (2009). Risk assessment of boron in glass wool insulation. *Environmental Science and Pollution Research*, 16(1), 73–78.
- Kudo, Y., Watanabe, M., Okada, M., Shinji, H., Niitsuya, M., Satoh, T., Sakai, Y., Kohyama, N., Kotani, M., & Aizawa, Y. (2003). Comparative cytotoxicity study of rock wool and chrysotile by cell magnetometric evaluation. *Inhalation Toxicology*, 15(13), 1275–1295. <https://doi.org/10.1080/08958370390241759>.
- Kumar, M. S., Sujata, M., Venkataswamy, M. A., & Bhaumik, S. K. (2008). Failure analysis of a stainless-steel pipeline. *Engineering Failure Analysis*, 15(5), 497–504. <https://www.sciencedirect.com/science/article/abs/pii/S1350630707000921>.
- Letourmy, A., Douce, J., Goletto, V., & Gilles, J. (2016). Product based on mineral fibers and process for obtaining It. US Patent, 9469563, Saint Gobain, 2011. <https://patents.google.com/patent/US20110111198A1/en>.
- Li, B.B., Chen, Z.F., Chen, Z., Qiu, J.L., Zhou Y.Q., & Zhou, J.M. (2012a) Glass wool prepared under various rotating speed by centrifugal-spinneret-blow process. *Advanced Materials Research*, 457–458, 1573–1576. <https://www.scientific.net/AMR.457-458.1573>.
- Li, B. B., Chen, Z., Qiu, J. L., Chen, Z. F., & Zhou, J. (2012b). Effect of service time of centrifugal pan on glass wool. *Advanced Manufacturing Processes*, 27(11), 1213–1216. <https://doi.org/10.1080/10426914.2012b>
- Li, X., Liu, J., Fan, X., Qin, J., Zhang, R., Cao, R., Wang, P., & Huo I. X. (2020). Simulating study on mechanical properties of rock wool board for thermal insulation on external walls. *Advances in Materials Science and Engineering*, (8), 1–11
- Mabru, M., Leveque, M. (1964). Manufacture of Fibers, Particularly Glass Fibers. United States Patent, US4420460A, Saint Gobain, France, <https://www.freepatentsonline.com/3152878.html>

- Marmoret, L. (2016). Assessment of hydrothermal performance by thermophysical characterization of a crimped glass wool building insulation. *Journal of Building Physics*, 40(5), 401–416.
- Moore, M. A., Boymel, P. M., Maxim, L. D., & Turim, J. (2002). Categorization and nomenclature of vitreous silicate wools. *Regulatory Toxicology and Pharmacology*, 35(1), 1–13. <https://doi.org/10.1006/rtph.2001.1509>
- Moore, T. (2014). Modelling the through-life costs and benefits of detached zero (net) energy housing in Melbourne, Australia. *Energy and Buildings*, 70, 463–471.
- Nakayama, Y., Kishimoto, K., Sugiyama, S., & Sakaguchi, S. (2002). Micro-structural design and function of an improved absorptive glass mat (AGM) separator for valve-regulated lead–acid batteries. *Journal of Power Sources*, 107(2), 192–200. <https://www.sciencedirect.com/science/article/abs/pii/S0378775301010059>.
- Stazi, F., Tittarelli, F., Politi, G., Pernac, C. D., & Munafõa, D. (2014). Assessment of the actual hydrothermal performance of glass inorganic wool insulation applied 25 years ago in masonry cavity walls. *Energy and Buildings*, 2014(68), 292–304. <https://doi.org/10.1016/j.enbuild.2013.09.032>
- Stelmah, J. (1968). Method and apparatus for processing heat softenable material. US, Patent US3395005A, Johns Manville. <https://patents.google.com/patent/US3395005A/en>.
- Wang, F., Chen, Z. F., Wu, C., & Yang, Y. (2019). Prediction on sound insulation properties of ultrafine glass wool mats with artificial neural networks [J]. *Applied Acoustics*, 146, 164–171.
- Wilson, R., Langer, A.M., & Nolan, R.P. (1999). A risk assessment for exposure to glass wool. *Regulatory Toxicology and Pharmacology*, 30(2 Pt 1), 96–109. <https://doi.org/10.1006/rtph.1999.1344>. PMID: 10536105. <https://www.sciencedirect.com/science/article/abs/pii/S0273230099913442>.
- Zeng, X. J., Wang, S. Y., Wang, H., Meng, L., & Wu, J. Q. (2002). *The simulation of thermal insulation property of ceramic fibers*. In *key engineering materials* (Vol. 224–226, pp. 825–830). Trans Tech Publications, Ltd. <https://doi.org/10.4028/www.scientific.net/kem.224-226.825>.
- Zhou, B. (2012). The application of glass wool and its products. *Plastics Manufacture*, 05, 74–75.
- Zou, C., Qian, X. M., Yang, R. L., & Liu, Y. (2020). Numerical simulation analysis of the influence of ultra-fine glass fiber production process on product homogeneity. *Journal of Industrial Textiles*, 152808372091245. <https://journals.sagepub.com/doi/https://doi.org/10.1177/152808372091245>.

# Chapter 6

## Characteristics of Bio-based Insulation Materials



Hartwig M. Künzel

**Abstract** The interest in low-energy, sustainable architecture and consequently, in buildings with minimized environmental impact has been growing over the years. As a result, the use of bio-based insulation, as well as construction materials, has become more and more prevalent in many countries around the world. Today the market share of bio-based insulation materials is well below 10% worldwide. In Germany, where the market share has increased by 2% points in the past 10 years, the share of bio-based building insulation reached 9% in 2020 which is among the highest in the EU. Almost 60% of these are wood fiber materials another 30% are based on cellulose fibers and the last 10% include all other bio-based insulation products. The hygrothermal performance of bio-based materials, especially their moisture buffering capacity and their high vapor permeability represent real benefits, while the moisture susceptibility is the most important downside.

### 6.1 Introduction

The use of bio-based insulation materials dates back at least to the Bronze Age. In Europe, walls made from wood wickerwork were filled with hay and roofs were covered by thick straw bundles—Eicke-Henning (2011). Other insulation materials used in the past include, e.g., sawdust, wood chives, seaweed, reed, cork, hemp and flax fibers as well as animal products such as sheep wool. These bio-based materials served not only as thermal insulation. Some of them were equally important to achieve a certain degree of airtightness. Cellulose fiber insulation is a more recent development because some decades ago old newspapers were mainly used as toilet paper or for food wrapping.

Today the market share of bio-based insulation materials is well below 10% worldwide. In Germany, where the market share has increased by 2% points in the past 10

---

H. M. Künzel (✉)

Department of Hygrothermics, Fraunhofer Institute for Building Physics IBP, Holzkirchen, Germany

e-mail: [hartwig.kuenzel@ibp.fraunhofer.de](mailto:hartwig.kuenzel@ibp.fraunhofer.de)



years, the share of bio-based building insulation reached 9% in 2020 which is among the highest in the EU. Almost 60% of these are wood fiber materials another 30% are based on cellulose fibers and the last 10% include all other bio-based insulation products.

The reasons why bio-based insulation materials have been replaced by organic foams and mineral fibers in the past are manifold. Fire protection is the most common explanation, however, this does not explain why organic foams have the largest market share today. Moisture susceptibility may be another reason. Both problems can be alleviated by additives or better constructional measures. The most likely explanations for the drop in bio-based materials are availability and cost. Organic foams contain more air and less solid matter than most other insulation materials. They are cheap, widely available and easy to install. However, their disposal may present problems, because they can contain listed compounds in the matrix polymers or fire retarding additives. On the other hand, many bio-based materials are not completely harmless. To reduce their flammability and moisture susceptibility as well as to protect them against insect attack, a variety of chemicals is often employed that may also pose some potential health risks. Sometimes, also polymeric glues or binding fibers are used which may impair recycling or composting.

However, there are also reasons why the application of bio-based insulation materials should be encouraged. Buildings made of bio-based materials represent long-term carbon storage facilities. Since buildings are meant to last, the CO<sub>2</sub> sequestered during growth is removed from the air for a long time. Other reasons are the lucrative use of waste materials left over from food production, environmental considerations, biodiversity aspects or moisture buffering properties.

Many bio-based insulation products have a limited applicability because they come either as loose fill or their compressive strength is too small to serve as insulating sheathing. Wood fiber products show the largest specialization for different applications among all bio-based insulation materials. There are flexible batts for cavity insulation and different rigid boards for exterior and interior wall insulation systems (see Fig. 6.1) as well as special weather resistive boards for roof top insulation and so on. In this chapter, the hygrothermal characteristics of bio-based insulation materials are addressed and evaluated.



**Fig. 6.1** Flexible wood fiber batt for cavity insulation (left) and wood fiber board for exterior wall insulation systems (EIFS)

## 6.2 Hygrothermal Properties of Bio-based Insulation Materials

As stated in Chap. 3, the thermal performance of insulation materials in the presence of moisture can only be adequately analyzed and described if heat and mass transfer are considered together. Since all bio-based insulation materials are hygroscopic—this includes materials that have been treated by silicones or equivalent compounds to render them water repellent—sorption moisture is always present under practical conditions. Therefore, care must be taken to determine their thermal conductivity in a way that excludes initial or reversible latent heat effects. Otherwise, bio-based materials would be penalized by overly conservative values (unreasonably high thermal conductivity listings due to vapor transfer with evaporation and condensation) compared to conventional insulation materials.

Since heat and moisture transfer in hygroscopic insulation materials are strongly coupled, the integral thermal performance of bio-based insulation materials can only be assessed by hygrothermal simulation (see Chap. 3). Apart from thermal properties, these calculations also require moisture transfer properties such as vapor permeability and moisture retention function. Liquid transfer is often less important in most bio-based insulation materials because they have been treated to repel water. Therefore, their liquid diffusivity is generally low compared to their vapor permeability. However, there are some materials, such as cellulose blow-in insulation, which must not get in contact with liquid water, because this may result in insulation settling. Generally, untreated (unprotected against liquid water absorption) bio-based insulation materials run the risk of rapid moisture degradation in case of unintended water entry.

To avoid damage and degradation, it is important to protect bio-based insulation materials from direct exposure to liquid water. Even small water leaks and condensation may pose problems if the water cannot dry out fast enough. Therefore, sophisticated moisture control strategies have to be pursued to ensure long-term system durability. Moisture tolerant design aided by hygrothermal simulation and professional installation checked by blower-door tests and thermography should be standard practice for all sustainable constructions.

## 6.3 Thermal Transfer Properties

The thermal properties which are part of the hygrothermal properties depend mainly on bulk density, homogeneity and fiber thickness resp. pore size of the insulation. The specific heat capacity in dry state is usually comparable to that of organic foams. Higher values found in literature are often due to sorption moisture which should be accounted for separately. The thermal conductivity of competitive bio-based insulation materials can reach similar levels as conventional mineral fiber or EPS insulation. However, bio-based materials are still not getting close to the low values achieved

**Table 6.1** Density and German design values for thermal conductivity of different bio-based insulation materials listed in FNR (2020)

Insulation material	Density (kg/m <sup>3</sup> )	Thermal conductivity [W/(m · K)]
Flax batts	30–40	0.039
Hemp batts	50–60	0.043
Wood fiber batts	40–50	0.038
Wood fiber boards	110–270	0.040
Cellulose fiber boards	70–145	0.042
Wood wool cement boards	350–500	0.090
Expanded cork boards	120	0.040
Reed boards	150	0.065
Seaweed boards	65–75	0.045
Straw bales	85–115	0.052

by modern high-performance insulation. Table 6.1 gives an overview of densities and design thermal conductivities of commonly used bio-based insulation batts and boards.

The German design value  $k$  is derived from the declared thermal conductivity  $k_D$  (90% confidence interval) measured at 10 °C mean temperature on samples conditioned at 23 °C and 50% RH according to the wood fiber products standard DIN EN 13171—see: DIN EN 13171 (2015). Compared to the dry thermal conductivity, the value at 50% RH of wood fiber insulation calculated as explained in Appendix D of this standard ranges between 1 and 2% and is therefore almost negligible (<1 mW/(m · K)). This can be explained by the calculation method in ISO 10456 which allows the determination of thermal conductivity in the hygroscopic range, between the dry state and an equilibrium moisture content at 50 or 80% RH, using an exponential approach and tabled coefficients. This method excludes explicitly all latent heat effect, i.e. the input values must also be determined in a way that excludes any interference by heat transfer related to vapor transport.

To arrive at the design conductivity (according to German technical approvals but there are similar approaches in other countries, e.g. European Technical Assessment ETA) a safety margin is added to the declared value which differentiates between quality controlled (third party monitoring) insulation materials and others. Without quality control the safety margin is at least 20%. For quality controlled materials 3% is added for non-hygroscopic and 5% for hygroscopic insulation materials. EPS and mineral wool are considered non-hygroscopic while all bio-based insulation materials are classified hygroscopic. The difference between declared and design value is believed to represent a safety margin bridging the performance measured under laboratory conditions to that in practice applications. It also includes the effect of moisture that is unavoidable in best practice constructions. The 2% difference between non-hygroscopic and hygroscopic insulation materials is explained by the

sorption moisture in equilibrium with in-situ climate conditions. The design values  $k$  of insulation materials without an ETA (European Technical Assessment) are determined by default according to ISO 10456 (2007). In case of wood fiber board  $k$  is  $0.07 \text{ W}/(\text{m} \cdot \text{K})$  which is so bad that all manufacturers apply for an ETA.

### 6.4 Moisture Transfer Properties

Fibrous bio-based insulation materials are generally very vapor permeable. Their vapor diffusion resistance is comparable to that of mineral fiber products, ranging from one to five times the diffusion resistance of stagnant air. Therefore, some kind of vapor control strategy is usually required. The main difference to the mostly non-hygroscopic mineral fiber products lies in their vapor sorption capacity. Figure 6.2 shows the moisture retention curves for widely used structural building materials. In the hygroscopic humidity range, wood has the highest vapor sorption capacity because cellulose can store large amounts of moisture.

The same holds for most bio-based insulation materials (see examples in Table 6.2). It is obvious that the moisture storage capacity depends on the bulk density of the material, because the water molecules are absorbed by the fibers and higher density means more fibers. Therefore, the equilibrium moisture content at 80% RH ambient conditions are also given in mass-%. This proves that the moisture fiber sorption properties of the different bio-based materials all end up in a narrow range between 15 and 18 mass-%. This is the same range as found for solid timber.

**Fig. 6.2** Moisture retention curves aka sorption curves in the hygroscopic range (below 95% RH) of fired clay brick, concrete and wood

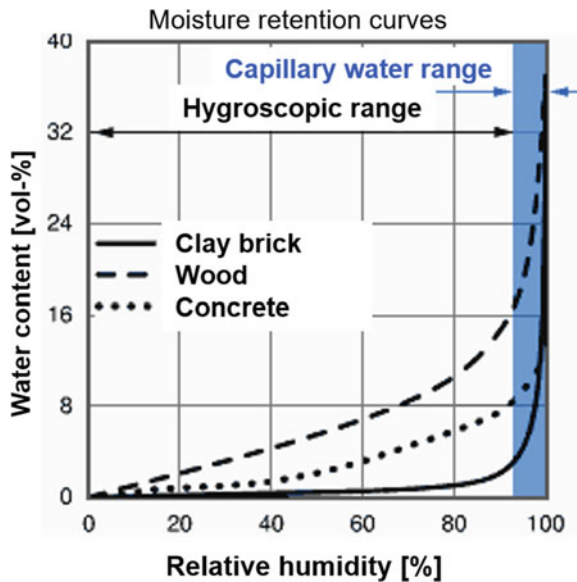


**Table 6.2** Moisture transfer properties of bio-based insulation materials from the Fraunhofer Institute for Building Physics, WUFI 6 material database ([www.wufi.com](http://www.wufi.com)) The vapor diffusion resistance factor is defined as the ration of vapor permeability in air to that in a porous material

Insulation material	Density (kg/m <sup>3</sup> )	Vapor diffusion resistance factor (–)	Equilibrium moisture content at 80% RH (kg/m <sup>3</sup> )	Equilibrium moisture content at 80% RH (mass-%)
Wood fiber batts	50	2	9	18
Wood fiber boards	140	3	21	15
Cellulose fibers	50	1	8	16
Seaweed batts	80	2	14	18
Wood wool cement boards	450	9	70	15
Straw bales	85	2	13	15

In contrast to concrete with its rather high vapor diffusion resistance, the sorption capacity of fibrous insulation is readily accessible for vapor in the air, due to their high porosity and vapor permeability. The combination of sorption capacity and vapor permeability describes the so-called moisture buffering performance of materials. This effect helps to dampen changes in RH in building assemblies or even in living rooms with moisture buffering interior lining and furnishing materials. To quantify the moisture buffering performance a moisture buffering value (MBV) has been defined that depends on the product of the material parameters vapor permeability and mean slope of the sorption curve in the range of indoor RH—see: Roels and Janssen (2006).

Among interior finishes, bio-based insulation materials show a strong dampening effect on the indoor RH fluctuations. Experimental investigation in twin rooms with different wall and ceiling finishing materials have demonstrated that wood fiber boards can reduce indoor RH peaks, resulting from moisture production cycles, by approximately 80% compared to the situation in a plastered reference room—Künzel et al. (2004). However, this remarkable RH dampening performance will only be achieved if the wood fiber boards are in direct contact with the indoor air. If the boards are coated, plastered or covered by gypsum board, the buffering effect is much smaller. In the same investigation acoustic panels that had wood fiber boards at the backside and perforated plywood at the front reduced the indoor RH peaks only by 15% in comparison to the reference room. This proves that the moisture buffering effect of bio-based insulation materials on the indoor RH is of little practical relevance because the insulation is rarely in direct contact with the indoor air.

The moisture buffering effect will also impact the hygrothermal conditions within the building assembly. Compared to the large daily RH cycles in flat roofs with non-hygroscopic insulation already discussed in Chapter 2, it can be expected that hygroscopic insulation materials will also act as RH dampening factor there.

Figure 6.3 compares the measured RH conditions in two identical light-weight flat roof constructions, one insulated with mineral fiber and the other with cellulose fiber loose fill between OSB boards—see: Pangratz and Holm (2004). The unvented roof constructions are part of a test building at the field test site of the Fraunhofer IBP in Holzkirchen (Bavarian alpine region). They are sealed by a dark roofing membrane at the top and rendered airtight by a second layer of OSB boards at the bottom. The indoor temperature is set to 20 °C. At the beginning of the 15 months test period the employed materials were dry (sorption moisture content in equilibrium at approx. 50% RH). At the end of the test period the moisture distribution in the roofs were very similar to the initial conditions, i.e. no net moisture gains or losses were recorded.

Looking at the daily mean RH at the top and bottom of both roofs in Fig. 6.3, demonstrates that even with little moisture in the assemblies there is a distinct seasonal migration between top and bottom, with peaks at the top in winter and at the bottom in summer. The impact of the insulation materials on the daily RH mean values is rather small. However, the daily fluctuations indicated by the daily RH maxima and minima are very different. While the measured humidity changes between day and night reach 40% RH at the bottom as well as on the top of the mineral fiber insulation layer, the moisture buffering effect of the hygroscopic cellulose fiber insulation is clearly visible, with diurnal humidity changes mostly below 10% RH.

The reduction of RH maxima and minima in construction assemblies by hygroscopic insulation materials renders mold growth due to humidity peaks less likely and

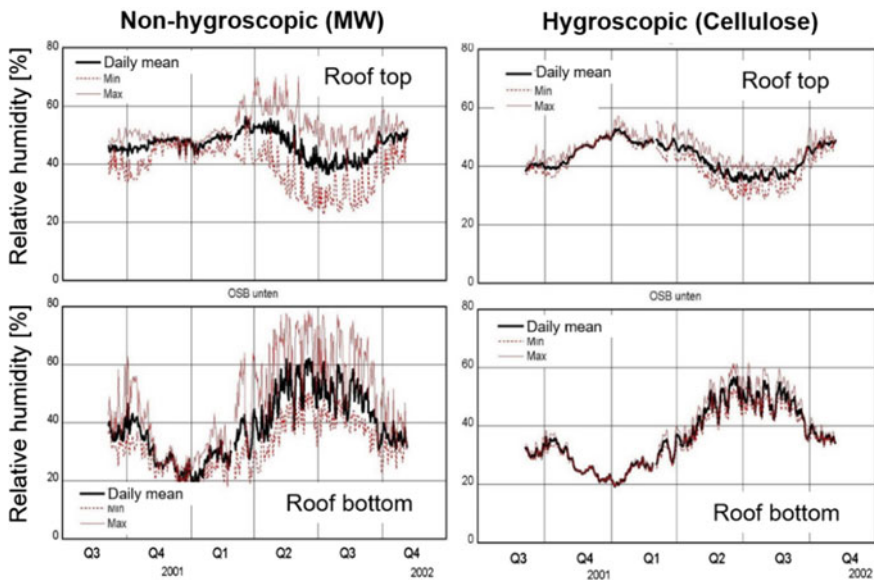


**Fig. 6.3** Moisture conditions recorded at top and bottom of the insulation layer in unvented flat light-weight roof constructions over a period of 15 months

may also prevent cracks caused by hygric dilatation (shrinkage and swelling). The moisture buffering capacity of hygroscopic bio-based materials may also accommodate moisture ingress due to humid indoor air infiltration into the assembly before it can dry out during the next season. This could be clearly beneficial because building assemblies are never completely airtight—see: Kölsch et al. (2016). On the other hand, any rainwater leak will be detected with delay, because much of the leaking water is absorbed, before the damage becomes apparent. Restoring such a water damaged roof by convective drying methods may be rather difficult, if not impossible.

In conclusion, the application of moisture buffering insulation materials has pros and cons, in any case it is important to be aware of them. The hygroscopic properties must also be taken into account for moisture control design. E.g., it is essential to ensure that hygroscopic materials are dry enough (in equilibrium with 50% RH) before they are installed, otherwise the moisture released after enclosure may cause damage. If they are really dry, they can also help to dry out a structure after water damage restoration, however, this should be carefully analyzed beforehand. Smart (humidity controlled) vapor retarders may not work as expected. The so-called hydrodiode, which relies on drying the assembly by wicking liquid water through a capillary active fabric, will not work if condensation doesn't occur and even if it occurs it will probably be absorbed by the insulation material before it reaches the wicking fabric—Künzel and Leimer (2001).

## 6.5 Hygrothermal Evaluation of Thermal Conductivity Measurements

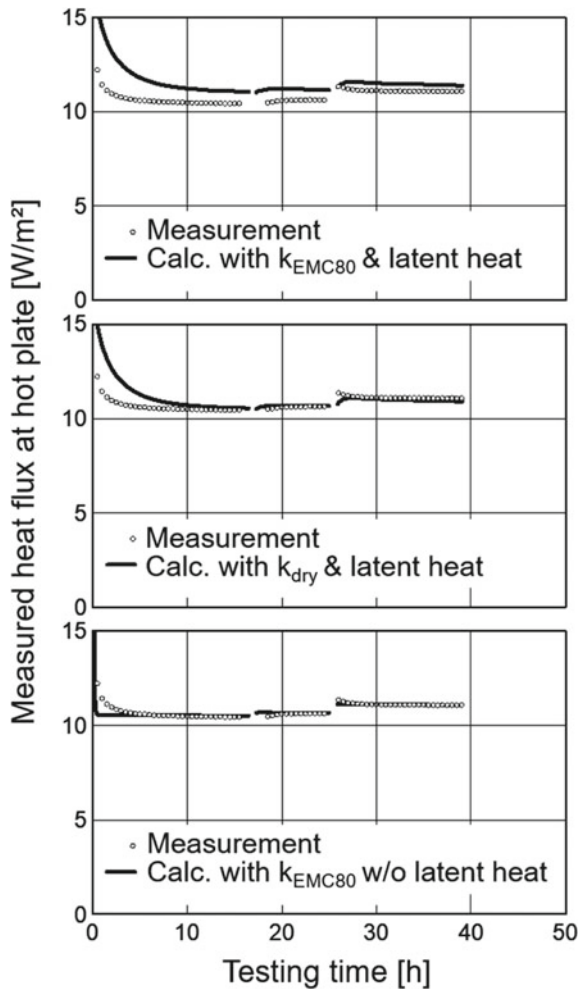
Thermal conductivity measurements of insulation materials are usually performed by installing a material sample between two temperature-controlled plates. The heat flow through the material is either determined by a heat flux transducer or by measuring the heating power supplied (guarded hot plate) with the latter method being slightly more accurate. For dry materials this is a well proven method which usually delivers reliable results. To make sure that the airflow resistance of the tested material sample is high enough to exclude buoyancy effects, it is recommended to either test the airflow resistance of the materials before, or to measure the heat flux horizontally and vertically with a temperature difference of at least 20 K. Some bio-based insulation materials may show considerably higher heat fluxes when installed vertically (horizontal heat flux) instead of horizontally, because their airflow resistance is too small. This may be the case with straw bales or other materials with connected open spaces of a certain size.

Determining the thermal conductivity of moist materials becomes rather challenging if they are very vapor permeable. This is due to the latent heat effect as already explained in Chapter 2. Since bio-based materials contain more sorption moisture than conventional mineral fiber insulation, also the latent heat effect will be

more pronounced. For this reason, the heat flux through moist cellulose fiber insulation has been measured by the hot-plate method and compared to hygrothermal simulation results employing the same boundary conditions in Kehrer et al. (2003). The heat flux was first measured at 20 °C, then at 25 °C and finally at 35 °C mean temperature in one test, each time with a temperature difference of 10 K.

Compared to the dry samples the cellulose fiber insulation samples conditioned to EMC<sub>80</sub> (equilibrium moisture content at 80% RH) showed an increase of 6% in the measured heat flux. When the heat flux was determined by hygrothermal simulation using the measured thermal conductivity of the moist cellulose fiber samples  $k_{EMC80\%}$  ( $k_{dry}$  multiplied by 1.06) the simulated heat flux curve proved to be somewhat higher than the measured one (see Fig. 6.4, top graph). When  $k_{dry}$  was used for the simulation instead of  $k_{EMC80\%}$ , measured and simulated heat flux corresponded very well (middle

**Fig. 6.4** Heat flux through cellulose fiber insulation sample, preconditioned to EMC at 80% RH, measured at the warm side of a hot plate apparatus (small circles indicating the same test results in all 3 graphs for 3 successive mean temperature steps) compared to hygrothermal simulation results (solid lines). The calculations were performed with the thermal conductivity determined from the same test (top graph), with the thermal conductivity of a dry sample of the same material (middle graph) and repeating the first simulation (top graph) without latent heat effect (bottom graph)





graph in Fig. 6.4). Repeating the calculations without latent effect (by setting the heat of evaporation to zero which is only possible in simulations, not in reality) and using  $k_{EMC80\%}$  again, resulted in almost the same heat flux curve as in the simulation using  $k_{dry}$  with latent heat effect, i.e. the results also show very good correspondence with the measured heat flux again.

As outcome of this exercise, it may be concluded, that the moisture related rise in the measured heat flux is caused by the latent heat effect only (i.e. by sorption moisture evaporating at the warm side and condensing on the cold side of the cellulose insulation sample). It is not caused by the impact of moisture on the real thermal conductivity of the material. Analogous results were also obtained with wood shavings as insulation material. If these results can be confirmed for other hygroscopic insulation materials, the consequence should be to abolish any moisture related thermal resistance penalty which is only applied to bio-based insulation materials and not to non-hygroscopic fiber insulation.

## 6.6 Life-Cycle Assessment of Bio-based Insulation Materials

At first sight, bio-based materials seem to be very eco-friendly. However, since the raw materials are generally flammable, fire-retardant compounds are often added to lower their natural flammability. Usually between 5 and 15 mass-% of fire protection salts such as borates, ammonium phosphates and sodium silicates are included in the final products—see: FNR (2008). The achievable fire rating according to ISO 11925-2 (2020) ranges between D and E—FNR (2008). However, flame retardants are not the only compounds that may raise some concern. Since bio-based insulation materials are often quite susceptible to mold growth, small quantities of fungicides may be employed to render them more mold resistant especially during the construction phase. Last but not least, with the exception of some wood fiber products (wet production process) manufacturing boards or batts requires up to 10% of chemical binders (e.g. polyurethane) or polymer fibers (e.g. polyester).

Assessing the environmental and health impacts of all these compounds is time consuming and all relevant information should be provided by the manufacturer. Sometimes compounds that are considered safe today may end up being reevaluated because of numerous concerns arising. There may be also differences in national classifications especially regarding safe limit concentrations. Therefore, no general assessment can be presented here, however, the progress in manufacturing technology and growing knowledge about potentially dangerous substances has improved the environmental quality of most bio-based materials. This also holds for emissions into the indoor air such as formaldehyde or other VOCs—FNR (2008).

Another important aspect of the life cycle assessment is the carbon footprint of building materials. This includes the carbon emissions for extracting, respectively farming the raw materials. Carbon sequestration during the growth process is

subtracted from this balance leading to a negative carbon footprint of many bio-based raw materials. However, arriving at the final product can offset the initial advantage of bio-based materials, because carbon emissions due to transport of the raw materials and during manufacturing process which often includes drying processes may exceed those of conventional insulation materials. In the end, the carbon equivalents of bio-based and conventional insulation materials are of the same magnitude—see: Reinhardt et al. (2019), and there is no clear advantage of either of them regarding their carbon footprint.

This comes as no real surprise because insulation materials contain mainly air which means their carbon footprint per kg is already pretty competitive. Applying insulation will always reduce the carbon footprint of buildings during operation by multiples of their own production emissions, regardless of the type of insulation material. Because of their low mass and high volume, long-distance transport is inefficient and manufacturing close to the construction site is preferable. This aspect could be beneficial for bio-based insulation materials because they are usually produced by small and medium size enterprises covering only regional markets.

## 6.7 Conclusions and Outlook

Due to perceived ecological reasons and homeowners' preferences, sales and applications of bio-based insulation materials are on the rise. Their thermal performance is generally comparable to conventional insulation materials, however, there is still room for improvements. The largest share in the building insulation market still belongs to polymeric foams and mineral fiber insulation products. Both have achieved significant reductions in their thermal conductivities in the past 20 years; e.g. EPS by diminishing radiant heat flow by adding graphite or other radiation absorbing dyes; mineral wool by optimizing fiber diameter and webbing structure. Similar approaches to improve the thermal performance could also be attempted by manufacturers of bio-based materials.

The hygrothermal performance of bio-based materials, especially their moisture buffering capacity and their high vapor permeability represent real benefits, while the moisture susceptibility is the most important downside. However, with up-to-date moisture control design, good solutions to protect bio-based insulation materials from damage and degradation are at hand. Sometimes, a combination of conventional and bio-based products with the conventional products being installed at the most critical positions in the building envelope, would be the best solution. However, experience with ecology minded homeowners shows that this option is often the least preferred, which will probably change when bio-based materials become more mainstream.

The high market share of wood fiber insulation among bio-based products in Europe, may be explained by the long history and experience of the wood processing industry. They have not only succeeded in turning their waste material into valuable products. They have also benefitted from their large customer base as well as from

established production lines that could be modified to generate new insulation products. The facts that foresting does not compete with agricultural cultivation and that timber products have a certain resistance against biodegradation may also have helped to push wood fiber insulation.

However, timber may not be a rare commodity yet, but its exploitation is increasing. At the same time, there are many countries with timber shortage. Therefore, alternatives for timber products should be more researched and promoted in future. This may include bamboo—see: Huang (2021), or plants growing in less valuable wetlands, e.g. reed or cattail (also called bulrush or *Typha* in Latin), the latter having stems with a natural spongy interior structure that may serve as natural insulation material with little further refinement—see: Georgiev et al. (2019).

The current voices calling for greener buildings, make believe that the future belongs to bio-based materials. However, it should not be forgotten that insulation materials, regardless of their sources, make buildings greener because they help to save operation energy and thus also carbon emissions. Considering their bulk density, even conventional insulation materials do not contain much embodied energy per mass. From an ecological point of view, carbon sequestration through the growth of bio-based materials is only beneficial if manufacturing and application of the final products are resource efficient (energy and water). Equally important is the question whether the variety of chemicals used for manufacturing and to protect the final product are acceptable from health perspectives and environmentally friendly. In order to arrive at fair assessments, more detailed analyses of the individual bio-based products are recommended prior to widespread applications.

## References

- DIN EN 13171. (2015). *Thermal insulation products for buildings—Factory made wood fibre (WF) products—Specification*. <https://shop.bsigroup.com/ProductDetail?pid=00000000030301854>.
- Eicke-Henning, W. (2011). Kleine Geschichte der Dämmstoffe. *History of insulation materials*. wksb (Wärme, Kälte, Schall, Brand) 65/2011, pp. 6–34. <https://doczz.com.br/doc/1059952/kleine-geschichte-der-d%C3%A4mmstoffe--hessische-energiespar>.
- FNR. (2008). Fachagentur Nachhaltige Rohstoffe (FNR) Report: Untersuchungen zur Optimierung und Standardisierung von Dämmstoffen aus nachwachsenden Rohstoffen. *Investigation concerning optimization and standardization of bio-based insulation materials*. <https://www.fnr.de/suche?q=Untersuchungen+zur+Optimierung+und+Standardisierung+von+D%C3%A4mmstoffen+aus+nachwachsenden+Rohstoffen>.
- FNR. (2020). Fachagentur Nachhaltige Rohstoffe (FNR): Marktübersicht Dämmstoffe aus nachwachsenden Rohstoffen. *Market overview of bio-based insulation materials* (pp. 13). <https://mediathek.fnr.de/dammstoffe-aus-nachwachsenden-rohstoffen.html>.
- Georgiev, G., Krus, M., Loretz, C., Theuerkorn, W. (2019). *Typha board in the restoration of historic Black Sea houses in Bulgaria*. MDPI sustainability, February 15, 2019, p. 13. <https://doi.org/10.3390/su11041000>.
- Huang, Z. (2021). *Resource-driven sustainable bamboo construction in Asia-Pacific Bamboo Areas*. Springer 2021, ISBN: 978-3-030-73535-7. <https://www.springer.com/gp/book/9783030735340>.

- ISO 10456. (2007). *Building materials and products—Hygrothermal properties—Tabulated design values and procedures for determining declared and design thermal values*. <https://www.iso.org/standard/40966.html>.
- ISO 11925-2. (2020). *ISO 11925-2:2020-07 Standard: Reaction to fire tests—Ignitability of products subjected to direct impingement of flame—Part 2: Single-flame source test*. <https://www.iso.org/standard/71204.html>.
- Kehrer, M., Künzel, H. M., & Sedlbauer, K. (2003). Ecological insulation materials—does sorption moisture affect their insulation performance? *Journal of Thermal Envelope Building Science*, 26(3), 207–212.
- Kölsch, Ph., Zirkelbach, D., Nusser, B., Wagner, R., Zegowitz, A., Künzel, H.M. (2016). Airflow through lightweight wall assemblies—influence of size and location of leakages. In: *Proceedings of the Buildings XIII Conference*, Clearwater, FL, USA, December 4–8, 2016 (pp. 459–484). ASHRAE.
- Künzel, H. M. & Leimer, H.-P. (2001). Performance of innovative vapor retarders under summer conditions. *ASHRAE Transactions 2001*, Part. 1, 417–420.
- Künzel, H. M. et al. (2004). Moisture buffering effects of interior linings made from wood or wood based products. *Fraunhofer IBP (Institute for Building Physics) Report HTB-04/2004/e* [http://publica.fraunhofer.de/eprints/urn\\_nbn\\_de\\_0011-n-267933.pdf](http://publica.fraunhofer.de/eprints/urn_nbn_de_0011-n-267933.pdf).
- Pangratz, O., Holm, A. (2004). Designing and testing a SIP (Structural Insulated Panel) with the help of WUFI®. In: *Proceedings of the Buildings IX Conference*, Clearwater, FL, USA (p. 8). ASHRAE. <https://www.designaid.at/2017/03/04/designing-and-testing-a-structural-insulated-panel-sip-wth-the-help-of-hygrothermal-model>.
- Reinhardt, J., Veith, C., Lempik, J., Knappe, F., Mellwig, P., Giegrich, J., Muchow, N., Schmitz, T., Voß, I. (2019). Ganzheitliche Bewertung von verschiedenen Dämmstoffalternativen. *Holistic evaluation of different insulation material alternatives*. DBU project report AZ 34426\_01, Heidelberg/Neckargemünd, 2019. [https://www.dbu.de/projekt\\_34426/01\\_db\\_2409.html](https://www.dbu.de/projekt_34426/01_db_2409.html).
- Roels, S., & Janssen, H. (2006). A comparison of the Nordtest and Japanese test methods for the moisture buffering performance of building materials. *Journal of Building Physics*, 30(2006), 137–161.

# Chapter 7

## Bio-based Foam Insulation



Sylwia Członka, Agnė Kairyė, and Anna Strakowska

**Abstract** The depletion of fossil feedstock, climate change, and environmental pollution push the scientific and industrial communities to focus their researches and production on more ecological materials using sustainable approaches. The substitution of fossil feedstock by renewable substances from biomass is driven by the development of new materials having different molecular architectures with greater or new performance characteristics. Innovative development based on ideas of circular economy and cleaner production requires new solutions in the production of bio-based components for the polymers industry, which could generate more benefits for the economics and environment. Natural oils are sustainable, eco-friendly renewable resources that can be applied to synthesize a new class of precursors such as polyols that can be implemented in the production of different polymeric materials, such as polyurethanes. Polyurethanes are commonly derived by the reaction of low molecular weight polyols with isocyanates. Both of the raw materials used contain at least two or more functional groups per molecule, which result in the formation of branched, linear or cross-linked polyurethane products. Nowadays, bio-based polyurethane foams from various vegetable- or waste-based oils and natural fillers as reinforcement are of great importance in order to increase the renewable content of the resultant products. Therefore, the chapter reveals the advantages of natural oil-based and natural filler reinforced polyurethane foams with improved performance characteristics and application possibilities in the building industry.

---

S. Członka (✉) · A. Strakowska  
Institute of Polymer Dye Technology, Lodz University of Technology, 90-924, Lodz, Poland

A. Kairyė  
Faculty of Civil Engineering, Institute of Building Materials, Laboratory of Thermal Insulating Materials and Acoustics, Vilnius Gediminas Technical University, Linkmenu st. 28, 08217 Vilnius, Lithuania

## 7.1 Introduction

According to the United Nations Environment Program, buildings and their construction account for 36% of global energy demand while 39%—of energy-related CO<sub>2</sub> emissions annually, therefore the energy performance of buildings is an important factor to reduce CO<sub>2</sub> emissions. Some studies have shown that increasing the amount of insulating material or even adding it within the building envelope reduces the heating demand by 20–60% (Martínez-Molina et al., 2016). According to statistics, the global rigid polyurethane (PUR) foam insulation market is foreseen to grow from USD 37.8 billion in 2020 to USD 54.3 billion in 2025. The long-term thermal benefits and energy efficiency improvement of such materials have been demonstrated, meanwhile, the total environmental quality of buildings is still a subject of continuing research.

To understand the benefits of using PUR and polyisocyanurate (PIR) insulation for increasing thermal comfort, Fig. 7.1 summarises the declared thermal conductivity values of common insulation materials. Data were collected from widely available declarations of performance (DoP) for products that conform the requirements of EN 13,162 for stone and glass wool (SW and GW, respectively) products, EN 13,163 for expanded polystyrene foam (EPS) products, EN 13,164 for extruded polystyrene foam (XPS) products and EN 13,165/EN 14,315-1 for factory-made and sprayed PUR and PIR foams. For new buildings that aim to achieve zero carbon emissions and existing buildings to alleviate fuel poverty, PUR and PIR foams offer higher potential for energy savings and thermal comfort compared to conventional thermal insulating materials existing in the market.

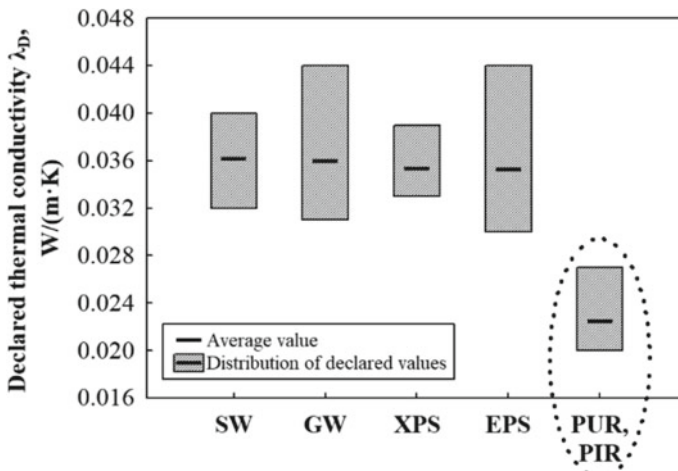


**Fig. 7.1** Declared thermal conductivity values of common commercially available thermal insulating materials

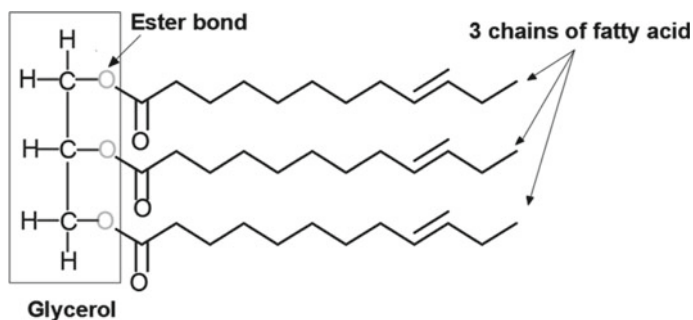


**Fig. 7.2** General representation of natural oil triglyceride

Extensive research on bio-based materials derived from agricultural crop has demonstrated their potential viability as building. Biobased materials can capture and store  $\text{CO}_2$  through photosynthesis, can be harvested annually, and are biodegradable at their end of service life. Notably, of all the available insulation materials PUR/PIR foams from renewable resources are the most potential ones because of their low cost, fairly high mechanical strength, and low thermal conductivity. It is noticed that tremendous attention in the scientific community is paid to the modification of PUR/PIR foams to obtain “greener” and more sustainable building material with improved thermal insulation and mechanical capacity (Choe et al., 2019; Oh et al., 2019). Currently, PUR/PIR foam found its alternative raw materials which had to be replaced with more sustainable solutions. Petroleum feedstock-based polyols were substituted with polyols from various natural oils, i.e. rapeseed (Kairyte et al., 2018a), soy (Dhaliwal et al., 2018), castor (Trovati et al., 2019), linseed (Czlonka et al., 2018a), etc.

All-natural oils, except castor oil, must be chemically modified to be suitable for the production of PUR/PIR foam products as they do not contain any hydroxyl groups. A general structure of natural oil triglyceride is presented in Fig. 7.2.

Most of the plant oils-based biopolyols are made from triglycerides, sometimes fatty acids, and some derivatives of fatty acids might be used as well. As it is seen from Fig. 7.2, triglycerides are made of three fatty acids that are connected to the glycerine backbone via ester linkages. The most abundant fatty acids have a length from 16 to 20 carbons and differentiate in unsaturation from 0 to 3 double carbon bonds. All plant oils, except castor oil, must be suspected to the chemical conversion of carbon-carbon double bonds or ester groups into reactive ones, i.e. hydroxyl groups. It can be achieved by epoxidation and oxirane ring-opening, ozonolysis and reduction, hydroformylation and reduction as well as various enzymes involves routes of natural oils double bonds. The reagents used for the preparation of biopolyols have the largest influence on the final chemical properties of the polyol and PUR/PIR foam itself. Biopolyols with secondary hydroxyl groups and functionality in the range of 2–3 are more suitable for flexible polyurethane foams production (Marcovich et al., 2017b). While biopolyols with a functionality of 3–5 deliver rigid PUR/PIR foams

(Szycher, 2017). Incorporation of a component containing long and linear chains into PUR/PIR foams causes a decrease in the packing degree of polymer macromolecules. Also, fatty acid residues have flexible segments with low or non-cross-linking ability which lead to open porosity, low mechanical performance and structural stability.

## 7.2 Requirements and Dimensional Stability of Biopolyol-Based Pur/Pir Foams

In-situ or factory made sprayed PUR/PIR foam products placed on the market must conform to strict requirements of harmonized product standards and the most important ones which can affect the building state and thermal comfort are presented in Table 7.1.

If water is used as a blowing agent, CO<sub>2</sub> gases generated during biopolyol and isocyanate reaction diffuse out of the foamed products instantly thus developing a pressure difference which causes the collapse of cell walls and dimensional instabilities in final PUR foam products obtained from low functionality rapeseed oil-based polyol (RP) as presented in Fig. 7.3.

From Fig. 7.3a, it can be observed that as the amount of water in the mixture increases from 1.0 parts by weight (pbw) to 5.0 pbw, the initial shrinkage increases as well. This means that the structure of the final product is not rigid enough to balance the pressure difference between the porous structure and the surrounding environment. The initial shrinkage occurs due to the faster diffusion of gas from the porous structure into the environment compared to the rate of air penetration into the porous structure. In this way, PUR foam goes through three main stages: the first stage is the process of formation of nucleus and cells, during which the atmospheric and internal pressures are the same. The second stage is the hardening of the foam, during which the molecular weight of the mixture increases and the process of cells

**Table 7.1** The most important requirements for in-situ and factory made sprayed PUR/PIR foam products placed on the market

Parameter	Target value
Apparent density, kg/m <sup>3</sup>	35–50
Closed cell content, vol.%	≥90
Thermal conductivity, W/(m·W)	Minimum
Compressive strength, kPa	≥100
Water absorption, %	≤4
Initial dimensional changes, %	Not standardized
Dimensional stability at 70 °C and 90%, %*	≤15
Fire resistance	class E

\* ≤ 5% in length and width and ≤ 10% in thickness according to EN 13,165 or ≤ 5% length and width and ≤ 0% thickness according to EN 14,315–1



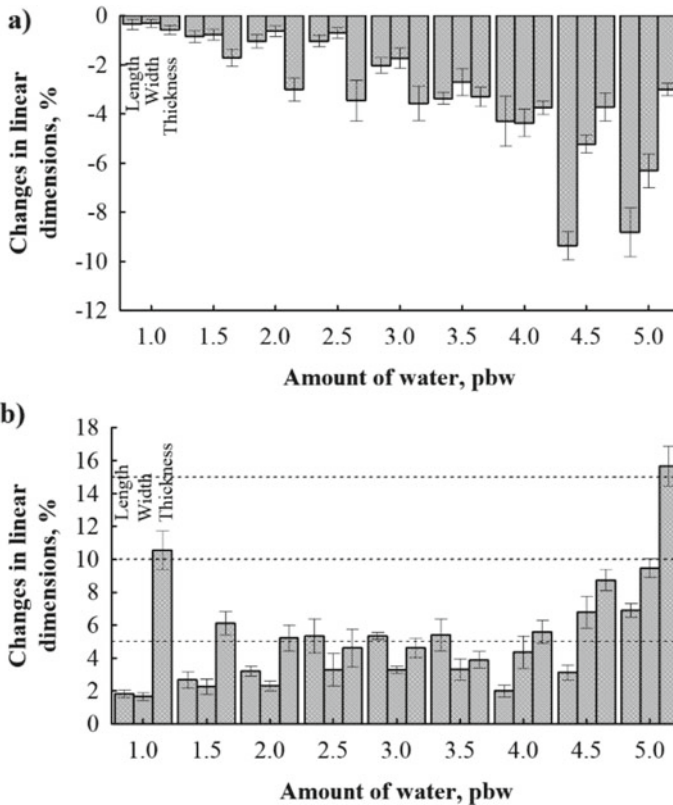


**Fig. 7.3** Dimensional changes of PUR foam at different amounts of water: **a** initial shrinkage and **b** dimensional stability at 70 °C temperature and 90% relative humidity

formation ends. While the foam reaches its final height, the internal temperature of the product and the internal pressure in the cells increases.

The third stage begins when the internal temperature of the product and the pressure in the cells begin to decrease. This means that when the internal pressure is lower than atmospheric pressure, initial shrinkage occurs in PUR foam products. The intensity and magnitude of these shrinkages depend on the amount of water used in the forming mixture and the nature of the porous structure (closed or open). The increase in water content results in a PUR foam structure with larger closed cells and thinner walls between them, which means that the diffusion of CO<sub>2</sub> gas through these walls is more intense and the shrinkage of the final product is higher.

As the temperature changes, all the materials expand or shrink more or less. The results presented in Fig. 7.3b can be divided into two main zones: from 1.0 pbw to 3.0 pbw and from 3.5 pbw to 5.0 pbw. Studies on dimensional stability under elevated temperature and humidity conditions show a decrease in the change in linear dimensions when the amount of water ranges from 1.0 pbw to 3.0 pbw. It

can be argued that the highest density PUR foam has a sufficiently rigid, thicker-walled porous structure that restricts the penetration of CO<sub>2</sub> gas into the environment, resulting in low initial shrinkage, but the residual gas trapped in cells escapes from the product at higher temperatures thus causing negative dimensional changes. The exact opposite trend is observed for products where the amount of water used varies from 3.5 pbw to 5.0 pbw. This is explained by the fact that lowering the density of the product requires more water. As a result, the cell walls become thinner, and the rate of CO<sub>2</sub> gas diffusion and the resulting changes in linear dimensions intensify both after production and during testing.

In order to assure the properties and structural parameters indicated in Table 7.1 and avoid any structural instabilities, it is desirable to use higher functionality polyols such as glycerol, sorbitol- or sucrose-based ones, etc. to stabilize the structure and increase cross-link potential of the final products (Fig. 7.4).

For comparison purposes, 3 pbw of water was used for the synthesis of PUR foam. It is seen from Fig. 7.4 that the addition of glycerol to polyol mixture reduces

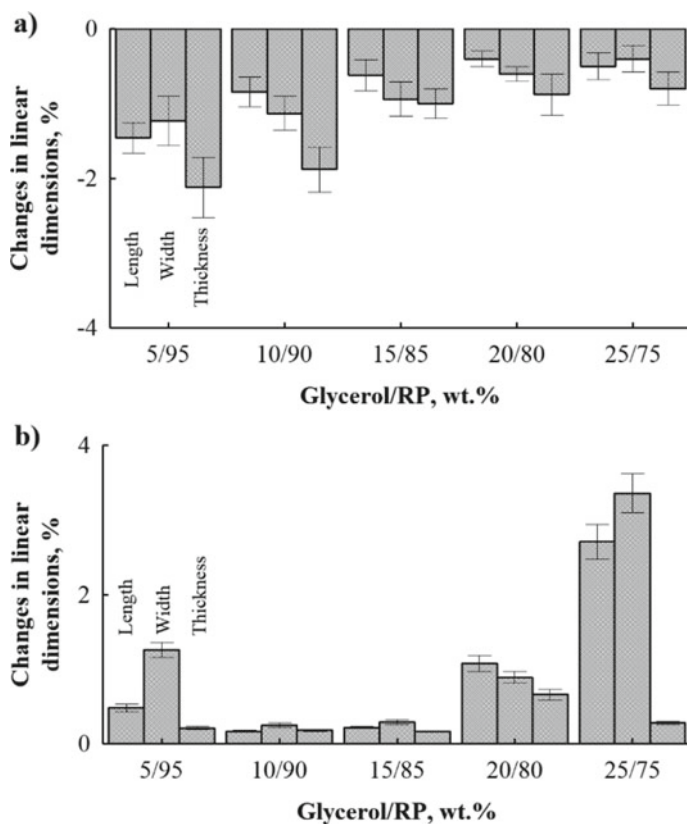


**Fig. 7.4** Dimensional stability of PUR foam at different weight ratios of glycerol/RP: **a** initial shrinkage and **b** dimensional stability at 70 °C temperature and 90% relative humidity

initial dimensional changes and the ones under increased temperature and humidity conditions. Even 5 pbw of glycerol reduced initial changes almost twice, i.e. from  $-4$  to  $-2\%$  in the thickness direction, while dimensional stability under increased temperature and humidity conditions was lowered from 5 to 0.5% in the thickness direction as well. It can be attributed to the increased cross-link density and the formation of thicker cell walls so the escape of  $\text{CO}_2$  gases is more aggravated.

### 7.3 Thermal Conductivity and Microstructure of Biopolyols-Based Pur Foams

The replacement of petroleum-based polyols with biopolyols has also a significant influence on the foaming reaction of PUR/PIR systems. The numerical values of cream, gel, tack-free times and maximum foaming temperature are presented in Table 7.2.

Table 7.2 shows that the replacement of petroleum-based polyol with 10–40% biopolyol determined slower reactivity of PUR mixtures. The study of (Kurańska & Prociak, 2016) showed that the addition of RP from 0 to 70% altered the main characteristic foaming times, i.e. cream, gel, and tack-free times. Cream and gel times were affected insignificantly while tack-free time was delayed by more than 2.5 min. at 70% of RP due to its secondary hydroxyl groups which reduce the reactivity of the overall system. Moreover, an even worse scenario was observed in (Kairyte & Vejelis, 2015) research where at 100% of RP-based PUR foam had a tack-free time equal to 10 min.

Thermal conductivity is influenced by three factors—conduction via polymer, conductivity via gas in a closed cell structure, and the radiation between cells (Septe-vani et al., 2015). For a rigid closed cell PUR foam with an apparent density of  $\sim 40 \text{ kg/m}^3$  using commercial blowing agent, conduction via cells, conduction via polymer struts/walls and radiation via foam represent respectively  $\sim 50\%$ , 15% and 35%. Therefore, gaseous blowing agent mainly determines the thermal conductivity value. Figure 7.5 shows the effect of biopolyol amount and the type of blowing agent on the thermal conductivity value of RP-based PUR foam.

**Table 7.2** Characteristic foaming times of PUR with different biopolyol amounts

Characteristic	RP amount (%)				
	0	10	20	30	40
Cream time, s	$9 \pm 2$	$11 \pm 2$	$16 \pm 3$	$18 \pm 1$	$20 \pm 2$
Gel time, s	$22 \pm 3$	$24 \pm 3$	$26 \pm 2$	$30 \pm 2$	$33 \pm 2$
Tack-free time, s	$110 \pm 3$	$132 \pm 4$	$151 \pm 3$	$160 \pm 3$	$175 \pm 2$
Max. temperature, °C	$162 \pm 3$	$158 \pm 5$	$152 \pm 4$	$144 \pm 3$	$137 \pm 3$

**Fig. 7.5** The impact of biopolyol amount and the type of blowing agent on thermal conductivity of PUR foam

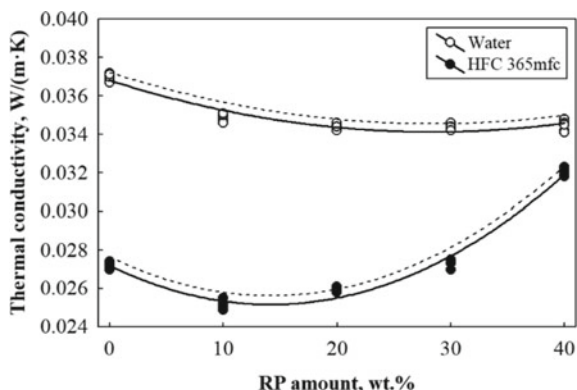


**Table 7.3** Statistical data of thermal conductivity results

Blowing agent	No. of samples	Equation coefficients			$R^2_{\lambda_{10^\circ\text{C}}}$	$S_{\lambda_{10^\circ\text{C}}}$
		$b_0$	$b_1$	$b_2$		
Water	25	0.036810	-0.000189	0.0000033	0.917	0.000317
HFC 365mfc		0.027197	-0.000286	0.0000101	0.982	0.000346

Equation— $\lambda_{10^\circ\text{C}} = b_0 + b_1 \cdot m_{bio} + b_2 \cdot m_{bio}^2$ , where  $\lambda_{10^\circ\text{C}}$ —average thermal conductivity, W/(m·K),  $b_0$ ,  $b_1$  and  $b_2$ —constant coefficients which were calculated from the experimental data,  $m_{bio}$ —biopolyol amount, %,. Note: one-sided prediction confidence interval of the results is presented with 90% probability, Student's criterion  $t_\alpha = 1.316$  when  $\alpha = 0.10$  (dotted lines in Fig. 7.5)

In order to quantitatively evaluate the impact of biopolyol amount on the changes in thermal conductivity values, mathematical–statistical analysis was implemented. It showed that the average values of thermal conductivity for both blowing agents blown PUR foams might be approximated by regression equation (Eq. 7.1).

The numerical values for Eq. 7.1 are presented in Table 7.3. Statistical evaluation shows that the obtained results of thermal conductivity of PUR foam blown with two types of blowing agent can be approximated by the regression equations. Additionally Table 7.3 presents the average standard deviation  $S_{\lambda_{10^\circ\text{C}}}$ , and the determination coefficient  $R^2_{\lambda_{10^\circ\text{C}}}$ . The data show that the determination coefficients for water and HFC 365mfc blown PUR formulations are 0.917 and 0.982, respectively. It means that the suggested regression models are suitably selected for the description of thermal conductivity values of water and HFC 365mfc blown PUR foams with different biopolyol amounts.

Thermal conductivity of PUR foam with both blowing agents decreased at 10% of biopolyol amount indicating that the partial replacement of petroleum-based polyol is beneficial for PUR foam formulation. Compared to fully petroleum-based foams, thermal conductivity at 10% of biopolyol amount reduced by 5.4% for water blown formulations and by 7.4% for HFC 365mfc blown ones. However, no significant effect can be observed for thermal conductivity of water blown PUR foam with

**Table 7.4** Structural parameters of PUR foams with different biopolyol amounts

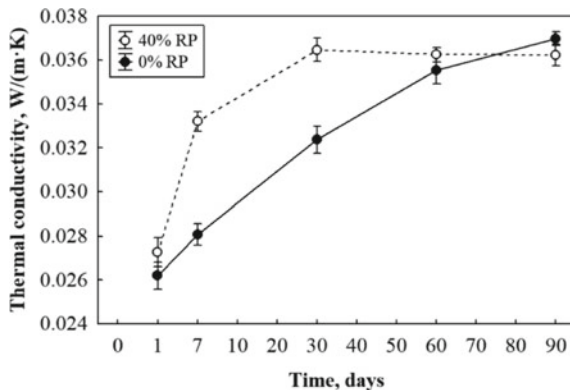
Parameter	RP amount (%)				
	0	10	20	30	40
<i>Water blown</i>					
Closed cell content, vol.%	94.2 ± 0.9	92.4 ± 1.2	90 ± 0.8	85.4 ± 1.3	76.6 ± 2.1
Average cell size, μm	311 ± 10	324 ± 10	365 ± 11	388 ± 12	390 ± 10
<i>HFC 365mfc blown</i>					
Closed cell content, vol.%	94.2 ± 0.9	96.4 ± 1.5	89.3 ± 1.2	86.4 ± 1.4	79.6 ± 1.4
Average cell size, μm	311 ± 10	309 ± 15	334 ± 9	345 ± 14	362 ± 13

a further increase of biopolyol amount from 10 to 40%. Contrary results can be observed for HFC 365mfc blown systems. The addition of biopolyol from 10 to 40% gradually increases thermal conductivity attributing to the deterioration of foam's cellular structure. It becomes irregular, partially open celled and ruptured (Chang et al., 2021) thus allowing a sudden replacement of HFC 365mfc with air which has greater thermal conductivity value. Similar observations were made by (Borowicz et al., 2020). They determined that the use of polyols based on white mustard oil resulted in a slight increase in the thermal conductivity up to 0.027 W/(m·K) for foams with 60% of biopolyol. This was mainly due to changes in the structure of PUR materials obtained after modification with plant-based polyols, i.e. a decrease in the content of closed cells and an increase in the average cell size in foams (Table 7.4).

It is obvious that the increase in average cell size causes parallel increase in heat transfer through radiation and therefore increase of total thermal conductivity value of PUR foam. Additionally, it is shown that the increase in an average cell size from 0.25 to 0.60 mm determines by 50% higher thermal conductivity value. Also, Table 7.4 shows the reduction of closed cell content with the addition of biopolyol. It means that partially open cell structure has a higher heat transfer through convection compared to a closed cell foam. Even though the obvious reduction in closed cell content and increase in thermal conductivity are observed at 40% biopolyol amount, authors (Hejna et al., 2017) showed that crude glycerol and castor oil-based biopolyol deteriorates the mentioned parameters only at amount of 70%

However, the impact of biopolyol and its content on cellular structure of PUR foams mainly depends on the initial raw materials used during the biopolyol synthesis as well as synthesis method itself. Research of (Kurańska et al., 2020) showed that it is possible to achieve sufficient thermal insulating properties for PUR foams with biopolyol amount of up to 30%. Also, it is determined that not all oils are suitable for the production of closed cell rigid PUR foams. The same authors (Kurańska et al., 2020) showed that incorporation of waste cooking oil-based polyol synthesized via epoxidation and oxirane ring opening method determine low content of closed cells (<5 vol.%) which mainly affected the thermal conductivity value that can be compared to commercial expanded polystyrene. Even though the thermal conductivity values are slightly higher than for the closed-cell foams, authors state

**Fig. 7.6** Thermal conductivity ageing of water blown PUR foams with 40% biopolyol



that these bio-based materials can still provide excellent thermal insulating and air barrier properties.

It is also worth mentioning that water blown PUR foams are more sensitive to time due to its fast ageing phenomena. As it can be seen from Fig. 7.6, thermal conductivity value was determined after 1, 7, 30, 60 and 90 days after production.

The replacement of the petroleum-based polyol with 40% of biopolyol increased the initial thermal conductivity of the foams by 0.001 W/(m·K). These changes are due to the alterations in cellular structure. The incorporation of 40% biopolyol increased the average cell size of the foams (Table 7.4) leading to a more rapid thermal conductivity increase after 7 and 30 days of production. Larger cells in the foams with biopolyols can facilitate the replacement of carbon dioxide with the air increasing the thermal conductivity faster. However, after 30 days the differences in the thermal conductivity of the foams with and without biopolyols are almost the same due to the same composition of the gas in the cells.

Previous study (Kairytė et al., 2018b) has shown that the reagents with different functionalities used to modify biopolyols have a great impact on structural parameters, thermal insulating as well as mechanical performance of PUR foams. The impact of the amounts of difunctional and trifunctional biopolyol modifiers, i.e. propylene glycol and glycerol, on the thermal conductivity and closed cell content of PUR foams is presented in Fig. 7.7. As can be seen from Fig. 7.7a, propylene glycol reduces closed cell content which is affected by slower polymer formation rate compared to blowing reaction rate.

In this case, ruptured cell windows form thus increasing the average value of thermal conductivity up to 0.038 W/(m·K) at 25 wt.%. Making PUR foams almost open celled it assures rapid outward diffusion of CO<sub>2</sub> and its substitution by atmospheric air. Contrary observations were done for glycerol which, as seen from Fig. 7.7b, maintains the closed cell content at 90 vol.% and decreases thermal conductivity from 0.032 W/(m·K) to 0.025 W/(m·K) due to increased cross-link density of the final PUR foam. It was also determined that propylene glycol by 100% increased the average cell size (Fig. 7.8b) while glycerol reduced it by 20% (Fig. 7.8c).

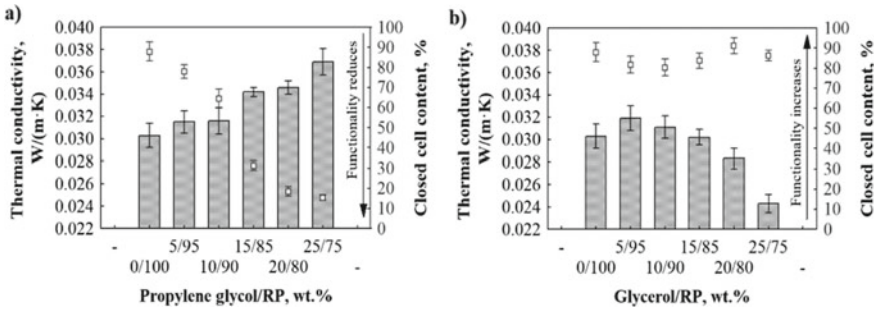


**Fig. 7.7** Thermal conductivity and closed cell content variation based on modifier type and its amount: **a** propylene glycol and **b** glycerol

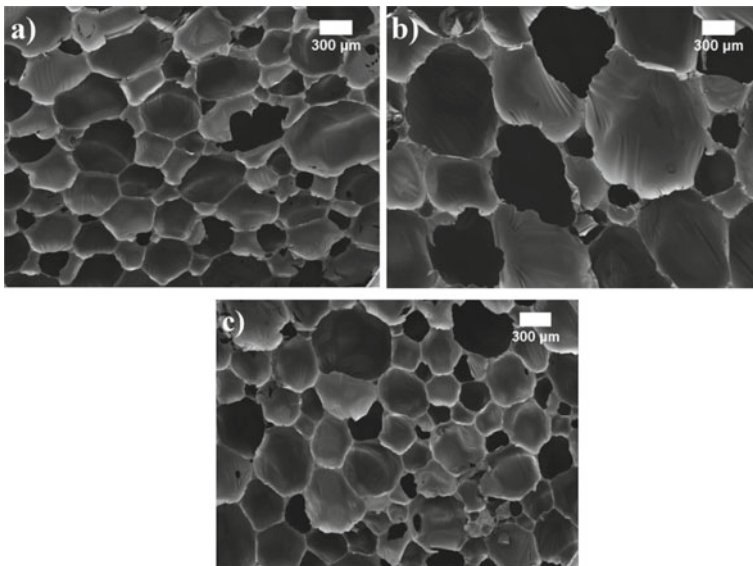


**Fig. 7.8** Cellular structure of RP-based PUR foam (magnification  $\times 35$ ): **a** unmodified; **b** 25 wt.% of propylene glycol and **c** 25 wt.% of glycerol

Apparently, the size of cells is greatly dependent on dynamic viscosity of the system. Other authors' works also show that incorporation of biopolyols with higher dynamic viscosity compared to petroleum-based ones leads to a formation of smaller cell size and sometimes nonuniform structure. (Ji et al., 2015) replaced 25 and 50% of petroleum based polyol with a soybean oil-based polyol and determined that the higher viscosity of the overall system has an effect on restraining the expansion of the cells. Moreover, the alteration of cell structures and the amount of open cells may also be due to the higher viscosity that affects the process of cell nucleation. (Borowicz et al., 2020; Hejna et al., 2017) made similar observations during the

synthesis of PUR foams based on biopolyols from castor oil and crude glycerol as well as mustard oil. They obtained a reduction in average cell size from 26 to 32% and increase in the closed cells content. Additionally, (Paciorek-Sadowska et al., 2018) investigated a new type oil from *oenothera biennis* seeds for the preparation of PUR foams with various fractions of the obtained biopolyol. The investigations have shown that the addition of biopolyols alters foam structure, i.e. increases cell size from 275  $\mu\text{m}$  to 408  $\mu\text{m}$  thus reducing the apparent density and mechanical performance. While (Borowicz et al., 2020) used sorbitol-based petrochemical and mustard oil-based polyols in ratios from 40:60 to 100:0% and obtained that the average cell size reduced by  $\sim 25\%$  with a slight addition of biopolyol.

Further on functionality of biopolyols, authors (Kirpluks et al., 2020) used four different chemical reagents, i.e. trimethylolpropane (TMP), diethylene glycol (DEG), triethanolamine (TEOA) and diethanolamine (DEOA) to synthesize high functionality tall oil-based biopolyols for c-pentane blown PUR foam products. They have also determined that chemical parameters of biopolyols such as functionality have a great impact on maintaining a high percentage of closed cell content as it is favourable in order to maintain high thermal resistance of PUR foam products. The study showed that the obtained biopolyols were characterized by functionality 5–9.3 and hydroxyl value 260–500 mg KOH/g. TMP-, DEG- and TEOA-based biopolyols resulted desirable  $\sim 90\%$  closed cell content while DEOA-based biopolyol was not suitable due to its high dynamic viscosity, miscibility with component problem and unsatisfactory dimensional stability of the final products.

## 7.4 Compressive Strength of Biopolyols-Based Pur/Pir Foams

Thermal conductivity is not the only property which can be affected by the amount and functionality of biopolyol. One of the most important characteristics for load bearing products is compressive strength. As it is noted, the amount of actual biopolyol has a great impact on mechanical performance of PUR/PIR foam products, therefore, Fig. 7.9 depicts the results of compressive strength obtained for RP-based PUR/PIR foams.

The compressive strength was measured in the two directions, perpendicular and parallel to the foaming direction due to the anisotropic cell structure of the rigid PUR/PIR foams (Fig. 7.10). The replacement of the petroleum-based polyol by the biopolyol up to 40% resulted in a slightly reduced compressive strength of the PUR/PIR foams. In the case of parallel direction, the compressive strength reduced by 18% while at perpendicular—by 15 at 40% biopolyol amount.

The parameter, evaluated in the perpendicular direction is much lower than the one determined in the parallel direction. This can be attributed to the elongated shape of the cells in the foam rise direction (Fig. 7.10b). In both cases, the replacement



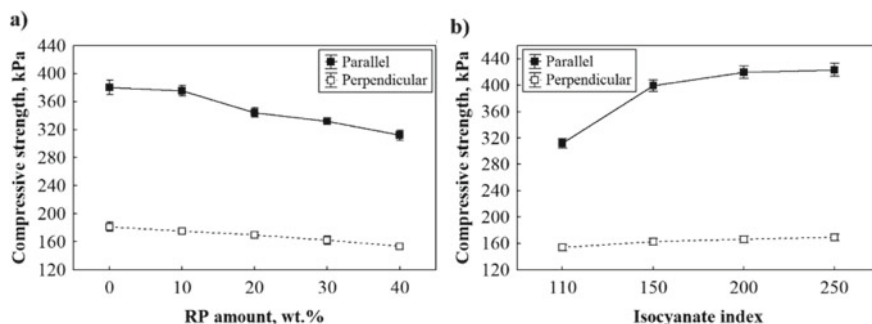


**Fig. 7.9** Parallel and perpendicular to foaming direction compressive strength of RP-based PUR/PIR foam: **a** at different amounts of biopolyol (isocyanate index 110) and **b** at 40% of biopolyol (isocyanate index 110–250)

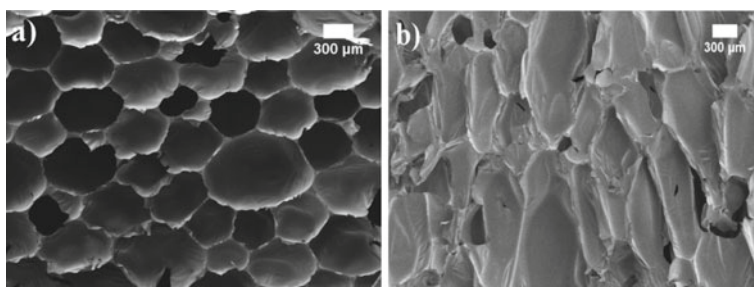


**Fig. 7.10** Microstructure of RP-based PUR/PIR foam: **a** in parallel foaming direction at 40% of biopolyol (magnification  $\times 100$ ); **b** in perpendicular direction at 40% of biopolyol (magnification  $\times 100$ )

of petroleum-based polyol with biopolyol leads to a decrease in mechanical performance. The decrease in the mechanical properties for all formulations is the result of lower cross-link density which is determined by the decreasing functionality of petroleum-based polyol and biopolyol premix ( $f = 4.5/2.3$ ) when the amount of biopolyol increases accordingly.

It was also observed that the increase in isocyanate index also affects the increase in rigidity of the PUR/PIR foams (Fig. 7.9b). It is worth mentioning that isocyanate index equal to 150 determined 28% increase in compressive strength parallel to foaming direction of PIR foam with 40% biopolyol. The obtained value became even greater than that of a control PUR foam without biopolyol. Regardless of the foaming direction, further increase in isocyanate index up to 250 does not give the tremendous impact as it was seen for PIR foams with 150 isocyanate index.

Additionally, in order to modify biopolyol as well as any polyol for the improvement of mechanical performance of PUR/PIR foams, it is possible to use difunctional and trifunctional low molecular weight materials. Difunctional materials form linear and extended structure and are called chain extenders while trifunctional and

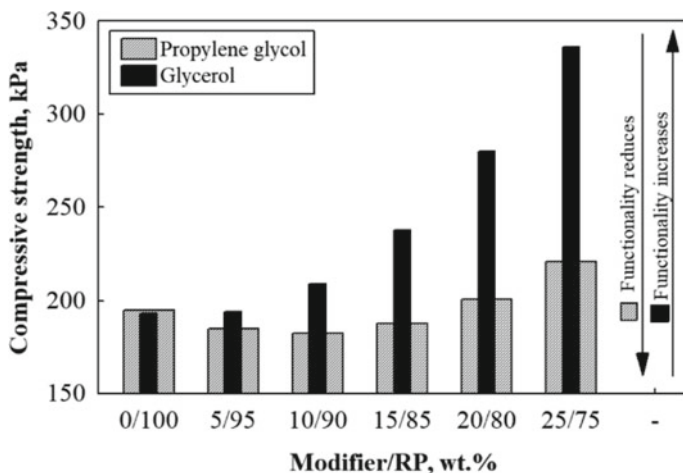


**Fig. 7.11** Compressive strength variation based on modifier type and its amount

higher functionality materials form cross-links and are called cross-linking agents. To investigate the impact of difunctional and trifunctional modifiers on mechanical performance of PUR/PIR foam, propylene glycol and glycerol were selected. The numerical value variations of compressive strength of PUR/PIR foams with different ratios of propylene glycol/RP and glycerol/RP are presented in Fig. 7.11.

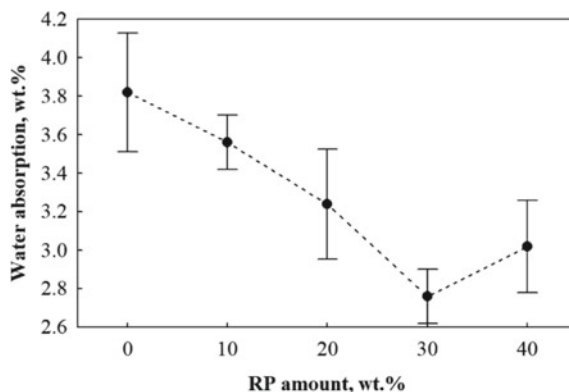
As expected, propylene glycol and glycerol altered mechanical performance of PUR/PIR foams. However, the compressive strength of propylene glycol modified PUR/PIR foams was only slightly higher at 25 wt.% while the highest influence is observed for glycerol. The parameter increased from ~200 kPa to ~350 kPa at 25 wt.% due to enhanced cross-link density of PUR/PIR foam matrix and enlarged functionality of polyols blend. Similar numerical values of compressive strength but at higher concentrations of high functionality, i.e. 9.3, TMP-based biopolyol was observed in (Kirpluks et al., 2020) as well.

## 7.5 Water Absorption of Biopolyols-Based Pur Foams

Another important parameter of foams, which are used in thermal insulation applications, is water absorption which is related to the percentage amount of water in the material after removal from total immersion in water. The impact of biopolyol amount on the water absorption of PUR foams is shown in Fig. 7.12.

It is determined that 30% of biopolyol reduces water absorption value by 26% compared to petroleum-based polyol. The addition of hydrophobic groups which are derived from vegetable oils improve water resistance of the final PUR foams. Such and similar tendencies have been observed in numerous studies with different vegetable oils-based PUR foams (Paciorek-Sadowska et al., 2018). Apparently, the

**Fig. 7.12** Short-term water absorption of RP-based PUR foam at different amounts of biopolyol



reduction of this parameter is crucial in order to maintain high thermal resistance of buildings. Additionally, reduced accumulation of water in building envelopes prevents from propagation of molds and other microorganisms. However, 40% of bio-polyol led to an increase of the parameter. It can be attributed to deteriorated microstructure and reduction in closed cell content (Table 7.4). Although, the final water absorption value at 40% is by 18% lower compared to petroleum polyol-based PUR foam.

## 7.6 Thermal Stability and Flammability of Biopolyols-Based Pur/Pir Foams

The mechanism of thermal degradation of PUR/PIR foams is a very complex process involving dissociation of the polyol and isocyanate, followed by the thermal decomposition and the formation of amines, transition components and  $\text{CO}_2$  (Piszczyk et al., 2014).

Figure 7.13 displays the thermogravimetric (TGA) and differential thermogravimetric (DTG) curves while Table 7.5 shows the average results of PUR foam with different amounts of biopolyol under the  $\text{N}_2$  atmosphere. It is seen that all foams are stable approximately up to 290°C and have two degradation stages. The first thermal degradation stage is in the range of 294–430 °C with maximum peak of 333 °C for petroleum polyol-based PUR foam, 336 °C for PUR foam with 20% biopolyol and 337 °C for PUR foam with 40% biopolyol. This stage of thermal degradation with more than 50% of mass loss is related to the urethane bond decomposition.

The second degradation stage ranges from 434 to 555 °C with maximum peaks at 502 °C for petroleum polyol-based PUR foam, at 479 °C for PUR foam with 20% biopolyol and at 480 °C for PUR foam with 40% biopolyol. This stage is associated to the degradation of other thermally resistant fractions which are available when RP-based polyol is incorporated into PUR foams (Kurańska et al., 2015). It is

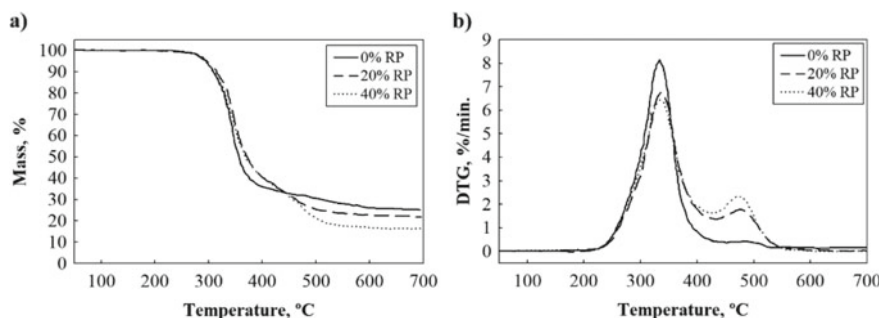


**Fig. 7.13** Thermal stability of RP-based PUR foam (isocyanate index 110): **a** TGA and **b** DTG

**Table 7.5** Thermal stability parameters for RP-based PUR foam

Biopolyol amount (%)	Temperature (°C)			Residue (wt.%)
	T <sub>5%</sub>	T <sub>1max</sub>	T <sub>2max</sub>	
0	294 ± 4	333 ± 4	502 ± 7	25.2 ± 1.5
20	296 ± 6	336 ± 8	479 ± 5	21.8 ± 1.8
40	294 ± 5	337 ± 6	480 ± 5	16.6 ± 1.1

worth mentioning, that RP-based polyol shifted T<sub>1max</sub> to a higher temperature but no significant changes can be observed for T<sub>2max</sub>. Moreover, the addition of RP-based polyol from 20 to 40% decreased the final content of residues.

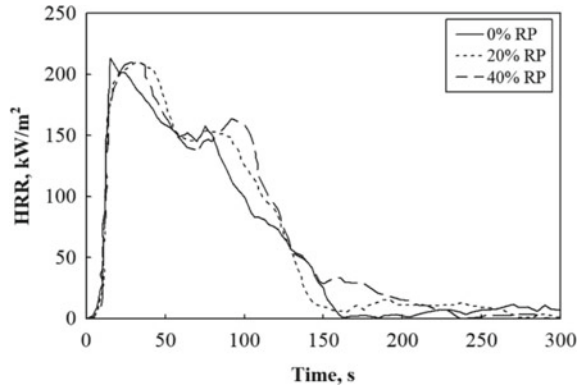
Overall observations from thermal stability measurements showed that there are no significant changes of PUR foams with petroleum-based polyol and RP-based polyol.

PUR/PIR foams have high flammability, and high smoke production during fire. Petroleum- and bio-based polyols are combustible and can be an additional fuel source in the case of a fire, therefore, this is a serious drawback which restricts the application of some PUR/PIR materials. Typically, a PUR/PIR foam may be subjected to a heat irradiation with intensity which is similar to that obtained during fire, i.e. from 25 to 75 kW/m<sup>2</sup> (Berta et al., 2006). Table 7.6 presents the values of the most important flammability parameters such as peak heat release rate (pHRR), total smoke released (TSR), carbon oxide and carbon dioxide yields (COY and CO<sub>2</sub>Y, respectively) and char residue, while Fig. 7.14 demonstrates the plots of HRR for

**Table 7.6** Flammability parameters of PUR foam a different amounts of biopolyol

Biopolyol amount (%)	pHRR, (kW/m <sup>2</sup> )	TSR (m <sup>2</sup> /m <sup>2</sup> )	COY (kg/kg)	CO <sub>2</sub> Y (kg/kg)	Char residue (%)
0	213 ± 10	750 ± 22	0.2 ± 0.03	3.4 ± 0.2	24.2 ± 1.2
20	209 ± 9.0	785 ± 36	0.2 ± 0.04	3.0 ± 0.3	20.6 ± 1.3
40	211 ± 14	898 ± 27	0.2 ± 0.03	2.4 ± 0.4	16.2 ± 0.9

**Fig. 7.14** Heat release rate of RP-based PUR foam at different amounts of biopolyol (isocyanate index 110)



prepared PUR foams with different biopolyol amounts.

Developed HRR plots are typical for materials which form thick char layer (Schartel & Hull, 2007). Additionally, the initial straightforward increase in HRR until effective char layer is formed can be noted as well. Other peaks in the HRR curves show the crack formation in char. As (Qian et al., 2014) observed, pHRR of fully unmodified foams typically reaches  $300 \text{ kW/m}^2$ , while for RP-based polyol modified ones it is slightly higher than  $200 \text{ kW/m}^2$ . Moreover, no significant effect in pHRR is seen for foams with greater biopolyol amounts while HRR curves have a broader shoulder meaning that heat is released for a longer time. Table 7.6 shows a slight impact of biopolyol amounts on TSR values. 20% of biopolyol increased the parameter by 4.6 and 40% of biopolyol—by 20% compared to petroleum polyol-based PUR foam.

Even though the TSR is greater for biopolyol modified PUR foams than for petroleum polyol-based foams, the added amount of biopolyol from 20 to 40% does increase the amount of combustion products in smoke and gas mixture. As it is seen, biopolyol does not alter the emission of CO and even reduce the yield of CO<sub>2</sub> by 12 at 20% biopolyol amount and by 29 at 40% biopolyol amount indicating a suppression ability of toxic gas release. Also, Table 7.6 shows the values of char residues after cone calorimetry test. It is clearly observed that the foam produced with petroleum-based polyol shows the highest char residue value compared to the ones that are modified with 20–40% biopolyol.

In addition, authors (Marcovich et al., 2017a) showed that further replacement of petroleum polyol with up to 70% biopolyol lead to the same conclusions regarding the amount of char residue. The scanning electron images of char residues after cone calorimeter test are presented in Fig. 7.15.

It is clearly seen from Fig. 7.15 that the replacement of petroleum-based polyol with biopolyol does not highly affect the structure of char residue. The outer surface is not dense, it has few spherical carbon residues and lots of holes, which formed due to the release of combustible gas and low capacity of forming solid char layer during fire. Therefore, it is of great importance to have an additional modification of such foams. The introduction of isocyanurate trimerisation structures into PUR foam

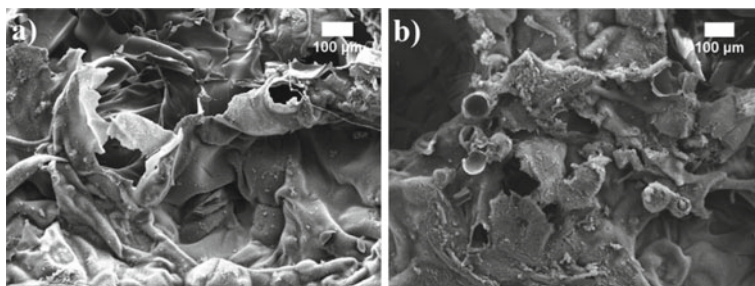
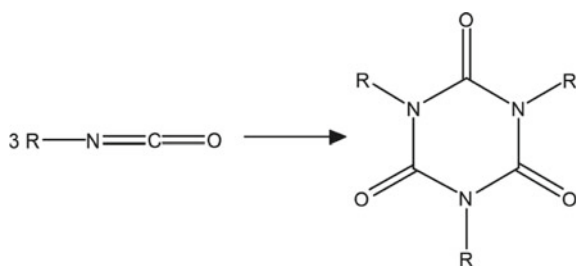


**Fig. 7.15** Images of char residues of PUR foam after cone calorimeter test (magnification  $\times 100$ ): **a** 0% RP-based polyol and **b** 40% RP-based polyol

**Fig. 7.16** General representation of isocyanate trimerisation reaction. Adapted from Modesti et al. (2001)



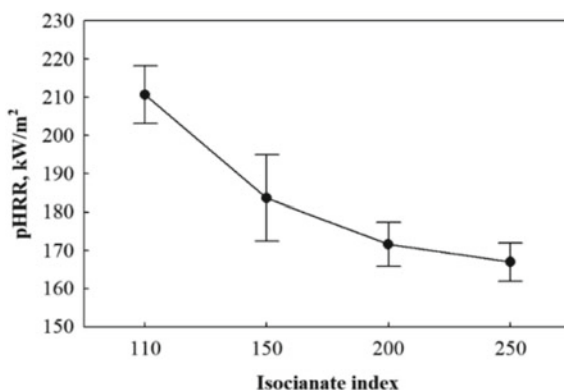
matrix may slightly improve the thermal stability and fire resistance of a so called PIR foam products. The trimerisation reaction of isocyanate groups into PIR rings is shown in Fig. 7.16. Thermodynamically, isocyanurates are more thermally stable than urethane bonds because urethane dissociates at  $\sim 200^\circ\text{C}$  while isocyanurates at  $\sim 350^\circ\text{C}$  (Modesti et al., 2001).

PIR foams are obtained in a large excess of isocyanate with a molar ratio of  $-\text{OH}$  and  $-\text{NCO}$  groups more than 1/1.5, which lead to a more complicated processing technology and equipment as the ratios of components are not equal. It is also observed that isocyanate trimerisation reaction occurs only when the reaction causes mixture to heat above  $140^\circ\text{C}$ . Such temperature determines a problematic application of PIR foams for in-situ sprayed thermal insulation (Kirpluks et al., 2016).

However, it has been found that the use of the higher isocyanate index has a significant effect on the pHRR during combustion (Fig. 7.17). It is demonstrated in Fig. 7.17 that increase of isocyanate index from 110 to 250 lead to by 20% lower pHRR value indicating better fire resistance. Same tendency was observed in other scientific works when isocyanate index equal to 250 led to by 14% reduced pHRR compared to control foams with isocyanate index of 110 (Kirpluks et al., 2016).

Apparently, according to (Kurańska et al., 2015), rigid foams with isocyanate index equal to 250 have the lowest heat release rate regardless of biopolyol type. It is very important during a fire because the rate at which heat is released results in a fire spread speed. Moreover, PIR foams with higher isocyanate index are able to develop denser char layer due to higher content of isocyanurate rings. Additionally,

**Fig. 7.17** The impact of isocyanate index on pHRR of PIR foam at 40% RP-based biopolyol



it was also showed that an increase in isocyanate index from 110 to 250 determine PIR foams with a higher thermal stability and increased char residue from 12.3 to 20.6% indicating that PIR foams are more thermally stable.

## 7.7 Rigid Polyurethane Foams Reinforced with Bio-fillers

The main concern when using renewable source-based products as the raw material for the preparation of polyurethane foams is their low mechanical strength. To enhance the mechanical strength of polyurethane foams, additives such as fibers, nanoparticles and particulate fillers have been used as reinforcement. Different researchers have worked on different types of fillers to enhance the mechanical strength of polyurethane products. Besides numerous inorganic fillers, such as nanoclay (Maharsia & Jerro, 2007; Nik Pauzi et al., 2014; Qi et al., 2018), expandable graphite (Guo et al., 2013; Modesti et al., 2002), silica (Członka et al., 2019a), talc (Sung & Kim, 2017) or polyhedral oligosilsesquioxanes (POSS) (Członka et al., 2019b; Strąkowska et al., 2019), fabrication of polyurethane foam composites with bio-based fillers from natural occurring recourses has attracted attention for their environment-friendly character. Incorporating bio-based fillers into polyurethane foams not only improves the mechanical properties but also provides reactive groups to react with isocyanates. In the literature, many different grades of particle-shaped agricultural waste fillers have been investigated (Table 7.7). The choice of filler depends on the local availability and the need to dispose of surplus biomass. The reinforcing efficiency of the natural fillers results from their geometry, chemical composition, the content of cellulose, hemicellulose, lignin, starch, proteins, and lipids, which all influence the ability to disintegrate, hardness and stiffness, as well as adhesion to selected polymers. It has been shown that depending on the used fillers, the incorporation of organic particles into a polyurethane composite matrix allows to obtain a modification of the mechanical, thermo-mechanical, physical, and thermal properties.

**Table 7.7** Recent works on filler reinforced polyurethane foams—effect of different fillers on selected properties of polyurethane composites

Filler used	Percentage of filler (wt.%)	Results
Kenaf fibre	20–50	Improvement of mechanical properties (El-Shekeil et al., 2012)
Pulp fibre	0–5	Deterioration of mechanical properties, improvement of thermal stability (Xue et al., 2014)
Rice husk ash	0–5	Improvement of mechanical properties and flame-retardancy, deterioration of thermal conductivity (Ribeiro da Silva et al., 2013)
Cellulose microfibrils	0–2	Improvement of mechanical properties (Zhu et al., 2011)
Egg shell waste	20	Improvement of mechanical properties and thermal stability (Zieleniewska et al., 2016)
Potato protein waste	0.1–5	Deterioration of mechanical properties and thermal stability with increasing filler content (Czlonka et al., 2018b)
Buffing dust waste	0.1–5	Deterioration of mechanical properties and thermal stability with increasing filler content (Czlonka et al., 2018c)
Keratin feathers	0.1–1.5	Mechanical properties and thermal stability decrease with increasing filler content (Czlonka, Sienkiewicz et al., 2018)
Forest based wastes	10	Deterioration of mechanical properties and thermal conductivity, improvement of flame-retardancy
Ground coffee	2.5–15	No significant influence on the mechanical and thermal properties, reduced brittleness and aging process (Soares et al., 2015)
Jute fibre	0.5–4	Deterioration of mechanical properties (Huang & Wang, 2017)

(continued)



Table 7.7 (continued)

Filler used	Percentage of filler (wt.%)	Results
Ramie fiber	0.2–0.8	Improvement of mechanical properties, thermal stability, and flame-retardancy (Nam & Netravali, 2004)
Rapeseed cake	30–60	Improvement of mechanical properties, thermal stability, and flame-retardancy (Paciorek-Sadowska et al., 2019)
Wood flour	0–15	Deterioration of mechanical properties, improvement of thermal conductivity and thermal stability (Mosiewicki et al., 2008)
Coir fibre	2.5	Improvement of mechanical properties (Shan et al., 2012)
Fly ashes	5–35	Improvement of mechanical properties and fire resistance (Paciorek-Sadowska et al., 2020)
Cinnamon extract, green coffee extract, cocoa extract	10	Improvement of susceptibility to biodegradation (Liszkowska et al., 2020)
Soy protein	2.4–9.6	Improvement of mechanical properties, deterioration of thermal stability (Zhang et al., 2018)

Despite these literature reports, the worldwide development and growth in the applications of bio-based PUR foams lead to the necessity of finding and establishing new sources of bio-fillers, that would be cheap and easily available throughout the world.

## 7.8 Polyurethane Composites Reinforced with Sugar Beet Pulp Filler Impregnated with Aminopropylisobutyl-Poss

Among different organic materials, solid residues of plants, such as sugar beet pulp fulfill the conditions to serve as sustainable bio-filler PUR foams. Sugar beet is one of the most commonly grown plants which is used in the sugar industry (Altundogan et al., 2007). According to the Food and Agriculture Organization (FAO), sugar production from sugar beet is the second largest production in the world. The greatest amount of sugar beet is produced in Europe, Asia, and North America (Altundogan et al., 2007). The main problem with sugar production from sugar beets is the formation of a huge amount of waste—sugar beet pulp (BP), which consisting of polysaccharides (~70–80%), cellulose (~20%), hemicelluloses (~30%), and pectin (~25%) (Vučurović & Razmovski, 2012).

Sugar beet pulp was proposed as a reinforcing filler for rigid polyurethane foams by (Strakowska et al., 2020). To improve the mechanical and thermal performances of the filler, BP filler was physically-modified with Aminopropylisobutyl-POSS (APIB-POSS) (1:1 w/w) using a planetary ball mill for 1 h (3000 rpm). Such prepared BP filler was incorporated into PUR at different percentages—1, 2, and 5 wt.%. The reference foam was labeled as PUR\_0, while the PUR composites reinforced with 1, 2 and 5 wt.% of BP filler, were labeled as PUR\_BP\_1, PUR\_BP\_2 and PUR\_BP\_5, respectively.

The cellular structure of PUR composites was examined using scanning electron microscopy (SEM) (Fig. 7.18). Generally speaking, with increasing the content of BP filler, the overall structure of PUR composite foams became less uniform with a higher number of cracked cells. This effect was the most prominent in the case of PUR composite foams with higher loading of BP filler. According to the presented results, the average cell diameter increased from 450 to 530  $\mu\text{m}$  with the increase of BP content from 1 to 5 wt.%.

The results presented in Fig. 7.19 revealed, that with the addition of 1, 2, and 5 wt% the density of PUR composite foams increased from 37  $\text{kg m}^{-3}$  to 40, 41, and 44  $\text{kg m}^{-3}$ , respectively, due to the incorporation of BP filler with a certain weight. Moreover, it was shown, that the changes in cellular structure and apparent density of PUR composite foams affected their insulating properties. The addition of 1 and 2 wt.% of BP filler did not affect  $\lambda$ , however, the addition of 5 wt.% of BP filler increased the value of  $\lambda$  to 0.035  $\text{Wm}^{-1} \text{K}^{-1}$ .

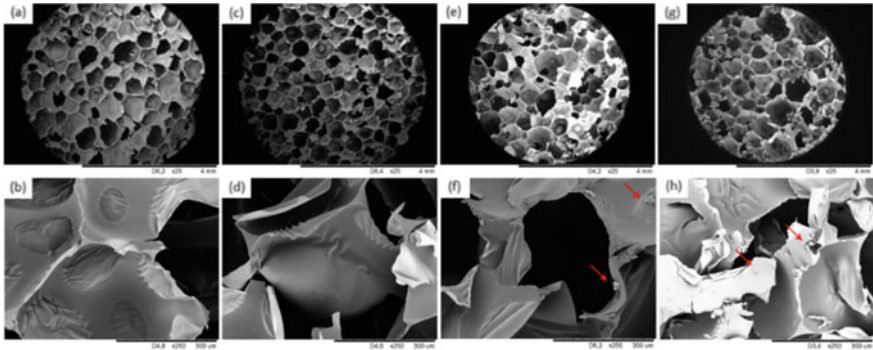


**Fig. 7.18** Cellular morphologies at different magnifications of **a, b** PUR\_0, **c, d** PUR\_BP\_1, **e, f** PUR\_BP\_2, **g, h** PUR\_BP\_5

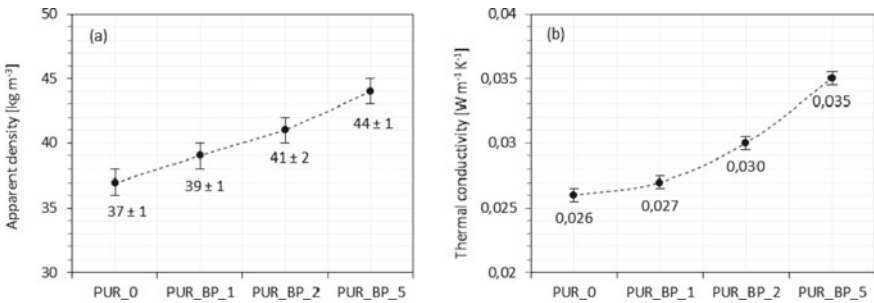


**Fig. 7.19** The results of **a** apparent density and **b** thermal conductivity of PUR composite foams

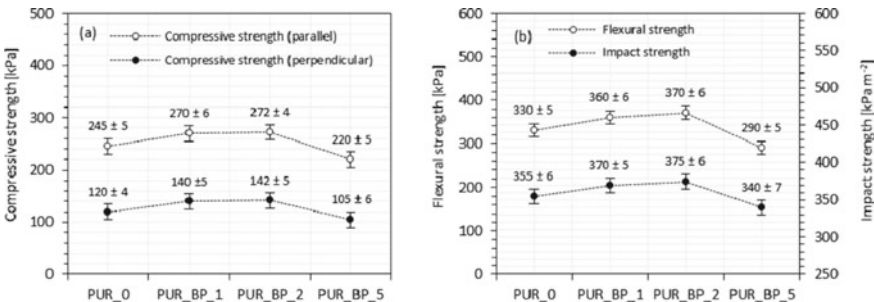


**Fig. 7.20** The results of **a** compressive strength and **b** flexural/impact strength of PUR composite foams

The impact of BP filler on the mechanical performances of PUR composites was determined by measuring the compressive strength, flexural strength and impact strength. Figure 7.20a presents the compressive strength of PUR composite foams containing various content of BP filler. Generally speaking, the compressive strength

of PUR composite foams increased initially with the addition of 1 and 2 wt.% of BP filler and then decreased slightly with the further increase of BP filler up to 5 wt.%. When compared with neat PUR foams, the greatest improvement in compressive strength was observed with the addition of 2 wt.% of BP filler—the value of compressive strength (measured parallel) increased by ~12%. A similar tendency was observed in the case of compressive strength measured perpendicular to the direction of foam growth—the greatest improvement was observed for PUR composite foams with the addition of 2 wt.% BP filler—compressive strength (measured perpendicularly) increased by ~18%. The authors explained that the greater number of smaller cells contributed to the superior mechanical behavior of PUR composite foams, since, the applied load is encountered by a greater number of cell walls per unit area. A similar observation was found in the case of flexural and impact strength of PUR composites. The addition of 1 and 2 wt.% of BP filler resulted in an improvement in flexural and impact strength, while an insignificant deterioration in mechanical properties was observed with the addition of 5 wt.% of BP filler. The greatest improvement in flexural and impact strength was observed with the addition of 2 wt.% of the filler—the value of flexural and impact strength increased by ~ 12 and ~6%, respectively.

The impact of BP filler on the fire behavior of PUR composites was examined using cone calorimeter test (Fig. 7.21). The intensity of the flame was determined by measuring the value of heat peak release (pHRR). When compared with the reference foam, the pHRR value decreased from 260 kW m<sup>-2</sup> to 170 and 155 kW m<sup>-2</sup> for

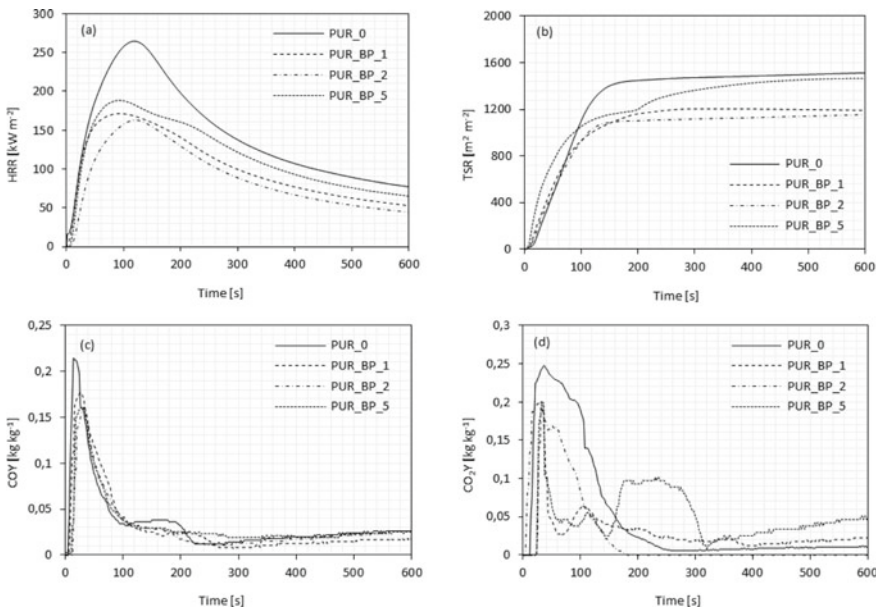


**Fig. 7.21** The results of the cone calorimeter test—**a** pHRR, **b** TSR, **c** CO release, and **d** CO<sub>2</sub> release

PUR\_BP\_1 and PUR\_BP\_2 and then increased to  $190 \text{ kW m}^{-2}$  with the incorporation of 5 wt.% of BP filler. The authors concluded that this improvement in the fire resistance of PUR composite foams is associated with the formation of a continuous char layer on the surface of PUR foams with the addition of BP filler, which acts as a physical barrier, effectively limiting the mass and heat transfer. Among all series of PUR composite foams, the greatest improvement was observed for PUR composite foams with 1 and 2 wt.% of BP filler—the value of pHRR decreased by  $\sim 35$  and  $\sim 40\%$ , respectively. In the case of PUR composite foams with 5 wt.% of BP filler, the value of pHRR decreased slightly by  $\sim 27\%$ , due to their more open-cell structure. Moreover, the incorporation of each amount of BP filler resulted in a lower value of total smoke release (TSR). When compared with neat PUR\_0, the value of TSR decreased by  $\sim 20$ ,  $\sim 27$ , and  $\sim 3\%$ , for PUR composite foams with 1, 2, and 5 wt.% of BP filler. The incorporation of BP fillers decreased the value of total heat release (THR). Comparing to neat PUR\_0, the addition of 1 and 2 wt.% of BP filler decreased the value of THR from  $21.5 \text{ MJ m}^{-2}$  (for PUR\_0) to 20.5 and  $20.9 \text{ MJ m}^{-2}$ , respectively. No significant difference was observed for PUR composite foams with 5 wt.% of BP—the value of THR decreased slightly to  $21.2 \text{ MJ m}^{-2}$ . Furthermore, the incorporation of BP filler decreased the ratio of carbon monoxide (CO) to carbon dioxide ( $\text{CO}_2$ ), which refers to the foam toxicity. The addition of BP filler reduced the value of the ratio, which means that the release of toxic smoke during the PUR foams combustion was reduced. The improvement of flame resistance of PUR composite foams with BP filler was also confirmed by the results of limiting oxygen index (LOI). The greatest improvement in LOI value was observed for PUR foams with 1 and 2 wt.%—the value of LOI increased from 20.2% (for neat PUR\_0) to 20.9 and 21.2%, respectively. A less noticeable improvement was observed for PUR foams with 5 wt.% of BP filler—the value of LOI increased to 20.5%. According to the presented results, the addition of 1 wt.% of BP filler did not affect the morphology of the char residue layer (Fig. 7.22). The difference was observed in the case of PUR composite foams with the addition of 2 and 5 wt.% of BP—the outer surface became denser and the spherical carbon residues were visible in the structure. This led to the conclusion, that BF particles can act as a flame barrier limiting the release of combustible gases.

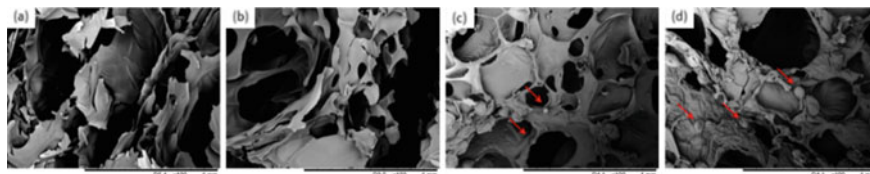


**Fig. 7.22** SEM images of char residues after the cone calorimeter test of **a** PUR\_0, **b** PUR\_BP\_1, **c** PUR\_BP\_2, **d** PUR\_BP\_5

## 7.9 Polyurethane Composites Reinforced with Maleic-, Alkali and Silane-Treated Eucalyptus Fibers

In another work, rigid polyurethane (PUR) foams were prepared by incorporating 2 wt.% of eucalyptus fibers (Czlonka et al., 2020). The eucalyptus fibers were surface-modified by maleic anhydride, alkali, and silane (triphenylsilanol) treatment. The reference foam was labeled as F\_EF\_0, while the PUR composites reinforced with non-treated, alkali-treated, maleic-treated and silane-treated eucalyptus fibers, were labeled as F\_EF\_NT, F\_EF\_A, F\_EF\_M and F\_EF\_S, respectively. The surface morphology of eucalyptus fibers before and after chemical treatments was investigated using an optical microscope (Fig. 7.23). According to the presented results, the non-treated eucalyptus fibers exhibited many impurities on the surface. After the alkali treatment, the surface of the fibers became clean and smooth. A similar effect was observed in the case of silanized and maleated fibers. This led to the conclusion that the chemical treatment improved the quality of the surface and all external impurities were removed.

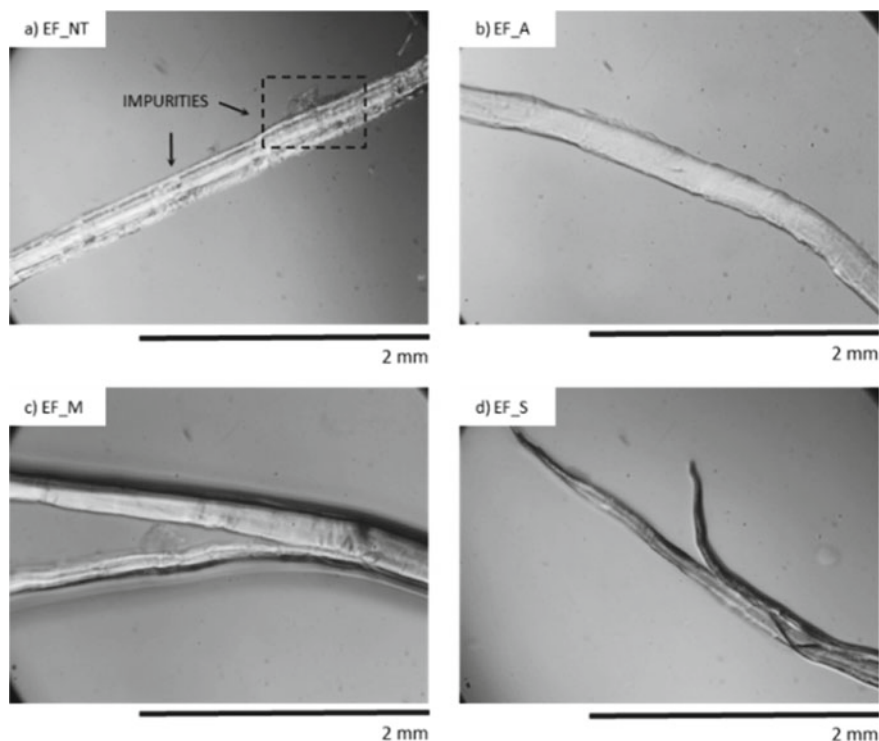


**Fig. 7.23** Optical images of **a** EF\_NT, **b** EF\_A, **c** EF\_M and **d** EF\_S observed at a magnification of 200

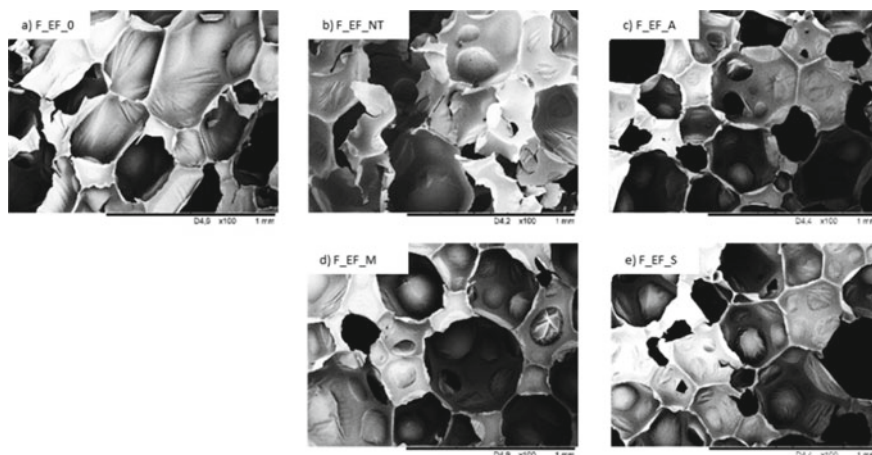


**Fig. 7.24** The morphology of **a** F\_EF\_0, **b** F\_EF\_NT, **c** F\_EF\_A, **d** F\_EF\_M, **e** F\_EF\_S

The impact of eucalyptus fibers on the cellular morphology of PUR composites was investigated using scanning electron microscopy (Fig. 7.24). The results revealed the cellular structure of PUR composites reinforced with non-treated eucalyptus fibers was more heterogeneous with a greater number of open cells. The porosity of PUR composites decreased from 91.5 to 89.2% due to the poor interfacial adhesion between eucalyptus fibers and the polymer matrix, which in turn disrupted the foaming process and resulted in the formation of more defective structure. A more uniform structure was observed in the case of foams with the addition of chemically-treated eucalyptus fibers. Most importantly, the addition of chemically-treated fibers did not affect the porosity of the foams—a high value of porosity (>90%) was observed for all series of modified foams. This led to the conclusion, that the chemical modification improved the interphase adhesion between eucalyptus fibers and polymer matrix which resulted in the more effective development of polyurethane structure.

The impact of the addition of non-treated and chemically treated eucalyptus fibers on the water uptake of PUR composites was evaluated. According to the results, the incorporation of non-treated eucalyptus fibers increased the water uptake of PUR composites. The authors concluded, that this may be connected with the more inhomogeneous open-cell structure of PUR foams reinforced with non-treated fibers as well as the hydrophilic character of the fibers, which was confirmed by the reduced value of the contact angle ( $\theta$ ) (Fig. 7.25). When compared with the reference foams, the incorporation of non-treated eucalyptus fibers decreased the value of contact angle from 125 to 120°. Interestingly, reduced water uptake was observed for PUR composites reinforced with chemically-treated fibers. Depending on the fibers, the water uptake decreased by 10–18%. Among all modified PUR composites the most

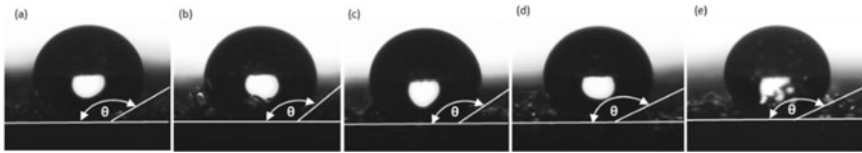


**Fig. 7.25** The contact angle of PUR foams **a** F\_EF\_0, **b** F\_EF\_NT, **c** F\_EF\_A, **d** F\_EF\_M, **e** F\_EF\_S

significant improvement was observed for PUR composites reinforced with silane-treated fibers. That was explained by the most hydrophobic character of the silane-treated fibers, which was also confirmed by the results of contact angle.

According to the results presented in the study, the incorporation of non-treated and chemically-treated eucalyptus fibers affected the mechanical performances of PUR composites. Compared to the reference foam, the value of compressive strength ( $\sigma_{10\%}$ ) increased by  $\sim 5\%$  for foams modified with non-treated eucalyptus fibers. The mechanical behavior increased after the chemical modifications. Alkali, maleic and silane treatment and of eucalyptus fibers resulted in improvement of  $\sigma_{10\%}$  by  $\sim 11$ ,  $\sim 15$  and  $\sim 20\%$ , respectively. Moreover, the incorporation of eucalyptus fibers influences flexural  $\sigma_f$  and impact strength of foams as well (Table 7.8). Compared to the reference foam, the abovementioned properties have been improved for all series of foams containing modified eucalyptus fibers. Only the introduction of non-treated fibers into the foam resulted in a deterioration of these properties. The greatest improvement of the mechanical properties was observed for PUR composites reinforced with silane-treated fibers. Comparing to the reference foam, the  $\sigma_f$  increased by  $\sim 6\%$ , while the impact strength increased by  $\sim 48\%$ . A slight decrease in mechanical behavior was observed for foams modified with non-treated fibers.

**Table 7.8** The results of the mechanical properties of polyurethane foams modified with eucalyptus fibers

Sample code	Compressive strength (parallel) $\sigma_{10}$ (kPa)	Compressive strength (perpendicular) $\sigma_{10\%}$ (kPa)	Flexural strength $\sigma_f$ (MPa)	Impact strength ( $\text{kJ m}^{-2}$ )
F_EF_0	260 $\pm$ 8	145 $\pm$ 9	0.405 $\pm$ 0.007	0.350 $\pm$ 0.004
F_EF_NT	273 $\pm$ 9	155 $\pm$ 9	0.370 $\pm$ 0.006	0.260 $\pm$ 0.004
F_EF_A	290 $\pm$ 9	160 $\pm$ 7	0.430 $\pm$ 0.004	0.400 $\pm$ 0.006
F_EF_M	298 $\pm$ 7	170 $\pm$ 8	0.420 $\pm$ 0.006	0.490 $\pm$ 0.007
F_EF_S	312 $\pm$ 8	170 $\pm$ 8	0.432 $\pm$ 0.006	0.006



## 7.10 Polyurethane Composites Reinforced with Lavender Filler Functionalized with Kaolinite and Hydroxyapatite

In another study polyurethane (PUR) composites were modified with 2 wt.% of lavender fillers functionalized with kaolinite (K) and hydroxyapatite (HA) (Członka et al., 2021). To lavender functionalization, selected amounts of lavender powder and kaolinite/hydroxyapatite (1:1 w/w) were weighed up and mixed intensively, using a high-energy ball milling process (1 h, 3000 rpm). Such developed lavender fillers were used as a reinforcing material in the synthesis of PUR composites. The reference foam was labeled as PUR\_REF, while the PUR composites reinforced with non-functionalized lavender, lavender functionalized with kaolinite, and lavender functionalized with hydroxyapatite were labeled as PUR\_L, PUR\_L\_K, and PUR\_L\_H.

It was found that the functionalization of lavender using a high-energy ball milling process affects the external morphology and size of filler particles. As presented in Fig. 7.26, the external morphology of non-functionalized lavender filler was quite rough, while the size of lavender particles oscillated between 950 nm and 3  $\mu\text{m}$  with an average value at  $\sim 1.5 \mu\text{m}$ . Due to the functionalization of the filler with kaolinite and hydroxyapatite, the overall structure of lavender particles became more uniform and smooth, while the average size of filler decreased to 712 and 615 nm, respectively.

According to the results presented in Fig. 7.27, the addition of lavender fillers increased the apparent density from  $36.8 \text{ kg m}^{-3}$  (for reference foam) to 37.4, 38.9, and  $38.6 \text{ kg m}^{-3}$ , for PUR composites reinforced with non-functionalized lavender, lavender functionalized with kaolinite and lavender functionalized with hydroxyapatite, respectively. Most importantly, on the incorporation of non-functionalized

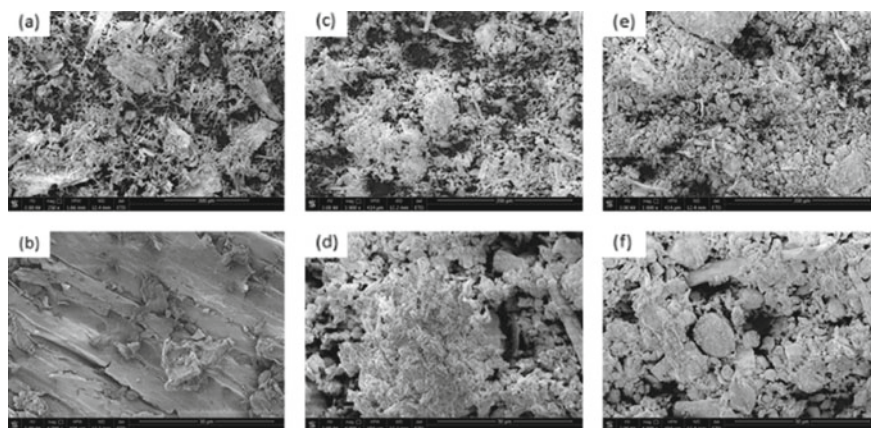


**Fig. 7.26** SEM images of lavender fillers: **a, b** non-functionalized lavender **c, d** lavender functionalized with kaolinite **e, f** lavender functionalized with hydroxyapatite

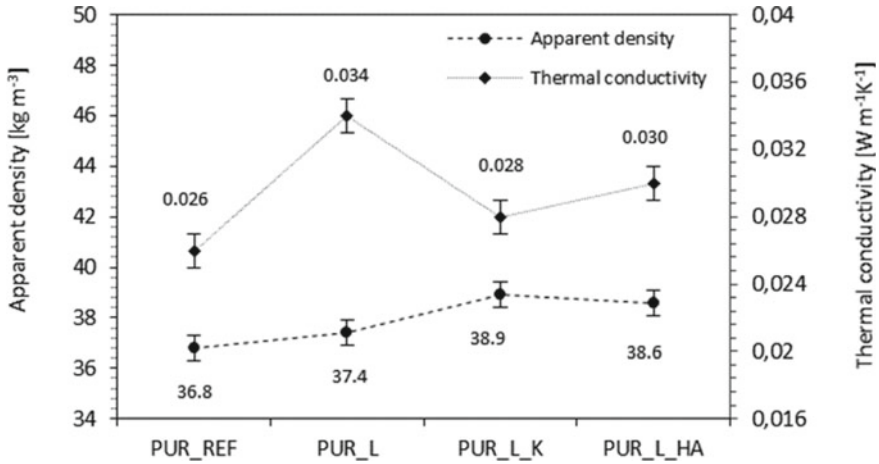


Fig. 7.27 The results of apparent density and thermal conductivity measured for PUR composites

lavender filler the value of thermal conductivity ( $\lambda$ ) increased from  $0.026 \text{ Wm}^{-1} \text{ K}^{-1}$  (for reference foam) to  $0.034 \text{ Wm}^{-1} \text{ K}^{-1}$ , while after the incorporation of functionalized lavender fillers, the value of  $\lambda$  increased insignificantly to  $0.028$  and  $0.030 \text{ Wm}^{-1} \text{ K}^{-1}$ .

The impact of lavender fillers addition on mechanical characteristics was evaluated by measuring the compressive strength ( $\sigma_{10\%}$ ), flexural strength ( $\sigma_f$ ) and impact strength ( $\sigma_I$ ). The results of mechanical performances are presented in Fig. 7.28. It was found, that the addition of non-functionalized and functionalized lavender fillers affects the value of  $\sigma_{10\%}$ . When compared with the reference foam,  $\sigma_{10\%}$  (measured parallel to the direction of foam expansion) increased by  $\sim 7$ ,  $\sim 15$ , and  $\sim 17\%$ , for PUR composites reinforced with non-functionalized lavender, lavender functionalized with kaolinite, and lavender functionalized with hydroxyapatite, respectively. An analog trend was observed in the case of  $\sigma_{10\%}$  measured perpendicular to the direction of the foam expansion—the value of  $\sigma_{10\%}$  increased by  $\sim 8$ ,  $\sim 18$ , and

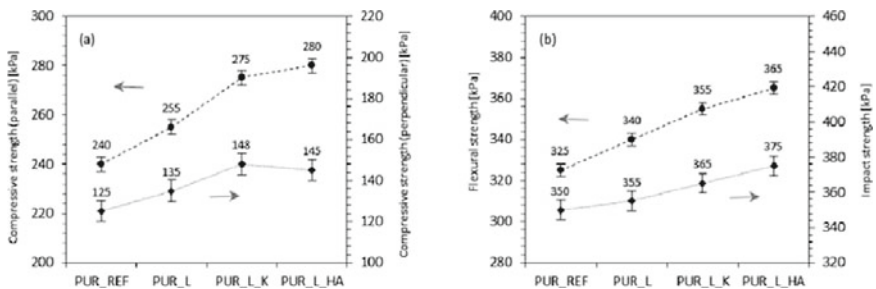


Fig. 7.28 The mechanical performances of PUR foams—**a** compressive strength, **b** flexural and impact strength

**Table 7.9** Antibacterial properties of PUR composites against selected bacteria and fungi

Sample	Bacteria		Fungi		
	<i>E. coli</i>	<i>S. aureus</i>	<i>B. subtilis</i>	<i>C. albicans</i>	<i>A. niger</i>
PUR_REF	–	–	–	–	–
PUR_L	+	+	+	–	–
PUR_L_K	+	+	+	–	–
PUR_L_HA	+	+	+	–	–

~16% for with non-functionalized lavender, lavender functionalized with kaolinite, and lavender functionalized with hydroxyapatite, respectively. To avoid the impact of apparent density on mechanical properties of PUR composites, the specific compressive strength was measured as well. According to the presented results, on the addition of lavender fillers, the specific strength of PUR composites slightly increased—the specific strength (measured parallel) calculated for the reference foam was 6.5 MPa/kg/m<sup>3</sup>, while due to the incorporation of lavender fillers, the value increased to 6.8, 7.1 and 7.3% for with non-functionalized lavender, lavender functionalized with kaolinite, and lavender functionalized with hydroxyapatite, respectively. A reinforcing effect of lavender fillers was also confirmed by the results of  $\sigma_f$  and  $\sigma_I$ . When compared with the reference foam, the addition of non-functionalized lavender filler increased the value of  $\sigma_f$  by ~5%, while the addition of lavender filler functionalized with kaolinite and hydroxyapatite increased the value of  $\sigma_f$  by ~9 and ~12%, respectively. A similar trend was observed for  $\sigma_I$ . The greatest improvement was observed for PUR composites reinforced with lavender filler functionalized with kaolinite and hydroxyapatite—the value of  $\sigma_I$  increased by ~4 and ~7%, respectively.

Considering the antibacterial and antioxidative properties of lavender, kaolinite and hydroxyapatite, the antibacterial properties of PUR composites filled with lavender fillers against *Escherichia coli*, *Staphylococcus aureus*, *Bacillus subtilis*, *Candida albicans*, and *Aspergillus niger* were evaluated (Table 7.9). The obtained results confirmed the antibacterial activity of PUR composites against bacteria, but no activity against fungi was observed. The authors reported, that a low antibacterial activity against fungi, may be connected with low concentration of lavender fillers in the PUR composites.

The flame retardant properties of PUR composites were performed using a cone calorimeter. The results of ignition time (IT), peak heat release rate (pHRR), total smoke release (TSR), total heat release (THR), average yield of CO (COY) and CO<sub>2</sub> (CO<sub>2</sub>Y), and limiting oxygen index (LOI) are presented in Table 7.10.

According to the presented results, the addition of lavender fillers affected the value of peak heat release rate (pHRR). Among all modified series of PUR composites, the lowest value of the pHRR parameter was observed for the PUR composites reinforced with lavender functionalized with hydroxyapatite, which was over 50% lower than for the reference foam. Furthermore, the incorporation of each filler resulted in a lower value of total smoke release (TSR). When compared with the

**Table 7.10** Flame retardant properties of PUR composites

Sample	IT (s)	pHRR (kW m <sup>-2</sup> )	TSR (m <sup>2</sup> m <sup>-2</sup> )	THR (MJ m <sup>-2</sup> )	COY/CO <sub>2</sub> Y (-)	LOI (%)
PUR_REF	4	263	1500	21.5	0.875	20.2
PUR_L	4	203	1400	21.1	0.844	20.5
PUR_L_K	6	144	1060	20.5	0.736	22.2
PUR_L_HA	6	130	1055	19.8	0.788	22.7

reference foam, the value of TSR decreased by  $\sim 7\%$  for PUR composites reinforced with non-functionalized lavender,  $\sim 29\%$  for PUR composites reinforced with lavender functionalized with kaolinite, and  $\sim 30\%$  for PUR composites reinforced with lavender functionalized with hydroxyapatite. This suggested that the incorporation of lavender fillers protects the PUR structure from further combustion and prevents the heat transfer through the PUR matrix. Furthermore, the incorporation of lavender fillers decreased the value of total heat release (THR). Comparing to the reference foam, for which the value of THR was  $21.5 \text{ MJ m}^{-2}$ , the addition of lavender fillers decreased the value of this parameter to  $21.1 \text{ MJ m}^{-2}$ ,  $20.5 \text{ MJ m}^{-2}$ , and  $19.8 \text{ MJ m}^{-2}$  for PUR composites reinforced with non-functionalized lavender, lavender functionalized with kaolinite, and lavender functionalized with hydroxyapatite, respectively. Moreover, the incorporation of lavender fillers decreased the carbon monoxide (CO) to carbon dioxide (CO<sub>2</sub>) ratio, which is related to the foam toxicity. The incorporation of lavender fillers effectively increased the value of limiting oxygen index (LOI). The greatest improvement was observed for PUR composites reinforced with lavender functionalized with hydroxyapatite and kaolinite—the value of LOI increased from 20.2% to 22.7% and 22.2%, respectively. A less noticeable improvement was observed for PUR composites reinforced with non-functionalized lavender filler—the value of LOI increases to 20.5%.

The char residue of PUR composites after the combustion process was evaluated using scanning electron microscopy. According to the images presented in Fig. 7.29, after the combustion process, the char residue of the reference PUR foams was loose and possessed a few fragments that were formed during the decomposition process. PUR composites reinforced with lavender fillers presented more compact char residue. The authors explained, that a more dense structure of PUR composites,

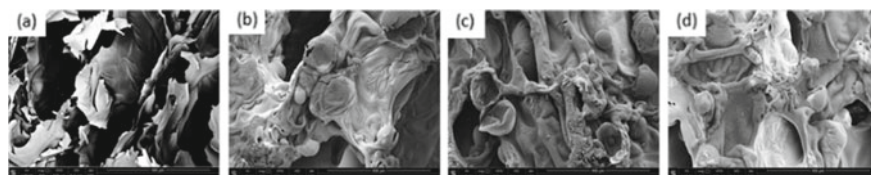


**Fig. 7.29** SEM images of char residue of **a** PUR\_REF, **b** PUR\_L, **c** PUR\_L\_K, and **d** PUR\_L\_HA (obtained after the cone calorimeter test)

may act as a physical barrier, effectively limiting the heat transfer through the PUR structure and successfully inhibiting the combustion process.

## 7.11 Soybean Oil-Based Polyurethane Composites Reinforced with Cloves

As another example of the use of organic fillers to reinforce the permanent polyurethane materials can be given *Syzygium aromaticum*, commonly known as cloves (Członka et al., 2020). Nowadays, cloves are cultured in different parts of the world including Indonesia or Brazil. Cloves are one of the richest sources of the phenolic extract. It consists mainly of eugenol (50–90%), eugenol acetate, thymol, and tanene. Due to this, cloves possess outstanding properties including antioxidant, antimicrobial, and antifungal activity. Clove extract is widely used as an additive in polymeric materials, for example, food packaging materials.

In presented study, grounded cloves were used as cellulosic filler for a novel polyurethane (PU) composite foams. Soybean oil-based PU composite foams were successfully reinforced with different concentrations (1, 2, and 5 wt.%) of clove filler. The reference foam was labeled as PU\_0, while the PU composite foams filled with 1, 2 and 5 wt.% of clove filler were labeled as PU\_1, PU\_2, and PU\_5, respectively.

The introduction of the clove filler leads to an elongation of the cream and an elongation time (Table 7.11). Compared to PU-0, the creaming time is increased from 43 to 60 s, while the expansion time is increased from 214 to 238 s for the PU-5 sample. The introduction of clove fillers affects the viscosity of the initial system, which affects the foaming process. The viscosity of the modified systems increases and the further growth of the resulting cells is limited. The foaming process can also be disturbed by the addition of clove extract with reactive groups that react

**Table 7.11** Selected properties of PU composite foams

	PU-0	PU-1	PU-2	PU-5
Temperature (°C)	125	123	122	119
Cream time (s)	43 ± 4	57 ± 2	58 ± 2	60 ± 2
Expansion time (s)	214 ± 10	228 ± 11	230 ± 8	238 ± 9
Tack-free time (s)	341 ± 14	347 ± 12	351 ± 12	368 ± 10
Cell size (µm)	390 ± 9	380 ± 8	330 ± 6	310 ± 8
Closed-cell content (%)	88	90	87	80
Apparent density [kg m <sup>-3</sup> ] (bottom)	36 ± 9	36 ± 9	37 ± 9	37 ± 9
Apparent density [kg m <sup>-3</sup> ] (middle)	39 ± 1	41 ± 1	42 ± 2	44 ± 2
Apparent density [kg m <sup>-3</sup> ] (upper)	38 ± 9	41 ± 9	42 ± 9	44 ± 9

with isocyanates, creating an imbalance in the ratio of NCO to OH groups. This relationship is also confirmed by the decrease in the maximum temperature ( $T_{max}$ ) measured during the foaming process. It can be concluded that the introduction of the clove filler leads to a decrease in the reactivity of the modified systems.

In the case of PU composite foams, a slight tendency to increase the apparent density is observed. The apparent density of PU-0 and PU composite foams depends not only on the concentration of the clove filler but is also influenced by the position of the PU foams and varies between different PU parts (upper/middle/lower) foam. Since the apparent density is affected by the filler density gradient, the lowest apparent density value is observed for the lower part of PU foams, which is characterized by an open-cell structure with visible voids and broken cells (Fig. 7.30). The middle part of the PU foams is characterized by the highest apparent density values as a result of a more homogeneous structure with a large number of closed cells. The apparent density decreases in the upper part of the PU foams due to more intense expansion and the presence of larger diameter cells. Basically, the incorporation of clove filler leads to an increase in apparent density.

Apparent density strongly affects the mechanical properties of porous materials. Compression strength ( $\sigma_{10\%}$ ) of PU composite foams was measured in a parallel and perpendicular direction in relation to the foam growth (Table 7.12). Compared to PU-

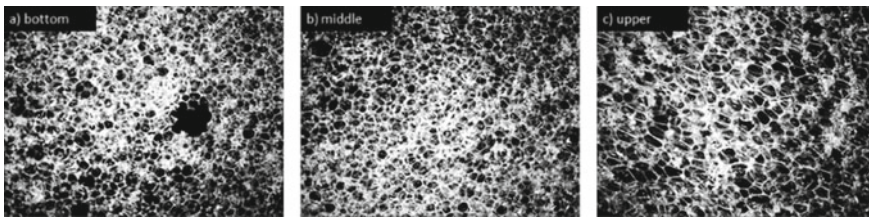


Fig. 7.30 The cellular structure of **a** bottom, **b** middle and **c** upper part of PU-1

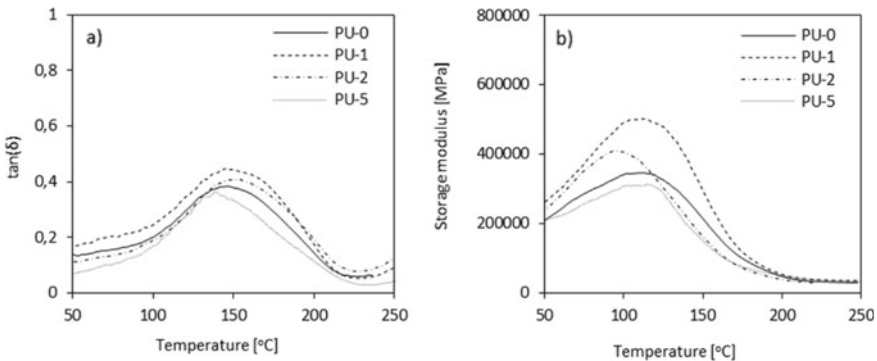


Fig. 7.31 Dynamic mechanical analysis of PU composite foams—**a**  $Tan\delta$  and **b** storage modulus in the function of temperature

**Table 7.12** Compressive strength, flexural strength, and elongation of PU composite foams

	Compressive strength $\sigma_{10\%}$ (parallel) (kPa)	Compressive strength $\sigma_{10}$ (perpendicular) (kPa)	Flexural strength $\epsilon_f$ (MPa)	Impact strength (MPa)
PU-0	250 $\pm$ 9	144 $\pm$ 4	0.402	0.389
PU-1	296 $\pm$ 8	176 $\pm$ 5	0.472	0.460
PU-2	283 $\pm$ 6	148 $\pm$ 4	0.440	0.431
PU-5	210 $\pm$ 6	130 $\pm$ 6	0.412	0.420

0, the incorporation of 1 and 2 wt.% of clove filler leads to significant improvement of  $\sigma_{10\%}$ . The value of  $\sigma_{10\%}$  (measured parallel) increases by  $\sim 18$  and  $\sim 13\%$  for sample PU-1 and PU-2, respectively. No further improvement of  $\sigma_{10\%}$  is observed for samples PU-5. Comparing to PU-0 the value of  $\sigma_{10\%}$  decreases by  $\sim 16\%$ .

An analog tendency is observed in the case of specific compression strength, which means that density is not the main factor that influences the mechanical properties of PU foams. Another factor may be found in characteristic features of PU foams structure.

The incorporation of clove filler influences the values of flexural strength ( $\sigma_f$ ) and impact strength of PU composite foams. Compared to PU-0 the aforementioned properties are improved, however, with increasing filler content the mechanical properties tend to decrease. Solid particles of clove filler act as reinforcing centers and generate localized stresses under the action of a loading force. Energy dissipation takes place when a growing crack encounters a filler particle distributed in a reinforced polymer matrix. During bending, an excess of solid particles acts as stress concentration centers that generate damage and cracking of the sample leading to the deterioration of the mechanical properties.

The dynamic mechanical analysis of PU composite foams as a function of temperature (0–600 °C) is shown in Fig. 7.31. The study of the  $\tan\delta$  value provides information on the damping properties of PU composite foams. The maximum value of  $\tan\delta$  corresponds to the glass transition temperature ( $T_g$ ). It was found that introducing 1 and 2 wt.% of clove filler does not affect the  $T_g$  value. A lower  $T_g$  value is observed for the PU-5 sample, which indicates that the addition of 5 wt.% of clove filler leads to a decrease in cross-link density and increased mobility of chain segments. Previous studies have shown that the  $T_g$  value depends on the aromaticity and cross-link density of PU materials. On this basis, it can be concluded that the introduction of clove filler at a high concentration, e.g. 5 wt.%, Reduces the cross-link density and increases the hollow fraction of the PU structure due to the limited interaction between the PU chains. As a result, the mobility of the PU chains increases and the  $T_g$  value is reduced. On the other hand, the introduction of clove filler may reduce the reactivity of the PU system due to the high viscosity of the PU blend and the disrupted foaming process.

The thermomechanical behavior of PU foams is a complex effect that involves a reinforcing effect of the filler and the structure of PU foams. In the case of PU-1

and PU-2, an improved thermos-mechanical behavior results from rigid structure of clove filler and well-developed closed-cell structure. Further increase of clove filler content results in open-cell structure with higher number of broken cells. It may be concluded that the incorporation of rigid particles of clove filler is not sufficient to compensate for negative changes in the morphology of PU foams.

The color change is the main parameter, which is a visual indicator of changes occurring in the polymer matrix due to the degradation process. PU composite foams samples were evaluated optically to determine the color change after the UV aging. The results of color analysis are presented in Table 7.13. A significant difference in total color change may be seen after the addition the clove filler. Compared to PU-0, with increasing concentration of clove filler, PU composite foams are characterized by a reduced value of  $L^*$  indicating on more intense color of PU composite foams. Increased values of  $a^*$  and  $b^*$  pointed out that comparing to PU-0, modified samples possess more intense yellow and red shades.

The results presented in Table 7.14 indicate that clove filler may be successfully used as an organic indicator of color change after the aging process. The color changes were evaluated in terms of the color parameters. According to the literature, the photodegradation process of organic compounds is mainly associated with the oxidation of chromophore groups and, consequently, with depolymerization of polymer chains. After the UV aging, organic fillers normally tend to lose red ( $<a^*$ ) and yellow ( $<b^*$ ) shades as a result of oxidation of organic compounds present in the PU chain.

**Table 7.13** Color analysis of PU foams before UV aging, where  $\Delta E^*$ —total color change,  $L^*$ —degree of lightness,  $a^*$ —red/green parameter,  $b^*$ —yellow/blue parameter

	Colorimetric Parameters			
	$L^*$	$a^*$	$b^*$	$\Delta E^*$
PU-0	11.7	22.4	−5.1	5.0
PU-1	25.3	72.5	−3.9	18.0
PU-2	49.5	75.6	−3.1	29.6
PU-5	58.5	77.9	0.2	34.1

**Table 7.14** Color analysis of PU foams after UV aging, where  $\Delta E^*$ —total color change,  $L^*$ —degree of lightness,  $a^*$ —red/green parameter,  $b^*$ —yellow/blue parameter

	Colorimetric Parameters			
	$L^*$	$a^*$	$b^*$	$\Delta E^*$
PU-0	18.7	24.2	−4.2	22.5
PU-1	28.3	75.4	−3.1	23.2
PU-2	49.5	75.1	−2.5	28.6
PU-5	60.5	79.2	0.3	30.4



The most visible change of total color changes ( $\Delta E^*$ ) after the UV aging process is observed for PU-0. With the increasing content of clove filler, the difference in  $\Delta E^*$  is reduced. Based on this result, it can be concluded that the addition of clove filler, which is a natural antioxidant compound, may protect the PU composite foams from UV radiation and high temperature. The incorporation of clove filler may significantly improve the stabilization of the PU composite foams and may be used as an anti-aging compound in the production of PU foams. The high resistance of cloves against high temperature and UV radiation should be justified by the chemical composition of cloves, including various extracts of cloves, such as eugenol, ether, or methanolic extracts which possess strong antioxidant activities and prevent a natural discoloration of PU composite foams.

## References

- Altundogan, H. S., Bahar, N., Mujde, B., & Tumen, F. (2007). The use of sulphuric acid-carbonization products of sugar beet pulp in Cr(VI) removal. *Journal of Hazardous Materials*, *144*, 255–264. <https://doi.org/10.1016/j.jhazmat.2006.10.018>
- Berta, M., Lindsay, C., Pans, G., & Camino, G. (2006). Effect of chemical structure on combustion and thermal behaviour of polyurethane elastomer layered silicate nanocomposites. *Polymer Degradation and Stability*, *91*, 1179–1191. <https://doi.org/10.1016/j.polymdegradstab.2005.05.027>
- Borowicz, M., Paciorek-Sadowska, J., Isbrandt, M. (2020). Synthesis and application of new biopolyols based on mustard oil for the production of selected polyurethane materials. *Industrial Crops and Products*, *155*, 112831. <https://doi.org/10.1016/j.indcrop.2020.113098>
- Chang, C., Liu, L., Li, P., et al. (2021). Preparation of flame retardant polyurethane foam from crude glycerol based liquefaction of wheat straw. *Industrial Crops and Products*, *160*, 113098. <https://doi.org/10.1016/j.indcrop.2020.113098>
- Choe, H., Choi, Y., & Kim, J. H. (2019). Threshold cell diameter for high thermal insulation of water-blown rigid polyurethane foams. *Journal of Industrial and Engineering Chemistry*, *73*, 344–350. <https://doi.org/10.1016/j.jiec.2019.02.003>
- Członka, S., Bertino, M. F., Kośny, J., et al. (2018a). Linseed oil as a natural modifier of rigid polyurethane foams. *Industrial Crops and Products*, *115*, 40–51. <https://doi.org/10.1016/j.indcrop.2018.02.019>
- Członka, S., Bertino, M. F., Strzelec, K. (2018b). Rigid polyurethane foams reinforced with industrial potato protein. *Polymer Testing*, *68*. <https://doi.org/10.1016/j.polymertesting.2018b>
- Członka, S., Bertino, M. F., Strzelec, K., et al. (2018c). Rigid polyurethane foams reinforced with solid waste generated in leather industry. *Polymer Testing*, *69*, 225–237. <https://doi.org/10.1016/j.polymertesting.2018.05.013>
- Członka, S., Kairyte, A., Miedzińska, K., & Strąkowska, A. (2021). Polyurethane Hybrid Composites Reinforced with Lavender Residue Functionalized with Kaolinite and Hydroxyapatite. *Materials (basel)*, *14*, 415. <https://doi.org/10.3390/ma14020415>
- Członka, S., Sienkiewicz, N., Strąkowska, A., & Strzelec, K. (2018). Keratin feathers as a filler for rigid polyurethane foams on the basis of soybean oil polyol. *Polymer Testing*, *72*, 32–45. <https://doi.org/10.1016/j.polymertesting.2018.09.032>
- Członka, S., Strąkowska, A., Pospiech, P., & Strzelec, K. (2020). Effects of Chemically Treated Eucalyptus Fibers on Mechanical, Thermal and Insulating Properties of Polyurethane Composite Foams. *Materials (basel)*, *13*, 1781. <https://doi.org/10.3390/ma13071781>

- Czlonka, S., Strakowska, A., Strzelec, K., et al. (2020). Bio-based polyurethane composite foams with improved mechanical, thermal, and antibacterial properties. *Materials (basel)*, *13*, 1–20. <https://doi.org/10.3390/ma13051108>
- Czlonka, S., Strakowska, A., Strzelec, K., et al. (2019a). Composites of rigid polyurethane foams and silica powder filler enhanced with ionic liquid. *Polymer Testing*, *75*, 12–25. <https://doi.org/10.1016/J.POLYMERTESTING.2019.01.021>
- Czlonka, S., Strakowska, A., Strzelec, K., et al. (2019b). Composites of Rigid Polyurethane Foams Reinforced with POSS. *Polymers (basel)*, *11*, 336. <https://doi.org/10.3390/polym11020336>
- de Avila, D. R., Magalhães, W. L. E., Petzhold, C. L., & Amico, S. C. (2018). Forest-based resources as fillers in biobased polyurethane foams. *Journal of Applied Polymer Science*, *135*, 1–7. <https://doi.org/10.1002/app.45684>
- Dhaliwal, G. S., Anandan, S., Chandrashekhara, K., et al. (2018). Development and characterization of polyurethane foams with substitution of polyether polyol with soy-based polyol. *European Polymer Journal*, *107*, 105–117. <https://doi.org/10.1016/j.eurpolymj.2018.08.001>
- El-Shekeil, Y. A., Sapuan, S. M., Abdan, K., & Zainudin, E. S. (2012). Influence of fiber content on the mechanical and thermal properties of Kenaf fiber reinforced thermoplastic polyurethane composites. *Materials and Design*, *40*, 299–303. <https://doi.org/10.1016/J.MATDES.2012.04.003>
- Guo, C., Zhou, L., & Lv, J. (2013). Effects of expandable graphite and modified ammonium polyphosphate on the flame-retardant and mechanical properties of wood flour-polypropylene composites. *Polymers and Polymer Composites*, *21*, 449–456. <https://doi.org/10.1002/app>
- Hejna, A., Kirpluks, M., Kosmela, P., et al. (2017). The influence of crude glycerol and castor oil-based polyol on the structure and performance of rigid polyurethane-polyisocyanurate foams. *Industrial Crops and Products*, *95*, 113–125. <https://doi.org/10.1016/j.indcrop.2016.10.023>
- Huang, G., & Wang, P. (2017). Effects of preparation conditions on properties of rigid polyurethane foam composites based on liquefied bagasse and jute fibre. *Polymer Testing*, *60*, 266–273. <https://doi.org/10.1016/j.polymeresting.2017.04.006>
- Ji, D., Fang, Z., He, W., et al. (2015). Polyurethane rigid foams formed from different soy-based polyols by the ring opening of epoxidised soybean oil with methanol, phenol, and cyclohexanol. *Industrial Crops and Products*, *74*, 76–82. <https://doi.org/10.1016/j.indcrop.2015.04.041>
- Kairyte, A., Vaitkus, S., Vėjelis, S., et al. (2018a). Rapeseed-based polyols and paper production waste sludge in polyurethane foam: Physical properties and their prediction models. *Industrial Crops and Products*, *112*, 119–129. <https://doi.org/10.1016/j.indcrop.2017.11.027>
- Kairyte, A., Vaitkus, S., Vėjelis, S., & Pundienė, I. (2018b). A Study of Rapeseed Oil-Based Polyol Substitution with Bio-based Products to Obtain Dimensionally and Structurally Stable Rigid Polyurethane Foam. *Journal of Polymers and the Environment*, *26*, 3834–3847. <https://doi.org/10.1007/s10924-018-1266-8>
- Kairyte, A., & Vėjelis, S. (2015). Evaluation of forming mixture composition impact on properties of water blown rigid polyurethane (PUR) foam from rapeseed oil polyol. *Industrial Crops and Products*, *66*, 210–215. <https://doi.org/10.1016/j.indcrop.2014.12.032>
- Kirpluks, M., Cabulis, U., Avots, A. (2016) Flammability of Bio-Based Rigid Polyurethane Foam as Sustainable Thermal Insulation Material. In: *Insulation Materials in Context of Sustainability*. InTech.
- Kirpluks, M., Vanags, E., Abolins, A., et al. (2020). High Functionality Bio-Polyols from Tall Oil and Rigid Polyurethane Foams Formulated Solely Using Bio-Polyols. *Materials (basel)*, *13*, 1985. <https://doi.org/10.3390/ma13081985>
- Kurańska, M., Pinto, J. A., Salach, K., et al. (2020a). Synthesis of thermal insulating polyurethane foams from lignin and rapeseed based polyols: A comparative study. *Industrial Crops and Products*, *143*, 111882. <https://doi.org/10.1016/j.indcrop.2019.111882>
- Kurańska, M., Polaczek, K., Auguścik-Królikowska, M., et al. (2020b). Open-cell rigid polyurethane bio-foams based on modified used cooking oil. *Polymer (Guildf)* *190*, 122164. <https://doi.org/10.1016/j.polymer.2020.122164>

- Kurańska, M., & Prociak, A. (2016). The influence of rapeseed oil-based polyols on the foaming process of rigid polyurethane foams. *Industrial Crops and Products*, 89, 182–187. <https://doi.org/10.1016/j.indcrop.2016.05.016>
- Kurańska, M., Prociak, A., Kirpluks, M., & Cabulis, U. (2015). Polyurethane-polyisocyanurate foams modified with hydroxyl derivatives of rapeseed oil. *Industrial Crops and Products*, 74, 849–857. <https://doi.org/10.1016/j.indcrop.2015.06.006>
- Liszkowska, J., Borowicz, M., Paciorek-Sadowska, J., et al. (2020). Assessment of photodegradation and biodegradation of RPU/PIR foams modified by natural compounds of plant origin. *Polymers (Basel)*, 12, <https://doi.org/10.3390/polym12010033>.
- Maharsia, R. R., & Jerro, H. D. (2007). Enhancing tensile strength and toughness in syntactic foams through nanoclay reinforcement. *Materials Science and Engineering A*, 454–455, 416–422. <https://doi.org/10.1016/j.msea.2006.11.121>
- Marcovich, N. E., Kurańska, M., Prociak, A., et al. (2017a). Open cell semi-rigid polyurethane foams synthesized using palm oil-based bio-polyol. *Industrial Crops and Products*, 102, 88–96. <https://doi.org/10.1016/j.indcrop.2017.03.025>
- Marcovich, N. E., Kurańska, M., Prociak, A., et al. (2017b). The effect of different palm oil-based bio-polyols on foaming process and selected properties of porous polyurethanes. *Polymer International*, 66, 1522–1529. <https://doi.org/10.1002/pi.5408>
- Martínez-Molina, A., Tort-Ausina, I., Cho, S., & Vivancos, J. L. (2016). Energy efficiency and thermal comfort in historic buildings: A review. *Renewable and Sustainable Energy Reviews*, 61, 70–85.
- Modesti, M., Lorenzetti, A., Simioni, F., & Camino, G. (2002). Expandable graphite as an intumescent flame retardant in polyisocyanurate–polyurethane foams. *Polymer Degradation and Stability*, 77, 195–202. [https://doi.org/10.1016/S0141-3910\(02\)00034-4](https://doi.org/10.1016/S0141-3910(02)00034-4)
- Modesti, M., Lorenzetti, A., Simioni, F., & Checchin, M. (2001). Influence of different flame retardants on fire behaviour of modified PIR/PUR polymers. *Polymer Degradation and Stability*, 74, 475–479. [https://doi.org/10.1016/S0141-3910\(01\)00171-9](https://doi.org/10.1016/S0141-3910(01)00171-9)
- Mosiewicki, M., A., Casado, U., Marcovich, N. E., Aranguren, M. I., (2008). Vegetable oil based-polymers reinforced with wood flour. *Molecular Crystals and Liquid Crystals*, 484, 509–516. <https://doi.org/10.1080/15421400801904344>.
- Nam, S., & Netravali, A. N. (2004). Characterization of ramie fiber/soy protein concentrate (SPC) resin interface. *Journal of Adhesion Science and Technology*, 18, 1063–1076. <https://doi.org/10.1163/1568561041257504>
- Nik Pauzi, N. N. P., & A. Majid R, Dzulkifli MH, Yahya MY., (2014). Development of rigid bio-based polyurethane foam reinforced with nanoclay. *Composites. Part b, Engineering*, 67, 521–526. <https://doi.org/10.1016/J.COMPOSITESB.2014.08.004>
- Oh, J. H., Bae, J. H., Kim, J. H., et al. (2019). Effects of Kevlar pulp on the enhancement of cryogenic mechanical properties of polyurethane foam. *Polymers Testing*, 80, 106093. <https://doi.org/10.1016/j.polymertesting.2019.106093>.
- Paciorek-Sadowska, J., Borowicz, M., Czupryński, B., & Isbrandt, M. (2018). Effect of Evening Primrose Oil-Based Polyol on the Properties of Rigid Polyurethane-Polyisocyanurate Foams for Thermal Insulation. *Polymers (basel)*, 10, 1334. <https://doi.org/10.3390/polym10121334>
- Paciorek-Sadowska, J., Borowicz, M., Isbrandt, M., et al. (2019). The Use of Waste from the Production of Rapeseed Oil for Obtaining of New Polyurethane Composites. *Polymers (basel)*, 11, 1431. <https://doi.org/10.3390/polym11091431>
- Paciorek-Sadowska, J., Czupryński, B., Borowicz, M., & Liszkowska, J. (2020). Rigid polyurethane–polyisocyanurate foams modified with grain fraction of fly ashes. *Journal of Cellular Plastics*, 56, 53–72. <https://doi.org/10.1177/0021955X19864391>
- Piszczyk, Ł., Strankowski, M., Danowska, M., et al. (2014). Rigid polyurethane foams from a polyglycerol-based polyol. *European Polymer Journal*, 57, 143–150. <https://doi.org/10.1016/j.eurpolymj.2014.05.012>

- Qi, X., Zhang, Y., Chang, C., et al. (2018). Thermal, Mechanical, and Morphological Properties of Rigid Crude Glycerol-Based Polyurethane Foams Reinforced With Nanoclay and Microcrystalline Cellulose. *European Journal of Lipid Science and Technology*, 120, 1–11. <https://doi.org/10.1002/ejlt.201700413>
- Qian, L., Feng, F., & Tang, S. (2014). Bi-phase flame-retardant effect of hexa-phenoxy-cyclotriphosphazene on rigid polyurethane foams containing expandable graphite. *Polymer (guildf)*, 55, 95–101. <https://doi.org/10.1016/j.polymer.2013.12.015>
- Ribeiro da Silva, V., Mosiewicki, M. A., Yoshida, M. I., et al. (2013). Polyurethane foams based on modified tung oil and reinforced with rice husk ash II: Mechanical characterization. *Polymer Testing*, 32, 665–672. <https://doi.org/10.1016/J.POLYMERTESTING.2013.03.010>
- Schartel, B., & Hull, T. R. (2007). Development of fire-retarded materials—Interpretation of cone calorimeter data. *Fire and Materials*, 31, 327–354. <https://doi.org/10.1002/fam.949>
- Septevani, A. A., Evans, D. A. C., Chaleat, C., et al. (2015). A systematic study substituting polyether polyol with palm kernel oil based polyester polyol in rigid polyurethane foam. *Industrial Crops and Products*, 66, 16–26. <https://doi.org/10.1016/j.indcrop.2014.11.053>
- Shan, C. W., Idris, M. I., Ghazali, M. I., (2012). Study of Flexible Polyurethane Foams Reinforced with Coir Fibres and Tyre Particles. *International Journal of Applied Mathematics*, 123–123. <https://doi.org/10.7763/IJAPM.2012.V2.67>.
- Soares, B., Gama, N., Freire, C. S. R., et al. (2015). Spent coffee grounds as a renewable source for copolyols production. *Journal of Chemical Technology and Biotechnology*, 90, 1480–1488. <https://doi.org/10.1002/jctb.4457>
- Strakowska, A., Członka, S., & Kairyte, A. (2020). Rigid polyurethane foams reinforced with poss-impregnated sugar beet pulp filler. *Materials (basel)*, 13, 1–15. <https://doi.org/10.3390/ma13235493>
- Strakowska, A., Członka, S., & Strzelec, K. (2019). POSS Compounds as Modifiers for Rigid Polyurethane Foams (Composites). *Polymers (basel)*, 11, 1092. <https://doi.org/10.3390/polym11071092>
- Sung, G., & Kim, J. H. (2017). Influence of filler surface characteristics on morphological, physical, acoustic properties of polyurethane composite foams filled with inorganic fillers. *Composites Science and Technology*, 146, 147–154. <https://doi.org/10.1016/j.compscitech.2017.04.029>
- Szycher, M. (2017). *Szycher's Handbook of Polyurethanes - 2nd Edition - Michael Szycher*. CRC Press.
- Trovati, G., Natali Suman, M. V., Sanches, E. A., et al. (2019). Production and characterization of polyurethane castor oil (*Ricinus communis*) foam for nautical fender. *Polymer Testing*, 73, 87–93. <https://doi.org/10.1016/j.polymertesting.2018.11.010>
- Vučurović, V. M., & Razmovski, R. N. (2012). Sugar beet pulp as support for *Saccharomyces cerevisiae* immobilization in bioethanol production. *Industrial Crops and Products*, 39, 128–134. <https://doi.org/10.1016/j.indcrop.2012.02.002>
- Xue, B.-L., Wen, J.-L., & Sun, R.-C. (2014). Lignin-Based Rigid Polyurethane Foam Reinforced with Pulp Fiber: Synthesis and Characterization. *ACS Sustain Chem Eng*, 2, 1474–1480. <https://doi.org/10.1021/sc5001226>
- Zhang, S., Xiang, A., Tian, H., & Rajulu, A. V. (2018). Water-Blown Castor Oil-Based Polyurethane Foams with Soy Protein as a Reactive Reinforcing Filler. *Journal of Polymers and the Environment*, 26, 15–22. <https://doi.org/10.1007/s10924-016-0914-0>
- Zhu, M., Bandyopadhyay-Ghosh, S., Khazabi, M., et al (2011) Reinforcement of soy polyol-based rigid polyurethane foams by cellulose microfibrils and nanoclays. *Journal of Applied Polymer Science*, 124, n/a-n/a. <https://doi.org/10.1002/app.35511>.
- Zieleniewska, M., Leszczyński, M. K., Szczepkowski, L., et al. (2016). Development and applicational evaluation of the rigid polyurethane foam composites with egg shell waste. *Polymer Degradation and Stability*, 132, 78–86. <https://doi.org/10.1016/j.polyimdegradstab.2016.02.030>

# Chapter 8

## Improvements of Polyurethane (PU) Foam's Antibacterial Properties and Bio-resistance



Natalia Sienkiewicz

**Abstract** Since there is a growing interest in using polymeric materials with antibacterial and antifungal properties, the present chapter is focused on the effect of natural compounds on the antibacterial and antifungal properties of polyurethane (PU) foams. These materials, in addition to great variety of traditional applications, can be used as antibacterial and antifungal agents both in shipping and storage of bio, pharmaceutical, and medical products, as well as in places where hygiene and sterile conditions are particularly required (e.g., in healthcare, hospitality, education, cosmetology, pharma, or food industries). As a result, they can become an alternative to commonly used mold growth inhibitors and disinfectants, which often show significant harmfulness, both to the environment and human health. Fungi grow in almost any environment, and they reproduce easily in dirt and wet spaces, and thus, the development of antifungal PU foams is focused on avoiding fungal infections and inhibiting growth. Polymers are susceptible to microorganism adhesion and, consequently, are treated and modified to inhibit fungal and bacterial growth. The ability of micro-organisms to grow on polyurethanes can cause human health problems during the use and storage of polymers, making it necessary to use additives that eliminate bacteria and fungi. It is also important for a healthy human life that building thermal insulation made of polyurethane foam have effective antibacterial and antifungal properties so it will not support the mold development and consequently, cause allergies and pulmonary or immune system problems. The results of the multidisciplinary research information presented in this chapter indicate that it is possible to modify and enhance bio-resistance of PU foams with either inorganic or bio-based compounds. Furthermore, such enhancements can also improve the foam cellular structure, leading to increased mechanical strength, and possibly reduce foam thermal aging.

---

N. Sienkiewicz (✉)

Institute of Polymer and Dye Technology, Faculty of Chemistry, Lodz University of Technology,  
Ul. Stefanowskiego 16, Lodz, Poland

e-mail: [natalia.sienkiewicz@p.lodz.pl](mailto:natalia.sienkiewicz@p.lodz.pl)

## 8.1 Introduction

Plastic foam insulation is a key in many industries that are essential for sustained economic growth, population health, and environment. This includes the building sector, as well as healthcare, hospitality, education, cosmetology, pharma, or food industries. Recently the COVID-19 pandemic has disrupted numerous industries worldwide, mostly due to common concerns over virus propagation in the building environment. In addition to widely discussed impacts of microbial- and mold-related processes in building enclosures and space conditioning systems, a growing interest can be observed. For the use of polymer materials with antibacterial and antifungal properties. The most important feature expected from materials with antibacterial properties is to inhibit the growth of bacteria and prevent their accumulation. The largest amounts of the most common colon *Escherichia coli*, *Klebsiella pneumoniae* and *Staphylococcus aureus* which cause the greatest number of infections and diseases in hospitals and other medical centers occur on objects that are near patients, such as bed rails, headboards, armchairs, and cabinets with contact surfaces from which bacteria can easily transfer to patients, their relatives, and employees. The type of used polymers is of a major importance for products that are expected to limit the growth of bacteria, fungi, and viruses. These polymers should demonstrate sufficient bacteriostatic activity to ward off the expansion of bacterial colonies in their proximity and destroy nearby bacteria by mitigating the progress of their cellular processes. For example, in buildings not using fungi-resistive materials, or without antifungal treatment, fungus and mold can contaminate walls, ceilings, insulation and other surfaces. This can often cause unaesthetic appearance and potential pulmonary and/or immune system problems for the buildings' inhabitants—see: Weinhold (2007), Curtis et al. (2004), Zainal Abidin (2017), Souza (2020), Annila et al. (2017). Mold and fungus usually grow in areas of high humidity, places with potential water–vapor condensation, and in materials of high moisture content, as well as in locations of past water/flood damage. Furthermore, in the case of many everyday-usage products, even a short-term exposure to fungi and various types of molds can cause the development of unpleasant black–green patterns on the product surface, which make them unaesthetic and unhygienic. Prolonged exposure to fungus and mold can cause building systems and materials to quickly deteriorate which impacts their long-term use, structural integrity, and for many direct consumption products it may shorten their shelf life. The use of antifungal materials can prevent growth. In the case of building envelope applications, the subsequent important feature to keep in mind are the overall cost, durability, thermal efficiency, and the amount of time a material surface will be used. A surface with antibacterial properties should be prepared with additives having a long lifespan and sustained efficiency. These additives should show resistance to a variety of environmental agents, so the leaching of antiseptic additives will not occur. Also, in the case of using antiseptics, the concentration of the active compound, the exposure time, and the pH of the environment, are important to maintain immunity for as long as possible—see: Desmet et al. (2009), Busscher et al. (2010), Jou et al. (2007).

## 8.2 Recent Developments of Polyurethane Foam Products with Antiseptic and Antimicrobial Characteristics

Polyurethanes are a group of polymers that are extensively used in construction, shipping, transportation, healthcare, and food industry, and in the manufacturing of industrial equipment. All these applications encounter humans during their use—Pivec et al. (2017). The first polyurethane products were made by the reaction between a diamine forming polyurea and an aliphatic diisocyanate. Later, the polyurea was replaced by glycol. Developed in 1937 by Otto Bayer of I.G. Farbenindustrie A.G. in Germany, polyurethane (PU) foam is a porous, cellular-structured, synthetic material made from the reaction of polyols and diisocyanates. Its structure is a composite of a solid phase and a gas phase. The solid phase is made from polyurethane elastomer while the gas phase is air and a low thermal conductivity gas which is introduced during formation of the foam. The huge gas phase of PU foams ascribes desirable properties such as good thermal and acoustic insulation, high compressive strength, low density, and sometimes material flexibility. Today, PU foams are most often produced from six following components: polyols, diisocyanates, blowing agents, surfactants, catalysts, and curatives (cross-linkers and chain extenders). The polyols and diisocyanates react to form the main polymer chain of the polyurethane foam. The blowing agent is responsible for creating the material's porous structure. The surfactants, catalysts, and curatives aid the polymer system to stabilize and maintain the desired rate of reaction of the polymer system. Additives are used to impart additional properties which can vary depending on a foam's intended application.

Numerous scientific and engineering reports indicate that the ability of bacteria, virus, or fungus to growth on the surface of polyurethanes can create a variety of human health problems that can arise during the building lifespan, product utilization, and material storage—see: Cosgrove et al. (2007), Lando et al. (2017), Magnin et al. (2019). That is why in many modern applications, polyurethanes are used with disinfectant and antiseptic additives or treatments. In buildings, mold, mildew, fungus, and bacteria can affect indoor air quality, penetrate thermal insulation, as well impacting the aesthetics of interior finish surfaces and façade systems.

When antimicrobial treatment is applied on the surface of polymeric products, the active agent usually penetrates the cellular wall of a microorganism, disabling its ability to grow and reproduce. The second path for the protection against the bio-growth is associated with surface properties of polyurethanes and focuses on mitigation of microbial adhesion. Unfortunately, in the case of even state-of-the-art applications, polyurethanes perform today only moderately well in reducing the bacterial adhesion. As a result, they are susceptible to bacterial colonization and have a high risk of infection. Typical strategies for antibacterial polyurethanes generally focus on designing antibacterial surfaces to repel or resist bacterial attachment through the incorporation of coatings with antibiotic agents or surface modification to generate anti-biofouling and/or bactericidal effects.

The use of antiseptic and simultaneously anti-adhesive properties of polyurethanes (PU) have been investigated by Kara et al. (2015). They immobilize chitosan and

heparin on specimens of polyurethane. Antibacterial functionalities against *Staphylococcus aureus*, *Staphylococcus epidermidis* (both Gram-positive), *Escherichia coli* and *Pseudomonas aeruginosa* (both Gram-negative) bacteria have been obtained by plasmas, modified with concentrations of chitosan from 0.5 to 2.0 wt.%, and heparin immobilization. Material samples prepared for analyses were modified by immobilizing chitosan (CH) and heparin (Hep) on samples of polyurethane via a stepwise process including plasma activation, acryl amide and glutaraldehyde treatment, and then sequential immobilization of CH and Hep. CH was used in two different concentrations to correlate its effect on each step with Hep used at constant concentration. Gram-negative *E. coli*, *P. aeruginosa*, and Gram-positive *S. aureus*, *S. epidermidis* exhibited a weak adhesion and proliferation on the modified surfaces compared to the control group. The results of this study showed that the surfaces with higher hydrophilicity and surface free energy enhanced anti-adhesion performance against bacteria. PU-CH-Hep samples had the most effective antibacterial and anti-adhesive properties and can be good candidates for applications which require medical purity. The bacterial adhesion results indicated a meaningful decrease in the quantity of bacteria. However, the polyurethane samples modified with chitosan as well as with heparin demonstrated significantly improved results (see: Figs. 8.1, 8.2, 8.3, 8.4 and 8.5). The above work demonstrated that polyurethane modified with different concentrations of chitosan with significant hydrophilicity can improve the efficiency of polyurethane against bacterial infections (*S. aureus* and *P. aeruginosa* bacteria).

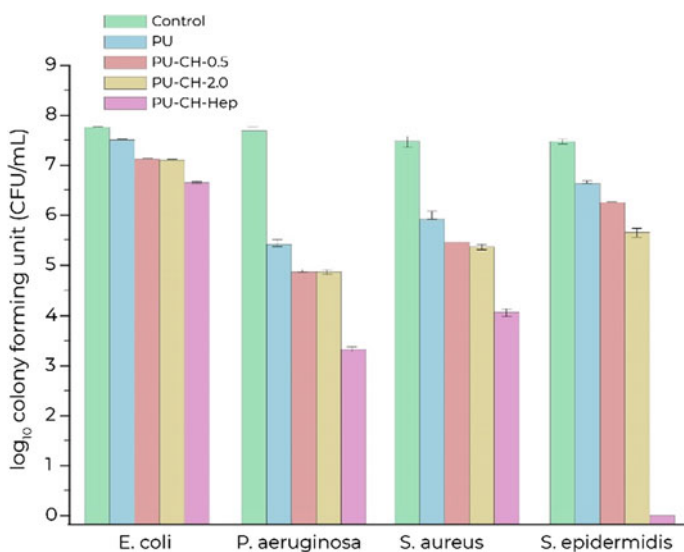


**Fig. 8.1** Antibacterial effects on control sample (Control), polyurethanes (PU), chitosan (CH), and heparin (Hep) immobilized on polyurethane films on survival of *E. coli*, *P. aeruginosa*, *S. aureus* and *S. epidermidis* bacteria—based on the work performed by Kara et al. (2015)



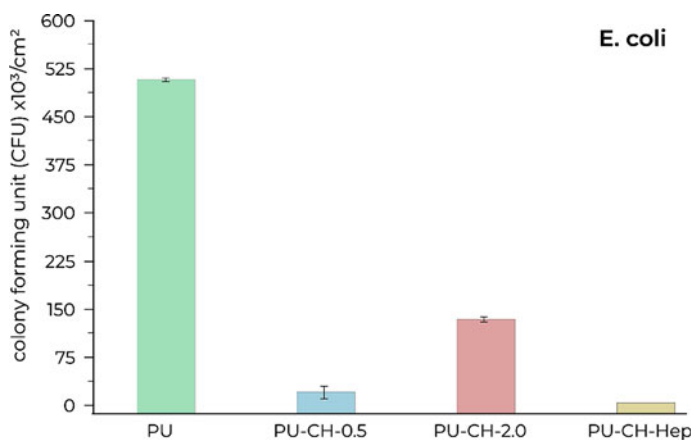


**Fig. 8.2** Number of feasible and adhesive *E. coli* on the polyurethanes (PU), chitosan (PU-CH-0.5; PU-CH-2.0) and heparin (PU-CH-Hep) immobilized on polyurethane films after a 4 h incubation period—based on the work performed by Kara et al. (2015)

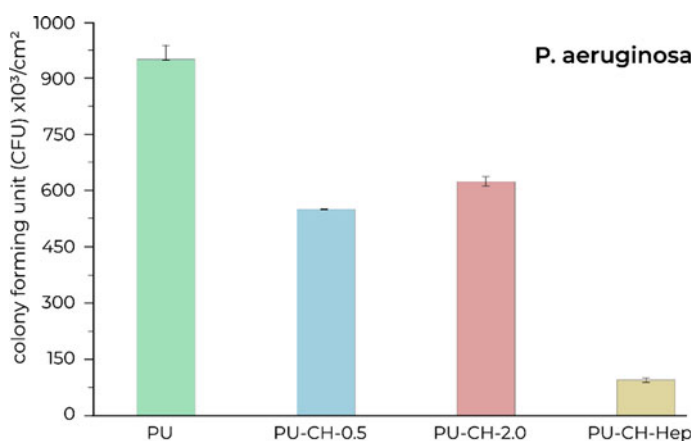


**Fig. 8.3** Number of feasible and adhesive *P. aeruginosa* on the polyurethanes (PU), chitosan (PU-CH-0.5; PU-CH-2.0) and heparin (PU-CH-Hep) immobilized on polyurethane films after a 4 h incubation period—based on the work performed by Kara et al. (2015)

Furthermore, the stability of immobilized CH and Hep was determined by spectroscopic analysis. In fact, no assessable signals of CH or Hep were obtained from the solution treated with PU-CH-0.5, PU-CH-2.0 and PU-CH-Hep. The results presented in Figs. 8.1, 8.2, 8.3, 8.4 and 8.5 show that CH as well as CH-Hep were stable and did not detach from the polyurethane surfaces. The results also show that CH and Hep were covalently linked to the surface by activating the surface with plasma and glutaraldehyde that provides reactive aldehyde groups that can easily react with the amine and hydroxyl groups of chitosan and heparin.

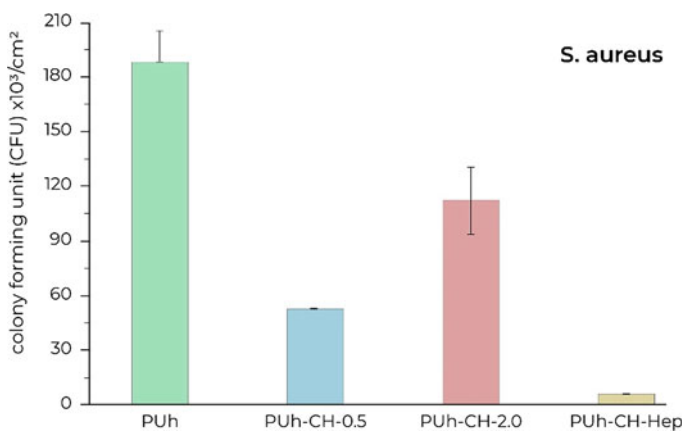


**Fig. 8.4** Number of feasible and adhesive *S. aureus* on the polyurethanes (PU), chitosan (PU-CH-0.5; PU-CH-2.0) and heparin (PU-CH-Hep) immobilized on polyurethane films after a 4 h incubation period—based on the work performed by Kara et al. (2015)

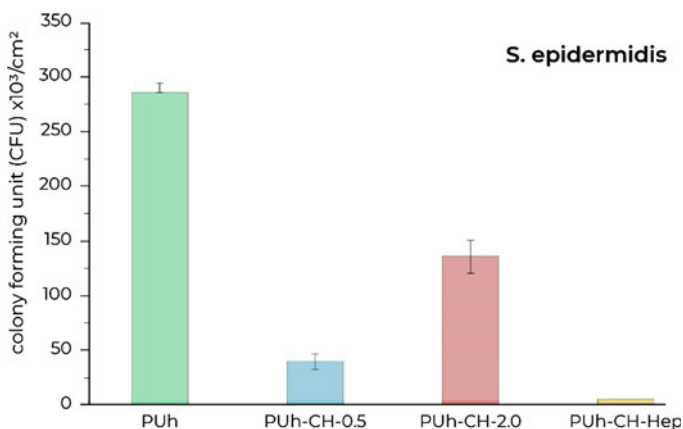


**Fig. 8.5** Number of feasible and adhesive *S. epidermidis* on the polyurethanes (PU), chitosan (PU-CH-0.5; PU-CH-2.0) and heparin (PU-CH-Hep) immobilized on polyurethane films after a 4 h incubation period—based on the work performed by Kara et al. (2015)

Prepared systems indicating that immobilization of chitosan and heparin was stable. They did not separate from the polyurethane surfaces—Kara et al. (2015).

In work performed by Xia et al. (2012), the cationic antibacterial polyurethane was prepared using soybean-oil with various molar ratios of polyols and hydroxyl groups from an amine diol. As presented in Tables 8.1 and 8.2, all polyurethane samples showed zone inhibition against foodborne pathogens such as: *Salmonella enterica*, *Salmonella typhimurium*, *Salmonella Minnesota* and *Listeria monocytogenes* and others. Polyurethane samples were analyzed both in the form of dispersion and as

**Table 8.1** Zone of inhibition (diameter) against two bacterial strains for polyurethane based on N-methyldiethanolamine as film and dispersion—see: Jeon et al. (2008)

Polyurethane prepared from N-methyldiethanolamine	<i>L. monocytogenes</i> (mm)	<i>S. typhimurium</i> (mm)
Film	12.52 ± 0.14	9.77 ± 0.08
Dispersion	12.66 ± 0.22	10.92 ± 0.03

**Table 8.2** Zone of inhibition (diameter) against three bacterial strains for polyurethane films prepared from different amino polyols—see: Jeon et al. (2008)

Polyurethane samples (PU)	<i>L. monocytogenes</i> (mm)	<i>S. typhimurium</i> (mm)	<i>S. Minnesota</i> (mm)
PU1 highest cross-link density	8.55 ± 0.17	None	12.28 ± 0.20
PU2 lowest ammonium ion content and a relatively high cross-link density	10.65 ± 0.14	7.58 ± 0.14	15.86 ± 0.19
PU3 highest ammonium ion content	None	8.88 ± 0.09	14.64 ± 0.09

a film. Results show that polyurethane had good antibacterial properties, specimens prepared as polyurethane dispersions show slightly better antibacterial activity than polyurethane films. This is most likely caused by higher diffusional mobility of the liquid phase or reduction in the accessibility or appearance of hydrophilic ammonium sites during the dispersion-to-film transition. Polyurethane incorporating N-methyldiethanolamine and other polyurethanes show better antibacterial properties on *Listeria monocytogenes* than *Salmonella typhimurium*. The results confirm generally approved mechanism for the antibacterial behavior of ammonium particles, that involves destructive interaction with the cell wall and/or cytoplasmic membranes. It can be also observed that increasing the ratio of ammonium cations improves antibacterial performance. The amount of isocyanate was calculated to have a stoichiometric ratio of 1:1 with respect to the hydroxyl groups. Moreover, results indicate a promising way to obtain effective antibacterial polyurethane coatings compared with other types of cationic materials reported in the literature. It is expected that these polymer coatings can be also effective against other microorganisms such as yeasts, molds, and viruses—see: Xia et al. (2012), Kenawy and Mahmoud (2003), Kenawy et al. (2002).

In research performed by Udabe et al. (2017) the functional quaternary ammonium monomers were used to obtain PU foams that demonstrated porous antimicrobial protection ability. In addition, the tri- and tetra-hydroxyl functional quaternary ammonium compounds were synthesized and used as a triol and tetraol monomer in a PU foam composition that caused the cationic ammonium group to be chemically incorporated into the polyurethane structure. The antiseptic features of these

new PU foams were investigated for *Escherichia coli* and *Staphylococcus aureus* Gram-negative and Gram-positive bacteria. The analyzed PU foams contained more than 20% of quaternary ammonium component. They demonstrated high antibacterial activity, which makes them good candidates for applications which require antiseptic properties (Fig. 8.6)—Udabe et al. (2017).

Ding et al. (2019) focused on obtaining imidazolium-type cationic foams with high antimicrobial and endotoxin adsorption features. Additionally, wound healing tests were performed with the use of *Pseudomonas aeruginosa* bacteria. Experiments on mice demonstrated that the imidazolium-type PU foams can be utilized in clinical applications as a new type of antibacterial dressings with intrinsically endotoxin adsorption activity. This new formulation of PU foams shows slightly higher efficiency against Gram-negative strains of bacteria than for Gram-positive one and significant absorbability of endotoxin or lipopolysaccharide. Gram-negative bacteria,

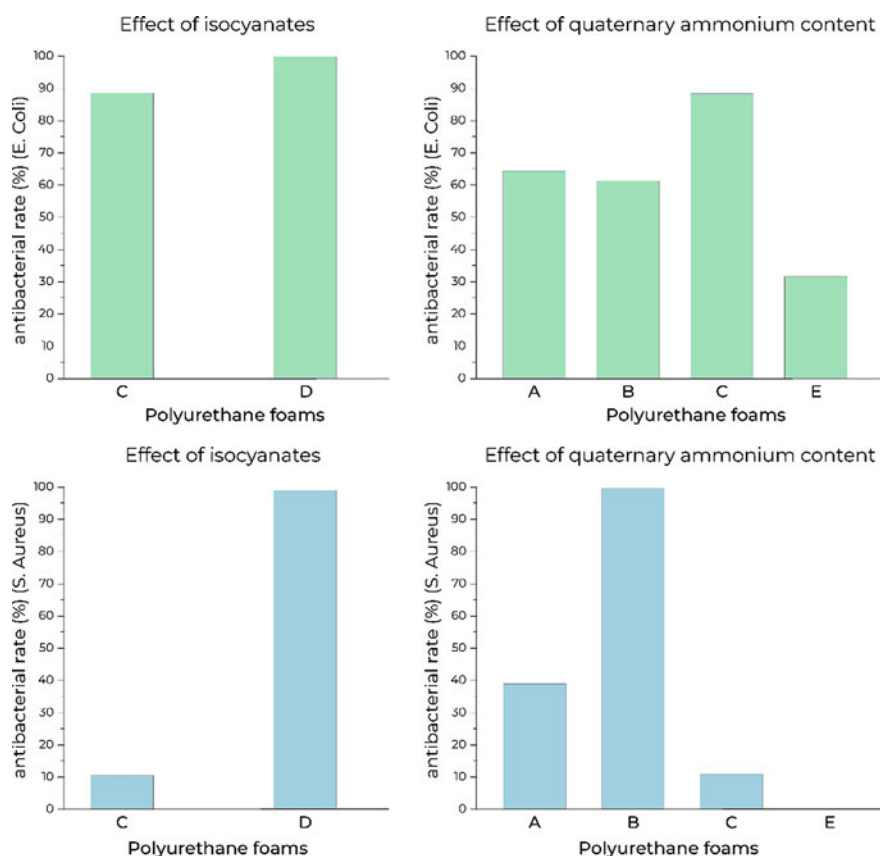


**Fig. 8.6** Antimicrobial rates of the PU foams toward *E. coli* and *S. aureus* containing different amounts of the quaternary ammonium functional group—based on work performed by Udabe et al. (2017)

including *Acinetobacter baumannii*, *Pseudomonas aeruginosa*, and Enterobacteriaceae belong to the group considered “critical” and high risk. Moreover, cell walls of Gram-negative bacteria also include a commonly known pathogenic component, lipopolysaccharide with highly toxic causing inflammation of a part of the body and inducing fever substance (Figs. 8.7, 8.8 and 8.9).

Antimicrobial copper nanoparticles were synthesized and used for controlled impregnation of industrial PU foams by Sportelli et al. (2016). Their research has demonstrated that copper nanoparticles can be effectively utilized as antiseptics against the Gram-negative and Gram-positive bacteria. This work also shows that copper particles can be useful as an antibacterial additive in various polymeric materials. Furthermore, copper nanoparticles, when reinforced with chitosan, demonstrate the ability to stabilize these nanoparticles, as well as the improvement of their

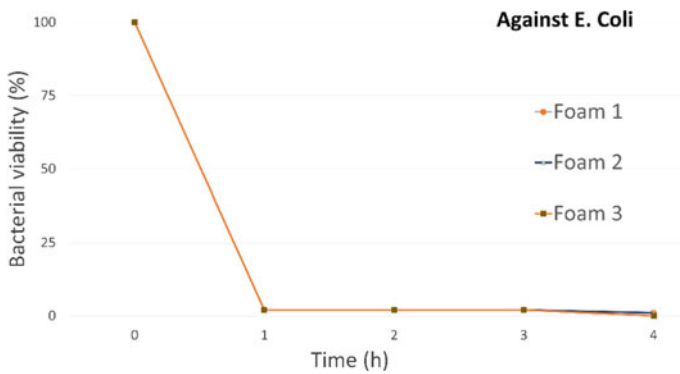


**Fig. 8.7** The time course of surviving *E. coli* upon contacting with the modified PU foams. Foam 1 contained 2 mmol of ionic diol; foam 2 contained 4 mmol of ionic diol; foam 3 contained 6 mmol of ionic diol—based on work performed by Ding et al. (2019)

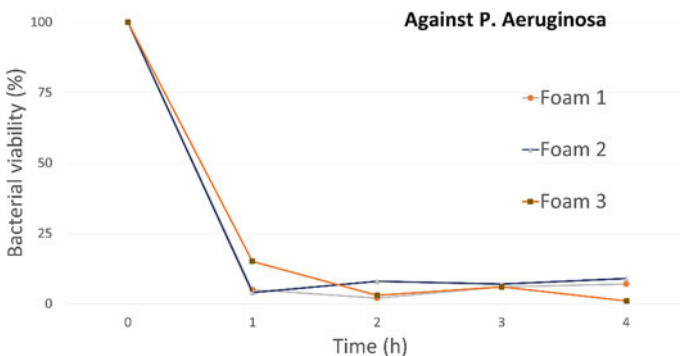


**Fig. 8.8** The survival time for *P. aeruginosa* upon contacting with the modified PU foams. Foam 1 contained 2 mmol of ionic diol; foam 2 contained 4 mmol of ionic diol; foam 3 contained 6 mmol of ionic diol—based on work performed by Ding et al. (2019)

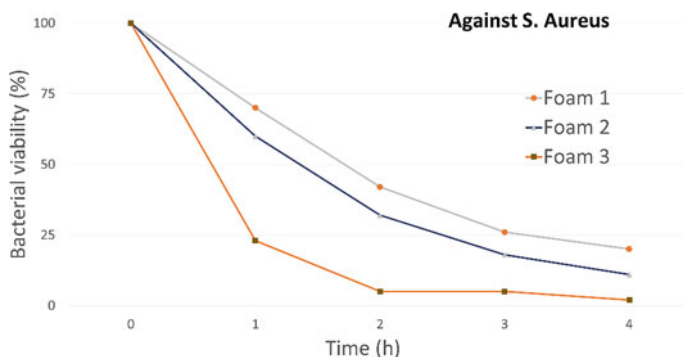


**Fig. 8.9** The time course of surviving *S. aureus* upon contacting with the modified PU foams. Foam 1 contained 2 mmol of ionic diol; foam 2 contained 4 mmol of ionic diol; foam 3 contained 6 mmol of ionic diol—based on work performed by Ding et al. (2019)

biocompatibility extending the operating time. This limits the bacterial ability for recolonization and is further reinforcing the material's antimicrobial characteristics. Moreover, the antimicrobial potential of copper nanoparticles, combined with their superior availability and low cost, make them valuable as an antiseptic component of future polymeric materials to enhance antibacterial, antiviral, and antifungal properties. In the same work of Sportelli et al. (2016) the enhancement of generally available PU foams by diluted coppers colloids was analyzed. These new enhanced antimicrobial capabilities were simultaneously validated against bacterium, virus, and fungus (*Staphylococcus aureus*, *Escherichia coli* and *Kluyveromyces marxianus*), demonstrating the colloidal copper's ability to inhibit bacterial growth and spread. As presented in Table 8.3, the following two open pore polyurethane formulations were used to evaluate the foam modification with CuNP-colloids: (i) foam samples type A PU (PUA) with large and irregular pores, typically used as a filling material for mattresses (density: 25 kg/m<sup>3</sup>, density tolerance  $\pm 5\%$ ) and (ii) foam samples Type B (PUB) with small and regular pores, used by the automotive industry (density: 21 kg/m<sup>3</sup>, density tolerance  $\pm 5\%$ ). Adsorption efficiency of PU foams with antimicrobial copper nanoparticles was done by weighing each sample before and after the modification process and observing the foam's morphology with the use of an optical microscope. Both samples showed the average weight increase equal to  $8.2 \pm 0.3$  mg for type A PU and  $7.8 \pm 0.2$  mg for type B PU. Pore sizes of initial foam samples were greater and more dispersed than in subsequent specimens, which had more regular porous structure. The morphology of the foams after the modification did not change—Sportelli et al. (2016).

Furthermore, research studies that focused on the enhancement of antiseptic, antibacterial, and anti-fungal properties have demonstrated that polyurethanes can not only be modified with copper nanoparticles, as discussed above, but also with different types of inorganic groups, such as silver particles [see: Amina et al. (2013), Nirmala et al. (2014), Jeon et al. (2008), Prabhakar et al. (2011), Yang et al. (2012), Toker et al. (2013), Pant et al. (2014)], carbon nanotubes [see: Subagia et al. (2014)],

**Table 8.3** Number of colony forming units (CFU) for the three target microorganisms, exposed to different samples for 24 h. Error on CFU counts is  $\pm 5$  in the last digit

Sample	<i>S. aureus</i> /CFU	<i>E. coli</i> /CFU	<i>K. marxianus</i> /CFU
Polyurethane (PU)	U	U	U
PUA + 0.1 M tetraoctylammonium chloride solution	0	U	U
PUA + 1:1,000 antimicrobial copper nanoparticles	0	0	30
PUA + 1:100 antimicrobial copper nanoparticles	0	0	25
PUB + 0.1 M tetraoctylammonium chloride solution	2	U	U
PUB + 1:1,000 antimicrobial copper nanoparticles	U	72	U
PUB + 1:100 antimicrobial copper nanoparticles	0	0	U

PUA: foam with large and irregular pores (density: 25 kg/m<sup>3</sup>, density tolerance  $\pm 5\%$ );

PUB: foam with small and regular pores (density: 21 kg/m<sup>3</sup>, density tolerance  $\pm 5\%$ );

U = Uncountable.

Source Sportelli et al. (2016)

zinc-silver bimetallic particles [see: Shamshi Hassan et al. (2013)], tourmaline [see: Tijjing et al. (2013) and (2016)], silica [see: Luo et al. (2012)] and zinc oxide [see: Anna et al. (2013)]. Please notice that, currently, silver particles are one of most used by industry as additives to both natural and synthetic materials, providing antiseptic properties against a wide range of microorganisms. The practice of enhancement of PU foams with silver particles is becoming quite common, because a usage of silver is able to simultaneously improve foam's antiseptic features, as well as mechanical and rheological characteristics, as discussed in Dumitriu et al. (2016).

During the development of polymeric materials for long-acting wound dressing applications, Morena et al. (2020) analyzed lignin-capped silver particles that were embodied in situ into PU foams through their polymerization. Lignin with growing phenolic addition, acquired through the enzymatic grafting of unaffected phenolic mixtures applications had a double ability of (i) a silver reducing factor in the synthesis of the lignin-capped silver nanoparticles and (ii) as a nano formulated polyol in the modified new composition capable to react with isocyanate. The PU foams with added nanoparticles demonstrated increases of over 4 or 5 decades of action against the Gram-positive *Staphylococcus aureus* and the Gram-negative *Pseudomonas aeruginosa*, imputed to both have strong contact and removal mechanisms. The swelling features of the foams as a wound dressing, resulting from the ability to delete the surplus of wound exudates comprising harmful oxidative species and enzymes, ranged from 585 to 1,145%, respectively, as a function of the amounts of nanoparticles. Available experimental data show that physicomachanical and antibacterial features of the PU foams, and their additional biocompatibility and

permanent excretion of silver, and show that these novel foams can become very valuable in medical applications—Morena et al. (2020). Similar research focused on the mold development mitigation that can be very useful for building thermal insulation applications.

### 8.3 A Use of Bio-based Additives for Enhancement of Antiseptic, Antimicrobial, and Physical Characteristics of PU Foams

As reported in numerous research publications, curcumin (diferuloylmethane), when added to polyurethanes, generates unique anti-inflammatory, anti-oxidant, anti-carcinogenic, anti-mutagenic, anticoagulant and anti-infective effects—see: Yangyang et al. (2018), Moghadamtousi et al. (2014), Chen et al. (2020), Ismail et al. (2019), Sharifi-Rad et al. (2020), Kunnumakkara et al. (2017), Jennings and Parks (2020). Curcumin is the main curcuminoid component of turmeric (*Curcuma longa*), a popular Oriental spice, that has been used for centuries in food and herbal medicine. It is responsible for turmeric's yellow color.

The research performed by Sienkiewicz et al. (2019) was focused on curcumin's application (Fig. 8.10) as a natural phenolic compound during the preparation of a polyurethane foam with good antibacterial, antiaging, mechanical, and physical features. Foam samples prepared with added (E,E)-1,7-bis(4-Hydroxy-3-methoxyphenyl)-1,6-heptadiene-3,5-dione as natural curcumin were subjected to microbiological tests (Disc Diffusion Method), color characteristic (CM-3600d Spectrophotometer), mechanical and thermal methods—Sienkiewicz et al. (2019). Since curcumin molecules are a natural phenolic compound having polar groups and hydrophilic properties, strong interfacial interaction, such as hydrogen bonding, can be formed between the curcumin molecules and isocyanate leading to the formation of a cross-linked structure (Fig. 8.11). Hydroxyl groups, which are present in curcumin molecules, can react with isocyanates even in the absence of catalyst—see: Mráz et al. (2004), Schwetlick et al. (1994), Arnold et al. (1957), Guo et al. (2013). The urethane bond is formed with these reactions. PU foams

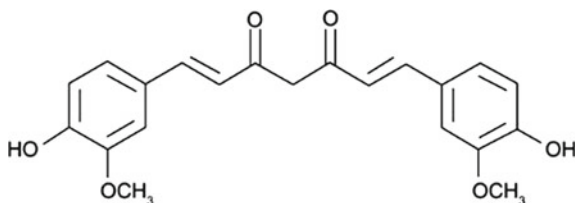
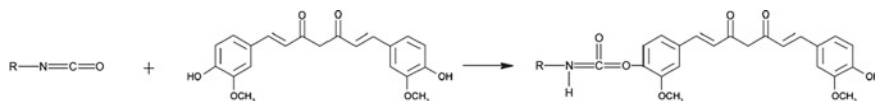


Fig. 8.10 Chemical structure of curcumin





**Fig. 8.11** Scheme reaction of isocyanate and curcumin

for special applications were prepared by a single-step method from a commercial two component mix (Izopianol 40/30/C and Purocyn B) which was modified with an addition of natural phenolic compound in the amount of 1, 2 and 5 wt.% in relation to the total polyol mass. Firstly, Izopianol 40/30/°C (containing polyester polyol, catalyst—Diethanolamine, flame retardant—Tris(2-chloro-1-methylethyl)phosphate, chain extender—1,2-propanediol, surfactant—polyether polydimethylsiloxane copolymer) and curcumin as natural antibacterial substance were weighed out in the required quantity and placed in a 1,000 ml polypropylene forms. Then, the mixture (component A with curcumin) was homogenized with an overhead stirrer at 500 rpm under the ambient conditions (temperature: 21 °C) for precisely 30 s. In the next step, the Purocyn B (polymeric diphenylmethane 4,4'-diisocyanate) was added to the previously prepared mixture and all components were then stirred for 15 s with an overhead stirrer at 2,000 rpm (as presented in Fig. 8.12). Next, the prepared reaction mixture was poured into an open container, which allowed the foam to rise freely in the vertical direction. As described in Sienkiewicz et al. (2019), the resulting samples were conditioned for 24 h in the ambient temperature.

It has been reported that curcumin exhibits hydrophobic characteristics, as well as physicochemical and biological instability, which may impact material properties plastic applications—see: Mahmood et al. (2015), Sun et al. (2013), Ziyun et al. (2020), O'Connor et al. (2018). That is why the impact of the different amounts of curcumin (1, 2, and 5 wt.%) on chemical structure (Table 8.4), physico-mechanical properties (compression strength, three-point bending test, apparent density, water absorption), and morphology of PU foams were explored. The results of this analysis indicate that the application of curcumin as a natural antibacterial compound (in the range between 1 and 5 wt.%) effects additionally the morphology of new foams, and correspondingly, their mechanical characteristics, as discussed in Sienkiewicz et al. (2019).

Component A: Izopianol 40/30/C + curcumin (1; 2; 5 wt.%)

Component B: Purocyn B

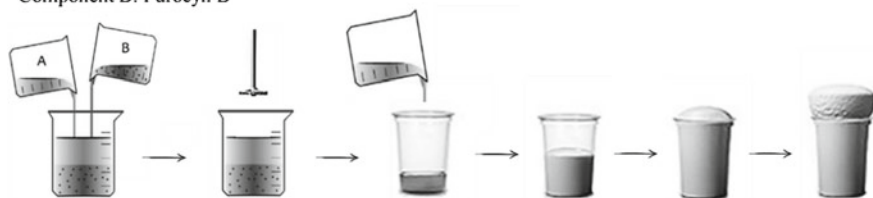


**Fig. 8.12** Schematic procedure of synthesis of curcumin modified PU foams. *Source* Sienkiewicz et al. (2019)

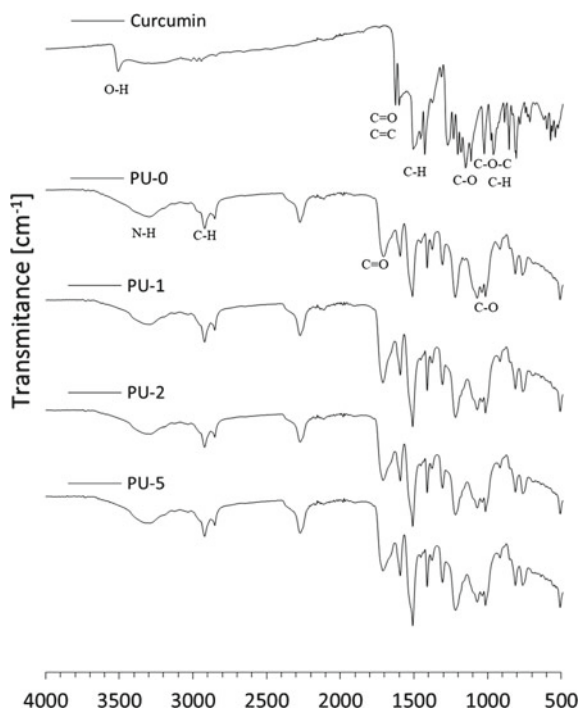
**Table 8.4** Polyurethane foam formulations.

Sample	Izopianol 40/30/C (by weight)	Purocyn B (by weight)	Curcumin (by weight)
Reference polyurethane foam (unmodified)	100	160	0
Foam with 1 wt.% of curcumin	100	160	1
Foam with 2 wt.% of curcumin	100	160	2
Foam with 5 wt.% of curcumin	100	160	5

Source Sienkiewicz et al. (2019)

Furthermore, as presented in Fig. 8.13, the FTIR analysis of the PU foam modified with antibacterial additives, showed that the addition of 1–5% of curcumin only insignificantly changed the chemical structure of the polyurethane foam. Only, insignificant shifts in the intensity and the values of wavenumbers of the characteristic bonds were noticeable in FTIR spectra of all tested foam samples. It is also interesting that the rise of the natural extract quantity causes that the absorbance

**Fig. 8.13** FTIR spectra of curcumin and PU foams for PU-0 non-modified polyurethane foam, PU-1 foam with 1 wt.% of curcumin, PU-2 foam with 2 wt.% of curcumin, PU-5 foam with 5 wt.% of curcumin. Source Sienkiewicz et al. (2019)



peak  $2,275\text{ cm}^{-1}$  (stretching vibration of residual isocyanate groups ( $-\text{N}=\text{C}=\text{O}$ ) to be more visible. This can be caused, to a large extent, by the hydroxyl groups of curcumin which can change the isocyanate index ( $R_{\text{NCO/OH}}$ ), that is the number of moles of NCO groups of the isocyanate per OH mole of the polyol in this way that influence on the use of NCO groups. The FTIR results shown the good incorporation of curcumin into the foam structure. A faint peak is observed in the same region at  $3,770\text{ cm}^{-1}$  in the spectra of all the samples containing curcumin are related to the mixed stretching vibrations of ( $\text{C}=\text{C}$ ), ( $\text{C}=\text{O}$ ) and phenyl rings of curcumin. In addition, by increasing the curcumin contents from 1 to 5 wt.% in foams, the absorption peak intensities at  $3,770\text{ cm}^{-1}$  are increased which confirmed the incorporation of curcumin in the structure of sample.

Additionally, it was observed that the insertion of natural curcumin extract into the foam yields more hydrogen bonds, compared to the non-modified PU foam, while the phase separation degree is not significantly changed. The Scanning Electron Microscopy (SEM) images shown in Figs. 8.14 and 8.15, present the specifics of foams cut parallel to the foaming direction. These images show the morphology of the foam sample, the cell size and cell distribution. It can be observed that the foam consists of closed cells with an insignificant quantity of cells with irregular walls. In comparison to the non-modified polyurethane foam samples, the natural curcumin extract notably modified foam internal structure, impacting a broad cell size and higher cell distribution frequency.

Moreover, it can be observed that pore sizes decrease with the increasing filler content. This allows a conclusion that curcumin can cause the reduction of the cell

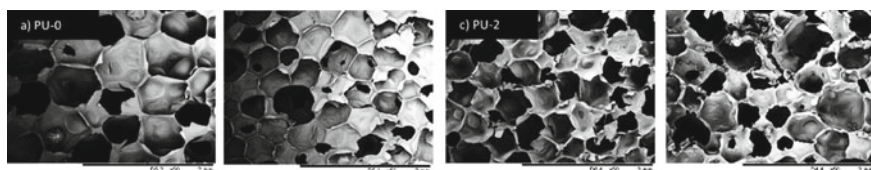


**Fig. 8.14** Morphology of **a** PU-0 non-modified polyurethane foam, **b** PU-1 foam with 1 wt.% of curcumin, **c** PU-2 foam with 2 wt.% of curcumin, **d** PU-5 foam with 5 wt.% of curcumin. All samples were observed at the same magnification. *Source* Sienkiewicz et al. (2019)

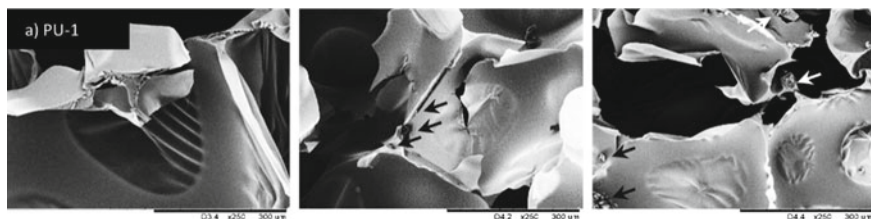


**Fig. 8.15** Morphology of **a** PU-1 foam with 1 wt.% of curcumin, **b** PU-2 foam with 2 wt.% of curcumin, **c** PU-3 foam with 5 wt.% of curcumin. All samples were observed at the same magnification. *Source* Sienkiewicz et al. (2019)

sizes in PU foam. This supports our earlier speculation that curcumin can impact cell sizes and cell distribution. As shown in Figs. 8.14 and 8.15, in currently analyzed PU foam samples, curcumin reduced the cell sizes, what can be associated with the increased viscosity of the system after the addition of the curcumin which inhibits the expansion of the cells. Additionally, the application of the natural fillers can modify the nucleation mode from homogenous to heterogeneous and reduce the nucleation energy, which in turn promotes the formation of large numbers of small cells. In comparison to the PU-0, the modified PU foams are characterized by a wider cell size range as well as the higher cell distribution frequency (as presented in Figs. 8.16, 8.17, 8.18 and 8.19).

The rheological properties of the polyol premixes with curcumin are shown as the viscosity versus shear rate in Figs. 8.20 and 8.21. In all examined samples, the viscosity is reduced at high shear rates. The viscosity of the obtained samples initially decreases sharply and then appreciably slower to reach a relatively stable value, since particles in the liquids reach the best practicable arrangement. Such a phenomenon is typical for non-Newtonian fluids with a pseudoplastic nature. In order to facilitate further analysis of the data, the graph of viscosity versus shear rate is converted to log viscosity versus log shear rate form. It can be seen from this graph, that the curvatures of viscosity versus shear rate can be made close linear using this log–log format with regression of 0.968–0.988. All results of power-law index ( $n$ ) and others other data are presented in Table 8.5. For the system PU-5, the power-law index is lower than that of their PU 1 and PU-2 counterparts, leading to highly non-Newtonian behavior.

It was observed that the addition of natural curcumin extract with biocidal properties impacts the compressive strength of the foam. In the case of the free-rising process, the PU foams shows favorable mechanical strength characteristics in a free-rising direction, relative to the cross course. This can result from the material position and deforming mechanisms in various directions. In our experiments, PU foam

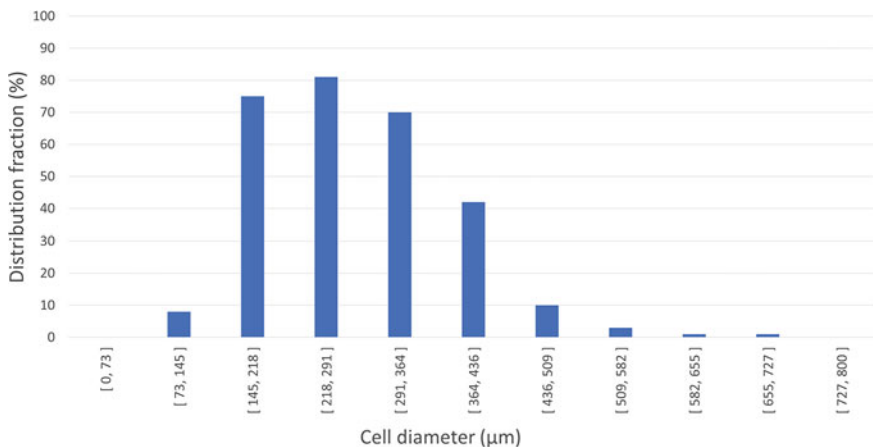


**Fig. 8.16** Cell size distributions of non-modified polyurethane foam. *Source* Sienkiewicz et al. (2019)

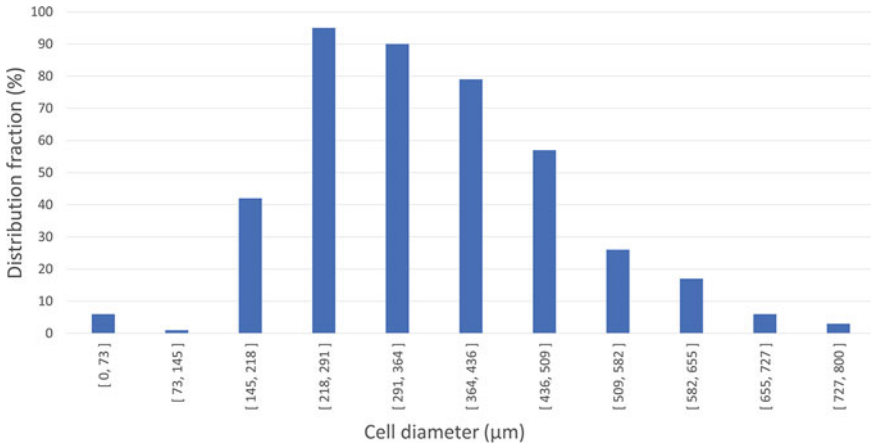


**Fig. 8.17** Cell size distributions of polyurethane foam with 1 wt.% of curcumin. *Source* Sienkiewicz et al. (2019)

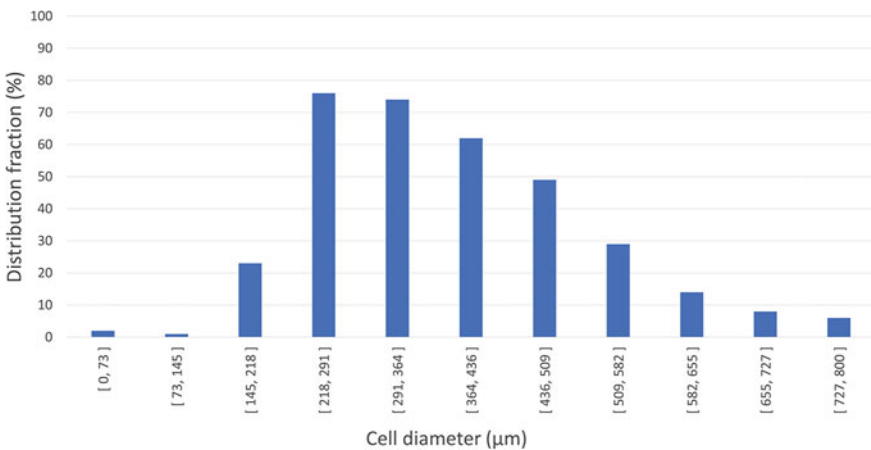


**Fig. 8.18** Cell size distributions of polyurethane foam with 2 wt.% of curcumin. *Source* Sienkiewicz et al. (2019)

samples have shown three stages of deformity in condensation. They are (i) the linear elastic region on the stress–strain curve, (ii) the second the plateau region, and (iii) the third densification area.

Based on the data presented in Figs. 8.16, 8.17, 8.18, 8.19, 8.20 and 8.21, it is worth mentioning that depending on the amount of used curcumin, the discussed above foam’s physical and mechanical strength characteristics can notably change. For example, foam modified with 1 wt.%, and 2 wt.% of the curcumin had considerable compressive strength (growth about of 10% and 7%, accordingly), better flexural strength (increase of 17% and 7%, accordingly). In the water uptake test,

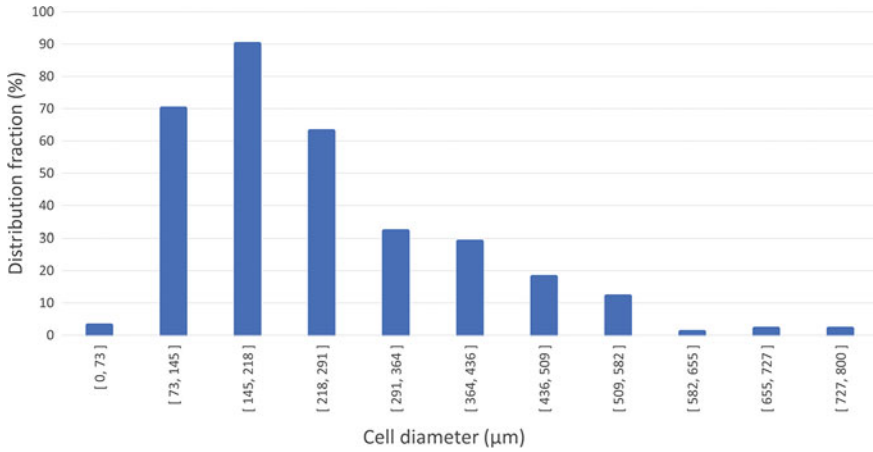
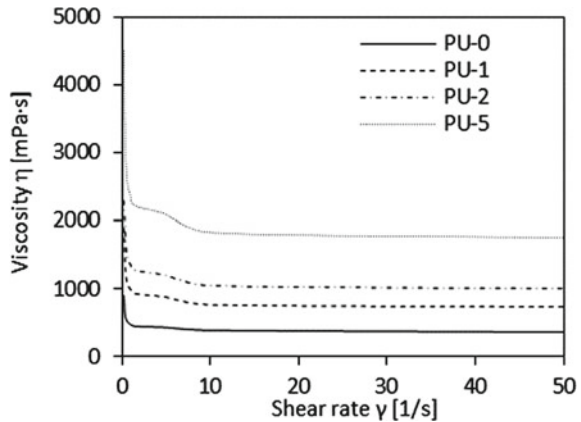


**Fig. 8.19** Cell size distributions of polyurethane foam with 5 wt.% of curcumin. *Source* Sienkiewicz et al. (2019)

**Fig. 8.20** Viscosity as a function of shear rate. PU-0 non-modified polyurethane foam; PU-1 foam with 1 wt.% of curcumin; PU-2 foam with 2 wt.% of curcumin; PU-5 foam with 5 wt.% of curcumin. *Source* Sienkiewicz et al. (2019)



the results show 10% and 12% reductions, compared to the non-modified reference foam samples.

Additionally, the results of antibacterial test confirmed that curcumin can be applied as a natural anti-ageing substance for PU foams and consequently other polymers. Disc diffusion test for antibacterial receptivity was performed according to the National Committee for Clinical Laboratory Standards (2003) to estimate the presence of antiseptic features of the PU foams with natural extracts. Selected bacteria such as *Escherichia coli* (Gram-negative) and *Staphylococcus aureus* (Gram-positive) were used to the disc diffusion tests. Antibacterial results shown that the addition of 5 wt.% of the curcumin is adequate for preparing PU foams with enhanced antimicrobial properties, as presented in Tables 8.6 and 8.7.

**Fig. 8.21** Log–log plot of the viscosity versus the shear rate for the polyol premixes with curcumin. PU-0 non-modified polyurethane foam; PU-1 foam with 1 wt.% of curcumin; PU-2 foam with 2 wt.% of curcumin; PU-5 foam with 5 wt.% of curcumin. *Source* Sienkiewicz et al. (2019)

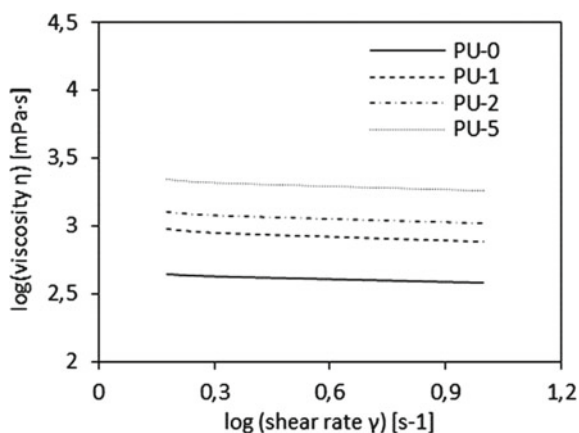


**Table 8.5** Dynamic viscosity and logarithmic plot of the fitting equations for polyol premixes

Sample	Dynamic viscosity $\eta$ 0.5 RMP (mPa·s)	Dynamic viscosity $\eta$ 5 RMP (mPa·s)	Dynamic viscosity $\eta$ 10 RMP (mPa·s)	Fitting equation	Power law index ( $n$ )	$R^2$
Reference polyurethane foam (non-modified)	628	424	380	$y = -0.060 + 0.305$	0.345	0.968
Foam with 1 wt.% of curcumin	1,418	885	772	$y = -0.061 + 0.308$	0.321	0.988
Foam with 2 wt.% of curcumin	1,934	1,207	1,053	$y = -0.059 + 0.310$	0.318	0.979
Foam with 5 wt.% of curcumin	3,342	2,086	1,819	$y = -0.058 + 0.308$	0.306	0.968

*Source* Sienkiewicz et al. (2019)

**Table 8.6** Antibacterial activity of PU foams against *E. coli*.

Time (h)	<i>E. coli</i> (CFU/ml)				
	Bacterial suspension	PU-0	PU-1	PU-2	PU-5
0	$74 \times 10^6$	$74 \times 10^6$	$74 \times 10^6$	$74 \times 10^6$	$74 \times 10^6$
6		$74 \times 10^6$	$58 \times 10^5$	$12 \times 10^5$	$82 \times 10^5$
12		$74 \times 10^6$	$34 \times 10^4$	$76 \times 10^4$	$15 \times 10^3$
24		$<74 \times 10^6$	$16 \times 10^4$	$31 \times 10^4$	$1.4 \times 10^3$

PU-0 non-modified polyurethane foam, PU-1 foam with 1 wt.% of curcumin, PU-2 foam with 2 wt.% of curcumin, PU-5 foam with 5 wt.% of curcumin

*Source* Sienkiewicz et al. (2019)

**Table 8.7** Antibacterial activity of PU foams against *S. aureus*

Time (h)	<i>S. aureus</i> (CFU/ml)				
	Bacterial suspension	PU-0	PU-1	PU-2	PU-5
0	$74 \times 10^6$	$74 \times 10^6$	$74 \times 10^6$	$74 \times 10^6$	$74 \times 10^6$
6		$74 \times 10^6$	$18 \times 10^5$	$18 \times 10^5$	$87 \times 10^4$
12		$74 \times 10^6$	$42 \times 10^4$	$63 \times 10^4$	$19 \times 10^3$
24		$74 \times 10^6$	$23 \times 10^4$	$12 \times 10^4$	$10.8 \times 10^3$

PU-0 non-modified polyurethane foam, PU-1 foam with 1 wt.% of curcumin, PU-2 foam with 2 wt.% of curcumin, PU-5 foam with 5 wt.% of curcumin

Source Sienkiewicz et al. (2019)

Furthermore, Członka et al. prepared polyurethane composite foams modified with different amount of ground clove filler (1–5 wt.%). The obtained results confirmed that the application of clove as natural fillers affect the rheological behavior, cellular structure, and mechanical and thermal properties of foams. The research results indicated that the addition of 1 and 2 wt.% of clove filler yields the foams with improved (i) compression strength, (ii) flexural strength and (iii) impact strength. Additionally, it was demonstrated that clove may be used as a natural anti-aging filler for polyurethane and other materials. The inclusion of clove as natural filler efficiently improved the stabilization of polyurethane composite foams. What is most important, it was shown that the application of clove filler considerably improved the antibacterial properties of PU foams compared to unmodified foam and proposed natural agent influencing the properties of the foam is suitable for the manufacturing of antimicrobial PU foams—see: Członka et al. (2020), Chaieb et al. (2007).

An increase in fragility occurs and as a result the enhancement establishes a more sudden change from the elastic region to the plateau, compared to the smooth transition observed in the non-modified PU foams. The elongation at break of the curcumin modified polyurethane foam grows with increasing natural extract volume, suggesting that filler application giving the foam structure more elasticity (Table 8.8).

## 8.4 Conclusion

Polyurethanes are one of the most universal polymeric materials. The chemical nature of polyurethanes allows different shapes and use in generally available products where there is required comfort, strength, heat and sound insulation.

The studies discussed show that chemical incorporation of modifying substances with proven antibacterial and antipsychotic properties into conventional polyurethane foam formulations can lead to the preparation of antimicrobial materials. The presented results confirmed that the addition of antibacterial filler influences the



**Table 8.8** Mechanical properties of modified PU foams

Sample code	Specific compressive strength (parallel) (kPa kg <sup>-1</sup> m <sup>-3</sup> )	Specific compressive strength (perpendicular) (kPa kg <sup>-1</sup> m <sup>-3</sup> )	Flexural strength $\varepsilon_f$ (MPa)	Elongation (%)
PU-0	6.6	3.8	0.402	11.2
PU-1	7.3	4.4	0.469	10.2
PU-2	7.0	3.9	0.432	10.8
PU-5	5.0	3.1	0.407	11.5

PU-0 non-modified polyurethane foam, PU-1 foam with 1 wt.% of curcumin, PU-2 foam with 2 wt.% of curcumin, PU-5 foam with 5 wt.% of curcumin

Source Sienkiewicz et al. (2019)

rheological behavior, cellular structure, and further mechanical properties of modified samples. The antimicrobial features of the foams were evaluated toward *E. coli* and *S. aureus* and others. The methods of foam modification presented in the paper allows fabrication of samples with the most effective antibacterial and antifungal properties. They can be good materials for applications which require medical purity and what's more they can be used as healthy household insulation on the surface of which fungi or bacteria dangerous to humans will not survive.

Moreover, significant amounts and methods for the formation of antibacterial and antifungal foams in different forms simplifies the future expansion of new safe and effective polyurethane materials in new applications.

The presented studies are part of the current research conducted by a number of researchers looking for materials with antibacterial, antiviral and antifungal properties. Fungus and mold can contaminate our walls, ceilings and other surfaces in commercial spaces, causing unsightly conditions and even breathing problems for the building's occupants. What more, mold and fungus grow in places where there is high humidity, water damage or dampness, making built-in antifungal and antibacterial agents key for preventing growth. Even everyday use products that are exposed to fungus and mold are affected by the appearance of ugly black and brown blots or greenish marks which can destroy the condition of materials if they are not protected with an antiseptic additive. Continuous exposure of fungus and mold can cause products to quickly weaken which will impact permanence, stability, and product shelf life. The presented works confirmed that chemical incorporation of modifiers with given antibacterial properties into conventional polyurethane foam formulations can lead to the preparation of antimicrobial materials with efficient alternatives to expensive technologies.

## References

- Amina, M., Amna, T., Hassan, M. S., Ibrahim, T. A., & Khil, M. S. (2013). Facile single mode electrospinning way for fabrication of natural product based silver decorated polyurethane nanofibrous membranes: Prospective medicated bandages. *Colloids and Surfaces a: Physicochemical and Engineering Aspects*, 425, 115–121.
- Amna, T., Hassan, M. S., Sheikh, F. A., Lee, H. K., Seo, K. S., Yoon, D., & Hwang, I. H. (2013). Zinc oxide-doped poly(urethane) spider web nanofibrous scaffold via one-step electrospinning: A novel matrix for tissue engineering. *Applied Microbiology and Biotechnology*, 97, 1725–1734.
- Annila, P. J., Hellemaa, M., Pakkala, T. A., Lahdensivu, J., Suonketo, J., & Pentti, M. (2017). Extent of moisture and mould damage in structures of public buildings. *Case Studies in Construction Materials*, 6, 103–108.
- Arnold, R. G., Nelson, J. A., Verbanc, J. J. (1957). Recent advances in isocyanate chemistry. *Chemical Reviews* 57, 47–76.
- Busscher, H. J., Norde, W., Sharma, P. K., & van der Mei, H. C. (2010). Interfacial re-arrangement in initial microbial adhesion to surfaces. *Current Opinion in Colloid & Interface Science*, 15(6), 510–517.
- Chaieb, K., Hajlaoui, H., Zmantar, T., Kahla-Nakbi, A. B., Rouabhia, M., Mahdouani, K., & Bakhrouf, A. (2007). The chemical composition and biological activity of clove essential oil, *Eugenia caryophyllata* (*Syzygium aromaticum* L. *myrtaceae*): A short review. *Phytotherapy Research*, 21, 501–506.
- Chen, Y., Lu, Y., Lee, R. J., & Xiang, G. (2020). Nano encapsulated curcumin: And its potential for biomedical applications. *International Journal of Nanomedicine*, 15, 3099–3120.
- Cosgrove, L., McGeechan, P. L., Robson, G. D., & Handley, P. S. (2007). Fungal communities associated with degradation of polyester polyurethane in soil. *Applied and Environment Microbiology*, 73(18), 5817–5824.
- Curtis, L., Lieberman, A., Stark, M., Rea, W., Vetter, M. (2004). Adverse health effects of indoor molds. *Journal of Nutritional & Environmental Medicine*, 14, 361–374
- Członka, S., Strąkowska, A., Strzelec, K., Kairyte, A., & Kremensas, A. (2020). Bio-based polyurethane composite foams with improved mechanical, thermal, and antibacterial properties. *Materials*, 13(5), 1108.
- Desmet, T., Morent, R., De Geyter, N., Leys, C., Schacht, E., & Dubruel, P. (2009). Nonthermal plasma technology as a versatile strategy for polymeric biomaterials surface modification: A review. *Biomacromolecules*, 10(9), 2351–2378.
- Ding, Y., Sun, Z., Shi, R., Cui, H., Liu, Y., Mao, H., Wang, B., Zhu, D., & Yan, F. (2019). Integrated endotoxin adsorption and antibacterial properties of cationic PU foams for wound healing. *ACS Applied Materials and Interfaces*, 11, 2860–2869.
- Dumitriu, R. P., Sacarescu, L., Macocinschi, D., Filip, D., & Vasile, C. (2016). Effect of silver nanoparticles on the dispersion, rheological properties and morphological aspect of solvent cast polyurethane/biopolymers bionanocomposite membranes. *Journal of Adhesion Science and Technology*, 30, 1716–1726.
- Guo, C., Zhou, L., Lv, J. (2013). Effects of expandable graphite and modified ammonium polyphosphate on the flame-retardant and mechanical properties of wood flour-polypropylene composites. *Polymers and Polymer Composites*, 21, 449–456.
- Ismail, N. I., Othman, I., Abas, F., Lajis N. H., Naidu R. (2019). Mechanism of apoptosis induced by curcumin in colorectal cancer. *International Journal of Molecular Sciences* 20(10), 2454.
- Jennings, M. R., & Parks, R. J. (2020). Curcumin as an antiviral agent. *Viruses*, 12(11), 1242.
- Jeon, H. J., Kim, J. S., Kim, T. G., Kim, J. H., Yu, W. R., & Youk, J. H. (2008). Preparation of poly( $\epsilon$ -caprolactone)-based polyurethane nanofibers containing silver nanoparticles. *Applied Surface Science*, 254, 5886–5890.
- Jou, C., Yuan, L., Lin, S., Hwang, M., Chou, W., Yu, D., et al. (2007). Biocompatibility and antibacterial activity of chitosan and hyaluronic acid immobilized polyester fibers. *Journal of Applied Polymer Science*, 104, 220–225.

- Kara, F., Aksoy, E. A., Yuksekdog, Z., Aksoy, S., & Hasirci, N. (2015). Enhancement of antibacterial properties of polyurethanes by chitosan and heparin immobilization. *Applied Surface Science*, 357, 1692–1702.
- Kenawy, E. R., & Mahmoud, Y. A. (2003). Biologically active polymers. *Macromolecular Bioscience*, 3, 107–116.
- Kenawy, E. R., Abdel-Hay, F. I., El-Shanshoury, A. E., & El-Newehy, M. H. (2002). Biologically active polymers. V. Synthesis and antimicrobial activity of modified poly(glycidyl methacrylate-CO-2-hydroxyethyl methacrylate) derivatives with quaternary ammonium and phosphonium salts. *Journal of Polymer Science Part A*, 40, 2384–2393.
- Kunnumakkara, A. B., Bordoloi, D., Padmavathi, G., et al. (2017). Curcumin, the golden nutraceutical: Multitargeting for multiple chronic diseases. *British Journal of Pharmacology*, 174(11), 1325–1348.
- Lando, G. A., Marconatto, L., Kessler, F., et al. (2017). UV-surface treatment of fungal resistant polyether polyurethane film-induced growth of Entomopathogenic fungi. *International Journal of Molecular Sciences*, 18(7), 1536.
- Luo, Z., Hong, R. Y., Xie, H. D., & Feng, W. G. (2012). One-step synthesis of functional silica nanoparticles for reinforcement of polyurethane coatings. *Powder Technology*, 218, 23–30.
- Magnin, A., Hoornaert, L., Pollet, E., Laurichesse, S., Phalip, V., et al. (2019). Isolation and characterization of different promising fungi for biological waste management of polyurethanes. *Microbial Biotechnology*, 2(3), 544–555.
- Mahmood, K., Zia, K. M., Zuber, M., Salman, M., & Anjum, M. N. (2015). Recent developments in curcumin and curcumin based polymeric materials for biomedical applications: A review. *International Journal of Biological Macromolecules*, 81, 877–890.
- Moghadamtousi S. Z., Kadir H. A., Hassandarvish P., Tajik H., Abubakar S., Zandi K. (2014). A review on antibacterial, antiviral, and antifungal activity of curcumin. *BioMed Research International*, 186864.
- Morena, A. G., Stefanov, I., Ivanova, K., & Pérez-Rafael S, Sánchez-Soto M, Tzanov T. (2020). Antibacterial PU foams with incorporated lignin-capped silver nanoparticles for chronic wound treatment. *Industrial and Engineering Chemistry Research*, 59, 4504–4514.
- Mráz, J., Šimek, P., Chvalová, D., Nohová, H., & Šmigolová, P. (2004). Studies on the methyl isocyanate adducts with globin. *Chemico-Biological Interactions*, 148, 1–10.
- National Committee for Clinical Laboratory Standards. (2003). *Approved standard: M2-A8, performance standards for antimicrobial disk susceptibility tests* (8th ed.). National Committee for Clinical Laboratory Standards.
- Nirmala, R., Kalpana, D., Navamathavan, R., Park, M., Kim, H. Y., & Park, S.-J. (2014). Antimicrobial activity of electrospun polyurethane nanofibers containing composite materials. *Korean Journal of Chemical Engineering*, 31, 855–860.
- O'Connor, N. A., Einbond, L. S., Redenti, S., Sauane, M., & Jitianu, A. (2018). Self-degradable curcumin polymer with anti-cancer activity. *Journal of Applied Polymer Science*, 135, 46867.
- Pant H. R., Kim, H. J., Joshi, M. K., Pant, B., Park, C. H., Kim, J. I., Hui, K. S., Kim, C. S. (2014). One-step fabrication of multifunctional composite polyurethane spider-web-like nanofibrous membrane for water purification. *Journal of Hazardous Materials*, 264, 25–33. Retrieved January 15, 2014.
- Pivec, T., Smole, M., Gašparič, P., & Stana-Kleinsche, K. (2017). Polyurethanes for medical use. *Tekstilec*, 10(14502), 60.
- Prabhakar, P. K., Raj, S., Anuradha, P. R., Sawant, S. N., & Doble, M. (2011). Biocompatibility studies on polyaniline and polyaniline-silver nanoparticle coated polyurethane composite. *Colloids and Surfaces. b, Biointerfaces*, 86, 146–153.
- Praditya, D., Kirchhoff, L., Brüning, J., Rachmawati, H., Steinmann, J., Steinmann, E. (2019). Anti-infective properties of the golden spice curcumin. *Frontiers in Microbiology*, 10, 912.
- Schwetlick, K., Noack, R., & Stebner, F. (1994). Three fundamental mechanisms of base-catalysed reactions of isocyanates with hydrogen-acidic compounds. *Journal of the Chemical Society. Perkin Transactions*, 2, 599–608.

- Shamshi Hassan, M., Amna, T., Sheikh, F. A., Al-Deyab, S. S., Eun Choi, K., Hwang, I. H., Khil, M. S. (2013) Bimetallic Zn/Ag doped polyurethane spider net composite nanofibers: A novel multipurpose electrospun mat. *Ceramics International* 39, 2503–2510.
- Sharifi-Rad, J., Rayess, Y. E., Rizk, A. A., et al. (2020). Turmeric and its major compound curcumin on health: Bioactive effects and safety profiles for food, pharmaceutical biotechnological and medicinal applications. *Frontiers in Pharmacology*, 11, 01021.
- Shimizu, K., Funamoto, M., Sunagawa, Y., et al. (2019). Anti-inflammatory action of curcumin and its use in the treatment of lifestyle-related diseases. *European Cardiology Review*, 14(2), 117–122.
- Sienkiewicz, N., Członka, S., Kairyte, A., Vaitkus, S. (2019). Curcumin as a natural compound in the synthesis of rigid PU foams with enhanced mechanical, antibacterial and anti-ageing properties. *Polymer Testing*, 79, 106046.
- Souza, E. (2020). *The threat of black mold to architecture and its inhabitants*. ArchDaily.
- Sportelli M. C., Picca, R. A., Ronco, R., Bonerba, E., Tantillo, G., Pollini, M., Sannino, A., Valentini, A., Cataldi, T. R. I., Cioffi, N. (2016) Investigation of industrial PU foams modified with antimicrobial copper nanoparticles. *Materials (Basel)* 7, 9(7), 544.
- Subagia, I. D. G. A., Jiang, Z., Tijjing, L. D., Kim, Y., Kim, C. S., Lim, J. K., & Lim, J. K. (2014). Hybrid multi-scale basalt fiber-epoxy composite laminate reinforced with Electrospun polyurethane nanofibers containing carbon nanotubes. *Fibers and Polymers*, 15, 1295–1302.
- Sun, Z.-J., Sun, B., Tao, R.-B., Xie, X., Lu, X.-L., & Dong, D.-L. (2013). A poly(glycerol-sebacate-curcumin) polymer with potential use for brain gliomas. *Journal of Biomedical Materials Research, Part A*, 101A, 253–260.
- Tijjing, L. D., Ruelo, M. T. G., Amarjargal, A., Pant, H. R., Park, C. H., Kim, D. W., & Kim, C. S. (2016). Antibacterial and superhydrophilic electrospun polyurethane nanocomposite fibers containing tourmaline nanoparticles. *Chemical Engineering Journal*, 197, 41–48.
- Tijjing, L. D., Amarjargal, A., Jiang, Z., Ruelo, M. T. G., Park, C. H., Pant, H. R., Kim, D. W., Lee, D. H., Kim, C. S. (2013). Antibacterial tourmaline nanoparticles/polyurethane hybrid mat decorated with silver nanoparticles prepared by electrospinning and UV photoreduction. *Current Applied Physics* 13, 205–210.
- Toker, R. D., Kayaman-Apohan, N., & Kahraman, M. V. (2013). UV-curable nano-silver containing polyurethane based organic–inorganic hybrid coatings. *Progress in Organic Coatings*, 76, 1243–1250.
- Udabe, E., Udabe, M., Sardon, H., Irusta, L., Salsamendi, M., Sun, Z., Zheng, Z., Yan, F., Mecerreyes, D. (2017). Antimicrobial PU foams having cationic ammonium groups. *Journal of Applied Polymer Science*, 134, 45473.
- Weinhold, B. (2007). A Spreading concern: Inhalational health effects of mold. *Environmental Health Perspectives*, 115(6), A300–A305.
- Xia, Y., Zhang, Z., Kessler, M. R., Brehm-Stecher, B., & Larock, R. C. (2012). Antibacterial soybean oil-based cationic polyurethane coatings prepared from different amino polyols. *Chem Sus Chem*, 5, 2221–2227.
- Yang, Z., Qiu, S., Wang, Y., Lv, H., Xing, X., & Luo, J. (2012). Synthesis and characterization of re-dispersible silver nanoparticles/polyurethane hybrid materials. *Polymeric Materials Science and Engineering*, 28, 118–121.
- Yangyang, Y., Qian, S., Yihong, L., Sun, P. Y., Xingmei, O., Dongxu, L., Meiling, J., & Weizhen, Z. (2018). Anti-inflammatory effects of curcumin in microglial cells. *Frontiers in Pharmacology*, 9, 386.
- Zainal Abidin, E. (2017). Review article dampness and mold exposure in buildings as a risk factor for health effects. *Malaysian Journal of Public Health Medicine*, 1, 28–40.
- Ziyun, L., Mingfei, S., Ning, L., & Ruodan, X. (2020). Application of functional biocompatible nanomaterials to improve curcumin bioavailability. *Frontiers in Chemistry*, 8, 929.

# Chapter 9

## Increased Thermal Stability and Reduced Flammability of Polyurethane Foams with an Application of Polyetherols



Jacek Lubczak and Renata Lubczak

**Abstract** In this chapter, the methods of synthesis of polyetherols with incorporated azacyclic rings are described. The polyetherols obtained by hydroxyalkylation of isocyanuric, uric, and barbituric acids, adenine, and melamine with oxiranes, formaldehyde, and alkylene carbonates are characterized. These hydroxyalkylated azacycles are shown as substrates to obtain rigid polyurethane foams of enhanced thermal resistance. Also, the current state of molecular modification of foam compositions in order to decrease the flammability of foams is described. The decrease of flammability can be achieved by azacycle-derived polyetherol modification with boron and silicon, as well as by addition of flame retardants. Additionally, it has been shown that natural polymers; starch and cellulose can be successfully hydroxyalkylated with glycidol and alkylene carbonates. The polyetherols obtained from cellulose and starch can be applied to obtain highly thermally resistant, biodegradable polyurethane foams, which are the milestones in green chemistry of polymers.

### 9.1 Introduction

Polyurethanes are widely used polymers in many branches of industry, like heat isolation materials in building, furniture production, car industry, machine production, electronic assemblies, and many others—see: Randall and Lee (2002), Oertel (1994), Wirpsza (1991). They are fabricated as rubbers, glues, lacquers, or fibers, and the most but not least as polyurethane foam (PUFs). 80% of polyurethanes are used as PUFs—Randall and Lee (2002). The substrates to obtain polyurethanes are polyols and diisocyanates. The physical and chemical properties of polyurethanes can be classified by kind of substrate, the molar ratio of substrates in the starting composition and fabrication conditions—see: Wirpsza (1991), Moss and Skinner (1976), Moss (1982).

---

J. Lubczak (✉) · R. Lubczak  
Department of Organic Chemistry, Rzeszów University of Technology, Rzeszów, Poland  
e-mail: [jml@prz.edu.pl](mailto:jml@prz.edu.pl)

Generally, PUFs have low thermal conductivities and therefore are good thermal insulations, with applications that can be increased provided that their thermal stability and flame resistance are increased. Traditional rigid polyurethane foams are flammable and have low thermal resistance, which limits their use. Attempts to improve their properties are currently of interest. The presence in foam of certain heterocyclic rings with nitrogen atoms may significantly improve its thermal stability. The PUFs obtained from them can be applied as thermal insulation for pipes for transmission of heating media or insulations for transporting liquid sulfur. However, the PUFs modified in that way are flammable.

Polyurethanes decompose at temperatures above 200 °C. Their combustion is accompanied by the release of toxic fumes and gases. The combustion products of polyurethanes include carbon dioxide, low molecular weight organic compounds, toxic gases such as carbon monoxide, hydrogen cyanide, hydrogen chloride, nitrogen oxides and other pyrolysis products, as discussed in Janowska et al. (2007). In order to protect the environment, research is being conducted on the flame retardation of plastics. By introduction of flame retardants, for example antipyrenes, the pyrolysis of polymeric materials as well as flame resistance can be considerably improved, and finally self-extinguishing materials can be obtained. This is especially important for foams that are to be used at high temperatures. Until recently, the most popular group of flame retardants were halogen compounds containing fluorine, chlorine and bromine atoms—see: Janowska et al. (2007), Cichy et al. (2003), Thirumal et al. (2008), Hilado (1998). Halogen antipyrenes during ignition emit acrid and toxic smoke, which threatens human life and health, and adversely affects the environment—Thirumal et al. (2008). Therefore, new, environmentally friendly flame retardants are being sought. An effective way to reduce the flammability of PUFs is to incorporate nitrogen, phosphorus, silicon, and boron atoms into their structure. As discussed by Zuchowska (2000), antipyrenes can be divided into two groups, namely: (i) reactive retardants, which are incorporated into the chemical structure of polymers at the stage of polymer synthesis or cross-linking, and (ii) additive flame retardants, which are incorporated into polymer as non-reacting compounds. Introducing phosphorus and nitrogen into polyurethane foams effectively increases PUF's flame resistance. The simultaneous modification of PUFs with nitrogen and phosphorus is desirable due to synergy between those two elements—see: Brzozowski et al. (2001), Gijnsman et al. (2002), Wilkie and Morgan (2009). Thus, the best-known flame retardants are melamine, ammonium phosphates and melamine polyphosphate (MPP)—Cichy et al. (2003). The addition of flame retardants decreases the percentage of flammable parts in composites. Moreover, upon decomposition at 350 °C the MPP degrades endothermally and releases phosphoric acid that deposits on the surface and forms a film, which is the thermal barrier for heat transfer into the polymer—Fuchs and Weiss (2014). Also, boron and its compounds are used as flame retardants. The products of reactions between boric acid and diols, derivatives of urea or oxiranes like glycerine epichlorhydrin were reported as flame retardants, when introduced into composites at the foaming step—see: Czupryński et al. (2002, 2006a, 2006b). Introduction of silicon-containing fillers into foaming compositions improves the thermal stability of polyurethane foams. Yang et al. (2006) demonstrated that colloidal silica

increased considerably the thermal stability of polyurethane foam in comparison with the non-modified foam. When talc, mica, or montmorillonite are used as fillers they need to intercalate with aminoacids, ammonium, or phosphonium salts (Kim et al., 2006), otherwise the fillers separate. Proper homogenization of silica nanoparticles with polyurethane led to materials of improved mechanical and thermal properties as well as the flame resistance, although these materials had diminished ability to form pores—see: Feng et al. (2013), Nikje and Tehrani (2010), that the addition of small amounts of reactive silicone compounds can improve thermal stability and flame resistance of PUFs. Polyurethane modifiers improve thermal resistance. The silsesquioxanes with many peripheral hydroxyl groups are able to facilitate the react with isocyanate groups of urethane prepolymers to give polyurethanes of improved thermal resistance—see: Levchik and Weil (2004), Zhang and Horrocks (2003), Mercado et al. (2006), Terraza et al (2008). They can also be modified by hydroxalkylation, epoxidation, amination etc. to give modified silsesquioxanes able to react with isocyanate groups. Hybrid foams formed from polyurethane and polysiloxanes were demonstrated as better thermal insulators than traditional PUFs, as discussed in Verdolotti et al. (2015).

## 9.2 Short Overview of Testing Methods for Rigid Polyurethane Foams

The following properties of rigid foams are usually studied: apparent density, water uptake, dimension stability and thermal conductivity. With regard to the foams that operated at a high temperature, their thermal stability as the weight loss at high temperature and compression strength are tested.

Per ISO 845 (2006), apparent density of PUFs is depth 3 cm calculated as the ratio of PUF mass to the measured volume of PUF specimen, a cube of 50 mm edge length. In order to estimate water volume uptake (N), a PUF cubic specimen of 30 mm edge length is weighed ( $m_1$ ) and placed in water and after 5 min, 3 and 24 h, the specimen is surface dried and weighs again ( $m_2$ )—ISO 2896 (2001):

$$N = \frac{m_2 - m_1}{V \cdot d} \cdot 100\% \quad (9.1)$$

where:  $d$ —water density ( $\text{g}/\text{cm}^3$ );  $V$ —the volume of sample ( $\text{cm}^3$ ).

Dimensional stability is tested on a  $100 \times 100 \times 25$  mm specimen, according to ISI O 2796 (1986). The linear Compressive sizes are measured with caliper before and after thermal exposure at  $150^\circ\text{C}$  for 20 and 40 h. The relative dimension change ( $\Delta L$ ) is calculated according to the formula:

$$\Delta L = 100 \cdot \frac{l_t - l_0}{l_0} \quad (9.2)$$

where:  $l_0$ —initial lengths (mm);  $l_t$ —the length measured after 20 or 40 h exposure.

Thermal conductivity is determined at room temperature using a IZOMET 2104 instrument from Applied Precision. The needle is inserted to a depth of 8 cm into a cylindrical PUF specimen of 8 cm diameter and 9 cm length and the thermal conductance coefficient is readout on the scale of the instrument. Compressive strength is determined from the load causing 10% compression of the PUF height..related to initial height (in accordance with the PUF growing direction) using a universal testing machine. Compressive strength is defined as the quotient of the maximum compressive force and the cross-sectional area of the sample—ISO 844 (2014). The thermal stability of foams is determined both by static and dynamic methods. In the static method, the foams are heated at 150, 175 and 200 °C with periodic measurements of mass loss and determination of mechanical properties before and after heat exposure. In the dynamic method, thermal analyses of foams are performed in a ceramic crucible in the 20–600 °C temperature range with approximately 100 mg of sample under an air atmosphere with a Thermobalance TGA/DSC 1 derivatograph, Mettler, with a 10 °C/min heating rate. The glass transition temperature is determined using a differential calorimeter Mettler Toledo 822e type with Staree system software. The results are registered as heat flow (in W/g) versus temperature.

The resistance of polymeric materials to burning can be determined by conventional qualitative indicators determined by many test methods, differing in terms of measurement, as well as the shape and dimensions of the samples. The most commonly used procedures are a combustion test and the oxygen index test. The flammability is determined in horizontal and vertical positions according to ISO 60695—see: ISO 60695–11-10 (1999). The foam samples (150 × 50 × 13 mm) are weighed, located on a horizontal support (wire net of 200 × 80 mm dimensions) and the line is marked at the distance of 25 mm from the edge. The sample is set on fire from the opposite edge using a Bunsen burner with the blue flame of 38 mm height for 60 s. Then the burner is removed and time for free burning of foam to reach the marked line or ceases burning is measured by a stopwatch. After that the samples are weighed again. The rate of burning is calculated according to the expression:

$$v = \frac{125}{t_b} \quad (9.3)$$

if the sample is burned totally: or

$$v = \frac{L_e}{t_e} \quad (9.4)$$

if the sample ceased burning,

where:



$L_e$ —the length of burned fragment, measured as the difference 150 minus the length of unburned fragment (in mm). According to norms, if the burned fragment has length 125 mm, then the foam is considered as flammable.

$t_e$ —the time of propagation of flame measured at the distance between starting mark up to the end mark or as the time the flame ceases.

The mass loss  $\Delta m$  after burning is calculated from the equation:

$$\Delta m = \frac{m_o - m}{m_o} \cdot 100\% \quad (9.5)$$

where  $m_o$  and  $m$ —mean the sample mass before and after burning, respectively.

The vertical flammability test is performed according to the standard ISO 60695–11–10, (1999). The sample is mounted vertically and exposed to a 25 mm height flame for 10 s. The time of flaming is measured starting from the point when initializing flame was removed until ceasing of the flame. Then the sample is ignited again, and the time until flame ceases is measured.

The flammability of foams is also characterized by oxygen index following ISO 4589–2 (2017). The limiting oxygen index test is performed using Concept Equipment LOI apparatus (Concept Equipment Ltd., Arundel, UK). The LOI value is the concentration of oxygen in a mixture of oxygen and nitrogen that is required to sustain the combustion of a sample. The LOI value is measured by changing the oxygen concentration in steps of 0.1%. According to the general classification, materials with an oxygen index below 21% are flammable, in the range of 21–28%—hardly flammable (self-extinguishing), and above 28% are considered non-flammable.

### Polyetherols and Foams with Azacyclic Rings

The presence of certain heterocyclic rings with nitrogen atoms in an organic polymer can significantly improve thermal stability. For typical PUFs, the upper temperature range for safe use is usually considered to be 90–110 °C—Wirpsza (1991). This limit can be improved in two ways:

- by making diisocyanates to trimerize during foam preparation (Fig. 9.1)—[see: Moss and Skinner (1976), Moss (1982)];
- by using a component, usually polyetherol, containing in its structure a thermostable heterocyclic ring with nitrogen atoms, such as 1,3,5-triazine (Fig. 9.2a)

**Fig. 9.1** Trimerization of isocyanates during the preparation of polyurethane foam

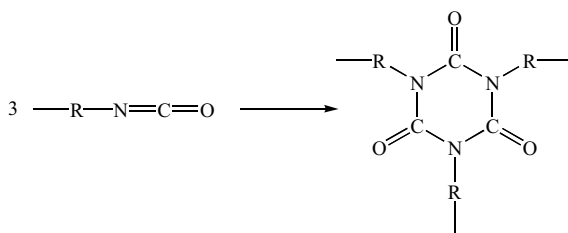
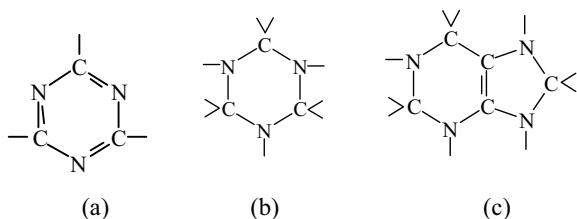


**Fig. 9.2** Thermostable heterocyclic rings with nitrogen atoms



perhydrotriazine (Fig. 9.2b) or purine ring (Fig. 9.2c) see: Lubczak (2011a, 2011b).

As discussed in Lubczak (2011a, 2011b), Goodman (1999) polyurethanes obtained from these polyetherols withstand temperatures up to 180 °C.

The method involving trimerization of diisocyanates often leads to increasing of foam fragility, and the disadvantage of the second method is the multistage process of preparation of suitable components and application of toxic and highly boiling solvents that have to be removed after synthesis. The polyetherols with heterocyclic rings were formerly obtained by hydroxyalkylation of the relevant heterocyclic compounds, e.g., isocyanuric acid (IA, Fig. 9.3a) (Frisch et al., 1980), melamine (M, Fig. 9.3b) (Langrish & Marklow, 1966), uric acid (UA, Fig. 9.3c), adenine (Fig. 9.3d) (Lubczak, 2002; Lubczak & Duliban, 2002) and barbituric acid (BA, Fig. 9.3e) or some of their derivatives with an excess of oxiranes and/or formaldehyde (Lubczak, 2011a, 2011b).

The azacycles of interest are insoluble in most organic solvents except dimethylsulfoxide (DMSO) or to some extent in water (like isocyanuric acid or melamine) others are practically insoluble (uric acid, adenine), therefore their functionalization by reaction in solution is precluded. N-hydroxymethyl derivatives of these azacycles usually are better soluble and readily react with hydroxyalkylating agents like oxiranes.

Hydroxyalkylation is a substitution of labile hydrogen with hydroxyalkyl group; usually the leaving hydrogen is bound to oxygen, nitrogen, or sulfur atom. The most common hydroxyalkylation agents are: formaldehyde (FA), oxiranes: ethylene oxide (EO) and propylene oxide (PO), and alkylene carbonates: ethylene (EC) or propylene carbonate (PC).

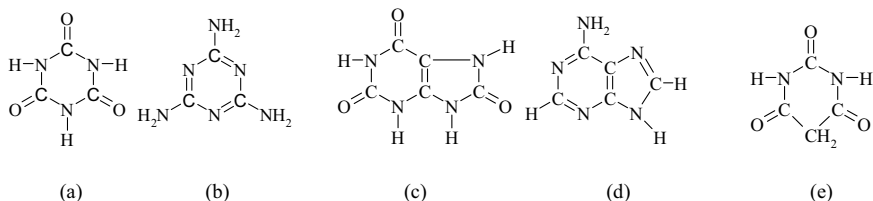
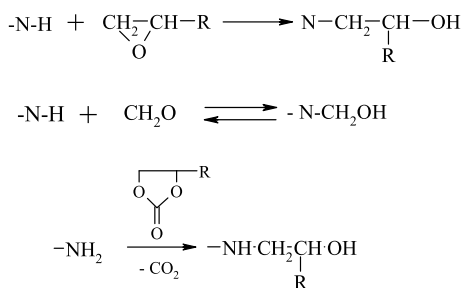


**Fig. 9.3** Azacyclic compounds used in the preparation of polyetherols suitable for the production of thermostable polyurethane foams



where R = -H, -CH<sub>3</sub>

**Fig. 9.4** Hydroxyalkylation of NH groups

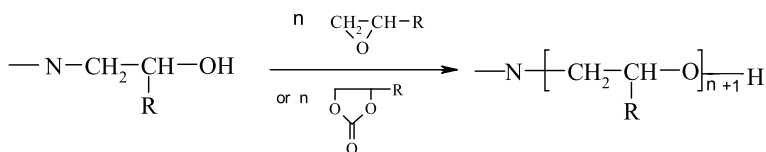


**Fig. 9.5** Reactions of polyetherols obtaining

Hydroxyalkylation of azacycles proceeds usually on the nitrogen atom of amine or imide group (Fig. 9.4):

The reaction requires an excess of hydroxyalkylation agent. The N-hydroxyalkylated derivatives are formed first with subsequent reaction to form oligo- or polyetherols (Fig. 9.5).

The process can proceed in two ways:

- in straightforward reaction of azacycle with oxiranes
- by initial reaction of azacycle with formaldehyde and later with oxiranes.

The methods of synthesis of polyetherols from isocyanuric acid, melamine and oxiranes differed in the type of catalyst used, kind of reaction medium (aliphatic or aromatic hydrocarbons, ketones, alcohols, dimethylformamide, DMSO), and the reaction conditions. The identified catalysts are oxides or hydroxides (often KOH) of metals of groups I or II of the Periodic Table. The latter, however, is not the most effective catalyst because of its limited solubility in organic solvents (including DMSO). Furthermore, dark-brown products are obtained in its presence, and products of high viscosity are formed. All these disadvantages are overcome when alkylammonium hydroxides such as tetrabutylammonium or tetraethylammonium hydroxides that dissolve in organic solvents much better than potassium hydroxide are used—see: Lubczak (2011a).

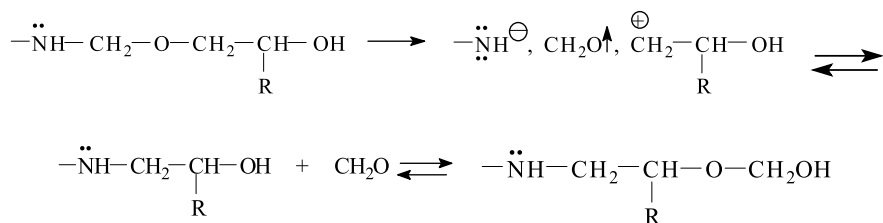


**Fig. 9.6** Elimination of formaldehyde blocked by one hydroxyalkyl group and shifts to the end of the chain

The insolubility of azacycles in organic solvents prompted a search to invent another pathway for polyetherols with azacycles. One of the possibilities took advantage of the better solubility of hydroxymethyl derivatives of azacycles in organic solvents and in water—see: Lubczak (2011a, 2011b).

The chemically blocked formaldehyde at nitrogen on the ring by one hydroxyalkyl group originating from ethylene oxide or propylene oxide is metastable and upon heating or in solution undergoes elimination and usually moves to the end of hydroxyalkyl chain (Fig. 9.6).

Permanent blocking of the formaldehyde molecule occurs when one equivalent of hydroxymethyl groups reacts with at least two equivalents of oxiranes. It is necessary, therefore, to increase the excess of ethylene oxide or propylene oxide to obtain polyetherols from hydroxymethyl derivatives in contrast to the straightforward reaction of azacycles with oxiranes.

The addition of (hydroxymethyl)melamines to ethylene or propylene oxide in DMSO or dimethylformamides accompanied by condensation of the hydroxymethyl groups occasionally leading to cross-linked products. The rationale of the condensation is the catalytic effect of the products of addition of oxirane; the highest for ethylene oxide and the lowest for propylene oxide-based products. It has been shown by Lubczak et al. (2002). That the condensation accompanying addition is caused by the formation of alcoholate anions  $\text{N}-\text{CH}_2-\text{O}-\text{CH}_2\text{CH}_2\text{O}^-$ , which are condensation catalysts (Fig. 9.7):

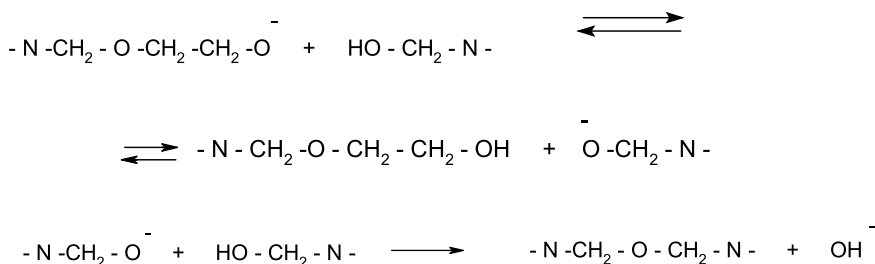


**Fig. 9.7** Formation of alcoholate and hydroxyl anions

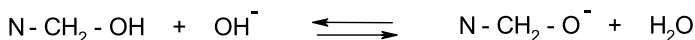


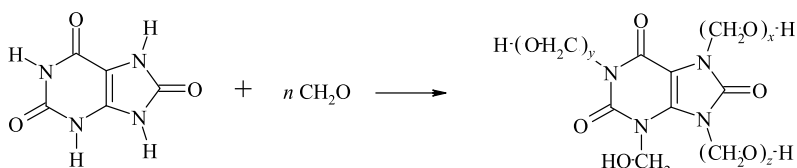
**Fig. 9.8** Catalytic action of hydroxyl anions

In reality, the last stage is more complicated, since hydroxyl anions take over the role of  $\text{N-CH}_2\text{-O-CH}_2\text{CH}_2\text{O-}$  anion and act as the catalyst of condensation (Fig. 9.8):

Suitable for polyetherol synthesis are the melamine derivatives containing four or more hydroxymethyl groups per molecule. Otherwise, cross-linked products and products containing unreacted amino groups are formed. Optimal conditions of the synthesis of 1,3,5-triazine polyetherols is reaction of  $\text{N,N,N',N'',N'''}\text{-pentakis-}$ (hydroxymethyl)melamine (PHMM) with oxiranes at 45–75 °C, respectively for 25–47 h.

The simplest way of preparing polyetherols with purine rings is the reaction of uric acid with oxiranes. Unfortunately, the lack of uric acid solvents precludes the reaction with oxiranes. The solubility problem is overcome by preparing soluble hydroxymethyl derivatives of uric acid (Fig. 9.9).

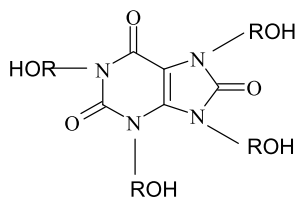
The products of addition at  $\text{UA:CH}_2\text{O}$  1: >6 are highly soluble in cold water, as discussed in Lubczak et al. (2002). When a small amount of water (5 wt.%) is introduced to the product of addition at  $\text{UA:CH}_2\text{O}$  1:7 (HMUA), liquid products are formed that dissolve in oxiranes like, ethylene oxide or propylene oxide upon slight heating (to 65–70 °C). In the presence of triethylamine catalyst oxiranes react with the derivative to give polyetherols containing thermostable purine rings (Fig. 9.10).



with  $x + y + z = n - 1$

**Fig. 9.9** Preparing soluble hydroxymethyl derivatives of uric acid

**Fig. 9.10** Polyetherol with purine ring



where R – oxyalkylene groups.



**Table 9.1** The properties of polyurethane foams obtained from polyols synthesized from THMI and ethylene oxide

Properties		Unit	Foam obtained from polyetherol	
			THMI:EO = 1:6	THMI:EO = 1:9
Density		kg/m <sup>3</sup>	44.3	41.6
Absorb. of water after 24 h		%	4.0	5.7
Linear post-shrinkage		%	0.2	0.3
Heat conductance coefficient		W/m K	0.0244	0.0261
Mass loss after 1 day exposure in temperature:	150 °C	% wt	2.0	2.6
	170 °C	% wt	4.8	6.0
	200 °C	% wt	5.2	14.2
Compressive strength		MPa	0.215	0.353
Compressive strength after 1 day exposure in temperature:	150 °C	MPa	0.227	0.359
	170 °C	MPa	0.303	0.387
	200 °C	MPa	0.223	0.426

Source Kucharski and Lubczak (1985)

treatment of IA-based PUFs resulted in increase of their compression strength due to additional crosslinking upon annealing. Other physical properties like apparent density, water uptake, polymerization shrinkage, and heat conductance of IA-based PUFs were typical for rigid PUFs.

Generally, the reaction of azacyclic compounds with oxiranes was most often carried out in DMSO. After completion the reaction, DMSO had to be removed under reduced pressure; nevertheless, heating of post-reaction mixture led to partial decomposition of DMSO and the product thus purified has a characteristic odor. Moreover, oxiranes themselves are low-boiling, toxic and flammable compounds, and form explosive mixtures with air. All these features render them hazardous chemicals—Kijowska (2005). The use of hydroxymethyl derivatives of azacycles instead of unsubstituted azacycles enables reactions with oxiranes due to the good solubility of derivatives in organic solvents and sometimes in neat oxiranes. The disadvantage of this method is a release of formaldehyde blocked with one oxirane, and migration of formaldehyde to the end of the etherol chain. This is the reason for occasional low thermal resistance of foams obtained from hydroxymethyl derivatives than directly from azacycles. The mass loss of PUF obtained from melamine derivative, PHMM and oxirane is larger than that of PUF obtained in straightforward reaction of melamine with oxirane even at low temperatures (Table 9.2)—Lubczak and Chmiel (1990). Recently alkylene carbonates were introduced as hydroxyalkyl agents. Alkylene carbonates are high-boiling, non-flammable and non-toxic substances called green chemistry solvents. Alkylene carbonates can be successfully used as hydroxyalkylating agents for such sparingly soluble azacyclic substrates like melamine (Lubczak et al., 2015; Kucharski & Kijowska, 2001), isocyanuric (Poplewska et al., 2004), and uric acids (Lubczak, 2006), and even melamine isocyanurate (Kijowska &

**Table 9.2** Comparison of the mass loss of polyurethane foams obtained from polyetherols sized with and without formaldehyde

Foam obtained from polyetherol	Temperature (°C)	Mass los in % after days				
		1	2	3	4	5
PHMM:EO = 1:6	175	26.2	29.3	30.2	30.3	30.4
M:PO = 1:9	200	16.7	20.5	23.0	24.0	24.8

Source Lubczak and Chmiel (1990)

Legocka, 2011), and three melamine ring-condensed compound (melem) (Ożóg & Lubczak, 2012). Thus, another method for synthesis of polyetherols without solvent, from azacycle and hydroxyalkylating agent was finally achieved by the use of alkylene carbonates, which give the same products as oxiranes. Alkylene carbonates can be the solvents and reagents at the same time, they do not have to be removed from post-reaction mixture, because they react to the end with azacycles. The apparent density of PUFs obtained from such polyetherols falls within 49–60 kg/m<sup>3</sup> region (Table 9.3, columns 3–5); very low or no polymerization shrinkage was observed. Water uptake of these PUFs is low, usually within 3.0–7.0 volume %. The PUFs have good thermal stability within 150 and 175 °C; one month of thermal exposure in these temperatures resulted in 6–7% and ca 20% mass loss respectively (Fig. 9.13) with concomitant increase of compression strength. However, one month of thermal exposure at 200 °C led to 31–37% mass loss ad lowered compression strength in such conditions—see: Kijowska and Kucharski (2004), Lubczak (2007). Additionally, some of these PUFs were deformed upon thermal exposure.

Sometimes the reactions of polyetherol synthesis with azacycles and alkylene carbonates requires an elevated temperature (180–190 °C), especially those with melamine or uric acid. This may result in partial decomposition of polyetherols and finally unpredictable worse properties of PUFs.

The search for compounds, which dissolve and react with azacycles to convert them into reactive hydroxyalkyl derivatives brought to glycidol as hydroxyalkylating agent—see: Cyzio and Lubczak (2011). The products of reaction between azacycles and glycidol are semisolid resins due to presence of a considerable number of hydroxyl groups. Every added glycidol equivalent introduces additional one hydroxyl group in the reaction shown in Fig. 9.14.

The further conversion of such derivatives into polyetherols, the hydroxyalkylation with alkylene carbonates can be performed. Alkylene carbonates are suitable solvents for these derivatives. They react with products obtained from azacycles GL at lower temperatures than that needed for reaction of azacycles with alkylene carbonates.

Polyetherols obtained by derivatization of azacycles with glycidol and alkylene carbonates have lower percentage of azacycle than described before. Therefore, the PUFs obtained from these polyetherols have lower thermal resistance and compressive strength than described before (Table 9.3, columns 6–9). Exceptionally, the PUFs obtained from carbazole (C)-derived polyetherols. Carbazole is the mono-functional



**Table 9.3** Properties of polyurethane foams obtained from polyetherols synthesized from various azacycles and alkylene carbonates

Properties	Units	Foam obtained from polyetherol									
		IA:EC = 1:9	M:PC = 1:22	UA:EC = 1:16	IA:GL:EC = 1:6:6	M:GL:PC = 1:8:12	UA:GL:EC = 1:6:10	BA:GL:PC = 1:4:12	C:GL:EC = 1:8:8	C:GL:PC = 1:7:6	
Density	kg/m <sup>3</sup>	49.3	60	56.2	49.5	45.6	53.9	48.1	57.7	38.9	
Absorb. of water after 24 h	%	7.0	1.7	3.0	4.8	9.0	5.4	6.3	5.3	3.4	
Linear post-shrinkage	%	1.6	0.6	0.0	0.0	0.0	0.2	2.9	2.6	0.2	
Heat conductance coefficient	W/m K	-	-	-	0.0484	0.0483	-	-	0.0402	0.0250	
Mass loss after 150 °C	% wt	6.0	7.0	7.0	9.0	13.5	24.4	13.1	5.4	3.9	
30 days exposure	% wt	19.3	23.0	23.0	27.4	23.4	28.3	30.2	13.3	10.1	
in temperature	% wt	31.0	37.0*	37.0*	40.1	35.1*	39.1	39.9	26.2	23.4	
Compressive strength	MPa	0.251	0.430	0.326	0.151	0.146	0.146	0.268	0.750	0.280	
Compressive strength after 30 days exposure in temperature:	MPa	0.266	0.318	0.318	0.178	0.246	0.173	0.818	1.430	0.300	
150 °C	MPa	0.309	0.402	0.402	0.159	0.205	0.256	0.407	0.540	0.220	
175 °C	MPa	0.224	*	*	0.101	0.166	0.125	0.556	0.200	0.090	
200 °C	MPa										

\* The foam deforms after annealing

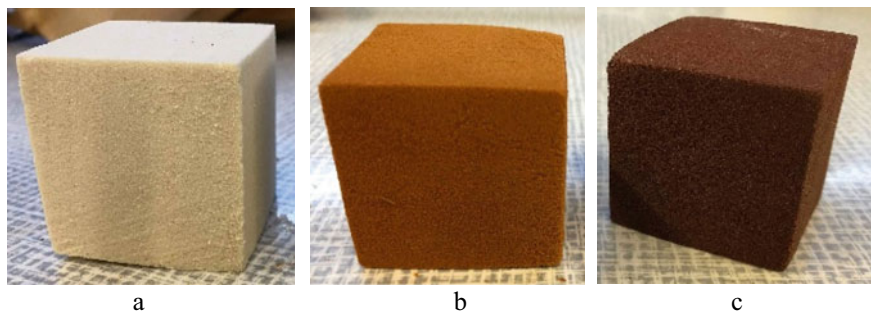


**Fig. 9.13** Polyurethane foam based on polyetherol obtained from melamine and propylene carbonate **a** unheated, and heated for one month at a temperature of **b** 150 °C and **c** 175 °C

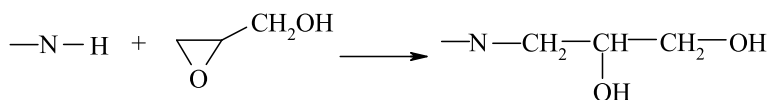


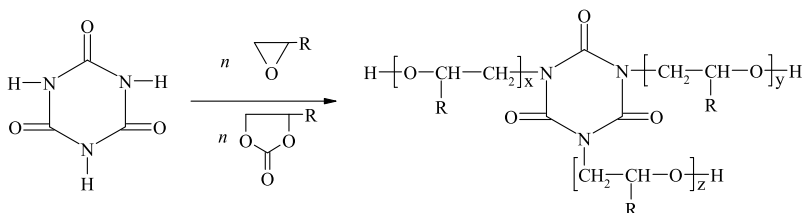
**Fig. 9.14** Reaction of NH group with glycidol

substrate, which cannot be used in a straightforward way to synthesize polyetherols by conversion with alkylene carbonates. However, if the carbazole is preliminarily converted with glycidol to increase the functionality of the substrate, polyetherols can be obtained by reaction with alkylene carbonates, which are suitable to get rigid PUFs, which have considerably increased thermal resistance and good mechanical properties in comparison to all PUFs described before (Table 9.3, columns 10, 11), as discussed in Lubczak (2015).

### 9.3 Reduction of Flammability of PUF with Azacyclic Rings

The polyurethane foams obtained from polyetherols synthesized in the hydroxyalkylation reactions of the aforementioned azacyclic compounds are flammable. The flammability of polymers can be diminished by introduction of phosphorus, boron, or silicone into their structure—see: Hilado (1998), Uhlig (1999). The methods of obtaining polyetherols with azacyclic rings described previously are based on reaction of azacycles e.g. isocyanuric acid with oxiranes or alkylene carbonates (Fig. 9.15).

There are no reports in the literature on the synthesis of polyetherols obtained from azacycles, containing boron. Up to now, the polyetherols for foam formation and hydroxyalkyl esters of boric acid were obtained separately, and further they were introduced into typical polyols as admixtures—see: Czupryński et al. (2002, 2006a, 2006b). It seems that the simplest way to obtain low flammability polyurethane foams with azacycles is addition of boric acid to polyetherol containing azacycle and further



where:  $x + y + z = n$

**Fig. 9.15** Obtaining polyetherol by hydroxyalkylation of isocyanuric acid with oxiranes or alkylene carbonates

reaction of such mixtures with isocyanates and water, as described by Blount (1991) in the patent for traditional polyurethane foams. Unfortunately, the PUFs obtained in that way are undercrosslinked, low foamed and have irregular pores.

Another method of polyetherols synthesis is based on reaction of azacycle with ethylene carbonate, followed by esterification of this product, containing terminal hydroxyl groups with boric acid and final foaming to obtain PUFs, as described in Lubczak et al. (2013). The obtained foams were under-crosslinked and low foamed. It was therefore decided to block side hydroxyl groups with alkylene carbonate. In the first step 2-hydroxyethyl derivatives of isocyanuric acid, melamine or uric acid were obtained. They were esterified with boric acid to obtain hydroborates. The hydroborate derivatives were then hydroxyalkylated with alkylene carbonates to obtain polyetherols. For example, in order to obtain hydroborates with a perhydro-1,3,5-triazine ring, the tris(2-hydroxyethyl)isocyanurate (THEI, Fig. 9.16) was synthesized and esterified with boric acid at a 1:3 molar ratio—Lubczak et al. (2013).

Hydroborates with azacyclic rings are soluble in hot alkylene carbonates, which is an important feature considering the possibility of further obtaining multifunctional

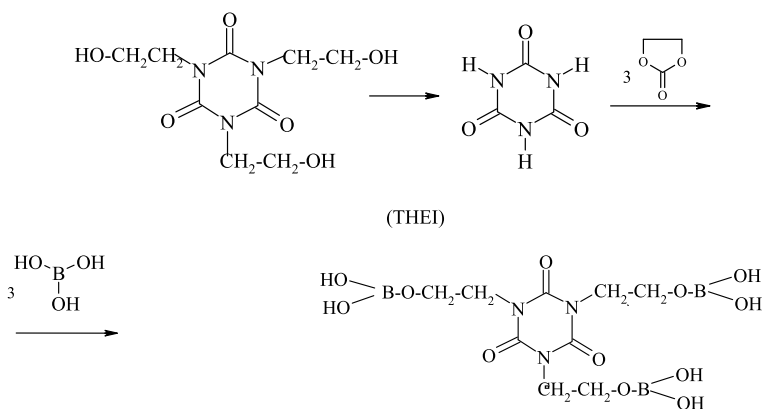


**Fig. 9.16** Obtaining of hydroborate with perhydro-1,3,5-triazine ring

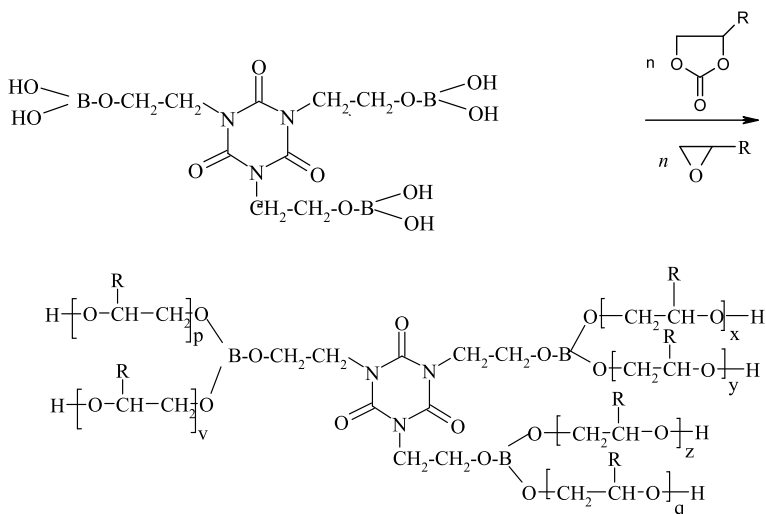


**Fig. 9.17** Preparation of polyetherol with perhydrotriazine ring and boron atoms

polyetherols with boron and azacycle, suitable for formation of polyurethane foams. The products showed increased functionality in comparison with hydroborates and contained azacyclic rings and boron incorporated (Fig. 9.17).

These foams are self-extinguishing or have lowered rate flammability, in relation to boron-free foams. The modification of foams obtained from isocyanuric acid, melamine, or uric acid with boron renders them better flame-resistant materials than non-modified analogues, which are flammable (Table 9.4). On the other hand, these PUFs have decreased thermal resistance and compression strength (cf. Tables 9.3 and 9.5). The PUFs have also increased water uptake presumably due to presence of boron atoms which can coordinate water molecules—see: Łukasiewicz and Lubczak (2012, 2014).

Multistep reaction and the necessity of separation and purification of intermediates is a disadvantage of this method of synthesizing polyetherols. Therefore, a less complex method leading to polyetherols as suitable substrates for thermally resistant and incombustible PUFs is desired. It seems that melamine diborate (MDB) might serve as a good candidate to synthesize such polyetherols due to presence of 1,3,5-triazine ring and boron. Polyetherol was obtained from the reaction MDB with EC = 1:22 (Fig. 9.18)—Chmiel and Lubczak (2017):

The resulting foam has similar properties to traditional rigid PUFs, except considerably higher thermal resistance and mechanical stability. It is also characterized by a higher water absorption than the foam obtained from polyetherol in reactions melamine with propylene carbonate (cf. Tables 9.3 and 9.5). The foam is self-extinguishing. Moreover, after thermal exposure the flammability of annealed PUF is further decreased, the flame ceases after the removal of the ignition source. This makes the resulting PUF a promising insulating material. The solvent-free

**Table 9.4** Flammability of some foams with azacyclic rings modified with flame retardants

No	Foam obtained from polyetherol	Flame zone* (mm)	Flame rate (mm/s)	Mass los (%)	Oxygen index (%)
1	M:PC = 1:22	150	6.2	62.2	19.6
2	THEI:H <sub>3</sub> BO <sub>3</sub> :EC = 1:3:12	30	0.4	9.6	–
3	THEI:H <sub>3</sub> BO <sub>3</sub> :EC:PC = 1:4:6:6	150	1.8	40.7	–
4	HHEM:H <sub>3</sub> BO <sub>3</sub> :EC = 1:3:15	25	1.1	14.6	–
5	HEUA:H <sub>3</sub> BO <sub>3</sub> :PC = 1:3:9	150	1.6	35.0	–
6	HEUA:H <sub>3</sub> BO <sub>3</sub> :PC = 1:4:17	150	0.9	69.7	–
7	MDB:EC = 1:22	49	0.5	15,9	21.2
8	M:H <sub>3</sub> BO <sub>3</sub> :GL:PC = 1:2:9:17	150	3.3	70.2	20.2
9	MSA:GL:EC = 1:4:3 (2% H <sub>2</sub> O)	150	2.0	80	–
10	MSA:GL:EC = 1:4:3 (4% H <sub>2</sub> O)	21	0.7	16.0.8	–
11	No 1 and no 9 (weight ratio = 1:1)	150	3.1	5.8	20.4

HHEM—N,N,N',N',N,"N"-hexakis(2-hydroxyethyl)melamine was obtained in reaction of cyanuric chloride with diethanolamine—Łukasiewicz and Lubczak (2012)

HEUA—hydroxyethyl derivative of uric acid obtained in reaction of uric acid with ethylene carbonate in molar ratio 1:5—Łukasiewicz and Lubczak (2014)

\*According to flammability test the PUF is considered as self-extinguishing if flame frontline does not reach 150 mm distance increased water uptake presumably due to presence of boron atoms which can coordinate water molecules

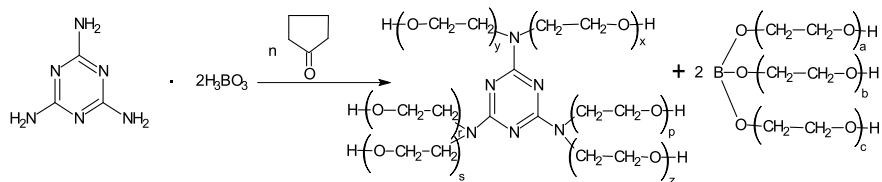
polyetherol synthetic method, the choice of substrate (ethylene carbonate) can be considered as an environmentally friendly process. The foams obtained from such polyetherols modified in reaction with boric acid have diminished flammability in comparison with those obtained from polyetherols made from azacycles and alkylene carbonates.

The flammability of PUFs obtained from azacycles, alkylene carbonate and boron showed flammability rate 0.4–3.3 mm/s, while those obtained from polyetherol synthesized from melamine and propylene carbonate indicated flammability 6.2 mm/s in the horizontal test. The number of steps for obtaining the polyetherol can be limited by hydroxyalkylation of the mixture of melamine and boric acid instead of melamine diborate (MDB). The functionality of polyetherol was deliberately increased by consecutive application of glycidol as hydroxyalkylating agent and, in the second step, the propylene carbonate as terminal hydroxyalkylating agent. A series of polyetherols were obtained with variable amounts of boron, namely using the mixture M:H<sub>3</sub>BO<sub>3</sub> = 1:2, 1:3, and 1:5 molar ratio—see: Chmiel and Lubczak (2019a). PUFs obtained from these polyetherols are flammable, but have decreased flammability in comparison with foams obtained from polyetherol synthesized from melamine and propylene carbonate only (Table 9.4, cf. No 1 and 8).

**Table 9.5** Properties of polyurethane foams modified with reactive flame retardants

Properties	Unit	Foam obtained from polyetherol						
		THEI:H <sub>3</sub> BO <sub>3</sub> :EC = 1:3:12	THEI:H <sub>3</sub> BO <sub>3</sub> : EC: PC = 1:3:6:6	HHEM:H <sub>3</sub> BO <sub>3</sub> : EC = 1:3:15	HEUA:H <sub>3</sub> BO <sub>3</sub> : PC = 1:3:9	HEUA:H <sub>3</sub> BO <sub>3</sub> : PC = 1:4:17	MDB:EC = 1:22	M:H <sub>3</sub> BO <sub>3</sub> :GL: PC = 1:2:9:17
Density	kg/m <sup>3</sup>	77.6	50.3	44.6	55.2	85.6	76.8	53.6
Absorb. of water after 24 h	%	12.7	7.7	15.8	10.2	13.5	14.5	6.2
Linear post-shrinkage	%	0.2	6.3	1.8	0.1	0.0	0.3	0.3
Heat conductance coefficient	W/m K			0.0357	0.0397	0.0387	0.0357	
Mass loss after 30 days exposure in temperature:	% wt	12.9	9.8	10.2	11.7	11	16.3	10.9
	% wt	30.7	27.8	22.0	20.1	19.0	35.2	27.1
	% wt	*	*	30.8	34.8	34.0	*	39.8
Compressive strength	MPa	0.118	0.249	0.248	0.098	0.435	0.268	0.203
Compressive Strength after 30 days exposure in temperature:	MPa	0.131	0.379	0.304	0.138	0.537	0.458	0.289
	MPa	0.300	0.425	0.478	0.248	0.638	0.309	0.140
	MPa	*	*	0.126	0.197	1.195	*	0.154

\*The foam deforms after annealing



(MDB) (XIX)

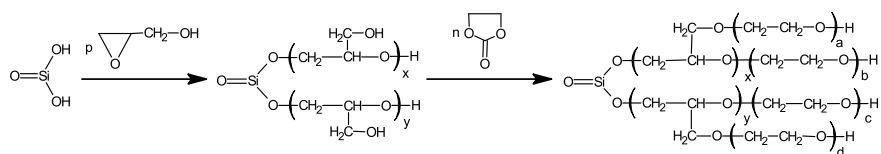
where: a, b, c, p, r, s, x, y, z – number of oxyalkylene units

$$a + b + c + p + r + s + x + y + z = n$$

**Fig. 9.18** Preparation of polyetherol in reactions MDB with ethylene carbonate

Introduction of silicon-containing fillers into foaming compositions improves also the thermal stability of polyurethane foams. Proper homogenization of silica nanoparticles with polyurethane led to materials of improved mechanical and thermal properties as well as the flame resistance, although these materials had diminished ability to form pores—see: Feng et al. (2013), Nikje and Tehrani (2010), Francés and Navarro Bañón (2014). The silica appears as an isolating layer on the surface of the PUF inhibiting heat flow. Moreover, silicone components are ecologically friendly, and combustion of such materials is not accompanied by corrosive smokes—see: Levchik and Weil (2004), Zhang and Horrocks (2003), Mercado et al. (2006). Silicon can be introduced into polyetherol in the following reaction steps. First, the metasilicic acid (MSA) can be obtained from sodium silicate by addition of hydrochloric acid. The method hydroxyalkylation of MSA with glycidol and ethylene carbonate leads to polyetherol (Fig. 9.19) useful to obtain polyurethane foams containing 9.5 mass % of poly(metasilicic acid) which is additive flame retardant.

The resulting foams show a very high compressive strength—Chmiel and Lubczak (2016). They withstand long term heating at 175 °C; additionally, after thermal exposure they gain compressive strength. The PUF obtained from polyetherol with silica atoms composition with 4% water are self-extinguishing. The PUFs after thermal



MSA

where:  $x + y = p$ 

$$a + b + c + d = n$$

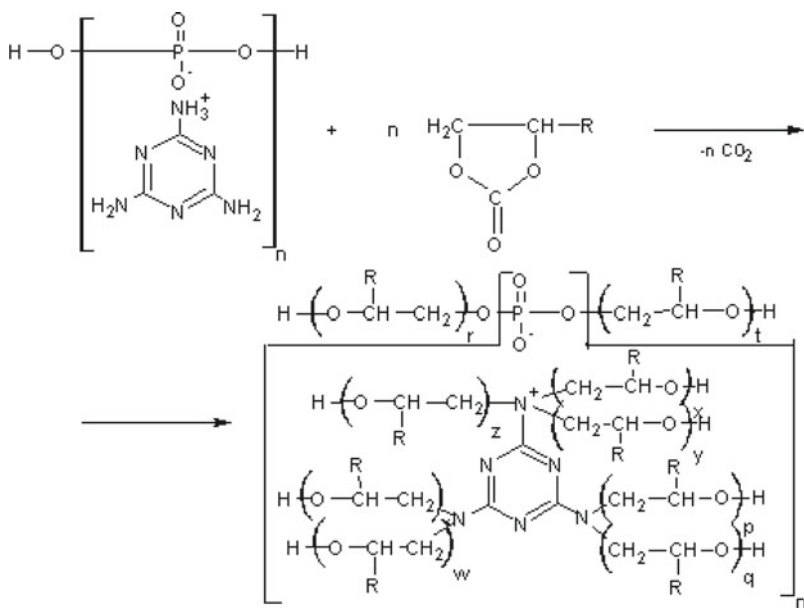
**Fig. 9.19** Preparation of polyetherol in reactions MA with glycidol and ethylene carbonate

exposure flamed only upon flame contact and self-extinguished after flame source removal (Table 9.4, No 10).

The PUFs with 1,3,5-triazine ring and silicon were obtained using mixture of polyetherols synthesized from melamine, propylene carbonate, metasilicic acid, glycidol, and ethylene carbonate. Foams with 1,3,5-triazine ring and boron, and silicon atoms are obtained from mixtures of polyetherols synthesized from ethylene carbonate, melamine diborate and ethylene carbonate and products of reaction between metasilicic acid, glycidol and ethylene carbonate. The properties of PUFs can be tuned into desired product (thermal resistance, compression strength, or flammability) by changing of the foaming composition.

The flame retardants discussed above were the nature of reactive agents. In experiments performed by Lubczak and Lubczak (2016) melamine polyphosphate (MPP) was applied as reactive and additive flame retardant for thermally resistant polyurethane foams. MPP was hydroxyalkylated with ethylene and propylene carbonates to get polyetherols with 1,3,5-triazine ring and phosphorus (Fig. 9.20).

The apparent density of the foams obtained from such a polyetherol is 60–64 kg/m<sup>3</sup>. The maximum water uptake maximum was 11.4%. This indicated that closed pores dominated in material obtained. The obtained PUFs had thermal conductivities between 0.026 and 0.043 W/m·K (Table 9.6). They are less



where:  $f + p + r + t + q + w + x + y + z = n$

$n$  – numbers of moles of alkylene carbonate which reacted with 1 mole of MPP.

**Fig. 9.20** Preparation of polyetherols with 1,3,5-triazine ring and phosphorus



**Table 9.6** Some properties of polyurethane foams with 1,3,5-triazine ring modified with flame retardants

Properties	Unit	Foam obtained from polyetherol									
		MPP:EC = 1:22 Source: MPP	MPP:EC = 1:22 + 16.5% MPP	MPP:EC = 1:22 + 20 %MP	MPP:EC = 1:10:6	MPP:EC = 1:10:6 + 16.5% MPP	MPP:EC = 1:10:6 + 20%MPP	MPP:EC = 1:22 + 11.5% MDB	MDB:EC = 1:22 + 20% M MDB	M:EC = 1:22 + 14% MPP	M:EC = 1:22 + 14% MI
Density	kg/m <sup>3</sup>	59.7	79.0	83.1	63.7	70.5	85.5	82.2	80.3	66.4	80.7
Absorb. of water after 24 h	%	5.6	20.9	17.5	11.4	15.4	18.7	19.8	1.4	1.9	1.2
Linear post-shrinkage	%	2.1	0.7	0.1	0.3	0.6	0.6	0.6	2.2	0.2	0.6
Heat conductance coefficient	W/m K	0.0260	0.0378	0.470	0.043	0.0370	0.0440	0.0393	0.0354	0.0395	0.0380
Mass loss after 30 days exposure in temperature:	% wt	11.4	15.0	13.3	11.3	14.5	13.8	19.1	7.4	6.0	6.3
	% wt	23.8	25.9	21.3	20.6	24.4	20.9	30.6	23.0	14.6	15.3
	% wt	*	33.7	34.7	38.8	*	*	*	34.0	23.0	24.5
Compressive strength	MPa	0.090	0.410	0.215	0.125	0.201	0.259	0.280	0.448	0.400	0.369
Compressive strength after 30 days exposure in temperature:	MPa	0.157	0.347	0.583	0.181	0.181	0.484	0.420	0.545	0.409	0.284
	MPa	0.365	0.025	0.344	0.216	0.092	0.202	0.762	0.151	0.377	0.243
	MPa	*	0.017	*	0.179	0.017	*	*	0.223	0.354	0.257

\* The foam deforms after annealing  
The weight percentage of additive flame retardant is given in columns 4, 5, and 7–12

**Table 9.7** Flammability of some foams with 1,3,5-triazine rings and boron or silicon atoms

No	Foam obtained from polyetherol	Flame zone* (mm)	Flame rate (mm/s)	Mass los (%)	Oxygen index (%)
1	MPP:EC = 1:22,	34	1.4	7.5	21.9
2	MPP:EC = 1:22 + 16.5% MPP	6.0	0.0	2.1	23.8
3	MPP:EC = 1:22 + 20%MPP	5.0	0.0	0.9	24.2
4	MPP:EC:PC = 1:10:6	35	1.3	4.9	21.9
5	MPP:EC:PC = 1:10:6 + 16.5% MPP	5.0	0.0	3.0	24.4
6	MPP:EC: PC = 1:10:6 + 20%MPP	7.0	0.0	1.5	24.6
7	MDB:EC = 1:22 + 11.5% MDB	0.0	0.0	0.0	25.4
8	M:EC = 1:22 + 20% M	5.0	0.0	1.8	24.2
9	M:EC = 1:22 + 14% MPP	10.5	0.7	2.2	23.5
10	M:EC = 1:22 + 14% MI	15.5	0.8	5.0	22.2

The weight percentage of additive flame retardant is given in column 2

\*According to flammability test the PUF is considered as self-extinguishing if flame frontline does not reach 150 mm distance

thermally resistant than those obtained from polyetherols synthesized from melamine and alkylene carbonates and those obtained from carbazole, glycidol, and alkylene carbonates. Horizontal flammability test results indicated that PUFs were self-extinguishing. Their flaming rate was low: 1.3–1.4 mm/s (Table 9.7). Characteristically, self-extinguishing was accompanied by low mass losses upon flaming: 4.9–7.5%. However, their oxygen index was not very promising being 21.9. The MPP was additionally used as an additive flame retardant. The foams with 16.5% MPP do not deform upon heating at 200 °C in contrast with PUFs with reactive MPP. On the other hand, these foams lose their compressive strength upon thermal exposure and also show high water absorption and apparent density. Introduction of MPP as an additive flame retardant to the foaming mixture resulted in diminished flammability in comparison with PUFs modified by reactive MPP. All of the foams studied were non-flammable as determined using the horizontal test (Table 9.7). Flaming reached 5–7 mm and the fire ceased after the ignition flame was removed. Mass loss during flaming test was at the level of 1.5–3.0 wt%. According to the general classification, materials with oxygen index above 28 are considered as non-flammable. The oxygen index for foams modified by the addition MPP was within 23.8–24.6, the value characteristic of self-extinguishing materials—see: Cogen et al. (2009). Similarly, the modification of the foaming composition obtained from polyetherol synthesized

from MDB and EC with addition of powdered MDB led to PUFs of considerably reduced flammability (Table 9.7)—Chmiel et al. (2019).

Thus, one of the solutions to reduce the flammability of thermo-resistant polyurethane foams is the addition of flame retardants during foaming. The additive flame retardants are usually highly dispersed solids (powders).

The best-known additives are melamine, melamine phosphate, melamine borate, melamine isocyanurate, and polyphosphates of melamine or ammonium—see: Brzozowski et al. (2001), Gijsman et al. (2002), Wilkie and Morgan (2009). These compounds influence the physicochemical properties of the final product and significantly decrease their flammability. Thermally resistant polyurethane foams with incorporated 1,3,5-triazine ring were modified with additive flame retardants: melamine, melamine polyphosphate and melamine isocyanurate (MI), see: Lubczak and Lubczak (2018). The resulting foams have enhanced thermal resistance and reduced flammability. All of the PUFs modified with MEL, MI, or MPP are self-extinguishing in the horizontal test (Table 9.4). The flame zone was 5–10 mm. After removal of the burner flame, the flame ceased (Fig. 9.21). The flame speed of flame retardant-modified PUFs until the flame goes out was lower (0.6–0.8 mm/s) than that of non-modified PUF (obtained from oligoetherol from melamine and PC (6.2 mm/s), and mass loss was 1.8–5.0 wt% in comparison with 52 wt% for non-modified PUFs. The vertical flammability test seems to be more practical in the sense of reflecting real fire conditions. The initializing flame not only sets the flame on the bottom part of tested specimen and leads to an increase of temperature of upper parts of

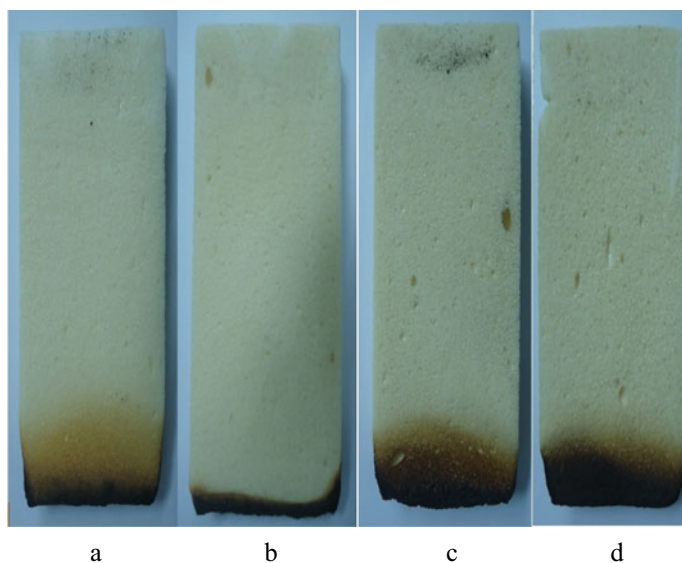


**Fig. 9.21** Photographs of PUF samples flamed by the horizontal test modified with melamine 6% H<sub>2</sub>O (a), melamine, 3% H<sub>2</sub>O (b), MPP (c), and MI (d). Source Lubczak and Lubczak (2018)

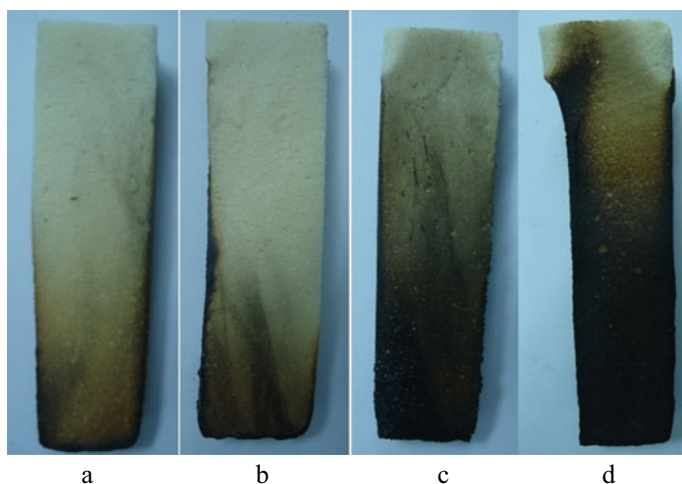


**Fig. 9.22** Photographs of PUF samples flamed in vertical test modified with: melamine, 6% H<sub>2</sub>O, melamine, 3% H<sub>2</sub>O (b), MPP (c), and MI (d). *Source* Lubczak and Lubczak (2018)

the specimen. Flame retardant-modified PUFs stopped burning after 10 s except MI-modified PUF (13 s). Similarly, the secondary firing showed short flame ceasing time (Fig. 9.22).

The oxygen index of modified PUFs was in the range 22.2–24.2% which is characteristic of self-extinguishing materials (Table 9.7, Fig. 9.23). The physical properties of modified PUFs are similar to classic rigid PUFs. Addition of MPP, MI or melamine into foaming mixtures additionally increases the thermal resistance of obtained PUFs in comparison with PUFs with 1,3,5-triazine ring obtained from polyetherols synthesized from melamine and propylene carbonate (cf. Tables 9.3 and 9.6).

#### 9.4 Polyetherols and Polyurethane Foams Based on Natural Products

Starch can also be hydroxyalkylated with oxiranes or alkylene carbonates, although the literature on such processes is limited. Hydroxyalkyl derivatives of starch can be obtained by grafting starch with ethylene or propylene oxides—see: Richter et al. (1968), Kesler and Hjermstad (1958), Villwock and BeMiller (2005a, (2005b), Ezra and Zilkha (1970). Hydroxyalkylation can also be accomplished in water with the addition of sodium hydroxide, which afterwards needs to be neutralized—Kesler and Hjermstad (1958). According to the Fuzesi and Klahs (1970) patent a hydroxyalkylation of starch with excess propylene oxide conducted in glycols in the presence of boron trifluoride, leads to polyols suitable for formation of PUFs, provided that

**Fig. 9.23** Combustion of foams using concept equipment LOI apparatus



the unreacted starch is removed from polyol. Starch can also be hydroxyalkylated with alkylene carbonates (AC). It has been claimed in a 1958 patent that potato starch was reacted with ethylene carbonate at 1:12 molar ratio starch unit (S):EC—Monson and Dickson (1958). The products of hydroxyalkylation were always a paste containing unreacted starch. The products of starch hydroxyalkylation can be used as substrates to obtain biodegradable foams provided that the starch substrate is liquid. Thus, the excessive hydroxyalkylation of starch with 18–19 equivalents of ethylene oxide related to unit of starch led to polyetherols suitable to obtain PUFs—see: Monson and Dickson (1958), Kwon et al. (2007), Shi and BeMiller (2000). Liquefaction of starch was achieved in polyglycol and glycerol—Ge et al. (2000). Obtained elastic foams based on plant-derived starch were biodegradable. It has also been reported that PUFs obtained from powdered starch added to polyol substrate also became biodegradable. However, PUFs containing more than 20% starch showed considerable decrease of compression strength—Cunningham et al. (2003). Starch is insoluble in organic solvents like oxiranes, alkylene carbonates or glycidol, which are used as hydroxyalkylating agents, while partially degraded starch is soluble in water. For the preparation of polyetherols a water-soluble starch was used which had number average molecular mass  $M_n = 5860$  g/mol, and weights-average molecular mass  $M_w = 36,910$  g/mol. The starch was dissolved in water at 80–85 °C. To this solution glycidol was added at 6:1 molar ratio in relation to unit of starch (Fig. 9.24)—Lubczak et al. (2020). The product of reaction was viscous semisolid resin unsuitable

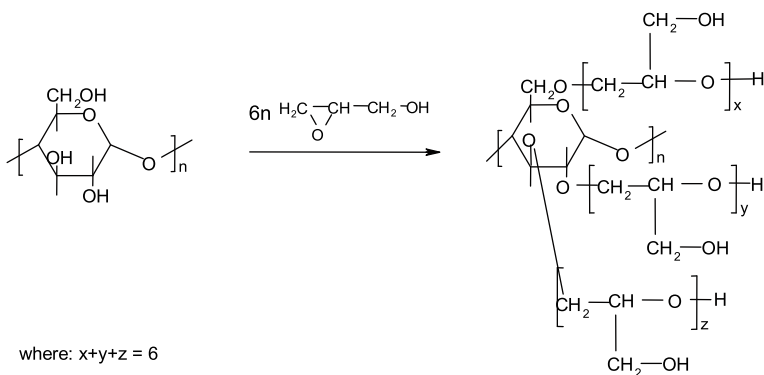


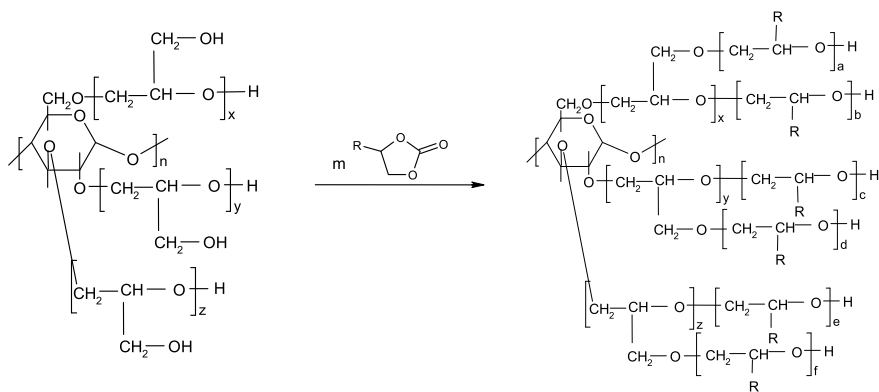
**Fig. 9.24** Reaction of starch with glycidol

for mixing with isocyanates. Therefore, it was further hydroxyalkylated by reaction with 9 equivalents of AC/starch unit (Fig. 9.25).

In such case, the alkylene carbonates were partially consumed in reaction with water to give glycols and polyglycols (Fig. 9.26).

In this way, liquid polyetherols were obtained, containing units of hydroxyalkylated starch, without solid starch.

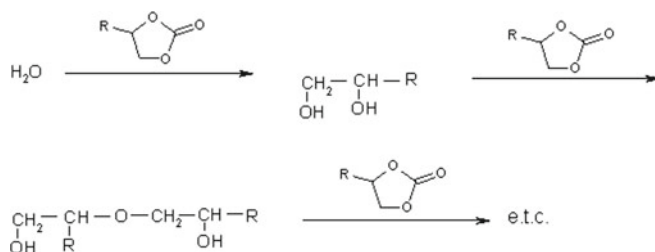
Also, the polyetherols were obtained by preliminary formaldehyde-treated starch and then converted by reaction with glycidol and alkylene carbonates—Lubczak and Szczęch (2019). A simple method of synthesis of polyetherols from starch and ethylene and propylene carbonates in aqueous solution also was elaborated. The products are mixtures of starch-derived polyols and products of hydroxyalkylation of



where:  $-R = -H, -CH_3$

$a + b + c + d + e + f = m$

**Fig. 9.25** Preparation of polyetherol with starch units



where: -R = -H, CH<sub>3</sub>

**Fig. 9.26** Reactions of alkylene carbonate with water and consecutive products

water. The elaborated method can be useful, ecology friendly synthetic route avoiding burdensome solvents. Starch-based polyetherols are good substrates to obtain rigid polyurethane foams—see: Lubczak et al. (2021), Rabek (2013). The PUFs obtained in such process have appropriate apparent density, low polymerization shrinkage, but also high thermal resistance and high compression strength before and after thermal exposure. They can stand long term thermal exposure at 200 °C (Table 9.8). Thermal exposure of PUFs resulted in increase of their compression strength. PUFs obtained from propylene carbonate and starch at 9:1 molar ratio of carbonate to starch unit, are partially biodegraded in a bioavailability test with *Bacillus subtilis* bacteria—Lubczak et al. (2021).

Cellulose (CL) is an ubiquitous natural polymer formed by a photosynthetic process. It is a basic component of plant cell walls—Rabek (2013). Cellulose (Fig. 9.27, R = H) is a polysaccharide comprising of glucopyranoses linked via β-1,4-glycoside bond. The polymer chain of cellulose is stabilized by hydrogen bonding between C3-hydroxyl group and ring oxygen. Hydroxyl groups are engaged in strong interchain bonds rendering this material almost insoluble in water and organic solvents. The solubility of cellulose can be increased by hydroxyalkylation to obtain hydroxyethyl- (HEC, Fig. 9.23, R = -H<sub>2</sub>CH<sub>2</sub>OH) and (hydroxypropyl)cellulose (HPC, Fig. 9.23, R = CH<sub>2</sub>CH(CH<sub>3</sub>)OH).

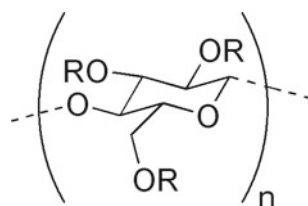
HEC can be obtained by reaction of alkali cellulose with ethylene oxide. When cellulose is dispersed in aqueous sodium hydroxide solution, a sodium alcoholates are formed, which are necessary for reaction with ethylene oxide. Finally, HEC can be isolated and purified after neutralization of solution. The level of substitution of HEC with ethylene oxide is 1.8–3.0. Further ethoxylation can be performed with excess of ethylene oxide to give oligoethoxyethylene derivatives—Florjańczyk and Penczek (1999). Cellulose is a good candidate to be a polyol component to produce polyurethane foams provided the method of liquefying is available, for instance by hydroxyalkylation of cellulose. No cellulose hydroxyalkylation with alkylene carbonates towards polyetherols obtaining are reported due to its insolubility. Instead, the cellulose powder has been described as admixed to liquid polyol in foaming composition—see: Florjańczyk and Penczek (1999), Macedo et al. (2017), Prociak et al. (2016), Pan and Saddler (2013), Kosmela et al. (2018).

**Table 9.8** Some properties of polyurethane foams obtained from polyetherols synthesized from starch and cellulose derivatives

Properties		Unit	Foam obtained from polyetherol					
			S:FA: GL:EC = 1:3:3:3	S:FA: GL:PC = 1:3:3:6	S:GL: PC = 1:6:6	S:PC = 1:9	HPC:GL:EC = 1:12:42	CL:GL:EC = 1:13:13
Density		kg/m <sup>3</sup>	46.8	51.6	26.0	43.2	58.1	72.9
Absorb. of water after 24 h		%	4.6	5.4	5.4	7.0	2.1	4.9
Linear post-shrinkage		%	2.3	2.0	0.4	1.4	4.6	0.8
Heat conductance coefficient		W/m K	0.0364	0.0342	0.0376	0.0459	0.0354	0.0364
Mass loss after 30 days exposure in temperature	150 °C	%wt	9.80	7.6	7.6	21.0	9.8	7.6
	175 °C	%wt	27.9	30.1	22.1	38.8	29.3	21.0
	200 °C	%wt	39.3	38.6	33.7	50.1	44.5	*
Compressive strength		MPa	0.233	0.270	0.101	0.121	0.279	0.212
Compressive strength after 30 days exposure in temperature	150 °C	MPa	0.413	0.443	0.127	0.676	0.350	0.325
	175 °C	MPa	0.349	0.388	0.108	0.596	0.549	0.410
	200 °C	MPa	0.254	0.346	0.094	0.393	0.725	*

\* The foam deforms after annealing

S, HPC and CL are starch, (hydroxypropyl)cellulose and cellulose units, respectively

**Fig. 9.27** Formula for a cellulose unit and its derivatives

Also, some cellulose derivatives were used as admixed polyetherols components in a one-step foaming process, like cellulose acetate, sulphate, carboxyethyl-, or trimethylsilylcellulose at the level of 11–44 wt % of polyol—Rivera-Armenta et al. (2004). According to the current state of the art, an addition of powdered cellulose into foaming composition resulted in a decrease of mechanical properties of polyurethane foams when non-reacted cellulose is present in the final PUF. The exceptions are compositions to which cellulose fibers were added at the level of foaming; the increase



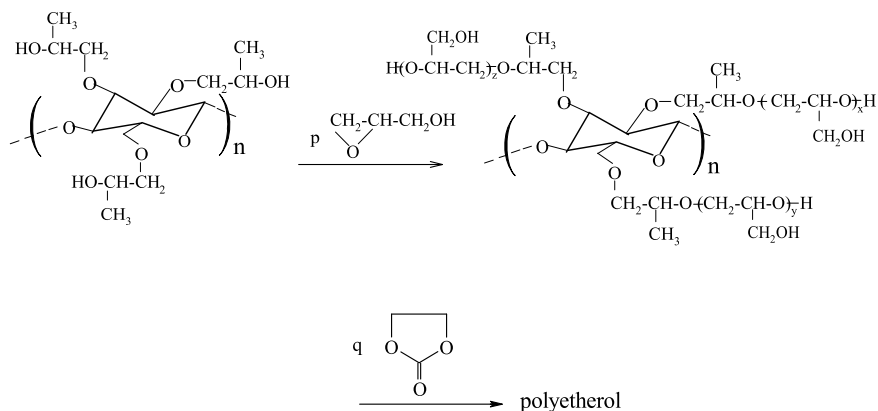


**Fig. 9.28** Preparation of polyetherol with cellulose units

of mechanical and thermal properties of PUFs was observed in those products—see: Lou et al. (2015), Septevani et al. (2017), Leng and Pan (2019). Polyetherols incorporating hydroxyalkyl cellulose derivatives units were obtained by reactions of HPC with glycidol and ethylene carbonate (Fig. 9.28)—Szpiłyk et al. (2021a).

A polyol synthesis based on cellulose hydrolyzate was also developed by reaction with glycidol and ethylene carbonate in the presence of potassium carbonate as catalyst without solvent—Szpiłyk et al. (2021b). Before hydrolysis, cellulose had particle size of 800–1200 nm. During hydrolysis, long chains are shortened with appearance of a large fraction of particles with a size of 50–200 nm. The obtained polyol contains hydroxyalkylated cellulose units incorporated into its structure. Foams obtained from these polyetherols can stand long term heating at 175 °C, while their compression strength increase upon annealing (Table 9.8). Both polyols as well as PUFs obtained are biodegraded in soil. In case of such polyols the complete degradation has been demonstrated.

## References

- Blount, D. (1991). Flame-retardant polyurethane foam utilizing boric acid. US Patent 50,075,343.
- Brzozowski, Z., Kijeńska, D., & Zatorski, W. (2001). Flammability of polymers. Part 2. Methods to reduce the flammability of plastics. *Plast Rev*, 9, 65–67.
- Chmiel, E., & Lubczak, J. (2017). Oligoetherols and polyurethane foams obtained from melamine diborate. *Journal of Polymer Research*, 24(6) 95, 1–12.
- Chmiel, E., & Lubczak, J. (2018). Oligoetherols and polyurethane foams obtained from metasilicic acid. *Polymer Bulletin*, 75, 1579–1596.
- Chmiel, E., & Lubczak, J. (2019). Synthesis of oligoetherols from mixtures of melamine and boric acid and polyurethane foams formed from these oligoetherols. *Polymer Bulletin*, 76, 2253–2275.

- Chmiel, E., Oliwa, R., & Lubczak, J. (2019). Boron-containing non-flammable polyurethane foams. *Polymer Plastics Technology and Engineering*, 58(4), 394–404.
- Cichy, B., Łuczowska, D., Nowak, M., & Władysław-Przybylak, M. (2003). Polyphosphate Flame Retardants with Increased Heat Resistance. *Industrial and Engineering Chemistry Research*, 42, 2897–2905.
- Cogen, J. M., Lin, T. S., & Lyon, R. E. (2009). Correlations between pyrolysis combustion flow calorimetry and conventional flammability tests with halogen free 530 flame retardant polyolefin compounds. *Fire and Materials*, 33, 33–50.
- Cunningham, L., Carr, M. E., & Bagley, E. B. (1991). Polyurethane Foams Extended with Corn Flour. *Cereal Chemistry*, 68, 258–261.
- Cyzio, K., & Lubczak, J. (2011). New possibilities of synthesis of oligoetherols with azacyclic compounds. *Polimery*, 56(11–12), 856–860.
- Czupryński, B., Paciurek-Sadowska, J., & Liszkowska, J. (2002). The effect of tri(1-chloro-3-etoxypropane-2-ol) borate on the properties of rigid polyurethane-polyisocyanurate foams. *Polimery*, 47, 727–729.
- Czupryński, B., Liszkowska, J., & Paciurek-Sadowska, J. (2006). Effect of selected boroorganic compounds on thermal and heat properties of rigid polyurethane-polyisocyanurate foams. *Journal of Applied Polymer Science*, 102, 768–771.
- Czupryński, B., Paciurek-Sadowska, J., & Liszkowska, J. (2006). Studies on effect of tri(2-hydroxypropyl), tri(2-hydroxybutyl) and tri(hydroxythiodiethylene) borates on thermal and heat properties of rigid polyurethane-polyisocyanurate foams. *Chinese Journal of Chemistry*, 24, 1796–1799.
- Ezra, G., & Zilkha, A. (1970). Anionic graft polymerization of propylene oxide on starch. *European Polymer Journal*, 6, 1305–1311.
- Feng, X. Y., Li, S. K., Wang, Y., Wang, Y. C., & Liu, J. X. (2013). The Effects of SiO<sub>2</sub>/PEG Suspension on Mechanical Properties of Rigid Polyurethane Foams. *Advances in Materials Research*, 815, 246–250.
- Florjańczyk, Z., & Penczek, S. (1999). *Polymer chemistry, Natural polymers and polymers with special properties* (Vol. III). Warsaw University of Technology Publishing House.
- Francés, A. B., & Navarro Bañón, N. V. (2014). Effect of silica nanoparticles on polyurethane foaming process and foam properties. *Conference Series: Materials Science Engineering*, 64, 1–6.
- Frisch, K. C., Tummars, D. M., & Nijenhuis, A. T. (1980). Preparation of tris(β-hydroxypropyl)isocyanurate. US Patent 4,198,505.
- Fuchs, S., & Weiss, T. (2014). Melamine phenylphosphinate flame retardant compositions. US Patent 8,877,838.
- Fuzesi, S., & Klahs, L. (1970). Polyurethane foams prepared from starch-based polyether polyols. US Patent 3541034.
- Ge, J., Zhong, W., Guo, Z., Li, W., & Sakai, K. (2000). Biodegradable Polyurethane Materials from Bark and Starch. I. Highly Resilient Foams. *Journal of Applied Polymer Science*, 77, 2575–2580.
- Gijsman, P., Steenbakkens, R., Furst, C., & Kersjes, J. (2002). Differences in the flame retardant mechanism of melamine cyanurate in polyamide 6 and polyamide 66. *Polymer Degradation and Stability*, 78, 219–224.
- Goodman, H. (1999). *Handbook of thermoset plastics* (2nd ed.). William Andrew Publishing.
- Hilado, C. J. (1998). *Flammability Handbook for Plastics*. Technomic Publishing C.
- ISO 2796. (1986). Cellular plastics, rigid. test of dimensional stability, European Standards EN ISO 2796:1986. <https://www.iso.org/standard/7786.html>.
- ISO 60695–11–10. (1999). Fire Hazard Testing—Part 11–10: Test flames –50 W horizontal and vertical flame test methods European Standards EN ISO 60695–11–10: 1999, <https://www.iso.org/standard/26271.html>.
- ISO 2896. (2001). Cellular plastics, rigid. determination of water absorption, European Standards EN ISO 2896:2001. <https://www.iso.org/standard/30408.html>.

- ISO 845. (2006). Cellular plastics and rubbers. Determination of apparent density, European Standards EN ISO 845:2006, <https://www.iso.org/standard/39408.html>.
- ISO 844. (2014). Cellular Plastics. Compression Test for rigid Materials, European Standards EN ISO 844:2014. <https://www.iso.org/standard/55473.html>.
- ISO 4589-2. (2017). Plastics. Determination of burning behavior by oxygen index – Part 2. Ambient-temperature test, European Standards EN ISO 4589-2:2017, <https://www.iso.org/standard/60786.html>.
- Janowska, G., Przygocki, W., & Włochowicz, A. (2007). Flammability of polymers and polymeric materials, WNT, Warsaw.
- Kesler, C., & Hjermstad, E. (1958). Hydroxyalkylation of ungelatinized starches and dextrans in aqueous, water-miscible alcohols. US Pat. 2,845,417.
- Kijowska, D., & Kucharski, M. (2004). Polyetherols from melamine and alkylene carbonates. Properties and application of foamed polyurethanes. *Journal of Applied Polymer Science*, *94*, 2302–2320.
- Kijowska, D. (2005). Alkylene carbonates with a five membered ring—production, properties and use. *Przemysł Chemiczny*, *8(9)*, 678–683.
- Kijowska, D., & Legocka, I. (2011). Polyetherols from melamine cyanurate and ethylene carbonate—synthesis and application. *Polish Journal of Chemical Technology*, *13(3)*, 42–46.
- Kim, B. S., Park, S. H., & Kim, B. K. (2006). Nanosilica-reinforced UV-cured polyurethane dispersion. *Colloid and Polymer Science*, *284*, 1067–1072.
- Kosmela, P., Hejna, A., Formela, K., Haponiuk, J., & Piszczyk, Ł. (2018). The study on application of biopolyols obtained by cellulose biomass liquefaction performed with crude glycerol for the synthesis of rigid polyurethane foams. *Journal of Polymers and Environment*, *26*, 2546–25.
- Kucharski, M., Lubczak, J., Rokaszewski, E. (1983). Addition of oxiranes to hydroxymethyl derivatives of isocyanuric acid. *Chemia Stos*, *27* (1–2), 65–77
- Kucharski, M., & Lubczak, J. (1985). Porous polyurethane materials based on the reaction products of ethylene oxide (oxirane) with 1,3,5-tris(hydroxymethyl)isocyanurate. *Polimery*, *30(9)*, 354–361.
- Kucharski, M., & Lubczak, J. (1991). Synthesis of polyetherols with s-triazine ring catalyzed by tetrabutylammonium hydroxide. *Acta Polymerica*, *42(4)*, 186–189.
- Kucharski, M., & Kijowska, D. (2001). Synthesis of polyetherols from melamine and ethylene carbonate. *Journal of Applied Polymer Science*, *80*, 1776–1784.
- Kwon, O. J., Yang, S. R., Kim, D. H., & Park, J. S. (2007). Characterization of polyurethane foam prepared by using starch as polyol. *Journal of Applied Polymer Science*, *103*, 1544–155381.
- Langrish, J., & Marklow, R. (1966). Polyurethanes. GB Patent 1,049,298.
- Leng, W., & Pan, B. (2019). Thermal Insulating and Mechanical Properties of Cellulose Nanofibrils Modified Polyurethane Foam Composite as Structural Insulated Material. *Forests*, *10(200)*, 1–12.
- Levchik, S. V., & Weil, E. D. (2004). Thermal decomposition, combustion and fire-retardancy of polyurethanes - a review of the recent literature. *Polymer International*, *53*, 1901–1929.
- Lubczak, J., & Kucharski, M. (1985). Reactions of melamine with oxiranes. *Synthesis of Polyetherols. Chemia Stos*, *29(3–4)*, 277–287.
- Lubczak, J. (1987). Addition of oxiranes to hydroxymethyl derivatives of melamine. Part III. Reactions of N, N'-bis(hydroxymethyl)melamine with an excess of oxiranes. *Polimery*, *32(8)*, 314–319.
- Lubczak, J., & Chmiel, E. (1990). Addition of oxiranes to hydroxymethyl derivatives of melamine. Part IV. Preparation of polyetherols from (methoxymethyl)melamines. *Polimery*, *35*, 194–199.
- Lubczak, J., Cisek-Cicirko, I., & Myśliwiec, B. (2002). Preparation and applications of the products of reaction of uric acid with formaldehyde. *Reactive and Functional Polymers*, *53*, 113–124.
- Lubczak, R., & Duliban, J. (2002). A study of the reaction of adenine with ethylene oxide or with ethylene carbonate. *Reactive and Functional Polymers*, *52*, 127–134.
- Lubczak, J. (2006). Reaction of Uric Acid with Excess of Propylene Carbonate. *Journal of Applied Polymer Science*, *101*, 2482–2487.
- Lubczak, J. (2007). Polyurethane foams with purine rings. *Polimery*, *52(7–8)*, 595–600.

- Lubczak, J., & Mendyk, E. (2008). Stable enol form of barbituric acid. *Heterocyclic Communications*, 14(3), 149–154.
- Lubczak, J. (2011a). Polyhydroxyalkyl derivatives and polyetherols obtained from azacyclic compounds. Part I. Reactions with Oxiranes. *Polimery*, 56(5), 360–368.
- Lubczak, J. (2011b). Polyhydroxyalkyl derivatives and polyetherols obtained from azacyclic compounds. Part II. Reaction with formaldehyde and alkylene carbonates. *Polimery*, 56(6), 452–460.
- Lubczak, R. (2015). Polyurethane foams with carbazole ring. *Cellular Polymers*, 34, 15–25.
- Lubczak, J., Chmiel-Szukiewicz, E., Duliban, J., Głowacz-Czerwonka, D., Lubczak, R., Zarzyka, I., Łukasiewicz, B., Łodyga, A., Tyński, P., Majerczyk, Z., Koziół, M., & Minda-Data, D. (2015). Method for preparing polyurethane foams with improved thermal resistance. *Polish Patent, PL Pat.*, 218, 727.
- Lubczak, J., & Lubczak, R. (2016). Melamine polyphosphate – the reactive and additive flame retardant for polyurethane foams. *Acta Chimica Slovenica*, 63, 77–87.
- Lubczak, J., & Lubczak, R. (2018). Thermally resistant polyurethane foams with reduced flammability. *Journal of Cellular Plastics*, 54(3), 561–576.
- Lubczak, J., Łukasiewicz, B., & Myśliwiec, B. (2013). Synthesis and applications of oligoetherols with perhydro-1,3,5-triazine ring and boron. *Journal of Applied Polymer Science*, 127, 2057–2066.
- Lubczak, R., & Szczęch, D. (2019). Polyurethane foams with starch. *Journal of Chemical Technology and Biotechnology*, 94, 109–119.
- Lubczak, R., Szczęch, D., & Lubczak, J. (2020). From starch to oligoetherols and polyurethane foams. *Polymer Bulletin*, 77(11), 5725–5751.
- Lubczak, R., Szczęch, D., Broda, D., Wojnarowska-Nowak, R., Kus-Liśkiewicz, M., Dębska, B., & Lubczak, J. (2021). Polyetherols and polyurethane foams from starch. *Polymer Test*, 93(106884), 1–12.
- Luo, F., Wu, K., Guo, H., Zhao, O., Liang, L., & Lu, M. (2015). Effect of cellulose whisker and ammonium polyphosphate on thermal properties and flammability performance of rigid polyurethane foam. *Journal of Thermal Analysis and Calorimetry*, 122, 717–723.
- Łukasiewicz, B., & Lubczak, J. (2012). Oligoetherols and polyurethane foams with 1,3,5-triazine ring and boron atoms. *Polimery*, 57(11–12), 819–829.
- Łukasiewicz, B., & Lubczak, J. (2014). Polyurethane Foams with Purine Ring and Boron. *Journal of Cellular Plastics*, 50(4), 337–359.
- Macedo, V., Zimmerman, M., Koester, L., Scienza, L., & Zattera, A. (2017). Flexible polyurethane foams filled with Pinnuselliotti cellulose. *Polímeros*, 27, 27–34.
- Mercado, L. A., Galia, M., & Reina, J. A. (2006). Silicon-containing flame retardant epoxy resins. *Polym Degrad Stabil*, 91, 2588–2594.
- Monson, N., & Dickson, W. (1958). Process for preparing oxyalkylated derivatives. *US Pat*, 2(854), 449.
- Moss, E. K., & Skinner, D. L. (1976). Modified Isocyanurate Foams. Part. 1. *Journal of Cellular Plastics*, 12, 332–336.
- Moss, E. K. (1982). Modified Isocyanurate Foams. Part VI. *J Cell Plast*, 18, 240–244.
- Nikje, M. M. A., & Tehrani, Z. M. (2010). Thermal and mechanical properties of polyurethane rigid foam/modified nanosilica composite. *Polymer Engineering and Science*, 50(3), 468–473.
- Nowak, M., Rostkowska, H., Łapiński, L., Kwiatkowski, J., & Leszczyński, J. (1994). Tautomerism N(9)H.dblharw. N(7)H of purine, adenine, and 2-chloroadenine: Combined experimental IR matrix isolation and Ab initio quantum mechanical studies. *Journal of Physical Chemistry*, 98, 2813–2816.
- Oertel, G. (1994). *Polyurethane Handbook* (2nd ed.). Carl Hanser Verlag, München.
- Ozóg, M., & Lubczak, J. (2012). The application of oligoetherol synthesized from melem and propylene carbonate to obtain polyurethane foams. *Technical Transactions*, 109(26), 181–192.
- Pan, X., & Saddler, J. (2013). Effect of replacing polyol by organosolv and kraft lignin on the property and structure of rigid polyurethane foam. *Biotechnology for Biofuels*, 6, 1–10.

- Poplewska, I., Węglowska, E., & Lubczak, J. (2004). Polyetherols from isocyanuric acid and ethylene carbonate. *Journal of Applied Polymer Science*, *91*, 2750–2755.
- Prociak, A., Malewska, E., & Bąk, S. (2016). Influence of isocyanate index on selected properties of flexible polyurethane foams modified with various bio-components. *J Renew Mater*, *4*, 78–85.
- Rabek J. (2013). *Polymers* PWN Warsaw.
- Randall, D., & Lee, S. (2002). *The polyurethanes book* ed. Wiley Ltd.
- Richter, M., Augustat, S., & Schierbaum, F. (1968). *Ausgewählte Methoden der Stärke chemie*. VEB Fachbuch-verlag.
- Rivera-Armenta, J., Heinze, T., & Mendoza-Martinez, A. (2004). New polyurethane foams modified with cellulose derivatives. *European Polymer Journal*, *40*, 2803–2812.
- Septevani, A., Evans, D., Annamalai, P., & Martin, D. (2017). The use of cellulose nanocrystals to enhance the thermal insulation properties and sustainability of rigid polyurethane foam. *Industrial Crops and Products*, *107*, 114–121.
- Shi, X., & BeMiller, J. N. (2000). Effect of sulfate and citrate salts on derivatization of amylose and amylopectin during hydroxypropylation of corn starch. *Carbohydrate Polymers*, *43*, 333–336.
- Szpiżyk, M., Lubczak, R., & Lubczak, J. (2021a). Polyetherols and polyurethane foams with cellulose subunits. *Polymer-Plastics Technology and Materials*, *60*(4), 440–452.
- Szpiżyk, M., Lubczak, R., Walczak, M., & Lubczak, J. (2021b). Polyol and polyurethane foam from cellulose hydrolysate. *Journal of Chemical Technology and Biotechnology*, *96*(4), 881–889.
- Ślącza, A., & Lubczak, J. (2007). Hydroxyalkylation of barbituric acid. Part II. Synthesis of polyetherols with pyrimidine ring. *Journal of Applied Polymer Science*, *106*, 4067–4074.
- Ślącza, A., & Lubczak, J. (2010). Polyurethane foams with pyrimidine rings in polymer molecules. *Polimery*, *55*(9), 681–684.
- Terraza, C. A., Tagle, L. H., Leiva, A., Poblete, L., & Concha, F. J. (2008). Poly(urethanes) Containing Silarylene and/or Germarlylene Units. *Journal of Applied Polymer Science*, *109*, 303–308.
- Verdolotti, L., Lavorgna, M., Lamanna, R., Di Maio, E., & Iannace, S. (2015). Polyurethane-silica hybrid foam by sole gel approach: Chemical and functional properties. *Polymer*, *56*(15), 20–28.
- Wilkie, C., & Morgan, A. (2009). *Fire Retardancy of Polymeric Materials*. London, New York, CRC Press.
- Wirpsza, Z. (1991). *Polyurethanes*, WNT, Warsaw.
- Thirumal, M., Khastgir, D., Singha, N. K., Manjunath, B. S., & Naik, Y. P. (2008). Effect of Expandable Graphite on the Properties of Intumescent Flame-Retardant Polyurethane Foam. *Journal of Applied Polymer Science*, *110*(5), 2586–2594.
- Uhlig, K. (1999). *Discovering polyurethanes*. Hanser Publishers.
- Villwock, V. K., & BeMiller, J. N. (2005a). Effects of salts on the reaction of normal corn starch with propylene oxide. *Starch Starke*, *57*, 281–290.
- Villwock, V. K., & BeMiller, J. N. (2005b). Influence of reaction conditions on MS values and physical properties of waxy maize starch derivatized by reaction with propylene oxide. *Carbohydrate Polymers*, *64*, 158–162.
- Yang, C. H., Liu, F. J., Liu, Y. P., & Liao, W. T. (2006). Hybrids of colloidal silica and waterborne polyurethane. *Journal of Colloid and Interface Science*, *302*, 123–132.
- Zhang, S., & Horrocks, A. R. (2003). A review of flame retardant polypropylene fibres. *Progress in Polymer Science*, *28*, 1517–1538.
- Zuchowska, D. (2000). *Construction polymers*, WNT, Warsaw.

# Chapter 10

## High Performance Thermal Insulations—Vacuum Insulation Panels (VIPs)



Phalguni Mukhopadhyaya

**Abstract** The spread of human civilization across the globe, including in the regions with extreme climatic conditions, is invariably linked with the development, availability and use of thermal insulation materials in built environment constructions. This chapter explains the fundamental mechanisms of heat transfer through thermal insulation materials used for building envelope constructions, with particular focus on high performance thermal insulations and Vacuum Insulation Panels (VIPs). There are opportunities and barriers, like all novel construction materials, associated with the application of VIPs in building envelope constructions. A close review of the available information and data shows that global concern about climate change adaptation and/or mitigation is fueling these opportunities, and persistent effort by researchers and engineering design communities across the world is bringing down the barriers.

### 10.1 Introduction

Energy used for space heating/cooling of built environment is a significant component of total energy consumption in developed countries around the world—Pérez-Lombard et al. (2008). Increased global focus on energy efficient buildings has been propelling the search for high performance thermal insulations in recent years. However, historically speaking, our search for thermal insulations with higher thermal resistance per unit thickness (in North America commonly referred as R-value/inch), is not a new phenomenon, and this eternal search has led to continuous improvement of R-value of insulation over the decades (Fig. 10.1) and it continues—see: Stovall (1999), Kollie et al. (1991).

It all started from the fundamental realization that the existence of life on our planet is very much dependent on insulation. The layer of air that encompasses our planet is essentially an effective insulation blanket keeping our planet inhabitable

---

P. Mukhopadhyaya (✉)  
Department of Civil Engineering, University of Victoria, 3800 Finnerty Road, Victoria, BC V8P 5C2, Canada  
e-mail: [phalguni@uvic.ca](mailto:phalguni@uvic.ca)

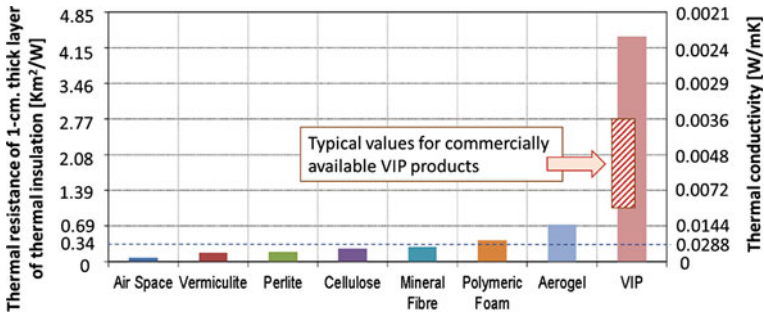


**Fig. 10.1** Increasing thermal resistance of thermal insulations

for us—Pelanne (1978). In the same way, introduction of still/static-air layer inside the building skin or envelope enhances the thermal resistance of building envelope. Hence, the air-gap can be seen as the most ancient form of thermal insulation in building envelopes. Incidentally, the maximum R-value that can be achieved by air gap is about  $R-0.15 \text{ m}^2 \cdot \text{K} / \text{W}$  for 1 cm thick layer of still air (at atmospheric pressure and temperature of  $\sim 20 \text{ }^\circ\text{C}$ ).

However, unlike other insulations, this value cannot be increased further by increasing the thickness of the air gap. In fact, the R-value decreases further due to the presence of convective heat transfer in a larger air gap. As shown in Fig. 10.1, the R-value per thickness of insulation has steadily increased over the time and the insulation that offers the highest R-values at this moment is Vacuum Insulation Panel (VIP). The potential scope of application of VIPs in building constructions in North America is enormous, particularly in regions with extreme climatic conditions (Fig. 10.2). However, it is to be noted that effectiveness of a thermal insulation material in a building is a complex phenomenon and it is significantly influenced by the construction details of the building envelope system and the surrounding

**Fig. 10.2** Installation of VIPs for exterior building envelope retrofit in Whitehorse, Yukon, Canada



boundary/environment conditions. Hence, functioning of thermal insulation as heat transfer barrier and the principles behind the development of high-performance thermal insulation cannot be fully explained without critical understanding of the basics of heat transfer mechanisms through thermal insulating materials.

## 10.2 Heat Transfer Mechanisms in Thermal Insulations

Three basic mechanisms of heat transfer through thermal insulation materials are: (i) Conduction, (ii) Convection, and (iii) Radiation. Conduction occurs when particles are in physical contact, and through these contacts higher energy (temperature) particles transfer heat to lower energy particles (Fig. 3a). Convection is due to the movement of air, vapor or dust particles which carry energy with them (Fig. 3b). The radiation mode of heat transfer happens, neither due to contact between particles nor because of movement of particles, but by means of electromagnetic waves from a higher energy surface to low energy surface, i.e. the same mode of heat transfer that carries energy from the sun to the earth (Fig. 3c). As mentioned earlier, the origin of building insulation started from the presence of an air gap inside the building envelope assembly. The three basic heat transfer mechanisms (i.e. conduction, convection and radiation) contribute significantly to the total heat flow through an air gap/layer inside the building envelope assembly (Fig. 4a)—Shircliffe (1972). However, when a reflective barrier layer/material is introduced inside the air gap the radiation component of the heat transfer reduces significantly, but conduction and convection components of heat transfer remain almost unaltered (Fig. 4b). Convection component can be reduced further by introducing some elements (e.g. fibers or particulate materials) that can block/resist the airflow inside the air gap (Fig. 4c). The conduction part of heat transfer comprises of solid conduction and air conduction (not to be mistaken as air convection). In traditional thermal insulation materials used in buildings and appliances, during heat transfer, the contributions made by conduction, convection and radiation would vary significantly depending on the insulation density, surrounding boundary conditions, pore structures etc. However, there is a generic relationship between the density of insulation materials and the quantity of heat transfer as shown in Fig. 10.5. As would be expected, the radiation component of heat flow reduces exponentially with the increase of insulation density, but the

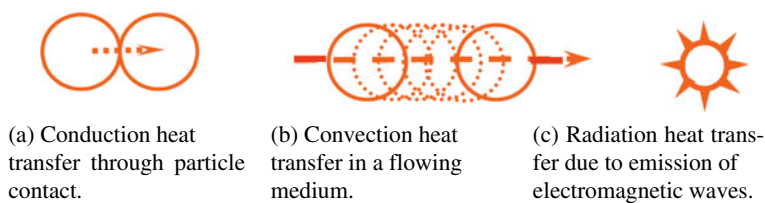


**Fig. 10.3** Basic heat transfer mechanisms



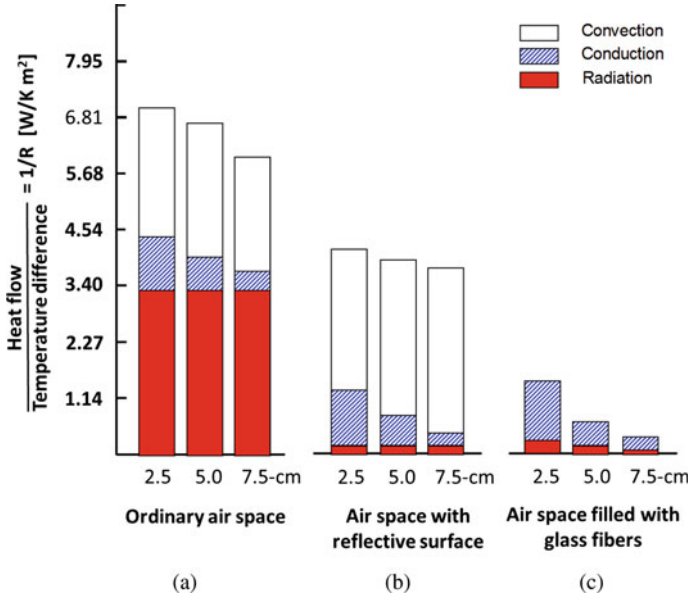
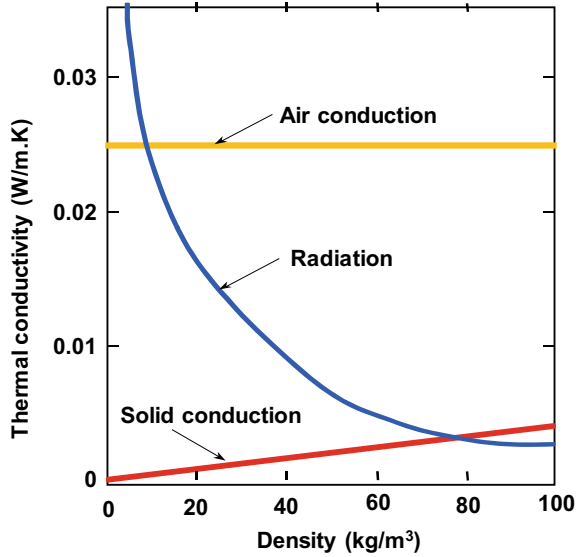


Fig. 10.4 Heat transfer across the air space

Fig. 10.5 Heat transfer mechanisms in conventional insulations



rate of this reduction slows down at a density of about  $40 \text{ kg/m}^3$ . On the other hand, solid conduction component of heat flow rises linearly with the increase of insulation density. These impacts of density on the radiation and solid conduction components of heat transfer limit the scope of reducing the thermal conductivity of an insulation material by changing its density. However, as shown in Fig. 10.5, for all practical purposes, the heat flow through still air (air conduction) is constant and not a function of insulation density. Hence, there lies the greatest opportunity to reduce the thermal conductivity of porous thermal insulations further by reducing the air conduction component of heat flow. Not surprisingly, almost all so called ‘high performance thermal insulations’ tread this path to augment heat flow resistance. There are three different approaches adopted by the thermal insulation industry to date: (1) Replace air in closed pores of a thermal insulation with a blowing agent that has lower thermal conductivity than air, (2) Develop nano porous thermal insulations (if other parameters remain same, a nano porous material has lower thermal conductivity than the same micro/macro porous material). (3) Remove air from pores by vacuuming. There are advantages and limitations in these three distinct approaches as outlined below.

### 10.2.1 Thermal Insulations with Blowing Agents

Most of the closed-cell polymeric foam insulations fall in this category. Typical cell structures of these type of insulations are shown in Fig. 6. The thermal conductivity closed-cell foam insulations vary significantly depending on the type of blowing agent used, as shown in Table 1 (Wu and Eury 2002). The thermal conductivity of most commonly used blowing agents is lower than half of the thermal conductivity of air. These insulations are widely used in buildings and refrigeration industry and known for versatility, durability and cost-effectiveness. Aging characteristics of these insulations and impact of blowing agent on the depletion of ozone layer were of concern during 1970s and 1980s but these issues have been addressed adequately in the recent past (Bomberg and Kumaran 1991; Kumaran et al. 1989). However, temperature dependent thermal conductivity of closed-cell foam insulations with captive blowing agent/s is a concern which would need special design considerations

**Fig. 10.6** Typical cell structure of closed-cell polymeric foam insulations with captive blowing agent

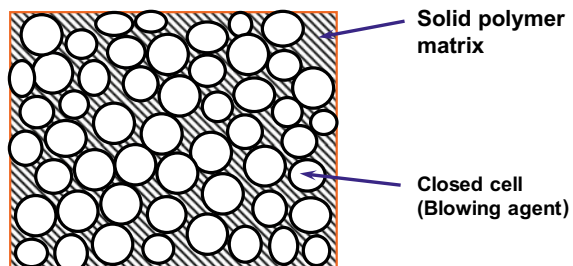


**Table 1** Thermal conductivity of blowing agents

Blowing agent	Thermal conductivity [ $K_{\text{gas}} @ 25(^{\circ}\text{C})$ mW/mK]
CFC-11	8.7
HCFC-141b	9.7
HCFC-142b	11.5
HCFC-22	11.0
Hydrocarbon c-C <sub>5</sub>	12.0
Hydrocarbon n-C <sub>5</sub>	15
HFC-134a	13.6
HFC-245fa	12.2
HFC-365mfc	10.6
Air	26

in extreme weather applications (Drouin et al. 2012; Jagdev and Mukhopadhyaya 2020).

### 10.2.2 Nano-Porous Thermal Insulations

It is well-known that pore diameter of nano porous material is smaller than the mean free path of the diffusing gas molecules and as a result the thermal conductivity of a nano porous insulation material is distinctively lower than that of micro/macro porous insulation materials. When the pore diameter of the material is less than the mean free path of gas molecules, the gas molecules do not collide with other gas molecules but with the pore surfaces without transferring energy, resulting in lower heat transfer rate, and this is known as the Knudsen effect—Kistler (1935), Simmler et al. (2005). A typical example of a nano porous thermal insulation material is silica aerogel (the lowest density solid material known to us) and fumed silica. As shown in Fig. 10.7, plots of thermal conductivity as a function of gas pressure inside the pore, even at atmospheric pressure the thermal conductivity of nano porous aerogel or fumed silica is lower than the other micro or macro porous insulation materials (R-value/inch is about twice that of the closed-cell foam insulations, see Fig. 10.1). Fumed silica, though an excellent insulator, is rarely used as a standalone thermal insulation material. However, flexible aerogel blanket (i.e. fine aerogel powders mixed with fibers) has many niche applications in buildings (e.g. thermal break) and infrastructures (e.g. pipe insulation).

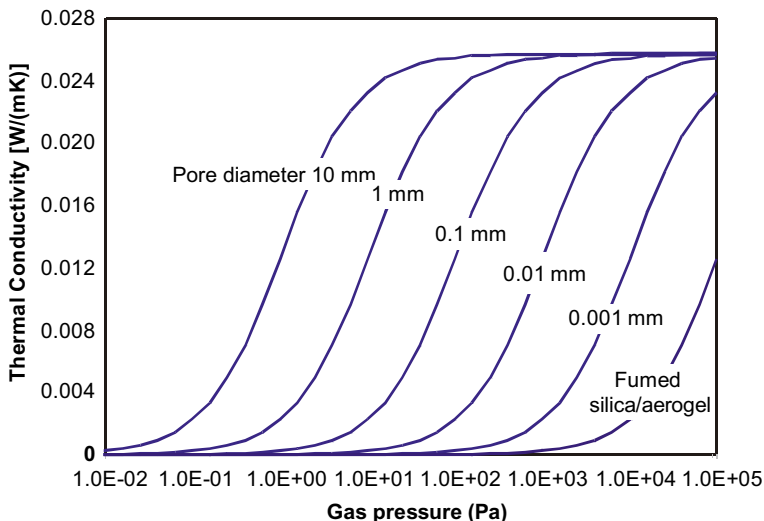


Fig. 10.7 Thermal conductivity of air as a function of pore diameter

### 10.2.3 Vacuum Insulations

Removing air altogether from the pores of an insulation material will bring the air conduction part of heat flow to ‘zero’ (Fig. 5b). Based on our existing knowledge and understanding of the fundamental physics of heat transfer, application of this approach would lead to ultimate high performance thermal insulations for generations to come. Incidentally the concept of vacuum insulation was first introduced more than a century ago in the form of a vacuum insulated container (i.e. Thermos or Dewar flask) by British Scientist Sir James Dewar in 1892—see: Bragg (1940). The most commonly used form of vacuum insulation is called Vacuum Insulation Panel or VIP, that can have thermal insulating efficiency five to ten times higher than traditional thermal insulation materials (Fig. 10.1). A VIP has three major components: (1) Barrier envelope, (2) Core, (3) Getter/Desiccant (Fig. 10.8).

The barrier envelope provides air and vapor-tight enclosure for the core material. Both aluminum and multi-layer metalized polyethylene foils are used as barrier materials. Thin, robust, puncture resistant and low thermal conductivity to reduce thermal bridging at VIP edges (Fig. 10.9) are some of the desirable characteristics of the barrier envelope. It is also to be noted that barrier foil is heat sealed to create the vacuum enclosure and effectiveness of the sealing is very important for short- and long-term performance of a VIP. The core component provides mechanical strength and thermal insulating capacity of a VIP and has open pore structure, very small (preferably nanoscale) pore diameter, ability to resist compression due to the pressure difference between vacuum (i.e. near zero pressure) and atmospheric pressure, and very high resistance to infrared radiation. Commonly used

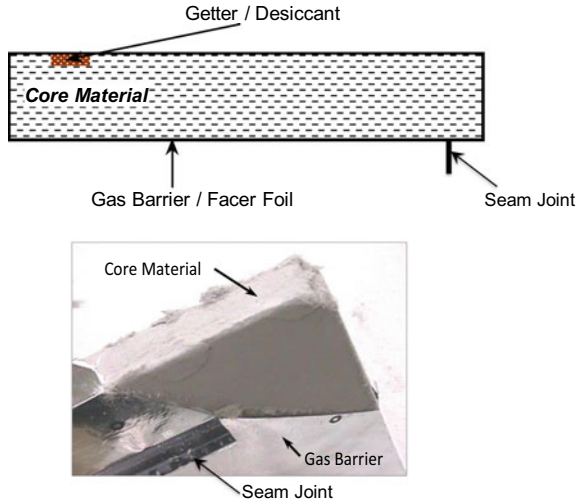
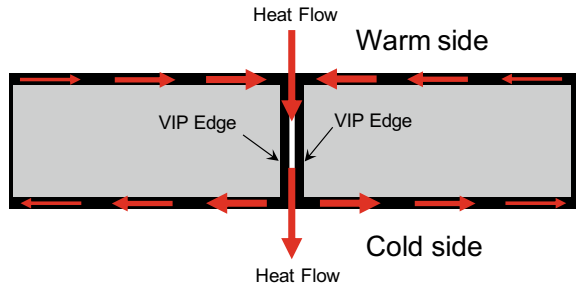


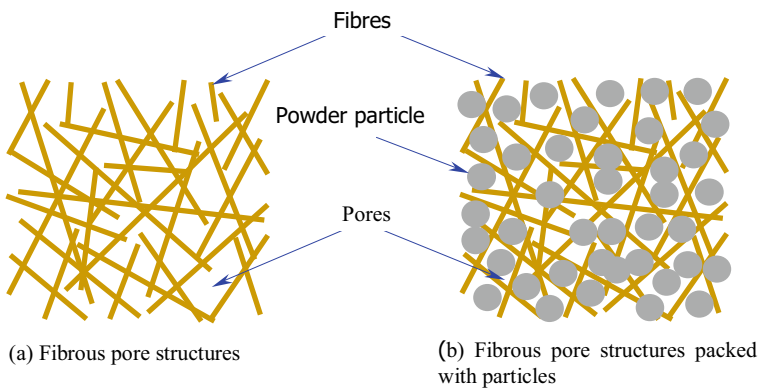
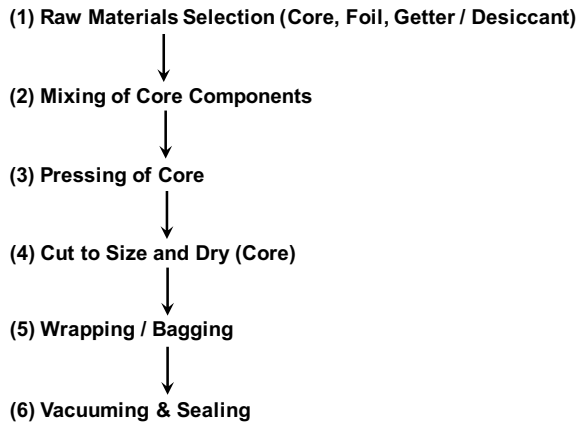
Fig. 10.8 Construction of vacuum insulation panel (VIP)

Fig. 10.9 Thermal bridge at VIP edges



core materials are fumed silica and glass fiber, however, alternative core materials including fiber-powder composite (Fig. 10.10), and bio-based materials have also been proposed—see: Mukhopadhyaya et al. (2008, 2009). The getter and desiccant are added inside the core material to adsorb residual or permeating atmospheric gases and water vapor, respectively, in the barrier envelope. It is to be noted that the VIP manufacturing process is not very complex. The primary manufacturing steps are shown in Fig. 10.11. The long-term performance of VIPs is very much dependent on the performance of the barrier envelope, core material and getter/desiccant. The addition of getter/desiccant increases the performance and longevity of VIPs. It is also to be noted that any damages which can compromise the physical integrity of the barrier foil or seam joint would reduce the thermal performance of VIP to that of the core material at atmospheric pressure. Hence, preserving the integrity of VIPs during the construction and operation would be one of the prime design considerations.

**Fig. 10.10** Alternative fiber-powder core composite for VIPs



**Fig. 10.11** Primary VIP manufacturing steps

### 10.3 Application of Vacuum Insulation Panels (VIPs)

In recent years, with the advent of vacuum technologies, sealing techniques, lightweight/thin barrier envelopes, innovative core materials, and global concerns about energy efficiency, VIP has become an attractive insulation option for both refrigeration and building construction industry. Reduced insulation thickness, due to the use of VIP, has made our refrigerators more spacious and high thermal resistance of VIP has made refrigeration units used in the healthcare/pharmaceutical industry more energy efficient and thermally stable. More recently, COVID-19 pandemic has created a surge in the demand for VIP insulated thermally stable cold storage containers—Kan et al. (2021). However, much anticipated mass applications of VIP in building construction industry is yet to be realized. There are three primary reasons which is keeping the VIPs away from the building construction and they are: (1) Long-term performance, (2) Construction details, and (3) Cost.

### 10.3.1 Long-Term Performance of VIPs

All construction materials deteriorate with time (i.e. aging phenomenon) and it is an unavoidable reality. The VIP is not an exception either. However, due to its unique construction and composition, the thermal performance of VIP can change more significantly over the time than other thermal insulation materials. The expected minimum service life of VIPs to be used in building construction is 25–50 years. Hence, design engineers need to know the aging characteristics of VIPs. To be more specific, the qualitative characteristics of VIPs are well established, but the challenges lie with quantification. The integrity of the VIP is of critical importance for its short- and long-term performance. The in-situ performance of VIP has two different aspects (see Fig. 10.12), aging and durability, both related to its long-term thermal performance, are identified as two different but interrelated phenomena. Aging of VIP is primarily due to very slow but continuous increase of gas/vapour pressure inside the VIP (Fig. 10.13). Durability is considered as a relatively sudden or rapid failure of the VIP, due to loss of vacuum, caused by mechanical failure of the facer or the seam joint, and can be prevented through appropriate design and stringent quality control during manufacturing and on-site construction. In essence, to a great extent, failure due to durability issues can be prevented but aging of VIP is a certainty. The aging of

Fig. 10.12 Aging and durability of VIP

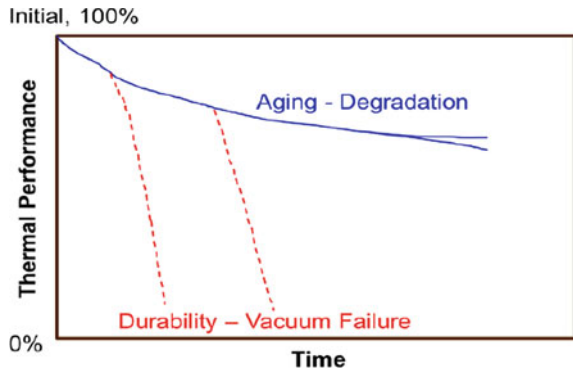
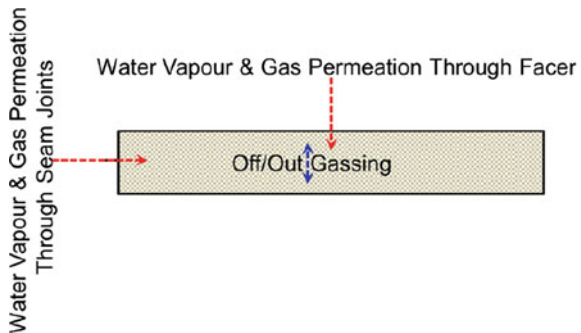


Fig. 10.13 Aging due to very slow but continuous increase of gas/vapour pressure inside the VIP



thermal insulation is not a new issue to the construction industry professionals who have dealt with the long-term thermal resistance (LTTR) of closed-cell foam insulation with a captive blowing agent and who are familiar with laboratory-based accelerated aging test procedure (i.e. thin-slicing), as discussed in Mukhopadhyaya et al. (2002). However, establishing an appropriate laboratory-based accelerated aging test method for the VIP is still a challenging job and in progress. Without a credible aging test protocol, validated by in-situ performance, the mass application of VIPs in building envelope construction will remain a distant pipedream. However, significant progress has been made during the last decade towards addressing the issues related to aging characteristics of VIPs through standardized test protocols and guidelines. In North America, Canadian Construction Materials Centre (CCMC) has developed guidelines for the evaluation of VIPs St-Onge et al. (2018) and in Europe, European Committee for Standardization (CEN) has developed technical specification standard EN 17,140:2020 for building envelope applications—EN 17140 (2020). These standards/guidelines recommend step-by-step methodologies to predict long-term performance of VIPs and both of them use accelerated aging for this purpose. Accelerated aging is a principle that uses intensified environmental conditions (e.g. temperature, humidity), to which the material/system would be exposed during the service life, to speed up the aging processes. While EN 17,140:2020 uses fundamental physics of heat-air-mass transfer mechanisms and results from accelerated aging tests, CCMC's technical guide uses field observations and results from accelerated aging tests to predict the long-term performance of VIPs. Though these two recent developments to predict the long-term performance of VIP complement each other and open up the door for mass integration of VIPs, further validations and fine-tuning of these methodologies using field performance data would be required in the coming years.

### ***10.3.2 Construction with VIPs***

VIP is a construction component that needs to be integrated in exterior building envelope constructions. The construction details involving this integration are of prime importance for design engineers and construction professionals. Inappropriate and/or ill-defined construction details can make the building envelope constructions with VIPs time consuming, labor intensive, expensive, thermally inefficient due to thermal bridging, and prone to damage during construction or operation. Over the years, standardized construction details have been developed for common building materials/components and helped to integrate these construction materials or components in the construction industry. However, the same has not happened for VIPs. Nevertheless, there exists numerous example case studies in the literature [see: Binz et al. (2005), Adl-Zarrabi and Johansson (2020)], which document construction details for integration of VIP in building envelope constructions. Apart from new constructions, these case studies also include application of VIPs for building envelope retrofits (Fig. 10.14)—Chan et al. (2019). The lack of standardized construction



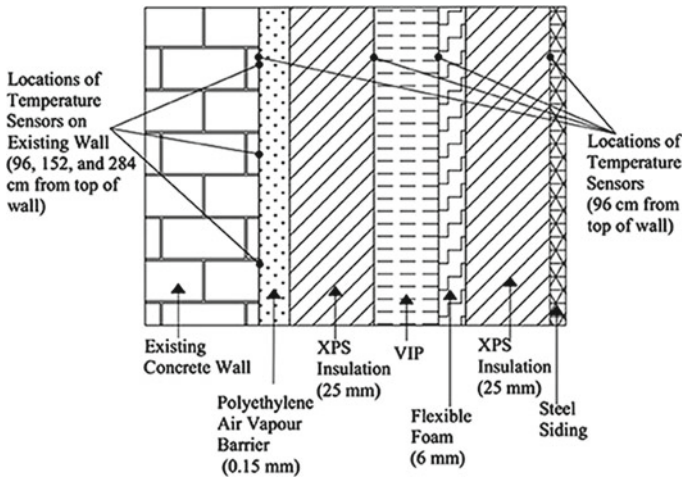


**Fig. 10.14** Retrofitted with VIPs—wall cross-section starting from cladding onwards and the locations of the temperature sensors. This drawing is not to scale

details remains one of the significant impediments for mass adoption of VIPs in the construction industry.

### 10.3.3 Cost of VIPs

Construction industry is sensitive to both time and cost escalation. Cost of VIPs used to be higher than the traditional thermal insulation materials. However, during last two decades, research and development on core, barrier materials, and increased market demand have helped to reduce the cost of vacuum insulation panels significantly. The cost of VIP, while considering its high thermal resistance, is not too far away from foam insulations. It is expected that cost will tumble down further with the development of cheaper core and barrier materials, and increased market volume.

## 10.4 Outlooks and Prospects

During last two decades, vacuum insulation panels (VIPs) have made significant inroads into the refrigeration industry and become an attractive thermal insulation option for the building envelope constructions. Recent developments of technical guidelines and standard specifications, in North America and Europe, for VIPs in building envelope applications are the steps in the right direction. The question about VIP's long-term performance is an issue which will likely to remain alive for the years to come, which is quite natural for any novel building material being introduced to the

construction industry. Further research in the laboratory and in-situ performance data will eventually provide a practical and satisfactory answer to this query. In addition, not only for VIP but for all building materials, there is a need to have a close look at the life cycle environmental impacts. It is becoming increasingly common for building materials manufacturers, including VIP manufacturers, to provide Environmental Product Declaration (EPD) in the public domain. This is a welcome step forward but lack of transparency about data sources is a serious concern which does not allow fair comparison of products or integrated systems—IEA/EBC (2020).

## References

- Adl-Zarrabi, B., & Johansson, P. (Eds). (2020) Long-term performance of super-insulating materials in building components and systems, report of subtask 3: Practical applications—Retrofitting at the building scale—Field scale. IEA/EBC Annex 65, 1–110.
- Binz, A., Moosmann, A., Steinke, G., Schonhardt, U., Fregnan, F., Simmler, H., Brunner, S., Ghazi Wakili, K., Bundi, R., & Heinemann, U. (2005). Vacuum insulation in the building sector—Systems and applications (Subtask B). *IEA/EBC Annex*, 39, 1–134.
- Bomberg, M. T., & Kumaran, M. K. (1991). Evaluation of long-term thermal performance of cellular plastics revisited. ASTM Special Technical Publication 1116. In *Proceedings of the Symposium on Insulation Materials: Testing and Applications ASTM* (pp. 123–141).
- Bragg, W. (1940). History of the vacuum flask. *Nature*, 145, 408–410.
- Chan, V. T. T., Ooms, M., Korn, J., MacLean, D., Mooney, S., Andre, S., & Mukhopadhyaya, P. (2019). Critical analysis of in situ performance of glass fiber core VIPs in extreme cold climate. *Frontiers in Energy Research*, 1–7.
- Drouin, M., Mukhopadhyaya, P., & Shirliffe, C. (2012). Insight into LTTR. In *Roofing Canada* (pp. 10–18). Spring/Summer.
- EN 17140 (2020) Thermal insulation products for buildings—Factory-made vacuum insulation panels (VIP)—Specification. CEN-CENELEC Management Centre, Rue de la Science 23, B—1040, Belgium.
- IEA/EBC, Wallbaum, H. (Ed.). (2020). Life cycle assessment: LCA—Life cycle cost: LCC, embodied energy: Report of subtask 4: Report of subtask IV: Sustainability. *IEA/EBC Annex*, 65, 1–40.
- Jagdev, G. S., & Mukhopadhyaya, P. (2020). Temperature dependent thermal performance of closed-cell foam insulation board in roof constructions. *ASCE Journal of Cold Region Engineering*, 34(3), 1–14.
- Kan, A., Zhu, W., Wang, T., Yuan, Y., & Zhang, X. (2021). Thermal performance assessment of cold chain chamber with vacuum insulation panel envelope layer. *Cleaner Engineering and Technology*, 4, 1–11.
- Kistler, S. S. (1935). The relationship between heat conductivity and structure in silica aerogel. *Journal of Physical Chemistry*, 39, 79–86.
- Kollie, T. G., McElroy, D. L., Fine, H. A., Childs, K. W., Graves, R. S., & Weaver, F. J. (1991). A review of vacuum insulation research and development in the building materials group of the Oak Ridge National Laboratory. In *Oak Ridge National Laboratory* (pp. 1–105). Tenn, USA.
- Kumaran, M. K., Bomberg, M. T., Marchand, R. G., Ascough, M. R., & Creazzo, J. A. (1989). A method for evaluating the effect of blowing agent condensation on sprayed polyurethane foams. *Journal Thermal Insulation*, 13, 123–137.
- Mukhopadhyaya, P., Bomberg, M.T., Kumaran, M.K., Drouin, M., Lackey, J., Van Reenen, D., & Normandin, N. (2002). Long-term thermal resistance of polyisocyanurate foam insulation with

- impermeable facers. In *Insulation Materials: Testing and Applications: 4th Volume, ASTM Special Technical Publication 1426* (pp. 351–365). ASTM International, West Conshohocken, USA.
- Mukhopadhyaya, P., Kumaran K., Normandin, N., van Reenen, D., & Lackey, J. (2008) High performance vacuum insulation panel: Development of alternative core materials. *ASCE Journal of Cold Regions Engineering*, 22(4).
- Mukhopadhyaya, P., Kumaran, Normandin, N., & Van Reenen, D. (2009). Fibre-powder composite as core material for vacuum insulation panel. In *Proceedings of 9th International Vacuum Insulation Symposium* (1–9).
- Pelanne, C. M. (1978). Thermal insulation: What it is and how it works. *Journal of Thermal Insulation*, 1(1978), 223–236.
- Pérez-Lombard, L., Ortiz, J., & Pout, C. (2008). A review on buildings energy consumption information. *Energy and Buildings*, 40(3), 394–398.
- Shirtliffe, C. J. (1972). Thermal resistance of building insulation. In *CBD-149, Institute for Research in Construction*. National Research Council.
- Simmler, H., Brunner, S., Heinemann, U., Schwab, H., Kumaran, K., Mukhopadhyaya, P., Quenard, D., Sallee, H., Noller, K., Kuecuekpinar-Niarchos, E., Stramm, C., Tenpierik, M., Cauberg, H., & Erb, M. (2005). Study on VIP-components and panels for service life prediction of VIP in building applications—Subtask A. *IEA/ECBCS Annex*, 39, 1–157.
- St-Onge, C., Mukhopadhyaya, P., Torok, G., & Moore, T. (2018). Canadian construction materials centre guidelines for the evaluation of vacuum insulated panels. In *Proceedings of 1st International Conference on New Horizons in Green Civil Engineering* (pp. 417–420). Victoria.
- Stovall, T. K. (1999). An introduction to VIP technology. In *Proceedings of the Vacuum Insulation Panel Symposium* (pp. 1–28).
- Wu, J., & Eury, S. (2002). HCFC and HFC alternative blowing agents. PU China, ©Arkema Inc.

# Chapter 11

## Application of Vacuum Insulation Panels (VIPs) in Buildings



Zhaofeng Chen and Qiong Wu

**Abstract** Vacuum insulation panels (VIPs) are widely regarded as one of the best performing thermal insulation materials, which have very low thermal conductivity. VIPs enable high thermal insulation performance—a measure to reduce the energy usage in buildings, cold-chain industry, and home appliances in general. This chapter discusses key materials used in VIPs, their structure, and compares the types and functions of key components, including core materials, envelopes, getters, and opacifiers. The heat transfer modes in VIP are discussed. Physical characteristics including thermal conductivity, inner pressure, durability, and predicted service life are reviewed as well. Applications of vacuum insulation in buildings and their effect over all energy consumption and building durability are also discussed. VIPs have successfully penetrated the building industry in China and manufacturing has matured. It is expected that due to the current pressure for cutting down carbon emissions, VIPs will certainly play a vital role in building energy conservation and sustainability projects. Furthermore, research and development of high performance and low-cost VIPs will be an important direction for future research efforts and industry technology development.

### 11.1 Introduction of VIP Technology

Thermal insulation is considered one of the basic needs for survival of life. A large amount of energy is being consumed for temperature maintenance in various sectors. Many insulation materials and systems have been developed since the beginning of 20th Century, but extensive research started after the oil crises in 1973. The International Energy Agency (IEA) was established in 1974 to control the energy crises

---

Z. Chen (✉) · Q. Wu  
College of Material Science and Technology, Nanjing University of Aeronautics and Astronautics,  
Nanjing 211106, P. R. China  
e-mail: [czf\\_msc@nuaa.edu.cn](mailto:czf_msc@nuaa.edu.cn)

Q. Wu  
e-mail: [wq941130@sina.cn](mailto:wq941130@sina.cn)

by reducing energy usage. Worldwide, consumption for space heating and cooling (about 40%). That is why, during the last few decades, generations of researchers have focused their development work on thermal insulation materials, and systems for building usage. Many traditional thermal insulation materials used so far are organic wool, expanded polystyrene (EPS), extruded polystyrene (XPS), polyurethane (PUR) and polyisocyanurate (PIR) foams, fiberglass, mineral wool, and cellulose fiber insulation, cork, and many others. In time, these traditional materials have significantly improved their thermal insulation characteristics, but following the continuously increasing building code requirements for thermal insulation, they still require significant amount of space for achieving the desired R-values. As architects prescribe more and more space for thermal insulation, it compromises the valuable real-estate area, especially in large cities. Besides this, a low fire resistance in the case of some insulations, high maintenance cost, and short service life, additionally reduce the scale of their applications—see: IEA/ECBCS (2005), OECD/IEA (2015), Alam et al. (2011), Chen et al. (2011), Kalnæs and Jelle (2014), Schiavoni et al. (2016), Lim et al. (2017).

The idea of vacuum insulation was developed from the concept proposed by Sir James Dewar in 1892. This type of thermal insulation has been well described by Fricke (2005), ASTM-C1484-10 (2018). Vacuum insulation panels were first introduced by the refrigerator industry during the 1980s (Johansson et al. 2016). In 1990s, the application of this technology was extended to building insulation (Johansson 2012). Germany and Switzerland pioneered in 1998/1999 in conducting early application performance tests of VIPs in buildings—Caps (2006). Later, the original Dewar’s idea was transitioned into the flat panels by placing the load-bearing core material between the evacuated impermeable envelope. The thermal conductivity of VIPs compared to other traditional insulation materials is shown in Fig. 11.1.

Figure 11.2 explains VIP structure. A VIP consists of three major parts, the highly porous core material, the envelope encapsulating the core, and the getter material. The core materials are mostly powders, fibers and/or foams. Envelopes usually consist

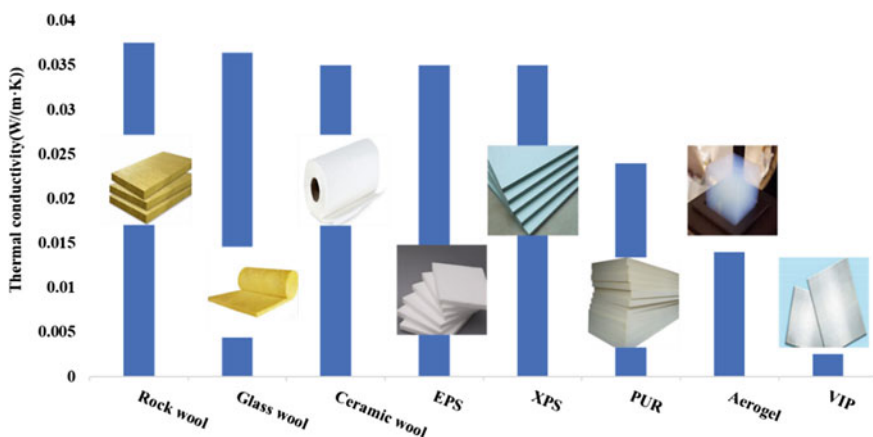
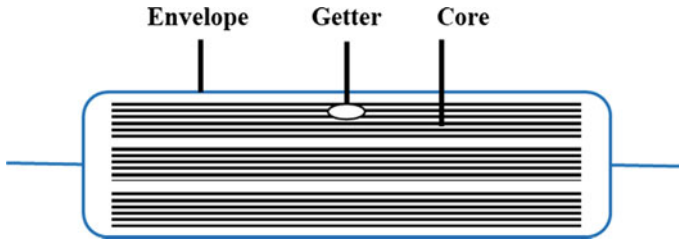


Fig. 11.1 Comparison of the thermal conductivity of various insulations



**Fig. 11.2** Schematic diagram of VIP

of metallic foils, polymeric films, or metalized polymeric films. Getters are added or placed in the core material.

So far, VIP technology has over 60-years long history and has gone through four main stages of development.

(1) The initial formation stage

In 1952, Bovenkerk filed the first patent for flat insulation and pioneered the development of a flat-shaped VIP filled with fine powder—see: Bovenkerk (1952). At that time, VIPs were mainly used in aviation, aerospace, and military fields to avoid the loss of control of aircraft and missiles in hot and cold environmental conditions.

(2) The rapid development stage

In the 1970s, NASA designed a two-inch thick vapor-phase silica VIP and used it in building walls that were six inches thick. Kaganer (1969) thoroughly investigated the heat transfer mechanism of fiber- and powder-based, and multi-layer materials through theoretical and experimental analysis. He specified the key advantages of VIPs, which played an invaluable role in the early development of this technology. Later, Shimada and Katto (1983) adopted the VIP concept into several other products, including for example a solar collector application. In the 1980s, VIPs packed with powders and fiber felt were used in high-temperature sodium-sulphur batteries—Caps et al. (1984). During this time, VIPs have been analysed and optimized for many times. Further, the VIP fabrication technology was greatly improved, as well.

(3) Multiple forms of development stage.

In 1990s, in Hanau, Germany, VIPs using a barrier plastic film coated with precipitated silica were developed for refrigerator insulation. Because of very low permeability and high durability, several companies used metal enclosures for VIPs at that time. Owens Corning developed a 75  $\mu\text{m}$  thick fibrous rigid VIP using steel sheet as envelope. Messerschmitt-Bolkow-Blohm GmbH (MBB) developed VIPs with a 100  $\mu\text{m}$  sheet steel casing and a diatomite filling ( $\rho \approx 400 \text{ kg/m}^3$ ). Dow Chemical has developed a low cost, easy to manufacture, easy to cut, and easy to process polystyrene and polyurethane foam core materials, as described by Bendergast and Malone (1999). Lyman and Neeser

(2005) designed the edges and corners of VIP into rounded corners to eliminate or reduce the deformation of the edges and corners caused by the stress concentration in the vacuum of VIP. In this stage, the preparation technology of VIP has been further improved. A large number of research and development institutions competed to join in the development of VIPs, supporting the growing industrial production of VIPs.

(4) Multi-field, cross-industry development and application stage.

At the beginning of the 21st century, Yamada (2005) used the block design technology to produce a “chip-vacuum” structure of VIP, composed of multiple independent vacuum cells. This structure is capable to not-only effectively avoid the failure of the whole VIP block caused by the damage of few vacuum cells, but also can be used in the thermal insulation equipment and containers with complex shapes through flexible design, thus expanding the application field of VIPs. Jung et al. (2014), developed a novel design of VIPs with double-core and double-membrane material structure, which greatly improved the service life of VIPs. In addition, a variety of specially shaped VIP configurations (such as cylinder, polygon, curved structure, back seal structure, vent structure, surface with edges, surface pits, surface with grooves, pre-anchorage holes and pre-set half-moon holes) have been developed. They can be applied in many fields where conventional flat vacuum panels cannot be easily used. Also, the application field of VIPs has been gradually extended to refrigerators, freezers, cold chain logistics, vending machines, medical refrigeration, high-performance, energy efficient water heaters, building energy conservation, and other fields. As a result, VIPs became a well-received product for wide range of customers.

## 11.2 VIP Basic Structure and Key Components

### 11.2.1 Most Commonly Used VIP Core Materials

In VIPs, the core material is responsible for providing the thermal insulation, as well as mechanical stability for the entire panel. For enhanced thermal performance, the internal structure of the core material must meet various requirements, to allow unique heat transfer phenomena. Per Alam et al. (2011), and Kalnæs and Jelle (2014), the above requirements are as follow:

1. The pore diameter of the core material should be tiny and fine. A very low inner pressure is required in the evacuated panel to maintain the low gas conductivity. Since, it is not possible for the polymeric envelopes to maintain the required vacuum level for a long time, metallic foils, or multilayer plastic-metal membranes are favoured for VIP envelopes. Also, core materials with nano-porous structures are preferred for control of gaseous and solid heat conduction.

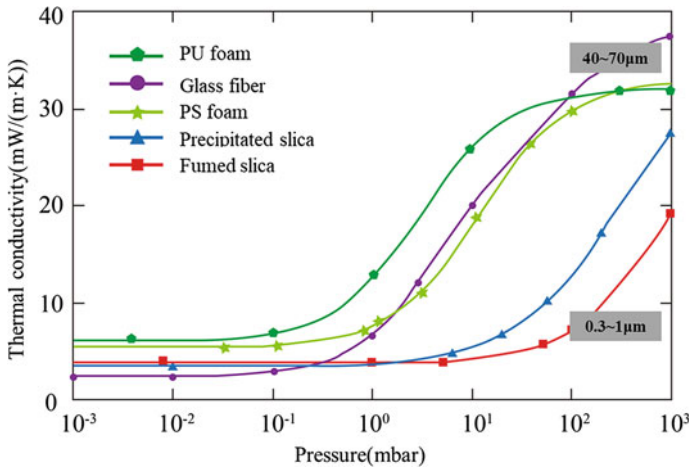


**Fig. 11.3** The relationship between thermal conductivity of VIPs and inner pressure for different core material. Sources: VIP, Bau-De,<sup>1</sup> Jung et al. (2014)

2. The pore structure of a core material should be 100% open, to evaporate the residual gases entrapped in the core material due to fabrication and variety of chemical reactions (depends on a type of the core material), which are taking place during the service time.
3. The core material should be capable of withstanding external compressive forces. The inner pressure of the VIP is significantly lower than the external atmospheric pressure. Therefore, the insulation materials that could resist such compressive forces and do not collapse under vacuum are preferred for a use in VIPs.
4. The core materials need to be opaque to the infrared radiation. This is essential to control radiative heat exchange across the panel.

Various types of insulation materials such as powders, foams, and fibers, etc. are used as a core material in VIPs. Figure 11.3 shows thermal conductivity of core materials, as a function of pore size, and at different gas pressure levels. It is noticeable that the critical pressure (at a point where thermal conductivity of the core sharply increases) can be significantly higher in the case of VIPs with smaller pore diameters (preferably nano size) core materials. This explains why VIPs with smaller pores usually exhibit longer service life. Very often, the core material selection is based on a type of application. Several commonly used VIP core materials are discussed in the section below.

<sup>1</sup> [http://vip-bau.de/e\\_pages/technology/vip/howtheywork.htm](http://vip-bau.de/e_pages/technology/vip/howtheywork.htm).



### 11.2.1.1 Powders Used as VIP Cores

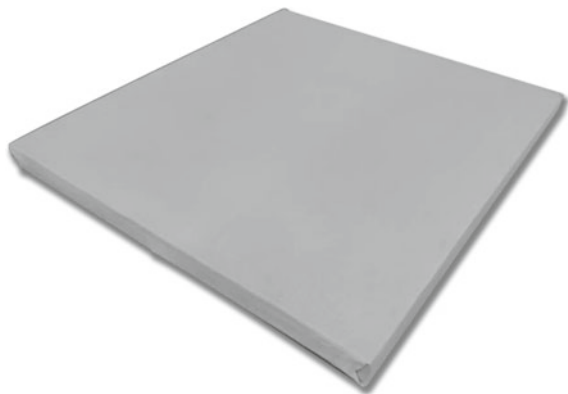
Powder core materials are most commonly used in VIPs serving as a building insulation. This is because of their relatively better insulation properties and service life, when compared to fiber or cellular plastic cores. The mainly used raw powder core materials include fumed silica, precipitated silica, or micro silica. Table 11.1 contains an example mixing formula used for production of the powder cores. Figure 11.3 shows that thermal conductivity of fumed silica, as a function of gas pressure, is much lower, compared to other types of core materials. The internal structure of a core material influences the overall thermal behavior of a whole panel. Figure 11.4 shows a VIP panel containing fumed silica core. The bulk density of the fumed silica core, compared to other conventional insulations, is nearly one order of magnitude higher. The specific surface area of fumed silica core materials is high because of its higher porosity ratio, which was ~90%.

The inner pressure of VIP, at which  $\lambda$  increases by half of the value of thermal conductivity of still air, is usually denoted as  $P_{1/2}$ —see: IEA/ECBCS (2005). A typical value of  $P_{1/2}$  for fumed silica is about ~630 mbar, while for a conventional PUR foam it is only ~2.6 mbar. This proves that fumed silica is very suitable for a usage as a core material in VIPs applied in buildings. But there are also many known shortcomings for its use as a core material. For example, (i) During the vacuum process, very light fumed silica particles are easy to extract, so they can block vacuum

**Table 11.1** An example formula of a silica-based VIP core

Component	Percent volume (%)
Micro silica	40–60
Fumed silica	20–40
Reinforced fibers	5–10
Opacifier	3–6
Getter	3–10

**Fig. 11.4** VIP with core material made of fumed silica



pump equipment; (ii) In the case when the drying of a core material is insufficient, the existence of large amount of moisture may compromise the process of vacuum packaging, and may also significantly reduce the heat insulation performance of a final VIP product, as well as its durability; (iii) As mentioned earlier, powders used in VIP production are very light, and subsequent the high amount of dust in the air may cause a variety of health problems.

### 11.2.1.2 VIPs Using Fiber Cores

A great variety of materials are today used in production of VIPs containing fiber cores. The most typical include glass fibers (glass wool and chopped strand glass fibers), rock wool, and variety of synthetic fibers. The thermal conductivity of VIPs with fiber cores is strongly related to the fiber average diameters, length, quantity, crimp degree, arrangement, and a pore structure in the fiber core. Fiber cores are usually produced as a laminated matter, formed by the lap laying of fibers. However, fiber directions/arrangement can vary in many different products.

Glass wool core materials (Fig. 11.5) are the most commonly used today. They have numerous advantages, which include a low cost, low density, and low thermal conductivity. At the same time, fiber cores show strong plasticity, which meant they can be easily fabricated into various shapes of VIPs. Figure 11.6 shows various VIP shapes using core materials made of glass wool.

The average diameter of glass wool used as core materials is between 1.6 and 3.0  $\mu\text{m}$ , and the average length of fibers ranges from 7 to 15 mm. Table 11.2 lists the example composition of glass wool in VIPs.

**Fig. 11.5** Core materials made of glass wool

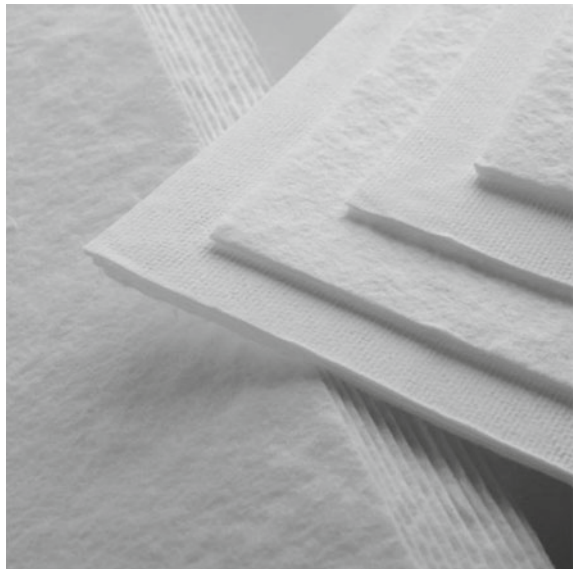


**Fig. 11.6** Various shapes of VIPs with cores made of glass wool

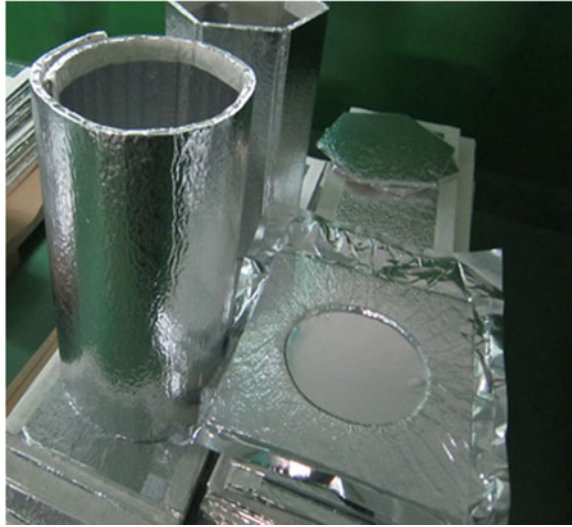


**Table 11.2** The example composition of glass wool used in VIP

Component	Percent weight (%)
SiO <sub>2</sub>	65
K <sub>2</sub> O + Na <sub>2</sub> O	16.5
CaO	7
MgO	2.6
Al <sub>2</sub> O <sub>3</sub>	2.8
B <sub>2</sub> O <sub>3</sub>	6
Fe <sub>2</sub> O <sub>3</sub>	0.6

Source Chen et al. (2015)

Comparing to glass wool, the chopped strand glass fibers are crude, with diameters ranging from 7 to 9  $\mu\text{m}$ . With the crude fibers, the pore sizes are larger than in the case of glass wool core materials. Thanks to this, it is easier to make vacuum cores from chopped strand glass fibers. This leads to lower thermal conductivity. However, because of high level of vacuum used, VIPs with these types of cores have a short service life.

The VIP cores using glass fibers have an open porous structure, they are flexible and have porosity level of  $\geq 90\%$ . Usually, the glass fiber cores are made of several laminated glass fiber blankets. The microstructure and performance parameters may significantly differ for different types of glass fiber mats, made by different manufacturers—Di et al. (2013). These differences in characteristics are usually due to fiber architecture and orientation, affecting the heat transfer mechanism. The heat transfer paths and solid skeleton microstructure of the constituent glass fibers highly

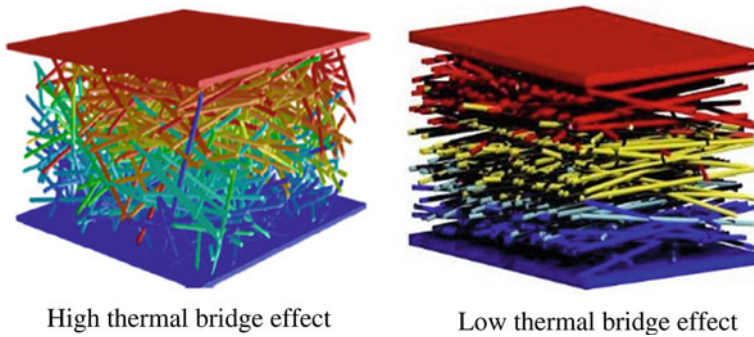


**Fig. 11.7** Structure of fiber core material

impact the performance of a core material as thermal insulation—see: Boafu et al. (2014), Wu et al. (2012).

The most favorable fiber alignment for thermal insulation is the one which is perpendicular to the direction of the heat transfer, as it increases the heat flow path, which weakens the thermal bridge effect. Besides this, the fiber's interfaces create a barrier to the heat flow—see: Wu et al. (2012), Alam et al. (2014), Kim and Song (2013). Figure 11.7 depicts the structure of the fiber core material. The vertical direction is the heat transfer direction, and the fibers in the core material are disorderly arranged. The fibers contact each other, and in the direction of heat transfer, they form a heat conduction path, so that the solid phase heat conduction increases, which is not conducive to core insulation.

Figure 11.3 shows that thermal conductivity of VIPs with glass fibers core materials may be as low as  $1.5 \text{ mW}/(\text{m K})$  under 1 mbar gas pressure. However, the thermal conductivity increases with the rise in inner pressure. This is mainly because of the larger pore sizes of the core material, where  $\lambda_g$  increases with the rise in gas pressure, which decreases the vacuum level (see: Kalnæs and Jelle (2014), Kim and Song (2013)]. This leads to the short service life this type of VIPs. The service life of VIPs with glass fibers core materials of and getter is about 15 years, which is significantly shorter compared to the building's lifespan. That is why VIPs with glass fibers core materials are mostly used in applications with lower lifespan requirements, such as, refrigerators, cold chain, and shipping container.

Figure 11.8 shows the influence of the fibers' length and diameter on the thermal conductivity of the VIPs with glass fiber core materials. When the dimension diameter is relatively thick, such as diameter for example  $7.0 \mu\text{m}$ , the thermal conductivity of the VIPs is less affected by the fibers length. With the increase or decrease of the fiber length, the thermal conductivity fluctuates less, and the thermal conductivity value is generally between  $2.9$  and  $3.5 \text{ mW}/(\text{m}\cdot\text{K})$ . In such material, the distribution of fibers appears to be anisotropic, and the number of fibers is relatively small. This shortens the heat transfer journey, which is not conducive to reducing solid heat transfer, so that the thermal conductivity increases.

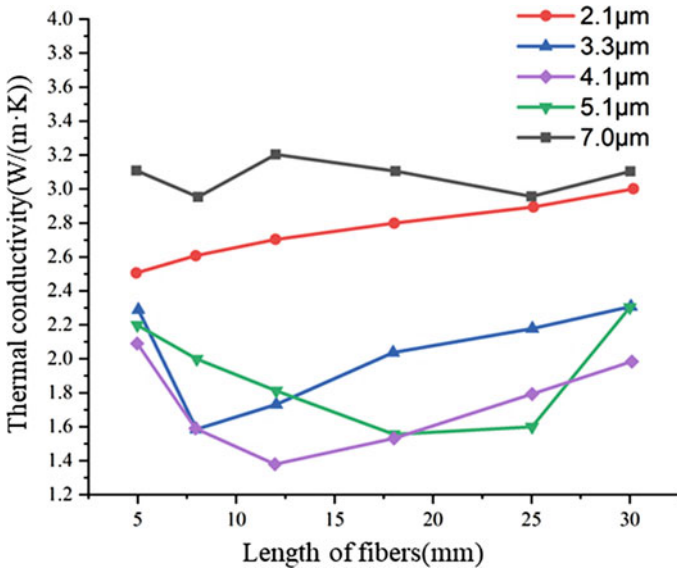


**Fig. 11.8** Influence of the fiber length and diameter on thermal conductivity of VIP with wet core material

When the fiber diameter decreased to below  $5.1 \mu\text{m}$ , the thermal conductivity of VIPs decreases. However, it is sensitive to the increase of the length of fibers, exhibiting the highest and lowest conductivity values of  $2.3 \text{ mW}/(\text{m}\cdot\text{K})$  and  $1.5 \text{ mW}/(\text{m}\cdot\text{K})$ , respectively. When the length of fibers is around  $5 \text{ mm}$ , more fibers are distributed along the thickness direction, which is the temperature gradient direction, which is not helping in reducing the solid heat transfer. When the fiber length increases to  $18 \text{ mm}$ , the thermal conductivity is the lowest. With the fiber length increasing, the fiber tend to be bended, and the content of the thermocline fiber increases, so that the thermal bridge effect between the layers of the core material is strengthened. As a result, the thermal conductivity is increased.

Oppositely, when the fiber diameter is  $4.1 \mu\text{m}$ , the thermal conductivity of the VIPs with the fiber length of  $12 \text{ mm}$  is the lowest, which is around  $1.3 \text{ mW}/(\text{m}\cdot\text{K})$  and, consequently, the overall thermal conductivity is the lowest.

However, when the fiber diameter continues to further decrease, the thermal conductivity is becoming to increase as well. For example, when the fiber diameter is only  $2.1 \mu\text{m}$ , the thermal conductivity of the VIPs is gradually increasing, following the increase of the fiber length, and the overall thermal conductivity is higher than  $2.0 \text{ mW}/(\text{m}\cdot\text{K})$ . The increase of the content of bent fiber is the main reason for this phenomenon.

It has also been shown that VIP internal pressure and resulting thermal conductivity are not fully stable—especially during the time period just after production. Figure 11.9 shows the relationship between thermal conductivity of VIPs with glass fibers core and the time of usage. All curves show wavy changes with the prolonging

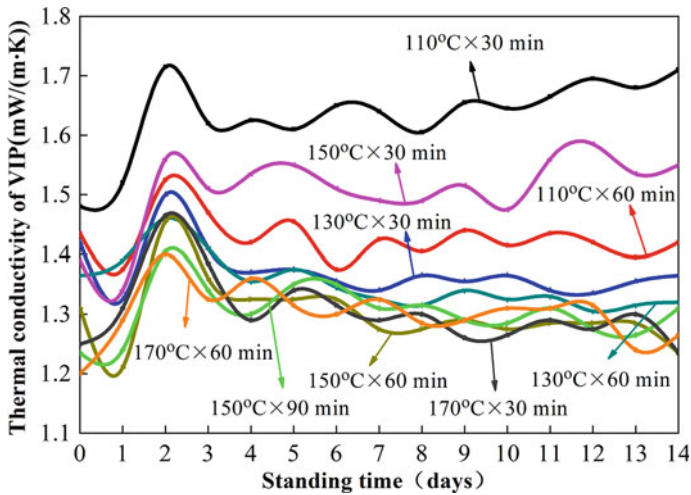


**Fig. 11.9** The relationship between thermal conductivity of VIP with glass fibers core and the time of usage

of the time of use. This is because in VIPs with glass fibers, degassing processes in the core material and the envelope are large under the vacuum. Thanks to the use of the CaO desiccant inside VIPs with glass fibers, the gas which is released by the envelope and the core is adsorbed by CaO. Since these processes are not fully constant (the periods of gas accumulation), the thermal conductivity of VIPs with glass fiber cores fluctuates. As shown in Fig. 11.9, during the second day, the gas content inside VIP with glass fibers reaches the highest value, and the thermal conductivity of VIP also reaches the maximum. However, the degassing capacity of the core and envelope materials is limited. With the prolongation of the time of the usage, the gas inside the VIP caused by the material degassing is almost completely absorbed by CaO.

It can be observed in Fig. 11.9 that thermal conductivity of the VIP with the glass fibers core prepared by the core material drying at 170 °C for 60 min is the lowest. Thermal conductivity of a VIP with glass fiber core, prepared by drying glass fibers at 110 °C for 30 min, is higher and increases in a fluctuating pattern, following the increase of the use time. It can be seen that thermal conductivities of VIPs with glass fibers cores, prepared under 7 different drying regimes, reach the maximum value during the second day and tend to stabilize with the prolonging usage time. Presented values of thermal conductivities along the usage time (where glass fibers core materials were dried for 60 and 90 min at 150 and 170 °C for 60 min) indicate that thermal conductivities are getting lower with the time of usage and quite stable. This is mostly due to the longer core drying time (more than or equal to 60 min) and higher drying temperatures (more than or equal to 150 °C) to ensure the core material is completely dry.

### 11.2.1.3 Utilization of Polymeric Foams as VIP Cores

Plastic foams are widely used as insulation without a need of being packaged as VIP cores. The most commonly used polymeric foam insulations are Polyurethane (PUR) and expanded polystyrene (EPS). The first core materials which were tried in VIPs were PUR foams. The pore size of open-cell for Polyurethane (PUR) and expanded polystyrene (EPS) ranging from 30 to 250  $\mu\text{m}$  made it suitable for VIP core applications—see: Alam et al. (2011), Kalnæs and Jelle (2014).

PUR foam can withstand high mechanical loads and has an open pore internal structure, which is required for the VP core materials. PUR foams typically have larger pore sizes, thus they require a lower vacuum level (below 1 mbar) to attain the expected thermal conductivity—Kalnæs and Jelle (2014). This thermal conductivity can be reduced by reducing the pore sizes. However, as discussed by Stec and Hull (2011), under the fire conditions, PUR foams release highly toxic gases such as carbon monoxide (CO), hydrogen cyanide (HCN) and other harmful emissions. Due to the flammable nature of these organic insulation materials, strict regulations were passed on their usage in buildings. In China, after the 2009 Beijing Television Cultural Centre fire<sup>2</sup> and 2010 Shanghai fire<sup>3</sup> new code regulations were introduced. Even though PUR foam core VIPs are less expensive to produce, they are now considered inappropriate for building applications, because of their short useful lifetime and high flammability.

In VIPs with foam cores, the inner core pressure is an important factor affecting the thermal insulation performance. When these VIPs are sealed, the foam brittleness, which causes local material breaking, and a content of closed cells (usually several per cent of a total) lead to reduced performance. With increased number of small foam fragments, gas slowly escapes over the time from their closed cells, which increases the inner pressure of the VIPs and thus increasing thermal conductivity. In addition, the in these closed cell foams, very small amounts of volatile components such as foaming agents and amine catalysts are dissolved in the foam skeleton. During the time, they slowly escape, resulting in the inner pressure increasing.

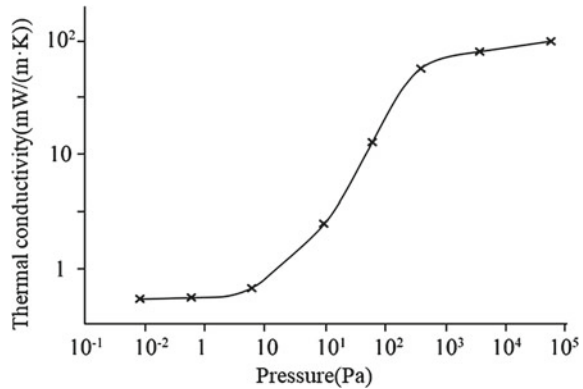
Figure 11.10 shows the variation of thermal conductivity as a function of gas for VIPs with cores made of the open-cell PUR foam. It can be observed that, when the residual gas pressure drops from the atmospheric pressure to 10 kPa, thermal conductivity remains constant. That means that in this pressure range, the inner gas pressure shows no serious impact on thermal conductivity. When the pressure is further reduced, that is, when the pressure is between 1 and 10<sup>3</sup> Pa, the thermal conductivity almost linearly changes with the pressure (with the decrease of the pressure, the thermal conductivity decreases). When the pressure is lower than 1 Pa, the thermal conductivity is completely dependent on the radiation heat transfer and solid thermal conductivity, which tend to be constant. Based on the data shown in Fig. 11.10, it can be concluded that the pressure in the panel should be lower than

---

<sup>2</sup> [https://en.wikipedia.org/wiki/Beijing\\_Television\\_Cultural\\_Center\\_fire](https://en.wikipedia.org/wiki/Beijing_Television_Cultural_Center_fire).

<sup>3</sup> [https://en.wikipedia.org/wiki/2010\\_Shanghai\\_fire](https://en.wikipedia.org/wiki/2010_Shanghai_fire).

**Fig. 11.10** The variation of thermal conductivity of VIPs with core materials of open-cell PUR with gas pressure



10 Pa if the foam VIPs were expected to exhibit the thermal conductivity below 0.8 mW/m·K.

### 11.2.2 VIP Envelope

The envelope is the outer skin of a VIP, which maintains the internal vacuum and prevents air and water permeation into the core. Envelope materials are expected to provide mechanical strength to the panel to withstand atmospheric pressure and handle stresses during transportation and installation. The thermal conductivity of the gas-insulated structural film is higher than that of the core material by 5–6 orders of magnitude, so there is usually a significant heat transfer present along the edge of the gas-insulated structural film, forming a thermal bridge effect. Although the gas-insulated structural envelopes perform the task of blocking the gas transport, they are not absolutely airtight. Gas penetrates into the vacuum panel through the surface of the diaphragm, and/or dissolves into the envelope through adsorption-diffusion, which has a great impact on the vacuum degree of the vacuum panel. This further affects the long-term VIP performance.

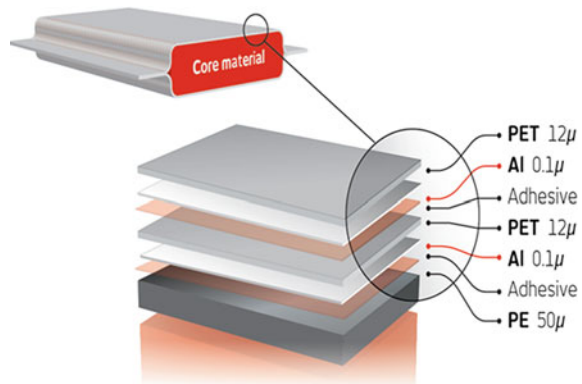
Usually, the envelope material needs to meet the following requirements:

1. Low water vapor transmission rate (WVTR) (less than 0.005 g/(m<sup>2</sup>·d)),
2. Low oxygen transmission rate (less than 0.002 cm<sup>3</sup>/(m<sup>2</sup>·d)),
3. Low thermal conductivity,
4. High mechanical strength, and
5. Ability to be thermally sealed.

For building applications, the water vapor transmission rate and oxygen transmission rate for the standard envelope should not exceed 0.0001 g m<sup>-2</sup> d<sup>-1</sup> and 0.001 cm<sup>3</sup> m<sup>-2</sup> d<sup>-1</sup> respectively to yield a useful lifetime of approximately 30–50 years—see; IEA/ECBCS (2005), Brunner et al. (2006).



**Fig. 11.11** The structure of VIP envelope



VIP envelope performance is highly dependent on its structure. Figure 11.11 shows a typical VIP envelope, which consists of three following material layers; (i) outer protective layer (ii) barrier layer (iii) inner sealing layer, each serving a distinct function—see: Alam et al. (2011), Kalnæs and Jelle (2014).

(1) VIP protective layer

It is the outmost layer of the envelope. It aims to make the panel more robust by protecting it from environmental and handling stresses. The material chosen for the envelope's protective layer should be able to resist the tearing or puncturing effect during transportation and installation. The protective layer usually includes polycarbonate film (PC), biaxially drawn polyester film (PET), biaxially drawn polyamide (BOPA) and biaxially drawn polypropylene (PP). Polyethylene terephthalate is the most commonly used material because of its low cost, as well as its tensile strength. Nylon-6, also known as polyamide, also is used; however, its high cost limits its application. It is also utilized as a substrate material for the barrier layer.

(2) Barrier layer

The middle layer of the multi-layered envelope that resists the gas and moisture permeation through the envelope is called a barrier layer. The number of barrier layers varies from one to three, depending on the application and anticipated the lifespan of the panel. Polypropylene (PP) and polyethylene terephthalate (PET) are commonly used for the barrier layer. Envelopes with Al foil (AF) barrier layer shows better WVTR and OTR index, but their higher thermal conductivity leads to the thermal bridging through the edge heat conduction. The edge thermal bridging can be reduced by replacing Al foil with a metalized polymer layer. However, the WVTR and OTR index for the metalized film (MF) is not as good as that of Al foil. It can be improved by increasing the number of MF barrier layers.

### (3) Sealing layer.

The sealing layer is the innermost layer of the multi-layered envelope that seals the core material into the laminated envelope. The sealing layer materials must have good sealing strength to withstand the panel's internal and external pressure. In the sealing process, a bond between two polymer layers is created by the hot-press method. For a stronger bond strength, a distinct balance between the temperature of the hot-pressing bars and applied pressing load is required. A good seal enhances the useful life of the panel by mitigating the leakage and puncturing effect. Conventionally Polyvinylidene chloride (PVDC), Low-Density Polyethylene (LDPE) and High-Density Polyethylene (HDPE) are used in VIPs as a reliable sealing layer—Brunner et al. (2006).

As the thermal performance of VIPs is highly dependent on the vacuum conservation inside VIPs, so the type and structure of the envelope are considered very important for maintaining the effectiveness of VIPs. The external environmental parameters, such as temperature and relative humidity, highly influence the gas and moisture permeation rates through the VIP envelope—Simmler and Brunner (2005). Thermal bridging around a VIP is also a factor that increases the panel's overall thermal conductance. The proportional decrease in the thermal bridging effects can be achieved by increasing the panel dimensions. In that case, a larger area is exposed to uniform heat losses—Wakili et al. (2004). The envelope structure and materials are usually selected based on application and environmental factors.

#### 11.2.2.1 Metal-Foil Envelopes

This type of envelope uses metallic foil as a barrier layer, which most often utilizes an aluminium foil. The research data has shown that if the thickness of the aluminium metallic layer in the range of 5–10  $\mu\text{m}$ , laminated in between PET as a protective layer and PE as a sealing layer, such envelopes show very high resistance to the gases and moisture permeation. This enhances the service life of such panels. These envelope structures are highly preferred for application in the regions where humidity ratio is high. However, high thermal conductivity ( $\lambda_{\text{Al}} = 210 \text{ W/m K}$ ) of aluminium, and its thickness contributes to the edge thermal conduction. The edge conduction of heat through the barrier layer led to the development of no-metallic and metalized materials that are alternatives of such metallic foils—see: Simmler and Brunner (2005), Wakili et al. (2004), Bouquerel et al. (2012).

#### 11.2.2.2 Metalized Polymer Film Envelopes

Metalized polymer film envelopes (MF) were designed to reduce the thermal bridging effect caused by the metallic barrier layer. A metalized polymer film is a barrier layer prepared by coating metals over the polymeric protective layer. The metalized film

has a lower thermal bridging value due to the thinner thickness of Al metalized. The number of MF varied in between 1 and 3 depending on the type of application. Multiple barrier layers of MF may show comparable protection from moisture and gases as that of AF. However, the reduced thickness of the metal barrier layer leads to the increase of the permeation rate with the time and thus to reduced service life of the VIP panel—Simmler and Brunner (2005).

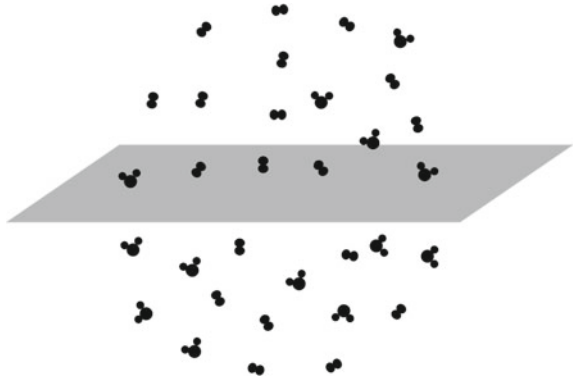
### 11.2.2.3 Fiberglass Cloth Envelopes

The dimensional stability and vacuum maintenance of the VIPs need highly careful handling during transportation and installation. The envelope material is exposed to mechanical stresses and has a high chance of being damaged during transportation or installation. Besides this, it will be corroded when exposed to alkaline environment. A fiberglass cloth (FGC) is added to the laminated envelope by hot press method as an additional protective layer. It has been used successfully in an increasing number of applications. A non-combustible FGC offers chemical and corrosion resistant, which withstand high mechanical stresses. It also provides surface and dimensional stability, and better acoustic properties. The FGC has better panel/wall surface interlocking ability and protects panels from localized alkaline cement—see: Chen et al. (2011), Caps (2006), Bofo et al. (2014). Especially, the VIPs with FGC are known in China as Super Thin Panel (STP, as shown in Fig. 11.12).



**Fig. 11.12** Photograph of VIP with fiberglass cloth envelope

**Fig. 11.13** Infiltration process of gas molecules



#### 11.2.2.4 Physical Properties of VIPs' Envelopes

##### Thermal Insulation Performance of Envelope

The thermal insulation performance of the envelope materials directly affects the overall thermal insulation performance of the VIP. The thermal conductivity of materials of envelope are usually as follows: (i) PVDC film is around  $0.13 \text{ W}/(\text{m}\cdot\text{K})$ , (ii) PET film— $0.15 \text{ W}/(\text{m}\cdot\text{K})$ , (iii) nylon film— $0.43 \text{ W}/(\text{m}\cdot\text{K})$ , (iv) polyethylene film— $1.005 \text{ W}/(\text{m}\cdot\text{K})$ , and (v) metal aluminum foil— $273 \text{ W}/(\text{m}\cdot\text{K})$ .

##### Permeability Principle

VIP envelopes are made of high molecular materials, which performs as a barrier to gas molecules, but they are not fully airtight. The gas-insulated structural envelope of polymer materials is mainly formed by the interweaving of polymer chains, which has the function of non-stop thermal motion. The thermal motion produces local fluctuations in the bond joints, which produces many intramolecular or intermolecular “gaps”.

With a concentration difference between the two sides of the VIP envelope, the gas phase molecules diffuse from the high concentration side to another side with lower concentration. Most researchers believe that the infiltration process of envelope is a single gas molecular diffusion process, belonging to the process of mass transfer, and following the permeation of gas molecules into solids, namely diffusion—stripping process (shown in Fig. 11.13): (1) Firstly, the gas molecules are adsorbed and dissolved on the surface of the envelope; (2) Subsequently, the gas molecules migrate and diffuse from the high concentration zone to the lower concentration zone; (3) Finally, the desorption process of gas molecules occurs on the other side of the envelope.

The adsorption of gas molecules on the surface of the gas barrier structural membrane is caused by the van der Waals force between the surface of the gas

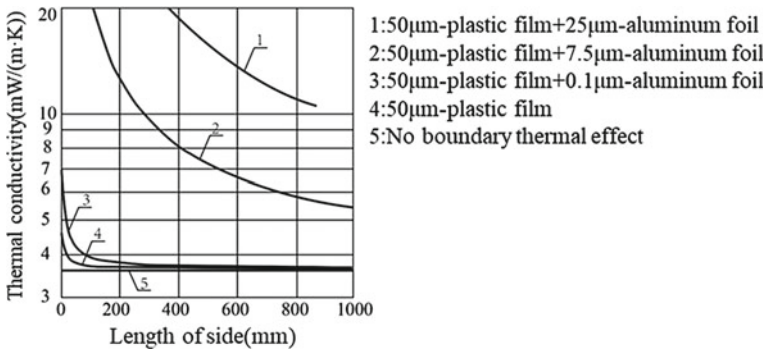


**Fig. 11.14** The relationship between side length and effective thermal conductivity of VIPs with different envelopes

barrier structural membrane and the gas molecules. Therefore, as long as the gas molecules contact the surface of the membrane, the adsorption phenomenon is generated. This adsorption phenomenon is reversible. When the environment changes after the adsorption, the adsorbed gas molecules may utilize energy from the surrounding, and then desorption occurs.

### Thermal Effect in Boundary

Assuming that the core material and boundary conditions of VIPs are the same, for a square VIP with a thickness of 25 mm, its effective thermal conductivity become a function of the side length of the VIPs. For the plastic film with a thickness of around 50  $\mu$ m, the boundary thermal effect can be ignored. Unfortunately, for VIPs with a plastic foam as the core material, the envelope of this thickness obviously can't meet the gas and vapor permeability requirements, and consequently, the service life expectation of the VIPs. Therefore, a metal and plastic composite membrane must be used as an envelope. For the thickness of metal coating in the envelope of around 0.1  $\mu$ m, the boundary thermal effect can be still ignored, when the side length of the VIP is greater than 150 mm. If the thickness of the metal film is increased in order to reduce the air permeability and prolong the VIP's service life, the thermal effect of the boundary will obviously reduce the thermal insulation performance. Figure 11.14 shows the relationship between the side length of a square VIP with several typical surface diaphragm materials and its effective thermal conductivity.

### 11.2.3 VIP Getter

The useful service life of the VIP is highly dependent on the vacuum maintenance inside the panel. Whereas the residual gases or moisture generated inside the panel

or permeated through envelope reduce the panel's internal vacuum which quickly reduces the service life of the panel.

The core materials and envelope with porous structure absorb water easily, and they release small amounts of water and gas ( $\text{CO}_2$ ,  $\text{H}_2\text{O}$ , etc.) due to the aging during an application time, thereby greatly reducing the internal vacuum of the VIPs. As the service time increases, the internal vacuum of the VIP gradually decreases, and the thermal insulation performance gradually deteriorates. Therefore, in order to prevent the variation of air pressure inside the VIP, from affecting the VIP's thermal insulation performance, an appropriate amount of getter is usually added to the VIP to absorb the internal gases.

Getters are generally added to core materials which are sensitive to internal pressure (i.e. plastic foams and core materials made of fibers). Getters reduce the core outgassing effects. After the VIPs are sealed, they absorb atmospheric gases and water vapor that may penetrate into the VIP through the envelope materials, as well as gases that can be released by the core and the envelope materials. After the core material of glass fibers is fully dried, the gas released is usually negligible, and the adsorption and precipitation of water vapor account for the main portion of thermal associated effects. Controlling the residual flux of the envelope material reduces the outgassing of the envelope materials. Inhalation speed, inhalation volume and powder particle size were the key factors in the getter design. The high inhalation speed ensures that the gas that penetrates into VIPs is absorbed in a short time. The inhalation volume is related to the service life of VIPs, and optimized particle sizes prevent the getters from failing before VIP being vacuumed. However, since thermal conductivity of the getter materials is usually high, the excessive addition of getters may lead to reduction of the VIPs overall thermal resistance. So, that factor needs to be carefully considered to optimize the panel performance and, at the same time, to control the amount of added getter.

Figures 11.15 and 11.16 are respectively showing the gas composition diagram in VIP at initial state and after two years. It can be seen on Fig. 11.15 that the residual gas composition in the panel at initial state is similar to the air composition, mainly including  $\text{N}_2$ ,  $\text{O}_2$ , a small amount of  $\text{H}_2\text{O}$ , and very low amounts of Ar and  $\text{H}_2$ .  $\text{H}_2$  is released by the VIP envelope, and other gases mainly come from the residual air after VIPs are vacuumed. Figure 11.16 shows that the residual gas composition in the panel is different from the initial state, with becoming higher presence of  $\text{H}_2$ , and keeping the presence of  $\text{H}_2\text{O}$ ,  $\text{N}_2$ ,  $\text{O}_2$ , CO and  $\text{CO}_2$ , as well as a trace of Ar. Among all of them,  $\text{H}_2$  is released by the core materials, the inner wall of envelopes, and internal organic matter. The weight of  $\text{H}_2$  is small and the release speed is relatively fast. Its thermal conductivity was about 7 times that of air. Therefore,  $\text{H}_2$  is very detrimental to the insulation performance of VIPs.  $\text{H}_2\text{O}$  mainly come from the penetration of water vapor form outside of the panels. The heat-sealing edge, the surface of envelope and the defects of corners have usually lower water blocking performance, which allows the moisture from the air to slowly infiltrate into the VIPs. Moisture is adsorbed in the core materials, which increases the solid phase thermal conductivity, and gaseous water heat transport level, which transfers the heat from the higher-temperature surface of a VIP to the low-temperature surface. It is happening

**Fig. 11.15** The gas composition diagram in VIP at initial state

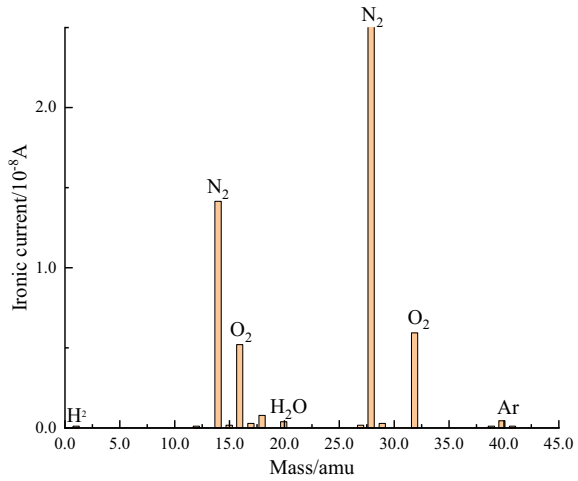
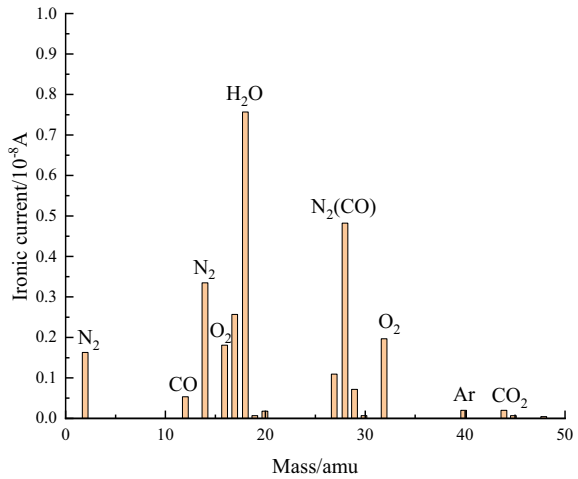


**Fig. 11.16** The gas composition diagram in VIP at initial state after 2 years



by absorbing the heat on the higher-temperature surface and transporting it to the low-temperature surface. Consequently, this process leads to the water condensation on the lower temperature side of the VIP and release of the heat, which represents a similar physical mechanism as in the heat pipe. This phenomenon significantly reduces the thermal insulation performance of VIPs. Other gases mainly come from the penetration of air, and some CO and CO<sub>2</sub> are released by the core materials and envelopes of organic origin.

**Table 11.3** Getters used in VIPs

Composition	Ingredient	Absorbed gas
Desiccant	Highly active CaO nano powder	H <sub>2</sub> O, CO <sub>2</sub>
Desiccant + Oxidant	Highly active CaO nano powder + Catalytic oxide	H <sub>2</sub> O, CO <sub>2</sub> , CO
Desiccant + Oxidant + Getter alloy	Highly active CaO nano powder + Catalytic oxide + Ba/Zr base alloy	H <sub>2</sub> O, H <sub>2</sub> , O <sub>2</sub> , N <sub>2</sub> , CO <sub>2</sub> , CO

### 11.2.3.1 Types of Getters

Getters used in VIPs mainly utilize chemical adsorption processes, while pure physical adsorption materials are not applicable due to a large amount of air released under the vacuum. Table 11.3 shows three main types of getters used in VIPs.

Among them, the oxides with catalytic effect exhibit high catalytic efficiency for the oxidation reaction of CO, H<sub>2</sub> and hydrocarbons. During this process the catalyst, CO and H<sub>2</sub> react with oxygen inside the VIP to generate CO<sub>2</sub> and H<sub>2</sub>O, which are later absorbed by CaO, and the alloy components mainly absorb N<sub>2</sub>.

The getters are highly selective. Before adding getter, the appropriate getter must be selected according to the core material and barrier film of the VIP, and the service life and internal gas volume of the VIPs must be predicted to determine the amount of getter added.

## 11.2.4 VIP Opacifier

### 11.2.4.1 Types of VIP Opacifiers

Some VIP core materials (i.e. powders) usually show low radiation resistance. Thus, opacifiers are often added to mitigate the penetration of radiation through the core.

The effect of opacifiers is to reduce the radiant heat transfer in VIPs. If VIPs are used at room temperature, it may be necessary to choose opacifiers with strong absorption and scattering of thermal radiation. If VIPs are used at high temperature, the opacifier also needs to have a high melting point and good heat resistance, as discussed by Jelle et al. (2014). The content of opacifier in VIPs should be optimized at the VIP's design stage. Too much opacifiers may increase the solid heat conduction of a core material. But too little, may show no visible effect on reducing thermal radiation.

Singh et al. (2015) studied the effect of the infrared inhibition property of carbon black, SiC and TiO<sub>2</sub> and their addition amount on the thermal conductivity of VNO<sub>2</sub> composite core material. The result showed that carbon black was the best opacifier, which made the thermal conductivity of VNO<sub>2</sub> VIP lower than 4 mW/(m K). Caps and Fricke (2000) studied the infrared inhibition property of carbon black, Fe<sub>3</sub>O<sub>4</sub>, SiC and



TiO<sub>2</sub> in the composite core material of perlite, silica and vaporous silica. The result showed that the initial thermal conductivity of VIPs with added opacifiers was about 3 mW/(m·K), and the thermal conductivity was still lower than 5 mW/(m·K) at 1000–2000 Pa. Feng et al. (2010) studied the high temperature heat insulation performance of gaseous silica composite core materials adding different amounts of SiC, ZrSiO<sub>4</sub>, KT<sub>6</sub> and BN, and the result showed that the composite core materials adding SiC had the best high temperature heat insulation performance. When the addition of SiC increased from 0 to 25 wt.%, the effective specific extinction coefficient of the composite core material increased greatly, and it had a very strong shading effect.

## 11.3 Heat Transfer Modes in VIPs

### 11.3.1 Heat Transfer Theory

There are three basic modes of heat transfer: heat conduction, convection and radiation. This section mainly introduces the modes of heat conduction and the heat transfer process in different modes of heat conduction.

#### 11.3.1.1 Heat Conduction

Heat conduction is one of the three basic modes of thermal energy transport and is involved in virtually all process heat-transfer operations. Heat conduction is the transfer of internal thermal energy by the collisions of microscopic particles and movement of electrons within a body. The microscopic particles in the heat conduction can be molecules, atoms, and electrons. Internal energy includes kinematic and potential energy of microscopic particles. For example, Fig. 11.17 depicts a case where the internal heat of the solid is transferred from the high temperature to the low temperature.

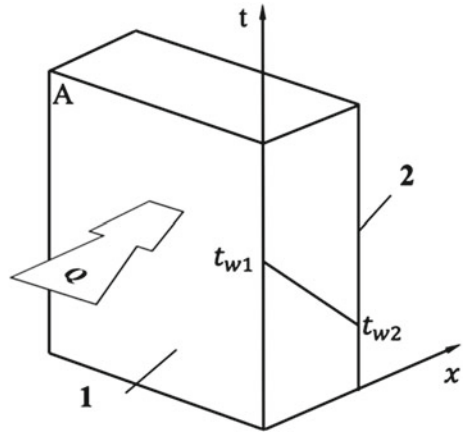
Heat conduction in homogeneous solid materials is governed by the Fourier's Law, which states that the time rate of heat transfer through a material is proportional to the negative gradient in the temperature and to the area, at right angles to that gradient, through which the heat flows. The rate of heat transfer by conduction can be expressed as follows:

$$Q = -\lambda \cdot A \frac{dt}{dx} \quad (11.3.1)$$

where,  $Q$  is the heat flow of a given area per unit time, and the unit is W;  $\lambda$  is the ratio coefficient (thermal conductivity), in units of W/(m·K);  $A$  is the area of given panel, and the unit is m<sup>2</sup>;  $\frac{dt}{dx}$  is the temperature gradient.

In engineering, heat flux is usually used to represent heat input, and Eq. (11.3.1) can be converted into the following equation:

**Fig. 11.17** One-dimensional thermal conductivity model of flat panel



$$q = \frac{Q}{A} = -\lambda \frac{dt}{dx} \quad (11.3.2)$$

where,  $q$  is the heat flux in units  $W/m^2$ .

Fourier's law is also called the fundamental law of heat conduction. The expressions of Eqs. (11.3.1) and (11.3.2) are expressions of Fourier's law under one-dimensional steady-state conditions.

Thermal conductivity is a basic parameter to characterize the thermal conductivity of materials, the unit of which is  $W/(m \cdot K)$ . The thermal conductivity value of different materials is different, even if it is the same material, the thermal conductivity value is still related to temperature and other factors. Generally speaking, metal materials have the highest thermal conductivity, and good conductive materials (such as silver and copper) are also good thermal conductivity, followed by liquid; the gas is the smallest.

### 11.3.1.2 Heat Transfer by Convection

The relative displacement between different parts of the fluid is caused by macro motion of the fluids, and the heat transfer process caused by the mutual mixing of cold and hot fluids is called heat convection. Heat convection can only occur in a fluid, and because the molecules in the fluid are moving irregularly at the same time, heat convection must be accompanied by heat conduction.

Convection heat transfer can be divided into natural convection and forced convection. Natural convection is a spontaneous mass diffusion exchange process, such as the spontaneous upward migration of hot air, due to the temperature gradient in each part of the fluid due to the non-uniformity of heat and cold. Forced convection is the flow of forced diffusion by pressure difference which caused by fans, pumps and so on.

The basic formula of convective heat transfer is Newton's cooling formula:

When the fluid is heated:

$$q = h(t_w - t_f) \quad (11.3.3)$$

When the fluid is cooled:

$$q = h(t_f - t_w) \quad (11.3.4)$$

Let  $\Delta t = |t_w - t_f|$ , then Newton cooling formula can be expressed as

$$q = h \cdot \Delta t \quad (11.3.5)$$

$$Q = h \cdot A \cdot \Delta t \quad (11.3.6)$$

The surface heat transfer coefficient is related to many factors in the process of convective heat transfer, including the shape of the heat transfer surface, flow rate, density and so on. Therefore, Eqs. (11.3.3)–(11.3.6) have no practical application value, and only the definition of surface heat transfer coefficient is given. In practical engineering application, it is necessary to calculate the surface heat transfer coefficient under the specific application environment of engineering application.

### 11.3.1.3 Heat Transfer by Radiation

The way an object transmits energy by radiating infrared light is called thermal radiation. All objects in nature are constantly radiating heat into space and absorbing heat radiation from other objects at the same time. The process of heat transfer between objects through radiation is called radiative heat transfer, also known as radiation heat transfer. When the object is in thermal equilibrium with its surroundings, the heat transferred by radiation is zero, but this is a dynamic equilibrium, and the process of radiation and absorption is still going on. Different from heat conduction and heat convection, which must rely on the medium to conduct heat, heat radiation can be transferred in vacuum and radiant energy is transferred most effectively in vacuum. This is the basic characteristic of heat radiation, which is different from heat conduction and convection.

The experimental results show that the radiation capacity of an object is related to the temperature, and the radiation and absorption capacity of different objects are also very different at the same temperature. In the process of exploring the law of thermal radiation, Stefan-Boltzmann introduced the concept of blackbody radiation. The so-called blackbody refers to an object that can absorb all the thermal radiation energy on its surface.

The heat radiated by a black body per unit time follows Stefan - Boltzmann's law:

$$Q = A \cdot \sigma \cdot T^4 \quad (11.3.7)$$

where,  $T$  is the thermodynamic problem of the black body, and the unit is  $K$ ;  $\sigma$  is Stefan-Boltzmann constant (blackbody radiation constant), with the value of  $5.67 \times 10^{-8} \text{ W}/(\text{m}^2 \cdot \text{K}^4)$ ;  $A$  is the radiation surface area, and the unit is  $\text{m}^2$ .

The radiation capacity of any actual object is less than that of a black body at the same temperature. The revised Stefan Boltzmann formula can be used to calculate the radiant heat flux of the actual object.

$$Q = \varepsilon \cdot A \cdot \sigma \cdot T^4 \quad (11.3.8)$$

where,  $\varepsilon$  is the emissivity of the object, also known as the blackness.

Stefan Boltzmann's law is the basis of radiant heat transfer calculation.

#### 11.3.1.4 Heat Transfer Equation

In the daily environment, as long as the indoor and outdoor temperatures are not the same, the indoor and outdoor air carries on the heat exchange through the walls all the time. In many industrial heat exchange equipment, the hot and cold fluids for heat exchange are often located on both sides of the solid wall. The transfer of heat by the fluid on one side of the wall to the fluid on the other side is called heat transfer. This is a typical heat transfer process often encountered in engineering technology, which requires necessary research and discussion.

For the heat transfer process in which hot and cold fluids exchange heat through a large flat wall, in the steady state, the heat transfer process involves three links in series: (1) Heat transfer from the hot fluid to the high temperature side of the wall; (2) Heat transfer from the high temperature side of the wall to the low temperature side of the wall, i.e. heat conduction through the solid wall; (3) Heat transfer from the low-temperature side of the wall to the cold fluid. Since it's a steady-state process, the heat flux  $Q$  is the same for each link in the series.

For the heat transfer process in Fig. 11.18, the heat flow can be expressed as follows:

$$Q = Ah_1(t_{f1} - t_{w1}) \quad (11.3.9)$$

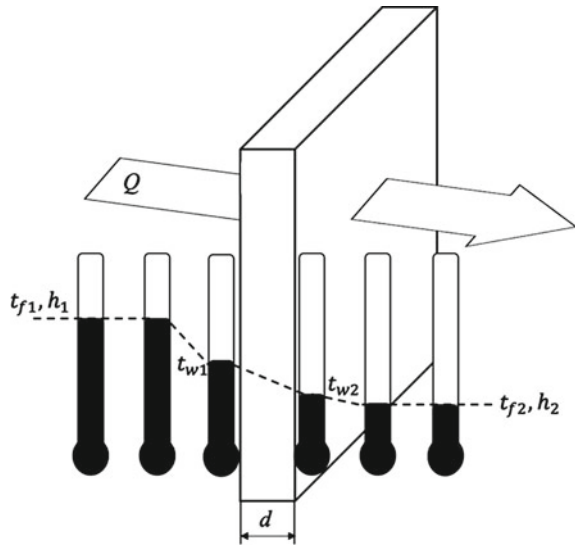
$$Q = A \frac{\lambda}{d}(t_{w1} - t_{w2}) \quad (11.3.10)$$

$$Q = Ah_2(t_{w2} - t_{f2}) \quad (11.3.11)$$

It can be obtained from Eqs. (11.3.9), (11.3.10) and (11.3.11):

$$Q = \frac{A}{\frac{1}{h_1} + \frac{d}{\lambda} + \frac{1}{h_2}} \cdot (t_{f1} - t_{f2}) \quad (11.3.12)$$

**Fig. 11.18** Infinite flat wall heat transfer process



Let  $\kappa = \frac{1}{\frac{1}{h_1} + \frac{d}{\lambda} + \frac{1}{h_2}}$ , then

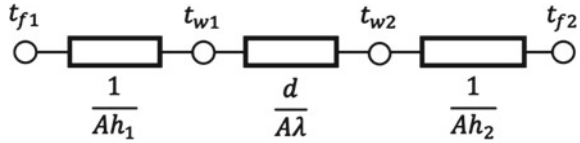
$$Q = A \cdot \kappa \cdot (t_{f1} - t_{f2}) \quad (11.3.13)$$

where,  $\kappa$  is the coefficient of heat transfer in  $\text{W}/(\text{m}^2 \text{K})$ .

The heat transfer coefficient is a scale to represent the intensity of the heat transfer process. The more intense the heat transfer process is, the greater the heat transfer coefficient will be, and vice versa. The heat transfer coefficient depends not only on the two types of fluids involved in the heat transfer process, but also the process itself (such as the size of the flow rate, whether there is a phase transition, etc.). If the radiant heat transfer between the fluid and the wall surface needs to be calculated, the surface heat transfer coefficient in Eq. (11.3.13) can be taken as the composite heat transfer surface heat transfer coefficient, which includes the surface heat transfer coefficient converted from radiant heat transfer, and its calculation method will be discussed later.

Equations (11.3.12) and (11.3.13) are called heat transfer equations and are the basic formulas for heat exchanger thermal calculation. As the heat transfer process always involves two stages of convective heat transfer, the in the heat transfer Eq. (11.3.13) is called the total heat transfer coefficient to distinguish it from the surface heat transfer coefficient of convective heat transfer.

**Fig. 11.19** Thermal resistance analysis in heat transfer process



### 11.3.2 Thermal Resistance

In the previous section, the concept of total heat transfer coefficient has been introduced, which can be obtained according to the calculation formula of heat transfer coefficient

$$\frac{1}{\kappa} = \frac{1}{h_1} + \frac{d}{\lambda} + \frac{1}{h_2} \tag{11.3.14}$$

The corresponding heat transfer equation can be written

$$Q = \frac{\Delta t}{\frac{1}{A\kappa}} \tag{11.3.15}$$

where,  $\Delta t = (t_{f1} - t_{f2})$ , compared with Ohm’s law ( $I = \frac{U}{R}$ ),  $\frac{1}{A\kappa}$  can be found that it is equivalent to the action of resistance R, so it will be denoted as the thermal resistance of heat transfer process. The heat transfer process in Fig. 11.19 can be expressed as Fig. 11.19. That is, in the process of heat transfer, the heat flow in each link is the same, and the total thermal resistance is equal to the sum of the thermal resistance of each link.

### 11.3.3 Heat Transfer Process in Porous Materials

Solid materials belong to a single continuous uniform medium, and the heat conduction process is relatively simple. Here the heat conduction process in porous materials will be discussed. Since porous materials are composed of solid and pores, and the pores contain a fluid medium, rather than a single continuous uniform material. Figure 11.20 showed that the heat conduction process of porous materials is more complicated.

Solid–gas porous materials are the most common porous materials and are widely used in many industries. For example, foamed plastics, porous concrete and foamed bricks used in heat insulation, foamed ceramics used in chemical industry, foamed aluminum and foamed metals used in load-bearing structures are all solid gas porous materials.

Since most of the porous insulation materials are considered to be solid–gas porous materials, this section will focus on the gas-phase heat conduction process in the solid–gas porous materials.

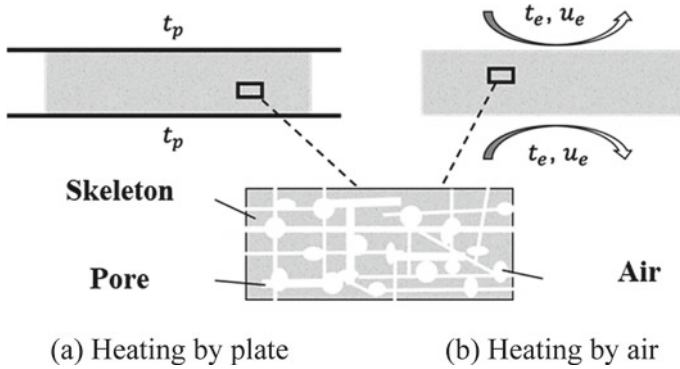


Fig. 11.20 Porous material heated by plate and air

### 11.3.3.1 Equivalent Thermal Conductivity

In-Series and Parallel Models: If the structure of the solid–gas porous material is considered as a simple series or parallel structure, the structure is the same as that of the calculated resistance network, so it is more convenient to calculate the thermal resistance network.

Figure 11.21 showed a simple series-parallel structure of porous materials. When the heat flow  $Q_L$  passes through the material vertically, the material is regarded as a parallel structure, and its thermal resistance network is shown in Fig. 11.22a. In Fig. 11.22a,  $R_s$  and  $R_a$  are the thermal resistance of solid phase and gas phase respectively. Figure 11.22a showed when the heat flow  $Q_L$  passes vertically through the material, the material is regarded as a parallel structure, and its thermal resistance network is the parallel network.

For the gas phase in Fig. 11.21a, the thermal resistance is

$$R_a = \frac{1}{\lambda_a} \times \frac{1}{A_a} = \frac{1}{\lambda_a} \times \frac{1}{\phi} \tag{11.3.16}$$

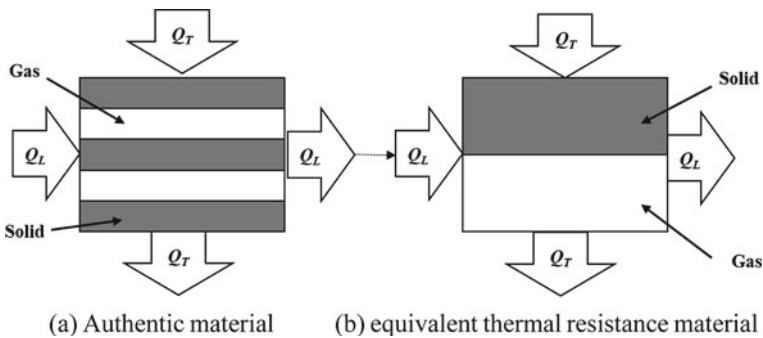
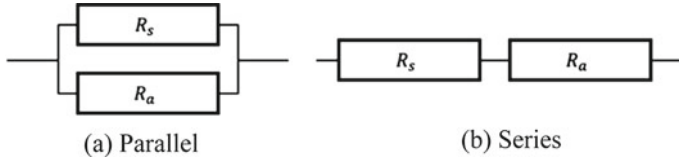


Fig. 11.21 A series–parallel structure of porous materials



**Fig. 11.22** Thermal resistance network of series and parallel structure

For the solid phase, the thermal resistance is

$$R_s = \frac{1}{\lambda_s} \times \frac{1}{A_s} = \frac{1}{\lambda_s} \times \frac{1}{1-\phi} \tag{11.3.17}$$

According to the parallel relation, the longitudinal thermal resistance  $R_L$  can be calculated as

$$R_L = \frac{R_a R_s}{R_a + R_s} = \frac{1}{\lambda_s(1-\phi) + \lambda_a \phi} \tag{11.3.18}$$

Combined with the definition of thermal conductivity of solid gas porous material, the longitudinal effective thermal conductivity of the material is

$$\lambda_L = \lambda_s(1 - \phi) + \lambda_a \phi \tag{11.3.19}$$

When the heat flow  $Q_T$  passes through the material laterally, the material is regarded as a series structure, and its thermal resistance network is shown as the series network in Fig. 11.22b.

For the gas phase in Fig. 11.21b, the thermal resistance is

$$R_a = \frac{\phi}{\lambda_a} \tag{11.3.20}$$

For the solid phase, the thermal resistance is

$$R_s = \frac{1-\phi}{\lambda_s} \tag{11.3.21}$$

According to the parallel relation, the longitudinal thermal resistance  $R_L$  can be calculated as

$$R_T = R_a + R_s = \frac{\phi}{\lambda_a} + \frac{1-\phi}{\lambda_s} \tag{11.3.22}$$

Combined with the definition of thermal conductivity of solid–gas porous material, the transverse effective thermal conductivity of the material is

$$\lambda_T = \frac{\lambda_a \lambda_s}{\lambda_a(1-\phi) + \lambda_s \phi} \tag{11.3.23}$$



Obviously, the difference between the series and parallel models is that, for vertical heat flow  $Q_L$ , the solid phase in the parallel model is connected, while for horizontal heat flow  $Q_T$ , the solid phase in the series model is separated by gas, and the contribution of the solid phase is only to reduce the thickness of the heat flow through the gas phase. Although the simple series and parallel model is too simplified and has a big gap with the actual porous materials, the application of this simple model can still effectively help us analyze the thermal conductivity of the actual materials, such as wood, continuous fiber reinforced resin composite materials with continuous texture.

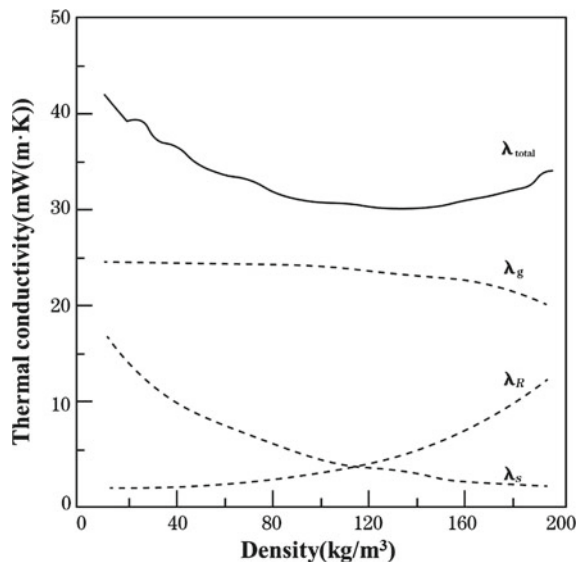
### 11.3.4 Heat Transfer in VIP

Under extremely low inner pressure, VIP faces three modes of heat transfer, including solid conduction, gaseous conduction, and radiation. All these modes sum up to give the total thermal conductivity of the panel, as given below—see: Fricke et al. (2006).

$$\lambda_T = \lambda_S + \lambda_R + \lambda_G + \lambda_{Cv} + \lambda_{coup} \tag{11.3.24}$$

where  $\lambda_S$  is the solid thermal conductivity (W/m·K);  $\lambda_R$  is the radiative thermal conductivity (W/m·K);  $\lambda_G$  is the gaseous thermal conductivity (W/m·K).  $\lambda_{Cv}$  is the gas convection inside the open pores, and  $\lambda_{coup}$  is the heat transfer from the coupled effect (W/(m·K)). Figure 11.23 showed that heat transfer modes vary concerning the density of the core materials—Changhai and Jianqiang (2016).

**Fig. 11.23** Comparison of the three heat transfer mechanisms in conventional thermal insulation materials—see: Changhai and Jianqiang (2016), Zimmermann and Bertschinger (2001)



### 11.3.4.1 Solid Conduction

The solid structure of the core material is responsible for the solid heat transfer ( $\lambda_S$ ) through the panel.  $\lambda_S$  occurs through the contact points between solid particles or fibers. The structure, density, and external pressure of the materials determines the magnitude of solid heat transfer. As from Fig. 11.11,  $\lambda_S$  increases with the increase in density, which can be better expressed by the following relation—Fricke (1993):

$$\lambda_S = \rho^\alpha \quad (11.3.25)$$

where  $\rho$  is the density ( $\text{kg/m}^3$ ) and index  $\alpha$  is a constant for foam and other materials in the range of 1.5–2 nm size.

Various methods have been adopted to reduce  $\lambda_S$ . Following the principles of Eq. (11.3.25), the density of core material can be reduced by increasing its porosity ratio and as a result,  $\lambda_S$  decrease. It is reduced by making heat transfer path more complex either by increasing path length or number of barriers. The alignment of the fibers or particles in a direction perpendicular to that of heat flow increases the path length. Besides this, the number of barriers in the heat flow path increase by increasing the number of interface regions at contact points. This can be done by using a very fine sized and a homogeneous shaped material.

### 11.3.4.2 Gaseous Thermal Conduction

The gaseous thermal conductivity consists of the sum of gaseous conduction and convection processes. The Knudsen number, i.e., the ratio of mean free path of gas molecules and the pore size of the material, defines the intensity of  $\lambda_g$ . A function of Knudsen Number was proposed in the following correlation Eq. (11.3.26)—Kreith and Black (1980):

$$\lambda_G = \lambda_o / (1 + 2\beta K_n) \quad (11.3.26)$$

where,

$$K_n = l_{\text{mean}} / \delta \quad (11.3.27)$$

where,  $\lambda_0$  is the thermal conductivity of air at atmospheric pressure;  $\beta$  is the coefficient which depends on accommodation coefficient and the adiabatic coefficient of the gas;  $K_n$  is the Knudsen Number,  $l_{\text{mean}}$  is the mean free path of air molecules and  $\delta$  denotes the characteristic size of the pore.

Whereas, gas thermal conductivity of air at room temperature ( $\beta = 0.0016/P$ ) is calculated by using the following equation:

$$\lambda_G = \lambda_o / (1 + (0.0032 / P\Phi)) \quad (11.3.28)$$

where  $P$  symbolizes the gas pressure (Pa) and  $\Phi$  is the pore size of the porous thermal insulation material (m). Equation (11.3.28) is used for calculating  $\lambda_g$  for insulating materials with a different pore size as a function of inner pressure. By reducing the pore diameter of core material,  $\lambda_g$  can be reduced up to higher gas pressure in the evacuated panels.

### 11.3.4.3 Radiation Thermal Conduction

Radiative heat  $\lambda_r$  transfers in the form of electromagnetic waves and does not require any medium to travel through it. This is the significant type of heat transfer mode, that can travel through a vacuum. Equation (11.3.29) can be used to calculate the radiation heat transfer through the VIP—Kreith and Black (1980):

$$\lambda_R = 16n^2 K_B T^3 / 3K \quad (11.3.29)$$

where,  $K$  is the extinction coefficient of materials ( $m^{-1}$ ), however,  $K = e(T) \cdot \rho$  and  $e(T)$  denotes the specific extinction coefficient ( $m^2/kg$ ),  $\rho$  is the material density ( $kg/m^3$ ), and  $n$  is the refractive index. where  $k_B$  is the Boltzmann constant ( $1.38 \times 10^{-23} J K^{-1}$ ).

Several solutions have been proposed for the reduction of radiative conductivity. One of the solutions is by making core material opaque to the infrared radiation by the addition of opacifier. The most commonly used opacifiers in VIP are Silicon carbide (SiC), titanium dioxide (TiO<sub>2</sub>), carbon black, and iron oxide (Fe<sub>3</sub>O<sub>4</sub>).

## 11.4 Physical Characteristics of VIPs

### 11.4.1 Thermal Conductivity

The thermal conductivity and resistivity are typically tested using a heat flow meter apparatus. This test method is based on the Fourier's law. The test sample is positioned between hot and cold plates at steady state conditions. Additionally, two heat flow sensors are mounted on the surface of the plates. By measuring the heat flow, the temperature difference between the plates and the sample thickness, the thermal conductivity can be determined. Figure 11.24 displays the diagram of the heat flow meter.

The heat flow through VIPs includes the one through core materials and envelope. If the parameters of envelope are known, the thermal resistance could be calculated by heat transfer coefficient:

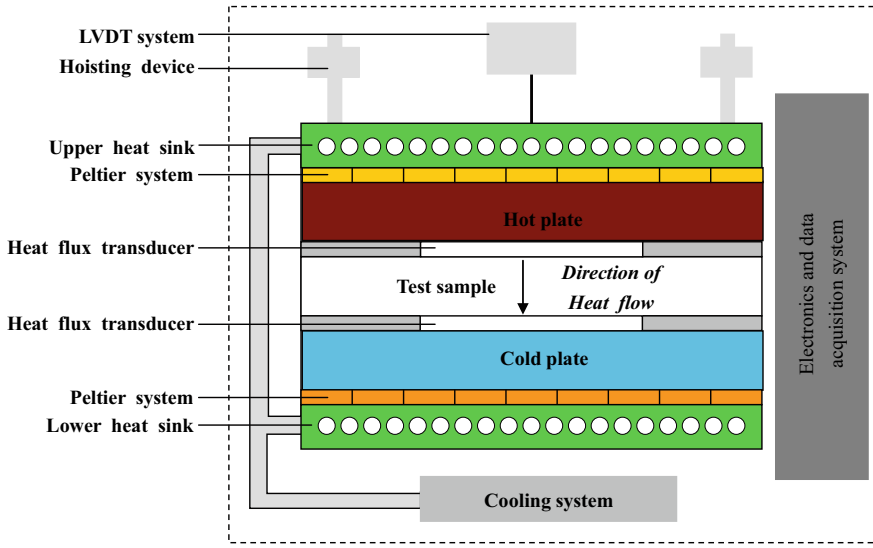


Fig. 11.24 Diagram of the heat flow meter

$$U_{\text{eff}} = U_{\text{cop}} + \frac{l_p}{S_p} \varphi_{\text{edge}} \tag{11.4.1}$$

$U_{\text{eff}}$  is the heat transfer coefficient of VIP;  $U_{\text{cop}}$  is the heat transfer coefficient of VIP centre;  $\varphi_{\text{edge}}$  is the linear coefficient of heat transfer of VIP;  $l_p$  is the perimeter of VIP;  $S_p$  is the area of VIP.

$$R_{\text{eff}} = \frac{1}{U_{\text{eff}}} - \frac{1}{7.8} - \frac{1}{25} \tag{11.4.2}$$

$$\lambda_{\text{eff}} = \frac{d}{R_{\text{eff}}} \tag{11.4.3}$$

### 11.4.2 Inner Pressure

According to Eq. (11.3.28) and Fig. 11.3, the inner pressure of VIP is significant for thermal insulation property of VIPs. It is necessary to test the inner pressure of VIPs.

Figure 11.25 describes the VIP inner pressure measuring method. It can be summarized as follows: with a pressure on the outside of the VIP that is equal to the inner pressure of the vacuum insulation, the envelope of the VIP is displaced. Laser range finder monitors displacement, when the change of displacement mutation, and the pressure of the outside of the VIP created is the inner pressure of VIP.

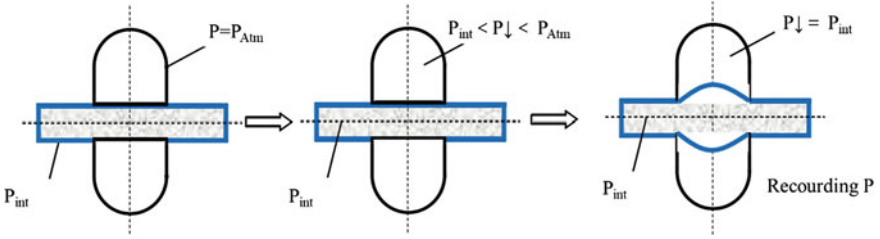


Fig. 11.25 The principle of VIP inner pressure measuring method



Fig. 11.26 Test equipment for measurements of the VIP’s inner pressure (NAPA, made by NUAU)

Figure 11.26 shows the test equipment for inner pressure of VIP. Figure 11.27 shows the relationship between the VIP’s internal pressure and the time of the test.

### 11.4.3 VIP Long Term Durability

Long-term performance of thermal insulation is indicated by its ability to sustain thermal properties during the expected service life. Usually mentioned as LTTR (long-term thermal resistance) value, it is a very important characteristic of an insulation material and used by the building envelope designers for energy calculations.

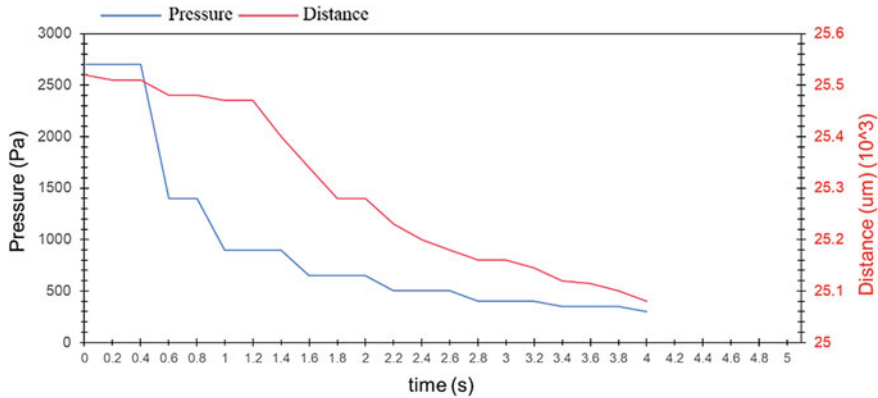


Fig. 11.27 A curve of the test for inner pressure of VIP

Diffusion of gas and/or vapor is the common phenomenon that governs ageing of VIP. For VIP, the ageing rate seems to be about constant, at least for the first 5–10 years, and ageing process appears to be a continuous process over a much longer duration of time. It is to be noted, even with continuous ageing, due to its extremely high initial R-value (measure of thermal resistance, as used e.g. in North America) VIP for a given thickness provides much higher thermal resistance than conventional thermal insulations (foam, fibre etc.) during its service life. Furthermore, even a totally failed (i.e. no more vacuum) VIP can have higher R-value than traditional insulations used for building envelope construction. Up to now, only limited research on the long-term performance is available. The popular way to estimate the long term performance of VIP is to conduct accelerated ageing tests in the laboratory. this part is to introduce the ageing method to test long term performance of VIP.

#### 11.4.3.1 Durability Testing and Testing Methodologies Used in Canada

A team of researchers from Canada proposed an accelerated ageing test protocol with performance requirements, as shown in Table 11.4.

It is to be noted that the proposed accelerated ageing test protocol and prediction of the long-term thermal performance of VIPs are based on the available information and authors’ experience with VIPs and other insulating materials. It is expected that the proposed test protocol and the performance requirements would be reviewed when more research and application outputs will be available in the coming years.

#### 11.4.3.2 Durability Testing Performed in China

In China, the ageing method was standardized in JG/T (2014) “Vacuum Insulation Panels for Buildings”. According to this standard, 9 test specimens soaked in water

**Table 11.4** Accelerated ageing test protocol with performance requirements in Canada—Mukhopadhyaya (2015)

No	Ageing conditions	Total duration (days)	%R-value reduction requirement
1	70 °C, 95%RH	30	≤20
2	95%RH, 22 °C	90	≤10
3	90 °C , ambient RH	90	≤10
4	−30 °C , ambient RH	90	≤5
5	70 °C (ambient RH), 95% RH (22 °C)—Alternate	98(1 week @ 70 °C, followed by 1 week @ 95% RH (22 °C)—7 cycles)	≤10
6	−30 °C (ambient RH), 50% RH (22 °C)—Alternate	98 (1 week @ −30 °C, followed by 1 week @ 50% RH—7 cycles)	≤5

for 1d among which 3 are done with thermal conductivity test. Remove water on their surfaces by wet towel when they are taken out. Treat test specimens with 30 damp-heat/freeze cycles in high/low temperature damp-heat tester. Keep them under standard testing conditions for 2 d. Conditions of damp-heat and freeze treatment are as follows:

- (a) Raise temperature to  $(70 \pm 5)$  °C relative humidity to  $(90 \pm 5)$  % within 1 h, and keep it for 3 h.
- (b) Lower temperature to  $(-20 \pm 5)$  °C within 1 h, and keep it for 3 h.

After the damp-heat and freeze treatment, according to thermal conductivity VIPs are classified to 3 types in Table 11.5.

### Germany

Several VIP products got a national approval for the use in buildings in Germany.

Beside others the testing procedure comprises following aspects:

- accelerated ageing at an elevated temperature in dry climate for half a year,
- several times thermal cycling,
- consideration of the thermal bridge effects for adjacent panels.

Based on scientific research from the accelerated ageing test the expected heat transfer for 25 years is calculated. Together with some add-on for safety this yields the value for the declared thermal conductivity for panels with minimum dimensions.

**Table 11.5** VIPs classified after the damp-heat and freeze treatment

Type	I	II	III
Thermal conductivity (W/(m K))	≤0.005	≤0.008	≤0.012

### 11.4.4 Service Life Predictions of VIPs

Successful application of VIPs in buildings depends greatly on their long-term durability. The service life of a VIP depends on the external environment where it is used, a rate of the VIP's inner pressure increase, water vapor permeability across the VIP's envelope, and the internal structure of used core material—Pons et al. (2017). In order to accurately validate the variation of the VIP's thermal conductivity over the time, and to predict the VIP's service life, the thermal aging tests are necessary. In aging standard testing used in China—GB/T (2019), the impact of the humidity of the VIP service environment is included in two following paths:

(1) **Humidity  $\leq 50\%$**

For humidity of the service environment below 50%, only incremental changes of thermal conductivity caused by the dry gas are considered.

To determine the relationship between thermal conductivity and the inner pressure and to determine the relationship between the inner pressure and the usage time, the VIP aging tests performed under different temperatures is recommended. The following test methodology is utilized.

Specifically, the VIP inner pressures are tested at different aging temperatures, once a month for half of a year. Then, the relationship between the inner pressure in time, at different test temperatures is computed using the following relationships:

$$P_{30^{\circ}\text{C},t} = P_0 P'_{30^{\circ}\text{C}} \times t \quad (11.4.4)$$

$$P_{50^{\circ}\text{C},t} = P_0 P'_{50^{\circ}\text{C}} \times t \quad (11.4.5)$$

$$P_{70^{\circ}\text{C},t} = P_0 P'_{70^{\circ}\text{C}} \times t \quad (11.4.6)$$

$P_{T,t}$  is the inner pressure under the aging test temperature of  $T$ ;

$t$  is the time (days);

$P_0$  is the initial inner pressure;

$P'_T$  is the rate of the inner pressure increase.

After taking into account  $P'_T$ , as well as considering Eq. (11.4.5), the linear fitting can be performed using the following Eq. (11.4.7):

$$\ln P'_T = \ln B - \frac{E_n}{R} \times \frac{1}{T} \quad (11.4.7)$$

$\ln B$  is the intercept of the fitting line;  $-E_n/R$  is the slope of the fitting line;  $E_n$  was the activation energy of envelope;  $R$  is the constant of air.



The service life of VIP is predicted according to the inner panel pressure, corresponding to the thermal conductivity value.

(2) **Humidity > 50%**

For humidity of the service environment over 50%, the increases of thermal conductivity caused by dry gas and vapour are considered.

To determine the relationship between thermal conductivity and inner pressure of a sample A and determine the relationship between the inner panel pressure and the usage time, the aging test is performed under different temperature conditions and in high humidity levels. The following test methodology is utilized.

The sample B (identical as sample A) is placed in the environment of  $70 \pm 2 \text{ }^\circ\text{C}$  and humidity of  $\pm 3\%$  for the aging experiment. The test includes analysis of thermal conductivity ( $\lambda_1\text{--}\lambda_6$ ) and quantity ( $m_1\text{--}m_6$ ) every 30 days, within half a year at  $23 \text{ }^\circ\text{C}$ , after sample conditioning for 24 h at  $23 \text{ }^\circ\text{C}$ , under 50% humidity. After the aging testing, the dry VIP test is performed to estimate the quantity ( $m_{\text{core,dry}}$ ).

To relate the thermal conductivity ( $\lambda_1\text{--}\lambda_6$ ) to inner pressure ( $P_1\text{--}P_6$ ), and to fit linearly the relation of inner pressure with time, the equation Eq. (11.4.8) is utilized:

$$P = P'_{\text{gas}(70,\varphi)} \times t \quad (11.4.8)$$

$P$  is the inner pressure;  $P'_{\text{gas}(70,\varphi)}$  is the rate of inner pressure increases under test condition of  $70 \text{ }^\circ\text{C}$  and humidity of  $\varphi$ .

To calculate the rate of the inner pressure increases caused by the dry gas  $P'_{\text{gas}(70)}$ , the equation Eq. (11.4.9) is used:

$$P'_{\text{gas}(70)} = P'_{\text{gas}(70,\varphi)} - P'_{w(70,\varphi)} \quad (11.4.9)$$

$P'_{w(70,\varphi)}$  is the rate of the inner pressure increases, caused by the water vapor. It is computed by the following formula:

$$P'_{w(70,\varphi)} = \frac{P_{wv,s,70}}{k} \times \frac{m'_{w(70,\varphi)}}{m_{\text{core,dry}}} \quad (11.4.10)$$

$P_{wv,s,70}$  is the saturated vapor pressure of water at  $70 \text{ }^\circ\text{C}$ ;  $k$  is a constant of 0.08;  $m'_{w(70,\varphi)}$  is the rate of quantity increases.

Then, to calculate the rate of the rate of the rate of inner pressure increasing under condition of  $23 \text{ }^\circ\text{C}$ , the following Eq. (11.4.11) is utilized:

$$P'_{\text{gas}(23)} = 0.135 - P'_{\text{gas}(70)} \quad (11.4.11)$$

To calculate the rate of the mass of water increases, the  $X_{w(23,\varphi),t}$  is calculated according to Eq. (11.4.12):

$$X_{w(23,\varphi),t} = 0.08 \times \varphi \times \left( 1 - \exp\left(\frac{-1.125 \times m'_{w(70,\varphi)}}{\varphi \times m_{\text{core,dry}}}\right) \right) \quad (11.4.12)$$

Thermal conductivity under condition of 23 °C and humidity of  $\varphi$   $\lambda_{(23,\varphi),t}$  is computed using Eg (11.4.13):

$$\lambda_{(23,\varphi),t} = \lambda_0 \frac{0.026}{1 + P_{1/2,\text{air}} / (P'_{\text{gas}(23)} \times t)} - 0.0005 X_{w(23,\varphi),t} \quad (11.4.13)$$

$P_{1/2,\text{air}}$  is the inner pressure of VIP, when its thermal conductivity is half of air.

To make the line of Equation, and  $t$  is the service life of VIP when  $\lambda_{(23,\varphi),t}$  is the invalid value.

## 11.5 VIPs' Application in Buildings

Traditional thermal insulations were grouped into two major classes; organic, and inorganic insulation materials. The organic insulation materials have higher thermal insulation properties as compared to the inorganic insulations, but they also exhibit considerably higher flammability, as discussed by Zimmermann and Bertschinger (2001). An application of traditional insulation materials of larger thickness in urban areas is another issue, where used internal space is considered to be an essential factor. Low thickness VIPs made it possible to achieve near zero energy building with high insulation standards and a very short payback period. The resulting lower energy consumption for heating or cooling promoted green environment and reduce expenses. The trend toward VIPs was developed because of their superior insulation performance, space-saving, fire resistance, and low gas emission and many others.

Although the first patent for VIP appeared as early as 1930, the first application of VIP in buildings was in 1999—see: Brunner et al. (2014). But, later, the VIP's technology for application in buildings has developed rapidly—Brunner (2012).

### 11.5.1 Examples of VIP Products Used in Buildings

To allow building applications, it is necessary to provide additional protection structure, preventing VIPs from being mechanically damaged. As mentioned before, fiberglass envelope wraps are becoming popular in VIPs, which are used in building. Also, plastic foams can be used for mechanical protection of VIPs, such as expanded polystyrene or polyurethane foam. Some VIP building products are listed in Table 11.6. Figure 11.33 shows VIPs with pits. The pits on the VIP surface improve the adhesion between VIPs and decorating layer—see Fig. 11.28.

**Table 11.6** Products of VIP in building

Manufacturer	Core	Protective materials	Thermal conductivity (mW/(m K))	Density (kg/m <sup>3</sup> )
Vaku-isotherm (SP-2)	Fumed silica	EPS	8	–
Vaku-isotherm (SP-2/E)	Fumed silica	EPS	8	–
Vaku-isotherm (BAUPLATTE)	Fumed silica	Plastic recycling panel and EPS	8	–
Porextherm (Vacupor PS-Bn-S)	Fumed silica	EPS	7	170–210
Weber Saint-Gobain (Weber.therm.LockPlate)	Fumed silica	EPS	7	190
Va-Q-tec(va-Q-vip B)	Fumed silica	Black fiberglass textile	7–8	180–210
Va-Q-tec(va-Q-vip F-EPS)	Fumed silica	EPS	7–8	180–210
Va-Q-tec(va-Q-vip F-GGM)	Fumed silica	Rubber granulate lamination	7–8	180–210
Variotec(VT-A-HYDRO)	Pyrogenic silica	Extruded polystyrene	7	190–220
Creek(STP-VIPB)	Microprousmaterial	Fiberglass	7	–

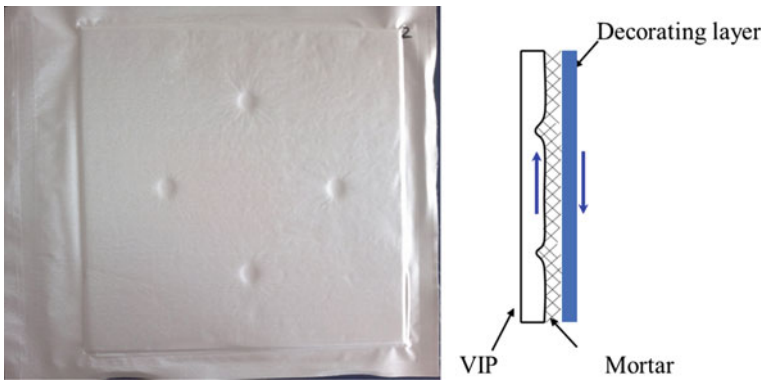


**Fig. 11.28** VIPs with pits

**Table 11.7** Standard specification documents in different countries or regions

Nation/ region	Document	Content
China	JG/T 438-2014 VIPs for building—see: JG/T (2014) GB/T 37,608-2019 Vacuum Insulation Panels—see: GB/T (2019)	According to this standard the thermal conductivity shall be measured in the centre of test specimen at average temperature of $(25 \pm 2)$ °C. Prior to these measurements the specimens have to undergo a durability test and ageing procedure
European	EAD 0,040,011-00-1201 for VIP with factory applied protection layers—see: EAD (2017)	These documents define characteristics for factory VIP for the thermal insulation of building. But VIPs with getters are not included
North America	ASTM C1484-10 Specification document for VIPs—see: ATM (2019)	Ageing due to outgassing and permeating gases are taken into account, and in the appendix as Nonmandatory information, panel aging calculations are described
Japan	JIS A141n-1 Test method for thermal resistance and related properties of thermal insulations-Guarded hot plate apparatus—see: JIS (2016)	Separately from the industrial specification document for VIP, testing method for measuring the thermal performance of VIP has been established steadily

### ***11.5.2 Standard Specification Documents for VIPs Used in Buildings***

In order to introduce VIPs to the market, standardizing product was necessary. Table 11.7 lists regional standard performance specifications for VIPs to be used in different countries and/or regions.

### ***11.5.3 Energy Performance of Building Installed with VIPs***

Great variety of case studies, focused on the VIPs energy performance, had been already carried out worldwide. A summary of energy use before and after renovation (when applicable) is given in Table 11.8. It can be observed that VIPs can notably improve the energy performance of buildings.

**Table 11.8** Date of energy performance before and after renovation for case studies using VIP

City, country	Energy performance before	Energy performance after	Total VIP area (m <sup>2</sup> )	Thickness of VIP (mm)
Fukushima, Japan	550 kWh/year/room	485 kWh/year/room	2576	8
Shiga, Japan	2.0 W/m <sup>2</sup> K	1.0 W/m <sup>2</sup> K (initial) 1.3 W/m <sup>2</sup> ·K (7 yr)	96	10
Osaka, Japan	16.3 kWh/day	9.9 kWh/day	128	10 (wall, roof) 8 (floor)
Osaka, Japan	2.29 W/m <sup>2</sup> K	1.36 W/m <sup>2</sup> K	3.3	10
Bottrop, Germany	72,000 kWh	900 kWh	60	50
Gothenburg, Sweden	158.7 kWh/m <sup>2</sup>	127.5 kWh/m <sup>2</sup>	83	20
Nantes, France	250 kWh/m <sup>2</sup>	115 kWh/m <sup>2</sup>	40	40
London, UK	3.03 W/m <sup>2</sup> K	0.18 W/m <sup>2</sup> K	13	40
Seongnam, Korea	0.21 W/m <sup>2</sup> K	0.16 W/m <sup>2</sup> K	250	20

Source Adl-Zarrabi and Johansson (2020)

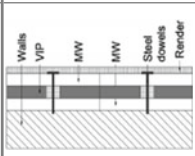
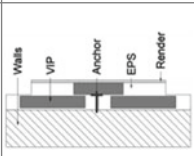
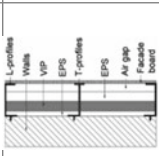
#### 11.5.4 Method of Installing VIPs in Building

Table 11.9 shows several case studies of VIPs application in new building. The applications in real building and test specimens were both included. Most of studies were carried in Central Europe, where VIP technology was better established. The installation and design of VIP in building impact not only the safety of the system, but also its thermal performance. Figures 11.34 and 11.35 illustrates the structure of thermal insulation system with VIP and installation method of VIP in Chinese buildings, respectively. Figure 11.36 shows several buildings installed with VIPs (Figs. 11.29, 11.30 and 11.31).

#### 11.5.5 Challenges of VIPs Applications in Buildings

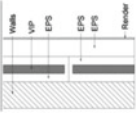
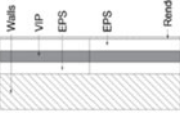
Due to the excellent thermal insulation performance, VIPs theoretically have a very strong potential for future building applications. However, a number of existing installation limitations and durability issues reduce market adoption of this technology. Today the application of VIPs in buildings is facing many challenges. On the one hand, there are the problems associated directly with the VIPs performance, and on the other hand there are issues reported on VIPs which are already installed

**Table 11.9** VIP application in new building

Location/reference	Illustration	Goals	Construction solution	Fixation	Main results/conclusions
Athens, Greece: Mandilaras et al. (2014)		Comparative assessment (experimental and numerical) of conventional and VIP mock-up two-storey Building	Lightweight steel-frame mock-up with gypsum boards (internally) and cement boards (externally) with drywall systems, using 20 mm VIP covered by 20 mm of mineral wool on both sides	Adhesive mortar with Two steel dowels for each board (VIP with two built-in holes)	Marked difference between predicted and achieved performance
Munich, Germany: Kubina (2010)		Demonstration of a new VIP system for BUILDING that was applied in a residential building	Wall with 20 mm VIP covered by EPS with overlapping plate	Adhesive with fasteners	The two insulation layers reduced the edge thermal bridges. If this system were to be replaced by thick insulation, a difference in room area of 6.5% is estimated
Stockholm, Sweden: Karami et al. (2015)		Illustration of a new VIP mounting system in a laboratory specimen	Aerated concrete with 20 mm thick VIP embedded between 20 and 10 mm thick EPS plus a façade board (with air space)	Adhesive and stainless-steel profiles (L and T profiles)	VIPs did not lead to high relative humidity in the wall or at the joint. Attention must be given to leakage at joints and penetrating rain

(continued)

Table 11.9 (continued)

Location/reference	Illustration	Goals	Construction solution	Fixation	Main results/conclusions
Bersenbrück, Germany: Johansson (2012)		Application of VIPs in a detached house	Wall with 20 mm VIP encapsulated on all sides within 20 mm EPS and additional layer of 80 mm EPS	Information not provided	The main disadvantage with encapsulation of the VIPs was the thermal bridges at the connections of the panels, which cannot be prevented
Trier, Germany: Johansson (2012)		Application of VIPs in 1.2 terraced houses	Wall with 20 mm VIP, with 20 mm EPS on both sides	Information not provided	Not available

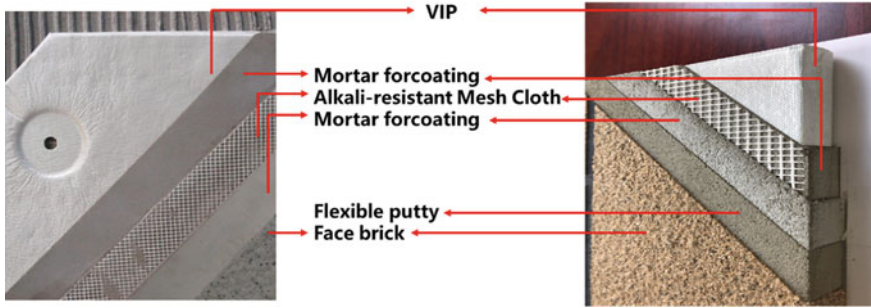


Fig. 11.29 The structure of thermal insulation system with VIPs in Chinese buildings

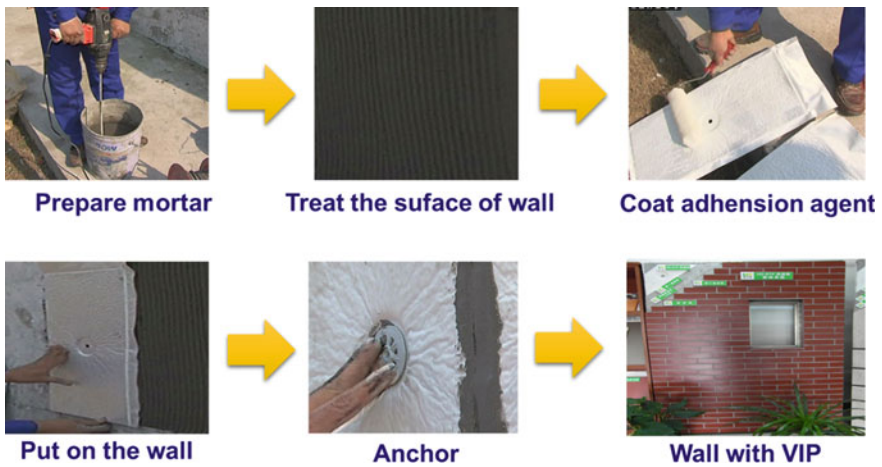
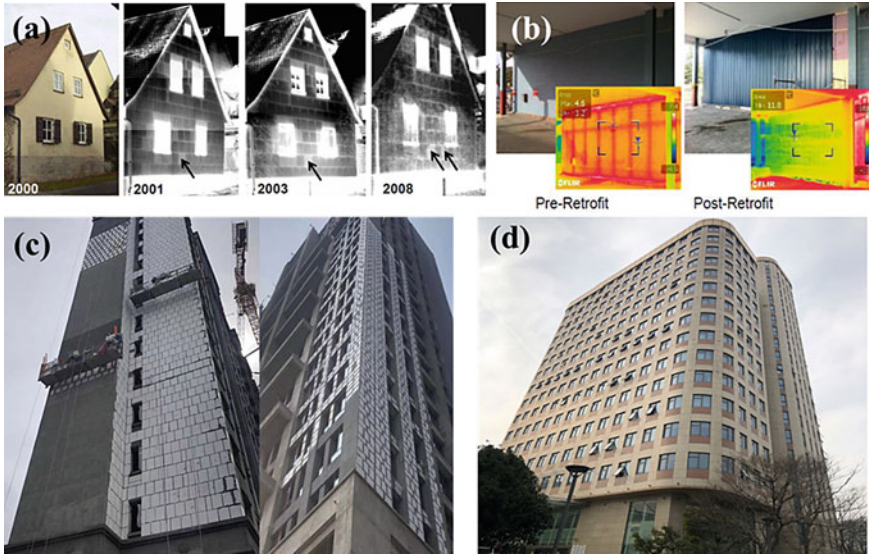


Fig. 11.30 Installation method of VIPs in Chinese buildings. *Source* Boafo et al. (2014)

on building. Thermal shorts generated by the VIPs enclosure as well as gas and H<sub>2</sub>O diffusion properties of a VIP membrane has been highlighted. In addition, the service life (shown in Table 11.10) of VIPs, and high material costs (shown in Table 11.11) are often listed as main challenges associated with VIPs’ applications in future buildings.





**Fig. 11.31** Applications of VIPs in building; **a** the gable of a listed building in Germany was retrofitted on the exterior with 15 mm VIPs using a special plastic rail system. The wall was afterwards investigated using thermography. From left: 2000, 2001, 2003 and 2008 (see: Heine- mann and Kastner (2010)); **b** VIPs retrofitted exterior wall in Canada and infrared images (see: Mukhopadhyaya et al. (2014)); **c** the buildings installing with VIPs; **d** the building with in Taicang, China

**Table 11.10** Service life estimates in building applications

Product	Estimated service life (years)
VIP with fumed silica core (single-layer metallized film)—Baetens et al. (2010)	10
VIP with fumed silica core (three-layer metallized film)—Baetens et al. (2010)	18–40
VIP with fumed silica core (three-layer metallized envelope)—Tenpierik (2009)	32
VIP with fumed silica core (aluminium foil laminate)—Tenpierik (2009)	45–50
VIP with glass fiber core—Tenpierik (2009)	5–20
VIP with expanded perlite core—Alam et al. (2017)	20

## 11.6 Short Overview of VIP Industry in China

### 11.6.1 Core Materials Suppliers and Products

**Table 11.11** Cost of VIP

Product	Thickness (mm)	Cost (€/m <sup>2</sup> )	Thermal conductivity (mW/(m K))	Cost per thermal resistance (€/ (m <sup>2</sup> K)/W)
VIP-fumed silica	60	200	6.2	20.7
VIP-fumed silica	10; 25–60	80.0; 91.4	4.0	32.0; 6.1
VIP-fumed silica	20; 30	49.4; 74.5	4.5	11.1; 11.2
VIP-fumed silica & expanded perlite	25	61.5	7.6	18.7
VIP-expanded perlite	25	51.7	13.0	26.9
VIP-glass fiber	25	41.8	2.8	4.7

Source Goncalves et al. (2020)

1. Nantong Yuanshun Fibers Co., Ltd

Nantong Yuanshun Fiber co., Ltd (Nantong Yuanshun) is located in Nantong, Jiangsu province, China. Nantong Yuanshun is a dynamic high-tech company and focuses on the production of glass wool core materials of VIP. The company is working hard to build a base which can produced 100,000 ton glass wool core materials per years. The thermal conductivity of VIPs used the company’s products is stable at 1.7–1.8 mW/(m·K), and the company has the ability to mass produce 1.5 mW/(m·K) VIP glass wool core materials. The products is popular in Chinese VIPs manufacturer.

2. Nantong Ecotherm Insulation Co., Ltd

Nantong Ecotherm Insulation Co., LTD (Ecotherm Insulation) was founded in 2018. The company is located in Nantong, Jiangsu province, China. Ecotherm Insulation is a professional supplier of fumed silica core materials. Figure 11.32 shows the fumed silica core materials produced by Ecotherm Insulation. Ecotherm Insulation’s annual capacity is 120,000 m<sup>3</sup> fumed silica core materials, and it is a vital supplier of fumed silica core materials in China. The properties of Ecotherm Insulations’ products are shown in Table 11.12.

**Fig. 11.32** Fumed silica core materials produced by Ecotherm Insulations

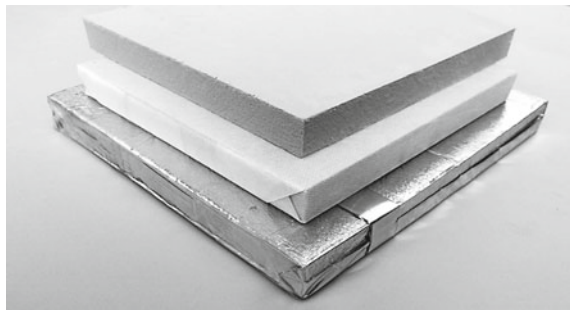


**Table 11.12** The properties of ecotherm insulations' products

Product type	K 200	K 200-L	K 500
Density (kg/m <sup>3</sup> )	~180	~170	~180
Specific heat capacity (KJ/kg K)	~0.9	~0.8	~0.9
Thermal conductivity At atmospheric pressure (mW/m k)	≤20.0	≤19.0	≤21.0
Thermal conductivity after sealing (mW/m k)	≤4.0	≤3.8	≤4.2
Fire protection class DIN ISO 4102	A1	A1	A1
Color	Grey	Grey	Grey
Thickness	5–50 mm		

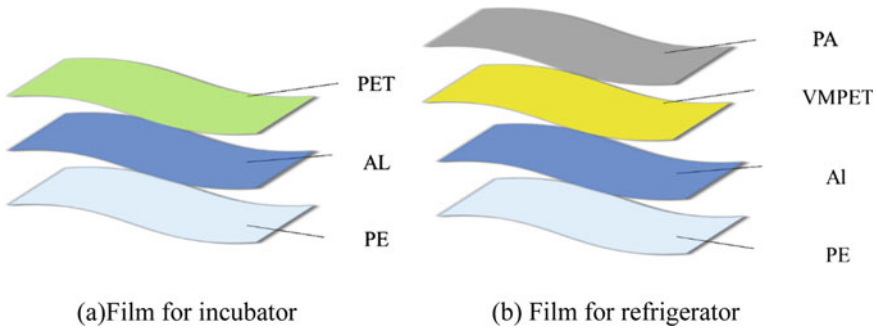


**Fig. 11.33** Major components of aluminum film

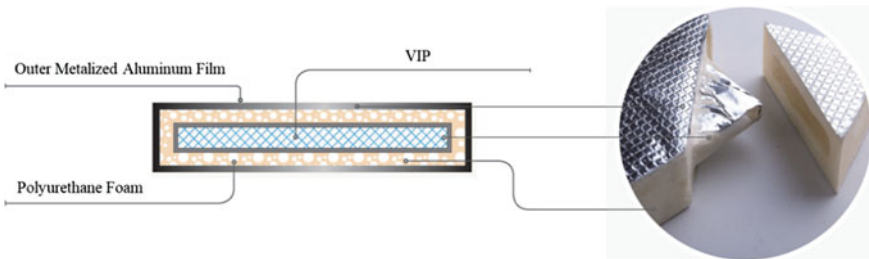


**Fig. 11.34** Structure of PV

3. Chuzhou Yinxing New Material Technology Co.,Ltd.

Chuzhou Yinxing New Material Technology Co.,Ltd. (Chuzhou Yinxing), located in Chuzhou, Anhui province, China, was founded in 2001 and it is one of the earliest domestic research and development, production of VIPs enterprises, Chuzhou Yinxing focuses on the production of VIP and core materials. Chuzhou Yinxing participated in the formulation standard specification documents for VIPs in China.



**Fig. 11.35** Application in of PV in refrigerated box and medical box

**Fig. 11.36** Typical VIP anchoring part



Chuzhou Yinxing's production are popular in Korea. Table 11.13 shows the core materials produced by Chuzhou Yinxing.

**Table 11.13** The Properties of Chuzhou Yinxing Insulations' products

Core material products	Glass wool	Chopped strand	Fumed Silica
Density after sealing ( $\text{kg}/\text{m}^3$ ) (%)	$260 \pm 10$	$310 \pm 10$	$150 \pm 10$
Thermal conductivity after sealing ( $\text{mW}/\text{m k}$ )	$\leq 3.0$ $\leq 2.5$ $\leq 2.0$	$\leq 2.5$ $\leq 2.0$	$\leq 4.5$
Maximum size (mm $\times$ mm)	$1880 \times 950$	$1880 \times 950$	$1880 \times 950$
Thickness (mm)	5–40	8–50	8–50

## 11.6.2 VIP Envelopes Produced in China

In China, each year there are 30 million square meters of envelopes is manufactured by Hanita, Toppan, Kinswee, Logos, etc., and the most common envelop are aluminum film, metalized film and glass fabric film. Aluminum films, metalized films are used for refrigerators and incubators, and glass fabric films are used for buildings.

### 11.6.2.1 Aluminum Film

In Chinese incubator and refrigerator, aluminum films are used as envelop of VIP. Figure 11.33a shows that the aluminum film for incubator include polyester film (PET), aluminum foil (Al) and polyethylene (PE), and the aluminum film for incubator include polyamide film (PA), PET vacuum metalized with aluminum (VMPET), Al and PE. Al foils in aluminum is 10–25  $\mu\text{m}$ . Thanks to thickness of Al foil, the water vapor transmittance and oxygen transmittance of aluminum film are below  $0.05 \text{ mg}/\text{m}^2\cdot\text{day}$  and  $0.05 \text{ cm}^3/\text{m}^2\cdot\text{day}$  which is at a low level, but boundary thermal effect is significant.

### 11.6.2.2 Metalized Film

Figure 11.33b shows that Metalized film is composed of multiple layers of VMPET and ultral-thin aluminum foil. Compared with aluminum film, the thickness of aluminum over PET in metalized film is nano scale. Therefore, the water vapor transmittance and oxygen transmittance of metalized film are below  $0.1 \text{ mg}/\text{m}^2\cdot\text{day}$  and  $0.1 \text{ cm}^3/\text{m}^2\cdot\text{day}$ , but boundary thermal effect of metalized film is weaker, causing higher performance in thermal insulation. The cost of metalized film is higher, so it is used in equipment requiring high thermal insulation performance.

### 11.6.2.3 Glass Fabric Film

Glass fabric film is a layer of fiberglass cloth added on the basis of aluminum film or metalized film, which is widely used in Chinese building insulation. Glass fabric film has a rough surface that the bonding force with mortar is stronger and resistance to puncture and fire. In China, the requirement of thermal conductivity of VIP for building is lower than others, so the water vapor transmittance and oxygen transmittance of glass fabric film is higher.

## 11.6.3 *VIP Product and Application in China*

In China, according to the classification of structure, there are three kinds of VIPs: Conventional VIPs, PU&VIPs (PV) and insulation decoration integrated board.

### 11.6.3.1 Conventional VIPs

Compared with other countries, glass wool core VIPs is more popular in China due to low cost and lower initial thermal conductivity. Glass wool cores VIPs are widely used in refrigerator. Thanks to long service life, fumed silica core VIPs are used in buildings. In addition, due to high service temperature, only fumed silica core VIPs can be used in electric water heater. In Chinese space industry, conventional VIPs are used in refrigerators to save room in space craft. When VIPs are equipped, to reduce heat leakage, PU is used to fill the space between VIPs and equipment.

### 11.6.3.2 PV

Figure 11.34 shows that the environment-friendly polyurethane (PU) is used to cover the surface of VIP to form a composite board (PV) of PU and VIP. The finished product not only has the high thermal insulation performance to increase use space, but also has the outstanding advantages of PU smooth surface, accurate size control, easy installation and adhesion, and high safety performance, which technically solves the defects existing in the use of VIP. PVs are widely used in refrigerated container, refrigerated truck, refrigerated box and medical box. Figure 11.35 shows application of PV in refrigerated box and medical box.

### 11.6.3.3 Insulation and Decoration Integrated Board

Traditionally, decorative materials and thermal insulation materials are independent products. Construction should be carried out separately. Insulation&decoration integrated board has the dual function of decoration and thermal insulation at the same

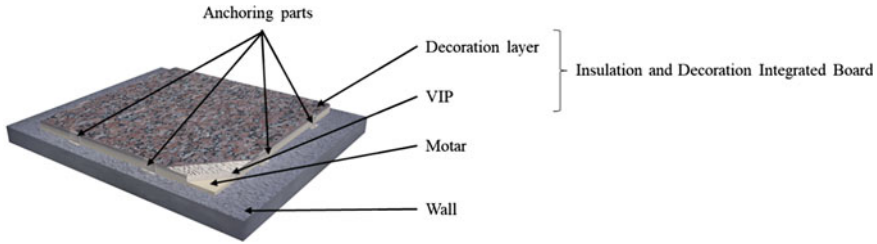


**Fig. 11.37** A way to install insulation& decoration integrated board

time. The user only needs to buy and install one time, and the decoration and thermal insulation of the facade can be completed. It is composed of decoration layer, VIP and anchoring parts. Decoration layer can be silicon calcium plates covered with paint or metal plates. To make it safety, insulation& decoration integrated boards usually are attached by sticking and anchoring. Figure 11.36 shows the anchoring parts, and Fig. 11.37 shows the way to install. Nowadays, processing and construction technology of the product is mature, and 80 million square meters insulation& decoration integrated boards are produced per year in China. They are widely used in projects of exterior wall thermal insulation.

## 11.7 Overview of Most Interesting Current VIP Application in Chinese Buildings

### 11.7.1 Winter Olympic Village Clinic, Beijing

Due to the high power consumption of medical equipment and the prevention of cross-infection in some rooms, medical buildings can only exhaust air independently without heat recovery, which has the characteristics of high energy consumption. Medical buildings are rarely selected as ultra-low energy consumption buildings. In order to demonstrate the determination of the Beijing 2022 Winter Olympic Games in energy conservation, emission reduction and low-carbon environmental protection, the Beijing Winter Olympic Village selected the polyclinic as the ultra-low energy consumption demonstration project. The building uses VIPs as thermal insulation materials, and this will reduce carbon dioxide emissions by about 42.4 tons per year (Fig. 11.38).



**Fig. 11.38** Winter Olympic Village clinic, Beijing

### ***11.7.2 Longcheng Guifu, Zibo, Shandong Province***

Longcheng Guifu located in Zibo, Shandong province is a senior community. Constructions adopted insulation & decoration integrated boards produced by Shandong Xintai as thermal insulation materials and decoration materials. The insulation & decoration integrated boards were composed by decoration plates of aluminum and VIPs, thickness of which is only 2.3 cm. Compared with other thermal insulation materials, insulation & decoration integrated boards increased the usable area by 5% (Fig. 11.39).

### ***11.7.3 Movable and Energy-Efficient Houses***

Thanks to the high performance of thermal insulation, VIPs can make more space buildings. Addition to lower density, VIPs are used in Movable and energy-efficient houses. Figure 11.40 shows a movable and energy-efficient houses with VIPs produced by Sanyou Dior. The thickness of thermal insulations is only 2 cm. The house are sold in Estonia.





**Fig. 11.39** Longcheng Guifu, Zibo, Shandong Province

**Fig. 11.40** A movable and energy-efficient houses with VIPs produced by Sanyou Dior



## 11.8 Conclusion

Following many years of research, application and development, VIP technology has achieved a technological maturity. It has been well-documented, that VIPs exhibit the lowest thermal conductivity among all thermal insulation products, which can be as low as  $1.5 \text{ mW}/(\text{m K})$ . In some world regions, VIPs become widely used by the cold chain industry in home appliances, and this technology is becoming more and more popular in building applications. VIPs are most often composed of core materials and envelopes (which are also using getters, and opacifiers). Mostly used core materials are fumed silica core materials, glass fibers core materials and polymeric foams core

material. Fumed silica VIPs are used in buildings and water heaters due to their long lifespan. Glass fibers VIPs are used in cold chain products and refrigerators due to their low thermal conductivity.

Keeping the insulation layer as thin as possible is challenging when one is also trying to keep high thermal resistance of the wall; this is exactly where VIPs are coming into service. The application of VIPs in buildings sector is spreading quickly around the world due to their excellent insulation performance, which means lower materials thickness and consequently, more living space to use. European companies were the first in VIP building applications. Furthermore, VIPs are gradually replacing the traditional foam applications in China, today. This is mostly due to the fact that, after three major high-rise building fires, between 2009 and 2011, Chinese standard fire performance requirements for building materials have been drastically reinforced.

In parallel with materials development, various install method blossom. Moreover, standardization is now in progress and several VIP-dedicated standards in different countries should be published very soon.

With more and more applications of VIPs in buildings, the global market is starting gradually recognizing this technology. In addition, China and other carbon GHG (greenhouse gas) emitters are under increasing pressure to cut their emissions. That is why VIP technologies are expected to certainly play a critical role in building energy conservation projects worldwide. Research and development of high performance and low-cost VIPs are expected to be a direction of the future research work in this area.

**Acknowledgements** Thanks to all those who supported writing and providing picture, the specific picture providers or units are as followed:

- Fig. 11.4 Sichuan Zerothermo Technology Co., Ltd
- Fig. 11.5 Nantong Yuanshun Fiber Co., Ltd
- Fig. 11.6 Nanjing University of Aeronautics and Astronautics
- Fig. 11.17 Sichuan Zerothermo Technology Co., Ltd
- Fig. 11.12 (left): Qingdao Jiuheshengye Energy Technology Co., Ltd
- Fig. 11.12 (right): Sichuan Zerothermo Technology Co., Ltd
- Fig. 11.26 Nanjing University of Aeronautics and Astronautics
- Fig. 11.28 (left): Nanjing University of Aeronautics and Astronautics
- Fig. 11.29 (right): Qingdao Jiuheshengye Energy Technology Co., Ltd
- Fig. 11.31 (d): Suzhou Super long Aviation heat Resistance material technology Co., Ltd
- Fig. 11.34 Jiangsu Sanyou Dior Energy-saving New Materials Co., Ltd
- Fig. 11.35 Jiangsu Sanyou Dior Energy-saving New Materials Co., Ltd
- Fig. 11.38 China Central Television
- Fig. 11.39 Shandong Cton Energy Saving Technologies Co., Ltd
- Fig. 11.40 Jiangsu Sanyou Dior Energy-saving New Materials Co., Ltd

## References

- Adl-Zarrabi, B., & Johansson, P. (2020). Practical applications retrofitting at the buildings scale-field scale. *IEA, Annex, 65*, Report. <https://research.chalmers.se/en/publication/515136>.

- Alam, M., Singh, H., & Limbachiya, M. C. (2011). Vacuum insulation panels (VIPs) for building construction industry—A review of the contemporary and future directions. *Applied Energy*, 88(11), 3592–3602.
- Alam, M., Singh, H., Brunner, S., et al. (2014). Experimental characterisation and evaluation of the thermo-physical properties of expanded perlite—Fumed silica composite for effective vacuum insulation panel (VIP) core. *Energy & Buildings*, 69, 442–450.
- Alam, M., Singh, H., Suresh, S., & Redpath, D. A. G. (2017). Energy and economic analysis of vacuum insulation panels (VIPs) used in non-domestic buildings. *Applied Energy*, 2017(188), 1–8.
- ASTM. (2019). ASTM C1484-10, Standard specification for vacuum insulation panels. ASTM. <https://www.astm.org/Standards/C1484.htm>.
- Baetens, R., Jelle, B. P., Thue, J. V., Tenpierik, M. J., Grynning, S., Uvsløkk, S., & Gustavsen, A. (2010). Vacuum insulation panels for building applications: A review and beyond. *Energy and Buildings*.
- Bendergast, P., & Malone, B. (1999). Characterization and commercialization of INSTILL vacuum insulation core. *Vuoto Scienza Et Tecnologia*, 28(1–2), 77–82.
- Boafo, F. E., Chen, Z., Li, C., et al. (2014). Structure of vacuum insulation panel in building system. *Energy and Buildings*, 85, 644–653.
- Bouquerel, M., Duforestel, T., Baillis, D., et al. (2012). Mass transfer modeling in gas barrier envelopes for vacuum insulation panels: A review. *Energy and Buildings*, 55(55), 903–920.
- Bovenkerk, H. P. (1952). Insulating structure and method of forming same. United States Patent, US2700633. <https://patents.google.com/patent/US2700633A/en>.
- Brunner, S., Gasser, P., Simmler, H., et al. (2006). Investigation of multilayered aluminium-coated polymer laminates by focused ion beam (FIB) etching. *Surface and Coatings Technology*, 200(20–21), 5908–5914.
- Brunner, S. (2012). Superinsulating materials present applications. In *Proceedings of the International Symposium Superinsulating Mater.* <https://www.aivc.org/sites/default/files/Flyer.pdf>.
- Brunner, S., Ghazi Wakili, K., Stahl, T., & Binder, B. (2014). Vacuum insulation panels for building applications. Continuous challenges and developments. *Energy Build*, 85, 592–596.
- Caps, R., Fricke, J., & Reiss, H. (1984). Improving the extinction properties of an evacuated high-temperature powder insulation. In *Proceedings of the European Conference on Thermophysical Properties* (pp. 225–232).
- Caps, R., & Fricke, J. (2000). Thermal conductivity of opacified powder filler materials for vacuum insulations. *International Journal of Thermophysics*, 21(2), 445–452.
- Caps, R. (2006). Vacuum insulation panels for buildings and technical applications. In *Proceedings of the EPIC conference*. USA. <https://www.epicpeople.org/wp-content/uploads/2014/09/2006-EPIC-Conference-Proceedings.pdf>.
- Changhai, P., & Jianqiang, Y. (2016). Structure, mechanism, and application of vacuum insulation panels in chinese buildings. *Advances in Materials Science and Engineering* (pp. 1–12).
- Chen, Z., Chen, Z. F., Qiu, J. L., et al. (2011). Vacuum insulation panel for green building. *Applied Mechanics and Materials*, 71–78, 607–611.
- Chen, Z., Chen, Z. F., Yang, Z., Hu, J., Yang, Y., Chang, L., Lee, J. L., & Xu, T. (2015). Preparation and characterization of vacuum insulation panels with super-stratified glass fiber core material. *Energy*, 93, 945–954.
- Di, X., Gao, Y., & Bao, C., et al. (2013). Optimization of glass fiber based core materials for vacuum insulation panels with laminated aluminum foils as envelopes. *Vacuum*, 97(Complete), 55–59.
- EAD. (2017). European standard—EAD 040011-00-120, vacuum insulation panels (VIP) with factory applied protection layers. ETA. [https://www.eota.eu/download?file=/2013/13-04-0011/ead%20for%20jeu/ead%20040011-00-1201\\_ojeu2018.pdf](https://www.eota.eu/download?file=/2013/13-04-0011/ead%20for%20jeu/ead%20040011-00-1201_ojeu2018.pdf).
- Feng, J., Chen, D., Ni, W., et al. (2010). Study of IR absorption properties of fumed silica-opacifier composites. *Journal of Non-Crystalline Solids*, 356(9–10), 480–483.
- Fricke, J. (1993). Materials research for the optimization of thermal insulations. *High Temperatures-High Pressures*, 25(4), 379–390.

- Fricke, J. J. Z.-D. (2005). From Dewars to VIPs—one century of progress in vacuum insulation technology. In *Proceedings of the 7th International Vacuum Insulation Symposium*. EMPA.
- Fricke, J., Schwab, H., & Heinemann, U. (2006). Vacuum insulation panels—Exciting thermal properties and most challenging applications. *International Journal of Thermophysics*, 27(4), 1123–1139.
- GB/T. (2019). GB/T 37608-2019 Standard China, Vacuum insulation panels.China, 2019. GB/T 37608-2019 English Version, GB/T 37608-2019 Vacuum insulation panels (VIP) (English Version)—Code of China.
- Goncalves, M., Simoes, N., & Serra, C., et al. (2020). A review of the challenges posed by the use of vacuum panels in external insulation finishing systems. *Applied Energy*, 257(Jan.1):114028.1–114028.15.
- Heinemann, U., & Kastner, R. (2010). VIP-PROVE: Vakuumisolationspaneele—Bewährung in der Baupraxis. Wissenschaftliche Begleitforschung. Schlussbericht Energieoptimiertes Bauen, ViBau Report ZAE 2-1210-11, (VIP-PROVE: Vacuum insulation panels—Testing in construction practice. Scientific evaluation. Final report energy optimized construction). Report ZAE 2-1210-11, [In German]. Retrieved from Würzburg, Germany. [http://vip-bau.de/pdf/literatur/BMWi\\_0327321N\\_Schlussbericht%20VIP-PROVE.pdf](http://vip-bau.de/pdf/literatur/BMWi_0327321N_Schlussbericht%20VIP-PROVE.pdf).
- IEA/ECBCS. (2005). Study on VIP-components and panels for service life prediction of VIP in building applications. HIPTI-High Performance Thermal Insulation, IEA/ECBCS Annex 39.
- Jelle, B. P., Gao, T., Sandberg, L. I. C., et al. (2014). Thermal superinsulation for building applications—from concepts to experimental investigations. *International Journal of Structural Analysis & Design*, 1, 43–50.
- JG/T. (2014). JG/T 438-2014, Standard China-Vacuum insulation panels for buildings.China. <https://jz.docin.com/p-1017798981.html>.
- JIS. (2016). Japanese Standard JIS A1412-1, Test method for thermal resistance and related properties of thermal insulations-Guarded hot plate apparatus. JIS. [https://infostore.saiglobal.com/en-us/Standards/JIS-A-1412-1-2016-623369\\_SAIG\\_JSA\\_JSA\\_1431863/](https://infostore.saiglobal.com/en-us/Standards/JIS-A-1412-1-2016-623369_SAIG_JSA_JSA_1431863/).
- Johansson, P. (2012). Vacuum insulation panels in buildings: Literature review. Chalmers University of Technology, Göteborg, Sweden 2012 Report 2012:1.
- Johansson, P., Adl-Zarrabi, B., & Sasic-Kalagasidis, A. (2016). Evaluation of 5 years' performance of VIPs in a retrofitted building façade. *Energy and Buildings*, 130, 488–494. <https://publications.lib.chalmers.se/records/fulltext/155961.pdf>.
- Jung, H., Yeo, I., & Song, T. (2014). Al-foil-bonded enveloping and double enveloping for application to vacuum insulation panels. *Energy and Buildings*, 84, 595–606.
- Kaganer, M. G. (1969). Teplovaia izoliatsiia v tekhnike nizkikh temperatur. Translation from Russian, Thermal insulation in cryogenic engineering. Israel Program for Scientific Translations. <https://searchworks.stanford.edu/view/692715>.
- Kalnæs, S. E., & Jelle, B. P. (2014). (2014) Vacuum insulation panel products: A state-of-the-art review and future research pathways. *Applied Energy*, 116, 355–375. <https://doi.org/10.1016/j.apenergy.2013.11.032>
- Karami, P., Gudmundsson, K., Björk, F., & Heymans, L. (2015). ETICS with vacuum insulation panels for retrofitting buildings from the great Swedish housing program “Miljonprogrammet”. In *Proceedings of the 12th International Vacuum Insulation Symposium—IVIS2015* (pp. 1–6). <https://vipa-international.org/uploads/kcFinder/files/Session%20III-1.pdf>.
- Kim, J., Song, T. H. (2013). Vacuum insulation properties of glass wool and pacified fumed silica under variable pressing load and vacuum level. *International Journal of Heat & Mass Transfer*, 64(sep.), 783–791.
- Kreith, F., & Black, W. (1980). *Basic heat transfer*. Harper & Row.
- Kubina, L. (2010). Etics with integrated vacuum insulation panels. In *Proceedings of the International Conference Central Europe towards Sustainable Building CESB* (pp. 2–5). [http://cesb.cz/cesb10/papers/3\\_materials/229.pdf](http://cesb.cz/cesb10/papers/3_materials/229.pdf).
- Lim, T., Seok, J., & Kim, D. (2017). A comparative study of energy performance of fumed silica vacuum insulation panels in an apartment building. *Energies*, 10(12), 1–12.

- Lyman, B. E., & Neeser, T. A. (2005). Vacuum insulation panel. United State, 5664396.
- Mandilaras, I., Atsonios, I., Zannis, G., & Founti, M. (2014). Thermal performance of a building envelope incorporating ETICS with vacuum insulation panels and EPS. *Energy Build*, 85, 654–665.
- Mukhopadhyaya, P. (2015). Long term thermal resistance of vacuum insulation panel (VIP)—Experimental observations & predictions. In *12th International Vacuum Insulation Symposium*.
- Mukhopadhyaya, P., Maclean, D., Korn, J., et al. (2014). Building application and thermal performance of vacuum insulation panels (VIPs) in Canadian subarctic climate. *Energy and Buildings*, 2014, 85.
- OECD/IEA. (2015). Building energy use in China—Transforming construction and influencing consumption to 2050. Tsinghua University. <https://webstore.iea.org/energy-use-in-the-chinese-building-sector>.
- Pons, E., Yrieix, B., & Brunner, S. (2017). Evaluation of VIPs after mild artificial aging during 10 years: Focus on the core behavior. *Energy and Buildings*, S0378778817329717.
- Schiavoni, S., D’Alessandro, F., & Bianchi, T., et al. (2016). Insulation materials for the building sector: A review and comparative analysis. *Renewable and Sustainable Energy Reviews*, 62, 988–1011.
- Shimada, M., & Katto, A. (1983). Solar heat collector assembly. United StatPatent, US4409964. <https://patents.google.com/patent/US4409964A/en>.
- Singh, H., Geisler, M., & Menzel, F. (2015). Experimental investigations into thermal transport phenomena in vacuum insulation panels (VIPs) using fumed silica cores. *Energy and Buildings*, 107, 76–83.
- Simmler, H., & Brunner, S. (2005). Vacuum insulation panels for building application: Basic properties, aging mechanisms and service life. *Energy & Buildings*, 37(11), 1122–1131.
- Stec, A. A., & Hull, T. R. (2011). Assessment of the fire toxicity of building insulation materials. *Energy and Buildings*, 43(2–3), 498–506.
- Tenpierik, M. (2009). Vacuum insulation panels applied in buildings constructions. Report, Technische Universiteit Delft. <https://repository.tudelft.nl/islandora/object/uuid%3Ae32e4540-e301-4015-aab9-b56feb5775d1>.
- Wakili, K. G., Bundi, R., & Binder, B. (2004). Effective thermal conductivity of vacuum insulation panels. *Building Research & Information*, 32(4), 293–299.
- Wu, W. P., Chen, Z. F., Zhou, J. M., & Cheng, X. Y. (2012). Thermal properties of vacuum insulation panels with glass fiber. *Advanced Materials Research*, 446–449, 3753–3756. <https://doi.org/10.4028/www.scientific.net/amr.446-449.3753>
- Yamada, M. (2005). Development on new vacuum insulation panel, “Chip-Vacume”. In *Proceedings of the 7th International Vacuum Insulation Symposium* (pp. 181–182).
- Zimmermann, M., & Bertschinger, H. (2001). High performance thermal insulation systems. Vacuum insulated products (VIP). In IEA, *Proceedings of the International Conference and Workshop, EMPA*, [http://www.iea-ebc.org/Data/publications/EBC\\_Annex\\_39\\_2001\\_1\\_hipti\\_proc.pdf](http://www.iea-ebc.org/Data/publications/EBC_Annex_39_2001_1_hipti_proc.pdf).

# Chapter 12

## The Concept of Nano Insulation Materials—Challenges, Opportunities, and Experimental Investigations



Bjørn Petter Jelle

**Abstract** The world of today is experiencing an ever-increasing interest and focus on material scarcity and abundance, energy efficiency and renewable and non-polluting energy harvesting. The main driving force of this increasing focus is global warming and climate changes due to emission of greenhouse gases to the atmosphere through various man-made processes. In this regard, the building sector represents one of the major sectors with a large potential for improvements, both for renovation of existing buildings and construction of new ones. Buildings which are thermally well insulated will have less energy demand for heating and cooling, i.e. energy-efficient buildings. Thus, there is a quest to invent and make thermal insulation materials with a low thermal conductivity and other suitable properties, to avoid undesirable thick building envelopes as would have been the case when applying traditional thermal insulation materials in situations where a large thermal resistance is required. This has led to an increased interest for today's state-of-the-art thermal insulation materials with low thermal conductivities, where especially commercial vacuum insulation panel (VIP) and aerogel products have experienced increased use during the last decades. However, VIPs and aerogels have several disadvantages, among them high costs for both VIPs and aerogels, and the loss of vacuum, either by perforations or long-term diffusion. One of the promising candidates for becoming the high-performance or super insulation material (SIM) of tomorrow is nano insulation materials (NIM). The utilization of the Knudsen effect in order to reach very low thermal conductivities represents the governing principle of NIMs. Wanting the SIM and NIM to be functioning with air at atmospheric pressure in their pores, the size of the pores should be made very small in the nano range well below 100 nm according to calculations exploiting the Knudsen effect. NIMs may be manufactured in several ways, and herein a few possible pathways will be discussed. A special focus will be given on the experimental synthesis and investigations of hollow silica nanospheres (HSNS) by applying a sacrificial template method, where the inner nanosphere diameter and

---

B. P. Jelle (✉)

Department of Civil and Environmental Engineering, Norwegian University of Science and Technology (NTNU), NO-7491 Trondheim, Norway

e-mail: [bjorn.petter.jelle@ntnu.no](mailto:bjorn.petter.jelle@ntnu.no)

the shell thickness can be controlled through the parameters of the syntheses. Thus, the HSNS may be tailor-made with the desired low thermal conductivity.

**Keywords** Nano insulation material · NIM · Hollow silica nanosphere · HSNS · Super insulation material · SIM · Knudsen effect · Thermal insulation · Thermal conductivity · Building

## 12.1 Introduction

Material resources scarcity and abundance, energy efficiency and renewable and non-polluting energy harvesting are key aspects to be dealt with in the years ahead in order to reduce global warming and climate changes caused by the emission of greenhouse gases to the Earth's atmosphere through many different man-made processes. During the last decades there has been an increased interest and pressure for changes concerning these issues, i.e. strong driving forces for decreasing the negative environmental impact.

The building sector represents one of the major sectors with a large improvement potential. This includes refurbishment of existing buildings and construction of new buildings. Heating and cooling loads are among the largest energy consumption loads in buildings. Buildings should be as energy-efficient as possible so that they can harvest their own demand for energy through exploitation of solar radiation by daylight utilization and electricity generation by solar cells.

Of special interest in this regard is the possibility of integrating solar cells into the exterior skin of the building envelope and hence functioning as both a weather protection screen and an electricity generator, i.e. denoted as building integrated photovoltaics (BIPV) (Andenæs et al., 2018; Andersson et al., 2017; Borrebæk et al., 2020; Breivik et al., 2013; Fasana & Nelva, 2013; Jelle, 2013c, 2016a; Jelle & Breivik, 2012a, b; Jelle et al., 2012; Jelle et al., 2016; Norton et al., 2011; Tripathy et al., 2016).

Furthermore, and of special interest with respect to the energy efficiency of buildings, is the possibility of dynamically regulating the solar transmittance through windows and other transparent or translucent parts of the building envelope. This may be accomplished by the utilization of smart windows and maybe in particular with electrochromic windows (Baetens et al., 2010d; Chiang & MacDiarmid, 1986; Deb, 2008; Granqvist, 1995, 2005, 2008, 2012; Granqvist et al., 2018; Huang et al., 1986; Jelle, 1993, 2013a, 2015; Jelle & Hagen, 1993, 1998, 1999a, b; Jelle et al., 1992a, b, 1993a, b, c, 1998, 2007, 2012a; Lampert, 1984, 1998, 2004; Monk et al., 1995; Mortimer, 1999; Mortimer et al., 2006; Tällberg et al., 2019).

Thermally well insulated buildings will have less energy demand for heating and cooling, and these buildings will thereby also be putting less strain on any renewable or other energy source. Thus, high-performance thermal insulation materials and systems (Annex 65, 2017, 2020; Baetens et al., 2010a, Gao & Jelle, 2019; Jelle, 2011a, 2016b; Jelle et al., 2010a, 2014a, b, 2019; Koebel et al., 2012, 2016; Li et al.,

2018; Rostam et al., 2015; Wang et al. 2017a, b) will be playing an important role in coming years.

In this respect, it should be noted that regarding abatement costs with respect to CO<sub>2</sub>, energy efficiency measures such as e.g. thermal insulation retrofitting are far more effective than e.g. energy harvesting measures like e.g. solar photovoltaics and wind energy (McKinsey, 2009). In addition, still concerning abatement costs with respect to CO<sub>2</sub>, it is seen that thermal insulation retrofitting, commercial and then residential, are more effective than building efficiency measures for new buildings (McKinsey, 2009).

Today's typical traditional thermal materials include mineral wool like glass wool and rock wool, and polystyrene products like expanded polystyrene (EPS) and extruded polystyrene (XPS), which all have thermal conductivities between 30 and 40 mW/(mK), then also including cellulose, cork and other variants which have somewhat higher thermal conductivity values between 40 and 50 mW/(m·K), and then also including polyurethane (PUR) and similar products with somewhat lower thermal conductivities between 20 and 30 mW/(m·K) (Jelle, 2011a). It should be noted that PUR products, when exposed to fire, will release highly toxic gases like hydrogen cyanide (HCN) and isocyanates. Furthermore, applying traditional thermal insulation materials may lead to undesirable thick building envelopes in order to achieve an adequate thermal resistance (to satisfy current building code requirements). Hence, there is a goal to invent and make thermal insulation materials with considerably lower thermal conductivities and other suitable properties.

Thus, this has led to an increased interest for today's state-of-the-art thermal insulation materials with substantially lower thermal conductivities, which include vacuum insulation panels (VIP) (Alam et al., 2011, 2014, 2017; Baetens et al., 2010a; Bouquerel et al., 2012; Grynning et al., 2011; Haavi et al., 2012; Jelle & Kalnæs, 2016; Kalnæs & Jelle, 2014; Sveipe et al., 2011; Wegger et al., 2011), gas-filled panels (GFP) (Baetens et al., 2010c; Mills & Zeller, 2008) and aerogels (Baetens et al., 2011; Buratti et al., 2014; Gao et al., 2014c, d; Jelle & Gao, 2019; Jelle et al., 2015; Sletnes et al., 2017). Furthermore, low-emissivity materials may play an important role for many building applications (Gao & Jelle, 2017; Jelle et al., 2015). Towards the ground part of the building envelope it is common to apply radon barriers (Jelle, 2012a; Jelle et al., 2011; Pacheco-Torgal, 2012), and in some cases it may be beneficial to combine radon barriers with low-emissivity coatings, i.e. reducing both the radon transport to the interior of the building and the thermal radiation towards the exterior ground. Moreover, phase change materials (PCM) (Baetens et al., 2010b; Demirbas, 2006; Jelle & Kalnæs, 2017; Kalnæs & Jelle, 2015) might also be a part of the thermal building envelope by exploiting the PCMs' ability by temperature activation to absorb and release heat energy when required.

The VIP product consists of an open-porous core of e.g. fumed (pyrogenic) silica enveloped by a metallized laminate or foil keeping a vacuum inside the VIP core. When breaking or perforating the VIP laminate, e.g. by cutting or driving a nail through, this will lead to a loss of vacuum and hence subsequent increased thermal conductivity. In any case, diffusion of air and moisture through the VIP laminate and into the VIP core will with time increase the thermal conductivity, typically from



about 4 mW/(mK) in the pristine, non-aged condition to about 20 mW/(mK) in the non-vacuum condition for VIPs with fumed silica cores.

The GFP products are in many ways similar to the VIP products, with the difference that instead of vacuum the GFPs have thermally low-conducting gases in their cores. Normally, the GFP pores are macroscopic voids or cavities and thereby considerably larger than the pores in the VIP cores which are in the micro and nano range. The GFPs' potential may seem high, however, up until now the GFPs have still not come into relatively widespread usage as compared with the VIPs. Hence, VIPs may currently seem to be the better choice between these two thermal insulation products.

Various aerogel products have thermal conductivities typically between 12 and 20 mW/(m·K). Aerogels have a very high porosity and are hence mostly consist of air (95–99 vol%). Thus, the aerogels can be cut, adapted and perforated as desired at the building site and during operation throughout their lifetime. However, aerogels are very brittle and the current commercial aerogel products are very expensive, even more costly than VIP products. Nevertheless, the aerogel products may be manufactured as opaque, translucent or transparent materials. Thereby, the aerogels may be able to fulfil several different functions in a building and hence the aerogels can find their applications in several areas. Thus, for such a versatile aerogel product one may also be willing to pay considerably more.

Hence, there is a quest to attempt to make new thermal insulation materials without the disadvantages of the state-of-the-art thermal insulation materials (VIPs, GFPs and aerogels), and with very low thermal conductivity values. Stagnant air has a thermal conductivity value of about 26 mW/(m·K), and an initial, major step will be to reach thermal conductivities below this value. Super insulation materials (SIM) may be defined in different ways, but normally they are defined with a thermal conductivity value of at least below 20 mW/(m·K).

Nano insulation materials (NIM) represent a promising candidate for becoming the future high-performance or super insulation material. The governing principle of NIMs is the exploitation of the Knudsen effect in a porous medium where the gas thermal conductivity, also including the interaction between the gas molecules and the pore walls, will be considerably lowered when the pore diameters of the porous thermal insulation material are decreased in the nano range so that the pore diameters become smaller than the mean free path of the gas molecules (Jelle, 2011a, 2016b; Jelle et al., 2010a, 2014a, b, 2019). As the SIMs and NIMs should be functioning with air at atmospheric pressure in their pores (i.e. without being based on vacuum, low pressure or any low-conducting gases), the size of the pores should then be made very small in the nano range well below 100 nm according to calculations utilizing the Knudsen effect.

It may be possible to fabricate NIMs in several ways, and a few possible pathways will be discussed. Herein, we will be elaborating more in detail the experimental synthesis and investigations of hollow silica nanospheres (HSNS) by applying a sacrificial template method. By manufacturing the HSNS, the inner nanosphere diameter and the shell thickness can be controlled through the parameters of the syntheses. Thereby and finally, the HSNS may be tailor-made with the desired low thermal conductivity, thus achieving the aim of making a SIM as a NIM.

## 12.2 Thermal Transport in Materials and Through Building Envelopes

In a material and through the building envelope there are several contributions to the thermal transport. The key property for a thermal insulation material is the thermal conductivity, where normally the strategy is to reach as low thermal conductivity as possible. Thus, a low thermal conductivity ( $W/(m \cdot K)$ ) will enable the utilization of relatively thin building envelopes with a high thermal resistance ( $m^2 \cdot K/W$ ) and a low thermal transmittance U-value ( $W/(m^2 \cdot K)$ ). The total overall thermal conductivity  $\lambda_{tot}$  may in principle be written in a simplified way as a sum of the following contributions (Jelle, 2011a, 2016b).

$$\lambda_{tot} = \lambda_{solid} + \lambda_{gas} + \lambda_{rad} + \lambda_{conv} + \lambda_{coupling} + \lambda_{leak} \quad (12.1)$$

where  $\lambda_{tot}$  is the total overall thermal conductivity,  $\lambda_{solid}$  is the solid-state thermal conductivity,  $\lambda_{gas}$  is the gas thermal conductivity,  $\lambda_{rad}$  is the radiation thermal conductivity,  $\lambda_{conv}$  is the convection thermal conductivity,  $\lambda_{coupling}$  is the thermal conductivity term accounting for second order effects between the various thermal conductivities given in Eq. 12.1, and  $\lambda_{leak}$  is the leakage thermal conductivity.

With the goal to reach as low a thermal conductivity as possible, each of the above contributions to the thermal transport processes must be minimized. Note that in this respect, the leakage thermal conductivity  $\lambda_{leak}$  representing an air and moisture leakage driven by a pressure difference, is normally not considered as one of insulation materials' properties and typical solutions are assumed to be without any holes which otherwise would have enabled thermal losses. The coupling term  $\lambda_{coupling}$  is included to account for second order effects between the various thermal conductivities in Eq. 12.1. Noteworthy, this coupling effect can be quite complex and will in general be neglected in the rest of this study. Also note that theoretical approaches to the thermal performance of vacuum insulation panels (VIP) usually assume this coupling effect to be negligible, where further information can be found in the work by e.g. Heinemann (2008). Nevertheless, another coupling term could also be included in Eq. 12.1, i.e. the interaction between the gas molecules and the solid state pore walls. This last coupling term is included through a factor in the expression for the gas conductivity as given in the simplified equation for the Knudsen effect (Eq. 12.2), which will be elaborated in our following discussions concerning the concepts of nano insulation materials.

The solid-state thermal conductivity  $\lambda_{solid}$  is directly connected to the thermal or heat transport between atoms by lattice vibrations, i.e. through chemical bonds between atoms. The gas thermal conductivity  $\lambda_{gas}$  is connected to the gas molecules colliding with each other and hence transferring thermal energy from one molecule to the other. The radiation thermal conductivity  $\lambda_{rad}$  is linked to the emittance of the electromagnetic radiation in the infrared (IR) wavelength region from a material surface. The convection thermal conductivity  $\lambda_{conv}$  is coming from the thermal mass transport or movement of air and moisture. Finally, all these thermal conductivity

contributions are driven by or dependent upon the temperature or temperature difference. Miscellaneous strategies are used and exploited to keep the specific thermal conductivities for different thermal insulation materials as low as possible.

As the thermal building insulation materials and solutions also must fulfil a series of requirements with respect to other properties than the thermal conductivity, these other requirements can and will induce various restrictions and challenges regarding how low thermal conductivities it may be possible to reach with specific materials and solutions.

## 12.3 Traditional Thermal Insulation

A short description of the most common traditional (conventional) thermal building insulation materials of today are given by Jelle (2011a, 2016b). These materials are not considered as super insulation materials, but they may still have a relatively low thermal conductivity. The overviews of traditional thermal insulation materials by Al-Homoud (2005) and Papadopoulos (2005) may also be mentioned in this regard.

The traditional thermal building insulation materials include mineral wool (glass wool and rock wool), expanded polystyrene (EPS) and extruded polystyrene (XPS) with typical thermal conductivity values between 30 and 40 mW/(m·K), cellulose and cork with typical thermal conductivities between 40 and 50 mW/(m·K), and polyurethane (PUR) with typical thermal conductivity values between 20 and 30 mW/(m·K), i.e. the lowest conductivity values considerably lower than the ones for mineral wool, polystyrene and cellulose products. However, it should be noted that although PUR is safe in its intended use it rises serious health concerns and hazards in case of a fire as PUR when burning will release hydrogen cyanide (HCN) and isocyanates, which are very poisonous. The toxicity of HCN is due to the cyanide anion (CN<sup>-</sup>) which is preventing cellular respiration.

Furthermore, one may also attempt to reduce the thermal conductivity of traditional thermal insulation materials by utilizing nano-based technologies, e.g. by synthesizing porous materials with the pores and voids located in the nano range. The traditional thermal insulation materials as of today have their pore and void volume mainly made up from pores and voids within the millimeter to the nanometer range.

## 12.4 State-of-The-Art Thermal Insulation

The state-of-the-art thermal building insulation materials and solutions of today are described and discussed by Jelle (2011a, 2016b). These are, the materials and solutions which are considered to be best ones existing today, i.e. the thermal building insulation materials with the lowest thermal conductivities as of today. These state-of-the-art thermal insulation materials are utilizing to a large extent porous material where the pores are within the nano range (except macropores for gas-filled panels).

Vacuum insulation panels (VIP) represent the state-of-the-art thermal building insulation material solution with the currently lowest thermal conductivity of a commercial thermal building insulation material. A VIP consists of an open porous core of fumed silica enveloped of several metallized polymer laminate layers. The VIP core may also consist of other materials than fumed (pyrogenic) silica particles, e.g. aerogels, polyurethane foam, polystyrene foam and various glass fibres, in addition to the commonly added desiccants, getters and opacifiers, the three latter ones for absorbing permeating water vapour, absorbing permeating gases and decreasing the radiative heat transfer, respectively (Jelle & Kalnæs, 2016; Kalnæs & Jelle, 2014). The centre-of-panel thermal conductivity values of VIPs are ranging from as low as 2 to 4 mW/(m·K) in the pristine (non-aged) condition to typically 8 mW/(m·K) after 25 years ageing due to water vapour and air diffusion through the VIP envelope and into the VIP core material which has an open pore structure. Depending on the type of VIP envelope, the aged thermal conductivity after 50 and 100 years will be somewhat or substantially higher than this value. This inevitable increase of the thermal conductivity represents a major disadvantage of all VIPs. Furthermore, if the VIP envelope is punctured, e.g. due to nails and similar, the centre-of-panel thermal conductivity will increase to about 20 mW/(m·K) for VIPs with fumed silica cores. Therefore, VIPs cannot be cut for adjustment at the building site or perforated without losing a large part of their thermal insulation resistance performance.

Both scientifically and commercially, VIPs have experienced an increasing interest where several authors have been investigating various aspects of this thermal insulation solution. These aspects include air and moisture penetration, ageing and service life, quality control, theoretical and analytical models, thermal bridges and their influence on the thermal conductivity, integration in building constructions including VIPs as exterior or interior thermal insulation retrofitting and various case studies. Examples of some of these investigations may be found in the studies by e.g. Alam et al., (2011, 2014, 2017), Alotaibi and Riffat (2014), Baetens (2013), Baetens et al. (2010a), Bataud et al. (2018), Beck et al. (2007), Biswas et al. (2019a, b), Bofo et al. (2014), Brunner and Simmler (2007, 2008), Brunner and Ghazi Wakili (2014), Brunner et al. (2006, 2012a, b, 2014), Caps (2005), Caps and Fricke (2000), Caps et al. (2001, 2008), Cho et al. (2014), De Masi et al. (2020), De Meersman et al. (2015), Fantucci et al. (2019), Fricke (2005), Fricke et al. (2006, 2008), Geng et al. (2021), Gonçalves et al. (2020), Grynning et al. (2011), Haavi et al. (2012), Heinemann and Kastner (2010), Heinemann et al. (2005), Jelle and Kalnæs (2016), Jelle et al. (2013, 2015), Johansson et al. (2014), Kalnæs and Jelle (2014), Kim et al. (2017), Lakatos and Kovács (2021), Li et al. (2015), Liang et al. (2017), Mandilaras et al. (2014), Mao et al. (2020), Miesbauer et al. (2014), Mukhopadhyaya et al. (2014), Pons et al. (2014), Pool (2009), Sallée et al. (2014), Schwab et al. (2005a, b, c, d, e), Simmler and Brunner (2005a, b), Simmler et al. (2005), Simões et al. 2021, Sprengard and Holm (2014), Sveipe et al. (2011), Tenpierik (2009), Tenpierik and Cauberg (2007), Tenpierik and Cauberg (2010), Tenpierik et al. (2007a, b, 2008), Uriarte et al. (2019), Van Den Bergh et al. (2011), Voellinger et al. (2014), Ghazi Wakili et al., (2004, 2005, 2011, 2014), Wegger et al. (2011), Yrieix et al. (2014) and Zwerger and Klein (2005). Among others, comprehensive reviews on VIPs for

building applications have been made by Baetens et al. (2010a), Gonçalves et al. (2020), Jelle and Kalnæs (2016), Kalnæs and Jelle (2014) and Tenpierik (2009).

With respect to forthcoming attempts to make nano insulation materials, it is important to note the thermal conductivity difference between 4 mW/(m·K) (pristine condition) and 20 mW/(m·K) (punctured) for VIPs, i.e. a difference of 16 mW/(m·K), which is entirely due to the changes in the gas thermal conductivity (then not accounting for any changes to the solid core due to the loss of vacuum). Hence, the combined solid state and radiation thermal conductivity of fumed silica in these VIPs is as low as 4 mW/(m·K) or in principle somewhat lower (as there is still a very small air residue inside a VIP it means that a small part of the 4 mW/(m·K) value is due to gas conduction). Thus, since it is possible to make thermal insulation materials with such a very low solid state and radiation conductivity, there should obviously be rather good opportunities to fabricate a super insulation material functioning at atmospheric air pressure by lowering the gas thermal conductivity.

Gas-filled panels (GFP) are representing another state-of-the-art thermal building insulation material solution. In principle, the GFPs are close to the technology of vacuum insulation panels (VIP). GFPs apply a gas less thermal conductive than air, such as e.g. argon (Ar), krypton (Kr) and xenon (Xe), instead of vacuum as in the VIPs. Among others, GFPs have been investigated by Desjarlais et al. (2016), Griffith et al. (1993, 1995) and Mills and Zeller (2008), and furthermore a review of GFPs for building applications has been given by Baetens et al. (2010c). Compared to the available literature and various studies for VIPs, there exists much less information on GFPs than VIPs, which may also be seen as a considerably less interest for GFPs than VIPs.

Crucial to the thermal performance of the GFPs is to avoid air and moisture penetration and thereby keep the low-conductive gas concentration inside the GFPs. Although low-conducting gases are applied in the GFPs, vacuum is nevertheless a better thermal insulator than these gases. However, then the GFP grid structure does not have to withstand the large pressure difference between the inner (near) vacuum as in the VIPs and the ambient atmospheric pressure. Moreover, applying low-emissivity surfaces inside the GFPs will decrease the radiative heat transfer. Thermal conductivity values for prototype GFPs are currently rather high, e.g. 40 mW/(m·K), although much lower theoretical values have been calculated. Thus, the GFPs hold many of the advantages and disadvantages of VIPs. GFPs as a future thermal building insulation solution may be questioned, and even doubtful some may claim, as compared to them the VIPs seem to offer a better solution both for today and the years ahead until new thermal insulation materials and solutions are developed.

Aerogels are also representing a state-of-the-art thermal insulation material solution, and perhaps the most promising with the highest potential of them all at the moment. The very low thermal conductivity of aerogels is due to a highly porous and air-filled (at atmospheric pressure) low-density silica skeleton with a typical air concentration as high as 95–99 vol%. Therefore, aerogels are sometimes denoted as frozen air.

There have been conducted numerous studies of aerogels, see e.g. the investigations by Aegerter et al. (2011), Baetens et al. (2011), Baillis et al. (2015), Berardi and Nosrati (2018), Bheekhun et al. (2013), Bi et al. (2014), Buratti (2019), Buratti and Moretti (2012a, b), Buratti et al., (2014, 2017a, b), Cotana et al. (2014), Cuce et al. (2014), Dowson et al. (2012), Fu et al. (2018), Gao et al. (2014c, d, 2016a, b), He and Xie (2015), Hostler et al. (2009), Ihara et al. (2015a, b, c), Jelle and Gao (2019), Jelle, Baetens et al. (2015), Koebel et al. (2012, 2016), Lamy-Mendes et al. (2021), Lee, Stevens et al. (1995), Lee, Kim et al. (1995), Lee, Stevens et al. (1995), Lee, Kim, et al. (1995), Levy and Zayat (2015), Li et al. (2017), Li et al. (2021), Moretti et al. (2017a, b, 2018), Nosrati and Berardi (2017, 2018), Schultz and Jensen (2008), Schultz et al. (2005), Smith et al. (1998), Stahl et al. (2012), Ghazi Wakili and Remhof (2017), Wong et al. (2014), Zhao et al. (2012) and Zhu et al. (2018) among many others.

When utilizing carbon black to suppress the radiative heat transfer, aerogels may reach thermal conductivities as low as  $4 \text{ mW}/(\text{m}\cdot\text{K})$  at a pressure of 50 mbar. However, the lowest thermal conductivity values for commercially available state-of-the-art aerogel products have been reported between 13 and  $14 \text{ mW}/(\text{m}\cdot\text{K})$  at ambient pressure (Aspen Aerogels 2008a, b). Then, higher thermal conductivities than these ones are common for various aerogel products, e.g. up to and also somewhat above  $20 \text{ mW}/(\text{m}\cdot\text{K})$ . Aerogels have a low tensile strength and are thereby very fragile, although with a relatively high compression strength. A carbon fibre matrix may be incorporated and hence increase the tensile strength. Furthermore, the production costs of aerogels are still very high.

Aerogels can be manufactured as either opaque, translucent or transparent materials, which makes it possible for aerogels to be used for many different building applications. Opaque aerogel products are often used to minimize heat bridges in buildings where the available space for thermal insulation is restricted. Compared to the opaque aerogel products, the translucent and transparent forms of aerogels have an added value as they can utilize the solar radiation as daylight and solar heat through windows and solar walls. That is, one may be able to pay for substantially larger costs when applying translucent and transparent aerogel products. In any case, the production costs have to be substantially reduced for aerogels to become a widespread thermal insulation material for opaque building applications. Note also the overview on past, present and future developments of transparent insulation materials by Paneri et al. (2019).

Furthermore, incorporating aerogels in the form of e.g. aerogel granules may be used to decrease the thermal conductivity of concrete, mortar, plasters, clay and similar material composites, see e.g. the studies by Berardi (2017), Buratti et al. (2014), Fickler et al. (2015), Gao et al. (2014a), Hostler et al. (2009), Huang et al. (2018), Fátima Júlio et al. (2016), Li et al. (2019), Liu et al. (2018), Ng and Jelle (2017), Ng et al. (2015a, b, 2016a, b), Schuss et al. (2017), Stahl et al. (2012), Ghazi Wakili et al., (2015, 2018), Wang et al. (2018), Wang et al. (2019), Welsch et al. (2018), Wernery et al. (2017), Yoon et al. (2020) and Zhu et al. (2019, 2020). For more general studies concerning nanotechnology with concrete see e.g. the studies by Raki et al. (2010), Sanchez and Sobolev (2010) and Sobolev and Gutiérrez (2005).

Phase change materials (PCM) are not really thermal insulation materials, but as they may play a role of the thermal building envelope, they are hence interesting for thermal building applications. As PCMs are heated, they change phase from solid state to liquid, thus absorbing energy in an endothermic process. Then, when the ambient temperature is lowered, the liquid PCMs will turn into solid state materials again and at the same time release the earlier absorbed heat in an exothermic process. Thereby, the indoor building temperature is stabilized by this phase change cycle, thus decreasing heating and cooling loads.

Various paraffins represent typical examples of PCMs, but a low thermal conductivity (Farid et al., 2004) and a large volume change during phase transition (Hasnain, 1998) restrict their building applications. Corresponding melting enthalpies and melting temperatures are given for different groups of PCMs by Dieckmann (2013). An overview of the main PCMs has been presented by Demirbas (2006). Miscellaneous other reviews on PCMs can be found in the investigations by Baetens et al. (2010b), Farid et al. (2004), Hasnain (1998), Jelle and Kalnæs (2017), Jurkowska and Szczygieł (2016), Kalnæs and Jelle (2015), Khudhair and Farid (2004), Leite da Cunha and Barroso de Aguiar (2020), Marani and Nehdi (2019) and Zhou et al. (2012). For some other investigations on PCMs, see e.g. the studies by Cao et al. (2010) and Kishore et al. (2021).

When choosing a specific PCM for building applications, the phase change temperature, and the ability to absorb and release large amounts of heat are important properties. Encapsulation is needed to avoid leaking problems of the liquid phase of PCMs to the surface and diffusing of low viscous liquids throughout the material (Özonur et al., 2006). Two PCM encapsulation techniques are denoted microencapsulation and macroencapsulation, and in addition nanoencapsulation has also been proposed. Note that the optimal phase change temperature for summer conditions will not be optimal for winter conditions and vice versa. To be able to partly counteract this, one may design systems with PCMs of different phase change temperatures by adding different layers of PCMs with different phase change temperatures working optimally at different temperatures (Jin & Zhang, 2011; Pasupathy & Velraj, 2008). One may also imagine creating a system with an adjustable phase change temperature where the efficiency could be substantially improved, which could either be performed through a controllable or an adaptive system and would thus enable a dynamical change of the phase change temperature in response to user preferences, different climates, and different seasons (Jelle & Kalnæs, 2017; Kalnæs & Jelle, 2015). It is referred to the studies by Jelle and Kalnæs (2017) and Kalnæs and Jelle (2015) for more details and state-of-the-art reviews on PCM products including further perspectives on various possible future research opportunities for PCMs.

## 12.5 The Nano Insulation Material Concept

The concept of nano insulation materials (NIM) was originating as a desire and an attempt to invent a thermal insulation material with as low thermal conductivity as

vacuum insulation panels (VIP) in their pristine and non-aged condition but without the disadvantages of VIPs related to keeping a (near) vacuum in their open-porous cores and thus the need of applying enveloping laminates (e.g. diffusion of air and moisture into the cores and that VIPs cannot be cut or perforated). Hence, the idea of making a material with an open or a closed pore structure at nanoscale was conceived, then by utilizing the already known Knudsen effect which we soon will elaborate further.

For a NIM the pore size within the material is reduced below a certain level, i.e. 40 nm or below for air, in order to reach an overall thermal conductivity of less than 4 mW/(m·K) in the pristine condition. That is, a NIM is defined as basically a homogeneous material with a closed or open small nanoporous structure with an overall thermal conductivity of less than 4 mW/(m·K) in the pristine condition (Jelle, 2011a; Jelle et al., 2010a). Naturally, the thermal conductivity may also of course be set to another low value, as 4 mW/(m·K) was originally chosen in order to have a very low value at the level of a VIP in its pristine condition. To illustrate the NIM idea conception and the development from VIP to NIM it is referred to Fig. 12.1.

The NIMs need to prevent air and moisture penetration into their pore structure during their service life for at least 100 years. The low thermal conductivity in NIMs is achieved without applying a vacuum in the nanoporous structure by utilizing the Knudsen effect, i.e. the NIMs will reach their low thermal conductivity with air at atmospheric pressure in their pores and thus the NIMs will be functioning at ambient pressure.

A thermal conductivity combining the gas thermal conductivity and the gas and solid state (pore wall) interaction, taking into account the Knudsen effect, may be denoted as  $\lambda_{gas+gas/solid\ state}$  or  $\lambda_{Kn}$  for short and written in a simplified way as (Baetens et al., 2010a; Bouquerel et al., 2012; Jelle, 2011a; Jelle et al., 2010a; Kaganer, 1969):

$$\lambda_{Kn} = \frac{\lambda_{gas,0}}{1 + 2\beta Kn} = \frac{\lambda_{gas,0}}{1 + \frac{\sqrt{2}\beta k_B T}{\pi d^2 p \delta}} \tag{12.2}$$

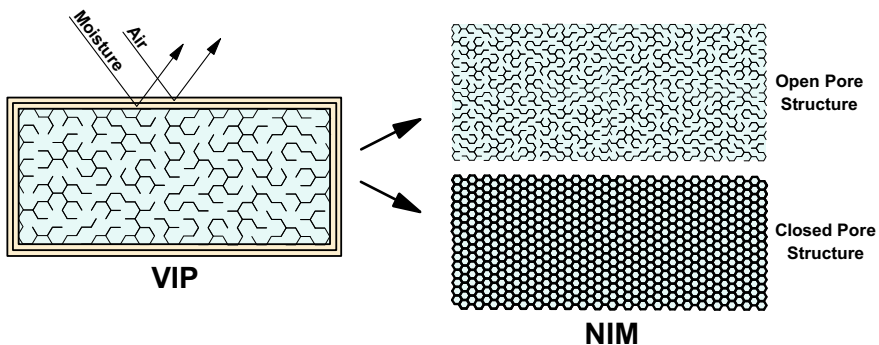


Fig. 12.1 The NIM idea conception and development from VIP to NIM (Jelle et al., 2010a)



where

$$Kn = \frac{\sigma_{mean}}{\delta} = \frac{k_B T}{\sqrt{2}\pi d^2 p \delta} \tag{12.3}$$

where  $\lambda_{Kn}$  is the Knudsen calculated thermal conductivity,  $\lambda_{gas,0}$  is the gas thermal conductivity in the pores at STP (standard temperature and pressure) (W/(m·K)),  $\beta$  is the coefficient characterizing the molecule-wall collision energy transfer (in)efficiency (between 1.5 and 2.0),  $k_B$  is the Boltzmann’s constant  $\approx 1.38 \cdot 10^{-23}$  J/K,  $T$  is the temperature (K),  $d$  is the gas molecule collision diameter (m),  $p$  is the gas pressure in pores (Pa),  $\delta$  is the characteristic pore diameter (m),  $\sigma_{mean}$  is the mean free path of gas molecules (m) and  $Kn$  is the Knudsen number.

Decreasing the pore size within a material below a certain level, i.e. a pore diameter of the order of 40 nm or below for air, the Knudsen calculated thermal conductivity (gas plus gas–solid interaction), and hence also the overall thermal conductivity, is becoming very low (<4 mW/(m·K) with an adequate low-conductivity solid state grid structure) even when the pores are filled with air at atmospheric pressure.

The background for this is the Knudsen effect where the mean free path of the gas molecules is larger than the pore diameter. Then, a gas molecule located inside a pore will impact on the pore wall and not hit another gas molecule (statistically, as there is a velocity distribution). In the expression for the Knudsen effect, the solid state and gas interaction is taken care of by the  $\beta$  coefficient in Eq. 12.2.

Finally, the resulting gas thermal conductivity also including the gas and pore wall interaction, i.e. the Knudsen calculated thermal conductivity, versus pore diameter and pore gas pressure, may be calculated in this simplified model and visualized as graphical plots as in Fig. 12.2. Moreover, it is referred to the works by Baetens et al. (2010a) and Jelle et al. (2010a) for further details and information.

The radiation part of the thermal transport processes also must be considered. Here, the Stefan-Boltzmann relationship can be used to demonstrate that the radiation

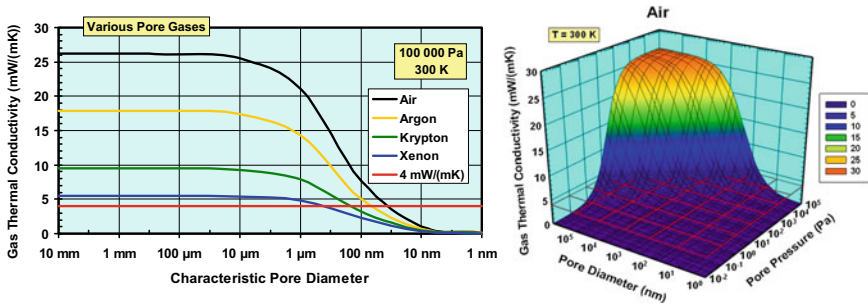


**Fig. 12.2** Knudsen calculated thermal conductivity (gas plus gas–solid interaction) with a (left) 2D-plot depicting the effect of the pore diameter for the gases air, argon, krypton and xenon and a (right) 3D-plot depicting the effect of the pore diameter and the gas pressure in air-filled pores (Jelle et al., 2010a)

thermal conductivity decreases linearly with decreasing pore diameter, and where the slope of the decrease is determined by the emissivity of the inner pore walls. Then, the smaller the pores, and the lower the emissivity, the lower the radiation thermal conductivity will be. However, these aspects do not encompass the complete story. Various investigations (e.g. Joulain et al., 2005; Mulet et al., 2002; Zhang, 2007) are describing a large increase in the thermal radiation as the pore diameter is decreasing below the wavelength of the thermal (infrared) radiation (e.g. 10  $\mu\text{m}$  for the ambient infrared radiation), where tunneling of evanescent waves may play an important role (near field radiation effects). The studies by Joulain et al. (2005) and Mulet et al. (2002) indicate that the large thermal radiation is only centered around a specific wavelength or a few wavelengths.

Thus, this may suggest that the total thermal radiation integrated over all wavelengths is not that large. How much this contributes to the overall thermal conductivity is not completely known at the moment, although it is assumed to be at least rather moderate, which is also indicated through our on-going (unpublished) research activities addressing these topics. More elaboration on these thermal radiation aspects is found in the study by Jelle et al. (2010a).

The solid-state lattice conductivity in the NIMs is also important to take care of, for example, to keep this part of the thermal conductivity as low as possible in order to obtain the lowest possible overall thermal conductivity. Then, on the condition and assuming that a thermal low-conductance solid state lattice and a low gas thermal conductivity are achieved, and which still are dominating the thermal transport (i.e., larger than the thermal radiation part), the way may be paved for the NIMs to become the chosen thermal super insulation material for application in our existing and future buildings.

Open-porous NIMs will be air-filled, therefore the NIM core structure must be resistant versus miscellaneous ageing degradation mechanisms, as air gases (also including different pollutions) will be admitted freely into the NIM cores and pores. A particular crucial issue is that water condensation in the nano pores has to be prevented, otherwise the thermal conductivity would increase considerably, which in turn, could ruin the whole concept of the NIMs.

## **12.6 Exploring Experimental Pathways of Nanoporous Thermal Insulation**

### ***12.6.1 Theoretical Concepts and Laboratory Experiments***

Exploiting theoretical concepts and principles, it has been demonstrated what future thermal super insulation materials may look like (Baetens et al., 2010a; Jelle et al., 2009, 2010a, b; Jelle, 2011a). The main core of these theoretical principles is the utilization of the Knudsen effect in nanoporous structures in order to achieve very low

thermal conductivities. However, to be able to make these super insulation materials is a much more challenging feat.

In any case, the exploration of this pathway from theoretical concepts to experiments has been started and may turn out to be fruitful and very rewarding in the end. Our laboratory experiments have so far been concentrating on synthesizing hollow silica nanospheres (HSNS) by the sacrificial template method (Gangåssæther et al., 2017a, b; Gao et al., 2012; Gao et al., 2013; Gao et al., 2014b; Gao et al., 2015; Grandcolas et al., 2013, 2019; Jelle, 2016b; Jelle et al., 2011; Jelle et al., 2013b, 2014a, b, d, 2015a, 2019; Ng et al., 2018; Sandberg et al., 2013).

To manufacture a bulk material with nanopores directly, might be viewed as a more ideal and efficient pathway of fabricating a super insulation material. That is, not to first synthesize hollow nanospheres which then afterwards need to be put together and assembled into a bulk material. Nevertheless, currently the HSNS may still be seen as a feasible and possible promising experimental pathway for being able to make a thermal super insulation material.

### ***12.6.2 The Membrane Foaming Method***

The main principle in the membrane foaming method is to produce foams with nanoscale bubbles, then follow with condensation and hydrolysis within the bubble walls to obtain a silica nanofoam as the final result. When applying this method, gas is pressed through a membrane to obtain bubbles with a controlled size, see e.g. the studies by Bals and Kulozik (2003) and Müller-Fischer (2007). Thereafter, hydrolysis and condensation of precursors at the bubble–liquid interface should result in formation of the desired gas capsules. This method was earlier used for obtaining nitrogen-containing capsules with titania-polypyrrole composite shells.

Preliminary experiments indicate that the preparation of silica nanofoams may be difficult to achieve, which was also supported by theoretical considerations. The gas pressure has to be adjusted very accurately. If the gas pressure is too low no bubbles will be formed, and if the gas pressure is too high a continuous gas stream will be the result. The bubble size may be reduced by decreasing the pore size of the membrane and then adjusting the membrane's surface properties for obtaining a large contact angle with the solvent so that the solvent should be repelled from the membrane's surface. Furthermore, the solvent mass density should be rather high and with a low surface tension. In principle, it should be possible to design a reaction system that fulfils these requirements, so that production of nanosized bubbles could become viable (Jelle et al., 2011).

In order to have a solid nanofoam production, it is required that the liquid foam is stable long enough for the reactions to proceed, e.g. hydrolysis and condensation of silane precursors to form the solid network. Furthermore, if the foam is to be of interest as a thermal insulation material, the foam walls must be thin as to keep the solid contribution to the overall thermal conductivity as low as possible. Wall thicknesses of about 20 nm may be obtained if surfactant bilayers are used to stabilize

the walls and the applied solvent has a low viscosity and is rapidly drained from the wall interior, which is possible to accomplish in water-based systems. However, the reactions are conducted in alcohol solutions like ethanol or isopropanol. Finally, in our initial experiments no surfactant was found that could stabilize the nanofoams long enough, thus the experimental explorations along these lines have so far been abandoned (Jelle et al., 2011).

### ***12.6.3 The Gas Release Method***

The gas release method requires a simultaneous formation of nanosized gas bubbles throughout the reaction system, thereafter, followed by hydrolysis and condensation to form a solid at the bubble perimeter. Such a bubble formation could be accomplished by either evaporation or decomposition of a component in the system. This method is similar to the process described by Grader et al. (1998), where crystals of the aluminum chloride isopropyl ether complex  $\text{AlCl}_3(\text{Pr}^i_2\text{O})$ , were heated to produce foams with a closed-cell structure. In this case, the crystals themselves decomposed. Upon further heating, the remaining solid dissolves in the generated solvent, where a polymerization reaction occurred at the temperature of solvent evaporation. Then, the solvent bubbles were trapped within the polymerizing gel, and after completing the reaction a stable foam is formed with pore sizes between 50 and 300  $\mu\text{m}$ .

It should be noted that the gas release process is followed by several challenges. To make nanosized bubbles with a sufficiently narrow size distribution, one has to maintain an equal temperature throughout the liquid phase, a task which is difficult to achieve at ordinary reaction conditions. Furthermore, the reaction to form the solid shell must proceed very fast if the shell is to be formed before the bubbles grow too large, which then would require very reactive chemicals where their application would require strict control of humidity both in the working environment and in the used solvents.

Thus, as a result of these practical challenges and difficulties, the experimental investigations along these directions became terminated (Jelle et al., 2011). However, if successful by applying these or similar methods, the potential for manufacturing nano insulation materials seems to be high.

### ***12.6.4 The Sacrificial Template Method***

The sacrificial template method starts with preparing a nanoscale structure in the form of a nano emulsion or polymer gel, thereafter, followed by hydrolysis and condensation to form a solid. This procedure is used for making e.g. catalysts and membrane materials.

In our laboratories, the current approach is to synthesize hollow silica nanospheres (HSNS), then followed by condensation and sintering to form macroscale particles

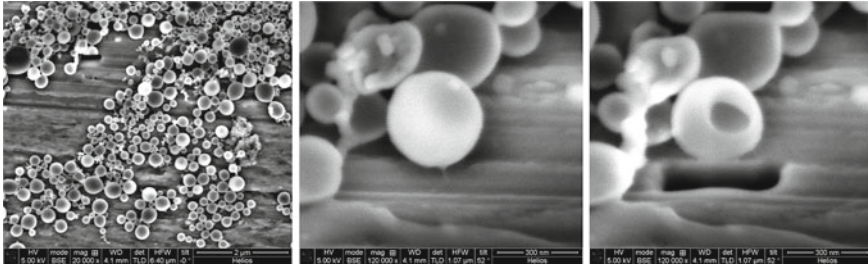


**Fig. 12.3** SEM images depicting an overview of a sample of HSNS (left, scale bar 2  $\mu\text{m}$ ) and an unetched silica sphere (middle, scale bar 300 nm), as well as the same silica sphere after extensive etching with a focused ion beam (right, scale bar 300 nm) (Jelle et al., 2011a)

or objects. To apply these materials as thermal insulation materials, it is desired and required to have small pore sizes combined with small wall thicknesses (Jelle et al., 2011).

In the literature, there are reported several methods for manufacturing of nanospheres. Initially, our starting point was based on the studies by Du et al. (2010) and Wan and Yu (2008), where the former study used the template method to prepare antireflection coatings, and the latter investigation described this method more in detail.

So far, our own experimental studies have been concentrated on synthesizing HSNS by utilizing polyacrylic acid (PAA) and polystyrene (PS) as sacrificial templates, where the PAA and PS templates (after having been coated with their silica shells) have been removed by a chemical washing process and a heating process, respectively. That is, the template materials have been diffusing and evaporating through the silica shells. In Fig. 12.3 there are scanning electron microscope (SEM) images of the very first HSNS we did synthesize.

## 12.7 Hollow Silica Nanosphere Experimental Investigations

### 12.7.1 Synthesis of Sacrificial Template Nanospheres

Utilizing the sacrificial template method, the template nanospheres have to be synthesized before making the hollow silica nanospheres (HSNS), i.e., a coating and deposition process of a silica shell around the template spheres, and thereafter a subsequent removal of the template spheres.

Then, there is a choice of what material to use for making the sacrificial templates. There are several choices for this task. The sacrificial template materials should be easy to make as nanospheres, be possible to make very small nanospheres well below 100 nm, allow the deposition of the silica shells around them, easy removal of the templates after formation of the silica shells, require only a low energy usage, overall

have a low negative environmental impact, and finally, have the possibility for reuse of the template materials which in turn will also lead to a low negative environmental impact. In our experimental studies so far, mainly two different materials have been used to make two different sacrificial template types, i.e., polyacrylic acid (PAA) and polystyrene (PS) template spheres.

In the following, the miscellaneous HSNS results presented here are based on different syntheses of HSNS by the sacrificial template method, where PS spheres have been utilized as the sacrificial templates for the various results shown herein. We have also employed PAA spheres as the sacrificial templates in other experimental investigations, but these ones are not shown here. The template sphere diameters, and then also the corresponding HSNS inner diameters, should be made to be well below 100 nm to obtain the full impact of the Knudsen effect. In our experimental laboratory investigations, though, it has been rather difficult and challenging to synthesize PS spheres with very small diameters.

From the Knudsen effect as given in Eqs. 12.2 and 12.3, it is shown that the further below 100 nm for the HSNS inner diameter one can reach, the lower thermal conductivity values may be expected. Furthermore, various parameters such as e.g., sphere packing density, sphere surface roughness and mesoporosity can also influence the thermal conductivity and other HSNS properties. Through our experimental explorations, the smallest PS template spheres (of uniform size) we have been able to synthesize so far have had sphere diameters of 85 nm, where SEM images of these ones are given in Fig. 12.4. Forthcoming experimental studies will attempt to further reduce the template sphere size, either for PS spheres or by exploiting other template materials than PS. In this regard it may be noted that we have made smaller template spheres utilizing the PAA material, but then with a non-uniform size distribution.

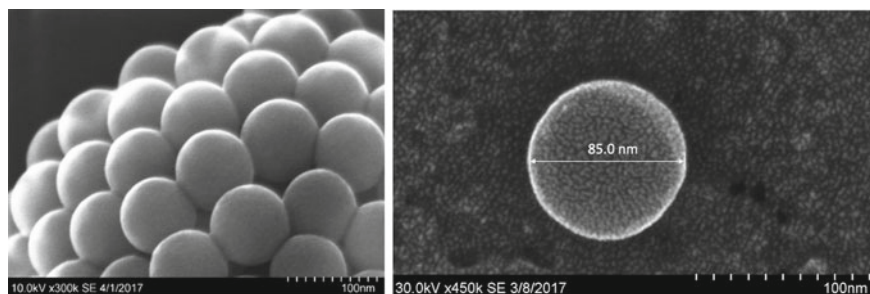


**Fig. 12.4** SEM images of (left, Mofid et al., 2020) several PS template spheres and (right) a single PS template sphere, all with a sphere diameter of 85 nm (uniform size)

## 12.7.2 *Synthesis of Hollow Silica Nanospheres*

Nano insulation materials (NIM) represent a very promising candidate in our quest for developing super insulation materials (SIM) with very low thermal conductivity values, where a possible pathway and stepping-stone may be represented by the sacrificial template method for developing hollow silica nanospheres (HSNS).

The sacrificial template method as briefly described earlier allows for a direct control of the inner sphere (pore) diameter (from the template diameter) and the silica shell (wall) thickness during the synthesis of the HSNS. Hence, we may then in principle be able to tailor-make our nano insulation materials with defined pore sizes and wall thicknesses according to our demands, and thereby also fabricating HSNS with tailor-made thermal conductivities.

Thus, in the following we will have a more detailed look on the experimental synthesis of the HSNS by the sacrificial template method, both about the manufacturing of the template spheres and the HSNS themselves. Different synthesis parameters may lead to different results, e.g., different surface morphologies of the HSNS.

A first and important choice to be made is to choose the bulk material for fabricating the NIMs and HSNS. This bulk material may be selected from among many different materials depending on our requirements and preferences. And in order not to forget, within the NIM definition and development, air at atmospheric pressure is already chosen as the preferred medium to fill the pores in the nano porous material to be developed. That is, there will be no vacuum or low-conducting gases in the NIMs. Then, the solid-state bulk material constituting the nano porous skeleton must be selected. Preferably, this solid-state material should be rather resistant and non-flammable. In our NIM investigations so far, we have chosen to focus on silica ( $\text{SiO}_2$ ) as our solid-state bulk material. In addition to being a resistant and non-flammable material, silica is also the most abundant chemical compound on Earth.

The next question and subsequent choice to be made will then be where to get the silica from? That means, finding a reliable, widely accessible, and inexpensive silica source for the synthesis of the NIMs and HSNS can be a key challenge. When applying the sacrificial template method for making HSNS, mainly two silica sources have so far been exploited, for example, the silica precursors tetraethyl orthosilicate (TEOS) and water glass ( $\text{Na}_2\text{SiO}_3$ ).

As described in the above, there was also a choice of what material to use for fabricating the sacrificial template nanospheres, where we in our experimental investigations so far have used mainly two different materials for making two different sacrificial template types, i.e., polyacrylic acid (PAA) and polystyrene (PS) template spheres.

With completed synthesis of the sacrificial templates, the stage has been set for coating the spherical template surfaces, where we in our laboratory have used silica as the final coating material. Then, after the PAA or PS templates have been coated with a layer of silica, either in the form as small silica particles or as a large, wrinkled silica sheet (depending on e.g., the silica precursor), the PAA or PS templates have been

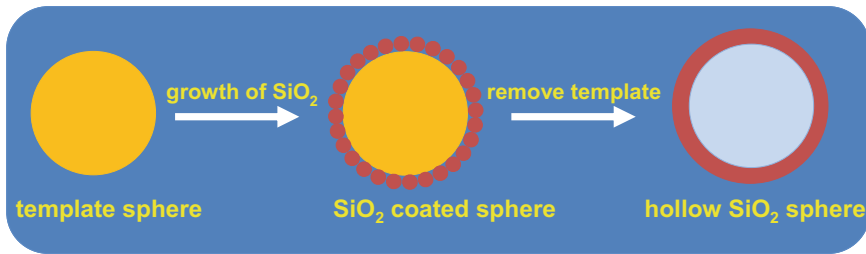


**Fig. 12.5** Cross-section illustration of the hollow silica nanosphere (HSNS) synthesis process by the sacrificial template method (Jelle et al., 2014a, b)

removed. The PAA templates have been removed by chemical treatment (washing) and the PS templates have been removed by heat treatment, where the template materials then have been diffusing and evaporating through the silica shells.

Finally, as the result, we have then manufactured a potential NIM in the form of HSNS. The HSNS synthesis process by the sacrificial template method is depicted in the cross-section illustration in Fig. 12.5. Then, we may move from the conceptual theory as illustrated in Fig. 12.5 to an actual example of HSNS synthesis as shown in Fig. 12.6. That is, scanning electron microscope (SEM) images of synthesized spherical PS templates, a PS template coated with small silica particles, and HSNS after removal of the PS templates, are shown in Fig. 12.6, hence demonstrating the illustrated and conceptual HSNS synthesis process in Fig. 12.5 with an actual experimental HSNS synthesis process in practice in Fig. 12.6. It is rather captivating to see such an enchanting example of the scientific step from theoretical concept to actual experimental results.

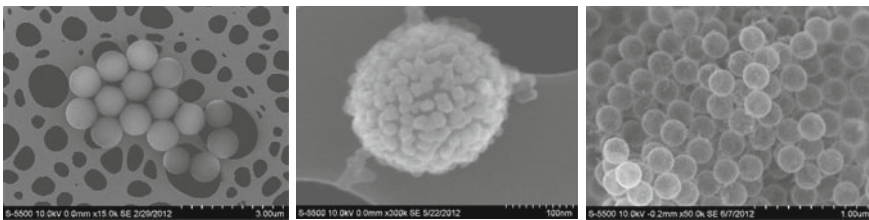


**Fig. 12.6** SEM images of an actual HSNS synthesis process with (left) spherical PS templates, (middle) small silica particles coated around a spherical PS template, and (right) HSNS after removal of PS templates (Jelle et al., 2014a, b). Compare with the illustrations in Fig. 12.5



### 12.7.3 Characterization of Hollow Silica Nanospheres

The visual appearance and dimensional attributes at nano level for the produced HSNS, and their corresponding PS sacrificial template spheres, have been characterized by using scanning electron microscopes (SEM) and transmission electron microscopes (TEM).

A Hot Disk apparatus has been utilized for measuring the thermal conductivity values for miscellaneous HSNS powder samples in our earlier presented HSNS studies.

In the HSNS results presented within this study, the thermal conductivity  $\lambda$  of the HSNS was determined by calculation according to

$$\lambda = \alpha \rho c_p \quad (12.4)$$

where the diffusivity  $\alpha$  was measured by a laser flash apparatus, the mass density  $\rho$  was calculated as  $\rho = m/V$  from mass  $m$  and volume  $V$  measurements, and the specific heat capacity  $c_p$  was measured by differential scanning calorimetry (DSC).

These HSNS syntheses including further information and details along with their corresponding thermal conductivity measurements are given in a more comprehensive HSNS study (Mofid et al., 2020). Herein, a few excerpts and highlights from this and other studies will be presented in the following.

### 12.7.4 Hollow Silica Nanosphere Results

As already mentioned, it is rather captivating to see the step from the theoretical concepts to the actual experimental synthesis results of the hollow silica nanospheres (HSNS). Thus, in this respect a principle drawing of a nano insulation material (NIM) alongside a TEM image of actual fabricated HSNS are depicted in Fig. 12.7, thereby demonstrating the close resemblance from theoretical concepts to experimental synthesis attempts.

Depending on the synthesis parameters, the produced HSNS may look quite different, both in size and surface/shell morphologies. Applying an SEM these aspects can be observed directly, i.e., the visual appearance and dimensional attributes of the HSNS.

Two examples of different HSNS samples are shown in the SEM images given in Fig. 12.8, where both HSNS samples have been synthesized by using sacrificial PS template spheres with diameters of 85 nm, hence also with resulting HSNS inner diameters of 85 nm, and with two different silica sphere shell (wall) thicknesses of 34 nm and 67 nm. The SEM images show that the sphere shells of these two HSNS samples are constituted by rather large silica particles, i.e., relatively large compared to the (larger) HSNS inner diameters. Moreover, it is also observed that some of the

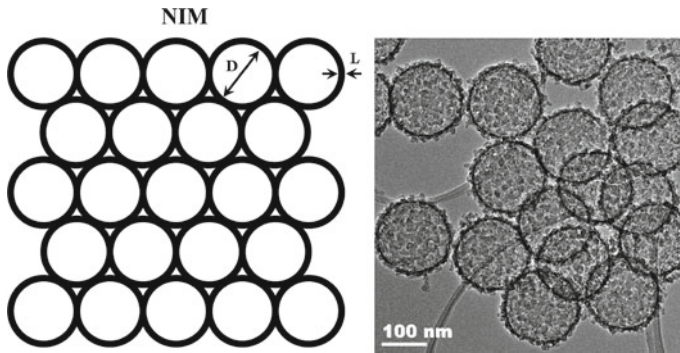


**Fig. 12.7** Demonstrating the close resemblance from theoretical concepts to actual experimental results with (left) a principle drawing of a NIM alongside (right) a TEM image of actual synthesized HSNS (Jelle et al., 2014a, b)

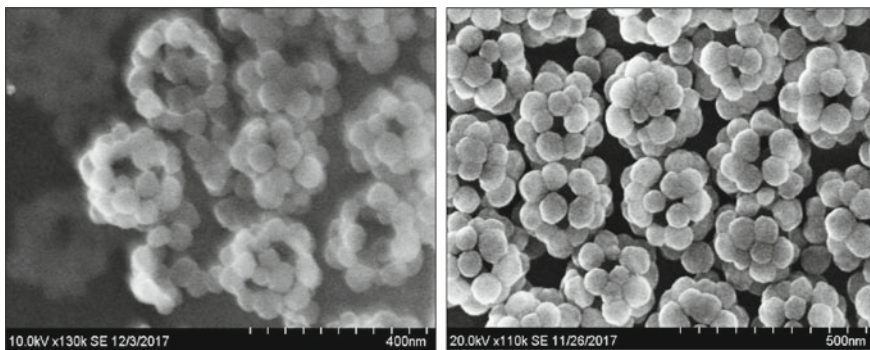


**Fig. 12.8** SEM images of synthesized HSNS with the same inner diameters of 85 nm, but with two different shell thicknesses of 34 nm (left) and 67 nm (right) (Mofid et al., 2020)

HSNS have larger holes where several silica particles are missing from the sphere shells.

HSNS from other syntheses may be made up from silica particles being relatively small compared to the (larger) HSNS inner diameters (Figs. 12.6 and 12.9), thus resulting in relatively smoother sphere (shell) surfaces, whereas in some other syntheses the silica sphere surface has been resembling a large, wrinkled sheet and thus resulting in relatively even smoother sphere surfaces (Fig. 12.9). In fact, Fig. 12.9 depicts a distinct difference in the silica shell surface morphologies when applying tetraethyl orthosilicate (TEOS) and water glass ( $\text{Na}_2\text{SiO}_3$ ) as the silica precursors, forming a rough silica shell as small silica particles and a smoother large, wrinkled silica sheet, respectively.

Earlier, applying the Hot Disk method to measure the thermal conductivity of the HSNS samples, the typical thermal conductivity values have been between 20 to 90 mW/(m·K), though, with some uncertainties with the Hot Disk method. Our latest

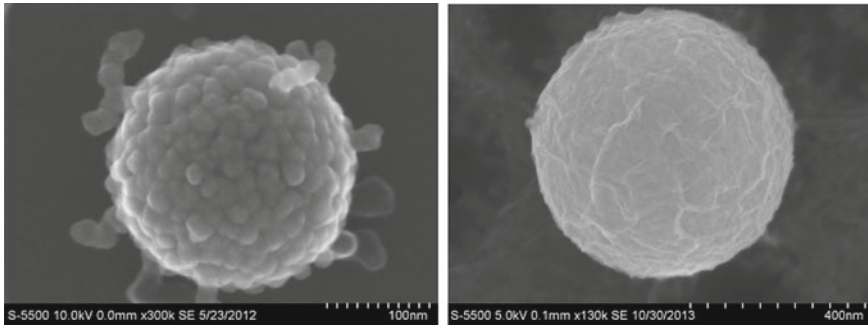


**Fig. 12.9** SEM images of (left, Sandberg et al., 2013) silica nanoparticles covering a PS template sphere and (right, Ng et al., 2018) a large, wrinkled silica sheet covering a PS template sphere, where the applied silica precursors were TEOS and water glass, respectively

HSNS results have demonstrated substantially lower thermal conductivities between 14 to 30 mW/(m·K) (Mofid et al., 2020), where these measurements involve the utilization of a laser flash apparatus and differential scanning calorimeter (DSC), and a calculation of the thermal conductivity according to Eq. 4. Furthermore, these latest HSNS results also indicate the possibility of reaching even lower thermal conductivities. That is encouraging news with respect to the possibility of developing SIMs as NIMs.

Thus, our latest HSNS results are summarized in Table 12.1, where four different HSNS samples with different inner sphere diameters have been presented with their measured (and calculated) inner diameter, thermal diffusivity, mass density, specific heat capacity and measured total thermal conductivity. These four HSNS samples have all the same sphere shell (wall) thickness of about 34 nm. The measured total

**Table 12.1** HSNS samples with four different inner sphere diameters and measured total thermal conductivities calculated according to measured values as  $\lambda = \alpha\rho c_p$  (Eq. 12.4). The sphere shell thickness is about 34 nm for all four samples (Mofid et al., 2020). For comparison, the calculated combined gas plus gas–solid interaction thermal conductivity  $\lambda_{Kn}$  according to the Knudsen effect is given, representing a lower limit for the thermal conductivity as the measured total one also includes solid state, convective and radiative thermal transport. See also Fig. 12.10

HSNS sample	Inner sphere diameter (nm)	Thermal diffusivity $\alpha$ (mm <sup>2</sup> /s)	Mass density $\rho$ (kg/dm <sup>3</sup> )	Specific heat capacity $c_p$ (J/(kgK))	Measured total thermal conductivity $\lambda$ (mW/(mK))	Knudsen calculated thermal conductivity $\lambda_{Kn}$ (mW/(mK))
1	85	0.102	0.190	740	14.3	6.78
2	100	0.144	0.180	740	19.2	7.63
3	150	0.195	0.175	740	25.3	9.99
4	213	0.236	0.170	740	29.7	12.2

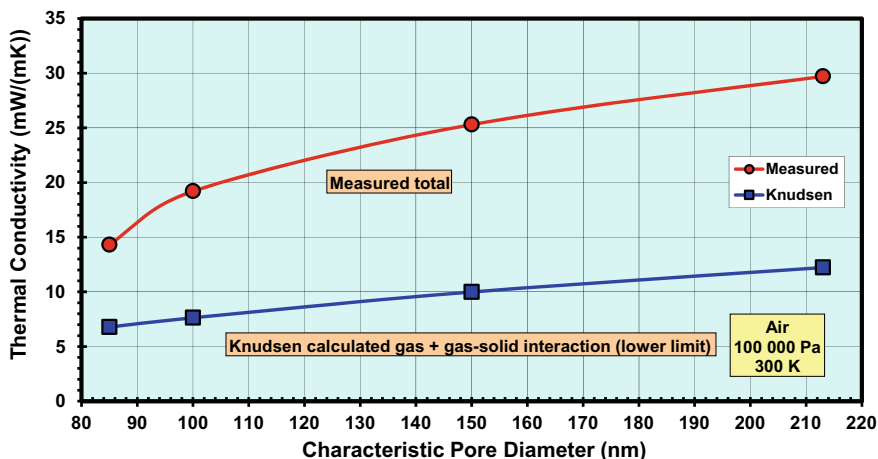


**Fig. 12.10** Measured total thermal conductivity for four HSNS samples with four different inner sphere diameters, and with a sphere shell thickness of about 34 nm for all four samples. For comparison, the calculated combined gas plus gas–solid interaction thermal conductivity according to the Knudsen effect is depicted, which represents a lower limit for the thermal conductivity as the measured total one also includes solid state, convective and radiative thermal transport. See also Table 12.1

thermal conductivities for these four HSNS samples have been graphically plotted versus their inner diameters in Fig. 12.10. Moreover, to compare with the theoretical limits, the combined gas plus gas–solid interaction thermal conductivities for these four HSNS samples with four different inner diameters have been calculated according to the Knudsen effect (Eqs. 12.2 and 12.3), which then are also given in Table 12.1 and Fig. 12.10. This calculated combined gas plus gas–solid interaction thermal conductivity  $\lambda_{Kn}$  as given by the Knudsen effect, represents a lower limit for the thermal conductivity as the measured total thermal conductivity also includes solid state, convective and radiative thermal transport.

From Table 12.1 and Fig. 12.10 it is observed that the measured thermal conductivity decreases with decreasing HSNS inner diameter, i.e. as also predicted by the Knudsen effect (Eqs. 12.2 and 12.3). Decreasing the inner diameter of the HSNS from 213 to 85 nm, the measured thermal conductivity is lowered from 29.7 mW/(m·K) to 14.3 mW/(m·K), respectively (Mofid et al., 2020).

Importantly, Fig. 12.10 clearly indicates that it would be highly interesting to attempt to fabricate PS spheres with smaller diameters and thereby HSNS with smaller inner sphere diameters than 85 nm, thus also probably being able to lower the thermal conductivity even further below the lowest one so far of 14.3 mW/(m·K) (Table 12.1).

Hence, for future HSNS developments, one should attempt to make smaller PS spheres with diameters further below 85 nm, even though it so far has been shown to be a challenging task to make PS spheres with such small diameters. However, if successful, one would then be able to make HSNS with smaller inner diameters

and thus also even lower thermal conductivities. That is, on the condition of being successful with keeping the solid state and in general also the radiative thermal conductivity sufficiently low, as the solid part (e.g. sphere shell thickness) and mass density may increase with decreasing HSNS inner diameter.

As already stated, it should be noted that the Knudsen calculated thermal conductivity is representing a lower limit for the thermal conductivity as the measured total thermal conductivity also includes solid state, convective and radiative thermal transport. Thus, although these lower limit values can never be achieved for measurements of real HSNS samples, it is illustrative and worthwhile to compare and study the relative thermal conductivity changes with variations in different experimental parameters and resulting properties and dimensions such as for example, inner sphere diameters. Furthermore, these calculated thermal conductivity values do also represent the lower values one may strive to achieve in the forthcoming experimental investigations.

These thermal conductivity calculations as discussed in the above are simplified and do not take into account miscellaneous aspects such as e.g., spherical geometry, voids of different geometries between the spheres and various coupling effects (except simplified gas and solid-state interaction through the  $\beta$  coefficient in the simplified equation for the Knudsen effect).

Looking at these aspects a bit more in detail, it may from a general viewpoint be stated that there is no direct, exact or clear relationship between the measured overall (total) thermal conductivity and the simplified Knudsen calculated thermal conductivity (the combined gas thermal conductivity also including the gas and solid state (pore wall) interaction), although one may find some simplified relationships in some specific cases and within limited parameter ranges. However, this matter is in general of a very complex nature and involves all the different thermal transport mechanisms to various degrees, and is also dependent on the miscellaneous parameters and what ranges they are within, e.g. including parameters like inner pore diameter, sphere shell (wall) thickness, sphere shell particle sizes and their different connections, sphere surface aspects like e.g. smooth or rough surfaces, mass density and mesoporosity, voids and porosity in general, and different packing effects of e.g. particles within the sphere shell and amongst or between the spheres themselves. Nevertheless, as is common and also exploited as a powerful tool in science, simplified models and relationships are often beneficially utilized and elaborated further to gain new insight and knowledge in the explored fields.

### ***12.7.5 Perspectives for Future Development of Hollow Silica Nanospheres***

In the quest to further lower the total thermal conductivity of the hollow silica nanospheres (HSNS) in the future, one may consider an attempt to reduce the solid state and radiative heat transport parts. Herein, one may assume a negligible thermal

transport from convection in the small nano pores. In addition, with respect to the thermal transport by gas conduction, one should also investigate if the dimensions of the voids between the individual HSNS are comparable to the HSNS inner diameters, and henceforth take measures to have all the voids within a suitable nano range and thus a reduced (gas and gas–solid interaction) thermal conductivity according to the governing Knudsen effect.

During the development of a new thermal insulation material, at some stage there will also be a question about the possibilities and opportunities of being able to take the large step from a research material in the laboratory to a commercial product. For this to actually happen, several properties of the material have to fulfil specified requirements, often after an optimization of these properties during the development process of the material. Naturally, the main key property for a thermal insulation material is the thermal conductivity which should be made to be as low as possible. For the HSNS to become a commercial thermal insulation material, one of the aspects to be investigated is packing or gluing, e.g. through a chemical reaction, of the HSNS to form a continuous solid bulk material, i.e. to piece together the individual nanospheres from its current powder form (Grandcolas et al., 2019).

Among several other aspects to be considered are robustness assessment (Jelle et al., 2014), durability and accelerated climate ageing (Jelle, 2012b) and life cycle analysis (Gao et al., 2013; Gao et al., 2014, Schlanbusch et al., 2014a, b). In any case, without having been able to synthesize and utilize very small inner HSNS diameters yet, i.e. without having fully exploited the Knudsen effect yet, then to actually have achieved as low thermal conductivity as  $14.3 \text{ mW}/(\text{m}\cdot\text{K})$ , is a very promising result. Thus, also promising with respect to future development and optimization attempts in the continued quest for making thermal super insulation materials.

Further information on synthesizing monodisperse PS nanospheres can be found in the study by Du and He (2008). In addition, more information on hollow silica nanospheres (and microspheres) may be found in the studies by e.g. Cheng et al. (2007), Du et al. (2010), Fan et al. (2011), Han et al. (2011), Kim et al. (2005), Le et al. (2004a, b), Liao et al., (2011, 2012), Liu et al. (2011), Meng et al. (2012), Peng et al. (2008), Pu et al. (2009), Rahman et al. (2017), Ruckdeschel et al., (2015, 2017), Teng et al. (2010), Wan and Yu (2008), Wang et al. (2010, 2012), Wu et al. (2012), Yang et al. (2008), Yuan et al. (2010), Yue et al. (2011), Zhang et al. (2004, 2009, 2012, 2013), Zhu et al. (2005) and Zou et al. (2018).

Nano capsules were used as building blocks for fabricating an air-containing polymer nanofoam with low thermal conductivity (far lower than that of stagnant air of  $26 \text{ mW}/(\text{m}\cdot\text{K})$ ) in the experimental studies by Luo and Ye (2012). Noteworthy, thermally insulating foams based on nanocellulose and graphene oxide with a thermal conductivity as low as  $15 \text{ mW}/(\text{m}\cdot\text{K})$  were explored by Wicklein et al. (2015). Furthermore, Li et al. (2014) studied the design, modelling and numerical validation of an ideal nano porous insulation material. In addition, miscellaneous interesting aspects can also be found amongst others in the investigations by Ruckdeschel and Retsch (2017) and Vaziri et al. (2019).

As examples of theoretical investigations, some of these also including experimental studies, including e.g. thermal transport and conductivity calculations, the

readers are referred to the studies by Baillis et al. (2015), Bi et al. (2014), Feng et al. (2021), He and Xie (2015), Joulain (2008), Joulain et al. (2005), Li et al. (2014, 2017), Liang and Li (2006), Mulet et al. (2002), Öchsner et al. (2009), Ruckdeschel et al. (2018), Sasihithlu and Agarwal (2018), Swimm et al. (2009), Wang et al. (2017a, b), Xu et al. (2008), Yang et al. (2012), Yarmohammadi (2016), Zhang (2007) and Zhao et al. (2012).

Concerning theoretical investigations, Wang et al. (2017) studied the modelling of the thermal transport through a nano cellular polymer foam with respect to the generation of new super insulation materials. In this work they illustrate the different forms of thermal transport modes through a closed-cell nano cellular polymer foam, e.g. in overall the various contributions to thermal conductivity in polymer foams (solid state, gas and radiation), significant phonon scattering at the boundaries of the nanoscale thin polymer film, confined gas molecule movements depicting the difference in macro/micro cells and nano cells, where the Knudsen effect takes place in the latter, and decreased reflected waves and hence enhanced transmitted waves due to the thin film interference (Wang, Zhao, et al., 2017). An experimental study at the same time by several of the same research scientists is also noted, where they investigated improvement of microcellular polymethylmethacrylate (PMMA) as a thermal insulation material (Wang, Wang, et al., 2017).

Thus, we are also reminded of the two cardinal backbones of all science, i.e. theory and experiment and their symbiotic interaction. Then, in addition to the theoretical insight, knowledge and deeper understanding such theoretical studies are providing, they may also prove to become very valuable in the forthcoming experimental attempts of tailor-making the thermal super insulation materials of the future.

## 12.8 The Path Ahead for Thermal Insulation Development

The thermal insulation materials and solutions already existing today, both the traditional and the state-of-the-art ones, will probably be used for many years. Moreover, several of these existing thermal insulation materials will experience various improvements in the years ahead. In addition, there will be a continuous development of new thermal insulation materials. Hence, in the coming years we will also see other thermal insulation materials and solutions than exist today. Then, as a summarization, we may conclude that the possible future research opportunities for thermal insulation materials may beneficially be sought and carried out along the following three pathways:

- (a) Improvement of the existing traditional thermal insulation materials and solutions.
- (b) Improvement of the existing state-of-the-art thermal insulation materials and solutions.

- (c) Exploration of the possibilities of discovering and developing novel high-performance thermal insulation materials and solutions with properties surpassing all of today's existing materials and solutions, such as super insulation materials (SIM) in the form of nano insulation materials (NIM).

With respect to discovery and development of new thermal insulation materials like for example, NIMs and any others, real breakthroughs may first happen through theoretical considerations or experimental explorations, or through a fruitful combination of both paths. That is, new discoveries occurring through the two crucial and cardinal backbones of all science, including, theory and experiment and their symbiotic interaction. Theoretical modelling and visualization possibilities have increased considerably the last decades and will continue to do so in the forthcoming years, both through increased theoretical insight and advances in computerized modelling hardware and software. It is anticipated that this insight and advances will become even more important in future modelling work at a molecular level and nanoscale resolution, such as for example nano insulation materials. Nevertheless, experimental investigations will always be at least equally important in these forthcoming studies, as these will demonstrate the real world in practice so to speak, also for the improvement and development of thermal insulation materials.

It is assumed that many new thermal insulation materials and products will be emerging in the foreseeable future. In the thermal insulation development, two major pathways may be sought, i.e., vacuum-based and non-vacuum-based thermal insulation materials/products.

Today, commercial products of vacuum insulation panels (VIP) already exist in many varieties, where recent collections of these can be viewed in the works by Gonçalves et al. (2020) and Kalnæs and Jelle (2014), where the former study is focused on applying VIPs for exterior thermal insulation of buildings. In VIPs the low thermal conductivity values are achieved due to a combination of exploiting vacuum, the Knudsen effect with voids in the nano range, and a low solid state and radiation conductivity. As noted earlier, the major disadvantage of VIPs is the need to maintain an intact vacuum in the VIP core material, which directly relates to the four cardinal weaknesses of VIPs, i.e., fragility, perforation vulnerability, lack of building site adaption cutting, and increasing thermal conductivity during time. Furthermore, heat bridge effects and high costs are also considered as important disadvantages of VIPs.

Aerogels (Levy & Zayat, 2015) are also exploiting the Knudsen effect (Jelle et al., 2015), then with pores filled with air at atmospheric pressure. In addition, the various aerogel forms as either an opaque, translucent, or transparent material can be utilized in miscellaneous building applications (Jelle & Gao, 2019). That is, for aerogels there are no concern for losing any vacuum as is the main disadvantage of VIPs. Major concerns to be addressed for aerogels are the fragility due to low tensile strength and the high production costs.

In any case and noteworthy, in their pristine non-aged condition the VIPs attain a substantially lower thermal conductivity value than today's aerogel products. Improvements of the VIPs may be found in e.g. the development of VIP cores being



able to keep a lower thermal conductivity even with air in their pores and the development of VIP envelope laminates being less fragile and better at minimizing the air and moisture diffusion into the VIP cores. Improvements of aerogels may be found in e.g. the development of an aerogel material with an even lower thermal conductivity and substantially lowered production costs. Furthermore, a decreased negative environmental impact for both VIPs and aerogels would also be beneficial.

One may claim that VIPs show great promise as a thermal building insulation solution for today and in the near future. Many building projects have already been completed with VIPs with initially good results, and many more are continuously being added. Improving the VIP technology further and thus being able to extend the current lifetime and guarantee it, could lead to VIP becoming a more trusted choice for thermal insulation. Even though the air and moisture diffusion through the VIP laminate could have been reduced to almost zero, which is far from the current situation, the risk of perforation and lack of building site cutting and adaption would still represent major disadvantages for the VIP applications.

Instead, other emerging high-performance thermal insulation materials and solutions may show greater promise, also including increased flexibility and the possibility of being able to be cut and adapted at the building site. If or when some of these are commercialized, they may eventually end up becoming a favourable choice over VIPs. Nanotechnology and its application for achieving and improving these super insulation materials (SIM) seems to represent a logical and promising pathway to follow in the years ahead, maybe less for vacuum but especially for non-vacuum based solutions.

The nano insulation materials (NIM) development attempts are ultimately aiming at achieving as low thermal conductivity values as VIPs in their pristine non-aged condition, e.g.  $4 \text{ mW}/(\text{m}\cdot\text{K})$ , with air at atmospheric pressure in the nanoporous material utilizing the Knudsen effect (Jelle, 2011a; Jelle et al., (2014b, 2019)). Thus, the NIMs could inherit the advantages of VIPs and aerogels and hopefully avoid their miscellaneous drawbacks. Attempting to commercialize NIMs, and noting that compared to the already existing and competitive VIP and aerogel products, there will naturally be several risks involved for any company with the aim of manufacturing a NIM product for the construction and building sector. On the other hand, the potential benefits seem to be very large.

Our experimental investigations so far on SIMs and NIMs have mainly been focused on miscellaneous attempts to tailor-make hollow silica nanospheres (HSNS) by manufacturing and applying different sacrificial template spheres, several parameter variations, synthesis processes/procedures, and various silica nanospheres with different inner sphere diameters, shell (wall) thicknesses and surface morphologies. An important aspect and challenge in the forthcoming development work will be how to assemble the individual HSNS into a coherent and practical thermal insulation bulk material. The future NIMs may not necessarily end up being based on HSNS, nevertheless the experimental HSNS studies represent a possible stepping-stone towards the ultimate goal of making a thermal SIM.

Although we currently are not attempting to fabricate NIMs by applying the membrane foaming method and the gas release method, these methods should clearly

not be forgotten as they might still represent feasible pathways well worth pursuing in the quest for making SIMs and NIMs, here also with the possibility of manufacturing SIMs and NIMs directly as a bulk material without the need of assembling individual nanospheres. Finally, it should also be emphasized that materials and methods not treated within this study, including hitherto unknown materials and methods, may hold the solution for the SIMs and NIMs of the future.

Naturally, safety and health aspects are very important in the development of new thermal insulation materials. For example, similar cases as the well-known asbestos case have to be avoided. Furthermore, it is also important to study the durability of building materials and components, including the newly developed ones, which may be conducted by carrying out accelerated climate ageing in the laboratory (Jelle (2011b, 2012b, 2013b), Jelle & Nilsen, 2011, Jelle et al., 2012). Moreover, performing a robustness assessment of these new materials and components may also be beneficial (Jelle et al., 2014). Hence, a durability and robustness evaluation of the newly developed SIMs should be carried out.

Thus, in the years ahead, miscellaneous attempts in various pathways and directions will be explored in the search for developing the high-performance thermal super insulation materials and nano insulation materials for the buildings aiming at taking the leap into a sustainable future. *The solutions for the grand scheme of things may very well be found in the very small scale of things.* That is, the solutions for the global situation may be found at nanoscale, e.g., nano insulation materials for energy-efficient and sustainable buildings.

## 12.9 Conclusions

Increased interest and demand for energy savings in buildings have led to increased focus on development of energy-efficient buildings. Hence, state-of-the-art thermal insulation materials and solutions like vacuum insulation panels (VIP) and aerogels with low thermal conductivities have experienced increased usage during the last decades. Thermal insulation materials with very low thermal conductivity values make it possible to avoid undesirable thick building envelopes as otherwise would have been the case when applying traditional thermal insulation materials in situations where a large thermal resistance is required.

However, the current state-of-the-art thermal insulation materials and solutions have several disadvantages, e.g., loss of vacuum by perforations or air and moisture diffusion with time for the VIPs. Thus, there is a quest for making new thermal insulation materials with very low thermal conductivities without any of the disadvantages of the state-of-the-art thermal insulation materials. A promising candidate in this respect is nano insulation materials (NIM) which are utilizing the Knudsen effect in order to reach very low thermal conductivity values. NIMs may be manufactured by several different experimental processes. A possible pathway for making NIMs is through the sacrificial template method by synthesis of hollow silica nanospheres (HSNS), where selected experimental results have been presented herein.

**Acknowledgements** This work has been supported by the Research Council of Norway within the Nano2021 program through the SINTEF and NTNU research project “High-Performance Nano Insulation Materials” (Hi-Per NIM, project no. 250159). Furthermore, the Research Council of Norway is acknowledged for their support to the “Norwegian Micro- and Nano-Fabrication Facility” (NorFab, project no. 245963/F50).

## References

- Aegerter, M. A., Leventis, N., & Koebel, M. M. (2011). *Aerogels Handbook*. Springer.
- Al-Homoud, M. S. (2005). Performance characteristics and practical applications of common building thermal insulation materials. *Building and Environment*, *40*, 353–366.
- Alam, M., Singh, H., & Limbachiya, M. C. (2011). Vacuum Insulation Panels (VIPs) for building construction industry—A review of the contemporary developments and future directions. *Applied Energy*, *88*, 3592–3602.
- Alam, M., Singh, H., Brunner, S., & Naziris, C. (2014). Experimental characterisation and evaluation of the thermo-physical properties of expanded perlite—Fumed silica composite for effective vacuum insulation panel (VIP) core. *Energy and Buildings*, *69*, 442–450.
- Alam, M., Singh, H., Suresh, S., & Redpath, D. A. G. (2017). Energy and economic analysis of vacuum insulation panels (VIPs) used in non-domestic buildings. *Applied Energy*, *188*, 1–8.
- Alotaibi, S. S., & Riffat, S. (2014). Vacuum insulated panels for sustainable buildings: A review of research and applications. *International Journal of Energy Research*, *38*, 1–19.
- Andenæs, E., Jelle, B. P., Ramlo, K., Kolås, T., Selj, J., & Foss, S. E. (2018). The influence of snow and ice coverage on the energy generation from photovoltaic solar cells. *Solar Energy*, *159*, 318–328.
- Andersson, P.-O., Jelle, B. P., & Zhang, Z. (2017). Passive snow repulsion: A state-of-the-art review illuminating research gaps and possibilities. *Energy Procedia*, *132*, 423–428.
- Annex 65, International Energy Agency (IEA). (2017). Long-Term performance of super-insulating materials in building components and systems. In U. Heinemann (Ed.), Report of Subtask 1: State of the Art on Materials & Components - Case Studies.
- Annex 65, International Energy Agency (IEA). (2020). Long-Term performance of super-insulating materials in building components and systems. In Adl-Zarrabi, B., & Johansson, P. (Eds.), Report of Subtask III: Practical Applications Retrofitting at the Building Scale - Field scale.
- Aspen Aerogels, Spaceloft 3251, 6251, 9251. (2008a). Flexible insulation for industrial, commercial and residential applications. Retrieved October 17, 2008 from <http://www.aerogel.com>.
- Aspen Aerogels, Spaceloft 6250. (2008b). Extreme protection for extreme environments. Retrieved October 07, 2008, from <http://www.aerogel.com>.
- Baetens, R. (2013). High performance thermal insulation materials for buildings. In Pacheco-Torgal, F., Diamanti, M. V., Nazari, A., & C.-G. Granqvist (Eds.), *Nanotechnology in eco-efficient construction* (pp. 188–206). Woodhead Publishing.
- Baetens, R., Jelle, B. P., Thue, J. V., Tenpierik, M. J., Grynning, S., Uvsløkk, S., & Gustavsen, A. (2010a). Vacuum insulation panels for building applications: A review and beyond. *Energy and Buildings*, *42*, 147–172.
- Baetens, R., Jelle, B. P., & Gustavsen, A. (2010b). Phase change materials for building applications: A state-of-the-art review. *Energy and Buildings*, *42*, 1361–1368.
- Baetens, R., Jelle, B. P., Gustavsen, A., & Grynning, S. (2010c). Gas-filled panels for building applications: A state-of-the-art review. *Energy and Buildings*, *42*, 1969–1975.
- Baetens, R., Jelle, B. P., & Gustavsen, A. (2010d). Properties, requirements and possibilities of smart windows for dynamic daylight and solar energy control in buildings: A state-of-the-art review. *Solar Energy Materials & Solar Cells*, *94*, 87–105.

- Baetens, R., Jelle, B. P., & Gustavsen, A. (2011). Aerogel insulation for building applications: A state-of-the-art review. *Energy and Buildings*, 43, 761–769.
- Baillis, D., Coquard, R., & Moura, L. M. (2015). Heat transfer in cellulose-based aerogels: Analytical modelling and measurements. *Energy*, 84, 732–744.
- Bals, A., & Kulozik, U. (2003). The influence of the pore size, the foaming temperature and the viscosity of the continuous phase on the properties of foams produced by membrane foaming. *Journal of Membrane Science*, 220, 5–11.
- Batard, A., Duforestel, T., Flandin, L., & Yrieix, B. (2018). Prediction method of the long-term thermal performance of vacuum insulation panels installed in building thermal insulation applications. *Energy and Buildings*, 178, 1–10.
- Beck, A., Frank, O., & Binder, M. (2007). Influence of water content on the thermal conductivity of vacuum panels with fumed silica kernels. In *Proceedings of the 8th International Vacuum Insulation Symposium*, ZAEBayern/UniWue, Würzburg, 18–19 September, 2007.
- Berardi, U. (2017). The benefits of using aerogel-enhanced systems in building retrofits. *Procedia Engineering*, 134, 626–635.
- Berardi, U., & Nosrati, R. H. (2018). Long-term thermal conductivity of aerogel-enhanced insulating materials under different laboratory aging conditions. *Energy*, 147, 1–15.
- Bheekhun, N., Talib, A. R. A., & Hassan, M. R. (2013). Aerogels in aerospace: An overview. *Advances in Materials Science and Engineering*, 18 pages, Article ID 406065.
- Bi, C., Tang, G. H., Hu, Z. J., Yang, H. L., & Li, J. N. (2014). Coupling model for heat transfer between solid and gas phases in aerogel and experimental investigation. *International Journal of Heat and Mass Transfer*, 79, 126–136.
- Biswas, K., Patel, T., Shrestha, S., Smith, D., & Desjarlais, A. (2019a). Whole building retrofit using vacuum insulation panels and energy performance analysis. *Energy and Buildings*, 203, 109430.
- Biswas, K., Gilmer, D., Ghezawi, N., Cao, P.-F., & Saito, T. (2019b). Demonstration of self-healing barrier films for vacuum insulation panels. *Vacuum*, 164, 132–139.
- Boafo, F. E., Chen, Z., Li, C., Li, B., & Xu, T. (2014). Structure of vacuum insulation panel in building system. *Energy and Buildings*, 85, 644–653.
- Borrebæk, P.-O. A., Jelle, B. P., & Zhang, Z. (2020). Avoiding snow and ice accretion on building integrated photovoltaics—Challenges, strategies, and opportunities. *Solar Energy Materials and Solar Cells*, 206, 110306, 1–12.
- Bouquerel, M., Duforestel, T., Baillis, D., & Rusaouen, G. (2012). Heat transfer modeling in vacuum insulation panels containing nanoporous silicas—A review. *Energy and Buildings*, 54, 320–336.
- Brevik, C., Jelle, B. P., Time, B., Holmberget, Ø., Nygård, J., Bergheim, E., & Dalehaug, A. (2013). Large-Scale experimental wind-driven rain exposure investigations of building integrated photovoltaics. *Solar Energy*, 90, 179–187.
- Brunner, S., & Simmler, H. (2007). In situ performance assessment and service life of vacuum insulation panels (VIP) in buildings. In *Proceedings of the 8th International Vacuum Insulation Symposium*, ZAEBayern/UniWue, Würzburg, 18–19 September, 2007.
- Brunner, S., & Simmler, H. (2008). In Situ performance assessment of vacuum insulation panels in a flat roof construction. *Vacuum*, 82, 700–707.
- Brunner, S., & Ghazi Wakili, K. (2014). Hints for an additional aging factor regarding the thermal performance of vacuum insulation panels with pyrogenic silica core. *Vacuum*, 100, 4–6.
- Brunner, S., Ph. Gasser, Simmler, H., & Ghazi, K. (2006). Investigation of multilayered aluminium-coated polymer laminates by focused ion beam (FIB) etching. *Surface & Coatings Technology*, 200, 5908–5914.
- Brunner, S., Stahl, T., & Ghazi Wakili, K. (2012a). An example of deteriorated vacuum insulation panels in a building facade. *Energy and Buildings*, 54, 278–282.
- Brunner, S., Stahl, T., & Ghazi Wakili, K. (2012b). Single and double layered vacuum insulation panels of the same thickness in comparison. In *Proceedings of the 3rd Building Enclosure Science & Technology (BEST 3 - 2012) Conference*, Atlanta, Georgia, USA, 2–4 April, 2012.
- Brunner, S., Wakili, K. G., Stahl, T., & Binder, B. (2014). Vacuum insulation panels for building applications—Continuous challenges and developments. *Energy and Buildings*, 85, 592–596.

- Buratti, C. (Ed.). (2019). *Translucent Silica Aerogel - Properties, preparation and applications*. Nova Science Publishers.
- Buratti, C., & Moretti, E. (2012a). Experimental performance evaluation of aerogel glazing systems. *Applied Energy*, *97*, 430–437.
- Buratti, C., & Moretti, E. (2012b). Glazing systems with silica aerogel for energy savings in buildings. *Applied Energy*, *98*, 396–403.
- Buratti, C., Moretti, E., Belloni, E., & Agosti, F. (2014). Development of innovative aerogel based plasters: Preliminary thermal and acoustic performance evaluation. *Sustainability*, *6*, 5839–5852.
- Buratti, C., Moretti, E., & Zinzi, M. (2017a). High energy-efficient windows with silica aerogel for building refurbishment: Experimental characterization and preliminary simulations in different climate conditions. *Buildings*, *7*, 1–12, Article no. 8.
- Buratti, C., Merli, F., & Moretti, E. (2017b). Aerogel-based materials for building applications: Influence of granule size on thermal and acoustic performance. *Energy and Buildings*, *152*, 472–482.
- Cao, S., Gustavsen, A., Uvsløkk, S., Jelle, B. P., Gilbert, J., & Maunuksela, J. (2010). The effect of wall-integrated phase change material panels on the indoor air and wall temperature - Hot box experiments. In *Proceedings of the Renewable Energy Research Conference - Renewable Energy Beyond 2020*, Trondheim, Norway, 7–8 June, 2010.
- Caps, R. (2005). Monitoring gas pressure in vacuum insulation panels. In *Proceedings of the 7th International Vacuum Insulation Symposium* (pp. 57–66), EMPA, Dübendorf, 28–29 September, 2005.
- Caps, R., & Fricke, J. (2000). Thermal conductivity of opacified powder filler materials for vacuum insulation. *International Journal of Thermophysics*, *21*, 445–452.
- Caps, R., Heinemann, U., Ehrmantraut, M., & Fricke, J. (2001). Evacuated insulation panels filled with pyrogenic silica powders: Properties and applications. *High Temperatures—High Pressures*, *33*, 151–156.
- Caps, R., Beyrichen, H., Kraus, D., & Weismann, S. (2008). Quality control of vacuum insulation panels: Methods of measuring gas pressure. *Vacuum*, *82*, 691–699.
- Cheng, X., Liu, S., Lu, L., Sui, X., Meynen, V., Cool, P., Vansant, E. F., & Jiang, J. (2007). Fast fabrication of hollow silica spheres with thermally stable nanoporous shells. *Microporous and Mesoporous Materials*, *98*, 41–46.
- Chiang, J. C., & MacDiarmid, A. G. (1986). 'Polyaniline': Protonic acid doping of the emeraldine form to the metallic regime. *Synthetic Metals*, *13*, 193–205.
- Cho, K., Hong, Y., & Seo, J. (2014). Assessment of the economic performance of vacuum insulation panels for housing projects. *Energy and Buildings*, *70*, 45–51.
- Cotana, F., Pisello, A. L., Moretti, E., & Buratti, C. (2014). Multipurpose characterization of glazing systems with silica aerogel: in-field experimental analysis of thermal-energy, lighting and acoustic performance. *Building and Environment*, *81*, 92–102.
- Cuce, E., Cuce, P. M., Wood, C. J., & Riffat, S. B. (2014). Toward aerogel based thermal superinsulation in buildings: A comprehensive review. *Renewable and Sustainable Energy Reviews*, *34*, 273–299.
- De Masi, R. F., Ruggiero, S., & Vanoli, G. P. (2020). Multi-layered wall with vacuum insulation panels: Results of 5-years in-field monitoring and numerical analysis of aging effect on building consumptions. *Applied Energy*, *278*, 115605, 1–15.
- De Meersman, G., Van Den Bossche, N., & Janssens, A. (2015). Long term durability of vacuum insulation panels: Determination of the Sd-Value of MF-2 foils. *Energy Procedia*, *78*, 1574–1580.
- Deb, S. K. (2008). Opportunities and challenges in science and technology of WO<sub>3</sub> for electrochromic and related applications. *Solar Energy Materials and Solar Cells*, *92*, 245–258.
- Demirbas, M. F. (2006). Thermal energy storage and phase change materials: An overview. *Energy Sources, Part B: Economics, Planning and Policy*, *1*, 85–95.
- Desjarlais, A., Shrestha, S., Chu, D., & Pagan-Vazquez, A. (2016). Thermal performance evaluation of walls with gas-filled panel insulation. Lecture presented at Buildings XIII Conference, 7

- December. Retrieved December 19, 2019 from [https://web.ornl.gov/sci/buildings/2016/docs/presentations/practices/practices-10/Practices10\\_Paper92\\_Desjarlais.pdf](https://web.ornl.gov/sci/buildings/2016/docs/presentations/practices/practices-10/Practices10_Paper92_Desjarlais.pdf).
- Dieckmann, J. H. (2013). Latent heat storage in concrete. Technische Universität Kaiserslautern, Kaiserslautern, Germany. Retrieved October 31, 2013 from [http://www.eurosolar.org/new/pdfs\\_neu/Thermal/IRES2006\\_Dieckmann.pdf](http://www.eurosolar.org/new/pdfs_neu/Thermal/IRES2006_Dieckmann.pdf).
- Dowson, M., Grogan, M., Birks, T., Harrison, D., & Craig, S. (2012). Streamlined Life Cycle Assessment (LCA) of transparent silica aerogel made by supercritical drying. *Applied Energy*, 97, 396–404.
- Du, X., & He, J. (2008). Facile size-controllable syntheses of highly monodisperse polystyrene nano- and microspheres by polyvinylpyrrolidone-mediated emulsifier-free emulsion polymerization. *Journal of Applied Polymer Science*, 108, 1755–1760.
- Du, Y., Luna, L. E., Tan, W. S., Rubner, M. F., & Cohen, R. E. (2010). Hollow silica nanoparticles in UV-visible antireflection coatings for poly(methyl methacrylate) substrates. *ACS Nano*, 4, 4308–4316.
- Fan, H., Lei, Z., Pan, J. H., & Zhao, X. S. (2011). Sol-Gel synthesis, microstructure and adsorption properties of hollow silica spheres. *Materials Letters*, 65, 1811–1814.
- Fantucci, S., Garbaccio, S., Lorenzati, A., & Perino, M. (2019). Thermo-economic analysis of building energy retrofits using VIP—Vacuum insulation panels. *Energy and Buildings*, 196, 269–279.
- Farid, M. M., Khudhair, A. M., Razack, S. A. K., & Al-Hallaj, S. (2004). A review on phase change energy storage: Materials and applications. *Energy Conversion and Management*, 45, 1597–1615.
- Fasana, S., & Nelva, R. (2013). Improvement of the water resistancy in the integration of photovoltaic panels on traditional roofs. *Construction and Building Materials*, 48, 1081–1091.
- Feng, T., Rai, A., Hun, D., & Shrestha, S. S. (2021). Molecular dynamics simulations of energy accommodation between gases and polymers for ultra-low thermal conductivity insulation. *International Journal of Heat and Mass Transfer*, 164, 120459, 1–10.
- Fickler, S., Milow, B., Ratke, L., Schnellenbach-Held, M., & Welsch, T. (2015). Development of high performance aerogel concrete. *Energy Procedia*, 78, 406–411.
- Fricke, J. (2005). From Dewars to VIPs - One century of progress in vacuum insulation technology. In *Proceedings of the 7th International Vacuum Insulation Symposium* (pp. 5–14). EMPA, Dübendorf, Switzerland, 28–29 September, 2005.
- Fricke, J., Schwab, H., & Heinemann, U. (2006). Vacuum insulation panels—Exciting thermal properties and most challenging applications. *International Journal of Thermophysics*, 27, 1123–1139.
- Fricke, J., Heinemann, U., & Ebert, H. P. (2008). Vacuum insulation panels—From research to market. *Vacuum*, 82, 680–690.
- Fu, J., He, C., Wang, S., & Chen, Y. (2018). A thermally stable and hydrophobic composite aerogel made from cellulose nanofibril aerogel impregnated with silica particles. *Journal of Materials Science*, 53, 7072–7082.
- Gangåssæter, H. F., Jelle, B. P., & Mofid, S. A. (2017a). Synthesis of silica-based nano insulation materials for potential application in low-energy or zero emission buildings. *Energy Procedia*, 122, 949–954.
- Gangåssæter, H. F., Jelle, B. P., Mofid, S. A., & Gao, T. (2017b). Air-filled nanopore based high-performance thermal insulation materials. *Energy Procedia*, 132, 231–236.
- Gao, T., & Jelle, B. P. (2017). Silver nanoparticles as low-emissivity coating materials. *Translational Materials Research*, 4, 015001 (9 pages).
- Gao, T., & Jelle, B. P. (2019). Thermal conductivity of amorphous silica nanoparticles. *Journal of Nanoparticle Research*, 21:108, 6 pages.
- Gao, T., Sandberg, L. I. C., Jelle, B. P., & Gustavsen, A. (2012). Nano insulation materials for energy efficient buildings: A case study on hollow silica nanospheres. In A. Mendez-Vilas (Ed.), *Fuelling the future: Advances in science and technologies for energy generation, transmission and storage* (pp. 535–539). BrownWalker Press.

- Gao, T., Jelle, B. P., Sandberg, L. I. C., & Gustavsen, A. (2013). Monodisperse hollow silica nanospheres for nano insulation materials: synthesis, characterization, and life cycle assessment. *ACS Applied Materials and Interfaces*, *5*, 761–767.
- Gao, T., Jelle, B. P., Gustavsen, A., & Jacobsen, S. (2014a). Aerogel-incorporated concrete: An experimental study. *Construction and Building Materials*, *52*, 130–136.
- Gao, T., Sandberg, L. I. C., & Jelle, B. P. (2014b). Nano insulation materials: Synthesis and life cycle assessment. *Procedia CIRP*, *15*, 490–495.
- Gao, T., Jelle, B. P., Ihara, T., & Gustavsen, A. (2014c). Insulating glazing units with silica aerogel granules: The impact of particle size. *Applied Energy*, *128*, 27–34.
- Gao, T., Jelle, B. P., Gustavsen, A., & He, J. (2014d). Lightweight and thermally insulating aerogel glass materials. *Applied Physics A: Materials Science & Processing*, *117*, 799–808.
- Gao, T., Jelle, B. P., Sandberg, L. I. C., & Gustavsen, A. (2015). Thermal conductivity of monodisperse silica nanospheres. *Journal of Porous Media*, *18*, 941–947.
- Gao, T., Ihara, T., Grynning, S., Jelle, B. P., & Lien, A. G. (2016a). Perspective of aerogel glazings in energy efficient buildings. *Building and Environment*, *95*, 405–413.
- Gao, T., Jelle, B. P., & Gustavsen, A. (2016b). Building integration of aerogel glazings. *Procedia Engineering*, *145*, 723–728.
- Geng, Y., Han, X., Zhang, H., & Shi, L. (2021). Optimization and cost analysis of thickness of vacuum insulation panel for structural insulating panel buildings in cold climates. *Journal of Building Engineering*, *33*, 101853, 1–15.
- Ghazi Wakili, K., & Remhof, A. (2017). Reaction of aerogel containing ceramic fibre insulation to fire exposure. *Fire and Materials*, *41*, 29–39.
- Ghazi Wakili, K., Bundi, R., & Binder, B. (2004). Effective thermal conductivity of vacuum insulation panels. *Building Research and Information*, *32*, 293–299.
- Ghazi Wakili, K., Nussbaumer, T., & Bundi, R. (2005). Thermal performance of VIP assemblies in building constructions. In *Proceedings of the 7th International Vacuum Insulation Symposium* (pp. 131–138). Dübendorf, Switzerland, 28–29 September, 2005.
- Ghazi Wakili, K., Stahl, T., & Brunner, S. (2011). Effective thermal conductivity of a staggered double layer of vacuum insulation panels. *Energy and Buildings*, *43*, 1241–1246.
- Ghazi Wakili, K., Binder, B., Zimmermann, M., & Tanner, Ch. (2014). Efficiency verification of a combination of high performance and conventional insulation layers in retrofitting a 130-year old building. *Energy and Buildings*, *82*, 237–242.
- Ghazi Wakili, K., Stahl, Th., Heiduk, E., Schuss, M., Vonbank, R., Pont, U., Sustr, C., Wolosiuk, D., & Mahdavi, A. (2015). High performance aerogel containing plaster for historic buildings with structured facades. *Energy Procedia*, *78*, 949–954.
- Ghazi Wakili, K., Dworatzky, C., Sanner, M., Sengespeick, A., Paronen, M., & Stahl, T. (2018). Energy efficient retrofit of a prefabricated concrete panel building (Plattenbau) in Berlin by applying an aerogel based rendering to its facades. *Energy and Buildings*, *165*, 293–300.
- Gonçalves, M., Simões, N., Serra, C., & Flores-Colen, I. (2020). A review of the challenges posed by the use of vacuum panels in external insulation finishing systems. *Applied Energy*, *257*, 114028, 1–15.
- Grader, G. S., de Hazan, Y., & Shter, G. E. (1998). Ultra light ceramic foams. *Sol-Gel Synthesis and Processing*, *95*, 161–172.
- Grandcolas, M., Etienne, G., Tilset, B. G., Gao, T., Sandberg, L. I. C., Gustavsen, A., & Jelle, B. P. (2013). Hollow silica nanospheres as a superinsulating material. In *Proceedings of the 11th International Vacuum Insulation Symposium (IVIS 2013)* (pp. 43–44). Dübendorf, Zürich, Switzerland, 19–20 September, 2013.
- Grandcolas, M., Jasinski, E., Gao, T., & Jelle, B. P. (2019). Preparation of low density organosilica monoliths containing hollow silica nanospheres as thermal insulation materials. *Materials Letters*, *250*, 151–154.
- Granqvist, C. G. (1995). *Handbook of inorganic electrochromic materials*. Elsevier.
- Granqvist, C. G. (2005). Electrochromic devices. *Journal of the European Ceramic Society*, *25*, 2907–2912.

- Granqvist, C. G. (2008). Oxide electrochromics: Why, how, and whither. *Solar Energy Materials and Solar Cells*, 92, 203–208.
- Granqvist, C. G. (2012). Oxide electrochromics: An introduction to devices and materials. *Solar Energy Materials and Solar Cells*, 99, 1–13.
- Granqvist, C. G., Arvizu, M. A., Pehlivan, I. B., Qu, H.-Y., Wen, R.-T., & Niklasson, G. A. (2018). Electrochromic materials and devices for energy efficiency and human comfort in buildings: A critical review. *Electrochimica Acta*, 259, 1170–1182.
- Griffith, B. T., Türlér, D., & Arashteh, D. (1993). Optimizing the effective conductivity and cost of gas-filled panel thermal insulations. In *Proceedings of the 22nd International Thermal Conductivity Conference*, Arizona State University, 7–10 November, 1993.
- Griffith, B. T., Arashteh, D., & Türlér, D. (1995). Gas-filled panels: An update on applications in the building thermal envelope. In *Proceedings of the BETEC Fall Symposium, Superinsulations and the Building Envelope*, Washington, DC, 14 November, 1995.
- Grynning, S., Jelle, B. P., Uvsløkk, S., Gustavsen, A., Baetens, R., Caps, R., & Meløysund, V. (2011). Hot box investigations and theoretical assessments of miscellaneous vacuum insulation panel configurations in building envelopes. *Journal of Building Physics*, 34, 297–324.
- Haavi, T., Jelle, B. P., & Gustavsen, A. (2012). Vacuum insulation panels in wood frame wall constructions with different stud profiles. *Journal of Building Physics*, 36, 212–226.
- Han, L., Gao, C., Wu, X., Chen, Q., Shu, P., Ding, Z., & Che, S. (2011). Anionic surfactants templating route for synthesizing silica hollow spheres with different shell porosity. *Solid State Sciences*, 13, 721–728.
- Hasnain, S. M. (1998). Review on sustainable thermal energy storage technologies, Part I: Heat storage materials and techniques. *Energy Conversion and Management*, 39, 1127–1138.
- He, Y.-L., & Xie, T. (2015). Advances of thermal conductivity models of nanoscale silica aerogel insulation material. *Applied Thermal Engineering*, 81, 28–50.
- Heinemann, U. (2008). Influence of water on the total heat transfer in ‘evacuated’ insulations. *International Journal of Thermophysics*, 29, 735–749.
- Heinemann, U., & Kastner, R. (2010). VIP-Prove, Vakuumisolationspaneele - Bewährung in der Baupraxis - Wissenschaftliche Begleitforschung, ZAE Bayern, Report ZAE 2 - 1210–11.
- Heinemann, U., Schwab, H., Simmler, H., Brunner, S., Ghazi, K., Bundi, R., Kumuran, K., Mukhopadhyaya, Ph., Quénard, D., Sallée, H., Noller, K., Küçükpinar-Niarchos, E., Stramm, C., Tenperik, M. J., Cauberg, J. J. M., Binz, A., Steinke, G., Moosmann, A., & Erb, M. (2005). Vacuum insulation. Panel properties and building applications. (Summary), *HiPTI - High Performance Thermal Insulation, IEA/ECBCS Annex 39*, September, 2005.
- Hostler, S. R., Abramson, A. R., Gawryla, M. D., Bandi, S. A., & Schiraldi, D. A. (2009). Thermal conductivity of a clay-based aerogel. *International Journal of Heat and Mass Transfer*, 52, 665–669.
- Huang, W. -S., Humphrey, B. D., & MacDiarmid, A. G. (1986). Polyaniline, a novel conducting polymer. morphology and chemistry of its oxidation and reduction in aqueous electrolytes. *Journal of the Chemical Society, Faraday Transactions 1: Physical Chemistry in Condensed Phases*, 82, 2385–2400.
- Huang, Y., Gong, L., Pan, Y., Li, C., Zhou, T., & Cheng, X. (2018). Facile construction of the aerogel/geopolymer composite with ultra-low thermal conductivity and high mechanical performance. *RSC Advances*, 8, 2350–2356.
- Ihara, T., Grynning, S., Gao, T., Gustavsen, A., & Jelle, B. P. (2015a). Impact of convection on thermal performance of aerogel granulate glazing systems. *Energy and Buildings*, 88, 165–173.
- Ihara, T., Gao, T., Grynning, S., Jelle, B. P., & Gustavsen, A. (2015b). Aerogel granulate glazing facades and their application potential from an energy saving perspective. *Applied Energy*, 142, 179–191.
- Ihara, T., Jelle, B. P., Gao, T., & Gustavsen, A. (2015c). Aerogel granule aging driven by moisture and solar radiation. *Energy and Buildings*, 103, 238–248.



- Jelle, B. P. (1993). Electrochemical and Spectroscopic Studies of Electrochromic Materials. *Ph.D. thesis*, 1993:131, Department of Applied Electrochemistry, The Norwegian Institute of Technology, Trondheim, Norway.
- Jelle, B. P. (2011a). Traditional, state-of-the-art and future thermal building insulation materials and solutions—Properties, requirements and possibilities. *Energy and Buildings*, *43*, 2549–2563.
- Jelle, B. P. (2011b). Evaluation of building products by conducting accelerated climate ageing in the laboratory. In *Proceedings of the 12th International Conference on Durability of Building Materials and Components* (pp. 311–319). Porto, Portugal, 12–15 April, 2011.
- Jelle, B. P. (2012a). Development of a model for radon concentration in indoor air. *Science of the Total Environment*, *416*, 343–350.
- Jelle, B. P. (2012b). Accelerated climate ageing of building materials, components and structures in the laboratory. *Journal of Materials Science*, *47*, 6475–6496.
- Jelle, B. P. (2013a). Solar radiation glazing factors for window panes, glass structures and electrochromic windows in buildings - measurement and calculation. *Solar Energy Materials and Solar Cells*, *116*, 291–323.
- Jelle, B. P. (2013b). The role of accelerated climate ageing of building materials, components and structures in the laboratory. In *Proceedings of the 7th Nordic Conference on Construction Economics and Organisation 2013* (pp. 111–122). Trondheim, Norway, 12–14 June, 2013.
- Jelle, B. P. (2013c). The challenge of removing snow downfall on photovoltaic solar cell roofs in order to maximize solar energy efficiency - research opportunities for the future. *Energy and Buildings*, *67*, 334–351.
- Jelle, B. P. (2015). Electrochromic smart windows for dynamic daylight and solar energy control in buildings. In R. J. Mortimer, D. R. Rosseinsky, & P. M. S. Monk (Eds.), *Electrochromic materials and devices* (pp. 419–502). Wiley-VCH.
- Jelle, B. P. (2016a). Building integrated photovoltaics: A concise description of the current state of the art and possible research pathways. *Energies*, *9*, 1–30, Article no. 21.
- Jelle, B. P. (2016b). Nano-based thermal insulation for energy-efficient buildings. In F. Pacheco-Torgal, E. Rasmussen, C.-G. Granqvist, V. Ivanov, A. Kaklauskas and S. Makonin (Eds.), *Start-up creation: The smart eco-efficient built environment* (pp. 129–181). Elsevier.
- Jelle, B. P., & Hagen, G. (1993). Transmission spectra of an electrochromic window based on polyaniline, prussian blue and tungsten oxide. *Journal of Electrochemical Society*, *140*, 3560–3564.
- Jelle, B. P., & Hagen, G. (1998). Electrochemical multilayer deposition of polyaniline and prussian blue and their application in solid state electrochromic windows. *Journal of Applied Electrochemistry*, *28*, 1061–1065.
- Jelle, B. P., & Hagen, G. (1999a). Performance of an electrochromic window based on polyaniline, prussian blue and tungsten oxide. *Solar Energy Materials and Solar Cells*, *58*, 277–286.
- Jelle, B. P., & Hagen, G. (1999b). Correlation between light absorption and electric charge in solid state electrochromic windows. *Journal of Applied Electrochemistry*, *29*, 1103–1110.
- Jelle, B. P., & Nilsen, T.-N. (2011). Comparison of accelerated climate ageing methods of polymer building materials by attenuated total reflectance fourier transform infrared radiation spectroscopy. *Construction and Building Materials*, *25*, 2122–2132.
- Jelle, B. P., & Breivik, C. (2012a). State-of-the-art building integrated photovoltaics. *Energy Procedia*, *20*, 68–77.
- Jelle, B. P., & Breivik, C. (2012b). The path to the building integrated photovoltaics of tomorrow. *Energy Procedia*, *20*, 78–87.
- Jelle, B. P., & Kalnæs, S. E. (2016). Nanotech based vacuum insulation panels for building applications. In F. Pacheco Torgal, C. Buratti, S. Kalaiselvam, C.-G. Granqvist & V. Ivanov (Eds.), *Nano and biotech based materials for energy building efficiency* (pp. 167–214). Springer.
- Jelle, B. P., & Kalnæs, S. E. (2017). Phase change materials for application in energy-efficient buildings. In F. Pacheco-Torgal, C.-G. Granqvist, B. P. Jelle, G. P. Vanoli, N. Bianco & J. Kurnitski (Eds.), *Cost-effective energy-efficient building retrofitting - materials, technologies, optimization and case studies* (pp. 57–118). Elsevier.

- Jelle, B. P., & Gao, T. (2019). Aerogel systems for miscellaneous building applications - experimental investigations. In C. Buratti (Ed.), *Translucent Silica Aerogel - Properties, Preparation and Applications*. Nova Science Publishers.
- Jelle, B. P., Hagen, G., Hesjevik, S. M., & Ødegård, R. (1992a). Transmission through an electrochromic window based on polyaniline, tungsten oxide and a solid polymer electrolyte. *Materials Science and Engineering B*, *B13*, 239–241.
- Jelle, B. P., Hagen, G., & Ødegård, R. (1992b). Transmission spectra of an electrochromic window based on polyaniline, tungsten oxide and a solid polymer electrolyte. *Electrochimica Acta*, *37*, 1377–1380.
- Jelle, B. P., Hagen, G., Sunde, S., & Ødegård, R. (1993a). Dynamic light modulation in an electrochromic window consisting of polyaniline, tungsten oxide and a solid polymer electrolyte. *Synthetic Metals*, *54*, 315–320.
- Jelle, B. P., Hagen, G., & Nødland, S. (1993b). Transmission spectra of an electrochromic window consisting of polyaniline, prussian blue and tungsten oxide. *Electrochimica Acta*, *38*, 1497–1500.
- Jelle, B. P., Hagen, G., Hesjevik, S. M., & Ødegård, R. (1993c). Reduction factor for polyaniline films on ITO from cyclic voltammetry and visible absorption spectra. *Electrochimica Acta*, *38*, 1643–1647.
- Jelle, B. P., Hagen, G., & Birketveit, Ø. (1998). Transmission properties for individual electrochromic layers in solid state devices based on polyaniline, prussian blue and tungsten oxide. *Journal of Applied Electrochemistry*, *28*, 483–489.
- Jelle, B. P., Gustavsen, A., Nilsen, T.-N., & Jacobsen, T. (2007). Solar Material Protection Factor (SMPF) and solar skin protection factor (SSPF) for window panes and other glass structures in buildings. *Solar Energy Materials and Solar Cells*, *91*, 342–354.
- Jelle, B. P., Gustavsen, A., & Baetens, R. (2009). Beyond vacuum insulation panels - How may it be achieved? In *Proceedings of the 9th International Vacuum Insulation Symposium (IVIS 2009)*, London, England, 17–18 September, 2009.
- Jelle, B. P., Gustavsen, A., & Baetens, R. (2010a). The path to the high performance thermal building insulation materials and solutions of tomorrow. *Journal of Building Physics*, *34*, 99–123.
- Jelle, B. P., Gustavsen, A., & Baetens, R. (2010b). The high performance thermal building insulation materials and solutions of tomorrow. In *Proceedings of the Thermal Performance of the Exterior Envelopes of Whole Buildings XI International Conference (Buildings XI)*, Clearwater Beach, Florida, USA, 5–9 December, 2010.
- Jelle, B. P., Tilset, B. G., Jahren, S., Gao, T., & Gustavsen, A. (2011a). Vacuum and nanotechnologies for the thermal insulation materials of beyond tomorrow - from concept to experimental investigations. In *Proceedings of the 10th International Vacuum Insulation Symposium (IVIS 2011)* (pp. 171–178). Ottawa, Canada, 15–16 September, 2011.
- Jelle, B. P., Noreng, K., Erichsen, T. H., & Strand, T. (2011b). Implementation of radon barriers, model development and calculation of radon concentration in indoor air. *Journal of Building Physics*, *34*, 195–222.
- Jelle, B. P., Hynd, A., Gustavsen, A., Arasteh, D., Goudey, H., & Hart, R. (2012a). Fenestration of today and tomorrow: A state-of-the-art review and future research opportunities. *Solar Energy Materials and Solar Cells*, *96*, 1–28.
- Jelle, B. P., Nilsen, T.-N., Hovde, P. J., & Gustavsen, A. (2012b). Accelerated climate aging of building materials and their characterization by fourier transform infrared radiation analysis. *Journal of Building Physics*, *36*, 99–112.
- Jelle, B. P., Breivik, C., & Røkenes, H. D. (2012c). Building integrated photovoltaic products: A state-of-the-art review and future research opportunities. *Solar Energy Materials and Solar Cells*, *100*, 69–96.
- Jelle, B. P., Sveipe, E., Wegger, E., Uvsløkk, S., Grynning, S., Thue, J. V., Time, B., & Gustavsen, A. (2013a). Moisture robustness during retrofitting of timber frame walls with vacuum insulation panels: experimental and theoretical studies. In V. P. de Freitas & J. M. P. Q. Delgado (Eds.), *“Hygrothermal Behavior, Building Pathology and Durability”*, Book Series *“Building Pathology and Rehabilitation”* (Vol. 1, pp. 183–210). Springer.

- Jelle, B. P., Gao, T., Tilset, B. G., Sandberg, L. I. C., Grandcolas, M., Simon, C., & Gustavsen, A. (2013b). Experimental pathways for achieving superinsulation through nano insulation materials. In *Proceedings of the 11th International Vacuum Insulation Symposium (IVIS 2013)* (pp. 99–100). Dübendorf, Zürich, Switzerland, 19–20 September, 2013.
- Jelle, B. P., Gao, T., Sandberg, L. I. C., Tilset, B. G., Grandcolas, M., & Gustavsen, A. (2014a). Thermal Superinsulation for Building Applications - From Concepts to Experimental Investigations. In *Proceedings of The International Conference On Advances in Civil, Structural and Mechanical Engineering (ACSME 2014)* (pp. 97–104). Bangkok, Thailand, 4–5 January, 2014.
- Jelle, B. P., Gao, T., Sandberg, L. I. C., Tilset, B. G., Grandcolas, M., & Gustavsen, A. (2014b). Thermal superinsulation for building applications—From concepts to experimental investigations. *International Journal of Structural Analysis and Design*, *1*, 43–50.
- Jelle, B. P., Sveipe, E., Wegger, E., Gustavsen, A., Grynning, S., Thue, J. V., Time, B., & Lisø, K. R. (2014c). Robustness classification of materials, assemblies and buildings. *Journal of Building Physics*, *37*, 213–245.
- Jelle, B. P., Gao, T., Sandberg, L. I. C., Tilset, B. G., Grandcolas, M., & Gustavsen, A. (2014d). The high performance thermal building insulation materials of beyond tomorrow - From concept to experimental investigations. In *Proceedings of TechConnect World Innovation Conference 2014 - Cleantech 2014 Energy and Efficiency Conference* (pp. 296–299). Washington DC, USA, 15–18 June, 2014.
- Jelle, B. P., Gao, T., Sandberg, L. I. C., Tilset, B. G., Grandcolas, M., & Gustavsen, A. (2015a). Experimental synthesis of hollow silica nanospheres for application as superinsulation in the buildings of tomorrow. In *Proceedings of the 4th Building Enclosure Science & Technology (BEST 4 - 2015) Conference*, Kansas City, Missouri, USA, 13–15 April, 2015.
- Jelle, B. P., Gao, T., Sandberg, L. I. C., Ng, S., Tilset, B. G., Grandcolas, M., & Gustavsen, A. (2015b). Development of nano insulation materials for building constructions. *Proceedings of 5th International Symposium on Nanotechnology in Construction (NICOM5)* (pp. 429–434). Chicago, Illinois, U.S.A., 24–26 May, 2015.
- Jelle, B. P., Kalnæs, S. E., & Gao, T. (2015c). Low-emissivity materials for building applications: A state-of-the-art review and future research perspectives. *Energy and Buildings*, *96*, 329–356.
- Jelle, B. P., Baetens, R., & Gustavsen, A. (2015d). Aerogel insulation for building applications. In D. Levy & M. Zayat (Eds.), *The Sol-Gel Handbook* (Vol. 3, pp. 1385–1412). Wiley-VCH.
- Jelle, B. P., Helgerud, S. C., Brunner, S., Gao, T. & Rognvik, E. (2015e). Experimental investigations of vacuum insulation panels in an alkaline environment. In *Proceedings of the 12th International Vacuum Insulation Symposium (IVIS 2015)* (pp. 302–306). Nanjing, China, 19–21 September, 2015.
- Jelle, B. P., Gao, T., Mofid, S. A., Kolås, T., Stenstad, P. M., & Ng, S. (2016). Avoiding snow and ice formation on exterior solar cell surfaces—A review of research pathways and opportunities. *Procedia Engineering*, *145*, 699–706.
- Jelle, B. P., Mofid, S. A., Gao, T., Grandcolas, M., Sletnes, M., & Sagvolden, E. (2019). Nano insulation materials exploiting the Knudsen effect. *IOP Conference Series: Materials Science and Engineering*, *634*, 012003.
- Jin, X., & Zhang, X. (2011). Thermal analysis of a double layer phase change material floor. *Applied Thermal Engineering*, *31*, 1576–1581.
- Johansson, P., Geving, S., Hagentoft, C.-E., Jelle, B. P., Rognvik, E., Kalagasidis, A. S., & Time, B. (2014). Interior insulation retrofit of a historical brick wall using vacuum insulation panels: Hygrothermal numerical simulations and laboratory investigations. *Building and Environment*, *79*, 31–45.
- Joulain, K., Mulet, J.-P., Marquier, F., Carminati, R., & Greffet, J.-J. (2005). Surface electromagnetic waves thermally excited: Radiative heat transfer, coherence properties and casimir forces revisited in the near field. *Surface Science Reports*, *57*, 59–112.
- Joulain, K. (2008). Near-field heat transfer: A radiative interpretation of thermal conduction. *Journal of Quantitative Spectroscopy & Radiative Transfer*, *109*, 294–304.

- de Fátima Júlio, M., Soares, A., Ilharco, L. M., Flores-Colen, I. & de Brito, J. (2016). Silica-based aerogels as aggregates for cement-based thermal renders. *Cement and Concrete Composites*, 72, 309–318.
- Jurkowska, M., & Szczygiel, I. (2016). Review on properties of microencapsulated phase change materials slurries (mPCMS). *Applied Thermal Engineering*, 98, 365–373.
- Kaganer, M. G. (1969). Thermal insulation in cryogenic engineering. IPST Press (Russian version 1966).
- Kalnæs, S. E., & Jelle, B. P. (2014). Vacuum insulation panel products: A state-of-the-art review and future research pathways. *Applied Energy*, 116, 355–375.
- Kalnæs, S. E., & Jelle, B. P. (2015). Phase change materials and products for building applications: A state-of-the-art review and future research opportunities. *Energy and Buildings*, 94, 150–176.
- Khudhair, A. M., & Farid, M. M. (2004). A review on energy conservation in building applications with thermal storage by latent heat using phase change materials. *Energy Conservation and Management*, 45, 263–275.
- Kim, K. D., Choi, K. Y., & Yang, J. W. (2005). Formation of spherical hollow silica particles from sodium silicate solution by ultrasonic spray pyrolysis method. *Colloids and Surfaces A: Physicochemical and Engineering Aspects*, 254, 193–198.
- Kim, J.-H., Boafó, F. E., Kim, S.-M., & Kim, J.-T. (2017). Aging performance evaluation of vacuum insulation panel (VIP). *Case Studies in Construction Materials*, 7, 329–335.
- Kishore, R. A., Bianchi, M. V. A., Booten, C., Vidal, J., & Jackson, R. (2021). Enhancing building energy performance by effectively using phase change material and dynamic insulation in walls. *Applied Energy*, 283(116306), 1–17.
- Koebel, M., Rigacci, A., & Achard, P. (2012). Aerogel-based thermal superinsulation: An overview. *Journal of Sol-Gel Science and Technology*, 63, 315–339.
- Koebel, M. M., Huber, L., Zhao, S., & Malfait, W. J. (2016). Breakthroughs in cost-effective, scalable production of superinsulating, ambient-dried silica aerogel and silica-biopolymer hybrid aerogels: From laboratory to pilot scale. *Journal of Sol-Gel Science and Technology*, 79, 308–318.
- Lakatos, Á., & Kovács, Z. (2021). Comparison of thermal insulation performance of vacuum insulation panels with EPS protection layers measured with different methods. *Energy and Buildings*, 236, 110771, 1–12.
- Lampert, C. M. (1984). Electrochromic materials and devices for energy efficient windows. *Solar Energy Materials*, 11, 1–27.
- Lampert, C. M. (1998). Smart switchable glazing for solar energy and daylight control. *Solar Energy Materials and Solar Cells*, 52, 207–221.
- Lampert, C. M. (2004). Chromogenic smart materials. *Materials Today*, 7, 28–35.
- Lamy-Mendes, A., Pontinha, A. D. R., Alves, P., Santos, P., & Durães, L. (2021). Progress in silica aerogel-containing materials for buildings' thermal insulation. *Construction and Building Materials*, 286, 122815, 1–32.
- Le, Y., Chen, J.-F., & Wang, W.-C. (2004a). Study on the silica hollow spheres by experiment and molecular simulation. *Applied Surface Science*, 230, 319–326.
- Le, Y., Chen, J.-F., Wang, J.-X., Shao, L., & Wang, W.-C. (2004b). A Novel pathway for synthesis of silica hollow spheres with mesostructured walls. *Materials Letters*, 58, 2105–2108.
- Lee, D., Stevens, P. C., Zeng, S. Q., & Hunt, A. J. (1995a). Thermal Characterization of carbon-opacified silica aerogels. *Journal of Non-Crystalline Solids*, 186, 285–290.
- Lee, K.-H., Kim, S.-Y., & Yoo, K.-P. (1995b). Low-density, hydrophobic aerogels. *Journal of Non-Crystalline Solids*, 186, 18–22.
- Leite da Cunha, S. R., & Barroso de Aguiar, J. L. (2020). Phase change materials and energy efficiency of buildings: A review of knowledge. *Journal of Energy Storage*, 27, 101083, 1–13.
- Levy, D., & Zayat, M. (Eds.), *The Sol-Gel Handbook*. Wiley-VCH.
- Li, Y.-H., Li, Z.-Y., & Tao, W.-Q. (2014). An ideal nano-porous insulation material: Design, modeling and numerical validation. *Applied Thermal Engineering*, 72, 34–40.
- Li, H., Chen, H., Li, X., & Duan, W. (2015). Degradation of VIP barrier envelopes exposed to alkaline solution at different temperatures. *Energy and Buildings*, 93, 208–216.

- Li, Z.-Y., Zhu, C.-Y., & Zhao, X.-P. (2017). A theoretical and numerical study on the gas-contributed thermal conductivity in aerogel. *International Journal of Heat and Mass Transfer*, *108*, 1982–1990.
- Li, T., Song, J., Zhao, X., Yang, Z., Pastel, G., Xu, S., Jia, C., Dai, J., Chen, C., Gong, A., Jiang, F., Yao, Y., Fan, T., Yang, B., Wägberg, L., Yang, R., & Hu, L. (2018). Anisotropic, lightweight, strong, and super thermally insulating nanowood with naturally aligned nanocellulose. *Science Advances*, *4*, eaar3724, 1–9.
- Li, P., Wu, H., Liu, Y., Yang, J., Fang, Z., & Lin, B. (2019). Preparation and optimization of ultra-light and thermal insulative aerogel foam concrete. *Construction and Building Materials*, *205*, 529–542.
- Li, C., Chen, Z., Dong, W., Lin, L., Zhu, X., Liu, Q., Zhang, Y., Zhai, N., Zhou, Z., Wang, Y., Chen, B., Ji, Y., Chen, X., Xu, X., Yang, Y., & Zhang, H. (2021). A Review of silicon-based aerogel thermal insulation materials: performance optimization through composition and microstructure. *Journal of Non-Crystalline Solids*, *553*, 120517, 1–18.
- Liang, L., & Li, B. (2006). Size-dependent thermal conductivity of nanoscale semiconducting systems. *Physical Review B*, *73*, 153303–1–153303–4.
- Liang, Y., Wu, H., Huang, G., Yang, J., & Ding, Y. (2017). Prediction and optimization of thermal conductivity of vacuum insulation panels with aerogel composite cores. *Procedia Engineering*, *205*, 2855–2862.
- Liao, Y., Wu, X., Liu, H., & Chen, Y. (2011). Thermal conductivity of powder silica hollow spheres. *Thermochimica Acta*, *526*, 178–184.
- Liao, Y., Wu, X., Wang, Z., Yue, R., Liu, G., & Chen, Y. (2012). Composite thin film of silica hollow spheres and waterborne polyurethane: excellent thermal insulation and light transmission performances. *Materials Chemistry and Physics*, *133*, 642–648.
- Liu, S., Wei, M., Rao, J., Wang, H., & Zhao, H. (2011). A controlled formation of cage-like nanoporous hollow silica microspheres. *Materials Letters*, *65*, 2083–2085.
- Liu, S., Zhu, K., Cui, S., Shen, X., & Tan, G. (2018). A novel building material with low thermal conductivity: Rapid synthesis of foam concrete reinforced silica aerogel and energy performance simulation. *Energy and Buildings*, *177*, 385–393.
- Luo, Y., & Ye, C. (2012). Using nanocapsules as building blocks to fabricate organic polymer nanofoam with ultra low thermal conductivity and high mechanical strength. *Polymer*, *53*, 5699–5705.
- Mandilaras, I., Atsonios, I., Zannis, G., & Founti, M. (2014). Thermal performance of a building envelope incorporating ETICS with vacuum insulation panels and EPS. *Energy and Buildings*, *85*, 654–665.
- Mao, S., Kan, A., Huang, Z., & Zhu, W. (2020). Prediction of thermal performance of vacuum insulation panels (VIPs) with micro-fiber core materials. *Materials Today*, *22*, 100786.
- Marani, A., & Nehdi, M. L. (2019). Integrating phase change materials in construction materials: Critical review. *Construction and Building Materials*, *217*, 36–49.
- McKinsey. (2009). Pathways to a low-carbon economy. Version 2 of the Global Greenhouse Gas Abatement Cost Curve. McKinsey & Company.
- Meng, Q., Xiang, S., Zhang, K., Wang, M., Bu, X., Xue, P., Liu, L., Sun, H., & Yang, B. (2012). A facile two-step etching method to fabricate porous hollow silica particles. *Journal of Colloid and Interface Science*, *384*, 22–28.
- Miesbauer, O., Kucukpinar, E., Kiese, S., Carmi, Y., Noller, K., & Langowski, H.-C. (2014). Studies on the barrier performance and adhesion strength of novel barrier films for vacuum insulation panels. *Energy and Buildings*, *85*, 597–603.
- Mills, G. L., & Zeller, C. M. (2008). The performance of gas filled multilayer insulation. *Advances of Cryogenic Engineering: Transactions of the Cryogenic Engineering Conference*, *53*, 1475–1482.
- Mofid, S. A., Jelle, B. P., Zhao, X., Gao, T., Grandcolas, M., Cunningham, B., Ng, S., & Yang, R. (2020). Utilization of size-tunable hollow silica nanospheres for building thermal insulation applications. *Journal of Building Engineering*, *31*, 101336, 1–9.

- Monk, P. M. S., Mortimer, R. J., & Rosseinsky, D. R. (1995). *Electrochromism: Fundamentals and applications*. VCH.
- Moretti, E., Merli, F., Cuce, E., & Buratti, C. (2017a). Thermal and acoustic properties of aerogels: Preliminary investigation of the influence of granule size. *Energy Procedia*, *111*, 472–480.
- Moretti, E., Zinzi, M., Carnielo, E., & Merli, F. (2017b). Advanced polycarbonate transparent systems with aerogel: Preliminary characterization of optical and thermal properties. *Energy Procedia*, *113*, 9–16.
- Moretti, E., Zinzi, M., Merli, F., & Buratti, C. (2018). Optical, thermal, and energy performance of advanced polycarbonate systems with granular aerogel. *Energy and Buildings*, *166*, 407–417.
- Mortimer, R. J. (1999). Organic electrochromic materials. *Electrochimica Acta*, *44*, 2971–2981.
- Mortimer, R. J., Dyer, A. L., & Reynolds, J. R. (2006). Electrochromic organic and polymeric materials for display applications. *Displays*, *27*, 2–18.
- Mukhopadhyaya, P., MacLean, D., Korn, J., van Reenen, D., & Molleti, S. (2014). Building application and thermal performance of vacuum insulation panels (VIPs) in Canadian subarctic climate. *Energy and Buildings*, *85*, 672–680.
- Mulet, J.-P., Joulain, K., Carminati, R., & Greffet, J.-J. (2002). Enhanced radiative heat transfer at nanometric distances. *Microscale Thermophysical Engineering*, *6*, 209–222.
- Müller-Fischer, N. (2007). Dynamically enhanced membrane foaming. *Ph.D. thesis*, Dissertation ETH Number 16939, Swiss Federal Institute of Technology, Zürich, Switzerland.
- Ng, S., & Jelle, B. P. (2017). Incorporation of polymers into calcined clays as improved thermal insulating materials for construction. *Advances in Materials Science and Engineering*, *2017*, 6 pages, Article ID 6478236.
- Ng, S., Sandberg, L. I. C., & Jelle, B. P. (2015a). Insulating and strength properties of an aerogel-incorporated mortar based on UHPC formulations. *Key Engineering Materials*, *629–630*, 43–48.
- Ng, S., Jelle, B. P., Sandberg, L. I. C., Gao, T., & Wallevik, Ó. H. (2015b). Experimental investigations of aerogel-incorporated ultra-high performance concrete. *Construction and Building Materials*, *77*, 307–316.
- Ng, S., Jelle, B. P., Zhen, Y., & Wallevik, Ó. H. (2016a). Effect of storage and curing conditions at elevated temperatures on aerogel-incorporated mortar samples based on UHPC recipe. *Construction and Building Materials*, *106*, 640–649.
- Ng, S., Jelle, B. P., & Stähli, T. (2016b). Calcined clays as binder for thermal insulating and structural aerogel incorporated mortar. *Cement and Concrete Composites*, *72*, 213–221.
- Ng, S., Jelle, B. P., Sandberg, L. I., Gao, T., & Mofid, S. A. (2018). Hollow silica nanospheres as thermal insulation materials for construction: Impact of their morphologies as a function of synthesis pathways and starting materials. *Construction and Building Materials*, *166*, 72–80.
- Norton, B., Eames, P. C., Mallick, T. K., Huang, M. J., McCormack, S. J., Mondol, J. D., & Yohanis, Y. G. (2011). Enhancing the performance of building integrated photovoltaics. *Solar Energy*, *85*, 1629–1664.
- Nosrati, R., & Berardi, U. (2017). Long-Term performance of aerogel-enhanced materials. *Energy Procedia*, *132*, 303–308.
- Nosrati, R. H., & Berardi, U. (2018). Hygrothermal characteristics of aerogel-enhanced insulating materials under different humidity and temperature conditions. *Energy and Buildings*, *158*, 698–711.
- Öchsner, A., Hosseini, S. M. H., & Merkel, M. (2009). Numerical simulation of sintered perforated hollow sphere structures (PHSS) to investigate thermal conductivity. In *Proceedings of the International MultiConference of Engineers and Computer Scientists 2009, Vol. II (IMECS 2009)*, Hong Kong, China, 18–20 March, 2009.
- Özonur, Y., Mazman, M., Paksoy, H. Ö., & Evliya, H. (2006). Microencapsulation of coco fatty acid mixtures for thermal energy storage with phase change material. *International Journal of Energy Research*, *30*, 741–749.
- Pacheco-Torgal, F. (2012). Indoor radon: An overview on a perennial problem. *Building and Environment*, *58*, 270–277.

- Paneri, A., Wong, I. L., & Burek, S. (2019). Transparent insulation materials: An overview on past, present and future developments. *Solar Energy*, *184*, 59–83.
- Papadopoulos, A. M. (2005). State of the art in thermal insulation materials and aims for future developments. *Energy and Buildings*, *37*, 77–86.
- Pasupathy, A., & Velraj, R. (2008). Effect of double layer phase change material in building roof for year round thermal management. *Energy and Buildings*, *40*, 193–203.
- Peng, B., Chen, M., Zhou, S., Wu, L., & Ma, X. (2008). Fabrication of hollow silica spheres using droplet templates derived from a miniemulsion technique. *Journal of Colloid and Interface Science*, *321*, 67–73.
- Pons, E., Yrieix, B., Heymans, L., Dubelley, F., & Planes, E. (2014). Permeation of water vapor through high performance laminates for VIPs and physical characterization of sorption and diffusion phenomena. *Energy and Buildings*, *85*, 604–616.
- Pool, M. (2009). Insulation of a mixed use building with 7 storeys in munich with VIP. In *Proceedings of the 9th International Vacuum Insulation Symposium (IVIS 2009)*, London, UK, 17–18 September, 2009.
- Pu, H., Zhang, X., Yuan, J., & Yang, Z. (2009). A facile method for the fabrication of vinyl functionalized hollow silica spheres. *Journal of Colloid and Interface Science*, *331*, 389–393.
- Rahman, Z. U., Wei, N., Li, Z., Sun, W., & Wang, D. (2017). Preparation of hollow mesoporous silica nanospheres: controllable template synthesis and their application in drug delivery. *New Journal of Chemistry*, *41*, 14122–14129.
- Raki, L., Beaudoin, J., Alizadeh, R., Makar, J., & Sato, T. (2010). Cement and concrete nanoscience and nanotechnology. *Materials*, *3*, 918–942.
- Rostam, N. G., Mahdavinjad, M. J., & Rostam, M. G. (2015). Commercializing usage of nano-insulating materials in building industry and future architecture. *Procedia Materials Science*, *11*, 644–648.
- Ruckdeschel, P., & Retsch, M. (2017). Interface and morphology control of the thermal conductivity in core-shell particle colloidal crystals. *Advanced Materials Interfaces*, *2017*, 1700963.
- Ruckdeschel, P., Kemnitzer, T. W., Nutz, F. A., Senker, J., & Retsch, M. (2015). Hollow silica sphere colloidal crystals: Insights into calcination dependent thermal transport. *Nanoscale*, *22*.
- Ruckdeschel, P., Philipp, A., & Retsch, M. (2017). Understanding thermal insulation in porous, particulate materials. *Advanced Functional Materials*, *2017*, 1702256.
- Ruckdeschel, P., Philipp, A., Kopera, B. A. F., Bitterlich, F., Dulle, M., Pech-May, N. W., & Retsch, M. (2018). Thermal transport in binary colloidal glasses: Composition dependence and percolation assessment. *Physical Review E*, *97*, 022612–1–10.
- Sallée, H., Quenard, D., Valenti, E., & Galan, M. (2014). VIP as thermal breaker for internal insulation system. *Energy and Buildings*, *85*, 631–637.
- Sanchez, F., & Sobolev, K. (2010). Nanotechnology in concrete—A review. *Construction and Building Materials*, *24*, 2060–2071.
- Sandberg, L. I. C., Gao, T., Jelle, B. P., & Gustavsen, A. (2013). Synthesis of hollow silica nanospheres by sacrificial polystyrene templates for thermal insulation applications. *Advances in Materials Science and Engineering*, 6 pages, Article ID 483651.
- Sasihithlu, K., & Agarwal, G. S. (2018). Dynamic near-field heat transfer between macroscopic bodies for nanometric gaps. *Nanophotonics*, *7*, 1581–1588.
- Schlanbusch, R. D., Jelle, B. P., Sandberg, L. I. C., Fufa, S. M., & Gao, T. (2014a). Life cycle assessment integrated in the design of a new nano insulation material. In *Proceedings of the 20th Annual International Sustainable Development Research Conference (ISDRC 2014)* (pp. 325–335). Trondheim, Norway, 18–20 June, 2014.
- Schlanbusch, R. D., Jelle, B. P., Sandberg, L. I. C., Fufa, S. M., & Gao, T. (2014b). Integration of life cycle assessment in the design of hollow silica nanospheres for thermal insulation applications. *Building and Environment*, *80*, 115–124.
- Schultz, J. M., & Jensen, K. I. (2008). Evacuated aerogel glazings. *Vacuum*, *82*, 723–729.
- Schultz, J. M., Jensen, K. I., & Kristiansen, F. H. (2005). Super insulating aerogel glazing. *Solar Energy Materials & Solar Cells*, *89*, 275–285.

- Schuss, M., Pont, U., & Mahdavi, A. (2017). Long-term experimental performance evaluation of aerogel insulation plaster. *Energy Procedia*, 132, 508–513.
- Schwab, H., Heinemann, U., Beck, A., Ebert, H.-P., & Fricke, J. (2005a). Permeation of different gases through foils used as envelopes for vacuum insulation panels. *Journal of Thermal Envelope & Building Science*, 28, 293–317.
- Schwab, H., Heinemann, U., Beck, A., Ebert, H.-P., & Fricke, J. (2005b). Dependence of thermal conductivity on water content in vacuum insulation panels with fumed silica kernels. *Journal of Thermal Envelope & Building Science*, 28, 319–326.
- Schwab, H., Heinemann, U., Wachtel, J., Ebert, H.-P., & Fricke, J. (2005c). Predictions for the increase in pressure and water content of vacuum insulation panels (VIPs) integrated into building constructions using model calculations. *Journal of Thermal Envelope & Building Science*, 28, 327–344.
- Schwab, H., Stark, C., Wachtel, J., Ebert, H.-P., & Fricke, J. (2005d). Thermal bridges in vacuum-insulated building facades. *Journal of Thermal Envelope & Building Science*, 28, 345–355.
- Schwab, H., Heinemann, U., Beck, A., Ebert, H.-P., & Fricke, J. (2005e). Prediction of service life for vacuum insulation panels with fumed silica kernel and foil cover. *Journal of Thermal Envelope & Building Science*, 28, 357–374.
- Simmler, H., & Brunner, S. (2005a). Vacuum insulation panels for building application—Basic properties, ageing mechanisms and service life. *Energy and Buildings*, 37, 1122–1131.
- Simmler, H., & Brunner, S. (2005b). Ageing and service life of VIP in buildings. *Proceedings of the 7th International Vacuum Insulation Symposium* (pp. 15–22). EMPA, Dübendorf, Switzerland, 28–29 September, 2005.
- Simmler, H., Brunner, S., Heinemann, U., Schwab, H., Kumaran, K., Mukhopadhyaya, Quènard, D., Sallée, H., Noller, K., Kücküpinar-Niarchos, E., Stramm, C., Tenpierik, M., Cauberg, H., & Erb, M. (2005). Vacuum insulation panels. Study on VIP-components and panels for service life prediction in building applications (Subtask A). *HiPTI - High Performance Thermal Insulation, IEA/ECBCS Annex 39*, September, 2005.
- Simões, N., Gonçalves, M., Serra, C., & Resalati, S. (2021). Can vacuum insulation panels be cost-effective when applied in building façades? *Building and Environment*, 191, 107602, 1–15.
- Sletnes, M., Jelle, B. P., & Risholt, B. (2017). Feasibility study of novel integrated aerogel solutions. *Energy Procedia*, 132, 327–332.
- Smith, D. M., Maskara, A., & Boes, U. (1998). Aerogel-based thermal insulation. *Journal of Non-Crystalline Solids*, 225, 254–259.
- Sobolev, K., & Gutiérrez, M. F. (2005, November). How nanotechnology can change the concrete world. *American Ceramic Society Bulletin*, 84, 16–20.
- Sprengard, C., & Holm, A. H. (2014). Numerical examination of thermal bridging effects at the edges of vacuum-insulation-panels (VIP) in various constructions. *Energy and Buildings*, 85, 638–643.
- Stahl, T., Brunner, S., Zimmermann, M., & Ghazi Wakili, K. (2012). Thermo-hygric properties of a newly developed aerogel based insulation rendering for both exterior and interior applications. *Energy and Buildings*, 44, 114–117.
- Sveipe, E., Jelle, B. P., Wegger, E., Uvsløkk, S., Grynning, S., Thue, J. V., Time, B., & Gustavsen, A. (2011). Improving thermal insulation of timber frame walls by retrofitting with vacuum insulation panels—Experimental and theoretical investigations. *Journal of Building Physics*, 35, 168–188.
- Swimm, K., Reichenauer, G., Vidi, S., & Ebert, H.-P. (2009). Gas pressure dependence of the heat transport in porous solids with pores smaller than 10  $\mu\text{m}$ . *International Journal of Thermophysics*, 30, 1329–1342.
- Tällberg, R., Jelle, B. P., Hamdy, M., Gao, T., & Loonen, R. (2019). Comparison of the energy saving potential of adaptive and controllable smart windows: A state-of-the-art review and simulation studies of thermochromic, photochromic and electrochromic technologies. *Solar Energy Materials and Solar Cells*, 200, 109828, 1–30.
- Teng, Z., Han, Y., Li, J., Yan, F., & Yang, W. (2010). Preparation of hollow mesoporous silica spheres by a sol-gel/emulsion approach. *Microporous and Mesoporous Materials*, 127, 67–72.



- Tenpierik, M. J. (2009). Vacuum insulation panels applied in building constructions (VIP ABC)", *Ph.D. thesis*, Delft University of Technology, Delft, The Netherlands.
- Tenpierik, M., & Cauberg, H. (2007). Analytical models for calculating thermal bridge effects caused by thin high barrier envelopes around vacuum insulation panels. *Journal of Building Physics*, *30*, 185–215.
- Tenpierik, M. J., & Cauberg, J. J. M. (2010). Encapsulated vacuum insulation panels: Theoretical thermal optimization. *Building Research & Information*, *38*, 660–669.
- Tenpierik, M. J., Cauberg, J. J. M., & Thorsell, T. I. (2007a). Integrating vacuum insulation panels in building constructions: an integral perspective. *Construction Innovation*, *7*, 38–53.
- Tenpierik, M., van der Spoel, W., & Cauberg, H. (2007b). Simplified analytical models for service life prediction of a vacuum insulation panel. In *Proceedings of the 8th International Vacuum Insulation Symposium*, ZAE Bayern/UniWue, Würzburg, 18–19 September, 2007.
- Tenpierik, M., van der Spoel, W., & Cauberg, H. (2008). An analytical model for calculating thermal bridge effects in high performance building enclosure. *Journal of Building Physics*, *31*, 361–387.
- Tripathy, M., Sadhu, P. K., & Panda, S. K. (2016). A critical review on building integrated photovoltaic products and their applications. *Renewable Sustainable Energy Reviews*, *61*, 451–465.
- Uriarte, A., Garai, I., Ferdinando, A., Erkoreka, A., Nicolas, O., & Barreiro, E. (2019). Vacuum insulation panels in construction solutions for energy efficient retrofitting of buildings. Two case studies in Spain and Sweden. *Energy and Buildings*, *197*, 131–139.
- Van Den Bergh, S., Uvsløkk, S., Jelle, B. P., Roels, S., & Gustavsen, A. (2011). Experimental and numerical investigations of polystyrene encapsulated vacuum insulation panels—Heat transfer results. In *Proceedings of the 10th International Vacuum Insulation Symposium (IVIS-X)* (pp. 29–34). Ottawa, Canada, 15–16 September, 2011.
- Vaziri, S., Yalon, E., Rojo, M. M., Suryavanshi, S. V., Zhang, H., McClellan, C. J. ... Pop, E. (2019). Ultrahigh thermal isolation across heterogeneously layered two-dimensional materials. *Science Advances*, *5*.
- Voellinger, T., Bassi, A., & Heitel, M. (2014). Facilitating the incorporation of VIP into precast concrete sandwich panels. *Energy and Buildings*, *85*, 666–671.
- Wan, Y., & Yu, S.-H. (2008). Polyelectrolyte controlled large-scale synthesis of hollow silica spheres with tunable sizes and wall thicknesses. *Journal of Physical Chemistry C*, *112*, 3641–3647.
- Wang, X., Miao, X., Li, Z., & Deng, W. (2010). Fabrication of mesoporous silica hollow spheres using triblock copolymer PEG-PPG-PEG as template. *Journal of Non-Crystalline Solids*, *356*, 898–905.
- Wang, F., Tang, Y., Zhang, B., Chen, B., & Wang, Y. (2012). Preparation of novel magnetic hollow mesoporous silica microspheres and their efficient adsorption. *Journal of Colloid and Interface Science*, *386*, 129–134.
- Wang, G., Zhao, J., Wang, G., Mark, L. H., Park, C. B., & Zhao, G. (2017a). Low-density and structure-tunable microcellular PMMA foams with improved thermal-insulation and compressive mechanical properties. *European Polymer Journal*, *95*, 382–393.
- Wang, G., Wang, C., Zhao, J., Wang, G., Park, C. B., & Zhao, G. (2017b). Modelling of thermal transport through a nanocellular polymer foam: Toward the generation of a new superinsulating material. *Nanoscale*, *9*, 5996–6009.
- Wang, L., Liu, P., Jing, Q., Liu, Y., Wang, W., Zhang, Y., & Li, Z. (2018). Strength properties and thermal conductivity of concrete with the addition of expanded perlite filled with aerogel. *Construction and Building Materials*, *188*, 747–757.
- Wang, Y., Huang, J., Wang, D., Liu, Y., Zhao, Z., & Liu, J. (2019). Experimental investigation on thermal conductivity of aerogel-incorporated concrete under various hygrothermal environment. *Energy*, *188*, 115999, 1–17.
- Wegger, E., Jelle, B. P., Sveipe, E., Grynning, S., Gustavsen, A., Baetens, R., & Thue, J. V. (2011). Aging effects on thermal properties and service life of vacuum insulation panels. *Journal of Building Physics*, *35*, 128–167.

- Welsch, T., & Schnellenbach-Held, M. (2018). High performance aerogel concrete. In D. Hordijk & M. Luković (Eds.), *High Tech Concrete: Where Technology and Engineering Meet* (pp. 117–124). Springer.
- Wernery, J., Ben-Ishai, A., Binder, B., & Brunner, S. (2017). Aerobrick—An aerogel-filled insulating brick. *Procedia Engineering*, 134, 490–498.
- Wicklein, B., Kocjan, A., Salazar-Alvarez, G., Carosio, F., Camino, G., Antonietti, M., & Bergström, L. (2015). Thermally insulating and fire-retardant lightweight anisotropic foams based on nanocellulose and graphene oxide. *Nature Nanotechnology*, 10, 277–283.
- Wong, J. C. H., Kaymak, H., Brunner, S., & Koebel, M. M. (2014). Mechanical properties of monolithic silica aerogels made from polyethoxydisiloxanes. *Microporous and Mesoporous Materials*, 183, 23–29.
- Wu, W., Cao, S., Yuan, X., Zhao, Z., & Fang, L. (2012). Sodium silicate route: Fabricating high monodisperse hollow silica spheres by a facile method. *Journal of Porous Materials*, 19, 913–919.
- Xu, Y., Wang, J.-S., Duan, W., Gu, B.-L., & Li, B. (2008). Nonequilibrium green's function method for phonon-phonon interactions and ballistic-diffusive thermal transport. *Physical Review B*, 78, 224303–1–224303–9.
- Yang, M., Wang, G., & Yang, Z. (2008). Synthesis of hollow spheres with mesoporous silica nanoparticles shell. *Materials Chemistry and Physics*, 111, 5–8.
- Yang, N., Xu, X., Zhang, G., & Li, B. (2012). Thermal transport in nanostructures. *AIP Advances*, 2, 041410–1–041410–24.
- Yarmohammadi, M. (2016). Dynamical thermal conductivity of the spin lieb lattice. *Solid State Communications*, 234–235, 14–20.
- Yoon, H.-S., Lim, T.-K., Jeong, S.-M., & Yang, K.-H. (2020). Thermal transfer and moisture resistances of nano-aerogel-embedded foam concrete. *Construction and Building Materials*, 236, 117575, 1–7.
- Yrieix, B., Morel, B., & Pons, E. (2014). VIP service life assessment: Interactions between barrier laminates and core material, and significance of silica core ageing. *Energy and Buildings*, 85, 617–630.
- Yuan, J., Zhou, T., & Pu, H. (2010). Nano-sized silica hollow spheres: Preparation, mechanism analysis and its water retention property. *Journal of Physics and Chemistry of Solids*, 71, 1013–1019.
- Yue, Q., Li, Y., Kong, M., Huang, J., Zhao, X., Liu, J., & Williford, R. E. (2011). Ultralow density, hollow silica foams produced through interfacial reaction and their exceptional properties for environmental and energy applications. *Journal of Materials Chemistry*, 21, 12041–12046.
- Zhang, C., Yan, H., Lv, K., & Yuan, S. (2013). Facile Synthesis of hierarchically porous silica nanocapsules and nanospheres via vesicle templating. *Colloids and Surfaces A: Physicochemical and Engineering Aspects*, 424, 59–65.
- Zhang, H., Zhao, Y., & Akins, D. L. (2012). Synthesis and new structure shaping mechanism of silica particles formed at high pH. *Journal of Solid State Chemistry*, 194, 277–281.
- Zhang, S., Xu, L., Liu, H., Zhao, Y., Zhang, Y., Wang, Q., Yu, Z., & Liu, Z. (2009). A dual template method for synthesizing hollow silica spheres with mesoporous shells. *Materials Letters*, 63, 258–259.
- Zhang, Y.-B., Qian, X.-F., Li, Z.-K., Yin, J., & Zhu, Z.-K. (2004). Synthesis of novel mesoporous silica spheres with starburst pore canal structure. *Journal of Solid State Chemistry*, 177, 844–848.
- Zhang, Z. M. (2007). *Nano/Microscale Heat Transfer*. McGraw-Hill.
- Zhao, J.-J., Duan, Y.-Y., Wang, X.-D., & Wang, B.-X. (2012). Effects of solid-gas coupling and pore and particle microstructures on the effective gaseous thermal conductivity in aerogels. *Journal of Nanoparticle Research*, 14:1024, 1–15.
- Zhou, D., Zhao, C. Y., & Tian, Y. (2012). Review on thermal energy storage with phase change materials (PCMs) in building applications. *Applied Energy*, 92, 593–605.
- Zhu, Y., Shi, J., Chen, H., Shen, W., & Dong, X. (2005). A facile method to synthesize novel hollow mesoporous silica spheres and advanced storage property. *Microporous and Mesoporous Materials*, 84, 218–222.

- Zhu, C.-Y., Li, Z.-Y., Pang, H.-Q., & Pan, N. (2018). Design and optimization of core/shell structures as highly efficient opacifiers for silica aerogels as high-temperature thermal insulation. *International Journal of Thermal Sciences*, *133*, 206–215.
- Zhu, P., Brunner, S., Zhao, S., Griffa, M., Leemann, A., Toropovs, N., Malekos, A., Koebel, M. M., & Lura, P. (2019). Study of physical properties and microstructure of aerogel-cement mortars for improving the fire safety of high-performance concrete linings in tunnels. *Cement and Concrete Composites*, *104*, 103414, 1–11.
- Zhu, P., Xu, X., Liu, H., Liu, S., Chen, C., & Jia, Z. (2020). Tunnel fire resistance of self-compacting concrete coated with SiO<sub>2</sub> aerogel cement paste under 2.5 h HC fire loading. *Construction and Building Materials*, *239*, 117857, 1–9.
- Zou, X., Tao, C., Yan, L., Yang, F., Lv, H., Yan, H., Wang, Z., Li, Y., Wang, J., Yuan, X., & Zhang, L. (2018). One-step sol-gel preparation of ultralow-refractive-index porous coatings with mulberry-like hollow silica nanostructures. *Surface and Coatings Technology*, *341*, 57–63.
- Zwerger, M., & Klein, H. (2005). Integration of VIP's into external wall insulation system. In *Proceedings of the 7th International Vacuum Insulation Symposium* (pp. 173–179), EMPA, Dübendorf, Switzerland, 28–29 September, 2005.

# Chapter 13

## Insulated Autoclaved Cellular Concretes and Improvement of Their Mechanical and Hydrothermal Properties



Anna Stepien, Ryszard Dachowski, and Jerzy Z. Piotrowski

**Abstract** Materials forming the external building envelope, and in particular, thermal insulation are important factors in mitigating heat losses from a building, and thus reducing the overall building energy usage (i.e., lower energy consumption and costs of space conditioning energy). They also contribute to the improvement of building environmental characteristics through lowering the Greenhouse Gas (GHG) emissions and are now the object of a growing interest associated with sustainable construction trends. Autoclaved aerated concrete (AAC) and autoclaved cellular concrete (ACC) are widely considered as structural materials of improved thermal insulation characteristics. They are made with fine aggregates, cement (or cement and lime), and an expansion agent that causes the fresh mixture to rise like a bread dough to create a porous, thermally insulating concrete structure. In fact, this type of concrete contains about 80% of air, where one m<sup>3</sup> of raw materials is sufficient to produce around five m<sup>3</sup> of AAC. Depending on the bulk density and humidity, aerated concretes exhibit very unique thermal performance and hygrothermal characteristics. This fact is of particular importance when designing building envelopes of optimized R-value (thermal resistance), or U-value (heat transfer coefficient). Typically, the thermal conductivities of AAC and ACC are a function of material density and moisture content that range from 0.1 to 0.7 W/(m·K) for material densities between 400 and 1700 kg/m<sup>3</sup>. This chapter discusses the physical properties of cellular concretes. Efforts to improve the mechanical and insulation performance characteristics using high-performance polystyrene (HIPS) are discussed. To analyze the geometry, size, and distribution of concrete pores in AAC with added HIPS, a series of measurements were performed by the authors. This includes analysis of concrete density, as well as porosity testing and Micro CT analysis (CT—computerized tomography). These tests show the presence of one nm pores, and the volume

---

A. Stepien (✉) · R. Dachowski

Faculty of Civil Engineering and Architecture, Kielce University of Technology, al. 1000-lecia PP 7, 25-314 Kielce, Poland

e-mail: [Ana\\_stepien@wp.pl](mailto:Ana_stepien@wp.pl); [a.stepien@tu.kielce.pl](mailto:a.stepien@tu.kielce.pl)

J. Z. Piotrowski

Faculty of Environmental, Geomatic and Energy Engineering, Kielce University of Technology, al. 1000-lecia PP 7, 25-314 Kielce, Poland

of voids in the material was estimated at approximately 50%. In addition, to better understand the internal structure of the AAC material, the following analyzes were performed: XRF, XRD and SEM with the EDS analyzer (Energy Dispersive X-ray Spectroscopy).

**Keywords** Autoclaved aerated concrete (AAC) · Thermal isolation · Micro CT · Pores · Microstructure · Autoclaved cellular concrete (ACC)

## 13.1 Introduction

The climate change, which was partly caused by extensive activities in the construction sector, is still progressing with constant intensification. That is why today, energy efficiency has become the mandatory point of interest during the design of modern, sustainable, and durable buildings. Sustainable building design practice and a usage of natural resources, combined with effective operation of mechanical systems and whole facilities, are essential for construction of so-called green, low-energy buildings—see: Birkenmajer (1967), Kozłowski (1975), Parker and Lilly (2005), Skalmowski (1966). They are also expected to reduce the occurrence of construction failures and extend overall building lifespan.<sup>1</sup>

In 2008, European Union countries introduced energy performance certificates for buildings (Directive 2002/91/EC of 16 December 2002<sup>2</sup>) for new and renovated buildings. All these steps are expected to contribute to beneficial environmental changes and optimization of manufacturing and construction processes—see: Boltyskii et al. (1995), Polyzois and Raftoyiannis Ioannis (2007), EU PN (2004). Building envelope materials, structural components, and construction methods play a very important role in this initiative. Lightweight aerated concretes can simultaneously serve as a thermal insulation and a structural support material. A building envelope should be designed to control the flow of air, heat, sunlight, radiant energy, liquid water, and water vapor. It should also provide many other attributes including fire protection, noise control, impact damage resistance, durability, aesthetic quality, and affordability—Szoke (2014).

Aerated concretes are materials that are characterized by low density, good thermal insulation characteristics and mechanical strength. They are non-flammable and are considered as natural due to their material composition. Autoclaved aerated concretes (AAC) or autoclaved cellular concretes (ACC) are made with fine aggregates, cement (or cement and/or lime), and an expansion agent that causes the fresh concrete mix to rise like a bread dough. In fact, this type of concrete may contain in its pores over 80% air. In concrete plants where AAC is made, the material is molded, expanded, and cut into blocks, panels, or beams (Figs. 13.1 and 13.3). During construction, AAC or ACC blocks or panels are usually joined together with a thin bead mortar. AAC or ACC components can be used for construction of walls, floors, and roofs. These

---

<sup>1</sup> <https://cembureau.eu/library/reports/2050-carbon-neutrality-roadmap>.

<sup>2</sup> <https://eur-lex.europa.eu/legal-content/EN/TXT/?uri=celex%3A32002L0091>.

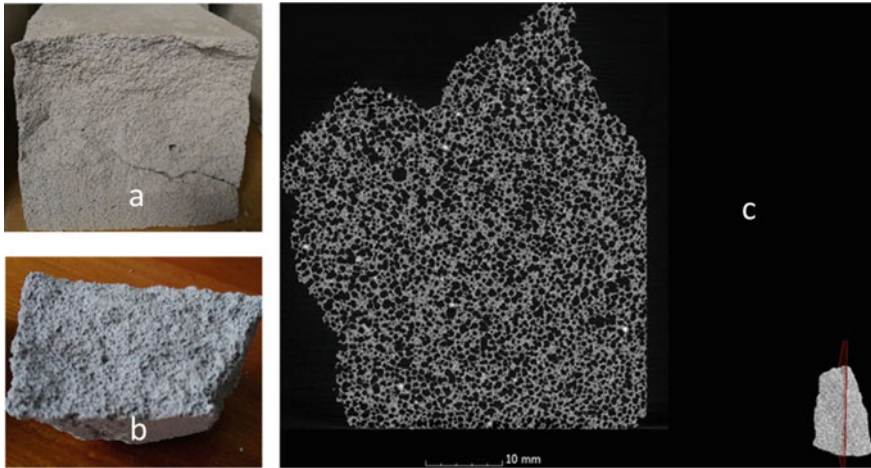


**Fig. 13.1** Autoclaved aerated concrete—**a** laboratory sample, **b** texture of AAC after the break, **c** relatively uniform micro-porous structure of AAC, visible in micro-CT analysis

lightweight construction materials offer excellent sound and thermal insulation, and like all cement-based materials, are mechanically strong and fire resistant.<sup>3</sup>

AAC is made mostly of natural materials such as quartz sand, water, lime, cement, i.e. with possible replacement of significant portions of cement by fly ash or other natural pozzolans. AACs are often considered as sustainable, or environmentally friendly. Furthermore, some researchers and AAC producers claim that manufacturing procedure requires lower energy input than the production of other construction materials or their components—Brelak and Dachowski (2017a).

The important early developments in the field of aerated concretes took place at the end of the nineteenth century. In 1880, a German researcher Michaelis was granted a patent on his concrete steam curing processes. A little bit later, Hoffman, a Czech, successfully tested and patented in 1889 the method of “aerating” concrete by carbon dioxide. Probably, the most meaningful event in history of cellular concrete, however, was the development of a method of scarifying cellular concrete using aluminum powder. This technology was patented in 1914 by two Americans, Aylsworth and Dyer. They used aluminum powder and calcium hydroxide to attain a porous cementitious mixture. This method is still used by almost all cellular concrete manufacturers, despite many years of research in this field. Following this development, in Europe, Axel Eriksson, a Swede, made several serious follow-on steps towards developing a modern AAC. In 1920, he patented the method of making an aerated mix of limestone and ground slate (a so-called “lime formula”). Next, in 1923, he invented the most advantageous way of curing cellular concrete in autoclaves using hot steam.

<sup>3</sup> <https://www.cement.org/cement-concrete/paving/buildings-structures/concrete-homes/building-systems-for-every-need/autoclaved-aerated-concrete>.

The emergence of autoclaved cellular concrete technology can be attributed to the energy crisis, which occurred in the 1930s in Sweden, when drastic restrictions were placed on the use of wood for building purposes. This was the first step towards the use of AAC, a material that combines some benefits of wood, such as good thermal insulation, natural origin of raw materials, lightness and ease of processing and construction, while being free of many wood disadvantages, i.e. AAC is resistive to decaying and it is non-flammable—see: Lothenbach et al. (2019), Błaszczyński and Król (2014). Due to its porous structure, cellular concrete is also a material with higher thermal insulation properties when compared to other types of concretes. It is also suitable for a usage as a load-bearing material, because it exhibits compressive strength in the range of 2–6 MPa.<sup>4</sup> Today, AAC masonry blocks are considered in many parts of the world as a prime construction material for residential and small commercial buildings. They are widely used in single-family homes as well as in other types of up to three-story commercial buildings, or other load-bearing structural applications. In addition, AAC, due to its ability to efficiently regulate the indoor air humidity, is widely regarded as a healthy material, showing a positive impact on the well-being of building residents. It is capable of absorbing the excess moisture from the room and return it back when the air becomes too dry. In addition, AAC exhibits a valuable resistance to bacteria, molds, and fungi. This is due to its chemical composition and resulting strong alkaline pH, which doesn't promote the growth of microorganisms.<sup>2</sup>

During the past century (mostly after WWII), the production technology of AAC products has been constantly improved. Today, specially designed, autoclave facilities are used worldwide to produce AAC building products. With small custom differences, AAC production procedures are similar in most production facilities worldwide. At the beginning of the production process, the lime is pre-homogenized with complete internal reaction for a period of time after ground.????? According to the example given by Li et al. (2020), the aluminum paste is dissolved in water at room temperature. It is later added to other components to create a concrete slurry, which is made at temperature of ~40 °C. During the next processing step, the slurry is cast into a mold preheated to a temperature of around 50 °C, where it later stays for about 30 min at a temperature of 64 °C, to complete the process of foaming, thickening, and hardening. After demolding, the blocks are placed into the autoclave for steam-curing for about three hours at pressure of 1.0 MPa and the temperature of 185 °C—Li et al. (2020).

Due to the growing awareness of environment problems, and the global sand supply deficit, many traditionally used AAC raw materials are being replaced now by various industrial by-products, and waste products (including waste concrete). That is why today, AAC products may embrace a waste containing mainly silicon and calcium, as well as other industrial by-products such as: fly ash, silica dust, bottom ash, waste from iron ore processing, copper waste, and slag blast furnace. It has been well researched and documented that a partial replacement of cement by the fly ash and/or other natural pozzolans significantly lowering the Global Warming Potential

---

<sup>4</sup> <https://www.solbet.pl/en/technical-parameters>.

(GWP) of concrete products—Wcislo (2018). Crushed waste concrete aggregates (fine) and concrete powder are sometimes used as a replacement of natural sand and fine aggregates in AAC.<sup>3</sup> In addition, studies show also that the use of rice husk ash can be utilized as a partial replacement for fine aggregate reduces the strength and density of AAC with a tendency to shorten the autoclaving time and the required autoclaving temperature.<sup>5</sup> Efforts have been made to improve the mechanical properties, especially fracture toughness, and increase the thermal insulation performance of AAC by using wood fiber and rubber powder—Szoke (2014). It was shown that the thermal conductivity of AAC with this modification increased linearly and was dependent on the basalt fiber content (the greater the amount of basalt fiber, the higher the strength parameters for the tested material). The strength parameters of AAC are closely related to its internal porous structure. Therefore, regardless of the substrates and modifiers used, AAC products are usually good thermal insulators, which exhibit sufficient strength (for non-load-bearing structures) and durability.

According to the American Concrete Institute (ACI)—ACI-122R-14 “Guide to Thermal Properties of Concrete and Masonry Systems” (Szoke (2014)) thermal conductivity of the AAC blocks ranges between 0.1 and 0.7 W/(m·K) for a density of 400–1700 kg/m<sup>3</sup>. The impact of moisture on the steady-state and dynamic thermal performance of AAC walls in residential and commercial buildings located in California, U.S. were analyzed by Gawin and Kośny (2000), Gawin et al. (2004). Thermal conductivities of five types of AAC and several lightweight walls, were measured in laboratory conditions, at various moisture contents. Then, the moisture distribution in AAC walls was simulated for California climate using the coupled heat and moisture transfer numerical model. Hygrothermal simulations were followed with whole building energy modeling for a single-story residential home. The whole building energy simulation results indicated a superior performance of AAC walls, compared to other types of lightweight systems of identical thermal resistance.

The following North American building standards regulate material characteristics and assembly methods for AAC masonry products:

- ASTM C1691-11 (2017) Standard Specification for Unreinforced Autoclaved Aerated Concrete (AAC) Masonry Units.<sup>6</sup>
- ASTM C1693-11 (2017) Standard Specification for Autoclaved Aerated Concrete (AAC).<sup>7</sup>

In Europe, the product standards for masonry units—including those for AAC units—have been under new regulation since April 1, 2006. Following the end of the coexistence period for the national and European standards, the harmonized European product standard DIN EN 771-4 was implemented. On November 1, 2015, Part 4 in the specification for masonry units was introduced: Autoclaved aerated

---

<sup>5</sup> <https://www.irjet.net/archives/V7/i2/IRJET-V7I2279.pdf>.

<sup>6</sup> <https://www.astm.org/Standards/C1691.htm>.

<sup>7</sup> <https://www.astm.org/Standards/C1693.htm>.



concrete masonry units (includes Amendment A1:2015). This standard specifies the characteristics and performance requirements of AAC masonry units.<sup>8</sup>

Similarly, in China, the thermal conductivity of AAC blocks used in civil construction ranges from 0.13 to 0.22 W/(m·K) for concrete density in the range 400–700 kg/m<sup>3</sup>. The national standard GB/T 11,969-2008, “Test Methods of Autoclaved Aerated Concrete” describes test methods for AAC masonry products.<sup>9</sup> According to Chinese building standards, the thickness of external walls built of AAC blocks should be no less than 400 mm and 300 mm, for residential buildings in a very cold climatic zone and a cold zone, respectively<sup>3</sup>—Li et al. (2020).

### 13.2 Fabrication of Autoclaved Aerated Concrete (AAC) and Description of the Autoclaving Process

There are two groups of concrete products manufactured by autoclaving: autoclaved aerated concrete (AAC) and lime-sand products commonly known as silicate bricks. In both cases, sand and water are basic raw materials used in their production. For aerated concrete, cement is also added. There is also a second category of lightweight cellular materials produced industrially. This second variant of lightweight cellular concrete is a foamed concrete, which is usually produced in field conditions. This technology, however, has not yet been used on a wide scale—Dachowski and Kapała (2016).

Aerated concretes are materials that are characterized by low density, good thermal insulation, flame resistance, and unique mechanical strength parameters. Masonry blocks that are made of ACC are usually about one-third of weight of similar products made from regular concrete. In addition, AAC products are flame resistance and do not contain any toxic gases or other toxic substances. They offer many advantages over traditional wood construction, while being free of many wood disadvantages. For example, AAC is dimensionally stable with no deflections or warping caused by changing moisture conditions. This improves the overall product durability—see: Lothenbach et al. (2019), Błaszczński and Król (2014). AAC panels and blocks are produced in factories to exact specified sizes. There is almost no need for on-site trimming since blocks and panels fit so well together, there is also little need for use of finish materials such as mortar. If needed, AAC products can be easily cut with hand tools on the construction site. Finally, because of low thermal conductivity, 24–36 cm thick walls, made of AAC blocks, can easily fulfill, building code requirements in many severe climates worldwide, without a need for additional sheathing thermal insulation—see: Lothenbach et al. (2019), Błaszczński and Król (2013), Zapotoczna-Sytek (2018). The major disadvantages of cellular concrete blocks include: high water absorption, and relatively low compressive strength, compared to other concrete products (up to 6 MPa on average). From the structural

---

<sup>8</sup> <https://standards.globalspec.com/std/9975426/DIN%20EN%20771-4>.

<sup>9</sup> <https://www.doc88.com/p-3854253232623.html>.

perspective, AAC is a material of mechanical strength allowing the construction of load-bearing structural walls in buildings for up to 3–4 floors (depends on the local country building standard regulations, specific for different product types). There is also a group of reinforced AAC technologies, allowing fabrication of a variety of structural building elements such as ceiling beams, columns, headers, and roof rafters.

The small-scale production of AAC masonry products started in Sweden in the 1930s. However, the real beginning of a widespread cellular concrete production on the industrial scale in Europe dates back to the 1940s and continued until the 1970s. Later, during the 1980s, numerous AAC plants built in Asia, the Middle East and Eastern Europe were based on four major technologies developed in Europe by Siporex and Ytong (Sweden), Durox (Netherlands), and Hebel (Germany). In the beginning of the 1990s, the first AAC production plant based on the Ytong technology was supplied to China. In Poland, this development is associated with a patented production method referred to as “the universal Polish method” called Unipol.<sup>10</sup> In spite of the fact that the AAC fabrication technology is similar worldwide (with several proprietary variations), depending on the manufacturer and the intended use, cellular concrete masonry and panel products are made in slightly different ways. In these processes, Portland cement, burnt lime, and some aggregates are used to prepare a binder, all together ground dry. When the fly ash (most often sourced from coal combustion) is utilized as the cement substitute, gypsum dihydrate (gypsum rock) is added as a dry additive. Quartz sand and/or fly ash are often used as aggregates. Water is the third, main component of the cellular concrete mix. It is added in the amount of 0.9 l/m<sup>3</sup> of semi-liquid concrete mix. A skimmed, flakey aluminum powder or aluminum paste is used for the foaming step (aeration). During the AAC production, gypsum can be also added to act as a setting regulator<sup>9</sup>—Zapotoczna-Sytek (2018).

Today, AAC manufacturing is carried out according to strictly followed material recipes and operation processes. The most important preparatory tasks include: (i) preparation of raw materials (this often includes drying, grinding, or heating materials, or mixing with water), (ii) dosing the ingredients in accordance with the specific company recipes, and (iii) mixing the whole batch. Examples of typical concrete formulations, used by major European AAC companies are presented in Table 13.1—Brelak and Dachowski (2017a).

Following the material mixing, the aerating agent reacts with the calcium hydroxide and causes the release of hydrogen, which escapes from the mix, causing it to rise, and creating thousands of small cells with air trapped in them. Today, cellular concretes of various bulk densities are produced following proprietary company-specific formulations and fabrication methods. The target AAC porosity is between 60 and 85%. That is why, the solids surrounding the pores shouldn't account for more than 40% of the total volume of used materials. At the end of this part of production, (v) an additional waiting period is needed for the concrete mix to harden, and later (vi) for slicing the hardened mass into pieces of appropriate dimensions. The surplus

---

<sup>10</sup> <http://www.eastlandchina.com/60-years-of-aerated-concrete-in-Poland-The-Past-and-the-future-id37144.html>.

**Table 13.1** Typical concrete mix formulations used by European AAC companies

Company	Basic substrates		Method of preparing ingredients
	Binder	Aggregates	
YTONG	Quicklime + cement (or blast furnace slag)	Quartz sand and, bottom ash	Dry milling of binder and aggregate or milling of aggregate with water and lime
SIPOREX	Cement	Sand or sand with blast furnace slag	Grinding sand and slag with water into sludge
HEBEL	Cement + quicklime	Quartz sand	Grinding sand with water into sand sludge
Calsilox	Cement + quicklime	Quartz sand	Common dry milling of binder and aggregates

Source Brelak and Dachowski (2017a)

concrete mix left over after the processing is returned to the component mixer, so the production is almost waste-free and consequently doesn't impact the environment through waste generation. The next production stage involves (vii) bringing the pallets with the hardened products to the autoclave, where the concrete is finally set. For this purpose, saturated autoclavation is associated with a process of curing the concrete mix in hermetically sealed autoclaves which are auxiliary heated for up to 12 h. Thanks to autoclaving, the chemical shrinkage of material is minimized. This improves the AAC frost resistance, increases durability and mechanical strength. At the final stage, hardened AAC products are subjected to a quality check and then stored in controlled environmental conditions—see: Stepień et al. (2019), Wcisło (2018), Lothenbach et al. (2019).

In autoclaves, under conditions referred to as hydrothermal, chemical reactions take place that guarantee the strength and quality of resulting products. As mentioned earlier, the combination of cement, lime, gypsum (anhydrite), finely ground sand and most importantly aluminum powder or paste causes the whole mix to considerably expand. During this process, the following three-step chemical reaction takes place (in simplified form):

1.  $\text{CaO} + \text{H}_2\text{O} \rightarrow \text{Ca(OH)}_2 + 65,2 \text{ kJ/mol}$
2.  $3\text{Ca(OH)}_2 + 2\text{Al} + 6\text{H}_2\text{O} \rightarrow \text{Ca}_3(\text{Al(OH)}_6)_2 + 3\text{H}_2$
3.  $6\text{SiO}_2 + 5\text{Ca(OH)}_2 \rightarrow 5\text{CaO} \cdot 6\text{SiO}_2 \cdot 5\text{H}_2\text{O}$ .

The final product of this process is Tobermorite or Hydrated Calcium Silicate  $\text{C}_5\text{Si}_6\text{H}_5$ —see: Van Boggelen (2014).

During AAC production the temperature in autoclaves depends on the pressure used. The increase of the autoclave pressure allows a usage of higher processing temperatures—Lothenbach et al. (2019).

As a part of ecological construction trends in cement and concrete industries, a new material solution, utilizing a geopolymeric cement binder has been introduced.<sup>11</sup> This alkaline-activated binder is not based on calcium carbonate chemistry—see: Matschei et al. (2007). It generates significantly lower CO<sub>2</sub> emissions and exhibits better strength than classic clinker-based cement. The procedure for production of geopolymer-based light-weight material similar to AAC blocks was recently developed—Kejkar Rupali and Wanjari Swapnil (2021). In this case, chemically aerated geopolymer material, resembling a foamed concrete was developed at a high alkaline solution concentration.

When compared to the conventional AAC manufacturing, this novel processing involves higher temperature, sometimes requires increased duration of the heat curing process, and higher pressure, which pose challenges for commercialization. In a recent study that focused on manufacturing of geopolymer-based aerated concrete, granulated blast furnace slag was utilized as an alternate to cement content (with 10–30% load). This new geopolymer-based foamed material is heat cured at 100 °C for a three-hour time period. The final product demonstrated 4.8 MPa compressive strength and contained 60% of fly ash, 30% of granulated blast furnace slag, and only 10% of Portland cement—Kejkar Rupali and Wanjari Swapnil (2021).

## 13.3 Basic Technical Characteristics of AAC

### 13.3.1 Density and Compressive Strength

Cellular concretes (Fig. 13.1a, b), depends on their average dry bulk density, are usually divided into the following concrete classes: 400, 500, 600 and 700 (Table 13.2). For these varieties, the lower and upper limits of volumetric density and corresponding product labels, i.e., the average values of compressive strength in the dry state, have been determined by AAC manufacturers. A comparison of the bulk density of cellular concrete with regular concrete products shows that it is 1/3–1/2 the density of regular concretes and has significantly lower thermal conductivity than regular concrete.

Autoclaved cellular concrete can therefore be used to manufacture large, light-weight products which can be combined with conventional masonry or other building envelope materials. The compressive strength of cellular concrete depends on its bulk density, and it is between 2 and 6 MPa (as discussed in Stepien et al. (2019), Nonat and Lecoq (1998)), while tensile strength represents 20–40% of compressive strength, similarly, shear strength is 20–30% of compressive strength. The modulus of elasticity is in the range 1.5 and 2.6 MPa. The water content of a specimen during testing and the direction of crushing in relation to the direction of the concrete growth in the mold are also important. In European standards, the compressive strength is

---

<sup>11</sup> <https://www.nbmcw.com/product-technology/construction-chemicals-waterproofing/concrete-admixtures/geopolymer-concrete-the-eco-friendly-alternate-to-concrete.html>.

**Table 13.2** Approximate amounts of components in the production of AAC by the Unipol method, for 500, 600 and 700 concrete classes (density classification)

Composition of the mixture	Unit	Sand technology			Ash technology		
		260	600	700	500	600	700
Sand	dcm <sup>3</sup>	260	350	440	–	–	–
Fly ash	kg	–	–	–	270	360	450
Binder	kg	240	260	280	230	240	255
Water	dcm <sup>3</sup>	80	75	62	250	300	350
Aluminum powder	kg	0.47	0.41	–	0.44	0,35	0.30
Surface active agent	dcm <sup>3</sup>	1.5	1.5	1.5	1.5	1.0	1.0

Source Lothenbach et al. (2019), Błaszczyński and Król (2014), Zapotoczna-Sytek (2018)

determined at a stabilized water content of approx. 6 wt.%. This is 80% of the compressive strength in the dry state, determined according to PN-89/B-06258,<sup>12</sup> EN 771-4,<sup>13</sup> and EN 772-16.<sup>14</sup>

### 13.3.2 Thermal Conductivity

The thermal conductivity of cellular concretes depends on their density and the water content. Several companies are currently able to produce AAC products with densities in the range 300–800 kg/m<sup>3</sup>, with lambda values as low as 0,08 W/(m·K)—Pruteanu and Vasilache (2013). Additionally, the required compliance with the strict EU standards (EN 771-4 and EN 772-16) results in high-precision products (tolerances of <1 mm for blocks and <3 mm for panels). This allows utilization of AAC products, which is associated with the on-site use of a thin bed mortar instead of a thick layer of conventional mortars. This reduces thermal bridging (improving thermal performance) and decreases the total cost of construction. Furthermore, the production of ultra-lightweight AAC blocks with thermal conductivity as low as 0,045 W/(m·K), at density of 145 kg/m<sup>3</sup>, has already become possible for some AAC producers—Van Boggelen (2014).

<sup>12</sup> <https://www.iso.org/standard/66185.html>.

<sup>13</sup> [https://infostore.saiglobal.com/en-us/Standards/EN-771-4-2011-A1-2015-331270\\_SAIG\\_CEN\\_CEN\\_761852/](https://infostore.saiglobal.com/en-us/Standards/EN-771-4-2011-A1-2015-331270_SAIG_CEN_CEN_761852/).

<sup>14</sup> <https://www.en-standard.eu/bs-en-772-16-2011-methods-of-test-for-masonry-units-determination-of-dimensions/>.

### 13.3.3 Frost Resistance

The water absorption of cellular concrete is between 40 and 60 vol.%, i.e. approx. 25% lower than would result from its total porosity. This means that the cells do not fill up completely when water is absorbed. This fact has a positive effect on frost resistance. The freezing water in the cell increases volume by about 10%. However, due to available extra cell volume, this does not exert pressure on the cell walls and thus does not induce undesirable stresses on the concrete structure.

### 13.3.4 Fire Resistance

Fire resistance is one of the most important building code requirements for construction products. The fire resistance is the ability of a structure element to withstand the action of fire under certain mechanical effects on one or more surfaces for a specified period of time without losing its load-bearing properties (PN-EN 13,501-2). Construction products manufactured and sold in the territory of the European Union are classified according to the PN-EN 13,501-1 standard, which provides for seven basic classes: A1, A2, B, C, D, E, F<sup>15</sup>—Macech (2020). Masonry walls made of cellular concrete blocks in the thickness range of 180–360 mm meet the requirements for the highest class of fire resistance of buildings as they withstand a 240 min fire test<sup>15, 16</sup>—see: Dachowski and Kapała (2016), Kapała and Dachowski (2016), Brellak and Dachowski (2017a), Macech (2020).

### 13.3.5 Natural Radioactivity

Building occupants are continuously exposed to radiation emitted by building materials. Construction materials produced from natural mineral sources such as rocks and/or soil, usually contain small amounts of natural radionuclides of the uranium (<sup>238</sup>U), thorium (<sup>232</sup>Th) series, and potassium (<sup>40</sup>K). These radionuclides can cause external and internal radiation exposure to occupants. While, the external exposure is usually caused by direct gamma radiation, the internal radiation exposure, often affecting the respiratory tracts, is due to radon and radon decay products, which radiate off from building materials. Good knowledge of the basic radiological characteristics such as radioactive content in building materials is important in the assessment of possible radiation exposure to the population. It is also essential for the development of building standards and material usage guidelines. In Poland,

---

<sup>15</sup> <https://www.en-standard.eu/bs-en-13501-1-2018-fire-classification-of-construction-products-and-building-elements-classification-using-data-from-reaction-to-fire-tests/>.

<sup>16</sup> <https://www.itb.pl/badania-ogniowe.html>.

**Table 13.3** The content of natural radioactive isotopes—Kapała and Dachowski (2016)

Building/construction material	$f_1 < 1.2^*$	$f_2 < 240 \text{ Bg/kg}^{**}$ (radioactive activity <sup>***</sup> )
Sand-lime brick	0.16	20
Aerated Autoclaved Concrete made with sand	0.16	20
Concrete	0.22	24
Expanded clay aggregate	0.36	32
Ceramic brick	0.54	70
Breezeblock (slag/cinder) block	0.56	80
Cellular ash concrete	0.60	90

\* Dimensionless coefficient  $f_1$  is expressing the content of natural isotopes of  $^{40}\text{K}$ ,  $^{226}\text{Ra}$ ,  $^{228}\text{Th}$

\*\* Content of  $^{226}\text{Ra}$  expressed in Bq/kg

\*\*\* Radioactive activity is a physical quantity equal to the rate of radioactive decay of atomic nuclei of a given sample, expressed in becquerel, Bq:  $1 \text{ Bq} = 1 \text{ decay/1 s}$ . [see: Piotr Jaracz: Promieniowanie jonizujące w środowisku człowieka. Fizyka, skutki radiologiczne, społeczeństwo. Ionizing radiation in the human environment. Physics, Radiological Effects, Society. Warsaw, Poland: Wydawnictwa Uniwersytetu Warszawskiego, 2001. ISBN 83-235-0146-7]

a systematic study of natural radioactivity of building products, including cellular concrete, has been carried out since 1980 (see: Table 13.3).

### 13.4 Enhancement of Mechanical Strength Characteristics of AAC by Use of High Impact Polystyrene (HIPS-High Impact Polystyrene)

When compared to regular density concretes, aerated concrete is characterized by relatively low compressive strength, typically ranging from 2 to 6 MPa. One of the methods of improving the compressive strength is the modification of aerated concrete with high-impact polystyrene (HIPS). HIPS is a thermoplastic polymer obtained by the block-suspension polymerization of styrene with an addition of synthetic rubber. As a result of polymerization, small particles of polybutadiene remain in the polystyrene matrix, changing its physical and mechanical properties<sup>17</sup>—see: Abdulrahman and Bruce (2004), Vilaplana et al. (2010), Alfarraj and Nauman (2004). HIPS thus achieves better temperature stability and plastic stiffness, which helps improve performance of building materials (e.g. concrete) modified by the addition of HIPS. Cellular concretes are not resistant to mechanical damage. That is why HIPS is used in AAC to increase the hardness of the material while maintaining its thermal performance. A recent study showed that the modification of AAC

<sup>17</sup> <http://www.plastics.pl/produkty/tworzywa-techniczne/polistyren-ps/polistyren-wysoko-udarowy-hips>.

**Table 13.4** Tests which were performed on AAC specimens enhanced with HIPS

Research	Characteristics of the study
Calorimetry	Measurement of heat generated by chemical reactions and various physical processes
Porosimetry	Pore size and distribution analysis using Mercury Porosimeter SYL & ANT Instruments, Micrometrics (AutoPore IV)
SEM—scanning electron microscope	Microscopic analysis to visualize the microstructure of the modified material. Microstructural characterization and elemental analysis of the samples were performed using Scanning Electron Microscopes (Quanta FEG 250 FEI)
X-ray diffraction (XRD)	XRD is a non-destructive test method used to analyze the structure of crystalline materials. XRD measurements of powdered samples were conducted with Empyrean PANalytical diffractometer using Ka radiation from a Cu anode
X-ray fluorescence	Elemental composition testing using the PANalytical instrument (XRF)
Micro CT analysis	Industrial computed tomography—non-surface analysis and visualization studies providing insight into the inside of the material (microscope Nikon XT H 225 ST—see: Fig. 13.1c)

with HIPS increased the compressive strength of the material by 27% and decreased the water absorption factor by 28% in comparison to a conventional product—see: Nonat and Lecoq (1998), Stepien et al. (2020). The material used in the tests was a re-granulate, pulverized to 630  $\mu\text{m}$  particle size, with a density of 1.05  $\text{g}/\text{cm}^3$ . A series of tests was performed on HIPS-modified AAC cube specimens (100 mm edge length), made under semi-industrial conditions in the aerated concrete manufacturing plant following a slow-setting silicate technology (SW) as a 500 concrete variant (gross dry density class).<sup>18</sup> The SW technology involves producing a slurry from adequately proportioned components (sand and gypsum jointly account for about 72% of the product mass, cement, and lime—about 20% and water—about 7%). At this stage, appropriate quantities of the HIPS were added. After mixing, the slurry was placed in tripart molds and stored in curing chambers at 60 °C for three hours. After that, the specimens were placed in autoclaves for 13 h at a temperature of 190 °C and a steam pressure of 1.2 MPa—see: Zapotoczna-Sytek and Balkovic (2013), Abdulrahman and Bruce (2004), Rybarczyk et al. (2015). Figure 13.3 shows samples of analyzed AAC material. Table 13.4 lists the tests which were performed to analyze the structure and properties of the AAC enhanced with HIPS:

<sup>18</sup> <https://www.solbet.pl/zalety-betonu-komorkowego/gestosc-betonu-komorkowego/>.



**Table 13.5** XRF analysis of AAC with HIPS

Formula	Concentration (%)
CaO	50.377
SiO <sub>2</sub>	39.280
Fe <sub>2</sub> O <sub>3</sub>	3.534
SO <sub>3</sub>	2.859
Al <sub>2</sub> O <sub>3</sub>	1.908
MgO	0.313
K <sub>2</sub> O	0.813
SrO	0.111
TiO <sub>2</sub>	0.527
P <sub>2</sub> O <sub>5</sub>	0.113
MnO	0.064
ZrO <sub>2</sub>	0.052
ZnO	0.049

The above tests were performed based on the CEN standards: PN-89/B-32250,<sup>19</sup> PN-EN 1008:2004<sup>20</sup> and based on the available construction regulations.

As presented in Table 13.5, the XRD analysis of elemental composition showed the main components of AAC are: SiO<sub>2</sub>, CaO, Fe<sub>2</sub>O<sub>3</sub>, Al<sub>2</sub>O<sub>3</sub>, SO<sub>3</sub>, MgO, K<sub>2</sub>O. The distribution and arrangement of pores that are present in the specimen of AAC that was tested using optical microscope, as well as XRD and micro-CT analyses.

AAC is a material that undergoes binder hydration. The next test that was performed was calorimetry.<sup>21</sup> The hydration process takes place immediately after the binder (cement, lime) is combined with water in the presence of other components of the raw mass (quartz sand, additives). However, hydration can also occur over time under certain hydrothermal conditions.

The thermal effect of many transformations is difficult to measure because it may be accompanied by other side processes, which themselves absorb or produce thermal energy—Van Boggelen (2014). A process of forming/setting of the AAC's internal microstructure is very dynamic and it is extremely important to understand the thermodynamic behavior of its components and phases that are formed. In ACC, hydrated calcium silicates are present, which are stable in certain temperature ranges and the stability of these products also depend on this factor (Calcium-Silicate-Hydrate phase or Tobermorite, although it is not always desirable in concretes, including ACC). Isothermal titration calorimetry (ITC) is a technique used to quantitatively study interactions between molecules. It directly measures the heat that is released or

<sup>19</sup> <https://sklep.pkn.pl/pn-b-32250-1988p.html>.

<sup>20</sup> <https://sklep.pkn.pl/pn-en-1008-2004p.html>.

<sup>21</sup> <https://apinstruments.pl/izotermiczna-kalorymetria-miareczkowa-itc/>.

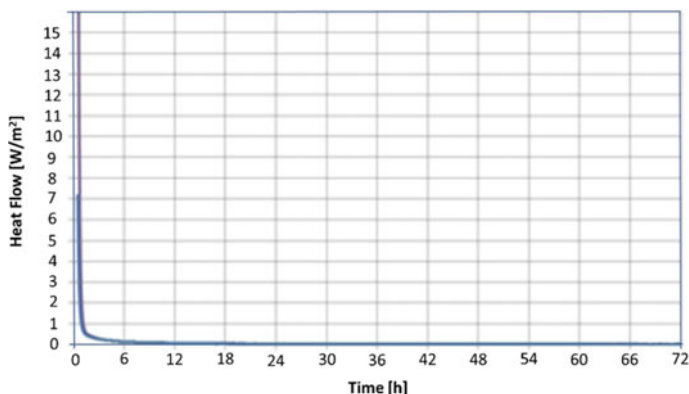


**Fig. 13.2** Heat flow recorded during the hydration process in AAC samples containing HIPS—measured using isothermal titration calorimetry (ITC)

absorbed during bond formation. ITC is the only method that simultaneously determines all binding parameters in a single experiment and does not require any modification of the reactants involved in the binding. Measurement of heat flow during binding enables accurate determination of the binding constant (KD), reaction stoichiometry (n), enthalpy change ( $\Delta H$ ) and entropy change ( $\Delta S$ ), which contributes to a complete thermodynamic profile of the interaction between molecules—see: Rybarczyk et al. (2015). The test data presented in Fig. 13.2 indicates that hydration occurred only during the first phase of the ACC setting process and any subsequent changes were not observed.

### 13.4.1 Mechanical Strength Properties and Porosity of ACC Modified with HIPS

In earlier studies, strength and water absorption measurements were used for conventional AAC and similar cellular concrete modified with HIPS (AAC with HIPS). Basic properties of both analyzed materials are presented in Table 13.6. The high-impact plastic used for AAC enhancement is a waste product that, as a result of this modification, positively improved the physical and mechanical properties of

**Table 13.6** Compression strength and water absorption for analyzed aerated concrete products

Materials (AAC)	Average compressive strength (MPa)	Average water absorption coefficient ( $\text{g/m}^2 * \text{s}^{0.5}$ )
AAC	3,35	105
AAC with HIPS	4,70	66

Source Dachowski and Kapała (2016)

the tested product. As shown in Table 13.6, the addition of HIPS to AAC yielded about a 40% increase in compressive strength and decreased the coefficient of water absorption of about 37% when comparing to conventional AAC without HIPS—see: Dachowski and Kapała (2016).

As shown in Fig. 13.3a, density tests were performed using the Quantachrome Ultracyc 1200e helium pycnometer. Irregularly shaped concrete specimens of 10–25 g were used for this purpose. For the porosimeter tests, the specimens were sequentially placed in the low-pressure port, where they were evacuated to 2.66 Pa and flooded with mercury at 0.035 MPa.—see: Fig. 13.3b.

Figures 13.4, 13.5, 13.6, 13.7 and 13.8, show the distribution and size of pores in the specimens R1, R2, R3, and R4. R1 is the reference AAC material while R2, R3, R4 is a modified HIPS material in the amount of 10, 20, 30%. In AAC production, it is not recommended to use a larger amount of the additive due to the possibility of cracking of the starting material (HIPS, like some mortars, may show high strength, which may result in cracking during operation). The tests showed that the specimens with HIPS addition showed a larger pore volume in the range (0.001–100), while the pore distribution was similar as in the reference material.

When analyzing the porosimetry results, it is important to remember that mercury is forced into pores of  $\sim 0.01 \mu\text{m}$  in diameter and smaller at very high pressures—over 100 MPa. Therefore, if the pores are connected by narrow passages and the specimen material cannot withstand this loading, the pores are sometimes crushed before mercury can penetrate. However, the possibility of injecting mercury into the bottle-neck pores without particularly destroying the material structure must not be overlooked. Otherwise, the theoretical calculation results may reflect the actual porosity values. Simply, the pore size distribution calculated from the MIP data will be inaccurate. In the case of large pores, with diameters around one  $\mu\text{m}$ , mercury is injected into them at a pressure of one MPa. A maximum pressure of 420 MPa

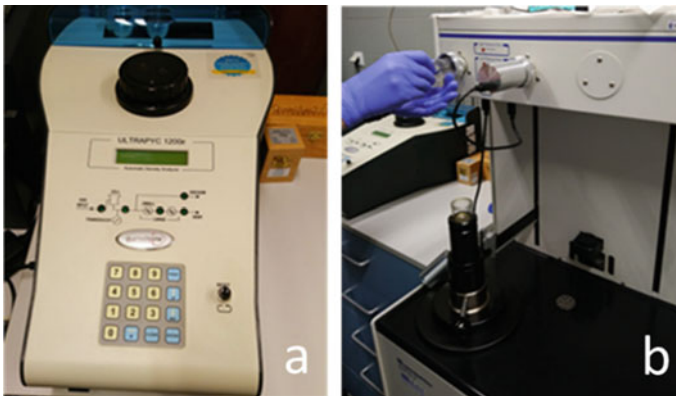


**Fig. 13.3** Analysis of AAC pore sizes performed with a use of **a** helium pycnometer (QUANTACHROME ULTRAPYC 1200e) and **b** mercury porosimeter SYL & ANT instruments

is needed to force the mercury into pores with diameters of  $0.006 \mu\text{m}$ . High pressures can destroy the internal skeleton and open access to pores that were completely isolated under natural conditions. If the assumption is made that the critical destructive pressure is close to the tensile strength of the material, when mercury is injected into pores with radius dimensions of  $\leq 0.02 \mu\text{m}$ , an intense damage process that changes the picture of the actual pore distribution will begin.

The present discussion of the results of mercury porosimetry measurements is usually interpreted in terms of long cylindrical capillary bundles. Tests (density and porosimetry—Figs. 13.4, 13.5 and 13.6) were performed on 4 independent samples of ACC with HIPS. The sample R1 was used for the pore size analysis (Figs. 13.7 and 13.8). The plots of the cumulative pore volume against its radius were developed using the results from four tests performed on specimens R1, R2, R3, R4, (Figs. 13.5 and 13.6). It can be observed on Fig. 13.7. that the pore size of  $10\text{--}50 \mu\text{m}$  has the largest volume in the sample, followed by  $0.0025\text{--}0.004$  and  $0.01\text{--}0.04 \mu\text{m}$ .

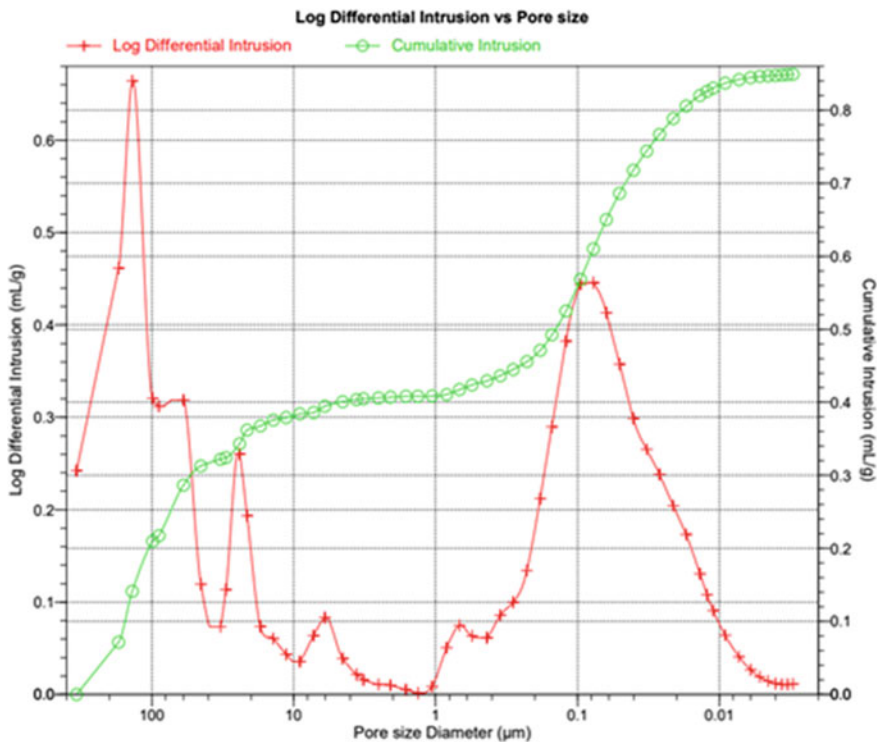


Fig. 13.4 Pore size distribution (reference AAC sample R1)

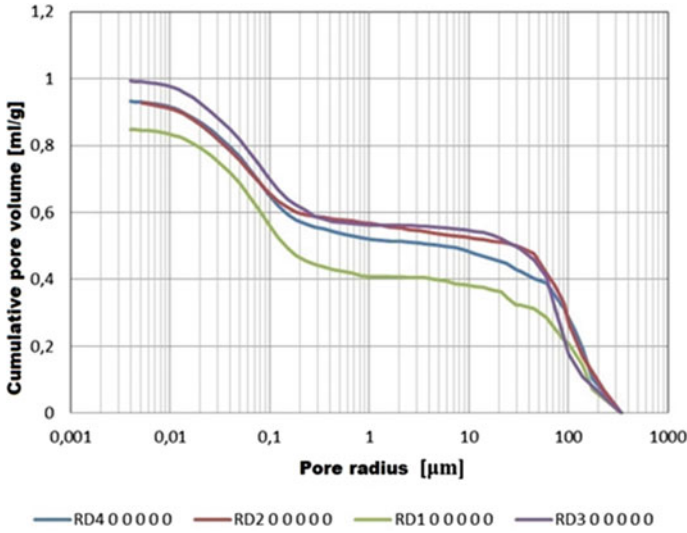


Fig. 13.5 AAC with added high-impact polystyrene (HIPS), distribution of pore geometry in relation to pore sizes

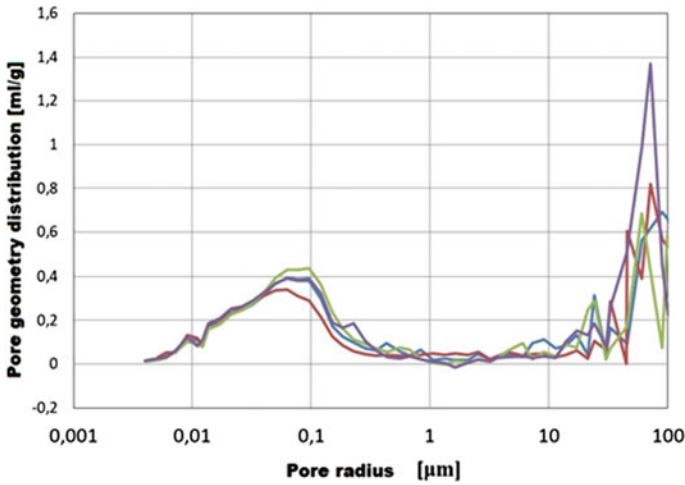


Fig. 13.6 Pore size distribution in AAC with added HIPS

### 13.4.2 Micro-structure Analysis of AAC Samples

The phase compositions and structure for AAC without and with HIPS was examined utilizing X-ray diffraction (XRD) and Scanning Electron Microscope (SEM) analyses. The area of the specimen was swept by electron probe under voltage of

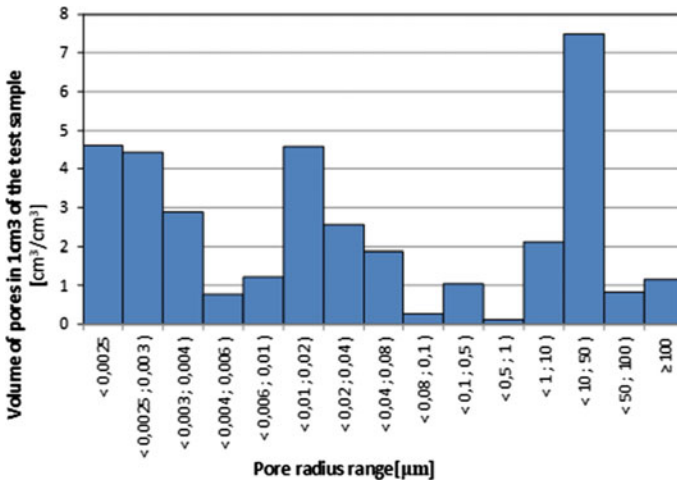


Fig. 13.7 Volume of pores in one m<sup>3</sup> of the test sample as a function of pore sizes

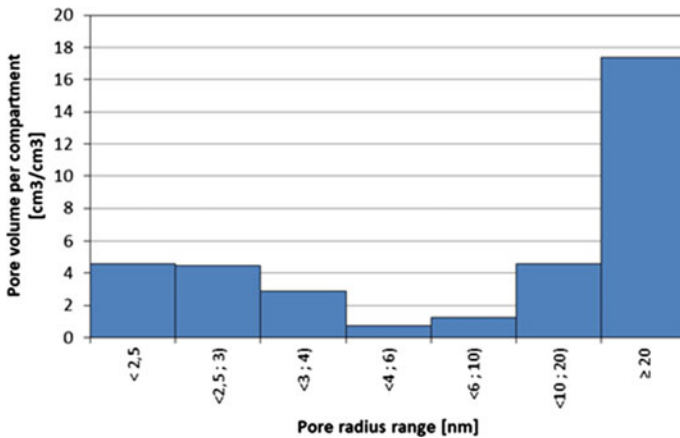
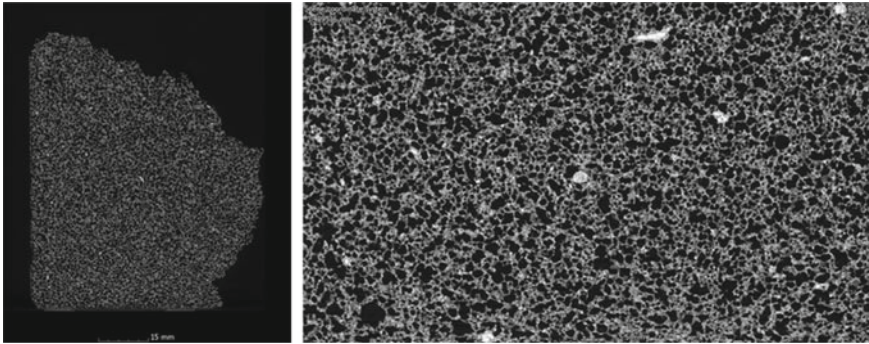


Fig. 13.8 Pore volume in AAC with HIPS in a given compartment as a function of pore radius

5–50 keV. The analysis of the distribution, number, and size of pores is important because this information allows the determination of the relationship between other physico-mechanical and structural values, as well as the durability of the material. Micro CT analysis was performed with the use of the Nikon XT H 225 ST CT scanner, which enabled measurements of external and internal geometry of AAC without and with HIPS (as presented in Fig. 13.9).

Results from measurements of the air void content for four aerated concrete specimens (R1, R2, R3, R4) versus density of the materials analyzed (Table 13.7).

Table 13.7 shows that the addition of HIPS did not significantly affect the number of voids in the modified material, so it certainly did not deteriorate its properties.



**Fig. 13.9** Measurements of pore geometry in the aerated concrete specimens using CT scan technique (computer tomograph)—analysis of distribution, volume, and size of pores in tested material

**Table 13.7** Summary of density and air void content in AAC with HIPS

Sample	Bulk density (kg/dm <sup>3</sup> )	Air void content (%)
R1	2.3589	52.53
R2	1.9222	47.33
R3	2.3241	55.06
R4	2.2654	55.16
Average value	2.21	52.52

Hydrated calcium silicates (including C-S-H, Tobermorite) are formed in the pores, i.e. phases whose quantity and quality also testify to the effectiveness and durability of the material. These tests showed the presence of pores with sizes of 0.1–100  $\mu\text{m}$ , and the volume of voids in the material was estimated at approximately 50% (RD1 52.53%; RD2 47.33%; RD3 55.06%; RD4 55.16%).

The phase compositions and structure for AAC without and with HIPS was examined utilizing X-ray diffraction (XRD) and Scanning Electron Microscope (SEM) analyses—see Fig. 13.10. The area of the specimen was swept by electron probe under a voltage of 5–50 keV. The analysis of the distribution, number and size of pores is important because this information allows to determine the relationship between other physico-mechanical and structural values, as well as the durability of the material.

The information on the C-S-H phase is particularly important due to the fact that there is an amorphous phase that is formed at the aggregate-binder interface and a metastable phase that strongly reacts to environmental changes (pressure, temperature, or even CO<sub>2</sub> concentration in the atmosphere), which is depends on the concrete pH. Any variations in pH (as a result of external or internal factors) are automatically reflected by the pore count, their sizes, which yields subsequent changes in the structural/physical characteristics of the material.

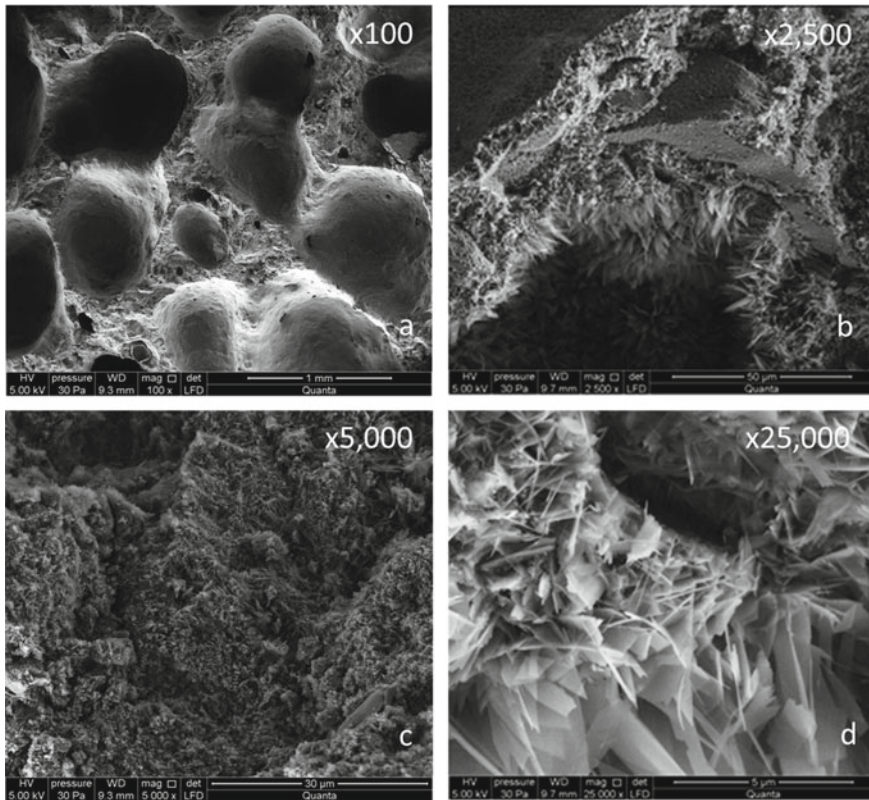


**Fig. 13.10** SEM images of the microstructure of ACC with added HIPS: **a** visible pores—100 × magnification, **b** 2,500 × magnification, **c** 5,000 × magnification, and **d** visible Tobermorite—25,000 × magnification

The C-S-H phase has a positive effect on the ACC strength. The following four morphological types of the C-S-H phase exist: (i) fibrous particles of C-S-H, (ii) honeycombs of C-S-H, (iii) flattened/isometric particles of C-S-H, and (iv) spherical agglomerates of C-S-H. Tobermorite has three phases varying by interlayer distances of 1.4; 1.13; and 0.97 nm. (Al + Na)-substituted Tobermorite structure contain well-developed hexagonal plates that may occur in spherical agglomerations—see: Brelak and Dachowski (2017b), Zapotoczna-Sytek and Balkovic (2013). The SEM analysis of the microstructures of specimens produced from modified AAC revealed the presence of the C-S-H phase and Tobermorite—Richardson (2004). Table 13.8 summarizes the results from the SEM microstructure analysis of AAC. The solid material skeleton, as well as microchannels and pores that constitute the microstructure of AAC materials are shown in Fig. 13.10. The phases that form the solid AAC structure are hydrated calcium silicates with varying degrees of order. The C-S-H phase is an amorphous phase with a sponge-like structure and fills the free spaces in the material.



**Table 13.8** Elemental quantitative analysis of sample R1 (AAC with HIPS)

Element	Wt.%	At.%	K-ratio	Z	A	F
C K	1.48	3.35	0.0035	1.0466	0.1793	1.0007
O K	44.42	60.68	0.0908	1.0289	0.1986	1.0003
Mg K	0.69	0.62	0.0037	0.9871	0.5481	1.0067
Al K	2.50	2.03	0.0166	0.9580	0.6857	1.0119
Si K	24.72	19.24	0.1901	0.9859	0.7770	1.0036
K K	0.59	0.33	0.0053	0.9359	0.9218	1.0448
Ca K	25.24	13.73	0.2311	0.9579	0.9556	1.0000
Total	100.00	100.00	–	–	–	–

Figure 13.11 shows the results of the SEM microstructure assessment with simultaneous elemental composition analysis (EDS spectrum for three randomly picked points on the AAC sample). It can be observed that all three analyzed points show very similar EDS spectra, which indicates high uniformity of tested AAC material. Please also notice that the existence of metallic elements such as aluminum, iron, and magnesium (Table 13.8 and Fig. 13.11) results from a use of industrial sand in the preparation of laboratory specimens of aerated concrete.

In concrete, the first phase to precipitate by chemical reaction is allite, which is responsible for the early strength of the concrete. Alite is calcium oxysilicate, the most important phase in Portland clinker. The reactivity of allite with water is responsible for the hardening of the slurry. Alite is more reactive than belite, due to its higher Ca content and the presence of oxide ions in the crystal lattice. Belite

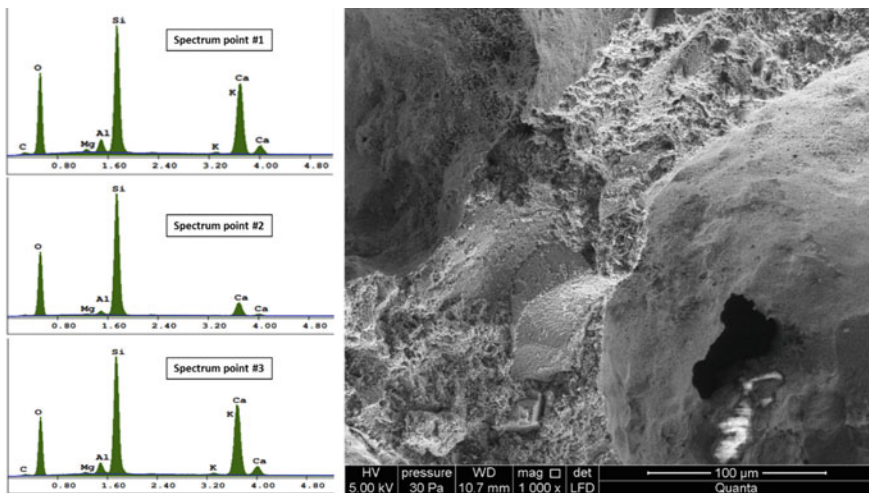


**Fig. 13.11** Energy Dispersive X-ray Spectroscopy (EDS) spectrum analysis for three randomly selected points on the AAC sample and SEM view of its microstructure at 1,000 × magnification

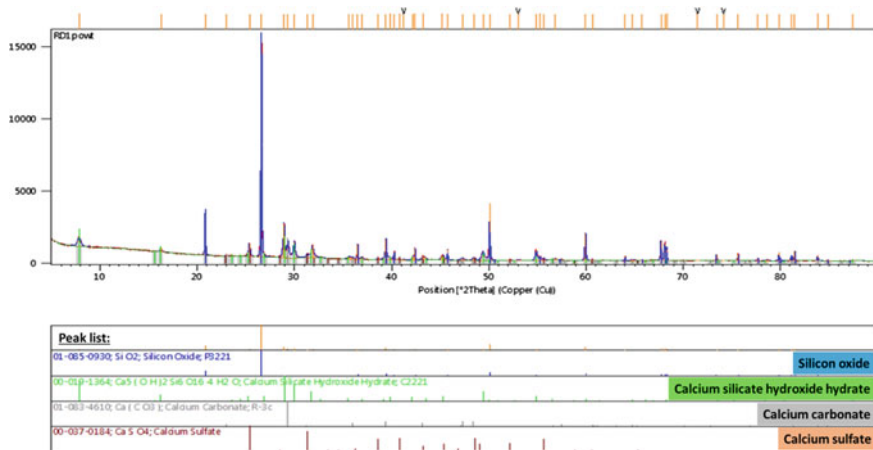
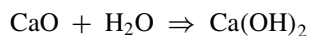
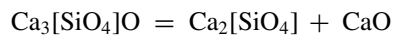


Fig. 13.12 XRD analysis of AAC specimens with HIPS

is a calcium orthosilicate and the second most important mineral component (after allite) in Portland clinker. Belite provides “late” concrete strength due to its lower reactivity—see: Taylor (1997), Matschei et al. (2007).



X-Ray Diffraction, frequently abbreviated as XRD, is a non-destructive test method commonly used to analyze the internal structure of crystalline materials. XRD analysis (Fig. 13.12), by way of the study of the crystal structure, is used to identify the crystalline phases present in a material and thereby reveal chemical composition information. Identification of phases is achieved by comparison of the acquired data to that in reference databases. X-ray diffraction is useful for evaluating minerals, polymers, corrosion products, and unknown materials. In most cases, the specimens are analyzed by powder diffraction using specimens prepared as finely ground powders.<sup>22</sup> The quartz peak, in particular, is visible in Fig. 13.11. Typically XRD is performed from 20 θ (theta), however some phases (including Tobermorite and C-S-H) are visible in the lower range of 10–20 θ. In that light, for autoclaved concrete materials, the specifications for the XRD testing may need to be changed in the future.

<sup>22</sup> <https://www.element.com/materials-testing-services/x-ray-diffraction#:~:text=X%2DRay%20Diffraction%2C%20frequently%20abbreviated,thereby%20reveal%20chemical%20composition%20information.>

Alite is a thermodynamically unstable mineral at temperatures below 1250 °C. But can be maintained in a metastable state at room temperature. Thermodynamically stable minerals do not have the ability to transform or change from one phase to another under optimal conditions. The C-S-H phase is particularly desirable in concretes, it usually contains a disordered and amorphous structure. C-S-H has a large specific surface area and is a thermodynamically stable phase at ambient temperature (20 °C). Toberomite (C-S-H (I) (Tobermorite) & C-S-H (II) (jennite)—are hydrated calcium silicates, with a crystalline structure (formed by the action of high temperature and/or pressure on the C-S-H phase. These phases are characterized by a low specific surface area—see: Dachowski and Kapała (2016), Balonis (2019). Phase transformations are related to so-called, hardening of the binder, i.e. the formation of a crystalline structure. C-S-H phase is responsible for 70–80% of the concrete strength. It is an amorphous phase that crystallizes over the years (concretes from the time of the Roman Empire still crystallize today).<sup>23</sup> When the C-S-H phase crystallizes, its specific surface area changes (decreases) creating free spaces in the pores, which allows e.g. water to interfere with the structure of the concrete and which consequently leads to the destruction of the concrete structure. C-S-H depending on the concentration of  $\text{Ca}(\text{OH})_2$  ions in the structure of concrete “takes” or “gives up”  $\text{Ca}^{++}$  ions, which is related to the appropriate alkalinity of concrete (preferably above 12.4pH),<sup>24,25</sup>—see also: Stepien et al. (2019), Lothenbach et al. (2019), Taylor (1997), Matschei et al. (2007), Balonis (2019).

### 13.5 Discussion and Conclusions

AAC products are thermally insulating structural materials that have been highly appreciated by construction industries, especially because of widespread applications in single-family housing. AACs are well-known because of their unique thermal insulation and environmental impact characteristics. They have become highly desired consumer products, which is reflected by numerous national building and energy standards, as well as sustainable construction specifications worldwide.

Autoclaved cellular concrete products exhibit compressive strengths up to 6 MPa. Our recent work demonstrated that use of high impact polystyrene (HIPS) additives can help with improvement of physical and mechanical properties (mainly stabilization of the compressive strength) and can cause significant reduction of the water absorption coefficient. The addition of HIPS to ACC acts in a similar way as the addition of fillers to the raw concrete mass. Performed internal structure analysis of AAC

---

<sup>23</sup> <https://www.wprost.pl/nauka/10063718/Cement-z-czasow-Imperium-Rzyskiego-pomoze-stworzyc-super-beton-Naukowcy-odkrywaja-karty.html>.

<sup>24</sup> <http://budmax.eu/solbet-blmoczki-z-betonu-komorkowego/>.

<sup>25</sup> <https://www.polskicement.pl/aktualnosci/cembureau-roadmap-2020-2050-ograniczenie-emisji-co2-o-ok-40-na-koniec-dekad>.

showed the presence of amorphous phases of the disordered structure C-S-H. Furthermore, micro-CT analysis demonstrated that the average content of air voids in tested AAC samples was around 52% with an average density from four measurements of 2.21 (kg/dm<sup>3</sup>). In addition to the component formulation, the internal structure characteristics were also affected by the employed AAC production method.

Performed porosity analysis of used materials (reference samples and modified with HIPS) made it possible to visualize the internal structure of the HIPS-modified AAC, especially the connections and distribution of micro-pores. This was important for better understanding the porosity test results. The analysis of mechanical strength characteristics was complemented with microstructure examination using a scanning electron microscope (SEM) and XRD, which in turn allowed the observation of hydrated calcium silicates formed in the tested materials. Research data discussed in this chapter demonstrated that the addition of HIPS did not change the microstructure of the material. Considering that cellular concretes are usually designed for a minimum of 20 years of use to further validate the long-term performance of AAC with added of HIPS thermal stability of concrete additives and durability of AAC under variable environmental conditions needs to be investigated.

**Acknowledgements** The authors would like to acknowledge to: Szmidt A. and Stepien K. for the opportunity to conduct joined analyses on the production of autoclaved materials; Sitarz M., Leśniak M. from AGH University in Cracow, Poland, as well as Skowera K. and Durliej M. from University of Technology in Kielce for cooperation and support.

**Funds** The Mirco CT analysis tomograph (CENWIS, University of Technology in Kielce), and some of the research done was performed thanks to the endowment funding.

## References

- Abdulrahman, A., & Bruce N. E. (2004). Super HIPS: Improved high IM pact polystyrene with two sources of rubber particles. *Polymer*, 45, 8435–8442.
- Alfarraj, A., & Nauman, E. B. (2004). Super HIPS: Improved high impact polystyrene with two sources of rubber particles. *Polymer*, 45, 8435–8442.
- Balonis, M. (2019). Thermodynamic modelling of temperature effects on the mineralogy of Portland cement systems containing chloride. *Cement and Concrete Research*, 120, 66–76. <https://doi.org/10.1016/j.cemconres.2019.03.011>.
- Birkenmajer, K. (1967). Lower Silesian basalts as monuments of inanimate nature—Nature protection No 32. Bazalty dolnośląskie jako zabytki przyrody nieożywionej. *Ochrona Przyrody* (nr 32, pp. 225–276). Kraków.
- Błaszczczyński, T. Z., & Król, M. (2013). Geopolimery w budownictwie/Geopolymers in construction. *IZOLACJE*, (5), 38–44.
- Błaszczczyński, T. Z., & Król M. (2014). Concrete production and the problem of reducing carbon dioxide emissions. *IZOLACJE*, (3). <https://www.izolacje.com.pl/artykul/chemia-budowlana/166160.produkcja-betonu-a-problem-redukcji-emisji-dwutlenku-wegla>. Accessed 01 July 2021.
- Boltyanskii, A. V., Bulakh, V. L., & Fedorova, L. S. (1995). Use of industrial waste for the production of building materials. *Refractories and Industrial Ceramics*, 36(8).

- Brelak, S., & Dachowski, R. (2017a). Multi-criteria comparative analysis of products made of autoclaved aerated concrete modified with recycling materials. *Wielokryterialna analiza porównawcza wyrobów z autoklawizowanego betonu komórkowego modyfikowanego materiałami recyklingowymi*. *Budownictwo o Zoptymalizowanym Potencjale Energetycznym*, 2(20), 29–36. <https://doi.org/10.17512/bozpe.2017a.2.04>.
- Brelak, S., & Dachowski, R. (2017b). Effect of autoclaved aerated concrete modification with high-impact polystyrene on sound insulation. *IOP Conference Series: Materials Science and Engineering*, 245.
- Dachowski, R., & Kapała, S. (2016). Modification of autoclaved aerated concrete with high-impact polystyrene. *Materiały Budowlane*, Wydawnictwo SIGMA-NOT Sp. z o.o., Redakcja Materiały Budowlane (Vol. 6, pp. 69–70), Warsaw.
- EU PN (2004) Directive 2002/91/EC of 16 December 2002 on the energy performance of buildings. Standard PN-EN ISO 13790, Standard PN-EN ISO 6946. <https://www.iea.org/policies/712-energy-performance-of-buildings-directive-200291ec>.
- Gawin, D., & Kośny, J. (2000). Effect of moisture on thermal performance and energy efficiency of buildings with lightweight concrete walls. In *Proceedings of the 2000 ACEEE Conference, ACEEE Summer Study on Energy Efficiency in Buildings: American Council for an Energy Efficient Economy*, Pacific Grove.
- Gawin, D., Kośny, J., & Wilkes, K. E. (2004). Thermal conductivity of moist cellular concrete—Experimental and numerical study. In *IX Conference—Thermal Performance of the Exterior Envelopes of Buildings*, Clearwater, Florida.
- Kapała, S., & Dachowski, R. (2016). The influence of the chalcedony on the properties of autoclaved aerated concrete. *Procedia Engineering*, 699–703.
- Kejkar Rupali, B., & Wanjari Swapnil, P. (2021). Feasibility study of commercially viable sustainable aerated geopolymeric foam based block. *Materials Today*, 45, 4398–4404 (Elsevier). <https://doi.org/10.1016/j.matpr.2020.11.916>.
- Kozłowski, S. (1975). *Rock raw materials of Poland/Surowce skalne Polski*-Wydawnictwo geologiczne/Geological Publishing House.
- Li, F., Chen, G., Zhang, Y., Hao, Y., & Si, Z. (2020). Fundamental properties and thermal transferability of masonry built by autoclaved aerated concrete self-insulation blocks. *Materials (Basel)*, 13(7), 1680. <https://doi.org/10.3390/ma13071680>.
- Lothenbach, B., Kulik, D. A., Matschei, T., Balonis, M., Baquerizo, L., Dilnes, B., Miron, J. D., & Myers, R. J. (2019). Cemdata18: A chemical thermodynamic database for hydrated Portland cements and alkali-activated materials. *Cement and Concrete Research*.
- Macech, J. (2020). Fire resistance of construction products. Association of silicate producers. White Bricklaying. <https://budownictwob2b.pl/przegrody/baza-wiedzy/sciany-i-stropy/22854-odpornosc-ogniowa-wyrobow-budowlanych>.
- Matschei, T., Lothenbach, B., Glasser, F. P. (2007). The role of calcium carbonate in cement hydration. *Cement and Concrete Research*.
- Nonat, A., Lecoq, X. (1998). The structure, stoichiometry and properties of C-S-H prepared by C3S hydration under controlled condition. In *Nuclear magnetic resonance spectroscopy of cement-based materials* (pp. 197–207). Springer, Berlin, Heidelberg. [https://doi.org/10.1007/978-3-642-80432-8\\_14](https://doi.org/10.1007/978-3-642-80432-8_14).
- Parker, P. M., Lilly, E. (2005). The 2006–2011 World Outlook for All Silica. Brick and shapes excluding Semi-Silica. INSEAD (Singapore and Fontainebleau, France) ICON Group International, Inc.
- Polyzois, D., & Raftoyiannis Ioannis, G. (2007). The effect of semi-rigid connections on the dynamic behavior of tapered composite GFRP poles. *Composite Structures*, 81(1), 70–79.
- Pruteanu, M., & Vasilache, M. (2013). Thermal conductivity determination for autoclaved aerated concrete elements used in enclosure masonry walls. *Bulletin of the Polytechnic Institute of Jassy, CONSTRUCTIONS. ARCHITECTURE Section*, LIX(LXIII)(3), 33–42.
- Richardson, I. (2004). Tobermorite/jennite- and tobermorite/calcium hydroxide-based models for the structure of C-S-H: Applicability to hardened pastes of tricalcium silicate, beta-dicalcium

- silicate, Portland cement, and blends of Portland cement with blast-fumace slag, metakaolin, or silica fume. *Cement and Concrete Research*, 34, 1733–1777.
- Rybarczyk, T., Chojnowski, J., Chruściel, W., Janiak, R., Kwaśniak, J., & Łaskawiec, K. (2015) Almost everything about cellular concrete/Prawie wszystko o betonie komórkowym. Zeszyt 1, Stowarzyszenie Producentów Betonów, Warszawa. ISBN 978-83-941005-1-3. <http://s-p-b.pl/img/upload/Prawie%20wszystko%20o%20betonie%20kom%C3%B3rkowym0.pdf>.
- Skalmowski, W. (1966). Technology of building materials/Technologia materiałów budowlanych Arkady, Tom II, Warszawa.
- Stepien, A., Leśniak, M., & Sitarz, M. (2019). A sustainable autoclaved material made of glass sand. *MDPI, Buildings*, 9(11), 232.
- Stepien, A., Potrzeszcz-Sut, B., Balonis, M., Prentice, D. P., Oey, T. (2020) The role of glass compounds in autoclaved bricks. *Buildings (MDPI)*, Tom: 10, Zeszyt: 3, Strony: 1–25.
- Szoke, S. S. (2014) Guide to thermal properties of concrete and masonry systems. American Concrete Institute, ACI 122R-14, ISBN: 978-0-87031-971-6.
- Taylor, H. F. W. (1997). *Cement chemistry* (p. 459). Thomas Telford. ISBN: 0 7277 2592 0.
- Van Boggelen, W. (2014). History of autoclaved aerated concrete—The short story of a long lasting building material.
- Vilaplana, F., Ribes-Greus, A., & Karlsson, S. (2010). Chromatographic pattern in recycled high-impact polystyrene (HIPS)—Occurrence of low molecular weight compounds during the life cycle. *Polymer Degradation and Stability*, 95, 172–186.
- Wcisło, A. (2018). Green construction of gray concrete/Zielone budownictwo z szarego betonu. Lafarge Cement S.A., DNI BETONU.
- Zapotoczna-Sytek, G., & Balkovic, S. (2013). Autoclaved aerated concrete. Technology, properties, application/Autoklawizowany beton komórkowy. Technologia, właściwości, zastosowanie- Wydawnictwo Naukowe PWN, Warszawa.
- Zapotoczna-Sytek, G. (2018). Durability of autoclaved aerated concrete based on Polish experience. In *ICAAC—6th International Conference on Autoclaved Aerated Concrete* (Vol. 2, No. 4, pp. 53–62). <https://doi.org/10.1002/cepa.850>.

# Chapter 14

## Dynamic Thermal Performance of Insulation Combined in Different Formations with Thermally Massive Components



Jan Kośny, Elisabeth Kossecka, and David W. Yarbrough

**Abstract** Today, thermal insulation is generally required to be used in building envelopes by building energy standards worldwide. It is also well-known that thermal insulation provides space conditioning energy savings and improvement of the internal thermal comfort. However, the impact of the placement of thermal insulation within the building envelope and insulation interaction with thermally massive components are not commonly understood. Static and dynamic thermal processes in buildings and building components, together with associated heat transfer, thermal mass effects, and thermal storage play an important role in overall building energy efficiency, utilization of renewable energy sources, and energy demand management. Building enclosures, which include both fenestration and the opaque portions of the envelope, effectively control the influence of the outdoor climate on the interior environment, reducing the heating, cooling, and lighting requirements to maintain the desired indoor conditions. The above factors directly affect the corresponding energy usage and its dynamics. Among all of the internal fabric and external enclosure of buildings, external walls are often one of the most dynamic components since they are exposed to intense solar radiation and temperature fluctuations that are subject to seasonal climatic conditions. Following the currently rising interests in demand-side management, building energy dynamics, and the thermal response characteristics of building components, the impact of the insulation placement and resulting wall material configuration on the dynamic thermal performance is theoretically and numerically analyzed in this chapter for typical wall material configurations. It is demonstrated that due to different arrangements of thermal insulation and structure-related, thermally massive layers, walls constructed of similar materials can present a wide range of dynamic thermal characteristics.

---

J. Kośny (✉)

University of Massachusetts, Lowell (UML), Lowell, MA, USA

e-mail: [Kosny\\_Jan@uml.edu](mailto:Kosny_Jan@uml.edu)

E. Kossecka

Polish Academy of Sciences (Retired), Warsaw, Poland

D. W. Yarbrough

R&D Services, Inc., Watertown, TN, USA

**Keywords** Heat transfer · Dynamic thermal performance · Building thermal response · Thermal insulation · Thermal mass · Decrement factor · Admittance response · Building thermal stability

## Nomenclature

$A_{Ti}, A_{Te}$	Interior and exterior temperature amplitude
$B(i\omega), D(i\omega)$	Elements of the transmission matrix
$I/B, D/B$	Transmittance and admittance response
$c_p$	Specific heat
$C, C_m$	Thermal capacity
$DF$	Decrement factor
$X(m\delta), Y(m\delta), Z(m\delta)$	Response factors with number $m$
$k$	Thermal conductivity
$L$	Thickness
$M$	Mass
$q_i, q_e$	Heat flux across the internal and external surface of a wall
$Q_i, Q_e$	Heat flow across the internal and external surface of a wall
$R_T$	Total resistance of a wall
$R_m$	Resistance of the wall layer $m$
$R_i, R_e$	Surface film resistance
$R_{i-x}, R_{x-e}$	Resistance from the interior and exterior air to the point $x$
$R_{i-m}, R_{m-e}$	Resistance from the interior and exterior air to the surface of the layer $m$
$t$	Time
$T_i, T_e$	Interior and exterior air temperature
$\delta$	Time decrement
$\varphi_{ii}, \varphi_{ie}, \varphi_{ee}$	Structure factors of a wall
$\rho$	Density
$\tau_{ii}, \tau_{ie}, \tau_{Ti}$	Time shift
$\omega$	Angular frequency

## 14.1 Introduction

Different types of thermal insulation and structural materials have been used in building construction since ancient times. Numerous advanced building envelope constructions, where thermal insulation is either placed between lightweight structural members, or sometimes it is layered between thermally massive components, can be found today in many locations worldwide. Unfortunately, many of these technologies still suffer from a lack of accepted standard measures of their excellent



thermal performance and unique dynamic thermal response characteristics. Kośny and Desjarlais (1994) investigated the impact of a variety of wall system architectural details on the overall thermal performance of the opaque wall. This work also introduced the terms “clear-wall” and “whole-wall” R-values. However, the steady-state R-value, that is commonly used today as a thermal performance measure for building envelopes, does not include dynamic behavior. To allow dynamic performance comparisons between different building envelope assemblies, the term “Dynamic Benefit for Massive Systems” (DBMS) was introduced by Kośny et al. (1998a, 1998b). In this analytical method, the thermal mass benefit is a function of the material configuration and climatic conditions. DBMS values are obtained by comparison of the thermal performance of thermally massive and lightweight envelopes of the same R-value.

Today, an in-depth understanding of combined performance of insulation and thermal mass can benefit modern, energy-efficient, sustainably built buildings. The annual energy demand for heating and cooling is affected to some extent by thermal stability of a building. Thermal stability is understood as the ability to maintain the internal building temperature within a certain time interval with normal external temperature oscillations and constant energy supply. The whole building thermal stability depends on the dynamic thermal responses of all building envelope components (exterior walls, internal partitions, ceilings, roofs, and floors) to external and internal temperature variations. These dynamic responses are determined by thermal properties, amounts of used materials (thermal mass), and their arrangement within the structure.

The important feature of the ambient temperature is its diurnal character. In spite of the importance of dynamic thermal characteristics of building components, they are less studied than, for example, the thermal resistance of building envelope elements, or heat conduction in individual systems or materials. The influence of thermal insulation on the static thermal performance, sustainability, and long-term durability of building envelopes has been thoroughly investigated for several decades, and it has been discussed in numerous technical publications—see: Hasan (1999), Ashouri et al. (2016), Ozel (2011), Axaopoulos et al. (2015), Yuan et al. (2017), and Feng et al. (2019). Furthermore, various studies have been initiated worldwide to estimate the heat transmission losses through building envelopes—see: Daouas (2011), Feng et al. (2019), Ramin et al. (2016), Saafi and Daouas (2018), and Cuce et al. (2014). When it comes to the dynamic thermal performance of building envelopes, however, the transient thermal characteristics of many, even simple structures (i.e. masonry units, insulated concrete foams, or prefabricated concrete panels), or basic structural materials such as wood, steel framed assemblies, or lightweight concretes are not fully understood. Consequently, dynamic performance, is not always reflected in national building energy standards—see: Peavy et al. (1973), Kusuda (1977), Van Geem et al. (1982), Kośny and Christian (1995), Kośny et al., (1998a, 1998b), Asan (2006), Gregory et al. (2008), Urban et al. (2013), Kośny et al. (2014), Tang et al. (2015), Balaji et al. (2019). Still, several consensus standards dealing with dynamic thermal performance of building components have been developed (i.e. ISO, 2005 and ISO, 2007). As described by Corrado and Paduos (2016), these standards are not

always correct in predicting desired thermal performance results when compared to the field data. This is perhaps due to a use of simplified periodic temperature algorithms in the heat-flow calculations. In terms of design and modeling, Košny and Kossecka (2002) demonstrated that some numerical models provide inadequate results for high-mass buildings. One of the reasons is that these standards have been developed for analysis of lightweight structures, and later, they were experimentally validated only on buildings with low thermal storage capacity.

In addition, several studies have focused on the influence of thermal mass on buildings utilizing different wall material configurations; for example, Aste et al. (2009) carried out a parametric study for a number of wall types for both heating and cooling scenarios. A small number of studies have evaluated the impact of insulation placement and the presence of thermal storage layers within a wall, usually relying on one-dimensional thermal analysis—see: Childs (1980), Bojic´ and Loveday (1997), Kossecka and Košny (2002). More accurate three-dimensional analysis of building envelopes became readily available after the development by Kossecka and Košny (1997), of the Equivalent Wall Theory (EWT). The EWT allows conversion of complex 3D geometry and multidirectional thermal effects in building envelopes into simplified 1D thermal representations. The conversion expedites the utilization of commonly used whole building energy simulation tools.

In different work, the dynamic thermal characteristics of building envelopes were analyzed, for the envelope cases, where the nominal performance of thermal insulation was compromised by heat conductive components. This work was conducted for the cold climates of British Columbia, Canada, by Ge and Baba (2017). The results of whole building energy simulations performed on a multifamily residential building show that a proper inclusion of thermal bridging positively impacts the whole building energy consumption, and it may reduce the annual space heating energy demand by up to 42% and decrease, the annual space cooling energy demand by up to 26% for interlayered concrete-insulation walls. The admittance method and finite difference heat transfer modeling were utilized by Balaji et al. (2019), to analyze the effects of various configurations of wall thermal insulation and structural materials on (i) the time lag and decrement factor (thermal decrement factor is a fractional measure of the relative reduction in cyclical temperature on the inside surface compared to the outside surface of a material due to thermal lag), (ii) interior surface instantaneous thermal load, and (iii) the impact of the exterior surface heat transfer coefficient on the time lag and decrement factors.

Kalinovic et al. (2019) studied non-stationary heat exchange processes between multilayer wall assemblies and the environment. The impact of material arrangements, including thermal insulation, structural components, and coating materials on the wall thermal inertia was analyzed. Experimental and numerical performance comparisons of advanced roofs and attic assemblies, using layered thermally massive and insulating components were performed by Košny et al. (2020). They showed over 90% reduction in roof-generated peak-hour cooling loads and close to 50% reductions in overall roof-generated cooling loads, when compared to traditionally constructed roofs using the same or similar levels of thermal insulation. Furthermore, unique design strategies, that were analyzed, yielded significant reductions of roof

peak daytime temperatures, reductions in peak thermal loads, and up to 10-h-long time shift of the peak load.

In this chapter, the impact of the insulation configuration within building envelope is illustrated by the results of theoretical and numerical analysis of both, the individual envelope component, as well as the whole building. The influence of the insulation placement and resulting wall material configuration on the dynamic thermal performance characteristics are analyzed for typical wall material configurations. Furthermore, a series of whole building simulations was completed for a one-story residential ranch house, for six representative U.S. climates, to analyze the thermal performance of multilayer wall assemblies containing different configurations of thermal insulation and structural materials.

## **14.2 Location and Distribution of Structural and Insulating Components Inside a Plain Wall as Major Factors Determining Its Dynamic Thermal Performance Characteristics**

Modern building envelopes are complex networks of thermal insulation, structural materials, and finish layers, where complex, multi-dimensional heat transfer processes take place. The impact of material arrangements, including thermal insulation, structural components, as well as finish, and coating materials on the wall thermal inertia has been analyzed in many research studies worldwide—see: Peavy et al. (1973), Kusuda (1977), Childs (1980), Van Geem et al. (1982), Košný and Christian (1995), Bojic´ and Loveday (1997), Košný et al. (1998a, 1998b), Kossecka and Košný (2002), Asan (2006), Gregory et al. (2008), Aste et al. (2009), Urban et al. (2013), Košný et al. (2014), Tang et al. (2015), Balaji et al. (2019), Košný et al. (2020). It was found that the major thermal design factors associated with the material/structural configuration of a wall are the overall thermal resistance (expressed as R-value), as well as the distribution of thermal resistance and heat capacity across its volume. Formal theoretical relationships, describing in a quantitative way the effect of structure on dynamic thermal behavior of building envelopes were initially introduced by Kossecka (1992, 1994). Following this work, thermal structure factors were defined, which represent the distribution of thermal resistance and heat capacity across the building envelope volume—see; Kossecka and Košný (1997). Thermal structure factors together with the total thermal resistance (function of material conductivity and thickness), and heat capacity (function of material volume and density), the basic thermal characteristics of building structures, where complex three-dimensional heat flow occurs. They can be derived from the integral formulae for the heat flow across the surfaces of a wall in a finite time interval. Thermal structure factors are similar to the identified by the ISO Standard 9869—ISO (1994), dimensionless quantities called thermal mass factors.

In addition, relationships between the structure factors, response factors and z-transfer function coefficients have been derived and analyzed by Kossecka (1996, 1998), Kossecka and Košny (1997). Thermal structure factors appear in expressions for the asymptotic heat flow across the surfaces of a wall, for boundary conditions independent of time.

To demonstrate these theoretical relationships (describing in a quantitative way the effect of structure on dynamic thermal behavior of building envelopes), let's consider a heat transfer case of a plane wall of thickness  $L$ , which separates a room at temperature  $T_i$  from the environment at temperature  $T_e$ . The thermophysical properties of this wall include: thermal conductivity  $k$ , specific heat  $c_p$  and density  $\rho$ , and as well surface film resistances,  $R_i$  and  $R_e$ . Let's also assume that they do not change with time and that  $\theta$  is the dimensionless temperature for the steady-state heat transfer through a wall, with boundary conditions  $T_i = 0$  and  $T_e = 1$ . For a plane wall, where one-dimensional heat flow conditions are satisfied, the function  $\theta(x)$  is given by:

$$\theta(x) = \frac{R_{i-x}}{R_T}, \quad 1 - \theta(x) = \frac{R_{x-e}}{R_T} \quad (14.1, 14.2)$$

where  $R_{i-x}$  and  $R_{x-e}$  denote the resistances for heat transmission from point  $x$  in a wall to the internal space and external environment, respectively, and  $R_T$  the total resistance for heat transmission across a wall.

$R_{i-x}$  and  $R_{x-e}$  can be expressed by the following integrals:

$$R_{i-x} = R_i + \int_0^x \frac{dx'}{k(x')}, \quad R_{x-e} = \int_x^L \frac{dx'}{k(x')} + R_e \quad (14.3, 14.4)$$

Let's assume that the transient heat transfer process for the ambient temperatures is constant for  $t > 0$  and the initial dimensionless temperature in the wall is zero.

For sufficiently large  $t$ , the asymptotic expressions for the total heat flow in the time interval  $[0, t]$ , across the internal and external surfaces of a wall, in the direction from the room to the environment,  $Q_i(t)$  and  $Q_e(t)$ , have the following form, as discussed in Kossecka (1992, 1993, 1996, 1998).

$$Q_i(t) = \frac{t}{R_T} [T_i - T_e] + C\varphi_{ii} + C\varphi_{ie} \quad (14.5)$$

$$Q_e(t) = \frac{t}{R_T} [T_i - T_e] - C\varphi_{ie} - C\varphi_{ii} \quad (14.6)$$

where  $C$  is the total thermal capacity of the wall element of the unit's cross-sectional area:

$$C = \int_0^L \rho c_p dx \quad (14.7)$$

and the quantities  $\varphi_{ii}$ ,  $\varphi_{ie}$  and  $\varphi_{ee}$  are given by:

$$\varphi_{ii} = \frac{1}{C} \int_0^L \rho c_p (1 - \theta)^2 dx = \frac{1}{C} \int_0^L \rho c_p \frac{R_{x-e}^2}{R_T^2} dx \quad (14.8)$$

$$\varphi_{ie} = \frac{1}{C} \int_0^L \rho c_p \theta (1 - \theta) dx = \frac{1}{C} \int_0^L \rho c_p \frac{R_{i-x} R_{x-e}}{R_T^2} dx \quad (14.9)$$

$$\varphi_{ee} = \frac{1}{C} \int_0^L \rho c_p \theta^2 dx = \frac{1}{C} \int_0^L \rho c_p \frac{R_{i-x}^2}{R_T^2} dx \quad (14.10)$$

The dimensionless quantities  $\varphi_{ii}$ ,  $\varphi_{ie}$  and  $\varphi_{ee}$  are called the “thermal structure factors” for a wall. For a plane wall they are determined directly by its structural configuration, represented by the thermal capacity and resistance distribution across its thickness. In transitions between two different states of steady heat flow, they represent fractions of the total variation of heat stored in the wall volume, which are transferred across each of its surfaces, due to the variation of the ambient temperature. The following identity is a consequence of Eqs. 14.8 through 14.10:

$$\varphi_{ii} + 2\varphi_{ie} + \varphi_{ee} = 1 \quad (14.11)$$

As discussed by Košny et al. (1998a, 1998b), the structure factors can be determined experimentally in processes with steady-state initial and final states of heat flow. Following the Eqs. 14.5 and 14.6, the structural factors are related to the measurable quantities, such as the heat flow, temperature, thermal resistance and heat capacity. Together with the total thermal resistance  $R_T$  and total heat capacity  $C$ , they constitute the basic thermal characteristics of a wall and have their counterparts for structures in which three-dimensional heat flow occurs—see: Kossecka and Košny (1996, 1997).

In multilayer assemblies, the structure factors for a wall composed of  $n$  plane homogeneous layers, numbered from 1 to  $n$  with layer 1 at the interior surface, are given as follows:

$$\varphi_{ii} = \frac{1}{R_T^2 C} \sum_{m=1}^n C_m \left[ \frac{R_m^2}{3} + R_m R_{m-e} + R_{m-e}^2 \right] \quad (14.12)$$

$$\varphi_{ie} = \frac{1}{R_T^2 C} \sum_{m=1}^n C_m \left[ -\frac{R_m^2}{3} + \frac{R_m R_T}{2} + R_{i-m} R_{m-e} \right] \quad (14.13)$$

$$\varphi_{ee} = \frac{1}{R_T^2 C} \sum_{m=1}^n C_m \left[ \frac{R_m^2}{3} + R_m R_{i-m} + R_{i-m}^2 \right] \quad (14.14)$$

where:  $R_m$  and  $C_m$  denote the thermal resistance and capacity of the  $m$ -th layer respectively, whereas  $R_{i-m}$  and  $R_{m-e}$  denote the resistances for heat transfer from surfaces of the  $m$ -th layer to inner and outer surroundings, respectively.

Please notice that the structure factor  $\varphi_{ii}$  is comparatively large, when most of the total thermal capacity is located near the interior surface  $x = 0$  and most of the insulating materials (resistances) reside in the outer part of the wall, located near the surface  $x = L$ . The opposite holds for  $\varphi_{ee}$ . The following relations are straightforward:  $0 < \varphi_{ii} < 1$ ,  $0 < \varphi_{ee} < 1$ . Similarly, the structure factor  $\varphi_{ie}$  is comparatively large, when most of the thermal mass is located in the center of the wall and the resistance is symmetrically distributed on both sides of it.

The following limitations on  $\varphi_{ie}$  result from Eq. 14.13:

- for a two-layer wall  $0 < \varphi_{ie} < 3/16$ ;
- for a  $n$ -layer wall, with  $n \geq 3$ ,  $0 < \varphi_{ie} < 1/4$ .
- For a homogeneous wall, with negligibly small film resistances  $R_i$  and  $R_e$ ,  $\varphi_{ii} = \varphi_{ee} = 1/3$ , as well as  $\varphi_{ie} = 1/6$ .

In the ISO Standard 9869—ISO (1994), dimensionless quantities  $C\varphi_{ii}$ ,  $C\varphi_{ee}$ , and  $C\varphi_{ie}$  for a multilayer wall are identified as thermal mass factors.

As explained in earlier sections, the structure factors for multilayer walls depend on the arrangement of wall materials. To demonstrate this effect, six differently configured multilayered walls of the same thermal resistance and heat capacity, were examined. The walls (1) through (6) are depicted in Fig. 14.1. As presented in Fig. 14.2, the theoretical wall material configurations c are very realistic and they reflect existing building envelope configurations t. Table 14.1 shows, thermophysical properties of wall materials used in analysis. The structure factors computed for the wall configurations considered are presented in Table 14.2 and compared to the structure factors of the wall made with a solid thermally massive core. The main part of each wall is a composition of heavyweight concrete layers, of the total thickness of 0.152 m, and thermal insulation layers, of the total thickness 0.102 m. The interior layer is the gypsum plaster board of 0.013 m thickness. The exterior layer is 0.019 m thick stucco layer. The total wall thickness  $L$  is 0.286 m. The structure factors for the wall with homogeneous core, of the same total thermal resistance and heat capacity, are added for comparison.

In thermal analysis of wall configurations presented in Fig. 14.1, the following wall surface film resistances are assumed:  $R_i = 0.12 \text{ m}^2 \cdot \text{K/W}$ ,  $R_e = 0.05 \text{ m}^2 \cdot \text{K/W}$ . The total thermal resistance for each wall is  $R_T = 3.21 \text{ m}^2 \cdot \text{K/W}$ . Overall heat transfer coefficient is  $U = 0.311 \text{ W/m}^2 \cdot \text{K}$ , total mass  $M = 390.27 \text{ kg/m}^2$  and wall heat

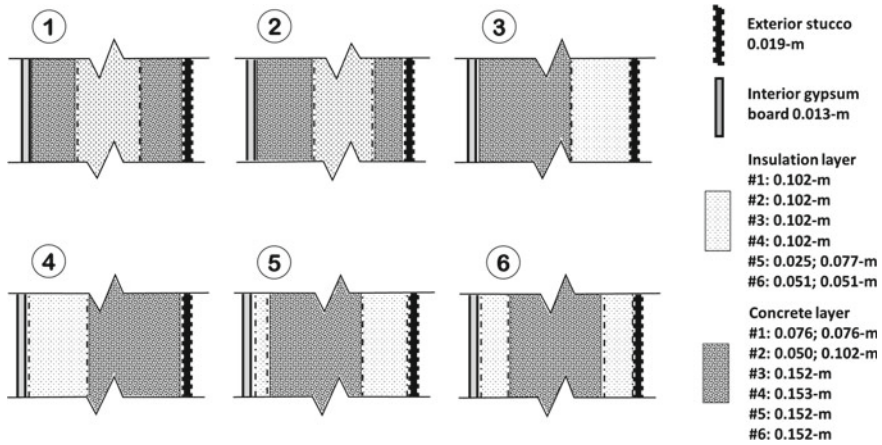


**Fig. 14.1** Schematics of six differently configured multilayered walls of the same thermal resistance and heat capacity and the total thickness of 0.286-m

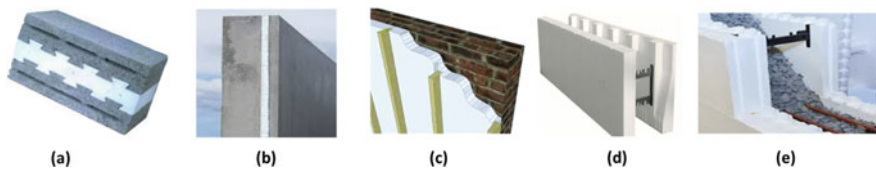


**Fig. 14.2** Several typical configurations of thermal insulation and thermally massive components which are presented in Fig. 14.1: **a** Mass-Insulation-Mass: configuration “1” in Fig. 14.1, **b** Mass-Insulation-Mass: configuration “2”, **c** Insulation-Mass: configuration “4”, **d** Insulated Concrete Form Technology (ICF): configuration “6”, **e** ICF wall filled with concrete; Insulation-Mass-Insulation: configuration “6.”

capacity is  $C = 329.93 \text{ kJ/m}^2\cdot\text{K}$ . Table 14.2 shows computed structure factors for the wall configurations under discussion.

**Table 14.1** Thermophysical properties of the wall materials used in analysis

Material	Density $\text{kg/m}^3$	Thermal conductivity $\text{W/m}\cdot\text{K}$	Specific heat $\text{kJ/kg}\cdot\text{K}$
Concrete	2240	1.44	0.838
Thermal insulation	16	0.036	1.215
Gypsum board	800	0.16	1.089
Stucco	1856	0.72	0.838

**Table 14.2** Structure factors for walls with cores composed of heavyweight concrete and insulation presented in Fig. 14.1

Wall	Wall configuration	$\varphi_{ii}$	$\varphi_{ie}$	$\varphi_{ee}$
Wall 1	Concrete-Insulation-Concrete	0.408	0.048	0.496
Wall 2	Concrete-Insulation-Concrete	0.530	0.053	0.363
Wall 3	Concrete-Insulation	0.770	0.068	0.094
Wall 4	Insulation-Concrete	0.034	0.040	0.885
Wall 5	Insulation-Concrete-Insulation	0.460	0.187	0.167
Wall 6	Insulation-Concrete-Insulation	0.234	0.222	0.322
Homogenous wall	Homogenous layer of material of averaged thermal properties	0.294	0.162	0.382

### 14.3 Relationships Between the Structure Factors and the Response Factors

The quantities  $C\varphi_{ii}$ ,  $C\varphi_{ie}$  and  $C\varphi_{ee}$ , in Eqs. (14.5) and (14.6) determine the role of thermal storage effects in transitions between different states of steady heat flow, affect particular modes of dynamic heat flux responses of a wall. As explained in Kossecka (1996, 1998), Kossecka and Košny (1997),  $C\varphi_{ii}$ ,  $C\varphi_{ie}$  and  $C\varphi_{ee}$  appear in the constraint conditions on dynamic thermal characteristics of walls such as the response factors, z-transfer function coefficients and also residues and poles of the Laplace transfer functions.

Additionally, corresponding to different heat flux response modes, the response factors for a wall can be denoted as  $X(m\delta)$ ,  $Y(m\delta)$  and  $Z(m\delta)$ . Please notice here that the response factor for number  $n$  represents the heat flux due to the unit, triangular temperature pulse of base width  $2\delta$ , at the time instant  $n\delta$ ; - see: Kusuda (1969), Clarke (1985). The relationships between the response factors  $X(m\delta)$ ,  $Y(m\delta)$ ,  $Z(m\delta)$  and structure factors  $\varphi_{ii}$ ,  $\varphi_{ie}$ ,  $\varphi_{ee}$  have the following form:

$$\delta \sum_{n=1}^{\infty} n X(n\delta) = -C\varphi_{ii} \quad (14.15)$$

$$\delta \sum_{n=1}^{\infty} n Y(n\delta) = C\varphi_{ie} \quad (14.16)$$

$$\delta \sum_{n=1}^{\infty} n Z(n\delta) = -C\varphi_{ee} \quad (14.17)$$

Analogous conditions are satisfied by the response factors for wall elements of complex structure, in which three-dimensional heat flow occurs, as discussed in Kossecka and Košny (1997). Equations 14.15 through 14.17 refer to the response factors with number  $n \geq 1$ , which represent the storage effects in form of surface heat



fluxes after the duration of the temperature pulse. They indicate that, for given total thermal capacity  $C$ , the sums of products of response factors of particular kind and their numbers increase with the appropriate structure factors. This means that the role of response factors having large numbers  $n$  increases with values of the appropriate structure factors.

#### 14.4 The Impact of Thermal Insulation Placement within Wall Assembly on Its Frequency Response

Equations 14.12 through 14.14 directly relate structure factors and wall responses to triangular ambient temperatures pulses. Wall responses to periodic temperature excitations also depend on the structure factors. This dependence is not represented by formal relations but appears in the form of significant correlations between the frequency dependent and structure dependent dynamic wall characteristics.

The general solution of the one-dimensional heat transfer problem in a multilayer wall assembly at periodic temperature conditions is presented in several publications, including Carslaw and Jaeger (1959) and Clarke (1985). The heat flux across the inside surface of a wall is given by:

$$q_i(t) = \frac{D(i\omega)}{B(i\omega)} T_i(t) - \frac{1}{B(i\omega)} T_e(t) \quad (14.18)$$

where  $D(i\omega)$  and  $B(i\omega)$  are the complex numbers, elements of the transmission matrix.

The term  $1/B$  represents the transmittance response, whereas  $D/B$  represents the admittance response. The decrement factor  $DF$  is here the amplitude of the transmittance response, multiplied by the total thermal resistance  $R_T$ . It represents reduction of the transmission cyclic heat flux amplitude, due to the external temperature excitation, at the inside surface of a wall, as compared to the steady state value, proportional to  $1/R_T$ . The time shifts of the transmittance and admittance response are denoted here by  $\tau_{ie}$  and  $\tau_{ii}$ , respectively.

$$DF = \frac{R_T}{|B(i\omega)|}, \quad \tau_{ie} = \frac{1}{\omega} \arg \frac{1}{B(i\omega)}, \quad \tau_{ii} = \frac{1}{\omega} \arg \frac{D(i\omega)}{B(i\omega)} \quad (14.19)$$

The time shift denoted as  $\tau_{ie}$ , is always negative; its absolute value is thus called the time lag, whereas  $\tau_{ii}$  is positive. For very thick walls  $1/B$  amplitude and  $DF$  tend to zero. Correspondingly, the admittance response amplitude tends to the finite value which, is equal to that for semi-infinite solids.

The effect of the structure factors, for given total resistance,  $R_T$ , and capacity,  $C$ , on wall responses to harmonic temperature variations, can easily be demonstrated on simple examples of multilayer wall configurations, as shown in Fig. 14.1. The decrement factors, amplitudes of the responses, and the appropriate time shifts, calculated

**Table 14.3** Decrement factors, amplitudes and time shifts of the transmittance and admittance response for walls with cores composed of heavyweight concrete and insulation depicted in Fig. 14.1

Wall	$\varphi_{ie}/\varphi_{ii}$	I/B response			D/B response	
		DF	Amplitude W/m <sup>2</sup> K	$\tau_{ie}$ [h]	Amplitude W/m <sup>2</sup> K	$\tau_{ii}$ [h]
Wall 1	0.048/0.408	0.270	0.08404	-8.831	4.3041	1.565
Wall 2	0.053/0.530	0.251	0.07836	-8.524	4.3382	1.231
Wall 3	0.068/0.770	0.205	0.06360	-7.478	4.3382	0.908
Wall 4	0.040/0.034	0.0196	0.11129	-6.761	0.8688	4.072
Wall 5	0.187/0.460	0.0038	0.02158	-8.237	1.2833	1.905
Wall 6	0.222/0.234	0.0032	0.01817	-8.288	0.9710	2.998
Homogenous wall	0.162/0.294	0.0021	0.01192	-20.548	2.2599	2.386

for harmonic oscillations of the exterior temperature with the period of 24 h, are summarized in Table 14.3. Results for the wall with homogeneous core, of the same total thermal resistance and capacity, are added for comparison.

It can be seen in Table 14.3 that for the same total resistance and heat capacity, the amplitude of the transmission heat flux response and its decrement factor decrease with the structure factor  $\varphi_{ie}$ . It is worth noticing that for configurations (5) and (6), which represent the type of configuration with thermal mass in the center, the value of  $DF$  is seventy to over eighty times lower than for configurations (1) through (3) and about six times lower from configuration (4). Configurations (1) and (2) have the insulation layer in the center and walls (3) and (4) have thermal insulation placed only on one wall side.

Correlations between the frequency responses and structure factors for building walls were examined by Kossecka (1999) for the set of 41 walls (selected to represent different groups of characteristic envelope assemblies with similar transient heat transfer properties) that were utilized for the development of the transfer function method calculation procedure, as presented in Harris and McQuiston (1988), Chapter 26 of the 1989 ASHRAE Handbook of Fundamentals. These correlations are represented in Fig. 14.3 by the plot of  $DF$  versus structure dependent time constant  $R_T C \varphi_{ie}$ . In general, it can be observed that the decrement factor decreases with  $R_T C \varphi_{ie}$ ;

- very rapidly, in the interval [0,10 h], from 1 to 0.5 approximately,
- less rapidly, in the interval [10 h, 30 h], from 0.5 to 0.1 approximately,
- above the  $R_T C \varphi_{ie}$  value of 30 h, it decreases very slowly.

The existence of such a correlation is not trivial, in light of a lack of a clear correlation between  $DF$  and the time constant  $R_T C$ . The nonlinear dependence of  $DF$  on  $R_T C \varphi_{ie}$  may be approximated by a smooth curve with good accuracy. The presented below formula for  $DF_{est}$ , gives a very good fit ( $r^2 = 0.985$  when transformed to the linear dependence):

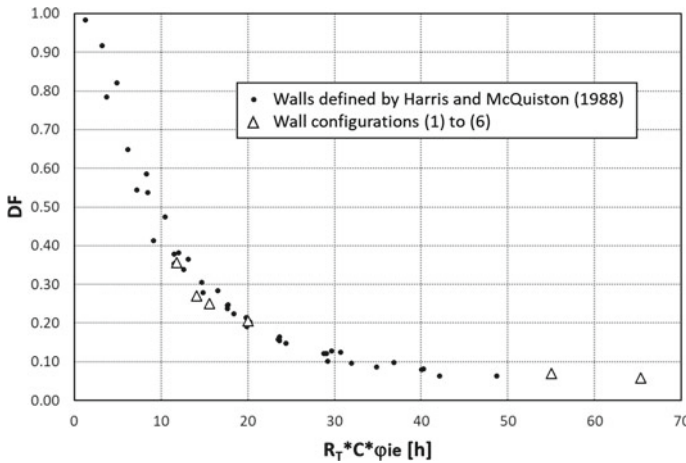


**Fig. 14.3** Relationship between decrement factor and structure dependent time constant  $R_T C \varphi_{ie}$

$$DF_{est}(x) = \frac{1}{\sqrt{1 + a x^b}}; \quad x = R_T C \varphi_{ie} \tag{14.20}$$

where:  $a = 0.014$  and  $b = 2.495$ .

Furthermore, as it can be seen in Table 14.3, amplitudes of the admittance response,  $D/B$ , are several times higher for walls (1), (2), (3), with massive concrete layers located at the inner side and comparatively high value of the structure factor  $\varphi_{ii}$ , than for walls (4) and (6), with insulation placed on the inner side and low value of  $\varphi_{ii}$  - Table 14.2. Wall (5), with thin insulation layer at the inner side, is an exception. It has almost as high a value of  $\varphi_{ii}$  as wall (2), but its admittance response amplitude is only 0.227 when for wall (2), it is 0.746.

Amplitudes of the heat flux responses to periodic temperature excitations depend on square roots of the products of  $k$ ,  $\rho$  and  $c_p$  (Carslaw & Jaeger, 1959; Shklover, 1961), which for light materials with low thermal conductivity, differ in order of magnitude from those for heavy materials with high thermal conductivity. The admittance response amplitude is sensitive to the values of  $\sqrt{k\rho c_p}$  for the innermost layers, with significant thickness.

### 14.5 Thermal Response of a Building Exposed to Periodic Temperature Changes

Accurate predictions of dynamic thermal performance of building envelopes is essential for control of the building’s energy demand, which, consequently, is critical for its interaction with the power grid. Depends on the complexity of the building

configuration, the analysis of its thermal response can be either based on approximate assessments using simple mathematical formulas (most cases of residential and small commercial buildings), or it may require an application of complex whole building numerical models. In the following section, a simplified analytical approach is discussed. For sake of demonstration how simplified analysis can be performed, let's consider a very simple model of a building in the form of a rectangular box, with walls identical to each other, exposed to the influence of the external temperature  $T_e$ . One-dimensional heat transfer through the walls is assumed. The building is ventilated, the air exchange velocity is constant in time. All other effects are neglected.

Let the external temperature  $T_e$  be a harmonic function of time, with angular frequency  $\omega$  and amplitude  $A_{T_e}$ . The steady-state periodic temperature  $T_i$ , is also a harmonic function of time with angular frequency  $\omega$ , but amplitude  $A_{T_i}$  and the time shift  $\tau_{T_i}$  with respect to the maximum of  $T_e$ :

$$T_e(t) = A_{T_e} e^{i\omega t}, \quad T_i(t) = A_{T_i} e^{i\omega(t + \tau_{T_i})} \quad (14.21)$$

The lower the value of the  $A_{T_i}/A_{T_e}$  ratio, the better the thermal stability of the system. Equation of the heat balance for this system has the following form:

$$C_V \frac{dT_i}{dt} = -S_w q_i - C_V n (T_i - T_e) \quad (14.22)$$

where:  $q_i$  is the heat flux across the internal surfaces of walls,

$S_w$  is the total surface area of the walls,

$C_V = \rho c_p V$  is the air volume thermal capacity and  $n$  [ $\text{h}^{-1}$ ] the air exchange frequency.

Solving Eq. (14.22) with respect to  $T_i$ , with  $q_i$  given by Eq. (14.18), the following expression is obtained:

$$T_i(t) = T_e(t) \frac{C_V n + \frac{S_w}{B(i\omega)}}{C_V [n + i\omega] + S_w \frac{D(i\omega)}{B(i\omega)}} \quad (14.23)$$

The response function  $1/B$  is in the numerator, whereas  $D/B$  is in the denominator, both multiplied by the wall area. Therefore, in general, amplitude of the temperature  $T_i$  increases with the amplitude of  $1/B$  and decreases with the amplitude of  $D/B$ . A simple recipe for the good thermal stability of this system is thus low response to the external temperature variations and high response to the internal temperature variations. Computed values of the amplitude ratio  $A_{T_i}/A_{T_e}$  and the time shift  $\tau_{T_i}$  calculated for walls (1)–(6), assuming room dimensions:  $4.5 \times 4.5 \times 2.7$ -m. and air exchange frequency  $n = 1$  [ $\text{h}^{-1}$ ], are presented in Table 14.4.

Results of the analysis shown in Table 14.4, for the simple building model, indicate that buildings having walls with massive concrete inside layers (structures 1, 2, 3) are stable. The amplitude ratio  $A_{T_i}/A_{T_e}$  for walls (1) through (3), with high values of

**Table 14.4** Amplitude ratio and time shift of the internal and external temperature oscillations for the one-room building with walls (1)–(6), as depicted in Fig. 14.1

Wall	$A_{Ti}/A_{Te}$	$\tau_{Ti}$
Wall 1	0.040	−2.878
Wall 2	0.041	−2.490
Wall 3	0.047	−1.996
Wall 4	0.222	−5.330
Wall 5	0.142	−2.087
Wall 6	0.184	−2.880
Homogenous wall	0.094	−2.101

the structure factor  $\varphi_{ii}$  and admittance response amplitude, is about 5.5 times lower than for wall (4) and about 4 times lower than for wall (6), with low values of  $\varphi_{ii}$  and  $D/B$  amplitude. Wall (5) is again an exception: comparatively high value of  $\varphi_{ii}$  does not guarantee a high value of the admittance response amplitude (Table 14.2) as well as low internal and external amplitude ratio (Table 14.3). Results presented in Tables 14.2 and 14.3 indicate that the high value of the internal admittance response amplitude of the external walls appears to be more important than the low value of the decrement factor for the transmission heat flux response. Modifications of the model, by adding interior massive walls and changing the air exchange velocity, have no effect on this general conclusion.

## 14.6 Impact of Wall Material Configuration on Dynamic Thermal Performance of Whole Buildings

It is a well-accepted common knowledge that thermal insulation, when installed in the building envelope can generate space conditioning energy savings. This fact is reflected in numerous building energy standards worldwide. However, it is not commonly understood that a placement of thermal insulation within building envelope and its configuration with thermally massive components plays important role as well. To analyze the influence of wall material configurations on their dynamic thermal performance and consequently, the whole building energy response, a series of whole building energy simulations is performed for a one-story residential ranch house. Six types of exterior walls, structures (1)–(6), as presented in Fig. 14.1, are considered.

The floor plan of the analyzed house is presented in Fig. 14.4, together with assumed material properties. This house has approximately 143 m<sup>2</sup> of the living area, around 123 m<sup>2</sup> of the exterior wall area, 8 windows, and 2 doors (one door is a glass slider; (its impact is included in modeling together with windows). The elevation wall area includes: 106 m<sup>2</sup> of the opaque wall area, 14.3 m<sup>2</sup> of the window area and 2.6 m<sup>2</sup> of the door area. Typical Meteorological Year data (TMY) for six following U.S. climates: Atlanta, Denver, Miami, Minneapolis, Phoenix, and Washington D.C.,

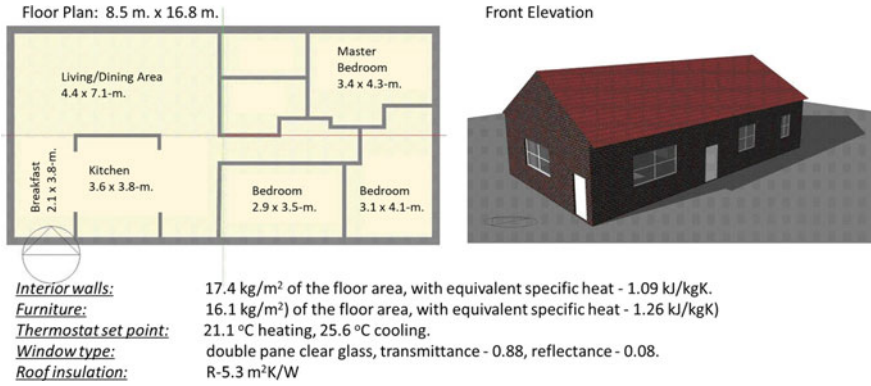


**Fig. 14.4** Schematic of the one-story ranch house used in the whole-building energy analysis

were used for the whole-building energy simulations. Resulted values of the annual heating and cooling energy demands are compared in Figs. 14.5 and 14.6., where best and worst performing wall material configurations were compared.

Formulas  $\% \Delta c_{max}$  and  $\Delta c_{max}$  show percent proportions and a difference between the worst performing (the highest cooling energy consumption) and best performing (the lowest cooling energy consumption) wall configuration in building cooling scenarios. Similarly, formulas  $\% \Delta h_{max}$  and  $\Delta h_{max}$  show percent proportions and a difference between the worst performing (the highest heating energy consumption) and best performing (the lowest heating energy consumption) wall configuration during building heating season.

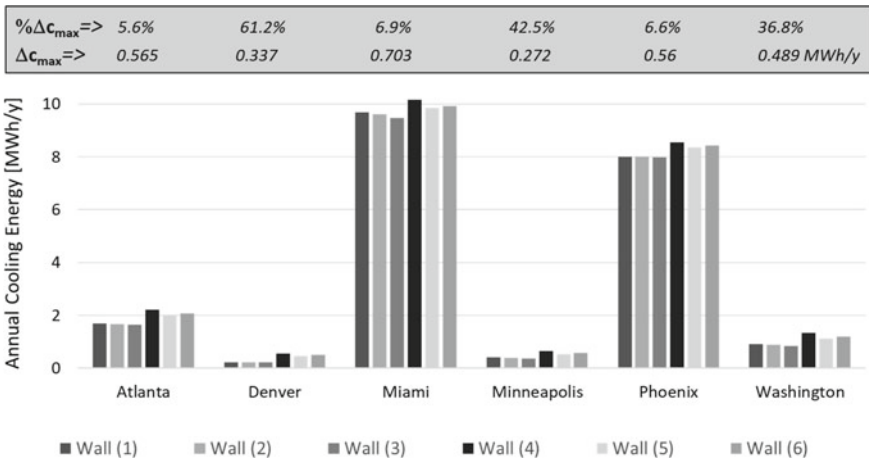


**Fig. 14.5** Annual cooling energy demands for the typical family ranch house with different types of exterior walls (in MWh per year)

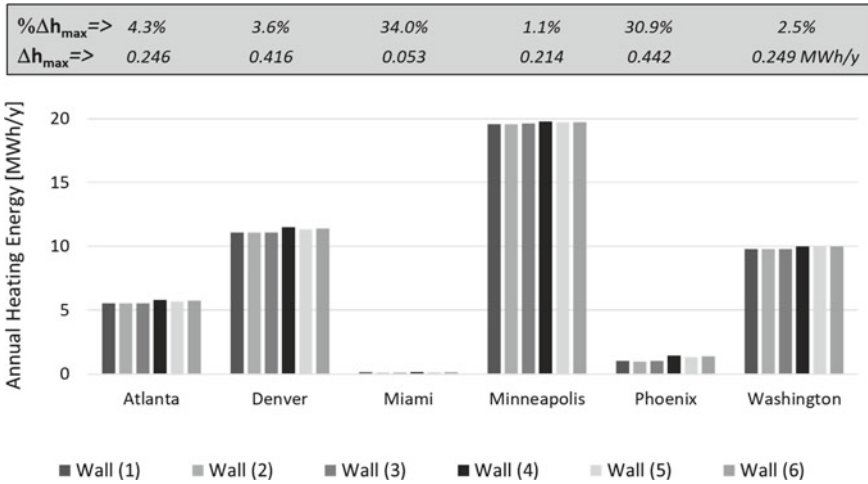


**Fig. 14.6** Annual heating energy demands for the typical family ranch house with different types of exterior walls (in MWh per year)

Results of the whole building dynamic modeling showed that walls containing thermally massive layers facing interior—cases (1), (2), (3), exhibit the best annual thermal performance for the climates considered. The lowest annual cooling energies are noticed for the wall configuration (3), where all the thermal mass is concentrated in its interior part of the wall. Similarly, wall configurations (1) and (2) generate the lowest heating energy demands, which are only slightly lower than for the wall case (3). In walls (1) and (2), insulation is located in the center of the wall and thermally massive layers are located on both sides. Wall (4), with insulation material concentrated on the interior side, generates the highest energy demands.

Figures 14.5 and 14.6 show that the maximum differences between total building space conditioning energies are for walls (3) and (4) for cooling, and (2) and (4) for heating. The highest differences in annual cooling energies are observed for Miami, Phoenix, and Atlanta climates. Please notice that the highest percent difference in annual cooling energies is for climatic conditions of Denver (61%), which means that significant proportional cooling energy savings are possible in the switch mountain climates in the case of optimized placement of thermal insulation and massive components within building envelopes. Analogously, the highest annual heating energy savings are available for climatic conditions of Phoenix and Denver, followed by Atlanta, Minneapolis, and Washington DC. In heating scenarios, potential annual energy consumption is less dependent on material wall configurations. The highest proportional heating energy savings are available for the wall configuration (2), for the Phoenix climate (30.9%). Practically, during performed whole building energy analysis, all three wall configurations (1), (2), and (3) yielded very similar annual heating energy predictions.

## 14.7 Conclusions

Analytical solution for the response of a simple building exposed to periodic temperature conditions indicates that the most effective wall assemblies are walls where thermal mass is in good contact with the interior of the building. These walls have high values of the structure factor  $\varphi_{ii}$  and the internal admittance heat flux response amplitude, that enter as parameter in the solution. A high value of the internal admittance response amplitude definitely improves the thermal stability of a building, expressed as the amplitude of internal temperature periodic oscillations, in response to the exterior temperature oscillations.

Whole building energy simulations were performed to predict annual heating and cooling energy demands for the one-story residential building. Results of the computer simulation lead to the conclusion that walls with massive internal layers, with high values of the structure factor  $\varphi_{ii}$ , show the best thermal performance for all U.S. climatic zones: minimum annual heating and cooling energy demand. Wall material configuration can significantly affect annual thermal performance of the whole building. There is the potential to save up to 11% of heating and cooling energy in U.S. residential buildings containing massive walls, only by optimization of the mass and insulation distribution in the walls.

## References

- ASHRAE *Handbook 1989: Fundamentals*; I-P Edition.
- Ashouri, M., Astaraei, F. R., Ghasempour, R., Ahmadi, M. H., & Feidt, M. (2016, August 05). Optimum insulation thickness determination of a building wall using exergetic life cycle assessment. *Applied Thermal Engineering*, *106*, 307–315. <https://doi.org/10.1016/j.applthermaleng.2016.05.190>.
- Asan, H. (2006). Numerical computation of time lags and decrement factors for different building materials. *Building and Environment*, *41*(5), 615–620.
- Aste, N., Angelotti, A., & Buzzetti, M. (2009). The influence of the external walls' thermal inertia on the energy performance of well insulated buildings. *Energy and Buildings*, *41*(11), 1181–1187.
- Axaopoulos, I., Axaopoulos, P., Panayiotou, G., et al. (2015). Optimal economic thickness of various insulation materials for different orientations of external walls considering the wind characteristics. *Energy*, *90*, 939–952.
- Balaji, N. C., Mani, M., & Venkatarama Reddy, B. V. (2019, January). Dynamic thermal performance of conventional and alternative building wall envelopes. *Journal of Building Engineering*, *21*, 373–395. <https://doi.org/10.1016/j.jobee.2018.11.002>.
- Bojić, M. L., & Loveday, D. L. (1997). The influence on building thermal behavior of the insulation/masonry distribution in a three-layered construction. *Energy and Buildings*, *26*(2), 153–157.
- Carlsaw, H. S., & Jaeger, J. C. (1959). *Conduction of heat in solids*. Oxford University Press.
- Childs, K. W. (1980). *Appraisal of the m factor and the role of building thermal mass in energy conservation*. Technical Report, DOE Oak Ridge National Laboratory, Oak Ridge, TN, USA.
- Clarke, J. A. (1985). *Energy simulation in building design*. Adam Hilger Ltd.



- Corrado, V., & Paduos, S. (2016). New equivalent parameters for thermal characterization of opaque building envelope components under dynamic conditions. *Applied Energy*, 163(February), 313–322.
- Cuce, E., Cuce, P. M., Wood, C. J., & Riffat, S. B. (2014). Optimizing insulation thickness and analysing environmental impacts of aerogel-based thermal superinsulation in buildings. *Energy and Buildings*, 77, 28–39.
- Daouas, N. (2011). A study on optimum insulation thickness in walls and energy savings in Tunisian buildings based on analytical calculation of cooling and heating transmission loads. *Applied Energy*, 88(1), 156–164.
- Feng, W., Huang, J., Lv, H., et al. (2019). Determination of the economical insulation thickness of building envelopes simultaneously in energy-saving renovation of existing residential buildings. *Energy Sources, Part a: Recovery, Utilization, and Environmental Effects*, 41(6), 665–676.
- Ge, K., & Baba, F. (2017, October). Effect of dynamic modeling of thermal bridges on the energy performance of residential buildings with high thermal mass for cold climates. *Sustainable Cities and Society*, 34, 250–263.
- Gregory, K., Moghtaderi, B., Sugo, H., & Page, A. (2008). 2008, Effect of thermal mass on the thermal performance of various Australian residential constructions systems. *Energy and Buildings*, 40(4), 459–465.
- Harris, S. M., & McQuiston, F. C. (1988). A study to categorize walls and roofs on the basis of thermal response, *ASHRAE Transactions*, 94(2).
- Hasan, A. (1999). 1999 Optimizing insulation thickness for buildings using life cycle cost. *Applied Energy*, 63(2), 115–124. [https://doi.org/10.1016/S0306-2619\(99\)00023-9](https://doi.org/10.1016/S0306-2619(99)00023-9)
- ISO. (1994). Standard ISO 9869. International Standard, Thermal Insulation - Building elements - In situ measurement of thermal resistance and thermal transmittance. International Organization for Standardization, Geneva, Switzerland.
- ISO 2007, Standard ISO 13786:2007: Thermal Performance of Building Components—Dynamic Thermal Characteristics—Calculation Methods. International Organization for Standardization, Geneva, Switzerland.
- ISO 2005, Standard, ISO 13792:2005: Thermal Performance of Buildings—Calculation of internal Temperatures of a Room in Summer without Mechanical Cooling—Simplified Methods. International Organization for Standardization, Geneva, Switzerland.
- Kalinovic, S., Djokovic, J., Nikolić, R., & Hadzima, B. (2019). Calculation of the thermal dynamic performance of the residential buildings' walls. In *13th International Conference Quality Production Improvement - QPI 2019*, Poland, 5–7 June 2019, (Vol. 1, pp. 212–221). Warsaw, Poland: Sciendo.
- Košny, J., & Desjarlais, A. O. (1994). Influence of architectural details on the overall thermal performance of residential wall systems. *Journal of Thermal Insulation and Building Envelopes*, 18, 53–69.
- Košny, J., & Christian, J. E. (1995, December). Steady-State thermal performance of concrete masonry unit wall systems—ASHRAE, BETEC, U.S.DOE VI thermal envelope conference, Clearwater, Florida.
- Košny, J., Kossecka, E., Desjarlais, A. O., & Christian, J. E. (1998a, December). Dynamic thermal performance of concrete and masonry walls. In *Proceedings of DOE, ASHRAE, ORNL Conference -Thermal Envelopes VII*, Clearwater, Florida, USA.
- Košny, J., Christian, J. E., Desjarlais, A. O., Kossecka, E., & Berrenberg, L. (1998a). The performance check between whole building thermal performance criteria and exterior wall; Measured clear wall R-value, thermal bridging, thermal mass, and air-tightness, *ASHRAE Transactions*, 104(2).
- Košny, J., & Kossecka, E. (2002). Multi-dimensional heat transfer through complex building envelope assemblies in hourly energy simulation programs. *Energy and Buildings*, 34(5), 445–454.

- Košny, J., Asiz, A., Smith, I., Shrestha, S., & Fallahi, A. (2014, April). A review of high R-value wood framed and composite wood wall technologies using advanced insulation techniques. *Energy and Buildings*, 72, 441–456.
- Košny, J., Miller, W. A., Yarbrough, D., Kossecka, E., & Biswas, K. (2020, September 30). Application of phase change materials and conventional thermal mass for control of roof-generated thermal loads. Applied Sciences, Special Issue Phase Change Materials in Buildings. *Applied Science*, 10(19), 6875. <https://doi.org/10.3390/app10196875>.
- Kossecka, E. (1992). Heat transfer through building wall elements of complex structure. *Archives of Civil Engineering*, 38(1), 117–126.
- Kossecka, E. (1993). Problem of the measured R-value error estimation. *Archives of Civil Engineering*, 39(4), 413–427.
- Kossecka, E. (1996). The effect of structure on dynamic thermal characteristics of multilayer walls. *Archives of Civil Engineering*, 42(3), 351–369.
- Kossecka, E. (1998). Relationships between structure factors, response factors and z-transfer function coefficients for multilayer walls. *ASHRAE Transactions* 104(1).
- Kossecka, E. (1999). Correlations between structure dependent and dynamic thermal characteristics of building walls. *Journal of Thermal Insulation and Building Science*, 22, 315–333.
- Kossecka, E., Košny, J., & Christian, J. E. (1994). A simple algorithm for determining the thermal resistance of a wall. *Building Research Journal*, 3(1), 57–66.
- Kossecka E., & Košny, J. (1996). Relations between structural and dynamic thermal characteristics of building walls. In *Proceedings of 1996 International Symposium of CIB W67 "Energy and Mass Flows in the Life Cycle of Buildings"*. Vienna, 4–10 August (pp. 627–632).
- Kossecka, E., & Košny, J. (1997). Equivalent wall as a dynamic model of the complex thermal structure. *Journal of Thermal Insulation and Building Envelopes*, 20, 249–268.
- Kossecka, E., & Košny, J. (2002). Influence of insulation configuration on heating and cooling loads in a continuously used building. *Energy and Buildings*, 34(4), 321–331.
- Kusuda, T. (1969). Thermal response factors for multi-layer structures of various heat conduction systems. *ASHRAE Transactions*, 75(1), 241–271.
- Kusuda, T. (1977). Fundamentals of building heat transfer. *Journal of Research of the National Bureau of Standards (NIST)*, 82(2), September–October.
- MEC. (1995). Council of American Building Officials “Model Energy Code.”
- Ozel, M. (2011). Thermal performance and optimum insulation thickness of building walls with different structure materials. *Applied Thermal Engineering*, 31(17–18), 3854–3863. <https://doi.org/10.1016/j.applthermaleng.2011.07.033>
- Peavy, B. A, Powell, F. J., & Burch, D. M. (1973). Dynamic thermal performance of an experimental masonry building, National Bureau of standards, Building Science Series #45, Library of Congress Catalog Card Number. 72–600347. Washington DC, July.
- Ramin, H., Hanafizadeh, P., & Akhavan-Behabadi, M. A. (2016). Determination of optimum insulation thickness in different wall orientations and locations in Iran. *Advances in Building Energy Research*, 10(2), 149–171.
- Saafi, K., & Daouas, N. (2018). A life-cycle cost analysis for an optimum combination of cool coating and thermal insulation of residential building roofs in Tunisia. *Energy*, 152, 925–938.
- Sherman, M. H, & Grimsrud, D.T. (1980, October). Measurement of infiltration using fan pressurization and weather data, LBL-10852, Lawrence Berkeley National Laboratory.
- Shklover, A. M. (1961). *Heat transfer at periodic thermal conditions*. Gosnizdat. [in Russian].
- Tang, D. L., Li, L. P., Song, C. F., et al. (2015). Numerical thermal analysis of applying insulation material to holes in hollow brick walls by the finite-volume method. *Numerical Heat Transfer, Part A: Applications*, 68(5), 526–547.
- Urban, B., Elliott, D., Shukla, N., Fallahi, A., & Košny, J. (2013). Thermal mass effect of solid block aerated autoclaved concrete. In *Proceedings of 2nd Central European Symposium on Building Physics, CESBP*, September, Vienna, Austria

- Van Geem M. G., Fiorato A. E., & Musser, D. W. (1982). Calibrated hot-box tests of thermal performance of concrete walls. In *Proceedings of the DOE, ASHRAE, ORNL Conference—Thermal Performance of the Exterior Envelopes of Buildings*, December, Clearwater, Florida, USA.
- Yuan, J., Farnham, C., & Emura, K. (2017). Optimum insulation thickness for building exterior walls in 32 regions of China to save energy and reduce CO<sub>2</sub> emissions. *Sustainability*, 9(10), 1711–1718.

# Chapter 15

## Thermal Efficiency of Insulation in Building Structures—The Impact of Thermal Bridging



Jan Kośny and David W. Yarbrough

**Abstract** In the construction industry, thermal insulations are construction materials used to reduce heat transfer between materials or structures of different temperatures. Theoretically, the exterior building skin should perform a variety of different roles that include keeping the exterior climate outside by limiting the transfer of heat, moisture, and air, which helps with maintaining comfortable interior conditions. A particular role is reserved here for thermal insulation, which is responsible for minimizing the heat exchange between the exterior environment and the interior space of a building. Mitigation of heat transport is the primary reason why thermal insulation materials are being used today in buildings. The use of thermal insulation materials greatly affects the following:

- Energy consumed for heating and/or cooling inside the building or houses (HVAC design)
- The thermal and hygrothermal performance of specific envelope and construction materials or structures that require thermal insulation such as opaque walls and roofs, damp-proof courses, waterproof membranes, related joints or sealants, and others.

In these applications, thermal insulation is a key component of the building interior fabric or exterior envelope. Often, additional functions provided by thermal insulation include: a visual and daylight connection to the outdoors, reduction of noise transmission, support of structural loads, and aesthetically pleasing appearance on both sides of building envelope. Furthermore, a number of configurations of thermal insulation and heat conducting components, generate thermal bridging effects in various parts of the building skin and architectural interfaces. They can not only significantly impact thermal performance of building envelopes, but also their long-term durability.

---

J. Kośny (✉)  
University of Massachusetts Lowell, Lowell, MA, USA  
e-mail: [Kosny\\_Jan@uml.edu](mailto:Kosny_Jan@uml.edu)

D. W. Yarbrough  
R&D Services, Inc., Watertown, TN, USA

## 15.1 Introduction

Thermal insulation, together with structural and finish elements, as well as moisture/air transport barriers are key components of building envelopes. Theoretically, the exterior building envelopes should perform a variety of different roles including keeping the exterior climate outside by limiting the transfer of heat, moisture, and air, which helps with maintaining comfortable interior conditions. A particular role is reserved here for thermal insulation, which is responsible for minimizing the heat exchange between the exterior environment and the interior space of a building. Additional functions provide, a visual and daylight connection to the outdoors, limit noise transmission, support of structural loads, and aesthetically pleasing appearance on both sides. Although building envelopes are usually effective in meeting these requirements, there are situations where they do not perform adequately. Shortcomings in thermal performance are often exhibited by excessive heat transfer (in and out) and unwelcome air or moisture transport across the building envelope that can lead to durability problems and increased energy consumption, as well as to poor thermal comfort within the occupied space. Sometimes, the presence of a thermal bridge results in discoloration on either the interior or exterior surface of the building envelope.

The effectiveness of thermal insulation in resisting the heat flow across building envelopes, in addition to the general design, depends also on how and where it is installed. The overall R-value of a wall, floor, or ceiling is usually notably different from the nominal R-value of the insulation itself, because heat flows more readily through beams, studs, joists, and other building materials, in a phenomenon known as thermal bridging. In addition, thermal insulation that, in framed constructions, fills building cavities densely enough to reduce air flow, can also reduce convective heat losses. While common cases of poor building envelope performance are associated with inadequate thermal insulation levels, other cases often occur because of construction imperfections, such as discontinuities in the thermal insulation or air barrier systems, compressed insulation, and air-leakage sites. Furthermore, discontinuities in the thermal insulation are often associated with a penetration of insulation by conductive structural members or installation members.

During the last century, numerous wall technologies have been introduced. Some of them are complex three-dimensional networks of structural components and thermal insulation. Moreover, building structural systems are advancing and every year a variety of new materials are introduced. Consequently, buildings often become unforgiving of design errors or assembly imperfections. At the same time, the overall energy efficiency of a building depends strongly on the thermal performance of exterior envelope elements (walls, roofs, windows), including the local heat losses that can occur around the envelope elements where they are penetrated by heat conducting building components. These areas of intense local heat flow, commonly known as thermal shorts or thermal bridges, can have a significant influence on how effective thermal insulation is, and consequently, they impact the overall thermal performance of the building envelope.

With the introduction of high-performance insulations, as well as advanced structural and finish materials, a single change in a building envelope configuration may compromise the local thermal performance and durability of exterior envelopes. That is why more and more frequently, only optimized combinations of structural subsystems and insulation materials are specified. In today's buildings, thermal bridges are responsible for a significant number of thermal performance and durability problems.

Thermal bridges, thermal shorts, or cold bridges (different names are used by building professionals in different parts of the world), are understood as unwanted paths for heat flow that bypass the envelope's thermal insulation. Often this happens when a heat conducting material is placed in the direction of heat flow and parallel to the thermal insulation, which yields an easy pathway for heat flow across the envelope. The most common forms are probably within the eyesight of every reader of this chapter: for example, concrete or metal elements crossing the exterior building skin, structural framing members, perimeters of building openings, and architectural connections.

This chapter discusses several configurations of thermal insulation and heat conducting components, which generate thermal bridging, and which can be spotted at various parts of the building skin and architectural interfaces. In order to minimize the resulting energy and durability problems, the eventual engineering solutions need to focus on designs that minimize thermal bridges and the resulting heat losses or gains, and, in many cases, to limit the risk of condensation. Sometimes, these measures occur in parallel with air-sealing efforts. Furthermore, to be widely implemented, the reduction of thermal bridges should be simple, inexpensive, and easy to apply. This chapter also discusses analytical and numerical methods used in the analysis and elimination of thermal bridges. In addition, major building standards regulating this subject are listed.

## **15.2 Definition of Thermal Bridges and Their Common Consequences**

In general, a thermal bridge is defined as a location within the building envelope or architectural component, which exhibits considerably more heat flow than surrounding areas. Thermal bridging refers to the loss or gain of energy by conduction through elements that "bridge" the insulation in building enclosure. While it is a common knowledge that most structural materials contribute to thermal bridging, it is good to remember that, in reality thermal shorts occur much more often than just when a conductive element passes through or bypasses a thermal insulation barrier. Considering that in building components with temperature gradients, heat flow has multidimensional character and taking into account the complexity of today's building envelopes, these thermal pathways often require complex three-dimensional numerical analysis.

The consequences of poorly selected connections between envelope components can produce severe thermal bridging. Taking into account that in some work assemblies, interface details can have an impact of as much as 50% of the overall wall area, the whole-wall R-value can be as much as 40% less than what is measured for the clear-wall section—see: Kośny and Desjarlais (1994), Christian and Kośny (1995). In addition, local heat losses through wall interface details may be twice that estimated by simplified design calculations that focus only on the clear wall. Poor interface details also may lead to excessive condensation of water that causes stains and dust markings on the interior finish, thus revealing thermal shorts in an unsightly manner. Moist surface areas can accelerate the propagation of molds and mildews, which can lead to degraded indoor air quality—Hens (2008). In addition, thermal bridging affects the dynamic thermal performance of a building—Kossecka and Kośny (2002).

It is good to remember that the exterior skin of a building provides a separation between the interior space and the exterior environment. In a perfect scenario, this separation should be as continuous as possible. This obligation equally applies to the building thermal insulation as well as to the air and moisture barriers. In the case of discontinuities in the thermal insulation layer, thermal bridges provide unwanted paths of least resistance for heat to move across the building envelope. Unwanted effects of thermal bridging include:

- Increased energy consumption; Due to the thermal outflow at the thermally bridged areas, heat is lost from every room (in heating dominated climates) or unwanted heat gains (in cooling dominated climates) resulting in a significant increase in whole-building energy consumption.
- Mold growth; In cold climates, interior wall temperatures can drop well below the dew point. This leads to condensation, deterioration of plaster and paintwork and conditions for harmful mold formation. Finally, if there is sustained exposure to condensation, a building can experience serious fungi grow that leads to health hazards.
- Compromised living space thermal comfort; Cold surface temperatures cause uncomfortable living space for occupants.

In most of buildings, even high-performance buildings, the existence of limited thermal bridging is unavoidable, mostly for structural reasons. However, good design and construction can reduce the number of thermal bridges and notably mitigate their effects.

### **15.3 Types of Thermal Bridges and Most Common Locations**

The most common flaws in building envelopes are discontinuities in the insulation layer or air/moisture barriers. These problems are caused by improper design, incorrect assembly, or occur over the building's lifetime when the design does not

provide adequate consideration of changes due to wind pressures and vibrations. Common imperfections in the thermal insulation barrier include both discontinuities in the insulation layer, installation of insulation in air cavities allowing air circulation around or across the insulation, compression of insulation, and other arrangements which decrease effectiveness. Envelope performance is then compromised by the increased heat-transfer rate. These assemblies usually show increased potential for moisture-related durability issues. Keep in mind that, local condensation and mold formation can be often caused by structural thermal bridges—Hens (2008), Trechsel and Bomberg (2009). For example, due to the compromised performance of thermal insulation, during the winter, interior temperatures of the adjacent interior space can drop well below the dew point. This may lead to water condensation on the interior surface and sometimes to deterioration of the interior finish. Considering common electrical penetrations in the exterior walls, plumbing and electrical line penetrations, and uninsulated spaces associated with space conditioning, it is very likely that water condensation can take place inside the envelope cavities causing decrease in the thermal performance of thermal insulation. Wet insulation, for example, conducts heat by as much as ten times the design value for dry insulation—Langlais et al. (1983), McFadden (1988), Kumaran (2006). If there is sustained exposure to water condensation inside the building envelopes as well as on the internal surfaces, the building may become a subject to serious material deterioration.

### ***15.3.1 Thermal Bridges Generated by Building Geometry and Architectural Details***

Thermal bridges most commonly occur at locations such as corners, overhangs, wall/floor, wall/roof, wall/internal interfaces, and window or door perimeters. Component connections are often high-strength, high-conductivity elements that serve to hold or connect building structural or architectural components. Some well-known examples include balconies, wall connections with terraces, perimeters of wall openings, window and curtain-wall mullions. Geometric thermal bridges do not form literal thermal shorts in the same way as, for example, construction thermal bridges. For instance, intense heat transfer can occur in the areas where nominal insulation thickness and insulation continuity are well maintained. Usually, geometric thermal bridges can be found in locations where the area of the external building surface is significantly different from the corresponding internal surface area. Identifiable thermal bridge effects occur at corners which accentuate two-dimensional heat-flow paths. As depicted in Fig. 15.1, some corner constructions may also lead to discontinuities in the envelope insulation and/or the air barrier. Geometric thermal bridges are often unavoidable. However, the energy impact of geometric thermal bridging increases with the complexity of the building form. Therefore, from the thermal and energy standpoint, as well from a long-term durability perspective, it is good to keep the building form as simple as possible.



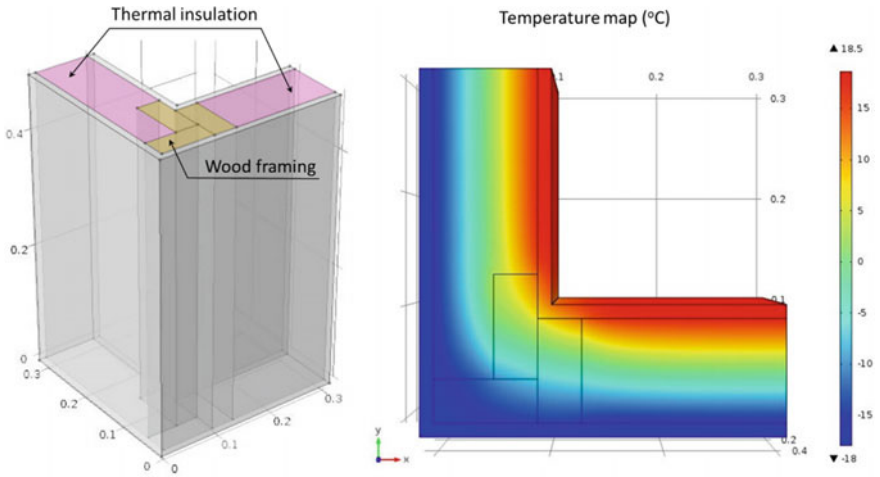


Fig. 15.1 Thermal insulation discontinuity in the corner design using wood studs

### 15.3.2 Thermal Bridges Characteristic of Building Materials and Construction Subsystems

Thermal bridging from heat flow through non-uniform construction elements occurs in two or three dimensions. These thermal bridges are localized and repetitive along the length of the structure. Examples of this type of thermal bridge is provided by metal connectors in concrete sandwich panels as shown in Fig. 15.2 and small connectors in curtain walls. In high-performance buildings with thick foam insulation installed to provide high R-value walls or roofs, the foam sheathing is often connected

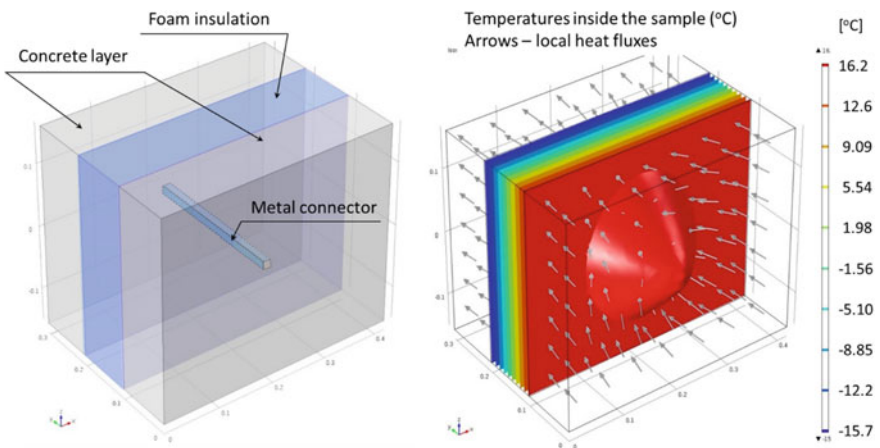
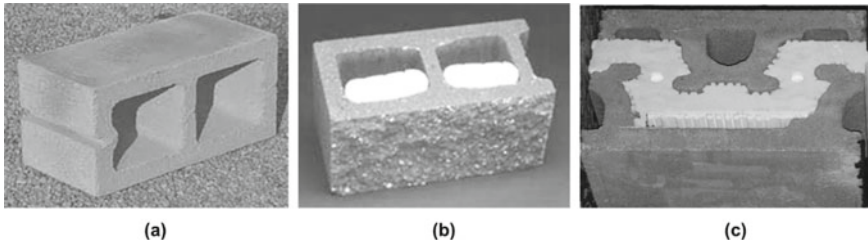


Fig. 15.2 Thermal bridge from metal connector used in concrete-foam-concrete panel



**Fig. 15.3** Concrete Masonry Units (CMUs)—Example of uninsulated concrete block (a), Ineffective- thermally bridged (b) and effective—Continues (c) thermal insulation inserts

to the structural substrate using long and relatively thick metal connectors. In addition to being expensive, these connectors often seriously compromise the overall system thermal and hygrothermal performance—Kośny et al. (2013). In longer-term, these thermal shorts often cause durability problems, which are commonly reported for these location, and which are typically caused by local water vapor condensation on thermally bridged cold-metal surfaces.

Insulated masonry units are a very good example of the system composition/design related thermal bridges. As depicted in Fig. 15.3, insulated concrete masonry units may have different foam insert designs, but high thermal conductivity concrete bridges remain due to two or three concrete webs joining the external and internal concrete skins. In that light, a concrete block filled with thermal insulation may still exhibit thermal bridging, resulting in effective thermal performance not very much improved, comparing to the concrete unit with empty cores. However, this thermal bridge effect can be reduced with a usage of interlocking inserts that create a continuous layer of insulation.

### 15.3.3 Structural Thermal Bridges Due to Construction

Structural thermal bridges due to construction are regularly spotted in buildings. This type of local thermal bridge is not only the easiest type to recognize, but also easy to comprehend and visualize. Construction thermal bridges occur wherever there is a material or component that conducts heat significantly better than thermal insulation and this material passes through the thermal insulation layer. Structural thermal bridging is usually associated with components like steel or concrete, combined with discontinuities in the thermal insulation layer.

Some examples of heat flow paths that result from a local design on the building structure:

- Reinforced concrete or steel frame beams and columns
- Roof rafters or floor joists that pass through the thermal envelope
- Wood, concrete, or metal framing members crossing the thermal insulation zone

- Cantilevered structures passing through or anchored in the thermal envelope
- Lintels and headers that interrupt envelope thermal insulation
- Structural connectors between metal-foam-metal sandwich panels.

Construction thermal bridges should be recognized and avoided as much as possible or mitigated by a careful design. Keep in mind that any construction thermal bridges may notably compromise local thermal and hygrothermal performance and contribute to the building energy use.

Figure 15.4 shows the wall-floor intersections for the cases of a light-gauge steel framed assembly, where the metal I-beam penetrates the vertical-wall insulation, significantly increasing the heat transmission. Significant disturbances in temperature fields can be observed in the case of the light-gauge steel wall-floor intersections. The floor-wall connections are often the site of significant thermal bridging when the metal floor joists, or concrete floor slabs pass through the wall insulation layer. The easiest fix for this problem is a usage of a continuous layer of external thermal insulation. In the case of building retrofits, a pillow of spray foam is also often used where the floor joists meet the wall bond beam (floor-wall intersections). It is not a perfect solution, but it helps in cutting thermal shorts, as well as reducing air movement through this detail.

The wall-floor intersections are not the only common locations of the construction related thermal bridges. The wall-roof connection is listed in engineering literature as another common location for thermal shorts and air leakage paths due to discontinuities between the wall and roof thermal and air or moisture barriers. In addition to discontinued thermal insulation, the wall air and moisture barriers often do not consistently extend to the roof deck level, and the roof membrane is not always sealed to the impermeable materials in the wall. Instead, the membrane is frequently turned up at the roof edge, leaving a discontinuity in the envelope air barrier. Depending on

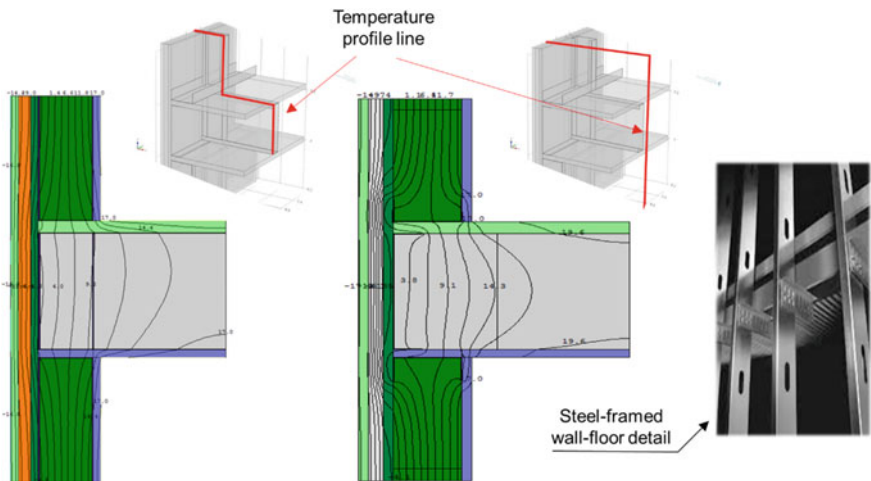


Fig. 15.4 Thermal bridge in wall-floor intersections in the case of steel framing

the building envelope technology, more or less complex detailing and installation of continuous thermal and air/moisture barriers are necessary.

Window-wall perimeters are associated with a number of probable thermal defects including highly conducting connectors/attachments, existing paths for air and moisture leakage, discontinuities in thermal insulation and insulation compression. Also, because of a very limited space there, there are also often observed cases of missing insulation or insulation displacement around the window frames, as well as a placement of the window thermal breaks in the way that air can easily bypass. Another common mistake is assembly design in which the width of the window frame exposed to the outdoors is greater from the width exposed to the indoors. In cold climates, the greater area for heat loss to the exterior air causes the inner frame to be cold, increasing the potential for local condensation.

In commercial building, the mullions of curtain walls have long been considered as key sources of thermal shorts associated with the installation of windows. This comes from the fact that most of curtain wall frames are made of extruded aluminum which is about four times more conductive than steel and couple hundred more than wood. Mullions usually connect the exterior surfaces of the building enclosure to the interior, creating a significant thermal bridge. A variety of thermal breaks (added thermal insulation crossing the heat flow paths), which are typically 1–2 cm thick inserts made of less conductive plastic foam or rubber, have become a characteristic component in modern curtain walls. These thermal breaks are typically located between the face plate and the structural part of the mullion, the rail, in line with the glazing pocket. Sometimes thermal insulation can be added along the backside of the spandrel panel.<sup>1</sup> This type of assembly keeps interior and exterior sides of the mullion rail well thermally separated; NIBS (2012).

### ***15.3.4 Combined Thermal Bridges***

In many cases, geometric thermal bridges also include an element of construction thermal bridging. For example, an external wall corner while being a geometric thermal bridge may also have structure creating construction thermal bridging. Similarly, ground floor and external wall junctions often involve a degree of construction thermal bridging. Very good examples of combined thermal bridges are corners with conducting studs or wall intersections with internal partitions. Figure 15.5 shows construction of the corner using light gage steel studs as structural members. In this case, increased heat flow through this architectural detail is caused by the heat transfer through the metal studs, as well as by the corner shape effect (different heat exchange areas on the interior and exterior surfaces).

---

<sup>1</sup> [http://www.forster-profile.ch/fileadmin/media/forster-profile/documents/Flyers/938366\\_curtain\\_walls\\_thermal\\_break.pdf](http://www.forster-profile.ch/fileadmin/media/forster-profile/documents/Flyers/938366_curtain_walls_thermal_break.pdf).

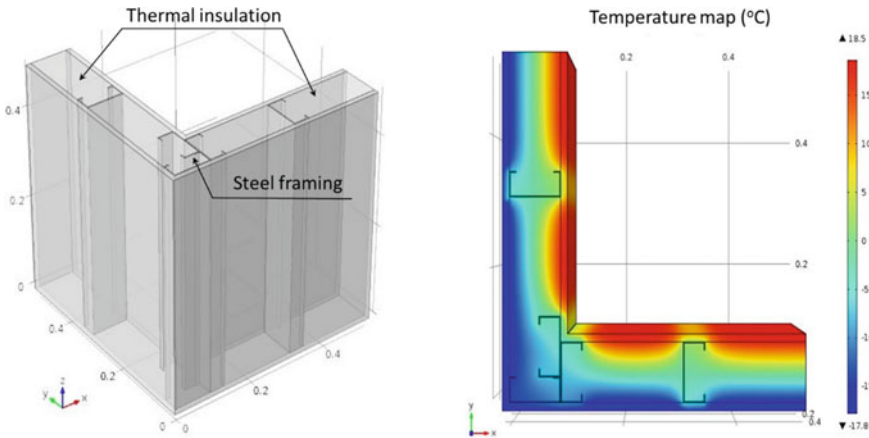


Fig. 15.5 Thermal bridge in corner with light-gauge steel framing

## 15.4 Thermal Efficiency of Insulation in Thermally Bridged Systems

R-values or U-values have been used for decades as measures of the thermal performance of building envelope components. The R-value depends on the type of insulation, its thickness, temperature and density. In perfectly designed building envelope applications with continuous layers of thermal insulation, R-values of the individual layers need only to be summed, when determining the R-value. However, in real life this is not the case. The continuity of thermal insulation is often broken by penetrating conductive structural materials or connectors. From the envelope designer's perspective, a thermal bridge is an element or location with missing thermal insulation, insufficient insulation, or reduced insulation performance, relative to adjacent areas of the thermal envelope. To better understand the interactions of different building envelope components the Whole-Wall Thermal Analysis Methodology was introduced by Košný and Desjarlais (1994). The "Whole-Wall R-value Procedure" has been used to estimate the opaque wall thermal performance, independently of a type of a wall system and construction materials.

The following set of thermal performance terms were introduced at that time:

- *Center-of-cavity R-value*: In-series sum of wall material R-values calculated at a point in the center of a wall cavity. This R-value does not include framing materials.
- *Clear-wall R-value*: R-value for the wall area containing only insulation and necessary framing materials for a region with no windows, corners, or connections between other envelope elements such as roofs, foundations, and walls.
- *Wall interface details*: A set of common structural connections between the exterior wall and other envelope components, such as wall/wall (corners), wall/roof,

wall/floor, window header, window sill, door jam, door header, and window jamb, that make up a representative residential wall.

- *Whole-wall R-value*: R-value estimation for the whole opaque wall including the thermal performance of the “clear wall” area with insulation and structural elements and typical envelope interface details, including wall/wall (corners), wall/roof, wall/floor, wall/door, and wall/window connections.

In the case of wood and steel framed constructions, there have always been many disagreements regarding thermal calculation methods, definitions used by building or energy standards, or design-required representative configurations. In both technologies, framing members represent significant thermal bridges compromising nominal thermal performance of the cavity insulation. That is why it is so important to correctly evaluate the amount of framing and its thermal impact on the surrounding area. As denoted in Eq. (15.1), the framing factor “ $f$ ” is expressed as a percent of the total wall area, which is occupied by the framing members. It is widely used today in experimental and theoretical performance analysis, as well as it is referenced in building code requirements.

$$f = \left[ 1 - \frac{R_{cw}}{R_n} \right] \times 100\% \quad (15.1)$$

where:  $R_{cw}$ —clear wall R-value and  $R_n$ —center of cavity nominal R-value.

Traditionally, in hot-box testing of wood-framed walls, the framing factor has been between 10 and 14%. In practice, however, the framing factor may be much larger. According to the reports prepared by Enermodal Engineering for the California Energy Commission (CEC) and ASHRAE, residential walls in California have an average framing factor of 27%. A similar study performed by ASHRAE in 2003 found an average framing factor of 25% for all U.S. residential buildings—see: Carpenter and Schumacher (2003), CEC (2001A), CEC (2001B).

The experimental and numerical analysis focused on the impact of the framing installation intensity on the overall wall thermal performance in wood and steel-framed walls was performed by Košny et al. (2007a). In addition, consequences of the installation imperfections in cavity insulation were investigated from the thermal perspective. A series of the hot-box tests and computer simulations were conducted for wall assemblies representing current residential construction practice in North America with 24% and 27% framing factors. It was concluded that center-of-cavity R-values are significantly higher than the measured clear-wall R-values. Furthermore, it was found that wood-frame walls are more sensitive than steel structures to imperfections in the wall-cavity insulation.

The second group of technologies, where thermal performance of insulation is often compromised by the system-design-based thermal bridging are concrete sandwich applications and masonry units. A large variety of new designs, higher performance insulations, as well as low-conducting structural connectors, available for production of these technologies can enable introduction of new products, where thermal insulation can be more effectively used.

Because thermal insulation inserts are always most expensive components of concrete masonry units (CMUs), knowing the fraction of thermal insulation that really works and affects the CMU's thermal performance is very useful. That is why Thermal Efficiency (TE) of insulation in CMUs was introduced by Kosny and Christian (1995). It is important to effectively use thermal insulation. There are available many masonry technologies containing several types of interstitial insulation inserts. Very often, if thermal resistance of used insulation and the increase of wall R-value (caused by this insulation) are compared, the actual increase of the wall thermal resistance is much lower from a nominal R-value of used insulation. This fact shows that thermal insulation must have been used in an ineffective way, with hidden thermal shorts causing undesired heat transfer.

The method of estimating TE value is based on comparison of R-values of the insulated ( $R_i$ ) and uninsulated ( $R_u$ ) CMUs, each having the same face area  $F_a$  (front/back side surface). The equivalent R-value of the insulation inserts ( $R_e$ ) can be calculated for a layer of insulation material having the same face surface area  $F_a$  as the analyzed CMU, and containing the same volume of thermal insulation  $V_{ins}$ , which is used to insulate this CMU. Therefore, TE can be expressed by the following equation:

$$TE = \frac{R_i - R_u}{R_e} 100\% \quad (15.2)$$

where:

$R_i$ —R-value of insulated CMU,

$R_u$ —R-value of uninsulated CMU.

$R_e$ —equivalent R-value of insulation material used in CMU.

Equivalent R-value of insulation material used in CMU— $R_e$  can be computed using the following formula:

$$R_e = \frac{d_e}{k_e} \quad (15.3)$$

where:

$d_e$ —equivalent thickness of the insulation material.

$k_e$ —thermal conductivity of the insulation material.

To calculate the equivalent thickness of used insulation  $d_e$ , the insulation volume  $V_{ins}$  is divided by the face surface area  $F_a$ , of the CMU. Equivalent thickness  $d_e$ , can be expressed as follows:

$$d_e = \frac{V_{ins}}{F_a} \quad (15.4)$$

In concrete masonry technologies, the TE value expresses the influence of the insulation and concrete parts of the CMU on the wall R-value. A series of 2-D and 3-D finite difference simulations were performed to analyze the thermal performance of concrete masonry technologies. These analyses were performed for a wide range of concrete densities and consequently thermal conductivities. Figure 15.6 summarizes the results of the TE simulations for five types of CMUs.

It can be observed that thermal efficiency of the insulation material in two-core, cut-web, and multicore units made of normal density concretes varies from 20 to 40%. This shows that as much as 60–80% of insulation is ineffective and does not increase the CMU R-value. An application of lightweight concretes in production of two-core, cut-web masonry units may enhance the thermal efficiency of insulation TE, which can reach even 90% for blocks made of lightweight concrete. However, the insulation placed in multicore CMUs is almost useless. For normal density concretes, TE is below 20%, and for multicore units made of lightweight concrete between 50 and 60%. It is important to notice that air-cores in units made of normal density concretes are not a good place for thermal insulation. Probably, the best thermal enhancement solution for a multicore CMU is the installation of a rigid foam sheathing on the external wall surface. As presented in Fig. 15.7, the best performing CMU technologies utilizing interlocking foam inserts (with herring tail interlocks) exhibits TE between 80 and 90% for all simulated types of concretes.

Vacuum insulation panel technologies (VIPs), because of a usage of a super-high-thermal performance core material are example of a very challenging design, which requires a careful consideration of very thin plastic foils (used for packaging of VIPs) or even conventional thermal insulations, like plastic foams. This is because, the intensity of a thermal bridge depends on differences in the apparent thermal

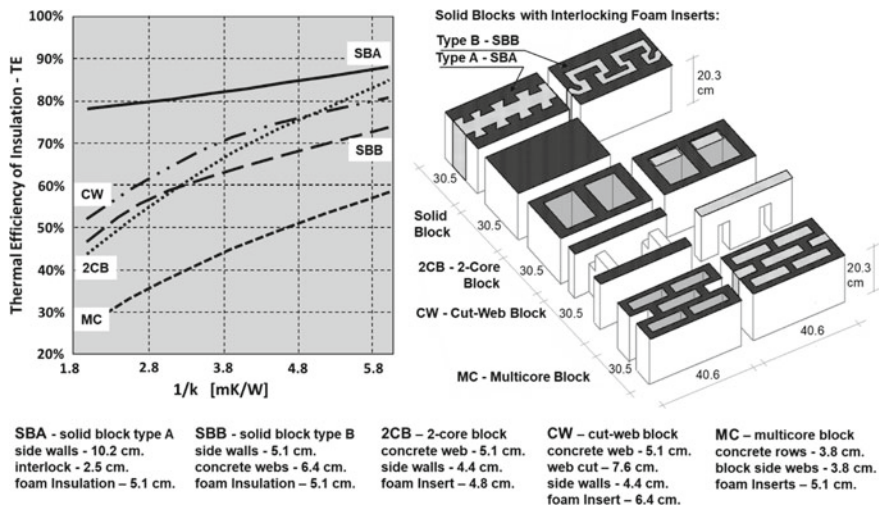
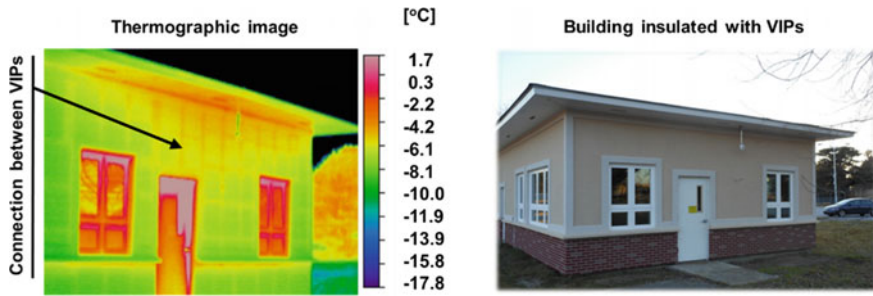


Fig. 15.6 Thermal efficiency of insulation material in different types of CMUs





**Fig. 15.7** Thermal bridging in a building insulated by vacuum panel insulation (VIP)

conductivity of neighboring materials. In this light, even thermal insulation materials can generate a thermal bridge effect. As shown in Fig. 15.7, high-resistance cellular plastic insulation can generate a thermal bridge effect. The infrared image of the building insulated with a use of the VIPs packed in the foam casing shows significantly different temperatures in places of VIP connections—Košný et al. (2014). Bear in mind that foam has about 10% to 20% of the thermally resistivity of the core of a VIP. So, if VIPs are encased with the plastic foam, it generates thermal bridges on the VIP edges.

## 15.5 Engineering Methods for Thermal Bridge Analysis

Heat transfer through envelope components is complex and dynamic. The steady-state thermal performance of building envelope technologies and architectural details can be established using engineering calculations, thermal simulations, or through different types of thermal tests. Typically this takes the form of either R-value or U-factor characterizations. Keep in mind that the direction and magnitude of heat flow in building envelope components are affected by solar gains from the sun, outdoor temperature, indoor temperature, and exposed surface area.

### R-value and U-factor of Building Assemblies

Thermal resistivity is a material property that is the reciprocal of the apparent thermal conductivity,  $k_a$ . Thermal resistance or R-value is defined as the thickness of a specimen divided by the apparent thermal conductivity. In either case, these terms are a measure of how effectively the material resists heat flow. R-values are used by the construction industry to describe insulation effectiveness and characterize steady-state heat flow across assemblies. Thermal resistance is identified by the term R-value with units,  $m^2 \cdot K/W$ , in SI units. Please notice that the insulation R-value does not describe the overall performance of an assembly. For overall assembly performance, the overall thermal resistance of the assembly which is determined from the resistances of the components of the assembly must be determined. The assembly

R-value of a multilayer structure with one-dimensional heat flow is the sum of the thermal resistances of the layers.

$$R = \sum_{i=1}^n \frac{t_i}{k_{ai}} = \sum_{i=1}^n R_i \quad (15.5)$$

Where:  $k_{ai}$  is the apparent thermal conductivity of material (layer)  $i$  and  $t_i$  is the thickness of layer  $i$ .

$R_i$  is the thermal resistance of the  $i$ th layer.

In a similar way U-factor (thermal transmittance) is used to calculate heat flow across an assembly. It can be calculated as the reciprocal value of the sum of the thermal resistance and the air-film resistance at the exterior and interior surfaces ( $h_e$  and  $h_i$ ). The quantities  $1/h_i$  and  $1/h_e$  are often referred to as air-film resistances.

$$U = \frac{1}{\frac{1}{h_e} + R + \frac{1}{h_i}} = \frac{1}{R_e + R + R_i} \quad (15.6)$$

The U-factor in Eq. 15.3 allows calculation of the rate of steady-state heat flow across an assembly. Most thermal insulations and a great majority of other building materials exhibit heat flow equally in both directions. However, some construction elements for example, wood, some cellular plastics, reflective insulations or panels using highly conductive materials have different thermal resistances and heat transfer rates in different directions.

$$Q = U \cdot A \cdot \Delta T \quad (15.7)$$

$Q$  is the heat flow in Btu/h or W,  $A$  is the cross-sectional area (constant in this case), and  $\Delta T$  is the temperature difference between the exterior air and the interior air.

There are several methods for determining thermal performance of building envelopes, and the appropriate method depends on the types of construction and thermal insulation. The ASHRAE Handbook of Fundamentals—ASHRAE (2021) provides several methods to determine clear-wall R-values and U-values. These methods are for assemblies with one or two-dimensional heat transfer.

### Parallel-Path Method

A commonly used approach is **the parallel-path method**. This method assumes that heat flows independently through regions that are in parallel and there is no heat exchange between regions as shown in Fig. 15.8.

Considering that some people are more comfortable working with the concept of thermal transmission ( $U$ ) than thermal resistance ( $R$ ), the equations are given below for both R-values and U-factors. The parallel-path calculations yield relatively accurate results for one-dimensional heat transfer, where there is little or no heat exchange between the “parallel” paths in the actual assembly. The parallel-path calculation is

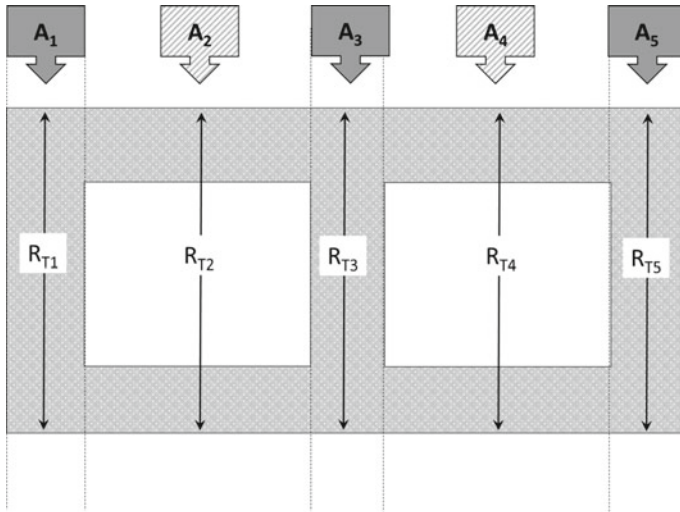


**Fig. 15.8** Calculation schematic for the parallel path method

useful in cases of simple sandwich constructions or wood-frame assemblies.

$$Q = (A_1/R_{T1} + A_2/R_{T2} + A_3/R_{T3} + \dots) \Delta T \tag{15.8}$$

$$Q = (U_1 \cdot A_1 + U_2 \cdot A_2 + U_3 \cdot A_3 + \dots) \Delta T$$

where:

$Q$  is the heat flow through a defined area with multiple adjacent assemblies.

$R_{Ti}$  is the thermal resistance for assembly “i”, generally obtained by summing the resistance of each layer of material in the assembly including inner and outer air films.

$U_i$  is the heat Transmission Coefficient in BTU/(h·ft<sup>2</sup>·°F) for assembly “i” including the effect of the interior and exterior surface films.

$A_i$  is the area of assembly “i”, in ft<sup>2</sup>.

$\Delta T$  is the difference between the indoor and outdoor air temperatures.

Effective R-value and U-factor can be computed using Eq. 15.5 for a region like that in Fig. 15.8.

$$R_{\text{eff}} = 1/U = (A_1/R_{T1} + A_2/R_{T2} + A_3/R_{T3} + \dots)/A_{\text{total}} \tag{15.9}$$

### Isothermal Planes (Series-Parallel Path) Method

In buildings with highly conductive structural members or other components made of concrete, steel, aluminum, or glass, the assumption of parallel heat flow is not likely to provide reliable results. In these cases, the **Isothermal Planes Method** provides an alternate procedure for calculating the U-value. The name comes from an assumption of uniform temperature (isothermal) for the highly-conductive planes separating less conductive layers. This method is used, for example, to analyze heat flow through wood-framed assemblies or masonry walls. The isothermal planes method divides the construction assembly into a series of layers. Hollow masonry units are a very good example of when this calculation method can be applied. The solid webs connecting the face shells are quite conductive compared to the air spaces in the hollow cores, and the face shells conduct heat laterally. As shown in Fig. 15.9, for a two-core masonry unit, the layer containing the webs and cores is treated with a parallel path calculation to arrive at an average R-Value for the layer. This is then added to the R-Values of the two face shells in series. In the isothermal planes method, the air-to-air R-value is calculated using Eq. 15.6.

$$R_{air-to-air} = \frac{1}{U} = R_e + R_{fe} + \left[ \frac{a_w}{R_w} + \frac{a_c}{R_c} \right] + R_{fi} + R_i \tag{15.10}$$

where:

$R_e$  and  $R_i$  are exterior and interior air-film resistances.

$R_{fe}$  and  $R_{fi}$  are exterior and interior face resistances.

$a_w$  and  $a_c$  are fractions of the total heat flow area for the webs and air-cores.

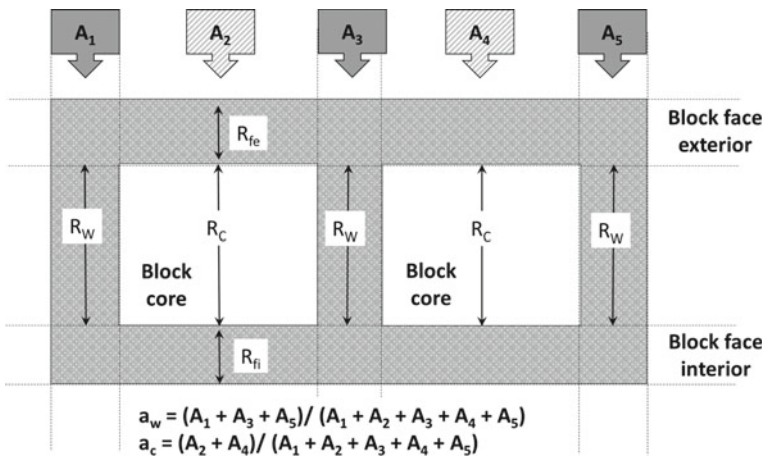


Fig. 15.9 Calculation schematic for the isothermal plane method

$R_w$  and  $R_c$  are R-values (calculated for the space between faces) for all webs and air-filled cores.

**Modified Zone Method**

Heat flow through construction assemblies with metal framing or sheathing is more complex and requires special consideration. For walls using light-gauge steel framing, the ASHRAE Handbook of Fundamentals recommends use of the ASHRAE Zone Method or Modified Zone Method—ASHRAE (2021). The Modified Zone Method was designed to improve the accuracy of clear-wall R-value calculations for light-gage steel-framed walls with insulated cavities containing steel C-shape studs with solid webs—Košný et al. (1995). The Modified Zone Method is similar to the Parallel Path Method and the ASHRAE Zone Method. All three methods are based on parallel-path calculations—the difference being how heat flow through the metal stud ( $w$  in Fig. 15.10) is estimated. In the Parallel Path Method, the “zone of influence  $w$ ” is assumed to be equal to the length of the stud flange—“ $L$ ” In the ASHRAE Zone Method  $w$  is assumed to be equal to the length of stud flange plus twice the total thickness of all finish material layers on the thicker side (can be exterior or interior)—as depicted in Fig. 15.10. In the Modified Zone Method  $w$  is determined by the following equation

$$w = L + z_f x d_t \tag{15.11}$$

where:

$w$ —the zone containing the metal stud.

$L$ —metal stud flange width.

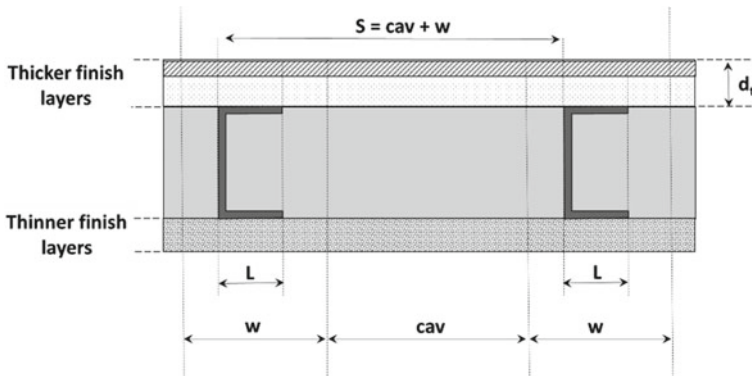


**Fig. 15.10** Calculation schematic for the modified zone method

$z_f$ —zone factor determined based on simulations of different steel-stud wall configurations. It depends on the ratio between thermal resistivity of finish material and cavity insulation, depth of stud, and thickness of finish material layers,

$d_t$ —total thickness of all wall finish material layers on the thick side.

The accuracy of the Modified Zone Method was verified by finite-difference modeling of over 200 metal frame walls with insulated cavities—Kośny and Desjarlais (1995). The Modified Zone Method results are within  $\pm 2\%$  of the results of the three-dimensional finite-difference evaluations. Furthermore, for six steel-framed wall assemblies tested at the Oak Ridge National Laboratory and 15 similar wall assemblies tested by Holometrix—see: Barbour (1994), the results of the Modified Zone Method calculations differed by less than 6.5 percent from test results—ASHRAE Research Project 785-TRP—see: Enermodal Engineering (1996).

### Linear Thermal Transmittance Method

The **Linear Thermal Transmittance Method** is a superposition of the local heat flows to calculate the overall heat flow in the building envelope assembly. The heat flows for full envelope assemblies are determined. The methodology for determining the linear thermal bridging coefficient is specified in several ISO standards, including- ISO 10211 (2007) and ISO 14683 (2007a, b), which deal with methods for determining the heat loss through linear thermal bridges at junctions of building elements. These ISO documents contain specifications for developing thermal models of thermal bridges, which can be utilized for determination of heat losses and surface temperatures—ISO 10211 (2007). The following types of thermal bridges are typically considered:

- Linear thermal bridges: where there is a thermal bridge with a specific length, for example, a lintel.
- Point thermal bridges: where there is a thermal bridge at specific points only, for example, masonry wall ties.
- Repeating thermal bridges: where there is a thermal bridge that repeats at regular intervals within an element of the thermal envelope, for example, timber studs in an insulated wall.
- Non-repeating thermal bridges: where there is a one-off thermal bridge, for example, a
- Structural column in an insulated wall.

In the Linear Thermal Transmittance Method, each construction detail containing a thermal bridge is represented by a heat flow. The thermal effect of the bridge is characterized by its linear thermal transmittance, which is expressed by  $\Psi$  [ $\text{W}/\text{m}^2 \cdot \text{K}$ ]. The  $\Psi$ -value represents the additional heat flow through the area of the linear thermal bridge, which is in addition to the heat flow for the adjacent, thermally undisturbed area. Two types of thermal bridges are specified in this method: linear and point thermal bridges. A linear thermal bridge is one with a uniform cross-section along one of the three orthogonal axes—ISO 14683 (2007a, b); ISO 10211 (2007). It is

commonly found in intersections and structural junctions. Examples of point thermal bridges can be visualized by a metal fastener penetrating an envelope assembly, shelf angles, slab edges, balconies, corner framing, parapets, and window interfaces.

A linear thermal bridge is defined mathematically as follows:

$$\psi = L^{2D} - \sum_{j=1}^{N_j} U_j * L_j \quad (15.12)$$

where:

$L^{2D}$  is the thermal coupling coefficient obtained from 2-D simulations—see: ISO 10211 (2007)

$U_j$  is the thermal transmittance of the 1-D component, “ $j$ ”, separating the two environments being considered.

$L_j$  is the length over which the  $\psi$ -value applies.

A linear thermal bridge coefficient can have a negative or positive value. If  $\psi$ -value for a specific building component has a negative value, this indicates that the thermal resistance of building envelope has been improved due to the introduction of that component. A positive  $\psi$ -value indicates that the presence of the component of interest has reduced the thermal resistance of the building envelope.

The overall thermal resistance  $R_{overall}$  [ $m^2 \cdot K/W$ ] of any type of building envelope can be computed with use of the following equation (assuming that there is only one type of clear field envelope assembly within the area considered for calculations):

$$R_{overall} = \frac{A}{\frac{A}{R} + \sum_{j=1}^J L_j \psi_j + \sum_{k=1}^K n_k \chi_k} \quad (15.13)$$

where:

$A$  is the total area of considered assembly [ $m^2$ ];

$R$  is the thermal resistance of the assembly without thermal bridge effects [ $m^2 \cdot K/W$ ].

$L_j$  is the length of linear thermal bridge [m];

$\psi_j$  is the linear thermal transmittance of linear thermal bridge [ $W/(m \cdot K)$ ];

$n_k$  is the number of the point thermal bridge components;

$\chi_k$  is the point thermal transmittance of the point thermal bridge “ $k$ ” [ $W/K$ ].

For building envelope assemblies containing multiple clear-field configurations “ $i$ ”, the Eq. 15.8 has the following form.

$$R_{overall} = \frac{A}{\sum_{i=1}^I \frac{A_i}{R_i} + \sum_{j=1}^J L_j \psi_j + \sum_{k=1}^K n_k \chi_k} \quad (15.14)$$

where:

$A_i$ —is the area of considered part of the assembly without thermal bridge effects [ $m^2$ ].

$R_i$ —is the thermal resistance of considered part of the assembly without thermal bridge effects [ $m^2 \cdot K/W$ ].

The same calculation methodology is used in ISO standard 6946 (2007) for calculation of the transmission heat transfer coefficients  $H$  [ $W/K$ ], where the contribution due to the thermal bridges is included according to the following equation.

$$H = \sum_{i=1}^I \frac{A_i}{R_i} + \sum_{j=1}^J L_j \psi_j + \sum_{k=1}^K n_k \chi_k = \sum_{i=1}^I A_i U_i + \sum_{j=1}^J L_j \psi_j + \sum_{k=1}^K n_k \chi_k \tag{15.15}$$

where:

$H$  is the object’s total heat transfer coefficient [ $W/K$ ].

$U_i$  is the thermal transmittance for each considered part of the assembly without thermal bridge effects [ $W/m^2 \cdot K$ ].

Figure 15.11 shows basic types of thermal bridges and describes the heat-transfer calculations using the linear transmission method.

**Numerical Tools Used in Thermal Bridging Analysis**

Thermal bridging and construction details in the building envelope impact the thermal performance. These features have both steady-state and dynamic repercussions.

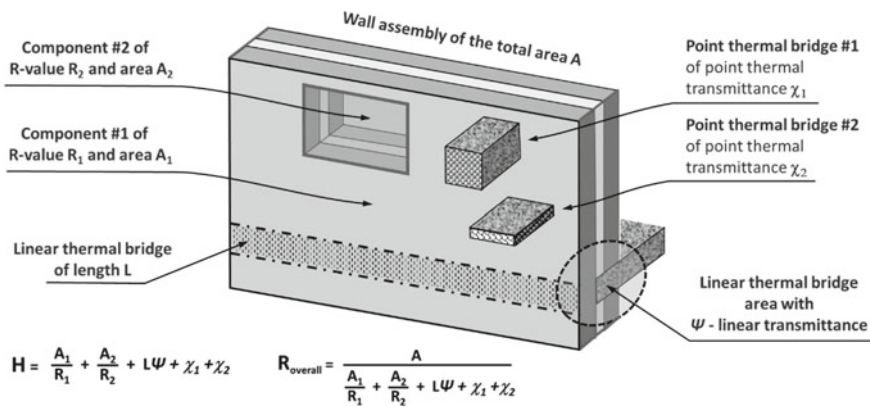


Fig. 15.11 Types of thermal bridges and the linear transmission method



Capability for reduction of building loads and successful whole-building integration are dependent, in large scale, on correct predictions of building thermal characteristics with building envelopes being one of the most important factors. In other words, building integration and load reductions are only possible when combined with accurate estimations of building envelope-generated thermal loads. Thermal and whole building energy simulation tools are often useful in determining the local thermal performance as well as the overall energy efficiency of buildings. The energy efficiency for the building enclosure is typically based on individual R-values of various building envelope components. The effects of thermal bridges are approximated in these calculations. Furthermore, the currently available whole-building energy modeling tools do not always accurately account for the real R-values of various interface configurations, such as window-to-wall, wall to partition, wall to foundation, and wall to interfaces—Hassid (1990), Košny and Desjarlais (1994), Kossecka and Košny (2002), Ben-Nakhi (2003), Al-Sanea and Zedan (2012), Martin et al. (2012). It is even more difficult to consider thermal bridges formed by steel framing—Kosny and Christian (1995), Martins et al. (2016). In these cases, two and three-dimensional heat transfer programs needs to be used to determine local R-values; the overall energy analysis can then be modified to consider these effects and arrive at an accurate picture of the overall energy efficiency of the building enclosure.

A great variety of numerical tools for this type of simulations are available and used by practitioners for two-dimensional thermal analysis—Comsol,<sup>2</sup> Heating<sup>3</sup> AnTherm,<sup>4</sup> BISCO (for 2D) and TRISCO (for 3D),<sup>5</sup> PSI Therm,<sup>6</sup> ANSYS Fluent,<sup>7</sup> and PHYSIBEL Voltra.<sup>8</sup> THERM is a free software developed by the Lawrence Berkeley National Laboratory (LBNL), which is commonly used in North America for this purpose.<sup>9</sup> Report from the European 2010 project funded by the Communities Intelligent Energy Europe Programme<sup>10</sup>; “Assessment and Improvement of the EPBD Impact (ASIEPI)” lists 29 numerical tools and 26, mostly national, thermal bridge atlases which can be useful in thermal bridge analysis.

---

<sup>2</sup> [https://www.comsol.com/heat-transfer-module?gclid=CJOBzYmq38wCFUFehgod\\_MgAHA](https://www.comsol.com/heat-transfer-module?gclid=CJOBzYmq38wCFUFehgod_MgAHA).

<sup>3</sup> <http://www.buildingphysics.com/index-filer/Page691.htm>.

<sup>4</sup> <http://www.antherm.at/antherm/EN/>.

<sup>5</sup> <http://www.physibel.be/index.htm>.

<sup>6</sup> <http://www.psitherm.uk/>.

<sup>7</sup> <http://www.ansys.com/Products/Fluids/ANSYS-Fluent>.

<sup>8</sup> <http://www.physibel.be/v0n2vo.htm>.

<sup>9</sup> <https://windows.lbl.gov/software/therm/therm.html>.

<sup>10</sup> [https://ec.europa.eu/energy/intelligent/projects/sites/iee-projects/files/projects/documents/asi\\_epi\\_access\\_the\\_results\\_en.pdf](https://ec.europa.eu/energy/intelligent/projects/sites/iee-projects/files/projects/documents/asi_epi_access_the_results_en.pdf).

## 15.6 Incorporation of Thermally Bridged Envelopes in Whole-Building Energy Simulations

Heat transfer through envelope components is complex (multidimensional) and dynamic—Ben-Nakhi (2003), Antretter et al. (2010), Martin et al., 2011, Ascione et al. (2012), Al-Sanea and Zedan (2012), Zedan et al. (2016). At the same time whole building simulation tools that are used today utilize simplified one-dimensional heat transfer models. In addition, recent developments in research (Kośny & Desjarlais, 1994; Enermodal, 1996; Tuluca et al., 1997; ASHRAE, 2002; ASHRAE, 2011) have shown that thermal bridging through building envelopes (structural framing at corners and junctions, and architectural details) can significantly reduce the thermal resistance of wall and roof assemblies. Many hourly calculation programs ignore this effect. Even for those that do account for the reduced thermal resistance, the transient or dynamic behavior of the thermal bridging is almost never taken into account in hourly building energy simulation programs. These whole-building programs can perform only one-dimensional heat flow simulations. In addition, they have been often calibrated using field data for buildings with lightweight exterior envelopes. Still, the material variations introduced by thermal bridging elements can affect the dynamic performance of the building envelope, by altering the temperature distribution and dynamic characteristics. These transient and multi-dimensional heat flow effects raise concern over the ability of the whole-building simulation programs to model the thermal performance of complex building envelopes (i.e. steel-framed, masonry, concrete) with significant thermal bridging.

Insulation installation imperfections, combined with thermal bridging, and the impact of construction details, greatly influence thermal performance of building envelopes, and consequently, the overall whole-building energy consumption. These features have both steady-state and dynamic repercussions. Capability for reduction of building loads and successful whole-building integration are dependent, in large scale, on correct predictions of building thermal characteristics with building envelopes being one of the most important factors. In other words, the building integration and load reductions are only possible when combined with accurate estimations of building envelope-generated thermal loads. This also helps with the optimization of a usage of thermal insulation (amount of insulation and its locations).

Thermal and whole building energy modeling tools are often useful in determining the local thermal performance, as well as the overall energy efficiency of a building. The energy efficiency for the building enclosure is typically based on individual R-values of various building envelope components. The effects of thermal bridges are approximated in these calculations. The currently available whole-building energy modeling tools, however, do not always accurately account for the real R-values of various interface configurations, such as window-to-wall, wall to partition, wall to foundation, and wall to interfaces. – Kośny and Desjarlais (1994), Kossecka and Kośny (2002). It is even more difficult to consider thermal bridges formed by steel framing. In these cases, two and three-dimensional heat transfer programs need to be used to determine local R-values; the overall energy analysis can then be modified to

consider these effects and arrive at an accurate picture of the overall energy efficiency of the building enclosure.

It has been known for some time that many thermally massive building envelope technologies, where complex multi-dimensional heat transfer occurs, may exhibit the strongly time-dependent behaviors—see: Burch et al. (1992), Kossecka (1992). As a result, their dynamic thermal performance cannot be accurately represented by simplified one-dimensional (layered) material configurations and static R-values in whole-building energy simulation programs. Yet, this is what is most commonly taking place. The result can be an imprecise computer model, generating inaccurate energy usage and building energy load profile predictions—see: Kosny and Kossecka (2002). In addition, inaccurate models may lead to a wrongly sized heating and/or cooling equipment during the design process.

The alternative way to perform whole building energy simulations is to employ a thermally equivalent one-dimensional model, which represents the identical steady-state and dynamic heat transfer characteristics as more complex, significantly more accurate, three-dimensional models of real structures. The Equivalent Wall Theory (EWT), developed by Kossecka and Košny (1996, 1997) can be used for this purpose. In the EWT a multi-layer Equivalent Wall (EW) is created with the same thermal resistance, capacity and structure factors, as in the three-dimensional wall assembly.

An EW has a simple one-dimensional multi-layer structure and the same thermal properties as the “complex”, real wall assembly (total resistance and thermal capacitance). Its dynamic thermal behavior is identical to the actual wall. The EWT for complex thermal structures expresses the role of heat storage effects in heat flow through an element. It leads to the definition of structure factors (dimensionless quantities representing the fractions of heat stored in the wall volume, in transition between two different states of steady heat flow, which are transferred across each wall surface). These quantities, together with total transmittance and capacity, provide the basic thermal characteristics of the structure. Even for a complex thermal bridge configuration, response factors, steady-state R-values and thermal structure factors have the same values for both walls (the “complex” real wall and the EW)—see: Kossecka and Košny (1997, 2002) and Košny et al. (1998).

The EWT uses, as its mathematical basis, conditions imposed on the response factors and z-transfer function coefficients by the thermal structure factors. Thermal structure factors are dimensionless quantities representing the fractions of heat stored in the wall volume, in transition between two different states of steady heat flow, which are transferred across each wall surface. Relationships of the structure factors with other dynamic thermal characteristics of walls are presented below. The validation of the EWT was performed by the Oak Ridge National Laboratory (ORNL) with a series of dynamic hot box tests of complex wall assemblies—Košny et al. (1998). In addition, the accuracy of the heat transfer predictions and precision of the EW generation with a usage of the EWT, were confirmed by the ASHRAE RP1145 research project, where a collection of 20 complex wall assemblies was analyzed—ASHRAE (2002).

The EW calculation method uses, as its mathematical basis, conditions imposed on the response factors and z-transfer function coefficients by the thermal structure

factors. Thermal structure factors are dimensionless quantities representing the fractions of heat stored in the wall volume, in transition between two different states of steady heat flow, which are transferred across each wall surface—see: Kossecka and Košný (1997, 2003, 2005), Košný and Kossecka (2002). Relationships of the structure factors with other dynamic thermal characteristics of walls are presented below.

The structure factors,  $\varphi_{ii}$  and  $\varphi_{ie}$ , for a composite wall element, adiabatically cut off from the surroundings, are given by:

$$\varphi_{ie} = \frac{1}{C} \int_0^V \rho c_p \theta (1 - \theta) dv \quad (15.16)$$

$$\varphi_{ii} = \frac{1}{C} \int_0^V \rho c_p (1 - \theta)^2 dv \quad (15.17)$$

where,  $C$  is the total thermal capacity of the wall element of volume  $V$ :

$$C = \int_0^V \rho c_p dv \quad (15.18)$$

$\theta$  is the dimensionless temperature for the problem of steady-state heat transfer, for ambient or surface temperatures  $T_i = 0$  and  $T_e = 1$ .

Structure factors  $\varphi_{ii}$  and  $\varphi_{ie}$  for a wall composed of  $n$  plane homogeneous layers, numbered from 1 to  $n$  with layer 1 at  $R$  is the total thermal resistance per the unit cross section area,  $R_m$  and  $C_m$  denote the thermal resistance and capacity of the  $m$ -th layer, whereas  $R_{i-m}$  and  $R_{m-e}$  denote the resistance for heat transfer from surfaces of the  $m$ -th layer to inner and outer surroundings, respectively.

the interior surface, are given as follows:

$$\varphi_{ii} = \frac{1}{R^2 C} \sum_{m=1}^n C_m \left[ \frac{R_m^2}{3} + R_m R_{m-e} + R_{m-e}^2 \right] \quad (15.19)$$

$$\varphi_{ie} = \frac{1}{R^2 C} \sum_{m=1}^n C_m \left[ -\frac{R_m^2}{3} + \frac{R_m R}{2} + R_{i-m} R_{m-e} \right] \quad (15.20)$$

where:

Conditions imposed by the structure factors on the response factors are as follows:

$$\delta \sum_{n=1}^{\infty} n X_n = -C \varphi_{ii} \quad (15.21)$$

$$\delta \sum_{n=1}^{\infty} n X_n = C \varphi_{ie} \quad (15.22)$$

There are several ways the EW technique may generate a simple one-dimensional multi-layer structure with the same thermal properties and dynamic behavior as the actual wall. The first step is to assume some number of ‘equivalent’ layers for the wall structure. For a set number of layers, a simple way to solve for equivalent layer properties is to first generate, either randomly or with some logic, a set of capacitances  $C_n$  for each layer, then seek the resistances  $R_n$  to satisfy Eqs. (15.19) and (15.20). The thermal structure factors and overall R-value must match those for the 3-D wall assembly. Thermo-physical properties of the layers may then be established, if necessary, to match  $R_n$  and  $C_n$  values and total thickness of the wall. Please notice that the relationship between the thermal structure factors and response factors play a pivotal role in the development of the EW model. The thermal structure factors, together with total thermal resistance  $R$  and capacity  $C$ , determine the dynamic thermal properties of a wall element—through the conditions they impose on the response factors. Those conditions, however, do not determine the response factors in a unique way, but rather play the role of constraints. Please notice that, the EW model is not unique; however different EWs have, in general, very similar dynamic thermal response properties.

## 15.7 Use of an Advance Insulation Technologies for Thermal Bridge Mitigation

As discussed in earlier sections, thermal bridging significantly influences the thermal performance of insulation used in building envelopes. In addition to the increased building space-conditioning energy consumption, undesired heat losses or gains through the thermally bridged areas often lead to the impaired long-term thermal performance, durability problems, and material deterioration, which are frequently associated with the local moisture condensation (locations of lower temperature where condensation occurs are common consequences of thermal shorts). Therefore, thermal bridges need to be correctly characterized and mitigated during the building design stage. The choice of construction method dictates how insulation continuity is approached. Components that form the principal insulation layers should be clearly identified on drawings, and their details developed to ensure continuity of these layers between elements of the construction.

Numerous design strategies are available to help ensure a building design contains as few as possible thermal bridges. In terms of thermal bridging, several general “rules

of thumb” have been developed. According to Ziegel (2010), as well as Kosny and Yarbrough (2018), they are as follows:

- the **Avoidance Rule** which states that discontinuities in the insulating layer should be avoided
- the **Breakthrough Rule** which say that any breaks in the insulating layer must have as high an insulating value as possible., and
- the **Geometry Rule** states that building geometry should be as simple as possible and corners in building intersections and architectural details should have a rounded shape, if possible.

From the practical standpoint, thermal bridging can be avoided by placing insulation in series with conductive material, instead of installing it in parallel. For example, you can place thermal insulation outside a framed wall or roof assembly instead of placing the insulation between the structural members. Thermal bridging can also be avoided by examining the elevation area for the lowest local R-value points and improving them through mitigation of thermal shorts. For instance, replacing metal facade connectors with plastic or composite elements.

Furthermore, simpler building geometries and simpler configurations of architectural details and intersection are more likely to be designed and built correctly. That is why the number of different types of construction technologies within the thermal envelope should be minimized, because thermal imperfections are most likely to occur where one type of construction meets another. Also, some construction details include areas that interrupt the insulation layer. These can be often found in areas of intersections of vertical and horizontal structural components. Although it is difficult to completely eliminate these thermal shorts, their effects can be minimized wrapping the conducting element with thermal insulation (even a thin one) and possibly by overlapping the insulating layers in vicinity of conducting elements, even though these insulations will not necessarily be in direct contact.

The most widespread, so far, and often the simplest method of thermal bridge mitigation in building envelopes is an application of the rigid foam sheathing across the entire opaque envelope area. Furthermore, installing exterior insulating sheathing is also one of the simplest ways to improve a thermal performance of wall systems. Thermal efficiency of the usage of insulating sheathing was previously analyzed by several authors (Barbour et al., 1994; Kośny, 1995; Christian & Strzepek, 1987; Strzepek, 1990; Trethowen, 1988, 1991). It can also improve building airtightness. Foam sheathing can be located on either the exterior or interior wall surfaces. It is important to remember that in case of wood or steel framed walls insulating sheathing is changing mean temperature for the cavity insulation. That is why, different nominal thermal conductivities of the cavity insulation have to be assumed for different sheathing locations and for walls without sheathing. Framing effect is another convenient measure of the sheathing thermal efficiency. It represents the R value reduction generated by the framing members (in case of framed wall technologies—studs and tracks)—Barbour et al (1994), Kośny (1995), Ohlsson (1998).

According to Christian and Kośny (1995), the clear wall R-value of a nominal  $2 \times 4$  in. wood-framed wall (cavity—8.9-cm thick) insulated with  $R_{SI}$ -1.9  $m^2 \cdot K/W$

fiberglass batts can be increased by as much as  $R_{SI}-0.6 \text{ m}^2\cdot\text{K}/\text{W}$  by the installation of 2.5-cm thick EPS (expanded polystyrene) foam sheathing. For detached single-family residential houses, this generates in average about 7.3% of savings in the whole house space conditioning energy consumption (considering representative U.S. climates).

In walls framed with light-gauge steel studs, in addition to improved overall thermal performance, the additional EPS foam sheathing reduces the temperature difference between the center of cavity and the stud area. The reduction in the temperature difference between the metal stud and the center-of-cavity diminishes the possibility of so-called “ghosting”—an aesthetic surface discoloration problem caused by the attraction of the dirt to cold areas of the wall surface. In this light, using of insulating sheathing can be recommended as an efficacious way of the improving the thermal performance of steel stud walls.

Since a large volume of research worldwide has been dedicated to the continues insulation sheathing, wrapping the entire building, the following sections are focused on the localized insulation applications.

### **Localized Insulation Systems for Thermal Bridge Mitigation**

From the building envelope designer perspective, a thermal bridge is an architectural detail or location, where thermally conductive structural components or connectors penetrate thermal insulation, or places with missing thermal insulation, insufficient insulation, or reduced insulation performance, relative to adjacent areas of the thermal envelope. The intensity of a thermal bridge depends on differences in the apparent thermal conductivity of neighboring materials. In this light, even thermal insulation materials can generate a thermal bridge effect.

Wood- and steel-framed wall systems are very common in U.S. residential and commercial buildings today. However, because metals exhibit significantly higher thermal conductivity than wood, the potential for thermal bridging, and consequent reduction in performance, is much more important in the case of metal-framed structures. Simply, in wood-framed buildings, the thermal bridge problem is not as severe. On the other hand, metal framed walls have certain advantages over the wood framing, such as noncombustible construction as well as superior termite and mold resistance. Further, if suitably designed, the metal stud walls can provide thermal performance close to the wood stud walls. Košny et al. (1997, 2002) explored methods to improve the steady-state thermal resistance of metal stud walls. These included adding exterior foam sheathing insulation, modified stud shapes, locally insulated steel studs with foam covers, etc. As showed in Fig. 15.12, the steel framed wall, containing 2.5-cm. thick foam shapes covering steel studs, was designed, and tested in the hot-box.

Usage of an insulating foam covering steel studs can be considered as one of construction methods helping in reduction of the contact area between studs and the sheathing. Such insulation also reduces a transverse heat transfer through stud flanges. Transverse heat transfer increases heat losses in steel framed structures and were measured and reported by Trethowen (1988). Covering foam shapes add highly efficient thermal insulation in locations only where it is strongly needed (steel stud

areas) - Kośny et al. (2010). This reduces thermal bridge effects. At the same time, the wall cavity is insulated by low-cost insulating batts.

As show on Fig. 15.12, foam insulation is placed only in the location of strong thermal shorts generated by the steel stud. With its simplicity, high R-value ( $R=2.8 \text{ m}^2\cdot\text{K}/\text{W}$ ), low Framing Effect (13%), and low cost, such walls can be a very good example how proper thermal designing can create an effective steel stud wall assembly. The authors concluded that foam-covered metal studs may perform as well as wood stud walls, while being cheaper than adding of rigid foam sheathing to conventional steel framing. It was found that the use of foam-covered studs is the simplest and an effective way of enhancing thermal performance of metal stud walls. Experimental hot-box test results presented in Table 15.1 document excellent thermal performance of the steel stud wall containing local stud insulation called Stud Snugglers.

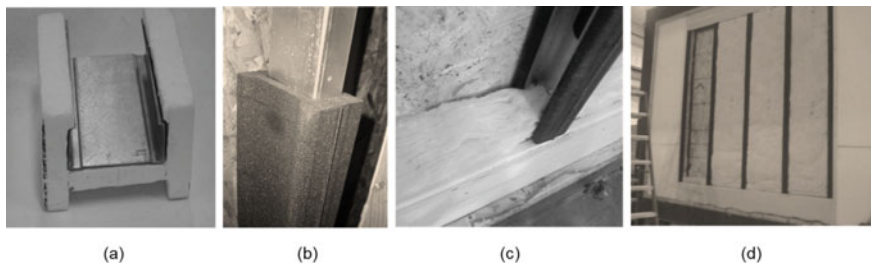


**Fig. 15.12** Foam stud insulation profiles for steel structures: **a** Stud Snuggler made of EPS foam, **b** Stud Snuggler made of Polyurethane foam, **c** wall cavity with the light-gauge steel stud and Stud Snuggler, **d** hot box test assembly of the steel stud wall with Stud Snuggler local insulation

**Table 15.1** Thermal performance of a steel-framed wall containing 2.5-cm. thick foam shapes covering the 8.9-cm. light-gauge steel studs

Wall construction	Cavity insulation R-value [ $\text{m}^2\text{K}/\text{W}$ ]	Hot-box test R-value [ $\text{m}^2\text{K}/\text{W}$ ]	R-value improvement [ $\text{m}^2 \text{K}/\text{W}$ ]	R-value improvement [%]	Framing effect [%]
Gypsum board, traditional, 8.9 -cm. steel studs, R-1.9 batts, OSB board	1.9	1.4			38.2
Gypsum board, 8.9 -cm. steel studs, 2.5-cm. foam profiles on studs, R-3.3 batts, OSB board	3.3	2.9	1.5	106.3	13.0



Additional, significant temperature variations on the envelope internal surfaces is a frequently reported problem associated with steel framing. Surfaces located over steel framing often have temperatures different than the areas adjacent to envelope cavities. Sometimes, a notable discoloration called “ghosting” can be observed in these areas. An application of insulation or tapes installed on the flange surfaces of steel structural members can be used to mitigate the above effect. The series of finite difference simulations and hot-box testing performed by Košný et al. (2010), demonstrated that the application of Stud-Snugglers on conventional 8.9-cm steel studs can reduce these surface temperature differences. Numerical analysis showed that, with a 27 °C temperature difference between the interior and exterior environments, the corresponding temperature differences between the center of cavity and the stud locations were 5.0 °C and 1.1 °C, for a conventional steel-stud wall and a similar wall with Stud Snugglers.

In a similar way, aerogel tapes or strips can be used to improve the thermal performance of steel-framed envelopes. The main advantages of using aerogel insulation are its flame resistance and about two times then thermal resistance in comparison with conventional plastic foams. A series of finite difference simulations and steady-state guarded-hot-box tests of commercial metal roofs using aerogel as a local thermal insulation have been performed—see: Košný et al. (2007b). The purpose of this analysis was to determine the potential for increase in the R-value of through-fastened metal roofs using aerogel insulation as a thermal block on the purlins. As shown in Fig. 15.13, the one-cm. thick aerogel strips were added to the compressed fiberglass insulation that was draped over and between the roofing purlins. Three assemblies were constructed to fit the 2.44-m wide metering area of the guarded hot box. Tests were performed with two purlins installed 1.22-m. on center. Two sizes of 7.6-cm and 12.7-cm wide aerogel strips were used on top of the steel purlins in areas where fiberglass blanket is compressed with associated thermal resistance reduction.

Figure 15.13 shows the hot-box test specimen of a commercial metal roof using aerogel as a local thermal insulation that demonstrated a notable thermal performance improvement. Wider aerogel strips performed slightly better. It was found that 12.7-cm. wide and ~1.0-cm. thick aerogel strips improved overall roof R-value by about 14%.

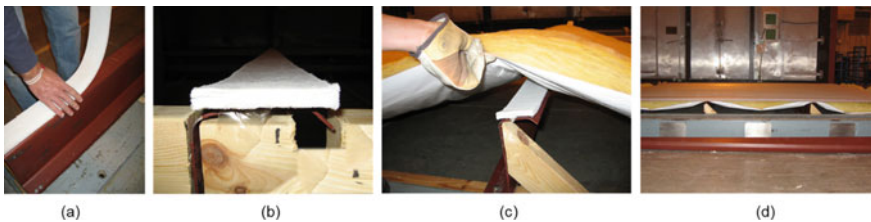


**Fig. 15.13** Installation of the 1-cm. thick aerogel strips and fiberglass blanket insulation on the test metal roof: **a** attachment of the aerogel strips to the purlin’s flange, **b** side view of the metal purlin with aerogel insulation, **c** installation of the fiberglass, and **d** a side view of the test metal roof before the installation of the metal roof top cover

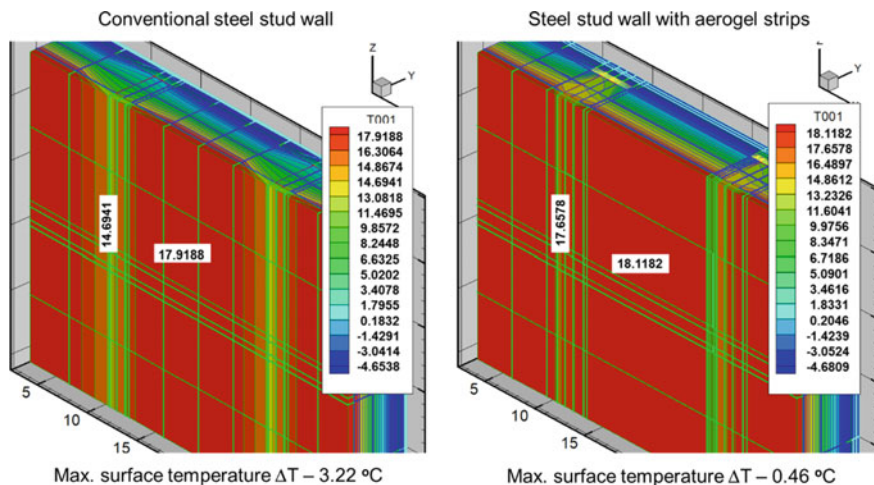


**Fig. 15.14** Simulated temperature fields on the interior surfaces in two configurations of steel framed walls using light-gage steel studs: conventional wall on the left, stud flanges insulated with aerogel strips on the right

The above research showed potential for an application of aerogel as a local insulation in commercial roofs. A similar aerogel application has been commercialized in the U.S. for steel stud walls. Košny et al. (2007b) performed a series of finite-difference simulations and steady-state guarded-hot-box tests of a steel-framed wall assembly using aerogel as a local thermal insulation of 8.9-cm. steel studs. The purpose of this analysis was to demonstrate the improvement of wall R-value and elimination of the “ghosting” on internal wall surfaces. Simulated temperature difference across both walls was 28 °C—with interior air temperature 21.1 °C and ambient air temperature -6.7 °C. As shown in Fig. 15.14, in the case of the wall using only fiberglass batt insulation, the surface temperature difference between center of the cavity and the stud location was 3.2 °C. For a wall with additionally installed aerogel strips, this difference was about 0.5 °C. Similarly, the hot-box measurements performed on the steel-framed wall (8.9-cm -studs) containing R-2.46 m<sup>2</sup>·K/W fiberglass insulation in the wall cavity and using 0.6-cm. thick aerogel strips installed on stud flanges, demonstrated a notable 29% R-value increase—see: Košny et al. (2010).

### 15.8 Mitigation of Thermal Bridging in Envelopes Using High Performance Vacuum Panel Insulation

Unwanted edge thermal bridge effects reduce the overall thermal resistance of VIPs. The thermal bridge in building envelope is most often defined as an element or location with missing thermal insulation, insufficient amount of insulation, or reduced

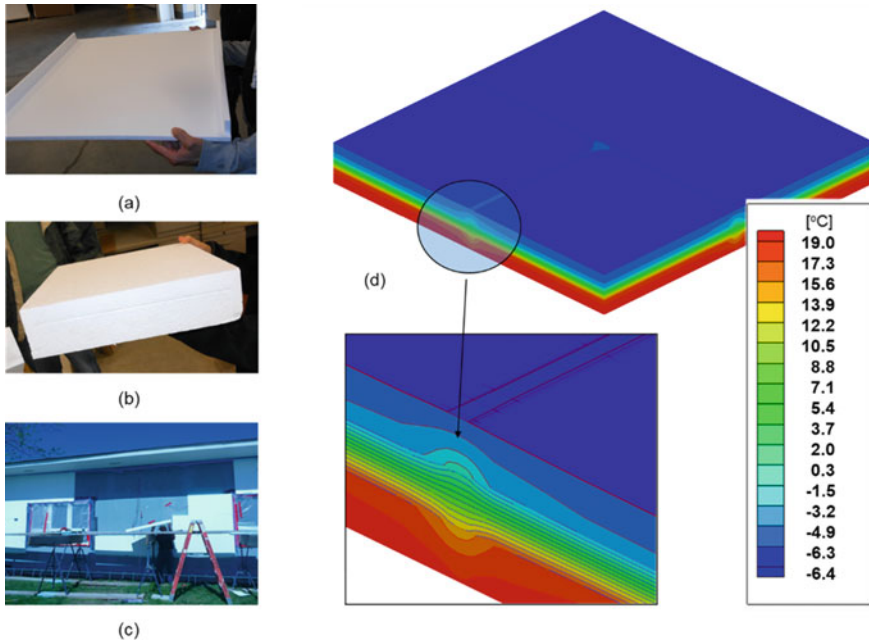


**Fig. 15.15** Thermal bridge effects generated by VIPs enclosed with plastic foam: **a** VIP foam encasement, **b** VIP packaged in the foam container, **c** wall thermal retrofit with VIPs packaged in a foam, and **d** thermal simulations of the VIP edge effects in the case of the foam packaging

insulation performance, relative to adjacent areas. Very frequently, however, it is an architectural or structural detail where materials of high thermal conductivity penetrate the thermal insulation in a direction perpendicular to the surface of the building facade. The intensity of a thermal bridge depends on a ratio of thermal resistance between neighboring conventional plastic foam can be a thermal bridge. Vacuum insulation panels (VIPs), with a center of panel thermal conductivity about 1/10th that of a conventional insulation is an example. As shown in Fig. 15.15, in the case of VIPs enclosed with cellular plastic foam, plastic foam insulation can be a thermal bridge. Infrared images of a building insulated with VIPs shows significantly different temperatures for VIPs that are packed in the foam casing—see: Fig 15.7. Figure 15.15 shows computer-generated temperature profiles near the VIP-batt connection. This demonstrates a distinct thermal bridge.

### 15.8.1 Influence of the VIP Edge Geometry and Edge Quality

As shown in Fig. 15.16 there are several VIP edge designs used today by the insulation industry. Since the VIP edge sometimes contains the panel seal, it usually includes several material layers. Considering that most of currently used VIP membranes

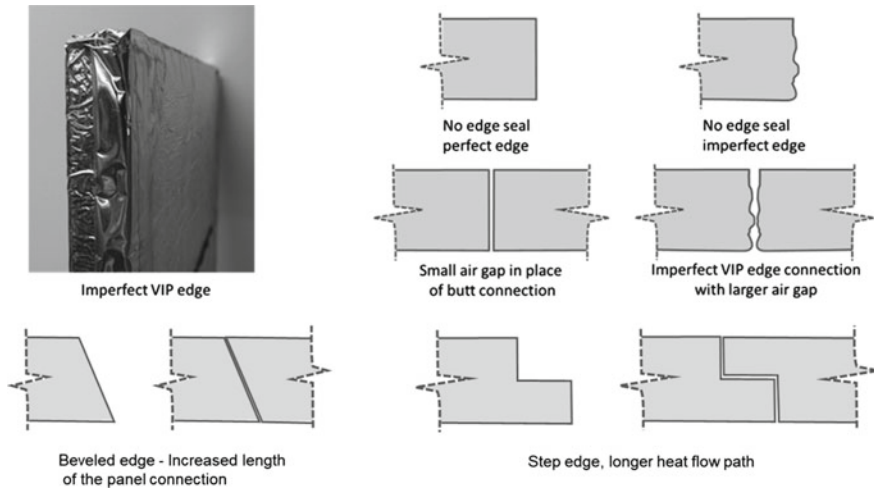


**Fig. 15.16** Examples how VIP edge quality effects the effective size of the butt connection between panels

have at least a single layer of a metal or metalized plastic film, the impact of the edge design on the overall VIP thermal performance can be significant. As discussed in numerous publications, a nominal center-of-the-panel R-value can be reduced by as much as 50% in external building envelope applications, depending on the VIP installation configuration—see: Tenpierik and Cauberg (2007), Childs et al. (2013), Sprengard and Holm (2014), Castro et al. (2017). These works combined numerical thermal analysis and testing of small-scale and whole-wall assemblies containing VIP insulation. It was also found that, due to high complexity of the edge material configurations (very thin material layers and differences in thermal conductivities up to a factor of 1000 times, numerical simulations don't always have sufficient accuracy in thermal performance predictions when compared to laboratory measurements performed with a heat-flow meter or the hot-box apparatus Van Den Bossche et al. (2010), Moore (2017). This makes it difficult to evaluate the thermal design of VIPs and development of new material configurations.

Selection of envelope materials is a key factor affecting VIP thermal performance. Both thermal and gas permeation characteristics of the external VIP skin structure are widely considered as challenges for growth of VIP technology market adoption. Reduction of gas transport through the envelope is needed to maintain the vacuum inside the VIP. This allows use of less-expensive core materials (i.e. fiberglass, fine powders, or plastic foams). That is why two or three thin aluminum layers or coatings are usually used to decrease the rate of gas transport through the VIP envelope. Wakili compared the results of heat transfer simulations with laboratory measurements of the thermal bridge effects generated by two types of enclosures on 20 mm thick VIPs with the following face area dimensions—500 × 500 and 500 × 250 mm. – see: Wakili et al. (2004) and (2011). The first film analyzed had a total aluminum

thickness of 90 nm and another one with 300 nm. It was found that the linear thermal transmittance was around  $7.0 \text{ mW}/(\text{m}\cdot\text{K})$  for the VIP using foil with 90 nm aluminum and  $9.0 \text{ mW}/(\text{m}\cdot\text{K})$  for the second case of the 300 nm aluminum foil. The increased heat flow through the film led to an increased apparent thermal conductivity of the VIP; 14% higher for the film with 90 nm aluminum and 19% higher for the film with 300 nm aluminum, when compared to the center-of-the-panel thermal conductivities, respectively for the VIP using the film with 90 nm aluminum, and VIP with the 300 nm aluminum foil.

Furthermore, VIP envelope materials are not robust and can be easily perforated or cut. Since thick membranes increase heat transfer through a VIP edge, a practical solution of using thick and as a result, strong membranes, is very limited unless metallic components like aluminum can be eliminated. These are some of the major technological challenges that need to be addressed in the close future in order to allow increased use of VIP in buildings.

Since, great number of publications and research reports associate the edge thermal bridging effects with thermal conductivity of membrane components, which are commonly using highly conductive aluminum, one of the key VIP improvement strategies is to develop an envelope system either completely without, or with a minimum thickness of aluminum layers. However, aluminum, which is used either as a solid film, or as a top coating on the PET film, is necessary to reduce the gas permeation through the envelope. This is because polymers do not exhibit similar levels of resistance to gas and water vapor transport. From this viewpoint, new developments of VIP membranes using inorganic oxide coatings, instead of a metal for decrease of the gas permeation, are particularly attractive—Bedoya et al. (2017).

The quality of the VIP edge is another rarely analyzed factor. The VIP edge should be flat to minimize the thermal bridge effect as can be seen in Fig. 15.17. This requirement, however, is extremely difficult to realize in the full-scale manufacturing practice. VIP core materials commonly shrink unevenly during evacuation of air thus changing the initially formed straight edge. The edge thermal bridge effect is also intensified by common membrane edge folds and geometrical imperfections, causing air gaps between adjacent panels—see: ECBCS/IEA Annex 39. (2005); Castro et al. (2017), Kosny and Yarbrough (2019).

In most VIP building applications, the arrays of panels are used rather than a single VIP. In these arrays, individual VIPs are often attached to each other by their edges. That is why the edge thermal bridge effect should not be determined for only a single panel—Pears et al. (1971), Childs et al. (2013), Castro et al. (2017). Air gaps between panels needs to be considered as well. A size of this gap is not only an installation-related factor since it is resulted from uneven or curved VIP edges. Schwab and the team performed steady-state heat transfer simulations to analyze the influence of air gaps in connections between VIPs—Schwab et al. (2005). The results of this numerical exercise showed that a five mm thick air gap can increase the overall U-value up to 360% for the case of the VIP using the laminated aluminum film, while only 44% increase was noted for the VIP with metalized multi-layered polymer film. Numerical analysis of thermal bridges associated with butt connections between VIPs, was performed by Castro et al. (2017) for different qualities of the VIP edge

surfaces that impact the size of the air gap between panels. In this research, variety of VIP membranes were analyzed including PET-metalized films and metallic foils. It was found that reductions in center-of-panel VIP R-values can vary even over 300%, when different VIP edge fabrication qualities, designs, and envelope materials are compared.

### **Thermal Impact of VIP Seals' Location on VIP Insulation Performance**

Significant research has been also dedicated to VIP envelope sealing techniques. A good understanding of methods, materials and equipment which can be utilized for VIP evacuation and sealing processes is necessary to achieve high quality seals, reduce the gas permeation through the membrane, and consequently extend the VIP lifespan. The heat-sealed flange is often considered the weak point in currently produced VIPs. In the case of polymeric membranes, a thin layer of low-melting-temperature insert is laminated to the inside of the envelope film, so than it can be heat-sealed around the VIP core during the encapsulating process. Especially designed seal films such, the best-known are ethylene vinyl alcohol copolymers are in use.<sup>11</sup> A significant portion, however, of currently-used heat-sealing plastics fail to demonstrate as good a gas permeation resistance as the envelope films.<sup>12</sup> In some cases, the edge diffusion through 50  $\mu\text{m}$  thick PET sealing layers can be responsible for more than 50% of the gas permeation into the encapsulated panel. To lessen this negative impact, some manufacturers use as thin as possible sealing inserts and combine them with wide seal lips. As shown in Fig. 15.17, variety of VIP seal locations is considered today.

Research has been focused on the optimization of the VIP seal location, i.e. either along the panel edges, or on one of the large area surfaces on the panel. As depicted in Fig. 15.17, there are many potential options for placement of the VIP vacuum seal. When these seals are located on the panel edge, several layers of highly conducting material are added to this location. This generates thermal shorts when two panels are connected. Based on the assumption that at minimum three layers of folded membrane are needed to make a folded edge seal, such connections contain at least six layers of the membrane (three layers from each panel). Considering that a three-layer membrane using aluminized PET foil with about 20–100 nm of metallization, the total thickness of aluminum that is part of such panel connection can be in a range between 0.4  $\mu\text{m}$  and 1.8  $\mu\text{m}$ . To avoid material concentration on the panel edges, several new VIP packaging methods have been developed and used, with the main focus on the main panel seal. In addition to improved thermal performance, these designs are expected to also simplify the VIP assembly processes and minimize the probability of undesired gas leaks. For example, Wakili et al. (2011) describes the VIP packaging and sealing method that reduces the number of seams to three on each panel and places the longest seam on a VIP face surface, instead of on the edges.

---

<sup>11</sup> [http://oisd.brookes.ac.uk/ivisnet/resources/papers/3A\\_Cynthia%20Teniers%20-%20revised%20copy.pdf](http://oisd.brookes.ac.uk/ivisnet/resources/papers/3A_Cynthia%20Teniers%20-%20revised%20copy.pdf).

<sup>12</sup> [https://cordis.europa.eu/docs/publications/1263/126376031-19\\_en.doc](https://cordis.europa.eu/docs/publications/1263/126376031-19_en.doc).

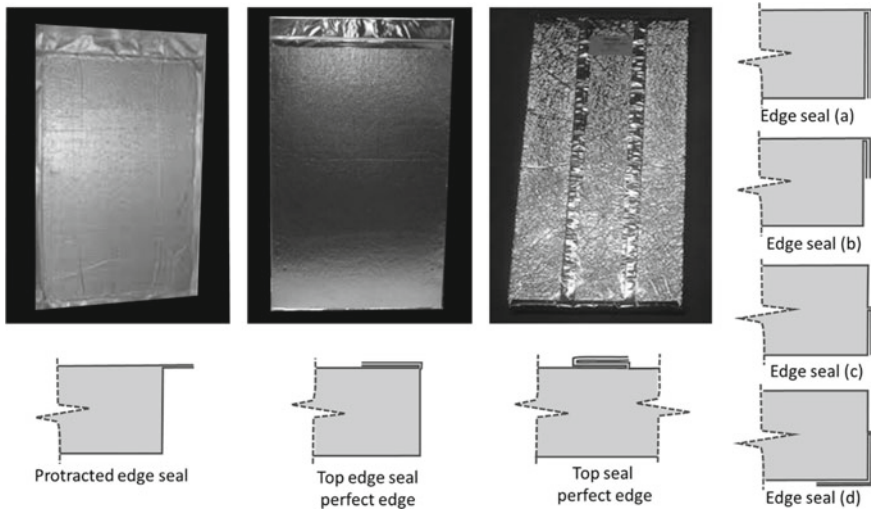


**Fig. 15.17** Different placements of the VIP seal, affecting the edge material configuration and consequently, the thermal bridge effects

## 15.9 Durability Problems Caused by Imperfections in Insulation and Thermal Bridging Generated by Structural and Finish Materials

Well designed and installed thermal insulation systems improve building energy efficiency, and often improve the lifespan of components. In addition to undesired heat losses and/or gains, thermal bridging in exterior envelopes may also lead to durability problems. Low-temperatures due to discontinuities in the thermal insulation and envelope penetrations by conductive materials may lead to water condensation and accumulation. Nearly all building materials are susceptible to durability problems associated with increased water content—see: Sedlbauer (2001); Kumaran (2006); Hens (2008) (i) wet thermal insulation may deteriorate and perform poorly (wet insulation is more conductive), (ii) uncontrolled high-water content in concretes, mortars, gypsum, or brick will cause material deterioration, (iii) wet bio-based building materials makes great nourishment for fungus and as a result the materials will deteriorate, (iv) steel components will corrode.

In commercial buildings, façade shading and decoration details frequently use numerous conductive components; including lintels, anchorage, and hangers that bypass the thermal barrier and produce thermal shorts, which often result in condensation on interior surfaces. Structural-steel framing that extends from the inside to the outside not only makes waterproofing and air barrier details difficult, but also forms areas of intense thermal bridges. Finally, a great number of commercial buildings are constructed today using light gauge or heavy gauge. This fact requires special attention during the design of the exterior envelope, because any design mistake,

coupled with highly conductive metal elements, may (most often it will) cause serious thermal shorts and resulting durability problems. Table 15.2 summarizes the most typical design problems associated with missing insulation, ill-performing insulation, and/or thermal bridging.

## 15.10 Building Performance Standards Dealing with Building Thermal Bridging

There are three energy performance standards focused on buildings in North America.

- ASHRAE 90.1 Energy Standard for Buildings Except Low-Rise Residential Buildings—ASHRAE 90.1 (2013)
- ASHRAE 189.1 Standard for the Design of High-Performance Green Buildings Except Low-Rise Residential Buildings—ASHRAE 189.1 (2013)
- National Energy Code of Canada for Buildings 2011 (NECB 2011)

In Europe, thermal bridge calculations are based on two ISO standards—ISO 10211 (2007); ISO 6946 (2007) “Thermal bridges in building construction—Heat flows and surface temperatures—Detailed calculations,” and “Building Components or Building Elements” which serves for:

- the calculation of minimum (lowest) surface temperatures in order to assess the risk of surface condensation and the calculation of heat flows in order to predict overall heat loss from a building (for the constant, steady state flow case; i.e. time independent temperature distribution) and determination of linear and point thermal transmittance and surface temperature coefficients (of thermal bridges).

The above specifications include geometrical boundaries and subdivisions, thermal boundary conditions, and thermal values and relationships to be used. The second important standard is ISO 6946 (2007) "Building Components or Building Elements—Calculation of Thermal Transmittance" is also available. According to this standard, calculation of heat transfer coefficients of parallel plane surface building components shall be performed based on one-dimensional calculations. For all other more complex heat flow cases with multidimensional heat transfer, the standard ISO 10211 (2007) “Thermal Bridges in Building Construction” requires the implementation of numerical methods.

Following is a list of ISO building standards which can be helpful in analysis of thermal bridges and building design.

- ISO 7345 (1987) “Thermal insulation—Physical quantities and definitions”.
- ISO 10456 (2007) “Building materials and products - Hygrothermal properties— Tabulated design values and procedures for determining declared and design thermal values”.
- ISO 13370 (2007)“Thermal performance of buildings—Heat transfer via the ground—Calculation methods”.



**Table 15.2** Typical design problems associated with missing thermal insulation and thermal bridging

<p>Typical consequences</p>	<p>Description of common energy-related problems associated with insulation imperfections and thermal bridging</p>
<p>Air gaps due to missing or compressed insulation</p>	<p>Air gaps created by missing or compressed insulation, may allow free air convection within building envelope cavities (reducing thermal performance). When connected, they may cause undesired air and moisture exchange between the interior and exterior of the building, causing moisture condensation and accumulation inside building envelopes. Consequently, this may yield a mold growth and material deterioration</p>
<p>Heat losses</p>	<p>Thermal bridges are the weakest points in the thermal envelope and so, in cold climates, they can contribute considerable heat losses. This reduces the overall building energy efficiency and increases heating costs</p>
<p>Unwanted heat gains</p>	<p>In cooling-dominated and mixed climates, thermal bridges allow unwanted solar heat gains. Roofs and attics are typical building envelope areas which may create intense solar gains if incorrectly designed</p>
<p>Cold internal surfaces</p>	<p>In winter, an intense heat transfer in a thermal bridge are, may cause the internal surface temperature to drop, creating a cold spot. The surface relative humidity will thereby increase, yielding a risk of condensation and potential for mold growth. In cold climates, metal window frames in commercial buildings are notorious sources of condensation problems caused by highly conductive materials and insufficient thermal break- see: Curcija et al. (2013)</p>

(continued)

**Table 15.2** (continued)

<p>Typical consequences</p>	<p>Description of common energy-related problems associated with insulation imperfections and thermal bridging</p>
<p>Discoloration marks on the interior and exterior surfaces</p>	<p>Depends on climatic conditions, intense thermal bridging (for example in case of metal framing) may cause internal or external cold spots, which can yield local condensation. On some surfaces, this may lead to development of unaesthetic discolorations (for example so-called ghosting on the internal gypsum board surfaces in case of steel framed buildings)</p>
<p>Risks to thermal comfort and health issues</p>	<p>Cold internal surfaces are uncomfortable to be near and can cause thermal discomfort and perception of draughts. In addition, local cold surfaces within building envelopes usually cause moisture condensation, which in longer-term can yield fungus grow, affecting the indoor air quality. It has been well documented in literature, that both moisture and mold growth can lead to building occupants' health problems—EPA (2013)</p>

- ISO 13786 (2007) "Thermal performance of building components—Dynamic thermal characteristics—Calculation methods".
- ISO 10211 (2007) "Thermal Bridges in Building Construction—Heat Flows and Surface Temperatures—Detailed Calculations";
- ISO 14683 (2007a, b) "Thermal Bridges in Building Construction—Linear Thermal Transmittance—Simplified Methods and Default".
- ISO 13788 (2012) "Hygrothermal performance of building components and building elements—Internal surface temperature to avoid critical surface humidity interstitial condensation—Calculation methods".
- ISO 13789 (2007) "Thermal performance of buildings—Transmission and ventilation heat transfer coefficient - Calculation method".
- ISO 14683 (2007a, b) "Thermal bridges in building construction—Linear thermal transmittance—Simplified methods and default values".

## References

- Al-Sanea, S., & Zedan, M. F. (2012). Effect of thermal bridges on transmission loads and thermal resistance of building walls under dynamic conditions. *Applied Energy*, 98, 584–593.
- Antretter, F., Radon, J., & Pazold, M. (2010). Coupling of dynamic thermal bridge and whole-building simulation. In *ASHRAE, Proceedings of Thermal Performance of the Exterior Envelopes of Whole Buildings XII International Conference*, Clearwater, FL, USA, 5–8 December.
- Ascione, F., Bianco, N., de' Rossi, F., Turni, G., & Vanoli, G. (2012). Different methods for the modelling of thermal bridges into energy simulation programs: Comparisons of accuracy for flat heterogeneous roofs in Italian climates. *Applied Energy*, 97, 405–418
- ASHRAE. (2002). Modeling transient performance of two-dimensional and three-dimensional building assemblies. Report, ASHRAE Research Project Report, RP-1145, Atlanta, Georgia, USA. [https://www.techstreet.com/standards/rp-1145-modeling-two-and-three-dimensional-heat-transfer-through-composite-wall-and-roof-assemblies-in-hourly-simulation-programs?product\\_id=1711769](https://www.techstreet.com/standards/rp-1145-modeling-two-and-three-dimensional-heat-transfer-through-composite-wall-and-roof-assemblies-in-hourly-simulation-programs?product_id=1711769).
- ASHRAE. (2011). Thermal performance of buildings envelope details for mid and high-rise buildings. Report, ASHRAE Research Project Report, RP-1365, Atlanta, Georgia, USA, July 6. [https://www.healthyheating.com/HH\\_Integrated\\_Design/Week%202/Thermal%20Performance%20of%20Buildings%20Envelope.pdf](https://www.healthyheating.com/HH_Integrated_Design/Week%202/Thermal%20Performance%20of%20Buildings%20Envelope.pdf).
- ASHRAE. (2021). Handbook of fundamentals. ASHRAE, Atlanta, Georgia, USA. <https://www.ashrae.org/technical-resources/ashrae-handbook/description-2021-ashrae-handbook-fundamentals>.
- ASHRAE 90.1. (2013). Energy standard for buildings except low-rise residential buildings. Retrieved May 27, 2016, from ASHRAE.org. <https://www.ashrae.org/resources-publications/bookstore/standard-90-1>.
- ASHRAE 189.1. (2014). Standard for the design of high-performance green buildings. Retrieved May 27, 2016, from ASHRAE.org. <https://www.ashrae.org/resources-publications/bookstore/standard-189-1>.
- Barbour, E., Goodrow, J., Košný, J., & Christian, J. E. (1994). Thermal performance of steel-framed walls - prepared for The American Iron and Steel Institute by NAHB Research Center, November 21.
- Bedoya, C., Lyons, C., Pollard, McClure, D., & Jones, S.J. (2017). High performance barrier films for vacuum insulation panels. In *Proceedings of the AIMCAL R2R Conference USA 2017, Roll 2*

- Roll Web coating and Finishing*, Tampa, Florida, October 15–18. <https://www.aimcal.org/2018-aimcal-r2r-conference-usa.html>.
- Ben-Nakhi, A. (2003). Development of an integrated dynamic thermal bridging assessment environment. *Energy Building*, 35, 375–382.
- Burch, D. M., Seem, J. E., Walton, G. N., & Licitra, B. A. (1992). Dynamic evaluation of thermal bridges in a typical office building. *ASHRAE Transactions*, Vol. 98, Pt. 1. ASHRAE, Atlanta, Georgia, USA.
- Carpenter, S. C., & Schumacher, C. (2003). Characterization of framing factors for wood-framed low-rise residential buildings. *ASHRAE Transactions*, 109, Pt 1. Feb.
- Castro Aguilar, J. L., Košny, J., & Shukla, N. (2017). Evaluating the impact of the edge thermal bridging on the overall thermal performance of vacuum insulation panel (VIP) assemblies. In *The 13th International Vacuum Insulation Symposium (IVIS 2017)*, Paris, France, 20–21 September.
- CEC. (2001A). Characterization of framing factors for lowrise residential building envelopes in California. Public Interest Energy Research Program: Final Report, Publication Number: 500-02-002, December.
- CEC. (2001B). 2001 energy standards for residential and non-residential buildings. California Energy Commission Title 24, August.
- Childs, K., Stovall, T., Biswas, K., Carbary, L. (2013). Thermal performance of exterior insulation and finish systems containing vacuum insulation panels. In *Proceedings of Thermal Performance of the Exterior Envelopes of Whole Buildings XII International Conference*, December.
- Christian, J. E., & Strzepek, W. R. (1987). Procedure for determining the optimum foundation insulation levels for new, low-rise residential buildings. *ASHRAE Transactions*, 93, Pt. 1, January.
- Christian, J. E., & Košny, J. (1995). Towards a national opaque wall rating label—ASHRAE, BETEC, U.S. DOE VI Thermal Envelope Conference, Clearwater, Florida, December.
- Curcija, C., Goudey, H., Mitchell R., & Dickerhoff, E. (2013). Highly Insulating Window Panel Attachment Retrofit. Report prepared for the General Services Administration by Lawrence Berkeley National Laboratory - Windows and Envelope Materials Group, March.
- ECBCS/IEA Annex 39. (2005). Vacuum insulation panels, study on VIP-components and panels for service life prediction of VIP in building applications (Subtask A). Retrieved from <http://www.ecbcs.org/annexes/annex39.htm>.
- Enermodal Engineering. (1996). Building insulation system thermal anomalies. Final report for ASHRAE Research Project 785-TRP – Waterloo, Canada.
- EPA. (2013). Moisture control guidance for building design, construction and maintenance. U.S. Environmental Protection Agency, December.
- Hassid, S. (1990). Thermal bridges across multilayer walls: An integral approach. *Building and Environment*, 25, 143–150.
- Hens, H. S. (2008). Building physics—Heat, air and moisture: fundamentals and engineering methods with examples and exercises. Ed. 2. John Wiley & Sons.
- ISO 10211. (2007). Thermal bridges in building construction—Heat flows and surface temperatures—Detailed calculations. Retrieved May 27, 2016, from iso.org. [http://www.iso.org/iso/home/store/catalogue\\_tc/catalogue\\_detail.htm?csnumber=40967](http://www.iso.org/iso/home/store/catalogue_tc/catalogue_detail.htm?csnumber=40967).
- ISO 14683. (2007a). Thermal bridges in building construction—Linear thermal transmittance—Simplified methods and default values. Retrieved May 27, 2016, from iso.org. [http://www.iso.org/iso/iso\\_catalogue/catalogue\\_tc/catalogue\\_detail.htm?csnumber=40964](http://www.iso.org/iso/iso_catalogue/catalogue_tc/catalogue_detail.htm?csnumber=40964).
- ISO 6946. [2007]. Building components and building elements—Thermal resistance and thermal transmittance—Calculation method. Retrieved May 27, 2016, from iso.org [http://www.iso.org/iso/iso\\_catalogue/catalogue\\_tc/catalogue\\_detail.htm?csnumber=40968](http://www.iso.org/iso/iso_catalogue/catalogue_tc/catalogue_detail.htm?csnumber=40968).
- ISO 7345. (1987). Thermal insulation—Physical quantities and definitions. Retrieved May 27, 2016, from iso.org [http://www.iso.org/iso/catalogue\\_detail.htm?csnumber=14024](http://www.iso.org/iso/catalogue_detail.htm?csnumber=14024).
- ISO 10456. (2007). Building materials and products—Hygrothermal properties—Tabulated design values and procedures for determining declared and design thermal values. Retrieved May 27, 2016, from iso.org [http://www.iso.org/iso/catalogue\\_detail.htm?csnumber=40966](http://www.iso.org/iso/catalogue_detail.htm?csnumber=40966).

- ISO 13370 (2007) - "Thermal performance of buildings - Heat transfer via the ground - Calculation methods," Retrieved May 27, 2016, from iso.org: [http://www.iso.org/iso/iso\\_catalogue/catalogue\\_tc/catalogue\\_detail.htm?csnumber=40965](http://www.iso.org/iso/iso_catalogue/catalogue_tc/catalogue_detail.htm?csnumber=40965)
- ISO 13786. (2007). Thermal performance of building components—Dynamic thermal characteristics—Calculation methods. Retrieved May 27, 2016, from iso.org [http://www.iso.org/iso/iso\\_catalogue/catalogue\\_tc/catalogue\\_detail.htm?csnumber=40892](http://www.iso.org/iso/iso_catalogue/catalogue_tc/catalogue_detail.htm?csnumber=40892).
- ISO 13788. (2012). Hygrothermal performance of building components and building elements - Internal surface temperature to avoid critical surface humidity interstitial condensation—Calculation methods. Retrieved May 27, 2016, from iso.org [http://www.iso.org/iso/iso\\_catalogue/catalogue\\_tc/catalogue\\_detail.htm?csnumber=51615](http://www.iso.org/iso/iso_catalogue/catalogue_tc/catalogue_detail.htm?csnumber=51615).
- ISO 13789. (2007). Thermal performance of buildings—Transmission and ventilation heat transfer coefficient—Calculation method. Retrieved May 27, 2016, from iso.org [http://www.iso.org/iso/iso\\_catalogue/catalogue\\_tc/catalogue\\_detail.htm?csnumber=40894](http://www.iso.org/iso/iso_catalogue/catalogue_tc/catalogue_detail.htm?csnumber=40894).
- ISO 14683. (2007b). Thermal bridges in building construction—Linear thermal transmittance - Simplified methods and default values. Retrieved May 27, 2016, from iso.org [http://www.iso.org/iso/iso\\_catalogue/catalogue\\_tc/catalogue\\_detail.htm?csnumber=40964](http://www.iso.org/iso/iso_catalogue/catalogue_tc/catalogue_detail.htm?csnumber=40964).
- Kossecka, E. (1992). Heat transfer through building wall elements of complex structure. *Archives of Civil Engineering*, 38(1–2), 117–126.
- Kossecka, E., & Košny, J. (1997). Equivalent wall as a dynamic model of a complex thermal structure. *Journal of Thermal Insulation and Building Envelopes*, 20, January.
- Kossecka, E., & Košny, J. (2002, April). Influence of insulation configuration on heating and cooling loads in continuously used building. *Energy and Buildings*, 34, 321–331
- Kossecka, E, & Košny, J. (2003). Z-Transfer function coefficients for simulation of three-dimensional heat transfer in building walls. August/September 2003 issue of *Archives of Civil Engineering*, vol. XLIX, 4, Warsaw, Poland.
- Kossecka, E, & Košny, J. (2005, March). Three-dimensional conduction Z-Transfer function coefficients derived from the response factors. *Energy and Buildings*.
- Košny, J., & Desjarlais, A. O. (1994). Influence of architectural details in the overall thermal performance of residential wall systems. *Journal of Thermal Insulation and Building Envelopes*, VIII, 53–69, July 1994, Clearwater, FL, USA.
- Kosny, J., & Christian, J. E. (1995). Reducing the uncertainties associated with using the ASHRAE zone method for R-value calculations of metal frame walls. *American Society of Heating, Refrigerating and Air-Conditioning Engineers (ASHRAE) Transactions*, 101, Pt 2.
- Košny, J, Christian, J. E., & Desjarlais, A. O. (1997). Thermal breaking systems for metal stud wall—Can metal stud walls perform as well as wood stud walls? *American Society of Heating, Refrigerating and Air-Conditioning Engineers (ASHRAE) Transactions*, 103 pt 1.
- Košny, J, Christian, J. E, Desjarlais, A. O, Kossecka, E, & Berrenberg, L. (1998). Performance check between whole building thermal performance criteria and exterior wall measured clear wall R-value, thermal bridging, and airtightness. *American Society of Heating, Refrigerating and Air-Conditioning Engineers (ASHRAE) Transactions*, 104 pt 2.
- Košny, J., & Kossecka, E. (2002). Multidimensional heat transfer through complex building envelope assemblies in energy simulation programs. *Energy and Buildings*, 34, 445–454
- Košny, J, Yarbrough, D. W, Childs, P., & Mohiuddin, S. A. (2007a-A). How the same wall can have several different R-values? Relations between amount of framing and overall thermal performance in wood and steel-framed walls. In *X Conference - Thermal Performance of the Exterior Envelopes of Buildings*, December, Clearwater, Florida.
- Košny, J., Yarbrough, D. W, Petrie, T, Childs, P, Mohiuddin, S. A, & Blair, C. (2007b-B). Nano-scale insulation at work. Thermal Performance of Thermally Bridged Wood and Steel Structures Insulated with Local Aerogel Insulation—X Conference—Thermal Performance of the Exterior Envelopes of Buildings, December, Clearwater, Florida.
- Košny, J., Stovall, T., Shrestha, S., & Yarbrough, D. (2010). Theoretical and experimental thermal performance analysis of complex thermal storage membrane containing bio-based phase-change material (PCM). In *Proceedings of DOE, ASHRAE, ORNL Conference—Thermal Envelopes XI*

- *Thermal Performance of the Exterior Envelopes of Buildings*, December 2010, Clearwater, Florida, USA.
- Košny, J., Fallahi, A., & Shukla, N. (2013). Cold climate building enclosure solutions – U.S. DOE Building America Program report, NREL/SR-5500–55875, January 2013, <http://www.nrel.gov/docs/fy13osti/55875.pdf>.
- Košny, J., Misiopcecki, C., Fallahi, A., Shukla, N., DuPont, W. C., & Carbary, L.D. (2014). Thermal design of window-wall interface in wall energy retrofits using high-performance vacuum insulation. *ASHRAE Transactions*, 120, SE-14–008, p. 90
- Košny, J., & Yarbrough, D. (2018). Thermal bridges in building structures. Chapter 4.10, Editor-in-Chief Raj P Chhabra - CRC Handbook of Thermal Engineering, Second Edition, Taylor & Francis Group, LLC. ISBN 9781315119717.
- Košny, J., & Yarbrough, D. (2019). Recent advances in vacuum thermal insulations used in building thermal envelopes. Chapter in vol 21. Annual Review of Heat Transfer, Begellhouse - ID "ARHT-30270.
- Kumaran, M. K. (2006). A thermal and moisture property database for common building and insulation materials. NRCC-45692, NRC, Institute of Research in Construction, Canada.
- Langlais, C., Hyrien, M., & Klarsfeld, S. (1983). Influence of moisture on heat transfer through fibrous-insulating materials. In *Proceedings of the Buildings III Conference*, December, Clearwater Beach, FL, USA.
- Martin, K., Erkoreka, A., Flores, I., Odriozola, M., & Sala, J. M. (2011). 2011, Problems in the calculation of thermal bridges in dynamic conditions. *Energy Building*, 43, 529–535.
- Martin, K., Campos-Celador, A., Escudero, C., Gómez, I., & Sala J. M. (2012). Analysis of a thermal bridge in a guarded hot box testing facility. *Energy and Buildings*, 50:S, 139–149.
- Martins, C., Santos, P., & da Silva, L. (2016). Lightweight steel-framed thermal bridges mitigation strategies: A parametric study. *Journal of Building Physics*, 39, 342–372.
- McFadden, T. (1988). Thermal performance degradation of wet insulations in cold regions. *Journal of Cold Regions Engineering*, 2(1), 25–34.
- Moore, T. V. (2017). *Evaluating the thermal resistance of a vacuum insulation panel wall assembly containing thermal bridges using industry standard calculation methods and numerical simulation techniques*. Thesis, Carleton University, Department of Mechanical Engineering, Ottawa, Ontario, Canada.
- NECB. (2011). National Energy Code of Canada for Buildings 2011. Retrieved May 27, 2016, from [nrc-cnrc.gc.ca](http://www.nrc-cnrc.gc.ca) [http://www.nrc-cnrc.gc.ca/eng/publications/codes\\_centre/2011\\_national\\_energy\\_code\\_buildings.html](http://www.nrc-cnrc.gc.ca/eng/publications/codes_centre/2011_national_energy_code_buildings.html).
- NIBS. (2012). Building envelope design guide—Curtain walls, National Institute of Building Sciences (NIBS), Washington DC, USA, 06–25–2012.
- Ohlsson, J. (1998). Measurements and calculations of the heat flow through walls with steel studs (in Swedish). Department of Building Physics, Lund University. P.O. Box 1 18, S221 00 Lund, Sweden.
- Pears, C. D. Touloukian, Y. S., Powell, R. W., Ho, C. Y., & Klemens, P.G. (1971). Thermophysical and electronic properties. Information and Analysis Center Lafayette In, TPRC Data Series Volume 2, pp. 145–6, Reference No. 144, page 1162>PDF. Retrieved from <http://oai.dtic.mil/oai/oai?verb=getRecord&metadataPrefix=html&identifier=ADA951936>.
- Schwab, H., Stark, C., Wachtel, J., Ebert, H.-P., & Fricke, J. (2005). Thermal bridges in vacuum-insulated building façades. *Journal of Thermal Envelope & Building Science*, 28(4), 345–355.
- Sedlbauer, K. (2001). *Prediction of mold fungus formation on the surface of and inside building components*. Fraunhofer Institute for Building Physics.
- Sprengard, C., & Holm, A. (2014). Numerical examination of thermal bridging effects at the edges of vacuum insulation panels (VIP) in various constructions. *Energy and Buildings*, Issue, 85, 638–643.
- Strzepek, W. R. (1990). Overview of physical properties of cellular thermal insulations. In D. L. McElroy & J. F. Kimpfen (Eds.), *Insulation materials, testing, and applications*, ASTM STP 1030 (pp. 121–140). American Society for Testing and Materials.

- Tenpierik, M. J., & Cauberg, H. (2007). Analytical models for calculating thermal bridge effects caused by thin high barrier envelopes around vacuum insulation panels. *Journal of Building Physics*, 30, 185–215.
- Trechsel, H. R., & Bomberg, M. (2009). *Moisture control in buildings: The key factor in mold prevention*—West Conshohocken, PA: ASTM International. <https://doi.org/10.1520/MNL18-2ND-EB>.
- Trethowen, H. A. (1988). Thermal insulation and contact resistance in metal-framed panels. *ASHRAE Transactions*, 94(2), 1802–1817, Corpus ID: 114783274.
- Trethowen, H. A. (1991). Sensitivity of insulated wall and ceiling cavities to workmanship. *Journal of Thermal Insulation*, 15, October 1991. <https://doi.org/10.1177/109719639101500205>.
- Tuluca, A. N. Lahiri, D., & Zaidi, J. H. (1997). calculation methods and insulation techniques for steel stud walls in low-rise multifamily housing. *ASHRAE Transactions: Technical and Symposium Papers*, Volume 103, Part 1; PB: 1136 p. CONF-9702141 - Journal ID: ISSN 0001–2505; TRN: IM9922%%192.
- Van Den Bossche, N., Moens, J., Janssens, A., & Delvoye, E. (2010). *Thermal performance of VIP panels: Assessment of the edge effect by experimental and numerical analysis*. Ghent University, Department of Architecture and Urban Planning.
- Wakili, G. K., Bundi, R., & Binder, B. (2004). Effective thermal conductivity of vacuum insulation panels. *Building Research and Information*, 32(4), 293–299.
- Wakili, G. K., Stahl, T., & Brunner, S. (2011). Effective thermal conductivity of a staggered double layer of vacuum insulation panels. *Energy and Buildings*, 43, 1241–1246.
- Zedan, M. F., Al-Sanea, S. A., Al-Mujahid, A., & Alsuhaibani, Z. (2016, June). Effect of thermal bridges in insulated walls on air-conditioning loads using whole building energy analysis. *Sustainability*, 8(6), 560. <https://doi.org/10.3390/su8060560>.
- Ziegel. (2010). Thermal Bridges. Retrieved December 07, 2020, from [www.ziegel.at](http://www.ziegel.at): <http://www.ziegel.at/gbc-ziegelhandbuch/eng/ressourcen/energie/prim/waermebruecken.htm>.